The 8.06 Physical Review

Foreword

This volume of *The 8.06 Physical Review* collects term papers written by 8.06 students in 2013. Physics 8.06 is the last semester of a three-semester sequence of courses on quantum mechanics offered at MIT. In 8.06, each student was required to write a paper on a topic related to but going beyond the content of 8.06. The topic could be a physical effect, a practical application, or further development of techniques and concepts of quantum mechanics. The paper was written in the style and format of a brief Physical Review article, aimed at fellow 8.06 students.

There are two main purposes for such a project. First, this gives our students the opportunity to research topics in modern physics on their own. Toward the end of 8.06, students should have the background and ability to understand many modern applications of quantum mechanics by themselves. The process of selecting a topic, understanding it, and then communicating it effectively to peers is a creative way of learning that effectively complements classroom lectures. A practicing physicist goes through such a process in his or her research.

Another important goal of the project is to help our students learn the art of effective technical writing. We expect later in life many of our students will often need to write technical reports or articles. Writing for *The 8.06 Physical Review* should provide a valuable starting point. Writing, editing, revising, and "publishing" skills are an integral part of the project. Each student was asked to choose another student to edit a first draft and then prepared a final draft on the basis of the suggestions of his "peer editor". In addition, each student was assigned a graduate student "writing assistant." The writing assistant's responsibilities include critiquing the proposal and the first draft of the paper and providing any additional help a student may seek. Typically papers improve enormously through this process. The quality of the papers collected here speak for themselves.

This year, fifty-five 8.06 students have written on a wide variety of fascinating topics, covering almost all major branches of modern physics, including astrophysics, condensed matter, particle physics, nuclear physics, relativistic quantum mechanics and quantum information. Some popular topics were addressed by more than one author, including, for example, graphene, the Dirac equation and path integrals. Many papers collected here were very well written and demonstrated clarity of thought and depth of understanding of their authors. This volume embodies the unfailing enthusiasm in quantum physics of 8.06 students.

ii

Acknowledgments

Contents

Dressed atom approach to laser cooling: dipole forces and Sisyphus cooling

Kamphol Akkaravarawong
Department of Physics
(Dated: May 3, 2014)

Today laser cooling is an important tool in atomic, molecular, and optical physics. The cooling mechanism can be explained by the interaction between an atom and an electromagnetic field. In this paper, we will use the dressed atom picture to explain how to use a standing electromagnetic wave to cool down atoms. In extremely small velocities regime, the resistive force is due to the dipole force. On the other hand, for intermediate velocity, the atom is cooled down by the Sisyphus mechanism.

I. INTRODUCTION

In 1997, the nobel prize was awarded to Steven Chu, Claude Cohen-Tannoudji and William D. Phillips for laser cooling. An important mechanism initially elucidated was Sisyphus cooling. Sisyphus cooling and dipole forces can be explained intuitively by using the dressed atom picture where the atom and light are treated in a coupled basis. This paper will focus on the scenario of a standing wave of a single laser mode inside a cavity. The formalism of the dressed atom picture will first be introduced. Then, the dressed atom will be used to explain the source of dipole forces in the extremely low velocity regime and Sisyphus cooling in the intermediate velocity regime.

II. DRESSED ATOM PICTURE

A. The Hamiltonian

Consider a system with a two-level atom in a standing wave of a single mode radiation. The total Hamiltonian of the system has three parts:

$$H = H_A + H_L + V_{AL} \qquad (1)$$

where H_A is the Hamiltonian of the atom, and H_R is the Hamiltonian of the radiation field, and V_{AL} is the atom-field coupling. H_A is the sum of kinetic energy and the internal energy. In calculation, because the atom is considered at any given point, the kinetic energy term $P^2/2m$ can be omitted.

$$H_A = \hbar\omega_o b^\dagger b \qquad (2)$$

where $\hbar\omega_o$ is the energy gap between two levels. $b^\dagger$ is a raising operator and b is a lowering operator. If $|e\rangle$ and $|g\rangle$ are the ground and the excited levels of the atom respectively, then the operators in this basis are

$$b^\dagger = |g\rangle\langle e|, b = |e\rangle\langle g| \qquad (3)$$

For the Hamiltonian of the radiation field, the laser will be treated as a quantized field.[4] The zero-point energy can be ignored without loss of generality. The Hamiltonian of the radiation field is then

$$H_R = \hbar\omega_L a^\dagger a = \hbar\omega_L N \qquad (4)$$

where $a^\dagger$ and a are a raising and a lowering operator of photons respectively, and N is a photon number operator.

In the absence of coupling, the eigenstates of the uncoupled Hamiltonian or the bare states are simply a ground or excited state with photons. For example, the bare states can be labeled as $|g, N\rangle$. Considering a case where the laser frequency is close to the atomic resonance frequency, the detuning $\delta = \omega_L - \omega_0 \ll \omega_0, \omega_L$. As a result, the bare state energy levels will be well-separated into manifolds, and each manifold will contain two states, see Fig. 1. The energy gap between two bare states in the same manifold is $E_{g,N+1} - E_{e,N} = \hbar\delta$. As a result, the position of the two levels can be switched if the sign of δ is changed. Later in this paper, the words manifold and dressed level will be used interchangeably when coupling is present.

The atom and the radiation field interact through the dipole interaction. The coupling Hamiltonian is

$$V_{AL} = -d \cdot E(r) \qquad (5)$$

where d is the atomic electric dipole moment and $E(r)$ is the electric field at position r. The atom does not have a dipole moment when it is in an energy eigenstate i.e. $\langle g| d |g\rangle = \langle e| d |e\rangle = 0$. For a two-level system, the dipole operator is purely non-diagonal. The Hermitian dipole operator can be represented as [2]

$$d = d_{eg}(|g\rangle\langle e| + |e\rangle\langle g|) = d_{eg}(b^\dagger + b) \qquad (6)$$

where $d_{eg} = \langle e| d |g\rangle = \langle g| d |e\rangle$. [?] The quantized electric field can be written as

$$E = \epsilon_L(a + a^\dagger) \qquad (7)$$

ϵ_L is product of the laser polarization and a scaling factor. Now the coupling Hamiltonian can be simplified, because the field frequency is close to the atomic resonance frequency. By moving from the Schrödinger picture into the interaction picture, the coupling Hamiltonian is evolved by a unitary operator of the atom and field Hamiltonian.[5] The unitary operator is

$$U = e^{i(H_A + H_L)t/\hbar} \qquad (8)$$
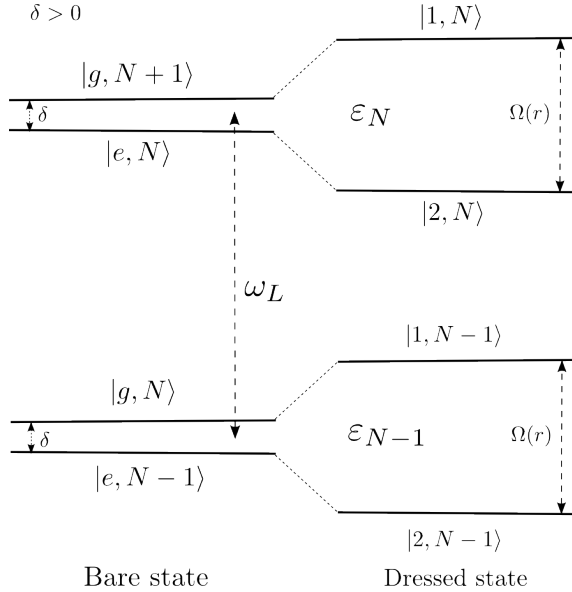
FIG. 1: Left)In the absence of coupling, the bare states are bunched into manifolds. Each manifold will contain two states. Two manifold ε_N and ε_{N-1} are shown here. When $\delta > 0$, state $|g, N+1\rangle$ has a higher energy than state $|e, N\rangle$. Right) In the presence of coupling, the new eigenstates still form manifolds with two dressed states inside each Unlike the bare state, the energy gap between two dressed state depends on the electric field strength, and despite the change in δ's sign, the energy levels do not change.

Thus, the coupling Hamiltonian in the interaction picture is

$$
\begin{aligned}
V_{AL}(t)^{inter} &= U V_{AL} U^\dagger \\
&= g(bae^{-i(\omega_o+\omega_L)t} + b^\dagger a^\dagger e^{i(\omega_o+\omega_L)t} \\
&\quad + b^\dagger a e^{i(\omega_o-\omega_L)t} + ba^\dagger e^{-i(\omega_o-\omega_L)t}) \quad (9)
\end{aligned}
$$

where $g = -d_{eg} \cdot \epsilon_L$. It follows that each term will oscillate with a frequency of either $\omega_L + \omega_0$ or $\omega_L - \omega_0$. Because $\omega_L \approx \omega_0$, the two frequencies are so different that the quickly oscillating terms will destructively interfere and cancel out when averaged, while the slowly oscillating terms will accumulate and contribute to the coupling Hamiltonian. Therefore, the quickly oscillating terms can be ignored. This approximation is called *the rotating-wave approximation*. The coupling Hamiltonian is then transformed back into the Schrödinger picture and combined with the atom and field Hamiltonian. The total Hamiltonian in the rotating wave approximation can be written as

$$
H = \hbar\omega_0 b^\dagger b + \hbar\omega_L N + g(b^\dagger a + ba^\dagger) \quad (10)
$$

B. Eigenenergies and eigenstates of dressed states

The coupling Hamiltonian, $g(b^\dagger a + ba^\dagger)$, can either raise the number of photons and de-excite the atom, or lower the number of photons and excite the atom. Therefore, the atom-laser coupling will only connect two states in the same manifold i.e. $|g, N+1\rangle \leftrightarrow |e, N\rangle$.

$$
\frac{2}{\hbar} \langle e, N | V_{AL} | g, N+1 \rangle = \frac{2}{\hbar} g\sqrt{N+1} = \Omega_1 \quad (11)
$$

Here the Rabi frequency, Ω_1, is introduced. For the manifold ε_N, the Hamiltonian in the matrix representation is

$$
H = \hbar\omega_0 \begin{bmatrix} 1 & 0 \\ 0 & 0 \end{bmatrix} + \hbar\omega_L \begin{bmatrix} N & 0 \\ 0 & N+1 \end{bmatrix} + \frac{\hbar}{2} \begin{bmatrix} 0 & \Omega_1 \\ \Omega_1 & 0 \end{bmatrix} \quad (12)
$$

where the basis vectors are $|e, N\rangle$ and $|g, N+1\rangle$. After diagonalizing the Hamiltonian matrix, the eigenenergies for the manifold ε_N are

$$
\begin{aligned}
E_{1n}(r) &= (N+1)\hbar\omega_L - \frac{\hbar\delta}{2} + \frac{\hbar\Omega(r)}{2} \\
E_{1n}(r) &= (N+1)\hbar\omega_L - \frac{\hbar\delta}{2} - \frac{\hbar\Omega(r)}{2} \quad (13)
\end{aligned}
$$

where

$$
\Omega(r) = [\Omega_1^2(r) + \delta^2]^{1/2} \quad (14)
$$

and the corresponding eigenstates (dressed states) are

$$
\begin{aligned}
|1, N\rangle &= \sin\theta |g, N+1\rangle + \cos\theta |e, N\rangle \\
|2, N\rangle &= \cos\theta |g, N+1\rangle - \sin\theta |e, N\rangle \quad (15)
\end{aligned}
$$

where the angle θ is defined by

$$
\cos 2\theta = \frac{-\delta}{\Omega}, \quad \sin 2\theta = \frac{\Omega_1}{\Omega} \quad (16)
$$

Here the splitting between dressed states depends on the laser frequency and and the magnitude of the electric field. Notice that the energy levels of uncoupled states outside the laser will be flipped when the sign of the detuning, δ, changes, see Fig. 2.

III. SPONTANEOUS EMISSION

In the previous section, the system is a combination of an atom and a radiation field. However, in quantum field theory, the vacuum is not truly empty but has fluctuation that can create electromagnetic waves that exists for a small period of time. To take this into account, the reservoir of empty modes, which is responsible for the spontaneous emission of fluorescence photons, is introduced. The coupling of the dressed atom with empty modes will cause transitions between two adjacent manifolds. The transitions between states are connected by the dipole operator d.
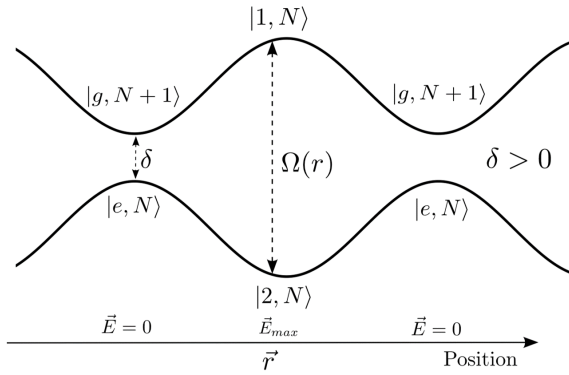
FIG. 2: This diagram represents the energy level of the manifold ε_N in a standing wave. At the middle of the diagram, the atom is in an anti-node of the laser where the field strength is maximal. The atom and the field are coupled here, so the eigenstates are the dressed states. On the other hand, at the laser node, the electric field vanished and there is no coupling. As a result, the eigenstates are bare states.

In the uncoupled basis the only transition is from $|e, N\rangle$ to $|g, N\rangle$. In the dressed atom basis, there are four allowed transitions. Because the laser frequency is close to the atomic resonance frequency, there are only three corresponding frequencies, see Figure (3). Considering transitions between manifold ε_N to ε_{N-1}, the transition rate is proportional to the square of the dipole matrix element d_{ij}. In the coupled basis, the matrix elements and the rates are

$$
\begin{aligned}
d_{ij} &= \langle i, N-1 |\, d_{eg}(b^\dagger + b)\, | j, N \rangle & (17) \\
\Gamma_{i \to j} &= \Gamma_{ij} = \Gamma_0 |d_{ij}|^2 & (18)
\end{aligned}
$$

Frequency	Transition	Transition rate
ω_L	$1 \to 1, 2 \to 2$	$\Gamma_0 \sin^2 \theta \cos^2 \theta$
$\omega_L + \Omega(r)$	$1 \to 2$	$\Gamma_0 \cos^4 \theta$
$\omega_L - \Omega(r)$	$2 \to 1$	$\Gamma_0 \sin^4 \theta$

where Γ_0 is the transition rate of uncoupled states $|e, N\rangle$ and $|g, N\rangle$. If a strong-intensity laser beam is used, the spectrum of the scattered light will form a triplet of lines, called *the Mollow triplet*.

The dressed atom picture also provides a physical interpretation of the radiative cascade where the dressed atom successively transitions from $\varepsilon_N \to \varepsilon_{N-1} \to \cdots$ In dressed atom basis, when the dress atom emits a photon, it can emit either on the carrier (ω_L) or one of the side bands ($\omega_L \pm \Omega(r)$). If it emits on a side band, the dressed atom will be in a different excitation of a lower manifold. As a result, it cannot emit the same side band photon successively.
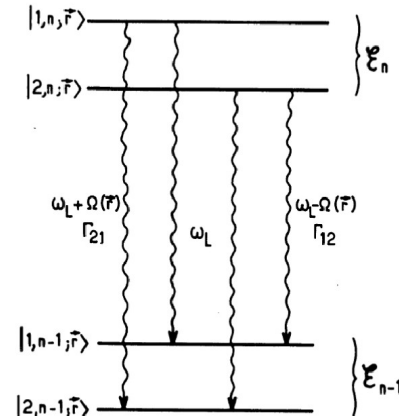
FIG. 3: This diagram represents the allowed transition between two adjacent manifold or dressed levels. The transitions correspond to three frequencies which from a triplet of spectrum line call *the Mollow triplet.* [1]

IV. EQUILIBRIUM POPULATIONS

Because the top and the bottom dressed states have different dynamics when interacting with the laser, it is important to know the number of population in each state.

$$
\Pi_i = \sum_N \langle i, N |\, \rho\, | i, N \rangle \tag{19}
$$

where ρ is the density matrix of the system. Π_i is the total population of the state i in the dressed atom basis. $|1, N\rangle$ is the top state, while $|2, N\rangle$ is the bottom state. The rate equation for the total population is

$$
\begin{aligned}
\dot{\Pi}_1 &= -\Gamma_{12}\Pi_1 + \Gamma_{21}\Pi_2 \\
\dot{\Pi}_2 &= \Gamma_{12}\Pi_1 - \Gamma_{21}\Pi_2
\end{aligned} \tag{20}
$$

At the equilibrium $\dot{\Pi}_1 = \dot{\Pi}_2 = 0$. As a result, the steady-state solution is

$$
\begin{aligned}
\Pi_1^{st} &= \frac{\Gamma_{12}}{\Gamma_{12} + \Gamma_{21}} = \frac{\sin^4 \theta}{\sin^4 \theta + \cos^4 \theta} \\
\Pi_2^{st} &= \frac{\Gamma_{21}}{\Gamma_{12} + \Gamma_{21}} = \frac{\cos^4 \theta}{\sin^4 \theta + \cos^4 \theta}
\end{aligned} \tag{21}
$$

V. LASER COOLING

As an atom travels in a standing wave, it will experience radiation pressure and dipole forces. However, this paper will focus only on dipole forces acting a atom with an extremely small velocity or at rest. When a velocity is no longer extremely small, an atom will be cooled down by Sisyphus mechanism.

A. Mean dipole forces of an atom at rest

Assuming the atom is at rest at r and the laser has strong intensity, the population is the steady-state solution. The splitting between dressed states in the same manifold is $\pm\frac{\hbar\Omega}{2}$. The force can be obtained from the negative of the gradient of the energy. The total force on the atom from the top and the bottom states are

$$F^{st}_{dip} = -\sum_i \Pi^{st}_i \nabla E_i = -\frac{\hbar}{2}(\Pi_1 - \Pi_2)\nabla\Omega \quad (22)$$

$$= -\hbar\delta\frac{\Omega_1^2}{\Omega_1^2 + 2\delta^2}\alpha \quad (23)$$

with

$$\alpha = \frac{\nabla\Omega_1}{\Omega_1} = \frac{\Omega}{\Omega_1^2}\nabla\Omega \quad (24)$$

Notice that the forces of the two states have opposite directions. Therefore, the total force depends on the difference in probability population of the two states.

The direction of the force of each state can be understood intuitively from the energy level diagram, see Fig. 4. Because the atom tends to move to regions with lower energies, the force of the top state will point towards nodes of laser because among every position in the top state, nodes have the lowest energy. With the same reasoning, the force will point towards anti-nodes in the bottom state.

The dressed states have unequal populations, because of spontaneous emission from $|e, N\rangle$ in ε_N to $|g, N\rangle$ in ε_{N-1}. Therefore, the dressed state that is more contaminated by $|e, N\rangle$ will be less populated due to more spontaneous emission. The admixture of $|e, N\rangle$ in the dressed states can be calculated from equation (15).

Alternatively the amount of admixture of $|e, N\rangle$ in each dressed state can also be found from the state with which the dressed states coincide in the absence of the electric field. $|e, N\rangle$ and $|g, N + 1\rangle$ will flip their energy levels if the detuning δ changes the sign. For blue detuned light, $\delta > 0$, the top coupled state $|1, N\rangle$ will coincide with $|g, N + 1\rangle$ in the absence of the laser beam, so the top state is less contaminated by $|e, N\rangle$ than the bottom state. It follows that the bottom state $|2, N\rangle$, with more $|e, N\rangle$, has more spontaneous emission than the top state. Therefore, the top state has more population ($\Pi_1 > \Pi_2$) and the force of the top state dominates (Fig.4)

In contrast, for red detuned laser, $\delta < 0$, $|1, N\rangle$ will coincide with $|e, N\rangle$ outside the laser beam, so it is more contaminated by $|e, N\rangle$ than the bottom state. With the same reasoning, the top state will have less population and the force will be dominated by the bottom state. At the resonance, the top and the bottom state are equally populated ($\Pi_1 = \Pi_2$), therefore the total force vanishes.
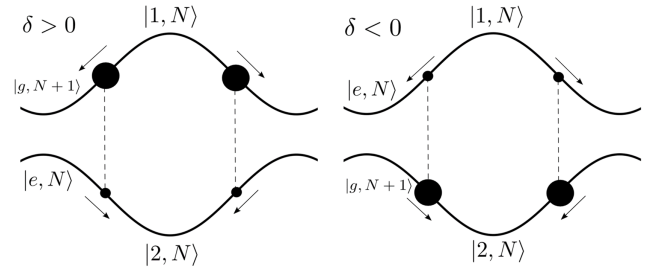
FIG. 4: These diagrams represent the energy level of two dressed states in the same manifold varying over a laser wavelength. Here the electric field is maximal at the antinodes and vanish at the nodes. The arrows represent the direction of the forces. The sizes of the black dots represent the population in each state. Left) for $\delta > 0$, ($\Pi_1 > \Pi_2$) and the total force points towards the node where there is no electric field. Right) for $\delta < 0$, ($\Pi_1 < \Pi_2$) and the total force points towards the anti-node or the region with strong electric field.

B. Mean dipole forces at small velocity

When the atom is moving, the populations are no longer in equilibrium. Here consider extremely small velocities such that

$$v\Gamma^{-1} \ll \lambda \quad (25)$$

where v is the velocity os the atom and Γ^{-1} is the spontaneous emission lifetime. In these conditions, the atom travels a small distance (compared with the laser wavelength) within its spontaneous emission lifetime. As a result, the population can reach the equilibrium before the atom covers a wavelength and the force is determined by local spontaneous transitions. At this limit, the Doppler effect can also be neglected in these conditions. When velocities are extremely small, the populations Π_i for a moving atom is approximately close to the steady state values. The populations take time to reach the equilibrium, therefore the populations will be delayed by τ_{relax} in time or $v\tau_{lag}$ in space where

$$\tau_{lag}(r) = \frac{1}{\Gamma(r)} = \text{time lag} \quad (26)$$

Because the velocity is small, the population Π_i can be expressed in a power series of $v\tau_{lag}$ and only the first-order term is kept.

$$\begin{aligned} \Pi_i(r) &= \Pi^{st}_i(r - v\tau_{lag}) \\ &\simeq \Pi^{st}_i(r) - v\tau_{lag}\cdot\nabla\Pi^{st}_i(r) \end{aligned} \quad (27)$$

Substituting the approximated populations back into the equation (23), the force is

$$F_{dip}(r, v) = F^{st}_{dip}(r) - \frac{2\hbar\delta}{\Gamma}\left(\frac{\Omega_1^2}{\Omega_1^2 + 2\delta^2}\right)^3(\alpha\cdot v)\alpha \quad (28)$$

The first term of the force is the the same as when the atom is at rest and only depends on the position. On the

other hand, the second term is proportional to the velocity of the atom. Here the atom is in a one dimensional standing wave where $\Omega_1(r) = \Omega_{10}\cos(2\pi r/\lambda)$. Therefore, the first term of the force will vanish when averaged over the wave length, because it is sysmetric. The averaged force seen by the atom will become

$$< F_{dip}(r,v) >= -\beta v \qquad (29)$$

where β is the friction coefficient. In this case, the friction force comes from the simple idea that the population will lag behind when the atom travels. From equation(27), the blue detuning $\delta > 0$ will slow down the atom, while the red detuning $\delta < 0$ will heat up the atom. To understand this, the dressed atom can provide a physical interpretation.
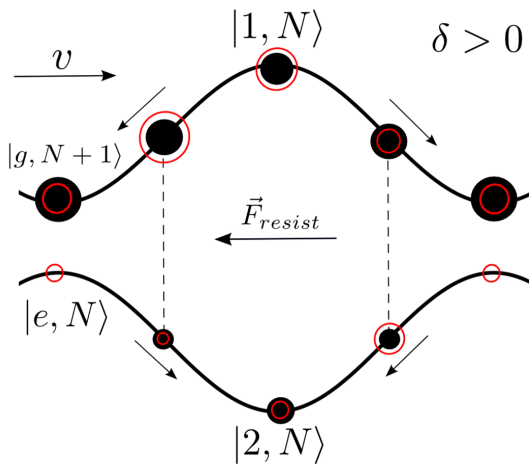
FIG. 5: The filled circles represent the populations at steady state, while the unfilled circles represent the real population of a moving atom. As an atom travels, the population will lag behind. The difference in population between the steady-state and the real population will create an extra resistive force which will not vanish when averaged over wavelengths.

Consider an atom entering a blue detuned laser beam i.e. $\delta = \omega_L - \omega_0 > 0$. With the same argument provided in the case of the atom at rest, the top state $|1,N\rangle$ coincides with $|g,N+1\rangle$ in the absence of the laser beam. $|1,N\rangle$ is then less contaminated by $|e,N\rangle$ than $|2,N\rangle$. Therefore $|1,N\rangle$ is more populated than $|2,N\rangle$: $\Pi_1^{st} > \Pi_2^{st}$. Furthermore, as the atom moves towards the laser node, Ω_1 and the admixture of $|e,N\rangle$ in $|1,N\rangle$ will also increase. It follows that the population of $|1,N\rangle$ decreases as the atom moves towards the laser beam or $\Pi_1^{st}(r-dr) > \Pi_1^{st}(r)$. Now consider an atom moving with a velocity v. Because of time lag, the population $\Pi_1(r)$ at r will be $\Pi_1(r - v\tau_{lag})$. It follows that

$$\Pi_1(r) = \Pi_1^{st}(r - v\tau_{lag}) > \Pi_1^{st}(r) \qquad (30)$$

The same argument gives

$$\Pi_2(r) = \Pi_2^{st}(r - v\tau_{lag}) < \Pi_2^{st}(r) \qquad (31)$$

Because of the shift in the populations, the top state is more populated and the bottom state is less populated than they would be in a steady state. As a result, there will be an extra force in the direction opposite to the movement, see Fig. 5. When the atom travels outwards from the anti-node, the force also points outwards from the anti-node. However, with the same argument, the force on the moving atom will be smaller than it would be if it were at rest, or there is an extra force resisting the movement. As a result, the force is averaged over a wavelength, only the extra force will accumulate and the total force will be a damping force. On the contrary, if a red detuned laser beam ($\delta < 0$) is used, the laser will heat up the atom instead of cooling it down.

VI. SISYPHUS COOLING

Now consider an atom in a high-intensity standing wave where $\delta > 0$ and the velocity is no longer extremely small. The condition for velocities is

$$v\Gamma^{-1} \geq \lambda \qquad (32)$$

This means that the atom covers several wavelengths within its spontaneous emission lifetime. It follows that the atom will have a small probability to emit fluorescence photons when it covers a wavelength, therefore the population is no longer determined by local transitions or the time lag mechanism as in the case of small velocities. Instead, the population is determined by the transition between dressed levels on average over wavelengths.

The physical interpretation of dipole forces can also be derived from the dressed atom picture. Consider the dressed atom in the $|1,N+1\rangle$ state. The allowed transitions are $|1,N+1\rangle \rightarrow |1,N\rangle$ and $|1,N+1\rangle \rightarrow |2,N\rangle$. We are more interred in the latter transition, because the former transition just puts the dressed atom in the same position of the lower manifold. Because the excited state $|e,N\rangle$ is unstable and will make a spontaneous transition to $|g,N\rangle$, the transition between dressed levels is most likely to happen at the position where the dressed state has the largest admixture of $|e,N\rangle$. With the blue detuning $\delta > 0$, anti-nodes of the laser beam are positions where the atom have the largest admixture of the excited state, so transitions are most likely to happen at anti-nodes or "the top of the (potential) hill."

After the transition, the dressed atom is in $|2,N\rangle$, we are interested in the next transition from $|2,N\rangle$ to $|1,N-1\rangle$. At a node of a laser beam, the bottom dressed state is in a pure excited state. With the same argument, it follows that the transition from the bottom state is most likely to happen at nodes of the laser beam. Interestingly, the transitions are likely to happen at "the top of the hill" for transitions from both the top and the bottom states. The cooling mechanism relies on the fact that after falling on the bottom of the potential hill, the atom will move up and down the hills before making a next transition at the top of the hill. As a result, the atom
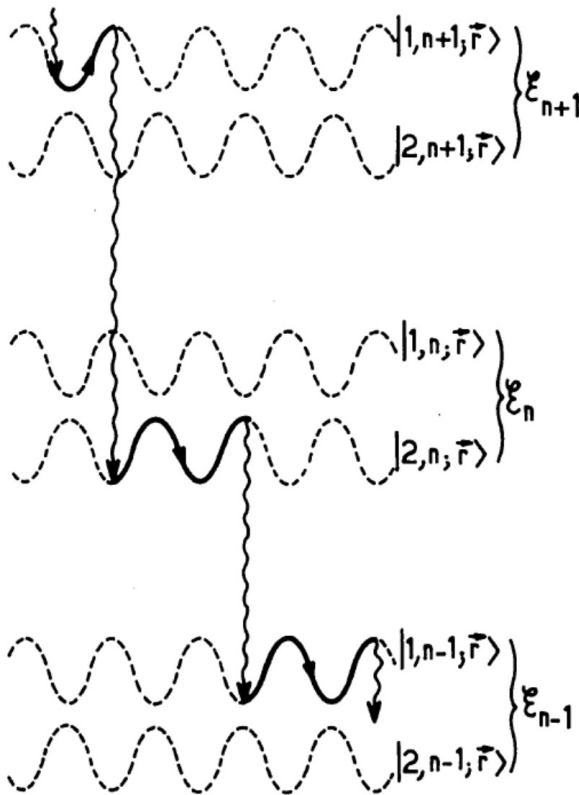
FIG. 6: Interpretation of Sisyphus cooling for $\delta > 0$. the transitions are most likely happen at the top of the "potential hill". As a result, the atom travels 'uphill' more than "downhill. [1]"

will go "uphill" more than "downhill". [6] The process implies cooling, because as the dressed atom go "uphill" its kinetic energy is converted to potential energy which is dissipated through spontaneous emissions.

The spontaneous emission can happen from the top and the bottom state. The dissipation rate is approximately proportional the transitions rate and the kinetic energy difference between the top and bottom of the standing wave potential hill.

VII.   CONCLUSION

The dressed states are eigenstate of the coupled Hamiltonian of an atom and an electric magnetic field. The splitting and the admixtures of uncoupled states in the dressed states are determined by the laser frequency and the electric field strength.

When the atom is at small velocity, the cooling mechanism is the time lag which causes the populations in dressed states to lag behind in space. As a result, the shift in population will create an extra force proportional to the velocity of the atom. The direction of the force depends on the detuning δ. If $\delta > 0$, the dipole force is damping, while if $\delta < 0$, the force is accelerating.

When the atom is at intermediate velocity, the cooling is due to spontaneous emissions between dress levels. Between two successive spontaneous emissions, the atom will climb up and down the potential hill. On average, the atom climb up more, so the kinetic energy will convert to potential energy which is dissipated through spontaneous emissions.

Acknowledgments

[1] J. Dalibard and C. Cohen-Tannoudji, J. Opt. Soc. Am .B 2, 1707 (1985)
[2] Claude Cohen-Tannoudji , Jacques Dupont-Roc, Gilbert Grynberg, *Atom-Photon Interactions: Basic Processes and Applications* (Wiley, 1998), chapter VI.
[3] The MIT Aomic Physics Wiki, `https://cua-admin.mit.edu/apwiki/wiki/Main_Page`.
[4] Here we consider a quantized radiation field in a coherent state. It can be shown that the quantized field behaves as if it were a classical field.
[5] It is also know as the Dirac picture and the rotating frame. In this case, the atom and field Hamiltonian is chosen to evolve the coupling Hamiltonian, so we can say that we move into the reference frame of the atom and field.
[6] In Greek mythology, King Sisyphus was punished for his deceitfulness by being compelled to roll a stone up a hill. When it reached the top it fell down again, and he then had to re peat it over and over again. This is how the mechanism gets its name.

Tunneling Electrons in Graphene Heterostructures

Trond I. Andersen

MIT Physics Department, 77 Massachusetts Ave., Cambridge, MA 02139-4307

(Dated: May 2, 2014)

In this paper we first consider the hexagonal honeycomb lattice structure of graphene to derive its band structure, featuring linear dispersion and no band gap. Subsequently, we use the band structure together with the WKB approximation and 2D Fermi-Dirac statistics to model photo-induced tunneling through vertical graphene-hBN-graphene heterostructures. The results from our simulations are consistent with the experimental data, suggesting a superlinear power law dependence of tunneling current on laser power. Finally, we report on theoretical predictions of an abrupt transition from tunneling to thermionic emission when reaching a certain temperature.

I. INTRODUCTION

Ever since graphene was discovered by Konstantin Novoselov and Andre Geim in 2004 [1], this atomically thin material has received much attention due to its wide range of possible applications, including desalination filters [2], solar cells [3] and transistors [4]. Not only is graphene the first ever discovered stable 2D material, but it also exhibits a plethora of unprecedented optic and electronic properties, mainly due to its linear dispersion relation and lack of band gap [5]. Recently, there has been a major focus on graphene heterostructures, which combine the properties of other materials with those of graphene to reveal novel physical phenomena [6]. Vertical graphene-hexagonal Boron Nitride-graphene (gr-hBN-gr) heterostructures have proven to be particularly interesting, because electrons tunnel through them when a bias voltage is applied [7]. While recent papers have created models that agree well with experiments on this phenomenon [8, 9], not much attention has been given to *photo-induced* tunneling, in which a laser is used to keep the electrons out of thermal equilibrium with the surroundings. In this paper, we consider the quantum physics behind this case, using the WKB approximation and 2D Fermi-Dirac statistics to model the process. We also compare our predictions with experimental data on the dependence on laser power.

II. THE BAND STRUCTURE OF GRAPHENE

In order to understand the theory of tunneling in a vertical graphene heterostructure, we first need to consider the band structure of graphene, which arises from its honeycomb lattice structure (fig.1). It is useful to consider this hexagonal structure as a combination of two triangular sub-lattices (A (red) and B (blue)), shifted by a vector $\Delta\vec{R}$ relative to each other. In graphene, the carbon atoms have three sp^2-orbitals and one p_z-orbital. The former ones are used to form bonds in the plane of the graphene sheet, so their electrons are not free to move and can be ignored when deriving the band structure. The p_z-orbitals on the other hand, are out of the plane, and have delocalized electrons. This means that the p_z-
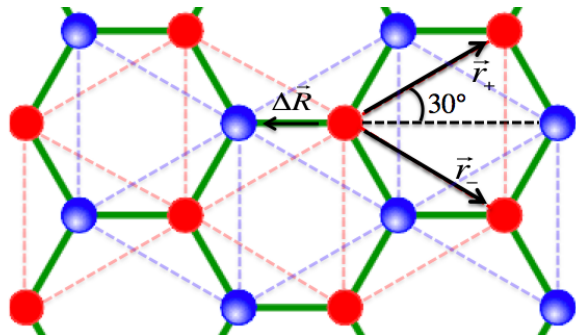
FIG. 1: The honeycomb lattice of graphene divided into its two sub-lattices A (red) and B (blue). $\vec{r}_+$ and $\vec{r}_-$ are the lattice vectors, and $\Delta\vec{R}$ is the displacement between the two lattices.

electrons are in a superposition of p_z-states belonging to multiple carbon atoms, and these electrons are those we need to consider. We define $\left|\vec{R}\right\rangle$ to be the p_z-state of a carbon atom at position $\vec{R}$, and use a Hamiltonian based on interactions between nearest neighbors only, which is commonly referred to as the tight-binding model. As can be seen from fig.1, this means that an electron in sub-lattice A only "feels" the three closest electrons in sub-lattice B. The Hamiltonian is then found from summing the three interaction terms at each carbon atom position $\vec{R}$:

$$
\begin{aligned}
H = -\,\gamma \sum_{\vec{R}} & \left|\vec{R}\right\rangle \left\langle \vec{R} + \Delta\vec{R}\right| \\
& + \left|\vec{R}\right\rangle \left\langle \vec{R} + \Delta\vec{R} + \vec{r}_+\right| + \left|\vec{R}\right\rangle \left\langle \vec{R} + \Delta\vec{R} + \vec{r}_-\right| \quad (1)
\end{aligned}
$$

where γ describes the strength of the interaction. Since the potential is periodic, the Hamiltonian is invariant under translation by $\vec{r}_+$ and $\vec{r}_-$. Thus, we introduce the translation operator $T_{\vec{R}}$ such that $T_{\vec{R}}\psi(\vec{r}) = \psi(\vec{r} + \vec{R})$ and observe that $\left[H, T_{\vec{r}_\pm}\right] = 0$, so H has the same eigenstates as $T_{\vec{r}_+}$ and $T_{\vec{r}_-}$. Furthermore, we know that $T_{\vec{r}_\pm}$ is unitary since $T_{\vec{r}_\pm} = \exp(-i\vec{p}\cdot\vec{r}_\pm/\hbar)$, so its eigenvalues must be complex exponentials. In other words, $|\psi(\vec{r} + \vec{r}_\pm)|^2 = |\psi(\vec{r})|^2$ for eigenstates ψ, which intu-
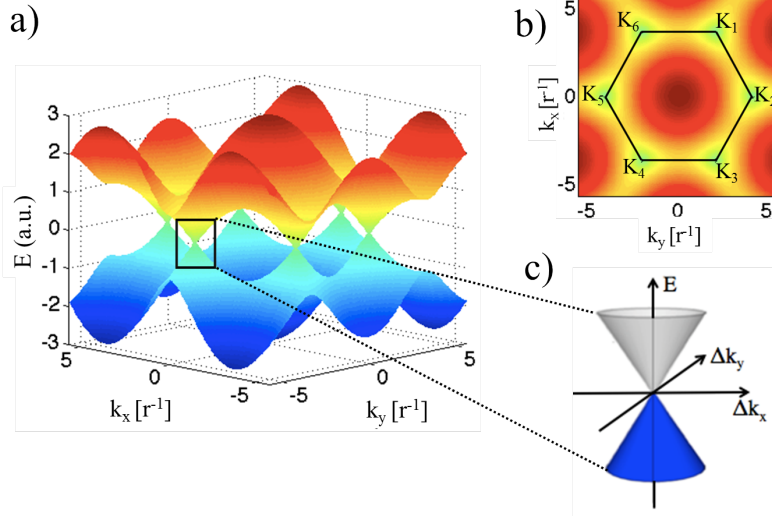
FIG. 2: a) Band structure of graphene, showing energy as a function of wavevector $\vec{k}$. b) Previous plot as seen from above, showing the 6 K-points. c) Zooming in on one of the K-points shows the famous Dirac cones featuring linear dispersion and no bandgap.

itively makes sense since we expect the probability density to be the same at two indistinguishable positions in an infinitely big, periodic lattice. Treating first only sub-lattice A and defining $\{\vec{R}_A\}$ as the positions of its carbon atoms, we observe that:

$$T_{\vec{r}_\pm}\sum_{\vec{R}_A}e^{i\vec{k}\cdot\vec{R}_A}\left|\vec{R}_A\right\rangle=\sum_{\vec{R}_A}e^{i\vec{k}\cdot\vec{R}_A}\left|\vec{R}_A-\vec{r}_\pm\right\rangle=$$

$$e^{i\vec{k}\cdot\vec{r}_\pm}\sum_{\vec{R}_A}e^{i\vec{k}\cdot(\vec{R}_A-\vec{r}_\pm)}\left|\vec{R}_A-\vec{r}_\pm\right\rangle=e^{i\vec{k}\cdot\vec{r}_\pm}\sum_{\vec{R}_A}e^{i\vec{k}\cdot\vec{R}_A}\left|\vec{R}_A\right\rangle \tag{2}$$

This state is clearly an eigenstate of $T_{\vec{r}_\pm}$ and therefore of H as well. States on this form are commonly referred to as Bloch states, with $\vec{k}$ being the crystal wave vector. After doing the same for sub-lattice B, we have normalized eigenstates for each sub-lattice:

$$\left|\vec{k},A\right\rangle=N^{-\frac{1}{2}}\sum_{\vec{R}_A}e^{i\vec{k}\cdot\vec{R}_A}\left|\vec{R}_A\right\rangle \tag{3}$$

$$\left|\vec{k},B\right\rangle=N^{-\frac{1}{2}}\sum_{\vec{R}_B}e^{i\vec{k}\cdot(\vec{R}_B-\Delta\vec{R})}\left|\vec{R}_B\right\rangle \tag{4}$$

Note that the extra term $-\Delta\vec{R}$ in the exponent of the B-state only gives a phase, but makes our calculations easier. We now consider the subspace of superpositions $\left|\vec{k}\right\rangle=\alpha\left|\vec{k},A\right\rangle+\beta\left|\vec{k},B\right\rangle$ for a specific wavevector $\vec{k}$ and write it in the $\{\left|\vec{k},A\right\rangle,\left|\vec{k},B\right\rangle\}$-basis. The diagonal terms of the Hamiltonian are then zero, since it shifts all terms on sub-lattice A to B, and vice versa. The off-diagonal terms, on the other hand, are easily found

using $\vec{u}\equiv\vec{R}_B-\vec{R}_A-\Delta\vec{R}$:

$$\left\langle\vec{k},A\right|H\left|\vec{k},B\right\rangle=$$

$$N^{-1}\sum_{\vec{R}_A,\vec{R}_B}e^{i\vec{k}\cdot(\vec{R}_B-\vec{R}_A-\Delta\vec{R})}\left\langle\vec{R}_A\right|H\left|\vec{R}_B\right\rangle=$$

$$-N^{-1}\sum_{\vec{R}_A,\vec{R}_B}e^{i\vec{k}\cdot\vec{u}}\cdot\gamma\left(\delta_{\vec{u},\vec{0}}+\delta_{\vec{u},\vec{r}_+}+\delta_{\vec{u},\vec{r}_-}\right)=$$

$$-\gamma(1+e^{i\vec{k}\cdot\vec{r}_+}+e^{i\vec{k}\cdot\vec{r}_-}) \tag{5}$$

Using $r=|\vec{r}_+|=|\vec{r}_-|$ and $\vec{k}\cdot\vec{r}_\pm=(\frac{\sqrt{3}}{2}k_x\pm\frac{1}{2}k_y)r$, it is now evident that the eigenvalues are

$$E_\pm=\pm\left|\gamma(1+e^{i\vec{k}\cdot\vec{r}_+}+e^{i\vec{k}\cdot\vec{r}_-})\right|=$$

$$\pm\sqrt{1+4\cos(\frac{\sqrt{3}}{2}k_xr)\cos(\frac{1}{2}k_yr)+4\cos^2(\frac{1}{2}k_yr)} \tag{6}$$

Fig.2a plots this expression as a function of $\vec{k}$, and shows that the energy becomes zero when $|k|=\frac{4\pi}{3r}$ and its angle to the x-axis is $\frac{(2n+1)\pi}{6}$ (fig.2b). These are commonly referred to as the K-points.

When we write $\vec{k}=\vec{K}+\Delta\vec{k}$ and expand the energy to first order around a K point, we find that the Hamiltonian is

$$H=\frac{\sqrt{3}}{2}\gamma r\begin{pmatrix}0 & \Delta k_x-i\Delta k_y\\\Delta k_x+i\Delta k_y & 0\end{pmatrix}=v_F\vec{p}\cdot\vec{\sigma} \tag{7}$$

where $\vec{p}=\hbar\Delta\vec{k}$ is the momentum of the electron and $v_F\approx10^6\mathrm{ms}^{-1}$ is the Fermi velocity.
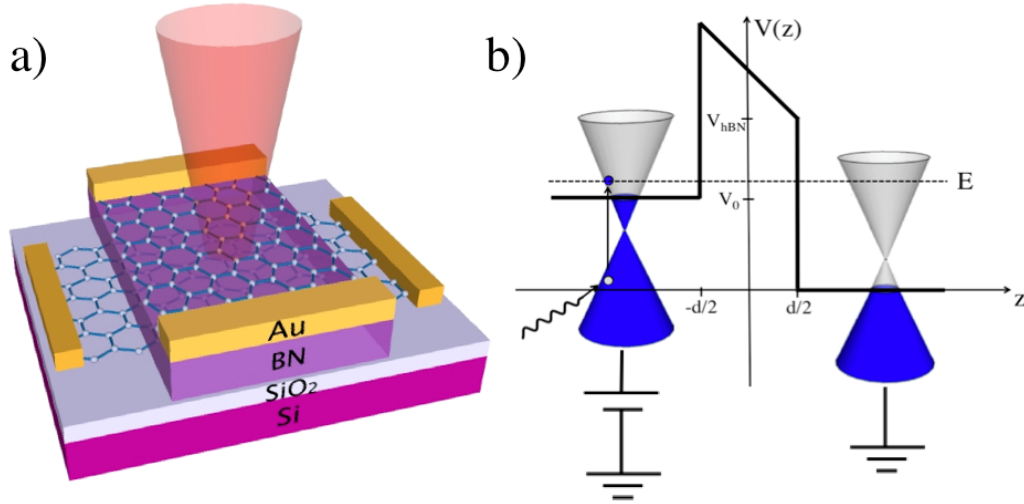
FIG. 3: a) Laser injected on vertical heterostructure. b) Potential $V(z)$ together with graphene band structure showing occupancy and a photo-excited electron. The right ($z > 0$) graphene electrode is grounded, and the barrier is slanted due to the applied bias voltage. Note that neither V_0 nor the z-axis are drawn to scale, so in reality, V_0 is significantly smaller, and the regions outside the barrier are much shorter (thickness of graphene).

Interestingly, this Hamiltonian is reminiscent of the kinetic term in the relativistic Dirac equation in that it contains $\vec{p} \cdot \vec{\sigma}$ rather than p^2. This has exotic consequences, including the fact that the effective electron mass $m^* \equiv \hbar^2 \left(\frac{\partial^2 E}{\partial k^2} \right)^{-1}$ is zero [5], and also that graphene can be used to realize unimpeded tunneling (Klein paradox) [10]. More important to us, however, is that such a Hamiltonian gives a band structure with a linear dispersion and no band gap, as depicted in fig.2c. The upper and lower cones correspond to the conduction and valence bands, respectively, and the point where they meet is referred to as the Dirac point. Since there is no band gap in graphene, all electron energies are allowed. This allows graphene to absorb all wavelengths because there will always be a vertical transition in the band structure that corresponds to the photon energy. Note that photo-induced transitions are vertical since the photons carry very little momentum (relative to its energy, in the sense that $\left(\frac{\partial E}{\partial p} \right)_{\text{photon}} = c >> v_{\text{F}} = \left(\frac{\partial E}{\partial p} \right)_{\text{electron}}$). Broadband absorption makes graphene an interesting alternative to silicon in photodetection devices, since the latter can only absorb photons with energies higher than its band gap of $\sim$1.1 eV, which corresponds to a wavelength of $\sim$1100 nm.

III. TUNNELING EXPERIMENTS

We are now prepared to consider photo-induced tunneling in vertical gr-hBN-gr heterostructures. Simply put, this involves applying a bias voltage V_0 between the top and bottom layers of a gr-hBN-gr "sandwich",

shining a laser beam on it, and measuring the current of electrons tunneling through the sandwich (fig.3a). Since hBN is an insulator, it works as a tunneling barrier, which is slanted due to the applied electric field, resulting in the following potential profile (fig.3b):

$$V(z) = \begin{cases} V_0 & z < -\frac{d}{2} \\ V_{\text{hBN}} + \frac{V_0}{d} \cdot (d/2 - z) & |z| < \frac{d}{2} \\ 0 & z > \frac{d}{2} \end{cases}$$

where V_{hBN} is the barrier height when no bias voltage is applied. Interestingly, the difference between the Dirac point energies (E_{DP}) of the graphene sheets is smaller than the applied bias potential (fig.3b), since the chemical potentials are shifted to account for the charge buildup that we expect in a capacitor. Fig.4 shows the tunneling current as a function of laser power. The linear log-log plot supports a power law relationship, and the slope of $\sim 3.3 > 1$ suggests a superlinear dependence on laser power. Interestingly, when using a laser to drive current *along* a graphene sheet rather than through a sandwich, one rather observes a *sublinear* relationship (slope< 1) [11]. In order to understand the difference between these two cases, we need to consider the quantum physics of the tunneling process, and we start by using the WKB approximation to find the transmission coefficient. Since the applied voltage V_0 is very small compared to V_{hBN} ($\sim 0.1\%$), very few electrons will have energies that intersect the slanted region of the barrier and travel through parts of the barrier classically. Thus, we only need to consider turning points at $\pm d/2$ [18],
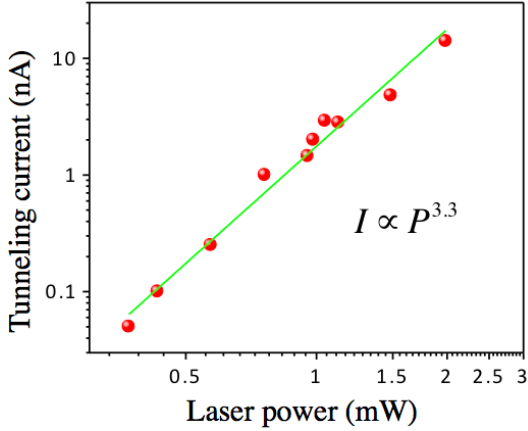
FIG. 4: Tunneling current vs. laser power plotted in log-log scale with linear fit (green). Linearity supports power law dependence, and the slope suggests an exponent of ~ 3.3.

which gives the transmission coefficient:

$$T(E) = \exp\left[-\int_{-d/2}^{d/2} \frac{2}{\hbar}\sqrt{2m^*(V(z)-E)}dz\right] =$$

$$\exp\left[-\frac{4d\sqrt{2m^*}}{3V_0\hbar}\left[(V-E)^{3/2}\right]_{V_{\mathrm{hBN}}}^{V_0+V_{\mathrm{hBN}}}\right] \approx$$

$$\exp\left[-\frac{2d}{\hbar}\sqrt{2m^*(V_{\mathrm{hBN}}-E)}\right] \qquad (8)$$

where the last approximation simply comes from Taylor expanding $(V_{\mathrm{hBN}} + V_0 - E)^{3/2}$ since V_0 is small, and m^* is the effective electron mass in hBN. The above expression provides us with some important insight; the transmission rate depends exponentially on the square root of the electron energy and is independent of the bias voltage at low V_0. We now need to combine this with the Fermi-Dirac statistics of the system to further understand the observed superlinear dependence on power. When an electron is excited, it will quickly cool through electron-electron interactions and optical phonon emission [13, 14], which reestablish a Fermi-Dirac distribution (F-D), although at a higher temperature than the surroundings. Subsequently, slower cooling processes (acoustic phonon emission) will bring the F-D distribution towards the surrounding temperature [15, 16]. Two-pulse correlation measurements have shown that the tunneling time scale (~ 1 ps) is much longer than that of the initial cooling mechanism (~ 10 fs), and we can therefore use a F-D distribution to further model the tunneling. Intuitively, the rate of tunneling from layer 1 to 2 of electrons with energy E is expected to be proportional to 1) the tunneling probability, 2) the number of electrons of energy E in layer 1, and 3) the number of available states at energy E in layer 2. Together, this gives $T(E) \cdot \rho_1(E) f_1(E) \cdot \rho_2(E)(1-f_2(E))$ where T is the transmission coefficient, ρ is the density of states and f is

the Fermi-Dirac distribution function. Note that we need the factor $\rho_2(E)(1 - f_2(E))$ to account for the fact that electrons are fermions and can thus only tunnel to available states in layer 2. The shifts of chemical potential and band structure are here included in the subscripts (1 and 2), giving individual functions for each graphene sheet. The linear dispersion gives $\rho \propto |E - E_{\mathrm{DP}}|$ where E_{DP} is the Dirac point energy. We now use three known relations to find an expression for E_{DP} of each sheet:

1. The chemical potential of a graphene sheet at position z is equal to the potential applied there: $\mu = V(z)$

2. 2D Fermi-Dirac statistics relate the chemical potential to the charge density n through: $\mu - E_{\mathrm{DP}} \propto n^{1/2}$

3. Looking upon the device as a capacitor allows us to relate the difference between the Dirac points to n: $\Delta E_{\mathrm{DP}} \propto n$

These together give a quadratic equation involving multiple device parameters that we can solve to find E_{DP} of each sheet. We can then sum the contributions from tunneling in both directions and integrate over all energies to get the total transmission rate:

$$r_T \propto \int_{-\infty}^{\infty} T(E)\rho_1(E)\rho_2(E)(f_1(E) - f_2(E))dE \propto$$

$$\int_{-\infty}^{\infty} \exp\left[-\frac{2d}{\hbar}\sqrt{2m^*(V_{\mathrm{hBN}}-E)}\right]|E - E_{\mathrm{DP},1}| \cdot$$

$$|E - E_{\mathrm{DP},2}| \cdot (f(E, \mu = V_0) - f(E, \mu = 0)) dE \quad (9)$$

In order to gain more intuition, we again assume that $V_0 \ll V_{\mathrm{hBN}}$ which gives $E_{\mathrm{DP},1} = E_{\mathrm{DP},2} = 0$ and $f(E, \mu = V_0) - f(E, \mu = 0) \approx V_0 \frac{df}{dE}|_{\mu=0}$. Then, we simply have:

$$r_T \propto \int_{-\infty}^{\infty} \exp\left[-\frac{2d}{\hbar}\sqrt{2m^*(V_{\mathrm{hBN}}-E)}\right] \frac{\beta V_0 E^2 e^{\beta E}}{(1+e^{\beta E})^2}dE =$$

$$\int_{-\infty}^{\infty} \frac{\beta V_0 E^2 e^{-\xi\sqrt{V_{\mathrm{hBN}}-E}+\beta E}}{(1+e^{\beta E})^2}dE \qquad (10)$$

where $\xi = \frac{2d}{\hbar}\sqrt{2m^*}$ and $\beta = (kT)^{-1}$.

As can be seen from fig.5d, simulations predict that the tunneling current is superlinear in T, as expected. However, further modeling of how T depends on laser power is needed to connect this completely to the observed power dependence in fig.4. Interestingly, the integral exhibits an abrupt transition as we increase T (fig.5d). At low temperatures, the decay rate of the F-D distribution with energy is higher than the exponential growth rate of the WKB transition probability, so the tunneling contribution from electrons with high energies (close to V_{hBN}, so almost classically allowed) is strongly suppressed (fig.5a). However, when we increase the temperature, the WKB term becomes dominant and the F-D statistics is not able
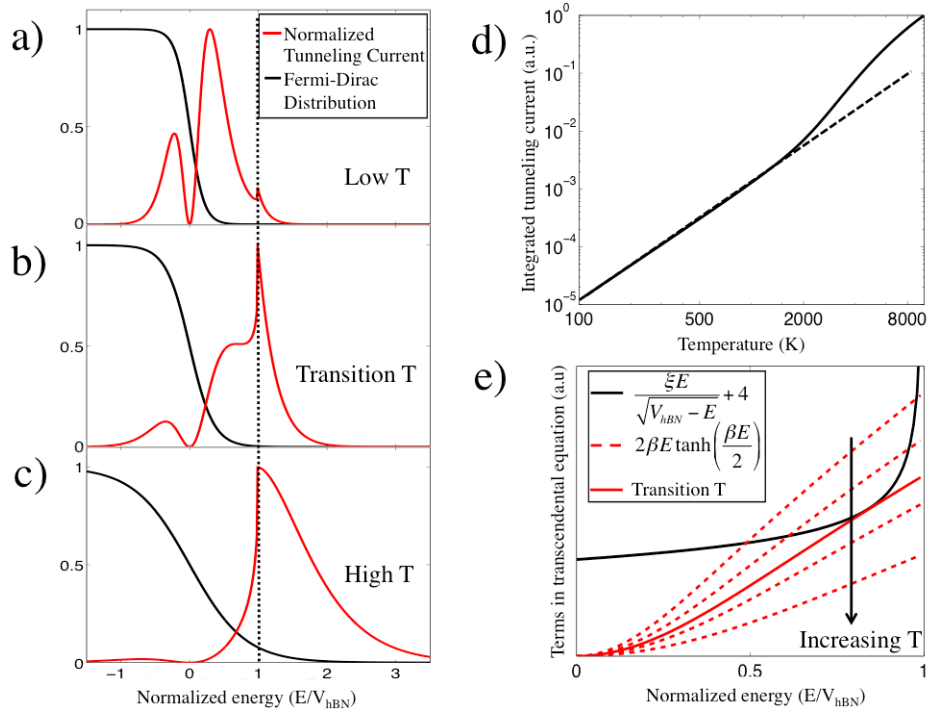
FIG. 5: a) Normalized contribution to tunneling from electrons with energy E at low temperature. Clearly, the main contribution comes from electrons at low energies, and there are two extrema for $E \in (0, V_{\text{hBN}})$ (maximum at $E \approx 0$ and minimum at E close to V_{hBN}). b) Same as previous plot, but at the transition temperature. The max and min points merge into a saddle point. c) Tunneling current contributions at high temperature. There are zero extrema for $E \in (0, V_{\text{hBN}})$, and the dominant contribution comes from electrons with energies above V_{hBN}, which can move through the barrier classically. d) Log-log plot of the total tunneling current (integrated over all energies) vs. temperature. The former is normalized by the maximum value in the plot. An abrupt transition is observed around 2000 K. e) Graphical solution of the transcendental equation governing the transition from tunneling to classical transmission (thermionic emission). The solid red line only gives one solution and thus corresponds to the transition temperature.

to prevent high-energy electrons from moving through the barrier *classically* (fig.5c). The latter is referred to as thermionic emission [17] and means that at high T, the main contribution to current through the heterostructure actually comes from electrons that are *not* tunneling. Note that we have here used $T(E) = 1$ for $E > V_{\text{hBN}}$. We now move on to finding the transition temperature by differentiating the integrand and solving for T such that it has exactly one zero in the interval $E \in (0, V_{\text{hBN}})$. From fig.5a-c, one can see that this corresponds to the transition temperature. After simplifying the derivative, it is evident that this is equivalent to only having one solution to the transcendental equation:

$$2\beta E \tanh \frac{\beta E}{2} = \frac{\xi E}{\sqrt{V_{\text{hBN}} - E}} + 4 \qquad (11)$$

We illustrate in fig.5e how the number of solutions to this equation goes from two to zero, and that there is a transition temperature at which there is exactly one solution. Below this temperature, the major contribution to interlayer current comes from tunneling, while thermionic emission dominates at higher T.

IV. CONCLUSION

In this paper, we used the honeycomb lattice structure of graphene to derive its famous Dirac cone band structure, exhibiting linear dispersion and lack of band gap. This dispersion relation was then used together with 2D Fermi-Dirac statistics to predict how tunneling through gr-hBN-gr heterostructures depends on electronic temperature, based on a WKB tunneling probability. Simulations suggested a superlinear dependence on temperature T, supporting the experimentally observed behavior with laser power P. However, a connection between T and P must be established to completely determine whether our model is consistent with the experimental data. We also predicted a transition from tunneling to thermionic emission as we enter a high-temperature regime, which has yet to be experimentally verified. Finally, we showed that the transition temperature can be found from a transcendental equation that is based on the observation that the number of extrema in the tunneling contribution function changes in the transition.

[1] K. S. Novoselov, A. K. Geim, S. V. Morozov, D. Jiang, Y. Zhang, S. V. Dubonos, I. V. Grigorieva, and A. A. Firsov, Science **306**, 666 (2004).

[2] D. Cohen-Tanugi and J. C. Grossman, Nano Letters **12**, 3602 (2012).

[3] X. Miao, S. Tongay, M. K. Petterson, K. Berke, A. G. Rinzler, B. R. Appleton, and A. F. Hebard, Nano Letters **12**, 2745 (2012).

[4] S. Vaziri, G. Lupina, C. Henkel, A. D. Smith, M. stling, J. Dabrowski, G. Lippert, W. Mehr, and M. C. Lemme, Nano Letters **13**, 1435 (2013).

[5] A. H. Castro Neto, F. Guinea, N. M. R. Peres, K. S. Novoselov, and A. K. Geim, Rev. Mod. Phys. **81**, 109 (2009).

[6] A. Geim and I. Grigorieva, Nature **499**, 419 (2013).

[7] L. Britnell, R. V. Gorbachev, R. Jalil, B. D. Belle, F. Schedin, A. Mishchenko, T. Georgiou, M. I. Katsnelson, L. Eaves, S. V. Morozov, et al., Science **335**, 947 (2012).

[8] L. Britnell, R. Gorbachev, A. Geim, L. Ponomarenko, A. Mishchenko, M. Greenaway, T. Fromhold, K. Novoselov, and L. Eaves, Nature communications **4**, 1794 (2013).

[9] R. M. Feenstra, D. Jena, and G. Gu, Journal of Applied Physics **111**, 043711 (2012).

[10] M. Katsnelson, K. Novoselov, and A. Geim, Nature physics **2**, 620 (2006).

[11] M. W. Graham, S.-F. Shi, D. C. Ralph, J. Park, and P. L. McEuen, Nature Physics **9**, 103 (2013).

[12] R. H. Fowler and L. Nordheim, in *Proc. R. Soc. London, Ser. A* (1928), vol. 119, pp. 173–181.

[13] H. Wang, J. H. Strait, P. A. George, S. Shivaraman, V. B. Shields, M. Chandrashekhar, J. Hwang, F. Rana, M. G. Spencer, C. S. Ruiz-Vargas, et al., Applied Physics Letters **96**, (2010).

[14] T. Ando, Journal of the Physical Society of Japan **75** (2006).

[15] J. C. Song, M. Y. Reizer, and L. S. Levitov, Physical review letters **109**, 106602 (2012).

[16] J. C. Song, M. S. Rudner, C. M. Marcus, and L. S. Levitov, Nano letters **11**, 4688 (2011).

[17] J. Schwede, T. Sarmiento, V. Narasimhan, S. Rosenthal, D. Riley, F. Schmitt, I. Bargatin, K. Sahasrabuddhe, R. Howe, J. Harris, et al., Nature communications **4**, 1576 (2013).

[18] For larger V_0, the Fowler-Nordheim extension [12] is needed

The Diffusion Monte Carlo Method

Bowen Baker

MIT Departments of Physics and EECS, 77 Massachusetts Ave., Cambridge, MA 02139-4307
(Dated: May 2, 2014)

We describe Monte Carlo methods for classical problems and a Quantum variant, the Diffusion Monte Carlo, for finding ground state energies of quantum many-body systems. We discuss the algorithm both with and without importance sampling. We go on to describe the problems that arise when calculating the ground state energy of a many-body fermion systems and the excited state energies for any many-body system. We then briefly discuss a few past applications of the Diffusion Monte Carlo.

I. INTRODUCTION

Finding exact values for the ground state energies of n-body quantum systems becomes nigh on impossible as n becomes very large. This is to be expected because the dimension of the Hilbert Space scales exponentially in n. For instance, representing 30 spin-$\frac{1}{2}$ particles requires a basis in 2^{30} (or roughly $\sim 10^9$) dimensions to fully specify the system.[1] However, do not fret! This seemingly large obstacle can easily be surmounted with the help of various numerical methods. In this paper we will discuss in detail one such method, the Diffusion Monte Carlo.

A. A Brief History of Monte Carlo Methods

The first algorithm similar to today's Monte Carlo was formulated in 1777 by the French naturalist Georges-Louis Leclerc, Comte de Buffon, in his imagined needle-throwing experiment to estimate the value of π. Then in the 1940's, Enrico Fermi postulated that the Schrödinger equation could be written in a form similar to the diffusion equation, establishing the basis for the Diffusion Monte Carlo.[2] Fermi did not publish his work on Monte Carlo methods for neutron diffusion, and so in 1947, John von Neumann and Stan Ulam proposed the same method, and thus the Monte Carlo method was born (officially).[3]

B. Monte Carlo Background

1. Direct Sampling

This section will follow the discussions in Refs. 2 and 5. Imagine you were on the beach and you and your friend got into an argument about the correct value for the area of the continental United States. You've been laying in the sun for quite a while so neither of you think to just look up the answer on a smartphone, but your friend just so happens to have a photographic memory for maps and you just got out of a lecture covering Monte Carlo methods. You tell him to draw the outline of the continental United States in the sand bounded by a box of known area (he can remember the scale of the

maps too). He draws something like Fig. 1:

FIG. 1: Continental United States with bounding box of total area 4,762,950 miles^2

As he is drawing you go and find N coconuts, where N is large. You come back and explain to him how you will calculate, almost exactly, the area. You both randomly throw coconuts so that the x and y coordinates of the throw act as random variables evenly distributed over the bounding box. After you are done, you go and count how many coconuts landed within the US, divide it by the total number thrown, and then multiply it by the area of the bounding box. This approach should seem fairly intuitive; we are randomly sampling a known probability distribution (the map) N times. We have a function f that maps samples inside the distribution to 1 and those outside to 0. To approximate the area in the map, we calculate the expectation of f, $<f>$, over the known distribution and multiplying it by the area of the bounding box. After N samples, some N_{in} coconuts will have landed inside the US. Thus

$$\text{area}_{US} = \frac{N_{in}}{N} * \text{area}_{boundingbox} \qquad (1)$$

One can see in Fig. 2 that as N increases so does the accuracy of our estimate.
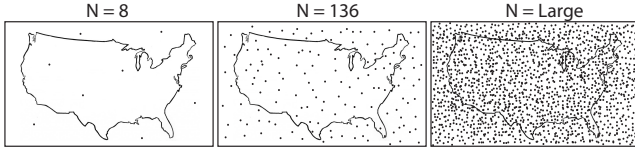
FIG. 2: Three different random samplings with varying N.

The actual area of the continental US is 3,095,993 miles^2.[4] In the first snapshot $\frac{N_{in}}{N} = \frac{3}{8} \rightarrow \text{area}_{US} = 1,786,106$ miles^2 which gives an error of 42.3%. In the second, $\frac{N_{in}}{N} = \frac{61}{136} \rightarrow \text{area}_{US} = 2,136,323$ miles^2, which is better with an error of 30.9%. For the last snapshot, $\frac{N_{in}}{N} \sim 64\% \rightarrow \text{area}_{US} = 3,048,288$ miles^2, which is much better with an error of 1.5%. Because we are randomly sampling over a constant distribution, $\lim_{N \to \infty} error = 0$, or more precisely $error \propto \frac{1}{N^2}$. The process we have just described is the Monte Carlo 2-d integral. The n-d version is performed in the same way but with n random variables; however, the error attenuates more slowly as n increases.[2]

2. Markov-Chain Sampling

Direct sampling, though simple, is computationally expensive in many cases. Consider the Boltzmann distribution,

$$p(E) = \frac{e^{-\frac{E}{k_B T}}}{Z} , \qquad Z = \sum_{i=0}^{\infty} e^{-\frac{E_i}{k_b T}} \qquad (2)$$

To directly sample $p(E)$ in order to approximate $< E >$, we would first have to calculate the partition function, Z, which could be extremely expensive if there is no efficient way of computing each E_i. If, however, we were sampling based on the relative probability between two states, then we would never have to explicitly calculate Z.

$$\frac{p(E_j)}{p(E_k)} = e^{-\frac{E_j - E_k}{k_B T}} \qquad (3)$$

We do just this in Markov-Chain sampling; each step is dependent only on the previous state. More generally, if we are trying to sample over some distribution $\pi(\mathbf{R})$, then direct sampling requires full knowledge of $\pi(\mathbf{R})$, whereas Markov-Chain sampling does not have this requirement and will converge to $\pi(\mathbf{R})$ in the long time limit.[5] For this reason Markov-Chain sampling is used for complex problems, such as high dimensional integrals.

Markov-Chain sampling is defined in the following way. Imagine that instead of randomly throwing rocks into the map with your friend, you recruit 50 friends to come help. Each person receives a bag of coconuts and starts in a sparse distribution inside the bounding box. Each throws a coconut to a random point (x, y) where Δx and Δy are picked randomly from the even distribution $[-\delta, \delta]$. If the point (x, y) is in the bounding box, then the thrower walks to the coconut. If (x, y) is not in the bounding box, then the person puts a coconut down where they are standing (now there is a stack of two or more coconuts at this point) and disregards the out-of-bounds coconut. After each walker repeats this process N times, the distribution of coconuts should look similar to that of the direct sampling approach (in the large N limit). To compute area_{US}, we simply reuse Eq. (1).

To rationalize dropping a coconut down in the out-of-bounds case, just think on what we are trying to accomplish. We are essentially trying to integrate the area of the United States using random sampling, so if we simply disregard throws out of the bounding box, the density of coconuts will be larger in the center of the box than near the edges. By having the random walker put a coconut down in this case, we are ensuring that the distribution of coconuts over the map be even for a large number of steps. In the Metropolis Algorithm, this step ensures we are satisfying the detailed balance condition; see Refs. 3, 5, and 6, for a more detailed description.

Furthermore, δ must be chosen very carefully. If δ is chosen too large, too many samples will land outside the bounding box and the walkers will never leave their original location, making the final distribution very skewed. Likewise if δ is small compared to $\frac{\text{range}(x_i)}{N}$, where $\text{range}(x_i)$ is the range of a random variable and N the number of steps, then the walker may never reach the other end of the space (in our example the map).[5]

At this point, one may wonder why we went through the trouble of introducing random variables into problems that could be easily solved by sampling over a regular array of points. For the US map example, we could certainly use a regular array of sample points as we were only doing a 2-d integral. However, the number of sample points we need to store goes up exponentially in dimension of the problem, making the use random variables necessary.[6,7]

3. Monte Carlo For Finding Minimums

Now imagine how we might modify the above method to, instead of integrating, find the minimum of some $f(x_1, \ldots, x_n)$. Assume that f only has one minimum. We will begin with the same sparse distribution of walkers and amplify walkers that are nearing the center, i.e. if $f(\mathbf{S}') < f(\mathbf{S})$ we should add a few walkers located at $\mathbf{S}'$. If the opposite is true, i.e. if $f(\mathbf{S}') > f(\mathbf{S})$, then we should remove the walker. Thus, as N increases, we will expect more and more walkers to approach the minimum. To retrieve our estimate of the minimum, we simply average over all final $\mathbf{S}_j$'s, where subscript j represents the jth walker. This modified algorithm resembles the Diffusion Monte Carlo at a very basic level, as we shall discover in the following sections.

The runtime of the algorithm outlined above for finding a minimum in f is attenuated from both the use random variables and the use of a Markov-Chain-like sampling,

which minimizes necessary data storage by ensuring that each iteration only depends on the previous state.

C. Diffusion Background

Processes that involve random walks, such as the minimization method in the previous section, can often be modeled with the diffusion equation and vice versa. The diffusion equation can be used to describe particles or heat dispersing in a material and takes the form

$$\frac{\partial p(\mathbf{R}, t)}{\partial t} = D\nabla^2_{\mathbf{R}} p(\mathbf{R}, t) , \qquad (4)$$

where $\nabla^2_{\mathbf{R}} = \sum_{i=1}^{n} \nabla^2_i$, $\mathbf{R}$ describes the position of each particle, $p(\mathbf{R}, t)$ is the probability of the particles being in position $\mathbf{R}$ at time t, and D is defined as the *diffusivity*, a constant that depends on the geometry and physical properties of the system.[12] If we introduce a spatially dependent force term, $\mathbf{F}(\mathbf{R})$, then the diffusion equation becomes the Focker-Planck equation,[13]

$$\frac{\partial p(\mathbf{R}, t)}{\partial t} = -\nabla_{\mathbf{R}}[\mathbf{F}(\mathbf{R})p(\mathbf{R}, t)] + D\nabla^2_{\mathbf{R}} p(\mathbf{R}, t) . \qquad (5)$$

In the long time limit, the state for which $p(\mathbf{R}, t)$ is maximum is the equilibrium state, or the state with lowest energy.

Diffusion processes describe the average motion resulting from an astronomical amount of small collisions (a single particle in a fluid experiences roughly 10^{20} collisions per second). Because it would be impossible to simulate all of these collisions, the motion of a particle can be modeled by a random walk where the distance and direction of displacement are picked from a Gaussian distribution with variance $2Dt$.[14]

II. DIFFUSION MONTE CARLO FOR n-BODY BOSON SYSTEMS

A. Algorithm Summary

To find the ground state energy of an n-boson system, we will initialize N starting states (each with defined particle positions) which we shall call snapshots. We will evolve each particle in each snapshot randomly. As with the algorithm for finding a minimum in some f, we will amplify the snapshots that "moved" closer toward the ground state and delete those that "moved" farther away.[7]

B. Diffusion Monte Carlo Without Importance Sampling

In this section we will follow the arguments made in Refs. 6 and 7. As Fermi postulated in the 1940's, when

utilizing the Schrödinger equation in imaginary time it resembles the diffusion equation. Let $\frac{it}{\hbar} \to \tau$ and the Schrödinger equation for n particles gives

$$-\frac{\partial \Psi(\mathbf{R}, \tau)}{\partial \tau} = [-D\nabla^2_{\mathbf{R}} + V(\mathbf{R})]\Psi(\mathbf{R}, \tau) , \qquad (6)$$

where diffusion constant $D \equiv \frac{\hbar^2}{2m}$. The particles will have some interaction potential given most generally by

$$V(\mathbf{R}) = \sum_{i \neq j} V(\mathbf{r}_i, \mathbf{r}_j) . \qquad (7)$$

Writing $\Psi(\mathbf{R}, 0)$ as a superposition of eigenstates of our Hamiltonian gives us

$$\Psi(\mathbf{R}, 0) = \sum_i c_i \phi_i(\mathbf{R}) , \qquad (8)$$

for $i \geq 0$ where

$$\hat{H}\phi_i(\mathbf{R}) = E_i \phi_i(\mathbf{R}) . \qquad (9)$$

We will assume that $\hat{H}$ is time independent, which is a reasonable assumption because we are only dealing with particle-particle interactions. We can therefore write

$$\Psi(\mathbf{R}, \tau) = \sum_i c_i e^{-E_i \tau} \phi_i(\mathbf{R}) . \qquad (10)$$

Notice that because we are working in imaginary time, $e^{-E_i \tau}$ is real valued, meaning that solutions to the Schrödinger equation will be growing or decaying exponentials. With this knowledge, we introduce a test energy into the Hamiltonian, shifting the the eigenvalues by E_T. Now

$$-\frac{\partial \Psi(\mathbf{R}, \tau)}{\partial \tau} = (\hat{H} - E_T)\Psi(\mathbf{R}, \tau) , \qquad (11)$$

which has solutions of the form

$$\Psi(\mathbf{R}, \tau) = \sum_i c_i e^{-(E_i - E_T)\tau} \phi_i(\mathbf{R}) . \qquad (12)$$

All elements $\phi_i(\mathbf{R})$ in $\Psi(\mathbf{R}, \tau)$ with $E_i < E_T$ will exponentially grow in amplitude with time and those with $E_i > E_T$ will decay in time. Thus if we choose $E_T \approx E_0$ and $\langle \Psi(\mathbf{R}, 0) | \phi_0(\mathbf{R}) \rangle \neq 0$, then

$$\lim_{\tau \to +\infty} \Psi(\mathbf{R}, \tau) = \phi_0(\mathbf{R}) . \qquad (13)$$

Because we rewrote the Schrödinger equation in imaginary time, the portion of $\Psi(\mathbf{R}, \tau)$ in the ground state will always have the most positive decay constant, i.e. $(E_0 - E_T) < (E_i - E_T) \, \forall i$. For this reason, the $\phi_0(\mathbf{R})$ portion of $\Psi(\mathbf{R}, 0)$ will always have the largest amplitude in the long time limit. In the full Diffusion Monte Carlo (DMC) we will update E_T to approach E_0.[2]

Now you may be wondering how we will actually go about evolving $\Psi(\mathbf{R}, 0)$ as we know little of $\phi_i(\mathbf{R})$ and

E_i. Here we shall define our time evolution operator, the Green's function

$$\hat{G} = e^{-(\hat{H} - E_T)\tau} .\qquad (14)$$

Our goal is to evolve $\Psi(\mathbf{R}, 0)$ to some $\Psi(\mathbf{R}', \tau)$; therefore we are interested the coordinate space representation of $\hat{G}$,

$$G(\mathbf{R}', \mathbf{R}, \tau) = \langle \mathbf{R}' | e^{-(\hat{H} - E_T)\tau} | \mathbf{R} \rangle .\qquad (15)$$

For the Hamiltonian given in Eq. (11), our time evolution Green's function is the solution to

$$-\frac{\partial G(\mathbf{R}', \mathbf{R}, \tau)}{\partial \tau} = [-D\nabla_{\mathbf{R}}^2 + V(\mathbf{R}) - E_T]G(\mathbf{R}', \mathbf{R}, \tau) .\qquad (16)$$

Now you may wonder why we chose to define $G(\mathbf{R}', \mathbf{R}, \tau)$ at all because solving Eq. (16) looks no better than solving the original Schrödinger equation in Eq. (6). In general the kinetic energy and potential energy components of the Hamiltonian do not commute, i.e. $[V(\mathbf{R}), \nabla_{\mathbf{R}}^2] \neq 0$, but for small enough time steps we may ignore this for the price of $O(\tau^2)$ error. Thus we define $\hat{G}_T \equiv e^{-\hat{T}\tau}$ where $\hat{T} = D\nabla_{\mathbf{R}}^2$ and $\hat{G}_V \equiv e^{-(\hat{V} - E_T)\tau}$ where

$$\hat{G} \approx \hat{G}_T \hat{G}_V, \text{ for } \tau \to 0 .\qquad (17)$$

Each $\Psi(\mathbf{R}, 0)$ has a unique set of $V(\mathbf{r}_i, \mathbf{r}_j)$, thus $V(\mathbf{R}) \neq V(\mathbf{R}')$. Therefore $\hat{V}$ is diagonal and we can write

$$\langle \mathbf{R}' | \hat{G}_V | \mathbf{R} \rangle = G_V(\mathbf{R}', \mathbf{R}, \tau) = e^{-(V(\mathbf{R}) - E_T)\tau} \delta(\mathbf{R}' - \mathbf{R}) .\qquad (18)$$

The elements of $\hat{G}_T$ are unfortunately not diagonal. This can be explained by imagining a free particle in one dimension with some average kinetic energy p. If we evolve the particle by some time t, it will move from $<\hat{x}> = x$ to $<\hat{x}> = x'$. Because there is no potential, $\hat{H} = \hat{T}$ and the particle will have the same $<\hat{p}>$ as before, indicating $\langle x' | e^{-\hat{T}} | x \rangle \neq 0$. Solving for $G_T(\mathbf{R}', \mathbf{R}, \tau)$ by inserting the identity twice we find

$$G_T(\mathbf{R}', \mathbf{R}, \tau)$$

$$= \langle \mathbf{R}' | e^{-\hat{T}\tau} | \mathbf{R} \rangle$$
$$= \langle \mathbf{R}' | e^{-D\tau\nabla_{\mathbf{R}}^2} | \mathbf{R} \rangle$$
$$= \iint d\mathbf{K}d\mathbf{K}' \langle \mathbf{R}' | \mathbf{K}' \rangle \langle \mathbf{K}' | e^{-D\tau\nabla_{\mathbf{R}}^2} | \mathbf{K} \rangle \langle \mathbf{K} | \mathbf{R} \rangle$$
$$= \iint d\mathbf{K}d\mathbf{K}' e^{-i\mathbf{R}'\cdot\mathbf{K}'} \langle \mathbf{K}' | e^{-D\tau\nabla_{\mathbf{R}}^2} | \mathbf{K} \rangle e^{i\mathbf{R}\cdot\mathbf{K}}$$
$$= \iint d\mathbf{K}d\mathbf{K}' e^{-i\mathbf{R}'\cdot\mathbf{K}'} e^{-D\tau\mathbf{K}^2} \delta(\mathbf{K}' - \mathbf{K}) e^{i\mathbf{R}\cdot\mathbf{K}}$$
$$= \int d\mathbf{K} e^{i\mathbf{K}\cdot(\mathbf{R}-\mathbf{R}')} e^{-D\tau\mathbf{K}^2}$$
$$= (4\pi D\tau)^{-3n/2} e^{-\frac{(\mathbf{R}-\mathbf{R}')^2}{4D\tau}} \qquad (19)$$

Each of the n particle represented in $\mathbf{R}$ takes 3 spacial dimensions to specify, (x_1, x_2, x_3), meaning that $G_T(\mathbf{R}', \mathbf{R}, \tau)$ is a $3n$ dimensional Gaussian distribution with variance $2D\tau$. Now that we have solutions to both the rate and diffusion equations we can write

$$G(\mathbf{R}', \mathbf{R}, \tau) = (4\pi D\tau)^{-3n/2} e^{-\frac{(\mathbf{R}-\mathbf{R}')^2}{4D\tau}} e^{-(V(\mathbf{R}) - E_T)} + O(\tau^2) ,\qquad (20)$$

which is our coordinate space representation of the evolution operator $\hat{G}$ for small τ, or more formally called the propagator.

Now given some $\Psi(\mathbf{R}, 0)$ we can calculate $\Psi(\mathbf{R}', \tau)$ as in Ref. 11. We want to find the overlap of some $|\mathbf{R}'\rangle$ with $|\Psi(\mathbf{R}, \tau)\rangle$. If

$$|\Psi(\mathbf{R}, \tau)\rangle = e^{-(\hat{H} - E_T)\tau} |\Psi(\mathbf{R}, 0)\rangle ,\qquad (21)$$

then

$$\langle \mathbf{R}' | \Psi(\mathbf{R}, \tau) \rangle = \langle \mathbf{R}' | e^{-(\hat{H} - E_T)\tau} | \Psi(\mathbf{R}, 0) \rangle$$
$$= \int d\mathbf{R} \langle \mathbf{R}' | e^{-(\hat{H} - E_T)\tau} | \mathbf{R} \rangle \langle \mathbf{R} | \Psi(\mathbf{R}, 0) \rangle$$
$$= \int d\mathbf{R} G(\mathbf{R}', \mathbf{R}, \tau) \langle \mathbf{R} | \Psi(\mathbf{R}, 0) \rangle .\qquad (22)$$

$\text{Dim}(\mathbf{R}) = 3n$, making this a very complex integral for large n. Thus we will employ the Markov-Chain Sampling Monte Carlo method outlined in Sec. I.B.2. to update the wave function from one time step to the next.

Now that we have laid the ground work, we are ready to run the algorithm. We start with an ensemble of N snapshots, or starting configurations, of the system each with n bosons (n random walkers) and pick an initial E_T. We calculate $V(\mathbf{R})$ for each snapshot and then make N_C copies of each snapshot where

$$N_C = int[e^{-\tau(V(\mathbf{R}) - E_T)} + \zeta] ,\qquad (23)$$

where $int[*]$ is the integer portion of $*$ and random variable $\zeta \in [0, 1]$. Next we evolve $\Psi(\mathbf{R}, 0)$ to $\Psi(\mathbf{R}', \tau)$ in the diffusion step by moving each of the n walkers according to

$$\mathbf{r}_i \to \mathbf{r}_i + \eta_i ,\qquad (24)$$

where η_i is a 3-dimensional random variable sampled from $G_T(\mathbf{R}', \mathbf{R}, \tau)$, a Gaussian with variance $2D\tau$. We then update E_T based on whether we had a net gain or net loss in the total number of snapshots and on our current guess on E_0. If we gained snapshots then we lower E_T and vice versa.

C. Diffusion Monte Carlo With Importance Sampling

The DMC as described above is not optimal; in fact it is rarely used as it has a major flaw. If the potential energy becomes very large and negative, as it may with an

electron moving very close to the nucleus (an electron is a fermion but we give this example out of accessibility), then our simulation in its current state will create an inordinate amount of snapshots because $e^{-\tau(V(\mathbf{R})-E_T)}$ will be huge. To prevent walkers from moving towards areas where $V(\mathbf{R}) \to \infty$ we introduce the method of importance sampling, which alters the underlying probability distribution in a way that pushes walkers away from dangerous regions.

Instead of solving for $\Psi(\mathbf{R}, \tau)$ we would like to solve for

$$f(\mathbf{R}, \tau) = \varphi(\mathbf{R})\Psi(\mathbf{R}, \tau) , \qquad (25)$$

where $\varphi(\mathbf{R})$ is an approximate ground state wave function (from a Hartree-Fock calculation for example) and will push our walkers away from unphysical regions.[7] Substituting $\frac{f(\mathbf{R},\tau)}{\varphi(\mathbf{R})} \to \Psi(\mathbf{R}, \tau)$, the Schrödinger equation reads

$$-\frac{1}{\varphi(\mathbf{R})}\frac{\partial f(\mathbf{R}, \tau)}{\partial \tau} = [-D\nabla_{\mathbf{R}}^2 + V(\mathbf{R}) - E_T]\frac{f(\mathbf{R}, \tau)}{\varphi(\mathbf{R})} . \quad (26)$$

Reorganizing this equation[2] we have

$$-\frac{\partial f(\mathbf{R}, \tau)}{\partial \tau} = \quad -D\nabla_{\mathbf{R}}^2 f(\mathbf{R}, \tau) + D\nabla_{\mathbf{R}} \cdot [\mathbf{F}(\mathbf{R})f(\mathbf{R}, \tau)]$$
$$+ [E_L(\mathbf{R}) - E_T]f(\mathbf{R}, \tau) , \qquad (27)$$

where the *drift force*

$$\mathbf{F}(\mathbf{R}) \equiv \nabla_{\mathbf{R}}\ln|\varphi(\mathbf{R})|^2 = 2\frac{\nabla_{\mathbf{R}}\varphi(\mathbf{R})}{\varphi(\mathbf{R})} , \qquad (28)$$

and the *local energy*

$$E_L(\mathbf{R}) \equiv \varphi(\mathbf{R})^{-1}\hat{H}\varphi(\mathbf{R}) . \qquad (29)$$

One usually calculates $\mathbf{F}(\mathbf{R})$ and $E_L(\mathbf{R})$ analytically before running the simulation. By doing this we can write a $G(\mathbf{R}', \mathbf{R}, \tau)$ that is independent of $V(\mathbf{R})$; we rely on the *drift force* and *local energy* to guide the snapshot away from problematic regions. Thus,

$$G(\mathbf{R}', \mathbf{R}, \tau) = (4\pi D\tau)^{-3n/2}e^{-\frac{(\mathbf{R}-\mathbf{R}'-\mathbf{F}(\mathbf{R})D\tau)^2}{4D\tau}}e^{-(E_L(\mathbf{R})-E_T)}$$
$$+ O(\tau^2) \qquad (30)$$

is one possible propagator and should look familiar as it is a modified version of Eq. (20). It is not unique because we do not know whether to diffuse the walkers or drift the walkers first, i.e. do we use $\mathbf{F}(\mathbf{R})$ or $\mathbf{F}(\mathbf{R}')$? Remember that diffusing the walkers corresponds to sampling over $G_T(\mathbf{R}', \mathbf{R}, \tau)$ from the previous section. We will disregard this point and take the ordering of drift then diffusion for our algorithm. We can now describe one possible procedure for the DMC:[2]

1. Initialize N configurations of our system where the n walkers are distributed according to $|\varphi(\mathbf{R})|^2$. We try to create a diverse ensemble of snapshots, so that at least some will remain after the first time step.

2. Update the ith walker in each snapshot according to

$$\mathbf{r}_i' = \mathbf{r}_i + D\tau\mathbf{F}(\mathbf{R}) + \eta_i , \qquad (31)$$

where η_i, as before, is a 3-d random variable sampled from a Gaussian with variance $2D\tau$.

3. Accept/reject step via a Metropolis question. This step essentially makes sure we are sampling the correct distribution by verifying that the step satisfies the detailed balance condition. Refer to Refs. 3,5, and 6 for more information.

4. Take each snapshot and make N_C copies where

$$N_C = \text{int}[e^{-\tau(E_L(\mathbf{R})-E_T)} + \zeta] , \qquad (32)$$

where once again the random variable $\zeta \in [0, 1]$. If $N_C = 0$ we kill the state.

5. Estimate E_0 by averaging E_L over all snapshots.

6. Adjust E_T so that it satisfies

$$E_T = E_0 + \kappa \ln\left(\frac{N(0)}{N(\tau)}\right) , \qquad (33)$$

where κ is a positive parameter small enough to avoid introducing bias into the calculation and $N(\tau)$ is the number of snapshots at time τ. A large κ would introduce bias because we would be updating based on a non-random process, which would cause more systemic error in our approximation.

III. DISCUSSION AND APPLICATIONS

A. Bosons vs. Fermions

You may have wondered why we limited our discussion to the ground state of an n-body boson system. Bosons are indistinguishable particles meaning that their wave functions are even. We can choose the ground state $|\phi_0(\mathbf{R})\rangle > 0 \ \forall \ \mathbf{R}$. Thus we can also choose our approximate ground state $|\varphi(\mathbf{R})\rangle > 0 \ \forall \ \mathbf{R}$. We therefore do not have to take into account any nodes in the wave function. Fermions, however, are distinguishable and have antisymmetric wave functions, meaning that when we choose $|\varphi(\mathbf{R})\rangle$, we must also choose a location for the node. Because we don't update $|\varphi(\mathbf{R})\rangle$ during the simulation, the accuracy of the result would be highly dependent on the choice of this node. Simulations of excited boson states suffer the same issue.

There are a couple methods, the fixed node and released node methods, for dealing with these problems as is discussed in Refs. 2 and 7. In both methods we replace $\varphi(\mathbf{R})$ with $|\varphi(\mathbf{R})|$ so that the drift term gives a correctly signed output. The fixed node method has exactly the problems mentioned above. We choose some $\varphi(\mathbf{R})$ and

do not change the node locations. If the node locations of $\phi_0(\mathbf{R})$ and $\varphi(\mathbf{R})$ differ, we will be under sampling regions of $\phi_0(\mathbf{R})$ near the true nodes. If, in some snapshot, a walker passed the approximated node, we reject this path and delete the snapshot; this rejection is reasonable because $\mathbf{F}(\mathbf{R})$, in Eq. (28), will push walkers away from nodes. In fact, $\mathbf{F}(\mathbf{R})$ is infinite at the node location so, under the fixed node approximation, it would be unphysical for the walker to pass this point. However, this leads to a highly biased result that's accuracy is reliant on the choice of $\varphi(\mathbf{R})$. The released node method allows walkers to pass nodes. The walkers essentially "pull" the node along with them (by a small amount as a one of n walkers in one of N snapshots does not have great statistical significance).

Neither of these methods are perfect. In fact, it has been speculated that these problems belong to the set of NP-Hard computational problems because the "sign problem" belongs to this class in complexity theory.[9] As such, DMC methods for fermions and excited states of bosons are still under investigation.

B.   Applications

DMC results have been shown to agree with experimental findings for many important systems. The list includes:

1. Calculating the ground state of a homogeneous Bose gas. Giorgini, Boronat, and Casulleras, verified that the energy per particle in a uniform gas of bosons can be expanded in powers of $\sqrt{na^3}$, where n is the density and a the s-wave scattering length, i.e. that

$$\frac{E}{N} = 4\pi na^3$$

$$\times \Big[1 \; + \; \frac{128}{15\sqrt{\pi}}\sqrt{na^3}$$

$$+ \; \frac{8(4\pi - 3\sqrt{3})}{3}na^3 \ln(na^3) + \dots \Big] . \quad (34)$$

This result is import because it verifies that at boson densities conducive to Bose-Einstein condensate magnetic trapping, the energy correction term to the mean field approximation is only dependent on na^3. Thus, future precision experiments may be able to infer na^3 from the measured energy of the Bose-Einstein condensate.[8,10]

2. Computing various properties of circular quantum dots. Production of quantum dots small enough to have atom-like properties is now feasible. It is possible to do exact diagonalization for dots with less than 8 free electrons, but these computations are only accurate up to $N = 3$, where N is the number of free electrons. Using the fixed node approximation, Pederiva, Umrigar, and Lipparini, found that the DMC results give better bounds on ground state energy, excitation energies, electronic correlation energy, chemical potential from addition of an electron into the dot, and spin density, for dots with $N \leq 13$.[15]

3. Computing the properties of a helium 0-temperature liquid. Whitlock et al. used the Lennard-Jones interaction potential of the form

$$V(r_{ij}) = 4\epsilon\Big[\Big(\frac{\sigma}{r_{ij}}\Big)^{12} - \Big(\frac{\sigma}{r_{ij}}\Big)^{6}\Big] \quad (35)$$

where $\epsilon = 10.22°$K and $\sigma = 2.556$Å. They reported an error of less than 1% for the DMC energy calculation and increases in accuracy for computations of equation of state and face-centered cubic crystal phase.[16]

4. Computing the electron configuration of the He atom ground state using a Hamiltonian of the form

$$\hat{H} = -\frac{1}{2}\nabla_1^2 - \frac{1}{2}\nabla_2^2 - \frac{2}{r_1} - \frac{2}{r_2} + \frac{1}{r_{12}} , \quad (36)$$

where the nucleus is approximated to have infinite mass and is placed at the origin. r_i refers to the distance of the ith electron from the nucleus and r_{12} refers the to the distance between the two electrons. Apaja chooses the trial wave function that of the 1S orbital. His calculation is used mostly as a tool to demonstrate the time step error in DMC's, which is linear in τ for small τ.[2]

IV.   CONCLUSION

In conclusion, the Diffusion Monte Carlo is a fast and simple way to calculate the ground state energies of n-body boson systems and an adequate way to approximate energy eigenvalues of n-fermion systems. Because the dimensionality of these systems scales exponentially in n, finding approximate solutions in time polynomial in n using the Diffusion Monte Carlo is extraordinary.

---

[1] Troyer, Matthias. Lecture. "Introduction to many-body quantum mechanics." Computational Quantum Mechanics. Institute For Theoretical Physics at Swiss Federal Institute of Technology Zurich. 2012.

www.itp.phys.ethz.ch/education/fs12/cqp/chapter04.pdf

[2] Apaja, Vesa. Lecture. "Monte Carlo Methods." University of Jyvskyl, Finland. 2009. users.jyu.fi/∼veapaja/Monte_Carlo/MC.lecture.vesa.pdf

[3] Metropolis, N. "The Beginning of the Monte Carlo Method." Los Alamos Science 15 (1987): 125.

[4] "Profile of the People and Land of the United States." Profile of the People and Land of the United States. N.p., 13 Jan. 2013. Web. 16 Apr. 2014.

[5] Krauth, Werner. *Statistical Mechanics: Algorithms and Computations* (Oxford: University Press, 2006).

[6] Metropolis, Nicholas, et al. "Equation of state calculations by fast computing machines." The journal of chemical physics 21.6 (2004): 1087-1092.

[7] Ceperley, David, and B. Alder. "Quantum monte carlo." Science. v231 555 (1986).

[8] Blume, Doerte, and Chris H. Greene. "Quantum corrections to the ground-state energy of a trapped Bose-Einstein condensate: A diffusion Monte Carlo calculation." Physical Review A 63.6 (2001): 063601.

[9] Troyer, Matthias, and Uwe-Jens Wiese. "Computational complexity and fundamental limitations to fermionic quantum Monte Carlo simulations." Physical review letters 94.17 (2005): 170201.

[10] Giorgini, S., J. Boronat, and J. Casulleras. "Ground state of a homogeneous Bose gas: A diffusion Monte Carlo calculation." Physical Review A 60.6 (1999): 5129.

[11] Elster, Charlotte. Lecture. "Green Functions and Propagators." Relativistic Quantum Mechanics. Ohio University. 2006. http://www.phy.ohiou.edu/∼elster/lectures/relqm_17.pdf

[12] Bernoff, Andrew J. Lecture. "Cooling of a Hot Bar: The Diffusion Equation." An Introduction to Partial Differential Equations. Harvey Mudd. http://www.math.hmc.edu/ ajb/PCMI/lecture2.pdf

[13] Hattovy, Scott. "The Focker-Planck Equation." University of Wisconsin-Madison. 2011. http://www.math.wisc.edu/ shottovy/NumPDEreport.pdf

[14] Ben-Naim, E., Krapivsky, P. L., and Redner, S. *Fundamental Kinetic Processes.* 2008. Chapter 2: Random Walk/Diffusion. http://physics.bu.edu/ redner/542/book/rw.pdf

[15] Pederiva, Francesco, C. J. Umrigar, and Enrico Lipparini. "Diffusion Monte Carlo study of circular quantum dots." Physical Review B 62.12 (2000): 8120.

[16] Whitlock, P. A., et al. "Properties of liquid and solid He 4." Physical Review B 19.11 (1979): 5598.

The Energetic Spectra of Rotational and Vibrational Modes in Diatomic Molecules

Bhaskaran Balaji

Quantum Mechanics III, 77 Massachusetts Ave., Cambridge, MA 02139-4307

(Dated: May 3, 2014)

In this paper, we determine the energetic spectra of rotational and vibrational modes in diatomic molecules. First, we use separation of variables and matrix methods, in addition to the alternative, simplifying method of transforming to center-of-mass coordinates, to determine the energies of the two modes in the most basic case. Then, we examine the effect of considering an anharmonic potential in the calculation of vibrational energies. Finally, we discuss the relevance of our calculations to the field of spectroscopy by looking at the total spectrum formed as the composite of those for rotations and vibrations.

I. INTRODUCTION

Diatomic molecules offer a contained environment in which to study molecular rotational and vibrational modes. Finding the energetic spectra of the two modes admits the use of elementary methods, such as diagonalization and separation of variables, as well as transformation to center-of-mass coordinates.

This problem serves as a stepping-stone to more complex phenomenology, such as the behavior of the spectra in the presence of external electromagnetic fields, as well as the spectra of larger polyatomic molecules. Additionally, while we begin with the usual harmonic approximation because it has a simple, exact solution, we can also analyze the system using the Morse potential, which quite accurately represents the observed potential and still has an analytic solution that is relatively easy to find.

We first solve the Schrödinger equations for rotation and vibration individually, in Sections II and III. Then in Section IV, we find the new vibrational energy levels in the Morse potential. In Section V, we look at the resulting spectra when rotations and vibrations are considered together. Finally, in Section VI we discuss what we have learned in the context of experimental results in spectroscopy.

II. ROTATION

To consider rotation alone, we assume that the molecule is a rigid rotor. This allows us to treat the problem, in the center-of-mass frame, as the movement of a single particle of mass

$$\mu = \frac{m_1 m_2}{m_1 + m_2} \quad (2.1)$$

on a sphere of radius r_0. We use the Hamiltonian in spherical coordinates [2]

$$-\frac{\hbar^2}{2\mu}\left[\frac{1}{r^2}\frac{\partial}{\partial r}\left(r^2\frac{\partial\psi}{\partial r}\right) + \frac{1}{r^2\sin\theta}\frac{\partial}{\partial\theta}\left(\sin\theta\frac{\partial\psi}{\partial\theta}\right) + \frac{1}{r^2\sin^2\theta}\left(\frac{\partial^2\psi}{\partial\phi^2}\right)\right] + V\psi = E\psi \quad (2.2)$$

and, as usual, look for solutions that separate into purely radial and purely angular components:

$$\psi(r,\theta,\phi) = R(r)Y(\theta,\phi). \quad (2.3)$$

But as stipulated above, $R(r) = r_0$, and since the rotation is free, $V = 0$, so we end up with

$$-\frac{\hbar^2}{2\mu r_0^2}\left[\frac{1}{\sin\theta}\frac{\partial}{\partial\theta}\left(\sin\theta\frac{\partial\psi}{\partial\theta}\right) + \frac{1}{\sin^2\theta}\left(\frac{\partial^2\psi}{\partial\phi^2}\right)\right] = E\psi. \quad (2.4)$$

The solutions to this Hamiltonian are the spherical harmonics Y_{jm} [1], with energies

$$E_j = \frac{\hbar^2}{2\mu r_0^2}j(j+1). \quad (2.5)$$

The energy E_j has degeneracy $2j+1$.

Thus the calculation of the rotational spectrum simplifies through a change of coordinates to a well known problem. Because of the dependence on reduced mass μ rather than individual masses, this result applies to the heteronuclear case as well as the homonuclear one. Thus we find that in general, the rotational spectra depend only on μ and r_0, or, more concisely, on the molecule's moment of inertia $I = \mu r_0^2$ about an axis perpendicular to the bonding direction.

III. VIBRATION

We start with the simplest model: two equal masses m connected by a spring of spring constant k. The values of these constants are enough to distinguish diatomic molecules from each other. The Schrödinger equation for this system is

$$H = T + V$$
$$= \frac{p_1^2}{2m} + \frac{p_2^2}{2m} + \frac{k}{2}(x_1 - x_2)^2. \quad (3.1)$$

In order to find the eigenenergies of this system, we want to diagonalize H, so we start by diagonalizing V. Given that $V = \frac{k}{2}(x_1 - x_2)^2$, we can rewrite it as a quadratic

20

form:

$$V = \vec{x}^T K \vec{x} = (\begin{array}{cc} x_1 & x_2 \end{array}) K \left(\begin{array}{c} x_1 \\ x_2 \end{array} \right) \qquad (3.2)$$

$$\text{where } K = \frac{k}{2} \left(\begin{array}{cc} 1 & -1 \\ -1 & 1 \end{array} \right).$$

This matrix K is easily diagonalizable; it has eigenvectors (yet unnormalized) $\left(\begin{array}{c} 1 \\ 1 \end{array} \right)$ and $\left(\begin{array}{c} 1 \\ -1 \end{array} \right)$, with eigenvalues 0 and k, respectively. Using this knowledge, we construct the rotation matrix

$$R = \frac{1}{\sqrt{2}} \left(\begin{array}{cc} 1 & 1 \\ -1 & 1 \end{array} \right) \qquad (3.3)$$

and use it to diagonalize K, so that

$$R^T K R = k \left(\begin{array}{cc} 1 & 0 \\ 0 & 0 \end{array} \right). \qquad (3.4)$$

Now we finish diagonalizing H. If we write T as a quadratic form, i.e.

$$T = \vec{p}^T S \vec{p} \qquad (3.5)$$

$$\text{where } \vec{p} = \left(\begin{array}{c} p_1 \\ p_2 \end{array} \right) \text{ and } S = \frac{1}{2m} I,$$

we note that S is proportional to the identity, so $R^T S R = S$. So, by rotating our coordinates into new momenta $\vec{q} = R^T \vec{p}$ and new positions $\vec{y} = R^T \vec{x}$, we find that

$$H = \frac{q_1^2}{2m} + \frac{q_2^2}{2m} + k y_1^2 \qquad (3.6)$$

or, rearranging and grouping,

$$H = \left(\frac{q_1^2}{2m} + k y_1^2 \right) + \frac{q_2^2}{2m}. \qquad (3.7)$$

Now we immediately see that this equation separates into the Hamiltonian of a simple harmonic oscillator of frequency $\omega = \sqrt{\frac{2k}{m}}$, and that of a free particle.

Of course, although our Hamiltonian takes into account all the possible modes of the system, we only care about the vibrational mode. Thus, we have our answer: the vibrational spectrum, when treated alone, is that of a harmonic oscillator, with energies

$$E_n = \hbar \omega \left(n + \frac{1}{2} \right) \qquad (3.8)$$

$$\text{where } \omega = \sqrt{\frac{2k}{m}}.$$

While this method is illuminating and simple enough, there is another that is still simpler: we can employ the change of coordinates that we did for studying rotations.

Another Approach to Vibrational Modes

We know from classical mechanics that by transforming to center-of-mass coordinates, we can treat the problem as that of a single particle of reduced mass μ (as defined in Eq. (2.1)) attached to a hard wall by a spring of constant k. We then know that the fundamental frequency is

$$\omega = \sqrt{\frac{k}{\mu}}, \qquad (3.9)$$

which is consistent with our result above, in the homonuclear case where $\mu = \frac{m}{2}$.

This simplification works because we are dealing with the problem of only two atoms, which easily contracts with classical arguments into that of a single atom. And we have learned something else along the way: by considering the reduced mass of the two atoms, we now do not have to assume that they have the same mass and can apply our result to heteronuclear diatomic molecules. Subject to our harmonic-oscillator approximation, the vibrational energies depend only on the reduced mass of the two atoms and the spring coefficient k of their bond.

However, the matrix method can also be used for atoms of differing mass and remains useful for molecules comprising more than two atoms.

IV. VIBRATIONS IN AN ANHARMONIC POTENTIAL

In all of our preceding treatment of vibrations, we approximated the potential between the two atoms as quadratic. A quadratic potential, however, goes to infinity for large separation x, while a Coulomb potential does not. A rather egregious result of our simplification is that we have bound states with unbounded energies (from the celebrated "ladder" of the harmonic oscillator). But this cannot be the case—if the vibrational energy were more than the dissociation energy of the molecule, it would break apart!

This inaccuracy suggests that we might improve our results if we choose a potential that behaves more like the Coulomb potential. However, we still want analytic solutions, which is why we chose the harmonic simplification in the first place. Luckily, there exists a potential that both is accurate for large x and admits (simple) analytic solutions to the Schrödinger equation. This is the Morse potential (Fig. 1)[3]:

$$V(x) = D_e \left(1 - e^{-\alpha(x - x_e)} \right)^2. \qquad (4.1)$$

Here D_e is the dissociation energy relative to the bottom of the potential, x_e is the equilibrium separation of the
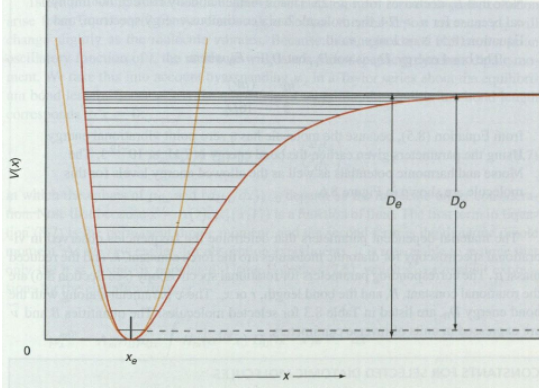
FIG. 1: The Morse potential. x_e is the equilibrium separation, D_e is the dissociation energy from the bottom of the well, and D_0 is the dissociation energy from the ground state. The horizontal axis marks separation distance of the two atoms, and the vertical axis marks the resulting potential energy of the system.[1]

two atoms, and

$$\alpha = \sqrt{\frac{k}{2D_e}}, \qquad (4.2)$$

$$\text{where } k = \left(\frac{d^2V}{dx^2}\right)_{x=x_e}$$

is defined in analogy to the quadratic potential. We now calculate the eigenenergies in the Morse potential. Our method is adapted from Morse's.[3]

The Schrödinger equation that we must solve is (again in center-of-mass coordinates)

$$-\frac{\hbar^2}{2\mu}\frac{d^2\psi}{dx^2} + D_e\left(1 - e^{-\alpha(x-x_e)}\right)^2\psi = E\psi. \qquad (4.3)$$

First we make the substitution $\alpha(x - x_e) = y$, so that

$$-\frac{\hbar^2\alpha^2}{2\mu}\frac{d^2\psi}{dy^2} + D_e\left(1 - e^{-y}\right)^2\psi = E\psi. \qquad (4.4)$$

Now define

$$\delta^2 = \frac{2\mu D_e}{\hbar^2\alpha^2} \quad \text{and} \quad \epsilon = \frac{2\mu E}{\hbar^2\alpha^2}, \qquad (4.5)$$

so that by rearranging, we end up with

$$\frac{d^2\psi}{dy^2} + \left(\epsilon - \delta^2\left(1 - e^{-y}\right)\right)^2\psi = 0. \qquad (4.6)$$

Now we make another substitution $u = e^{-y}$, yielding the new equation

$$u^2\frac{d^2\psi}{du^2} + u\frac{d\psi}{du} + \left(\epsilon - \delta^2 + 2\delta^2 u - \delta^2 u^2\right)\psi = 0 \qquad (4.7)$$

Now that we have simplified the presentation of the equation, we make a guess, following Morse, about the dependence of ψ on u:

$$\psi(u) = e^{-\delta u}(2\delta u)^{b/2}f(u), \qquad (4.8)$$

for some function $f(u)$ and some number b. Making this substitution, we arrive at the new equation in f:

$$e^{-\delta u}(2\delta u)^{\frac{b}{2}-2}\Big((2\delta u)^2\frac{d^2f}{du^2} + 2\delta(2\delta u)(b+1-2\delta u)\frac{df}{du}$$
$$+ \delta^2\left(b^2 + 4\left(\epsilon - \delta^2\right) - 2(2\delta u)(b+1-2\delta)\right)f\Big) = 0. \qquad (4.9)$$

Since $u \neq 0$, we can cancel out the prefactors. Additionally, we now find that imposing a condition on b simplifies this equation, namely

$$b^2 = -4\left(\epsilon - \delta^2\right), \qquad (4.10)$$

giving

$$(2\delta u)^2\frac{d^2f}{du^2} + 2\delta(2\delta u)(b+1-2\delta u)\frac{df}{du}$$
$$- 2\delta^2(2\delta u)(b+1-2\delta)f = 0. \qquad (4.11)$$

Next we let $z = 2\delta u$ and cancel out an extra z present in each term to give us

$$4\delta^2 z\frac{d^2f}{dz^2} + 4\delta^2(b+1-z)\frac{df}{dz} - 2\delta^2(b+1-2\delta)f = 0, \qquad (4.12)$$

or, dividing out $4\delta^2$,

$$z\frac{d^2f}{dz^2} + (b+1-z)\frac{df}{dz} - (\frac{b}{2} + \frac{1}{2} - \delta)f = 0. \qquad (4.13)$$

We now consider power-series solutions $f(z) = \sum_{m=0}^{\infty} a_m z^m$ to Eq. (4.13). In order for such a solution to be meaningful, it must be normalizable, and so it must terminate. Plugging this form for f into Eq. (4.13), we find the recurrence relation

$$a_{m+1}(m+b+1)(m+1) = a_m\left(m + \frac{b}{2} + \frac{1}{2} - \delta\right). \qquad (4.14)$$

In order for the power series to terminate, then, we need

$$n + \frac{b}{2} + \frac{1}{2} - \delta = 0 \qquad (4.15)$$

under the condition $2\delta \geq 1$. Solving for b and plugging the result into our earlier condition (4.10), we find

$$\epsilon = \delta^2 - \frac{(2\delta - 2n - 1)^2}{4}$$
$$= \delta^2 - \left(\delta - n - \frac{1}{2}\right)^2$$
$$= 2\delta\left(n + \frac{1}{2}\right) - \left(n + \frac{1}{2}\right)^2. \qquad (4.16)$$

We want to return dimensions to these quantities to know the energy levels we have calculated. First, combine Eqs (3.9) and (4.2) to find

$$\frac{2\mu}{\hbar^2 \alpha^2} = \frac{4D_e}{\hbar^2 \omega^2}. \tag{4.17}$$

(Note that our use of ω here is still general, because of its definition in terms of k, which in turn is defined generally in Eq. (4.2).) Then by dividing Eq. (4.16) by this factor, we arrive at our final result for the energy levels in the Morse potential:

$$E_n = \hbar\omega\left(n + \frac{1}{2}\right) - \frac{(\hbar\omega)^2}{4D_e}\left(n + \frac{1}{2}\right)^2. \tag{4.18}$$

The quadratic "correction term" in the Morse energies (4.18) is of order $\frac{\hbar\omega}{D_e}$ relative to the harmonic oscillator energies. For the H_2 molecule, since the bond energy $D_0 \approx D_e$, this is about (values from [1])

$$\frac{h\nu}{D_0} = \frac{\left(6.626 \times 10^{-34}\right)\left(8.29 \times 10^{14}\right)}{7.24 \times 10^{-19}} \approx 0.121, \tag{4.19}$$

quite significant!

In this paper, we are primarily concerned with the eigen*energies* of the Morse potential, but for some more context, we can note here that the eigen*functions* of f are the generalized Laguerre polynomials.[6] Knowing this, we can construct the bound-state wavefunctions by reverting all of our substitutions.

When we first introduced the Morse potential, we remarked that we did not want bound states with arbitrarily high energy. In the Morse potential, the quadratic term serves to limit the number of possible states, so that we not only have all states bounded in energy, but we also have only a finite number of such states. To see this, note that in order to exist as a bound state in this potential, a state must have energy satisfying $0 \le E_n \le D_e$. This translates into the condition

$$0 \le n \le \frac{4D_e}{\hbar\omega} - \frac{1}{2}. \tag{4.20}$$

Due to the quadratic term in (4.18), we can calculate that the maximum energy is achieved by the state with n that best approximates

$$n \approx \frac{2D_e}{\hbar\omega} - \frac{1}{2} \tag{4.21}$$

with energy

$$E_{max} \le D_e \tag{4.22}$$

with equality if n actually makes (4.21) exact.

The Morse potential offers a remarkably accurate approximation to real, observed potentials, and as a result, its eigenenergies also closely match the observed quantities.[3] However, from here we no longer require its level of precision, so we will return to using the harmonic-oscillator potential by default.

V. COMBINED ROTATIONAL-VIBRATIONAL SPECTRA

Now that we have calculated the spectra for rotations and vibrations each individually, we seek to combine them. At first glance, this is quite a difficult task, in which we must solve the Schrödinger equation for the Hamiltonian that incorporates both the harmonic-oscillator potential and the potential caused by the centrifugal force from rotation.

$$H = \frac{p^2}{2\mu} + \frac{k}{2}r^2 + \frac{\hbar^2}{2\mu r^2}j(j+1). \tag{5.1}$$

The Schrödinger equation for this Hamiltonian is not solved easily, and in fact it cannot be done exactly[4]. However, we can make a fairly accurate approximation.

Let us compare, using our models from Sec. II and III, the energy spacing between the two lowest rotational states with the spacing between the two lowest vibrational states (indeed, the spacing between any two adjacent harmonic-oscillator states):

$$\frac{\Delta E_j}{\Delta E_n} = \frac{\hbar^2/\mu r_0^2}{\hbar\sqrt{k/\mu}} = \frac{\hbar}{r_0^2\sqrt{\mu k}}. \tag{5.2}$$

This number is quite small, usually of order 10^{-2}.[4] It is also known that the eigenfunctions for this Hamiltonian have the same form as those for the Hamiltonian in which the rotational term is neglected.[5] So, as a preliminary approximation, valid for small values of j, we regard the new term as constant:

$$\delta H = \frac{\hbar^2}{2\mu r_0^2}j(j+1). \tag{5.3}$$

With this constant perturbation to the Hamiltonian, we can simply add the rotational energies to each vibrational energy level, resulting in a nested double-spectrum (Fig. 2)

$$E_{nj} = \hbar\omega\left(n + \frac{1}{2}\right) + \frac{\hbar^2}{2\mu r_0^2}j(j+1). \tag{5.4}$$

To be more general, we could treat the new rotation term as a *non*-constant perturbation. The first order correction to the energy of state n would then be, for each j (that is small enough to be treated as a perturbation),

$$E_n^1 = \frac{\hbar^2}{2\mu}j(j+1)\langle n|\frac{1}{r^2}|n\rangle. \tag{5.5}$$

But this inner product causes problems because of the divergence of $\frac{1}{r^2}$ as $r \to 0$. Instead, the standard approach is to expand the denominator in a Taylor series around the equilibrium separation. Any terms of degree less than or equal to 2 can be combined with the existing harmonic-oscillator potential for exact results. Any higher-order terms can then be treated as perturbations, whose matrix elements may then be computed.[4]
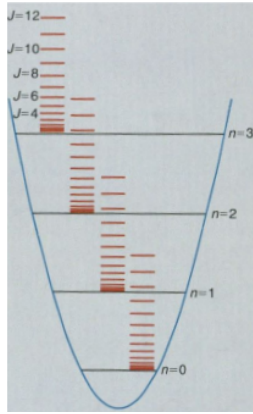
FIG. 2: The rotational energy levels, superimposed on each vibrational energy level.[1]

VI.   APPLICATION: INFRARED SPECTROSCOPY

We can observe the energy levels of rotational and vibrational modes by studying light absorption and emission from diatomic molecules. A photon can be absorbed only if it imparts to the molecule exactly enough energy for the molecule to transition to another one of its discrete energy levels. So the absorption spectrum can tell us certain physical parameters of the molecule under observation, based on the spacing between absorbed frequencies.

Let us consider the restrictions on allowed transitions (called "selection rules") upon absorption of a photon. The probability of transition from state n to state m is nonzero only if the transition dipole moment in the direction of the electric field

$$\mu_x^{mn} = \langle \psi_m(x)| \mu_x(x) |\psi_n(x)\rangle = \int \psi_m^*(x)\mu_x(x)\psi_n(x)dx \tag{6.1}$$

is nonzero [1], where x is the spatial coordinate in the direction of the field and $\mu_x(x)$ is the dipole moment in the same direction. Taking into account the molecule's vibration, we can expand the dipole moment in a Taylor series around the equilibrium bond length. To first order in x, which represents the displacement from equilibrium,

$$\mu_x(x) = \mu_x(0) + x \left(\frac{d\mu_x}{dx} \right)_{x=0}. \tag{6.2}$$

Taking m and n as distinct states, the inner product with the constant term $\mu_x(0)$ disappears, as different eigenstates are orthogonal. Thus with this Taylor approximation, we find that the selection rule depends only on the "dynamic dipole moment," i.e. the coefficient to the first-order term in the Taylor expansion (6.2). Homonuclear diatomic molecules like H_2 do not have a dynamic dipole moment, so their vibrational modes are not excited by

photons. But we can consider heteronuclear molecules like HCl, which *do* have a dynamic dipole moment. For these molecules, the same Taylor approximation gives us $\Delta n = +1$ for absorption.[1]

Now that we have found the selection rule for transitions between vibrational states, it remains to consider transitions between rotational states. We recall that a photon carries one quantum of angular momentum. It follows that absorption of a photon changes the molecule's quantum number of angular momentum by 1, i.e. $\Delta j = \pm 1$.

What are the energies corresponding to these selection rules? For the vibrational states, as we know well from studying the simple harmonic oscillator, the energy levels are equally spaced by $\hbar\omega$, so

$$\Delta E_n = \hbar\omega. \tag{6.3}$$

For the rotational states, $\Delta j = +1$ yields

$$\begin{aligned}\Delta E_{j+} &= \frac{\hbar^2}{2\mu r_0^2}(j+1)(j+2) - \frac{\hbar^2}{2\mu r_0^2}j(j+1) \\ &= \frac{\hbar^2}{\mu r_0^2}(j+1),\end{aligned} \tag{6.4}$$

and $\Delta j = -1$ yields

$$\begin{aligned}\Delta E_{j-} &= \frac{\hbar^2}{2\mu r_0^2}(j)(j-1) - \frac{\hbar^2}{2\mu r_0^2}j(j+1) \\ &= -\frac{\hbar^2}{\mu r_0^2}j.\end{aligned} \tag{6.5}$$

As we should expect from the quadratic dependence of E_j on j, the energy differences are *not* equal. But recall from Eq. (5.2) that the rotational energy differences are relatively small, compared to the vibrational energy differences. Knowing this, we can expect that the absorption spectrum will look like a comb centered around the fundamental frequency ω, with spacing between the comb teeth equal to $\frac{\hbar}{\mu r_0^2}$ (Fig. 3). The left branch, called the "P branch," corresponds to $\Delta j = -1$, while the right branch, the "R branch," corresponds to $\Delta j = +1$. There is, of course, a gap between the two branches, as a tooth there would correspond to $\Delta j = 0$, which is disallowed.
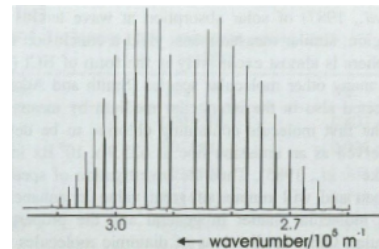
FIG. 3: The rotational-vibrational spectrum of HCl.[4]

It is worth calculating ΔE_n for the energy levels of the

Morse oscillator.

$$\Delta E_n = \hbar\omega - \frac{(\hbar\omega)^2}{4D_e}\left(n^2 + 3n + \frac{9}{4} - n^2 - n - \frac{1}{4}\right)$$

$$= \hbar\omega - \frac{(\hbar\omega)^2}{4D_e}(2n + 2)$$

$$= \hbar\omega - \frac{(\hbar\omega)^2}{2D_e}(n + 1). \tag{6.6}$$

VII.   DISCUSSION

The diatomic molecule offers a simple system in which to study molecular vibrations and rotations, and due to the prevalence of such molecules, this study lends itself to multiple applications. The characteristic spectra of different diatomics can be used to identify the composition of various astronomical substances, such as planetary and stellar atmospheres. Additionally, from our work in Sec. VI, we know that homonuclear diatomics, such as H_2, O_2, and N_2, which compose the great majority of the Earth's atmosphere (99.93

The methods and results we learn from diatomic molecules can sometimes be applied to molecules with more atoms. For example, in order to study vibrational spectra, we can often treat pairs of bonded atoms in polyatomic molecules as if they were each separate diatomic molecules. The covalent bond between the two atoms is strong enough compared to non-bonding interactions with other nearby atoms in the molecule that such two-atom systems can be isolated as if they were diatomic molecules.[1]

In much the same way as one can use elementary methods to simplify the analysis of modes in diatomic molecules, diatomic molecules themselves can serve to simplify more complex problems in quantum chemistry. Thus they are a useful analytical tool, both as a means to study further problems and as an end in themselves.

[1] Engel, T. (2010). Quantum Chemistry & Spectroscopy (2nd ed.). Upper Saddle River, NJ: Pearson Prentice Hall, pp. 115-117, 138-149.

[2] Griffiths, D. J. (2005). Introduction to Quantum Mechanics (2nd ed.). Upper Saddle River, NJ: Pearson Prentice Hall, p. 133.

[3] Morse, P. M. Diatomic Molecules According to the Wave Mechanics II. Vibrational Levels. *Phys. Rev.*, 34:57-64, Jul 1929.

[4] Ogilvie, J. F. (1998). The Vibrational and Rotational Spectrometry of Diatomic Molecules. San Diego, CA: Academic Press, pp. 148-152.

[5] Pekeris, C. L. The Rotation-Vibration Coupling in Diatomic Molecules. *Phys. Rev.*, 45:98-103, Jan 1934.

[6] See [3] for a more detailed discussion of the Laguerre polynomials and their appearance in this problem.

The Dipolar Interaction in Nuclear Magnetic Resonance

Arunima D. Balan

MIT Department of Chemistry, MIT Department of Physics,
77 Massachusetts Ave., Cambridge, MA 02139-4307

(Dated: May 2, 2014)

This paper describes the basics of nuclear magnetic resonance, and delves into the influence of dipole-dipole interactions on nuclear magnetic resonance spectroscopy. The dipole-dipole coupling interaction is first treated as a time-independent perturbation, through first order perturbation theory and can be used to determine internuclear distances. Time-dependence of dipolar coupling in liquids is then used to describe transition rates. Using first order kinetics, population dynamics of the states and the Overhauser effect is explained.

I. INTRODUCTION

Nuclear Magnetic Resonance (NMR) is a powerful tool that probes the energy gap between nuclear spin levels. In biology and chemistry NMR is often used for structure determination of both molecular and extended systems, including organic molecules, proteins [1], and synthetic polymers [2]. A standard NMR experiment probes the local electronic environment of NMR-active nuclei via application of an oscillating radiofrequency pulse in the xy-plane to a sample experiencing a strong magnetic field in the z-direction. This tips some of the spin into the xy-plane, which precess about the z-axis at a frequency that is related to the chemical environment, known as the Larmor frequency, which is then measured, appearing as a frequency peak in the spectra.

One complication to traditional NMR spectroscopy is the inclusion of dipole-dipole interactions between two nuclei or between electrons and nuclei [3]. This paper will describe the theory behind NMR and the results of including dipolar interactions in the nuclear Hamiltonian to first order in perturbation theory, which is used to study internuclear distances in the solid state. I will then explore transitions induced by dipolar interactions in liquid NMR, and use kinetic arguments to heuristically describe decoherence. This connects to the Overhauser effect, which describes the transfer of spin polarization from one spin-1/2 particle to another [4]. The Overhauser effect is utilized in a number of advanced NMR techniques, which will be explored briefly [4].

II. GENERAL NMR

In this section, the basics behind NMR spectroscopy, will be described to form a basis for future discussions of dipolar coupling in NMR.

A. The Constant Magnetic Field

Given a collection of identical, noninteracting nuclear spins, a constant magnetic field in the z-direction, B_o is applied. Depending on the electronic environment, nuclei are partially shielded from the applied magnetic field [5]. Rather than experiencing the full field, nuclei experience

$$B_{eff} = B_o\sqrt{1-\sigma} \tag{1}$$

where σ is the shielding constant and is dependent on the local chemical environment. One complication is that the value of σ often spans a relatively small range; therefore a NMR spectra of complex species are likely to have a number of overlapping peaks, impeding structure determination [5].The resulting Hamiltonian (only including the Zeeman effect) is

$$H_o = -\gamma B_{eff} I_z = \omega_o I_z$$
$$\omega_o = -\gamma B_{eff} \tag{2}$$

where γ is the gyromagnetic ratio, ω_o is the Larmor frequency and I_z is the spin projection along the z-axis, with the corresponding quantum number being m_I [6]. After a sufficiently long time, the spins can be described via a thermal density matrix [6]

$$\rho_{th} = \frac{e^{-\beta H_o}}{\text{tr}[e^{-\beta H_o}]} \tag{3}$$

where $\beta = \frac{1}{kT}$, and kT is the thermal energy. For a typical NMR experiment the difference in populations of the thermal state is one spin in 10,000 or less, due to the small energy splittings of the nuclear spin states [7]. Because of the small energy splitting, ρ_{th} is approximated to first order in its taylor expansion.

$$\rho_{th} \approx \frac{1}{2}\left(\mathbf{I} - \beta H_o\right) \tag{4}$$

Using the approximation in (4), the magnetization along the z-axis (also known as the longitudinal magnetization) can be determined

$$\left\langle I_z^{th} \right\rangle = \text{tr}\left[I_z \rho_{th}\right] = \frac{\hbar^2}{4}\beta\gamma B_{eff} \tag{5}$$

B. A Transverse Magnetic Field Induces Transitions

A small oscillating magnetic field transverse to the static field is then applied to the sample. The Hamil-

tonian, H_1, that describes this perturbation is

$$H_1 = -2\gamma B_1 I_x \cos(\omega_e t) = 2\omega_1 I_x \cos(\omega_e t)$$
$$\omega_1 = -\gamma B_1 \tag{6}$$

where B_1 indicates the strength of the magnetic field, and I_x is the nuclear spin projection along the x-axis [5]. I can then move into the rotating frame of the interaction picture. If the system is on resonance, which means $|\omega_e| + \omega_o = 0$, H_1 in the interaction picture is

$$H_1^{int} = U_R^\dagger(t) H_1 U_R(t) \tag{7}$$

where

$$U_R(t) = \exp\left\{\frac{-iH_o t}{\hbar}\right\} = \exp\{-i\omega_o t \sigma_z\} \tag{8}$$

and σ_i corresponds to the i$^{\text{th}}$ Pauli matrix. The matrices $U_R(t)$ and $U_R^\dagger(t)$ rotate H_1 into the interaction picture. Applying these two rotation operators yields

$$H_1^{int} = \omega_1\{I_x + I_x\cos(2\omega_e) - I_y\sin(2\omega_e t)\} \tag{9}$$

The latter two terms in (9) can be neglected, since they involve a larger frequency scale, which will time average to zero during the course of the NMR experiment [5]. After applying H_1 for a time t, the density matrix in (4) evolves to

$$\rho_R(t) = U(t)U_R^\dagger(t)\rho_{th}U_R(t)U^\dagger(t) \tag{10}$$

with $U_R(t)$ defined in (8) and

$$U(t) = \exp\{\frac{-iH_1^{int}t}{\hbar}\} = \exp\{-i\omega_1 t\sigma_x\}$$

$U_R(t)$ and $U_R^\dagger(t)$ rotate the density matrix into the interaction picture, as they did for H_1. $U(t)$ and $U^\dagger(t)$ describe the time evolution with respect to H_1^{int}. Since the approximation for ρ_{th} given in (3) commutes with $U_R(t)$, $\rho_R(t)$ is simple to compute. For a so-called $\frac{\pi}{2}$ pulse, which is designed to tip the maximum magnetization into the xy-plane, $t^* = -\frac{\pi}{2\omega_o}$ and

$$\rho_R(t^*) = \frac{1}{2}\left(\mathbf{I} - \beta\hbar\omega_o\left[\cos^2(\frac{\pi}{2}\frac{\omega_1}{\omega_o})\sigma_z + \sin(\pi\frac{\omega_1}{\omega_o})\right]\right) \tag{11}$$

Transitioning back to the stationary frame, and neglecting terms that are second order in ω_1,

$$\rho(t^*) = \frac{1}{2}\left(\mathbf{I} - \beta\hbar\omega_o\left[\sigma_z - \pi\frac{\omega_1}{\omega_o}\sigma_y\right]\right) \tag{12}$$

After the $\frac{\pi}{2}$ pulse, H_1 is removed. The spin then precesses at the Larmor frequency, ω_o. The signal in NMR comes from the spin in the xy plane. At $t = t*$ the spin is along the y-axis so the spin in the xy-plane is

$$\langle I_y \rangle = \text{tr}[I_y\rho(t^*)] \tag{13}$$

which is proportional to $\beta\hbar\omega_1$. Since this value is much less than one, typical NMR signals are extremely weak. This is another major source of difficulty in NMR experiments.

Another representation of the interaction with the tranverse magnetic field in NMR is the absorption of radiation model. In this case, the average transition rate, W_{fi}, from initial state $|i\rangle$ to final state $|f\rangle$ is given by Fermi's golden rule [8],

$$W_{fi} = \frac{1}{T}\frac{1}{\hbar^2}\left|\int_{-T/2}^{T/2}\langle f|H_1(t')|i\rangle e^{\frac{i}{\hbar}(E_f-E_i)t'}dt'\right|^2 \tag{14}$$

where E_f and E_i are the corresponding energies. The integral over T is over a period of the potential, in order to accurately average the transition rate. subsituting (6) simplifies (14) to

$$W_{fi} = \frac{2\pi}{\hbar}\left|\langle f|H_1^{t.i}|i\rangle\right|^2 \delta(E_f - E_i - \hbar\omega_e) \tag{15}$$

where $H_1^{t.i}$ is time independent, and does not include the $\cos(\omega_e t)$ dependence. Therefore, a transition is allowed in NMR if

$$|\langle f|\omega_1 I_x|i\rangle| \neq 0 \tag{16}$$

and if the applied transverse field matches the energy difference between the two m_I levels. For NMR of non-interacting spin-1/2 nuclei, transitions are allowed if $\Delta m_I = \pm 1$.

After considering NMR from a general perspective, the dipolar coupling Hamiltonian and its effects on NMR will be examined.

III. THE DIPOLAR COUPLING HAMILTONIAN

Classically, the energy of the dipole-dipole interaction between two magnetic point dipoles $\vec{\mu}_1$ and $\vec{\mu}_2$ takes the form

$$E_{12} = \frac{\mu_o}{4\pi}\left(\frac{\vec{\mu}_1 \cdot \vec{\mu}_2}{r_{12}^3} - \frac{(\vec{\mu}_1 \cdot \vec{r}_{12})(\vec{\mu}_2 \cdot \vec{r}_{12})}{r_{12}^5}\right) \tag{17}$$

where $\vec{r}_{12}$ is the vector between dipole 1 and 2, and μ_o is the vacuum permeability [7]. In quantum mechanics, this interaction can be decomposed into the so-called alphabetic decomposition of the Hamiltonian. For simplicity, spin operators I_z and S_z are defined such that I_z acts on dipole 1, and S_z acts on dipole 2, with γ_1 and γ_2 as their respective gyromagnetic ratios.

$$H_d = d(A + B + C + D + E + F) \tag{18}$$

where

$$A = I_z S_z (1 - 3\cos^2(\theta))$$

$$B = -\frac{1}{4}(1 - 3\cos^2(\theta))(I_+ S_- + I_- S_+)$$

$$C = D^* = -\frac{3}{2}\sin(\theta)\cos(\theta)e^{-i\phi}(I_z S_+ + S_z I_+)$$

$$E + F^* = -\frac{3}{4}\sin^2(\theta)e^{-2i\phi}(I_+ S_+)$$

$$d = \frac{\mu_o \gamma_1 \gamma_2}{4\pi r_{12}^3} \tag{19}$$

where $I_\pm = I_x \pm I_y$ and the analog is true for the second spin [7]. Here, θ and ϕ refer to the polar and azimuthal angles of $\vec{r}_{12}$. A is a classically familiar term that describes the effect of a magnetic dipole interacting with a local field created by a neighboring dipole [7]. B is known colloquially as the "flip-flop" term and switches the spin for each nuclei, which means $\Delta M \equiv m_I + m_S = 0$ [5]. For the C and D terms $\Delta M = \pm 1$, and for terms E and F $\Delta M = \pm 2$.

IV. THE DIPOLAR INTERACTION AND DISTANCE DETERMINATION

In the solid state, when two nuclei are coupled via the dipolar coupling interaction, the initial NMR peaks are split into doublets. The energy difference between the two peaks in the doublet is directly related to the distance between the two nuclei in the sample. Using dipole-dipole interactions to determine internuclear distances is of particular interest for materials which are not crystalline but have short-range order such as glasses, proteins, and polymers [7]. Since information about the structure of such species is almost impossible to get via diffraction techniques, dipolar interactions in NMR can be used to probe the structure. One example of this is an NMR study that used dipolar couplings to determine relevant structures in a membrane-bound protein [9].

To describe this effect, the dipolar interaction can be treated to first order in perturbation theory. The first order dipolar splitting will be derived for two identical spins and for two different spins.

A. Two Non-Identical Spins

For two non-identical spins, the Hamiltonian is the same Hamiltonian as (18), with $\gamma_1 \neq \gamma_2$. For two spins with the same nuclei but different chemical environments, the γ parameter implicitly includes the chemical shielding parameter, $\sqrt{1 - \sigma}$. Using the basis,

$$|++\rangle = |1; +\rangle \otimes |2; +\rangle$$
$$|+-\rangle = |1; +\rangle \otimes |2; -\rangle$$
$$|-+\rangle = |1; -\rangle \otimes |2; +\rangle$$
$$|--\rangle = |1; -\rangle \otimes |2; -\rangle \tag{20}$$

where $|1; \pm\rangle$ represents the $\pm\frac{1}{2}$ eigenstate of I_z and $|2; \pm\rangle$ is the same for S_z, the Zeeman Hamiltonian is

$$H_Z = \frac{\hbar}{2}\begin{pmatrix} \omega_o^{(1)} + \omega_o^{(2)} & 0 & 0 & 0 \\ 0 & \omega_o^{(1)} - \omega_o^{(2)} & 0 & 0 \\ 0 & 0 & -\omega_o^{(1)} + \omega_o^{(2)} & 0 \\ 0 & 0 & 0 & -\omega_o^{(1)} - \omega_0^{(2)} \end{pmatrix} \tag{21}$$

with $\omega_o^{(1)}$ corresponding to the Larmor frequency of the first dipole, and $\omega_o^{(2)}$ the Larmor frequency of the second dipole. Since there are no degenerate states, only the on-diagonal terms of the dipolar Hamiltonian give a nonzero first order perturbation. This is only the A term. The first order dipolar perturbation is then [7],

$$H_d = \frac{d\hbar^2}{4}Y\begin{pmatrix} 1 & 0 & 0 & 0 \\ 0 & -1 & 0 & 0 \\ 0 & 0 & -1 & 0 \\ 0 & 0 & 0 & 1 \end{pmatrix} \tag{22}$$

where $Y = (1 - 3\cos^2(\theta))$. Allowed transitions among this manifold of states are those for which (15) holds. In the case of two spins, H_1 affects each spin. Therefore,

$$H_1 = -2B_1(\gamma_1 I_x + \gamma_2 S_x)\cos(\omega_e t) \tag{23}$$

Substituting (23) into (15) and neglecting constants yields

$$|\langle f| - \gamma_1 I_x - \gamma_2 S_x |i\rangle| \neq 0 \tag{24}$$

The allowed transitions and their energies are

$$|++\rangle \Leftrightarrow |+-\rangle \qquad E = -\hbar\omega_o^{(2)} - \frac{\hbar^2 d}{2}Y$$

$$|++\rangle \Leftrightarrow |-+\rangle \qquad E = -\hbar\omega_o^{(1)} - \frac{\hbar^2 d}{2}Y$$

$$|+-\rangle \Leftrightarrow |--\rangle \qquad E = -\hbar\omega_o^{(1)} + \frac{\hbar^2 d}{2}Y$$

$$|-+\rangle \Leftrightarrow |--\rangle \qquad E = -\hbar\omega_o^{(2)} + \frac{\hbar^2 d}{2}Y$$

This corresponds to two doublets, centered around $-\hbar\omega_o^{(1)}$ and $-\hbar\omega_o^{(2)}$, with a splitting of $\hbar^2 d$, thus allowing the distance between nuclei to be determined, as d is related to r_{12}, given by (19). Additionally, as the two correlated spins have the same energy splitting for their NMR peaks, the peak splitting can be used to determine which spins are near each other. One complication is the fact that the orientation with respect to the magnetic field does influence the splitting. This can be resolved by using a single crystal in a fixed orientation. However, for a number of the species being studied a single crystal is impractical if not impossible to make. In this case, a powder average will be present, as all possible values of θ are integrated. This results in broadening and a more complex pattern, but still can be used to determine internuclear distances [5].

B. Two Identical Spins

For two identical spin-1/2 particles, the dipolar Hamiltonian is (18), with $\gamma_1 = \gamma_2$. The Zeeman Hamiltonian in the basis given by (20) is

$$H_Z = \hbar\omega_o \begin{pmatrix} 1 & 0 & 0 & 0 \\ 0 & 0 & 0 & 0 \\ 0 & 0 & 0 & 0 \\ 0 & 0 & 0 & -1 \end{pmatrix} \tag{25}$$

This is slightly more complicated than the case with two different spins, as $E_{+-} = E_{-+}$. To treat this system to first order in perturbation theory, terms that introduce interactions between the $|+-\rangle$ and $|-+\rangle$ must also be included. The term from the alphabetic decomposition that inolves this interaction is the B term. The resulting first-order dipolar Hamiltonian is

$$H_D = \frac{d\hbar^2}{4}Y \begin{pmatrix} 1 & 0 & 0 & 0 \\ 0 & -1 & -1 & 0 \\ 0 & -1 & -1 & 0 \\ 0 & 0 & 0 & 1 \end{pmatrix} \tag{26}$$

Diagonalizing the sum of (25) and (26) gives

$$H_{Z+D} = \frac{d\hbar^2}{4}Y \begin{pmatrix} \hbar\omega_o + \frac{d\hbar^2}{4}Y & 0 & 0 & 0 \\ 0 & -\frac{d\hbar^2}{2}Y & 0 & 0 \\ 0 & 0 & 0 & 0 \\ 0 & 0 & 0 & -\hbar\omega_o + \frac{d\hbar^2}{4}Y \end{pmatrix} \tag{27}$$

The basis states in this representation are

$$|1\rangle = |1;+\rangle \otimes |2,+\rangle$$

$$|2\rangle = \frac{1}{\sqrt{2}}(|1;+\rangle \otimes |2;-\rangle + |1;-\rangle \otimes |2;+\rangle)$$

$$|3\rangle = \frac{1}{\sqrt{2}}(|1;+\rangle \otimes |2;-\rangle - |1;-\rangle \otimes |2;+\rangle)$$

$$|4\rangle = |1;-\rangle \otimes |2;-\rangle \tag{28}$$

The basis in (28) has a triplet manifold of states ($|1\rangle$, $|2\rangle$, and $|4\rangle$) and a singlet state ($|3\rangle$). For this reason, the problem is treated as that for a spin-1 particle, as the singlet state does not interact with the magnetic field [7]. Allowed transitions are those for which the transition rate is nonzero, given by (24). Since $\gamma_1 = \gamma_2$, allowed transitions occur only for states for which

$$|\langle f| I_x + S_x |i\rangle| \neq 0 \tag{29}$$

The allowed transitions and corresponding energies are

$$|1\rangle \Leftrightarrow |2\rangle \qquad E_{12} = -\left(\frac{3d\hbar^2}{4}Y + \hbar\omega_o\right)$$

$$|2\rangle \Leftrightarrow |4\rangle \qquad E_{24} = -\hbar\omega_o + \frac{3d\hbar^2}{4}Y$$

This yields a doublet centered at the Zeeman splitting energy of $-\hbar\omega_o$ and split by $\frac{3d\hbar^2}{2}Y$, which is again related to the internuclear distance. This again has the dependence on θ, addressed previously.

V. DIPOLE-DIPOLE EFFECTS IN DOUBLE RESONANCE

In a liquid sample, the molecules are free to translate and rotate. H_1 must then be treated as a time-dependent perturbation to the spin system, as r, θ, and ϕ are implicitly functions of time due to molecular motion [10]. For a time-dependent perturbation to the Zeeman Hamiltonian, (14) can be used to calculate transition rates. From these transition rates, first order kinetics can be used to model decoherence and spin population transfer [10]. This population transfer occurs without applying any transverse magnetic field, differing from the solid-state case. One note is that this treatment does not consider the energy splitting due to dipolar coupling from the A term, which broadens the peaks.

A. Transition Rates

The effects of terms B through F from the dipolar coupling Hamiltonian will now be described. For a set of two different spins, these terms induce transitions between spin states. They are collected into a transition Hamiltonian matrix in (30), which only includes off-diagonal elements, in the same basis given in (20).

$$H_{dd}^{trans} = \begin{pmatrix} 0 & w_1 & w_1' & w_2 \\ w_1^* & 0 & w_0 & w_1 \\ w_1'^* & w_0 & 0 & w_1' \\ w_2^* & w_1^* & w_1'^* & 0 \end{pmatrix} \tag{30}$$

where

$$w_0 = -\hbar^2 d\frac{1}{4}(1 - 3\cos^2(\theta))$$

$$w_1 = w_1' = -\hbar^2 d\frac{3}{4}\sin(\theta)\cos(\theta)e^{-i\phi}$$

$$w_2 = -\hbar^2 d\frac{3}{4}\sin^2(\theta)e^{-2i\phi}$$

These transitions are also shown in fig. 1. (14) can be
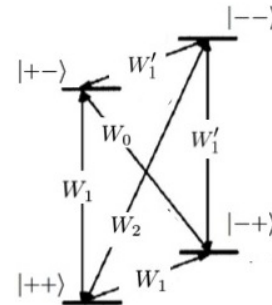
FIG. 1: Energy levels and transition rates for the dipole-dipole coupling Hamiltonian perturbation. Adapted from [11]

used to calculate the transition rates, substituting the implicitly time-dependent Hamiltonian of (18) for H_1. To

complete this calculation, the physics of random molecular motion is necessary, which is beyond the scope of this paper. Interested readers can consult [10] for the full derivation. After performing the necessary calculations, the resulting transition rates are

$$W_0 = \frac{\hbar^2 d^2}{10} \tau_c J(\omega_I - \omega_S)$$

$$W_1 = \frac{3\hbar^2 d^2}{20} \tau_c J(\omega_I)$$

$$W_1' = \frac{3\hbar^2 d^2}{20} \tau_c J(\omega_S)$$

$$W_2 = \frac{3\hbar^2 d^2}{5} \tau_c J(\omega_I + \omega_S) \qquad (31)$$

where τ_c is the correlation time, which is describes the rotational time scale, and $J(\omega_x) = (1 + \tau_c^2 \omega_x^2)^{-1}$ is the correlation function. W_0 corresponds to the transition probability of flipping both spins such that $\Delta M = 0$, resulting from the B term in (19). Similarly W_1 and W_1' correspond to $\Delta M = \pm 1$, from the C and D terms and W_2 to $\Delta M = \pm 2$ from the E and F terms in (19). These equations simplify greatly in the regime in which $\tau_c \omega_x \ll 1$, where molecules rotate quickly compared to their Larmor frequencies, as $J(\omega_x) \approx 1$. Assuming this approximation is valid, (31) simplifies to

$$W_0 = \frac{\hbar^2 d^2}{10} \tau_c$$

$$W_1 = W_1' = \frac{3\hbar^2 d^2}{20} \tau_c$$

$$W_2 = \frac{3\hbar^2 d^2}{5} \tau_c \qquad (32)$$

Included implicitly in (31) and (32) is the time average over the distance between dipoles, because $\langle d^2 \rangle \propto \langle \frac{1}{r^6} \rangle$.

The transition rates for all first-order transitions have now been determined. This information can now be used to derive the rates of longitudinal decoherence.

B.   Population Kinetics and the Overhauser Effect

Using the rates derived in the previous section, spin relaxation processes along the z-axis can be determined. This can then be used to describe the Overhauser effect. The subsequent derivation is simplified by defining

$$k = \frac{(\hbar d)^2}{20} \tau_c \qquad (33)$$

This simplifies (32) to

$$W_0 = 2k$$
$$W_1 = W_1' = 3k$$
$$W_2 = 12k \qquad (34)$$

The relaxation is derivated assuming first order kinetics for the populations, which means that for a given transition the rate of change is proportional to the initial state population. Analyzing the spin states by taking into account decreases in populations due to transitions to all other states, and increases in population due to transitions from all other states yields

$$\frac{dN_{++}}{dt} = -(3k + 3k + 12k)N_{++} + 3k(N_{+-} + N_{-+} + 12kN_{--}) + c_{++}$$

$$\frac{dN_{+-}}{dt} = -(3k + 3k + 2k)N_{+-} + 3k(N_{--} + N_{++}) + 2k(N_{-+}) + c_{+-}$$

$$\frac{dN_{-+}}{dt} = -(3k + 3k + 2k)N_{-+} + 3k(N_{--} + N_{++}) + 2k(N_{+-}) + c_{-+}$$

$$\frac{dN_{--}}{dt} = -(3k + 3k + 12k)N_{--} + 3k(N_{+-} + N_{-+} + 12kN_{++}) + c_{--}$$

$$(35)$$

where the various N represent the population of a given state. The average longitudinal spin for each dipole is

The spin population of the first dipole and the population of the second dipole can be evaluated independently, as the Larmor frequencies for the two spins are different. The average spin component for each dipole can be described as

$$\langle I_z \rangle = \frac{\hbar}{2} [N_{++} + N_{+-} - N_{-+} - N_{--}]$$

$$\langle S_z \rangle = \frac{\hbar}{2} [N_{++} + N_{-+} - N_{+-} - N_{--}] \qquad (36)$$

Differentiating (36) with respect to time, and substituting (35) gives

$$\left\langle \frac{dI_z}{dt} \right\rangle = -20k\langle I_z \rangle - 10k\langle S_z \rangle + c$$

$$\left\langle \frac{dS_z}{dt} \right\rangle = -20k\langle S_z \rangle - 10k\langle I_z \rangle + c \qquad (37)$$

Noting that the constants in (35) reflect the final, thermalized state of the system, (37) becomes

$$\left\langle \frac{dI_z}{dt} \right\rangle = -20k \left(\langle I_z \rangle - \langle I_z^{th} \rangle \right) - 10k \left(\langle S_z \rangle - \langle S_z^{th} \rangle \right)$$

$$\left\langle \frac{dS_z}{dt} \right\rangle = -20k \left(\langle S_z \rangle - \langle S_z^{th} \rangle \right) - 10k \left(\langle I_z \rangle - \langle I_z^{th} \rangle \right)$$

$$(38)$$

where $\langle I_z^{th} \rangle$ and $\langle S_z^{th} \rangle$ represent the average longitudinal spin of the thermal states for dipole 1 and dipole 2. Note that the decay of these spins is a biexponential decay, not a simple exponential decay as is assumed in Bloch's equations.

One limit to consider is the homonuclear case, where the two dipoles are the same. In this case, it is impossible to measure $\langle I_z \rangle$ and $\langle S_z \rangle$ separately, as both have the same Larmor frequency. Only the sum can be measured.

$$\left\langle \frac{dI_z}{dt} + \frac{dS_z}{dt} \right\rangle = -30k \left(\langle I_z + S_z \rangle - \langle I_z^{th} \rangle - \langle S_z^{th} \rangle \right) \quad (39)$$

This recovers the standard exponential decay of the magnetization, as described in Bloch's equations [7]. The

parameter T_1 measures the exponential decay of the longitudinal magnetization. In this situation

$$T_1 = \frac{1}{30k}$$

A second limit to consider is that of a nucleus coupling to an electron. Electrons can relax via a number of pathways in addition to dipolar coupling, at a much faster rate than nuclei [7]. Since this is the case, it is assumed that the electron spin, defined here to be S_Z is at its thermal state, $\langle S_z^{th} \rangle$. In this case, (38) simplifies to

$$\left\langle \frac{dI_z}{dt} \right\rangle = -20k(\langle I_z \rangle - \langle I_z^{th} \rangle)$$
$$\left\langle \frac{dS_z}{dt} \right\rangle = 0 \tag{40}$$

Again, a simple exponential decay is recovered. However, in this situation

$$T_1 = \frac{1}{20k}$$

The derived rates of population change will now be used to explain the steady-state Overhauser effect. The first step to observe the Overhauser effect is to apply an oscillating radiofrequency field to saturate one of the spins, S_z in this case, such that the populations of the $|2; +\rangle$ and $|2; -\rangle$ states are equal [12]. This means that $\langle S_z \rangle = 0$ [12]. Substituting this into (38) and recognizing that at steady state the change in populations are 0 results in,

$$0 = -20k(\langle I_z \rangle - \langle I_z^{th} \rangle) + 10k \langle S_z^{th} \rangle \tag{41}$$

Solving for $\langle I_z \rangle$ gives

$$\langle I_z \rangle = \langle I_z^{th} \rangle + \frac{1}{2} \langle S_z^{th} \rangle \tag{42}$$

Since, at the steady state, without polarization transfer, $\langle I_z \rangle = \langle I_z^{th} \rangle$, a fractional polarization enhancement of I due to S is defined as

$$f_I[S] = \frac{\langle I_z \rangle - \langle I_z^{th} \rangle}{\langle I_z^{th} \rangle} \tag{43}$$

Since $\langle I_z^{th} \rangle$ and $\langle S_z^{th} \rangle$ can be approximated using (5) (implicitly including the chemical shielding term in γ), the relationship between the two expectation values is

$$\langle I_z^{th} \rangle = \frac{\gamma_1}{\gamma_2} \langle S_z^{th} \rangle \tag{44}$$

. Substituting (44) into (43) yields

$$f_I[S] = \frac{1}{2} \frac{\gamma_2}{\gamma_1} \tag{45}$$

The fractional enhancement can be very large depending on the ratio between the gamma values. One technique that takes of advantage of the Overhauser effect

is cross-polarization from protons to carbon-13 nuclei. Carbon-13 NMR, if the sample has not been enriched, suffers from the limited elemental abundance of carbon-13 [11]. To increase intensity, spin from the protons is transferred to carbon-13 nuclei via an Overhauser effect. The theoretical limit is approximately a two-fold increase in polarization, corresponding to a four-fold increase in signal intensity [11]. Another technique that applies the Overhauser effect is 2D Nuclear Overhauser Effect Spectroscopy (NOESY). In NOESY, transfer of polarization from one nuclei to another via dipolar interactions is used to determine the proximity of the nuclei to each other. This is useful in elucidating structural information from very complicated systems, such as proteins [1].

VI. CONCLUSION

One major difficulty with using NMR for structure determination is its small signals, attributable to the very small energy splitting between m_I states in the nuclei. It is cleary shown in section II in the density matrix formulation of NMR that the component of the spin in the xy-plane, which is what NMR measures, depends linearly on $\beta\hbar\omega_1$, which is much less than one. This indicates that the xy-plane component of the spin is quite small, highlighting this difficulty. An additional issue is the small range of chemical shfits, resulting in overlapping peaks.

The dipolar coupling Hamiltonian can be used to ameliorate both of these issues, as well as to provide new information. In the solid state, the dipolar coupling Hamiltonian is time-independent. Treating this Hamiltonian as a perturbation to first order in time-independent perturbation theory yields information about internuclear distances, as shown in section IV.

Dipolar interactions in liquids are time-dependent, as the molecules in solution are free to rotate and translate. For this reason, the dipolar coupling Hamiltonian induces transitions between states. Using Fermi's Golden Rule, the transition rates can be derived. From these rates, using first order kinetic arguments, the change in the longitudinal spin is examined. It is shown that dipolar interactions in liquids can be tailored in order to maximize polarization transfer between two spin species, via the Overhauser effect. This solves the problem of small signals in NMR. 2D spectroscopy techniques, such as NOESY, take advantage of the Overhauser effect to help determine which peaks correspond to close nuclei, increasing the information from the spectrum and partially resolving the problem of overlapping chemical peaks. Dipolar interactions serve as very welcome perturbation in NMR, as they have significant uses in structure determination.

[1] J. Fiaux, E. Bertelsen, A. Horwich,and K. Wüthrich, Nature **418**, 207 (2002).

[2] T. Nakano and T. Yada. J. Am. Chem. Soc. **125**, 50, (2003).

[3] A. Overhauser, Phys. Rev. **89**, 689 (1953).

[4] R. Ernst, G. Bodenhausen and A. Wokaun *Principles of Nuclear Magnetic Resonance in One and Two Dimensions*, (Clarendon, 1987).

[5] A. Abragam *The Principles of Nuclear Magnetism*, 1st ed. (Clarendon, 1961).

[6] A. Harrow. 8.06 Course Notes, (2014).

[7] J. Hennel and J. Klinowski *Fundamentals of Nuclear Magnetic Resonance*, 1st ed. (Longman, 1993).

[8] R. Shankar *Principles of Quantum Mechanics*, 2nd ed. (Springer, 1994).

[9] F. Castellani, B. van Rossum, A. Diehl, M. Schubert, K. Rehbein, and H. Oschkinat, Nature **420**, 98 (2002).

[10] I. Solomon, Phys. Rev. **99**, 559 (1955).

[11] T. Maly, G. Debelouchina, V. Bajaj, K. Hu, C. Joo, M. Mak-Jurkauskas, J. Sirigiri, P. van der Wel, J. Herzfeld, R. Temkin, and R. Griffin, J. Chem. Phys. **128**, 052211 (2008)

[12] D. Neuhaus, "The Nuclear Overhauser Effect" *Encyclopedia of Magnetic Resonance*, (Wiley, 1996).

Squeezed Light: Two Photon Coherent States

Nicolas M. Brown

Center for 8.06 Physics, 77 Massachusetts Ave., Cambridge, MA 02139-4307

(Dated: May 2, 2014)

I. INTRODUCTION

Coherent light one photon formulation, in the focus of optics and the statistics of the fields, has been in the literature since Glauber's paper *Coherent and Incoherent states of the Radiation Field* [1] in 1963. By 1963, Quantum electrodynamic theory [QED] had been developed but its usefulness absent to physicists who dealt with optics. This is due to QED's inherent limitation in describing many stationary states of the field (photon states) to only a few before computations become prohibitively difficult. Glauber describes an approach using a basis which "arises in a natural way in the discussion of correlation and coherence properties of fields." [1] Glauber calls these states coherent states whose formulation has become invaluable to the experimental physics and the electrical engineering communities in recent decades in a regimen where one must worry about approaching the quantum mechanical limit.

In 1976, Yuen, an electrical engineer at the Massachusetts Institute of Technology, published a paper [2] describing two photon coherent states and how their counting statistics could be shown to display characteristics of the one photon states that we now call squeezed states. The paper was not highly appreciated until Caves published his formalism [3][4] for two photon quantum optics. We will proceed to entertain this formalization in Sec. III.

II. SINGLE PHOTON COHERENT AND SQUEEZED LIGHT

Here I present a overview of single photon coherent and squeezed light formulation.

A. Coherent Light

The traditional approach to describing the electromagnetic radiation field is to treat the field as a continuous distribution of harmonic oscillators with different frequencies ω. Each ω we will call a particular mode of the electromagnetic field. To get a description of the field you then integrate over the frequency bandwidth you are interested in.[3] We then write the mode of the electric field as

$$E(t) = x\cos(wt) + p\sin(wt) \qquad (1)$$

keeping with the convention used by Teich [5]. Teich uses units where $\hbar=1$, but we will keep explicit our $\hbar$.
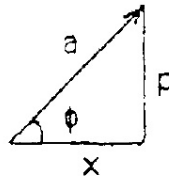
FIG. 1: Polar and quadrature-component representations of the electric field for monochromatic classical light. Figure from Teich [5]
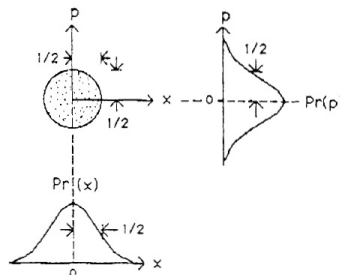
FIG. 2: Quadrature-component uncertainties for the vacuum state. Figure from Teich [5].

We discussed in 8.05 [6] that the ground state of the harmonic oscillator, which we will treat as the vacuum state of the electromagnetic field for a particular mode ω, satisfies the lower bound of the Heisenberg uncertainty relation. It therefore has expectation value 0 for both quadratures x and p, i.e.:

$$\langle x \rangle = 0, \ \ \langle p \rangle = 0, \ \ \sigma_x \sigma_p = \frac{\hbar}{2} \qquad (2)$$

These equations imply that the electromagnetic vacuum field is inherently noisy; because the vacuum state has nonzero energy, there are fluctuations in σ_x and σ_p. By equation 1, $E(t)$ is therefore also noisy. We call x and p quadrature components because they differ by 90 degrees.

We can analyse this noise in the polar representation of our uncertainties: the photon-number and phase representation. In the ground state we have

$$\langle n \rangle = 0, \ \ \langle \phi \rangle = undef, \ \ \sigma_n \sigma_\phi = \hbar \qquad (3)$$

We can construct excited states by attaching them to a phasor with amplitude $|\alpha| = \sqrt{\langle n \rangle}$ and phase e^{-iwt}.

When in a excited coherent state it is important to notice that the uncertainties are time independent and independent of uncertainties at different frequencies.

B. Squeezed Light

There are two types of squeezed light that I will address: quadrature-squeezed and photon-number-
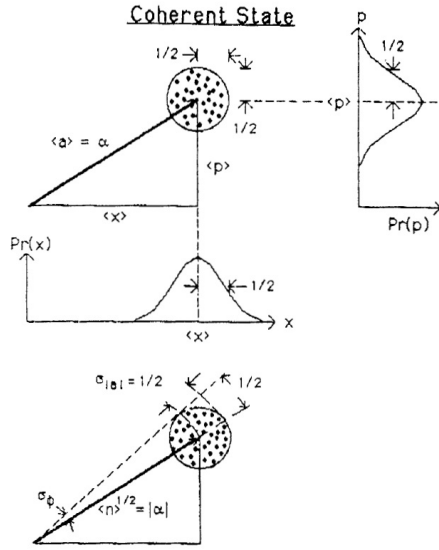
FIG. 3: Quadrature-component and number-pase uncertainties for the coherent state. Figure from Teich [5].

FIG. 4: (a) Quadrature squeezed state. (b)Right: partially squeezed photon-number-squeezed state; Left: fully squeezed photon-number-squeezed state.

squeezed.

A quadrature-squeezed state is when one of the quadratures has an uncertainty that is less than $\sqrt{\hbar/2}$. We can 'squeeze' one quadrature at the expense of the other, thereby still satisfying the uncertainty principle but perhaps giving us experimental advantages.

A photon-number-squeezed state is when σ_n is below $\sqrt{\hbar}$, the photon-number uncertainty in the coherent state. Squeezing the photon-number means that the associated uncertainty in phase must increase. Photon-number-squeezed light is sometimes called amplitude squeezed light and when the phase uncertainty wraps around the whole graph, as on the right side of (b), the state is called a number state because $\sigma_n = 0$ and $\sigma_\phi = \infty$.[5] (Not to be confused with the excited levels of the harmonic oscillator.)

C.   Examples of states of light

Now imagine we are able to alter the two quadrature components of E(t), we will see some methods that do so in Sec. IV. We then affect a change: $E_s(t) = xe^{-\gamma}e^{i\zeta}\cos(wt) + pe^{\gamma}\sin(wt)$, where γ is the squeezing parameter.[5] γ is similar to γ in [6] but it is not defined according to two different harmonic oscillator potentials. Here γ is a given parameter, which depends on the non-linear elements in the system that provide squeezed light. (See references [7] [8]) Our $e^{i\zeta}$ is only present for convenience. It allows us to affect a change $e^{-\gamma}\sigma_x$ and $e^{\gamma}\sigma_p$ in the uncertainties of x and p, effectively 'squeezing' them. See figures 5 and 6 for illustrations.

We must be careful as the statistics of our vacuum state have changed[5]:

$$\langle n \rangle = \sinh^2(r) > 0 \tag{4}$$
$$\sigma_n^2 = 2\hbar(\langle n \rangle + \langle n \rangle^2) \tag{5}$$

Our state no longer has zero average photon number and its variance is no longer Poisson.

The coherent state changes accordingly. [5]

$$\langle n \rangle = |\alpha|^2 + \sinh^2(r) \tag{6}$$

If we look at figure 6 we expect that σ_n will be largest when θ is integer multiples of π and it will be smallest when θ equals odd integer multiples of $\pi/2$. Where θ is the angle between the major axis of the squeezing ellipse and the phasor, α. We can change θ by changing ζ relative to $\angle\alpha$.[5] The expression when $|\alpha|^2 \gg e^{2\gamma}$ is:

$$\sigma_n^2 = \langle n \rangle (e^{2\gamma}\cos^2(\theta) + e^{-2\gamma}\sin^2(\theta) \tag{7}$$

See figure 7 for a plot of the magnitude of σ_n^2 when θ is varied for a given γ.

Now let's turn to a concrete example taken from Teich [5]. Assume you have a 50/50 beamsplitter and you input coherent light on one end and leave the other input port open. We can model this system as the unused open port inputing a vacuum state which is combined with a coherent state from an ideal gas laser. Since the two states are uncorrelated their means and variances add. The beamsplitter has a transmission coefficient $T = 1/2$
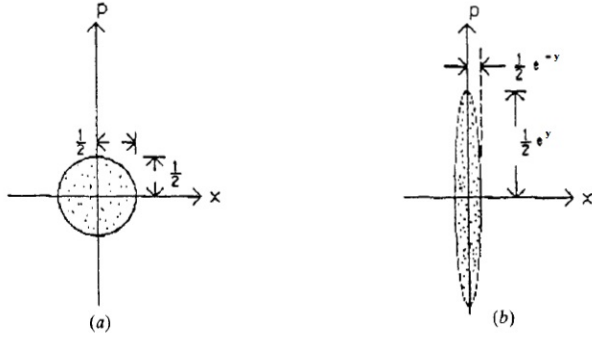
FIG. 5: Comparison of quadrature-component uncertainties for the vacuum and squeezed vacuum states: (a) vacuum state, (b) squeezed vacuum state. Figure from Teich, [5].

FIG. 7: Dependence of the squeezed coherent state photon-number variance, σ_n^2, on the angle θ. The light is super- or sub-Poisson depending on θ. Figure from Teich, [5].

reduced because of losses to the other open output port the beamsplitter.

Now let us imagine we squeeze the input vacuum state somehow. (See Sec. IV) Our vacuum state now has $\langle x_v \rangle = \langle p_v \rangle = 0$ and $\sigma_{xv}^2 = \hbar e^{-2\gamma}/2$, $\sigma_{pv} = \hbar e^{2\gamma}/2$ so we get

$$\langle x \rangle = \langle x_c \rangle / \sqrt{2} \tag{16}$$

$$\langle p \rangle = \langle p_c \rangle / \sqrt{2} \tag{17}$$

$$\sigma_x^2 = \frac{\hbar}{4}(1 + e^{-2\gamma}) \tag{18}$$

$$\sigma_p^2 = \frac{\hbar}{4}(1 + e^{2\gamma}) \tag{19}$$

In the end, we have squeezed light whose mean is the same as the unsqueezed case. This has been illustrated in Figure 8.

An interesting thought experiment is to change t to a larger value. We then have an output amplitude of $A = \sqrt{T}a_v + \sqrt{1-T}a_c$. As T increases, the amount of squeezing picked up by our coherent state increases at the expense of a decrease in α; to get a coherent state squeezed as much as our squeezed vacuum state would require an arbitrarily large a_c.

FIG. 6: Comparison of quadrature-component uncertainties for the coherent and squeezed coherent states: (a) coherent state, (b) squeezed coherent state. Figure from Teich, [5].

and transmittance $t = 1/\sqrt{2}$ so we get the following.

$$\langle x \rangle = \langle x_c \rangle t + \langle x_v \rangle t \tag{8}$$

$$\langle p \rangle = \langle p_c \rangle t + \langle p_v \rangle t \tag{9}$$

$$\sigma_x^2 = \sigma_{xc}^2 T + \sigma_{xv} T \tag{10}$$

$$\sigma_p^2 = \sigma_{pc}^2 T + \sigma_{pv}^2 T \tag{11}$$

Where the subscripts c and v stand for coherent and vacuum states. For the regular vacuum state, whose $\langle x_v \rangle, \langle p_v \rangle = 0$ and $\sigma_{xv}, \sigma_{pv} = \sqrt{\hbar/2}$, we get

$$\langle x \rangle = \langle x_c \rangle / \sqrt{2} \tag{12}$$

$$\langle p \rangle = \langle p_c \rangle / \sqrt{2} \tag{13}$$

$$\sigma_x^2 = \sqrt{\frac{\hbar}{2}} \tag{14}$$

$$\sigma_p^2 = \sqrt{\frac{\hbar}{2}} \tag{15}$$

So for unsqueezed vacuum input into the unused port we get coherent light of reduced mean. The mean is

III. TWO PHOTON FORMULATION

Here I present the traditional two photon formulation as discussed by Caves. [3]

We denote the annihilation operators for the two modes as a_+ and a_- which satisfy the commutation relations.

$$[a_+, a_-] = [a_+, a_-^\dagger] = 0 \tag{20}$$

$$[a_+, a_+^\dagger] = [a_-, a_-^\dagger] = 1 \tag{21}$$

The free Hamiltonian is

$$H_o = (\Omega + \epsilon)a_+^\dagger a_+ + (\Omega - \epsilon)a_-^\dagger a_- \tag{22}$$
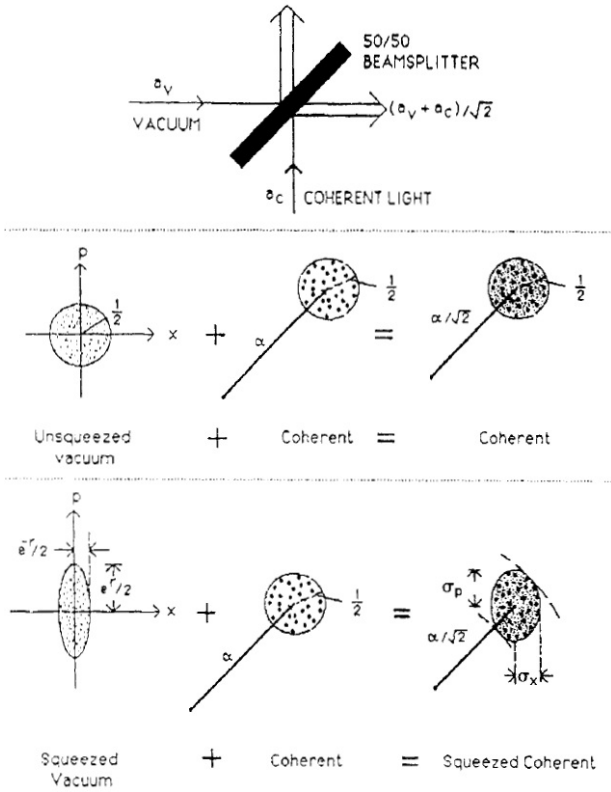
FIG. 8: Quadrature-component uncertainties for the superposition of a coherent field with unsqueezed and squeezed vacuum fields at a 50/50 beamsplitter. Figure from Teich, [5].

We can create our two-mode coherent states by displacing each mode using our two-mode displacement operator, a combination of two one-mode displacement operators from 8.05.

$$D(a_+, \alpha_+)D(a_-, \alpha_-) = e^{(\alpha_+ a_+^\dagger - \alpha_+^\star a_+ + \alpha_- a_-^\dagger - \alpha_-^\star a_-)}$$
$$(23)$$

Here I have adapted somewhat the notation of Caves, instead of using $\mu_\pm$ I am using α for the eigenvalue as we did in 8.05.

To introduce the two-mode squeezing operator S we will consider the Hamiltonian for an ideal two photon process

$$H = H_o + i\kappa(t)[a_+ a_- e^{-2i(\phi - \Omega t)} - a_+^\dagger a_-^\dagger e^{2i(\phi - \Omega t)}] \quad (24)$$

Where κ is any real time dependent function. The interaction part, given by the operators, creates or destroys a pair of photons in the two modes we are considering, and never only one. The unitary time evolution operator for eq. 24 is

$$U(t,0) = e^{-iH_o t}S(\zeta, \phi) = S(\zeta, \phi - \Omega t)e^{-iH_o t} \quad (25)$$

where

$$\zeta \equiv \int_0^t \kappa(t')dt' \quad (26)$$

$$S(r, \phi) \equiv exp[\gamma(a_+ a_- e^{-2i\phi} - a_+^\dagger a_-^\dagger e^{2i\phi})] \quad (27)$$

Where γ is the squeeze factor introduced in 8.05. A key feature of S is that

$$S(\gamma, \phi)a_\pm S^\dagger(\gamma, \phi) = cosh(r)a_\pm + a_\mp^\dagger e^{2i\phi}sinh(r) \quad (28)$$

The two photon formulation can readily be ported to our single photon formulation if you consider the sum of the two photons to act as one (see figure 9), but the formulation is still important to understanding two photon devices. Two photon devices in general create two photons at different frequencies but ones that are nevertheless correlated. This is an indicator that we must in part abandon the one photon picture because it relies on the independence of the modes of the electric field from each other.
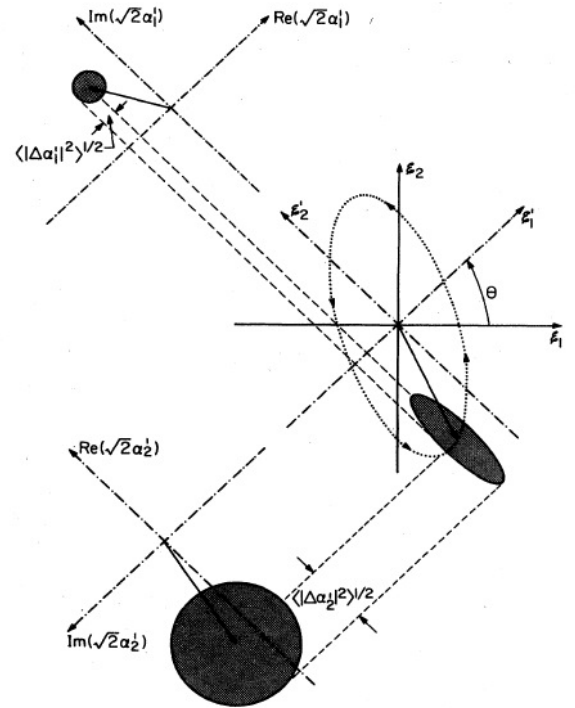
FIG. 9: Combination of the two photon modes. From Caves. [3]

IV.   METHODS OF PRODUCING SQUEEZED LIGHT

Coherent light is the light emitted from an ideal one photon laser while squeezed light usually is from two-photon processes. The mathematical descriptions of the

two photon processes that create squeezed light require a inherent non-linearity between, usually, two modes of the electric field and for this reason it will be too involved for analysis in this paper. Those interested can read the general literature on quantum optics. (See [7] [8]) I will proceed to present two typical systems that create squeezed light: one type of crystal squeezing and ponderomotive squeezing.

Crystal squeezing is a type of squeezing where you pass high intensity light through a nonlinear medium in a cavity to create a coupling between two quadratures. One method is parametric down conversion. This method takes light from one mode Ω and converts it into two correlated modes usually centred around $\omega_c = \Omega/2$. Giving:

$$\omega_{new} = \omega_c \pm \epsilon \qquad (29)$$

Where $\epsilon \ll \omega_c$. These two new modes are created in a squeezed state due to actions of the nonlinear element. [9]

Ponderomotive squeezing is where one uses a spring to couple two quadratures together. Normally an optical spring is used versus a mechanical one due to its high resonant frequency and decreased susceptibility to introduce thermal noise into the spectrum, which would swamp the squeezing. To create an optical spring, one operates a cavity with dynamic mirrors on the side of a resonance. By changing the mirrors, the intra-cavity power, and therefore force from radiation pressure, changes approximately linearly in position. Just like a spring. Because the test mass motion creates a phase shift of the reflected light dependent on the intensity fluctuations we have a coupling between radiation pressure and phase. This coupling is used to squeeze the radiation pressure noise versus phase noise. [15]

V. APPLICATIONS OF SQUEEZED LIGHT

Possible applications of quadrature-squeezed and photon-number-squeezed light include areas of spectroscopy, interferometry[16], precision measurement, and communications [10][11][12].

A particular case of squeezing in interferometry is the Laser Interferometer Gravitational-wave Observatory [LIGO]. LIGO is a large observatory that measures the positions of end mirrors on a interferometer very precisely. They are attempting to detect passing fluctuations of space caused by gravity waves. In many parts of the noise spectrum they are dominated by quantum limits and squeezed state injection is one way they hope to increase their sensitivity.

Squeezed vacuum state is injected into an unused port of the beamsplitter. This reduces noise in one quadrature at the expense of additional noise in the orthogonal quadrature. The squeeze angle, the orientation of the major axis of the squeezing ellipse, is rotated at the input to adjust for differences in the interferometer over time, such as temperature fluctuations, that change the squeeze angle.[13] For LIGO the interested quadratures are the phase and amplitude (number) quadratures. The phase is inherently responsible for shot noise while the amplitude quadrature is inherently connected to radiation pressure noise. Radiation pressure noise taints the measurement of the end mirror positions. At low frequencies (e.g. 100Hz for LIGO) the noise attributed to radiation pressure dominates while at higher frequencies the shot noise dominates. Squeezing seems tobe a promising adaptation to the system to increase sensitivity. There are many other ways that LIGO reduces their quantum limited measurements, such as using power recycling cavities, but inputting squeezed vacuum has been studied vigorously over the past couple of years and will be implemented in the next upgrades to the observatory under the AdvancedLIGO project, a testament to its viability.

VI. CONCLUSION

We have seen that fluctuations in each mode of the electric field are independent of each other and that two photon processes, in general, do not follow this rule. We then discussed a new formulation that can explain these phenomenon and in some cases can be simplified to the one photon characterization. This two photon representation was provided by Caves.

There are many methods of producing squeezed light, each having different effects in different regimes, and having an even more variety of applications. It is important to understand these standard quantum mechanical limitations to measuring accurately the electric field and its implications for increasing precision in experiments.

[1] R. J. Glauber, Phys. Rev. **131**, 2766 (1963), URL http://link.aps.org/doi/10.1103/PhysRev.131.2766.
[2] H. P. Yuen, Physical Review A **13**, 2226 (1976).
[3] C. M. Caves and B. L. Schumaker, Physical Review A **31**, 3068 (1985).
[4] B. L. Schumaker and C. M. Caves, Physical Review A **31**, 3093 (1985).
[5] M. C. Teich and B. E. Saleh, Quantum Optics: Journal of the European Optical Society Part B **1**, 153 (1989).
[6] B. Zwiebach, *8.05 notes ch.5*.
[7] D. F. Walls and G. J. Milburn, *Quantum optics* (Springer, 2007).
[8] M. O. Scully, *Quantum optics* (Cambridge university press, 1997).
[9] J. L. H. Ling-An Wu, H. J. Kimble, Physical Review Letters **57**, 2520 (1986).

[10] H. P. Yuen and J. H. Shapiro, Information Theory, IEEE Transactions on **24**, 657 (1978).

[11] J. H. Shapiro, H. P. Yuen, and A. Mata, Information Theory, IEEE Transactions on **25**, 179 (1979).

[12] H. P. Yuen and J. H. Shapiro, Information Theory, IEEE Transactions on **26**, 78 (1980).

[13] T. Corbitt and N. Mavalvala, Journal of Optics B: Quantum and Semiclassical Optics **6**, S675 (2004).

[14] C. M. Caves, Physical Review D **23**, 1693 (1981).

[15] Information taken from talk slides by Thomas Corbitt (Louisiana State University) and posters by the LIGO group.

[16] LIGO is a prime example. See [13] [14]

Quantum Noise and Error Correction

Daniel Bulhosa

Massachusetts Institute of Technology, 77 Massachusetts Ave., Cambridge, MA 02139-4307

(Dated: May 9, 2014)

We present a formalism for describing quantum noise and quantifying its effects. We introduce classical linear error correction, and present a procedure for using classical codes to create quantum error correction codes. In particular we discussed the codes developed by Calderbank, Shor, and Steane.

I. INTRODUCTION

Over the last two decades quantum computation has become a research field of high interest. Following Shor's publication of a quantum algorithm capable of factoring large prime numbers in polynomial time, it became understood that the quantum effects of superposition and interference could be exploited to carry out certain calculations exponentially faster than conventional computers.

One of the challenges when dealing with any kind of signal is the introduction of noise. In the last century effective error correcting techniques have been developed in order to alleviate this issue in classical systems. After Shor's publication, one of the biggest problems facing the prospect of practical quantum computation was quantum noise. Due to the seeming complexity of this kind of noise it was initially thought that no protocols could be developed to remedy it. Further research showed that this noise admitted a simple description, and thus error correcting techniques could be developed to handle quantum noise. In this paper we introduce the idea of quantum noise, different measures of the fidelity of quantum information after being corrupted, and introduce a formalism for deriving quantum error correction codes from classical ones.

II. CLASSICAL LINEAR CODING AND ERROR CORRECTION

Suppose we have a classical bit 0, and we wish to transmit it over some signal line. Furthermore, suppose that there is some probability p that an error will occur and this bit will be flipped to 1. We would like to come up with a scheme that reduces this error.

Consider the following proposition. Rather than sending a single bit we send three bits, two of them containing redundant information. So, for example, rather than sending 0 we would send 000. If the string contains no errors the receiver leaves the string as is, and if one of the bits differs from the others the receiver assumes the value of the remaining two was the intended message and corrects the error by flipping the erroneous bit. Assuming that the errors on different bits occur independently of each other and with sufficiently small probability this scheme is sensible, since it is much more likely that no error or a single error would occur in the bit string rather than two or three.

Given that this is our protocol for transmitting information, the receiver will only receive the wrong message when two or three bits are flipped. This occurs with probability:

$$\binom{3}{2}p^2(1-p) + p^3 = 3p^2 - 2p^3 \tag{1}$$

Since the probability of error without error correction is p we see that this error correction code improves the fidelity of our information transfer when $p < 1/2$.

This idea of redundancy of information can be generalized into what are called classical linear error correction codes. In the theory of classical linear codes we represent strings of k bits as k-dimensional vectors with entries in the integers modulo 2. The value of each entry in one of this vectors is equal to the value of the corresponding bit. Thus for example, for five bits:

$$10010 \rightarrow \begin{bmatrix} 1 & 0 & 0 & 1 & 0 \end{bmatrix}^T \tag{2}$$

In order to protect such strings of k bits from noise we map, or *encode*, the k-dimensional basis that spans all such strings to the k-dimensional basis of a subspace of an n-dimensional bit string vector space. We call such a subspace $\mathcal{C}$ an $[n,k]$ *code*. Since $k < n$, $\mathcal{C}$ carries redundant information about our original bit string. We call the $n \times k$ matrix G that maps our original bit string x to the encoded bit string Gx the *generator matrix* for the code. Thus, for example, the generator matrix mapping our single bit ($k = 1$) from the previous example to the three bit encoding is:

$$G = \begin{bmatrix} 1 \\ 1 \\ 1 \end{bmatrix} \tag{3}$$

It is easy to see that this matrix maps 0 and 1 to $[0,0,0]^T$ and $[1,1,1]^T$ respectively. The generator characterization of a code is very intuitive when dealing with transforming the bit strings we wish to encode to their encoded versions. However, for the purpose of carrying out error correction it is easier to characterize a code by its *parity check matrix*. If H is the parity check matrix of some $[n,k]$ code $\mathcal{C}$, we define the code to be the set of n-dimensional vectors x such that:

$$Hx = 0 \qquad (4)$$

Here H is an $n - k \times n$ matrix. It can be shown [1] that we can convert between generator matrices and parity check matrices, and vice-versa. Thus the two characterizations are equivalent. In the case of our previous example the parity check matrix is:

$$H = \begin{bmatrix} 1 & 1 & 0 \\ 0 & 1 & 1 \end{bmatrix} \qquad (5)$$

It can be shown that the unique vectors satisfying $Hx = 0$ for this equation are $[0, 0, 0]^T$ and $[1, 1, 1]^T$.

In order to develop the classical linear theory of error correction we must first introduce the concept of the *Hamming distance* $d(x, y)$ between two bit strings x and y. This is defined to be the number of places where the entries of the two bit strings differ. For a code $\mathcal{C}$, define $d(\mathcal{C})$ to be the smallest distance between any two different codewords in the code:

$$d(\mathcal{C}) = \min_{x, y \in \mathcal{C}, x \neq y} d(x, y) \qquad (6)$$

Error detection is accomplished as follows [1]. Recall that any n-dimensional bit string x contained in the code $\mathcal{C}$ obeys Eq. 4. Suppose that as we transmit the bit string x it incurs some errors, so that the bit string x' is received at the other end of the channel. Define $e = x' - x$ to be the *error vector* of the transmission, which tells us the places at which the original and final bit strings differ. If the probability of error on each bit is assumed to be small and independent, then with very high probability e will not lie in $\mathcal{C}$ so if the receiver applies H on the received bit string he will get a non-zero answer $Hx' = Hx + He = He$.

A code with $d(\mathcal{C}) \leq 2t + 1$ can correct up to t errors on a bit string. This condition guarantees that for any erroneous bit string x' with up to t errors there exists a unique codeword x such that $d(x', x) < t$. The erroneous bit string x' is corrected by transforming it back to x. The receiver can then map the codeword back to the original k-dimensional bit string.

III.   QUANTUM NOISE

When describing quantum noise we use the language of density operators and quantum operations. For a review of density matrices and their properties please refer to [2].

Although most of the qubit systems we treat theoretically are in isolation, the systems we encounter in reality are far from isolated. They are often coupled to an external system, which we call the *environment*, whose detailed properties we are ignorant about. Such a system is

called an *open* system, and systems in isolation are called *closed*.

If our qubits are in isolation we can evolve their state by multiplying their initial state vector by a unitary operator U. However if the qubits are in contact with some environment we cannot in general evolve them separately with a unitary operator. What we can do is make the open qubit system closed by adjoining the environment to our description. For example, if our qubits and the environment are initially in the uncoupled states ρ and ρ_e respectively, we can describe the full closed initial system as $\rho \otimes \rho_e$. We can then evolve this closed system with some unitary operator U.

In quantum computation we can think of the sources of noise as the environment of the qubits. We can then characterize the effect of the environment on our qubit over time by evolving the full qubit-environment state, and then taking the partial trace over the environment to get the ensemble describing only the qubits. The final state resulting from the noise is thus:

$$\mathcal{E}(\rho) = tr_e[U(\rho \otimes \rho_e)U^\dagger] \qquad (7)$$

The map $\mathcal{E}$ is a quantum operator. Mathematically, a general quantum operation $\mathcal{E}$ is a completely positive, convex linear map from density matrices to density matrices such that $0 \leq \mathrm{tr}[\mathcal{E}(\rho)] \leq 1^{[i]}$. This particular quantum operation describes the effect of noise of a system of qubits ρ.

Though this representation of the noise quantum operator is physically intuitive, it is not the most useful for computation. For that purpose we use the *operator-sum representation* of this quantum operator. This can be derived from Eq. 7 as follows. Let $\{|e_k\rangle\}$ be a basis for the environment state space. Without loss of generality[ii] assume that the environment starts in a pure state so that $\rho_e = |e_0\rangle \langle e_0|$. Then Eq. 7 reduces to:

$$\sum_k \langle e_k| U(\rho \otimes |e_0\rangle \langle e_0|)U^\dagger |e_k\rangle = \sum_k E_k \rho E_k^\dagger \qquad (8)$$

Here $E_k = \langle e_k| U |e_k\rangle$ is an operator on the state space of ρ, which in general obeys:

$$\sum_k E_k E_k^\dagger \leq 1 \qquad (9)$$

This is equivalent to the condition on the trace of $\mathcal{E}(\rho)$, with equality occurring under the same circumstances. Thus we can use 8 along with some set of $\{E_k\}$ to describe

————

[i] The inequality is due to the fact that in general quantum operators can describe the process of measurement. When no measurement is done we simply have the equality $tr[\mathcal{E}(\rho)] = 1$.

[ii] See section 2.5 of [3].

the effect of any kind of noise on quantum bits. The E_k's are called the *operation elements* for the noise operation $\mathcal{E}$.

For concreteness we present an example of noise. Another term for an environment that introduces noise into a qubit system is a *noise channel*. Consider a single qubit. Since the state of a quantum bit can be determined by two numbers on the unit sphere we can think of it as having a particular direction, that is, a particular polarization. We say the qubit is depolarized when it has equal probability to point in any direction. We also call this state the maximally mixed state. The noise channel with probability p of depolarizing some quantum state and probability $(1 - p)$ of leaving it alone is called the depolarizing channel. Its noise operation can be written as:

$$\mathcal{E}(\rho) = \frac{pI}{2} + (1 - p)\rho \qquad (10)$$

In the formalism of density matrices this equation is the statement that the resulting state $\mathcal{E}(\rho)$ is equal to the maximally mixed state $I/2$ with probability p, and equal to the input state ρ with probability $1 - p$. This operation can be re-expressed as:

$$\mathcal{E}(\rho) = (1 - p)\rho + \frac{p}{3}\left(\sigma_x\rho\sigma_x + \sigma_y\rho\sigma_y + \sigma_z\rho\sigma_z\right) \qquad (11)$$

Here the σ_i's are the Pauli spin matrices. Thus in the operator sum representation the $\mathcal{E}$ has operation elements $\{I, \sigma_x, \sigma_y, \sigma_z\}$.

IV. FIDELITY

When considering classical information we used the Hamming distance to quantify the differences between two different bit strings. We would like to like to have an analogous construction for quantum information. Unfortunately because of the probabilistic nature of quantum mechanics the concept of the Hamming distance does not extend naturally into the field of quantum information.

In probability theory there exist different measures to quantify the difference between two probability distributions. One of these is called the *fidelity*. Suppose p and q are probability distributions for discrete random variables. The fidelity of p and q is defined as:

$$F(p, q) = \sum_x \sqrt{p_x q_x} \qquad (12)$$

Here we sum over all values of the random variables. Note that when the two probability distributions p and q are equal then the fidelity equals 1, and zero when the distributions are non-zero exclusively on different values of x. Geometrically, we can think of $\sqrt{p}$ and $\sqrt{q}$ as unit vectors, and we can interpret $F(p, q)$ to be their inner product. Thus the arccosine of the fidelity measures the angular separation of these two vectors along the unit sphere.

The definition of fidelity commonly used in quantum information theory is motivated by Eq. (12). Given two density matrices ρ and σ describing a quantum system we define their fidelity to be [3]:

$$F(\rho, \sigma) = \text{tr}\sqrt{\rho^{1/2}\sigma\rho^{1/2}} \qquad (13)$$

Here $\rho^{1/2}$ is the matrix square root of ρ. That is, $\rho^{1/2}$ is a matrix such that $\rho^{1/2}\rho^{1/2} = \rho$. Though it is not apparent from the above definition, the fidelity is symmetric in its entries and its values range between 0 and 1. A value of 1 is obtained when $\rho = \sigma$. The quantum fidelity also has a geometric interpretation as the inner product of state vectors on the unit sphere. This interpretation, however, requires some rigorous motivation[iii].

We can use the fidelity to measure to what extent a noise channel corrupts quantum information. For example, let $\rho = |\psi\rangle\langle\psi|$ and consider the effect of the depolarization operator on this state. Note that $(|\psi\rangle\langle\psi|)^2 = |\psi\rangle\langle\psi|$ so $\rho^{1/2} = |\psi\rangle\langle\psi|$. Let:

$$\sigma = (1 - p)|\psi\rangle\langle\psi| + \frac{p}{3}\sigma_x|\psi\rangle\langle\psi|\sigma_x \qquad (14)$$
$$+ \frac{p}{3}\sigma_y|\psi\rangle\langle\psi|\sigma_y + \frac{p}{3}\sigma_z|\psi\rangle\langle\psi|\sigma_z$$

Then:

$$F(|\psi\rangle, \mathcal{E}(|\psi\rangle)) = F(|\psi\rangle\langle\psi|, \mathcal{E}(|\psi\rangle\langle\psi|)) \qquad (15)$$
$$= \sqrt{(1 - p) + \frac{p}{3}\sum_i |\langle\psi|\sigma_i|\psi\rangle|^2}$$
$$= \sqrt{1 - \frac{2}{3}p}$$

So as the probability of the noise occurring increases, the agreement between the initial and final states decreases.

V. QUANTUM ERROR CORRECTION

A. The Shor 9-Qubit Code

Now that we have a formalism for describing noise and a means of quantifying the magnitude of the effect of noise on a state we can consider protocols for correcting quantum errors and their effectiveness.

[iii] See section 9.2.2 of [3], in particular the proof of Uhlmann's theorem.

Early in the study of quantum noise it was thought that creating a quantum error correction scheme would be impossible. This is because of the large set of values a quantum bit can take on. As opposed to a classical digital bit, which can take on only two values, a quantum bit has an infinite set of states, which can be parametrized by the coordinates of the unit sphere. There can be no physical error correction scheme that could correct for an infinite set of possible errors in finite time.

However, it was eventually realized that although qubits can take on an infinity of states, the errors that a particular qubit can undergo admit a discrete, finite description after error detection has occurred. We illustrate how this is accomplished by considering the Shor 9-qubit code [4], which is capable of correcting an arbitary error on a single qubit. Consider a generic pure state $\alpha |0\rangle + \beta |1\rangle$, and the encoding:

$$|0\rangle \rightarrow |0_L\rangle = |a^+\rangle^{\otimes 3} \qquad (16)$$
$$|1\rangle \rightarrow |1_L\rangle = |a^-\rangle^{\otimes 3}$$

Here $|\psi\rangle^{\otimes n}$ denotes the tensor product of $|\psi\rangle$ with itself n times, and:

$$|a^\pm\rangle = \frac{(|000\rangle \pm |111\rangle)}{\sqrt{2}} \qquad (17)$$
$$|b^\pm\rangle = \frac{(|100\rangle \pm |011\rangle)}{\sqrt{2}}$$

The space spanned by the orthonormal vectors $|0_L\rangle$ and $|1_L\rangle$ is our quantum code $\mathcal{C}$. Note that just like the classical codes, this quantum error correction code relies on the use of redundant qubits. Suppose a single error occurs on the first qubit. Any operation on a single quantum bit can be written as a linear combination of Pauli matrices with some complex coefficients:

$$E^1 = e_0 I^1 + e_1 \sigma_x^1 + e_2 \sigma_y^1 + e_3 \sigma_z^1 \qquad (18)$$

The upper index 1 denotes that these operators are acting on the first qubit. The error E_1 maps the state $\alpha |0_L\rangle + \beta |1_L\rangle$ to:

$$E^1(\alpha |0_L\rangle + \beta |1_L\rangle) \qquad (19)$$
$$= \alpha \left(e_0 |a^+\rangle + e_1 |a^-\rangle + ie_2 |b^-\rangle + e_3 |b^+\rangle\right) |a^+\rangle^{\otimes 2}$$
$$+ \beta \left(e_0 |a^-\rangle + e_1 |a^+\rangle + ie_2 |b^+\rangle + e_3 |b^-\rangle\right) |a^-\rangle^{\otimes 2}$$

For brevity we have suppresed the tensor product symbols that should be written between the superposition in parathensis and the tensored states to the right of them. Note that:

$$\sigma_x^1 \sigma_x^2 \sigma_x^3 |a^\pm\rangle = \pm 1 |a^\pm\rangle, \; \sigma_x^1 \sigma_x^2 \sigma_x^3 |b^\pm\rangle = \pm 1 |b^\pm\rangle \quad (20)$$
$$\sigma_z^1 \sigma_z^2 |a^\pm\rangle = +1 |a^\pm\rangle, \; \sigma_z^1 \sigma_z^2 |b^\pm\rangle = -1 |b^\pm\rangle$$

As examination of the equations above shows, measurement of the operator $\sigma_z^1 \sigma_z^2$ tells us whether the first and second qubits match. If we measure +1, then the superposition collapses to a state in which the first two qubits match, and thus in effect no bit flip error occurred:

$$E^1(\alpha |0_L\rangle + \beta |1_L\rangle) \qquad (21)$$
$$\rightarrow \alpha \left(e_0 |a^+\rangle + e_1 |a^-\rangle\right) |a^+\rangle^{\otimes 2}$$
$$+ \beta \left(e_0 |a^-\rangle + e_1 |a^+\rangle\right) |a^-\rangle^{\otimes 2}$$

On the other hand, if we measure -1 then the superposition collapses to a state in which the first two qubits differ, and thus in effect a bit flip did occur:

$$E^1(\alpha |0_L\rangle + \beta |1_L\rangle) \qquad (22)$$
$$\rightarrow \alpha \left(ie_2 |b^-\rangle + e_3 |b^+\rangle\right) |a^+\rangle^{\otimes 2}$$
$$+ \beta \left(ie_2 |b^+\rangle + e_3 |b^-\rangle\right) |a^-\rangle^{\otimes 2}$$

In this sense we can think of the act of measurement determining which error occurs, and given the knowledge of what error this is we can correct it. In the first case no action is necessary, and in the second case application of σ_x^1 to the state will correct the bit flip error.

Suppose we have detected any bit flip errors and corrected them, so the problem reduces to consideration of state in Eq. (21). Inspection of Eq. (20) reveals that measurement of the operator $\sigma_x^1 \sigma_x^2 \sigma_x^3 \sigma_x^4 \sigma_x^5 \sigma_x^6$ compares the first two kets in the tensor product of state (21)[iv]. If measurement of this operator yields +1 the first two kets are the same. On the other hand, if the measurement yields -1 the two kets are opposite. Thus, for example, $|a^+\rangle |a^+\rangle |a^+\rangle$ has eigenvalue +1 with respect to this operator, and $|a^-\rangle |a^+\rangle |a^+\rangle$ has eigenvalue -1.

For example, assume we measure $\sigma_x^1 \sigma_x^2 \sigma_x^3 \sigma_x^4 \sigma_x^5 \sigma_x^6$ for (21) and the measurement yields -1. Then the superposition collapses to:

$$\rightarrow \alpha e_1 |a^-\rangle |a^+\rangle^{\otimes 2} + \beta e_1 |a^+\rangle |a^-\rangle^{\otimes 2} \qquad (23)$$

If we eliminate the e_1 factor by renormalizing and apply σ_z^1 to flip the sign of the first state in the tensor product we arrive at the state:

$$\rightarrow \alpha |a^+\rangle^{\otimes 3} + \beta |a^-\rangle^{\otimes 3} = \alpha |0_L\rangle + \beta |1_L\rangle \qquad (24)$$

Thus after detecting and correcting as necessary we have returned to the original state. The procedure we

―――――

[iv] In fact this operator compares the relative sign between the terms implicit in this two states. Thus, the state $|b^+\rangle |a^+\rangle |a^-\rangle$ has eigenvalue +1 with respect to this operator, and the state $|a^+\rangle |b^-\rangle |a^-\rangle$ has eigenvalue -1.

followed is not particular to our assumption that an error occurred on the first qubit, it can be carried out for other qubits by carrying out an analogous set of measurements. Also, we chose to consider a pure state for the sake of simplicity, but the same analysis can be carried out for ensembles described by density matrices. The only key assumption we made was that an error occurred on a single qubit. Hence the Shor code is capable of remedying any single qubit error.

Note that the error operator E^1 has four complex degrees of freedom so the image of $\alpha \left|0_L\right\rangle + \beta \left|1_L\right\rangle$ under it is an infinite set. However, the process of measuring the operators $\sigma_z^1 \sigma_z^2$ and $\sigma_x^1 \sigma_x^2 \sigma_x^3 \sigma_x^4 \sigma_x^5 \sigma_x^6$ eliminates these degrees of freedom, reducing the set of all possible errors to a single element. It is this fact which makes quantum error correction possible.

B.   Calderbank-Shor-Steane Codes

As can be seen from consideration of the effect of σ_z, qubits can suffer from bit flip errors just like classical bits. However, qubits can also suffer from phase flip errors. This kind of error is described by the action of σ_z, and is unique to quantum information channels[v]. Given the added complexity of quantum errors it is perhaps a surprising result that classical error correction codes can be used to create quantum error correction codes. The class of quantum error correction codes created in this manner are named *Calderbank-Shor-Steane Codes* (or *CSS codes*) after their inventors. In order to understand how these codes are constructed we must first introduce some mathematical definitions.

1.   Mathematical Background

The following are some definitions and theorems from group theory:

Definition 1: We define a *group* to be a set $\mathcal{G}$ along with an operation · which combines two elements of the group to produce a third. A group must obey the following axioms:

- *Closure*: If a and b are elements of $\mathcal{G}$, then $a \cdot b$ must be an element of $\mathcal{G}$.

- *Associativity*: For every a, b, and c in $\mathcal{G}$, $(a \cdot b) \cdot c = a \cdot (b \cdot c)$.

————

[v] Note that the action of σ_y on qubits can be described as a joint bit flip and phase flip, since $\sigma_y = i\sigma_z \sigma_x$. Thus all quantum errors can be described as a combination of these two types of errors.

- *Identity Element*: There exists an element $\mathbb{1}$ in $\mathcal{G}$ such that for each a in $\mathcal{G}$ we have that $\mathbb{1} \cdot a = a \cdot \mathbb{1} = a$.

- *Inverse Element*: For each element a in $\mathcal{G}$ there exists an element a^{-1} in $\mathcal{G}$ such that $a \cdot a^{-1} = a^{-1} \cdot a = \mathbb{1}$

Definition 2: Suppose $\mathcal{G}$ is a group with operation ·. We say a subset $\mathcal{H} \subset \mathcal{G}$ is a *subgroup* of $\mathcal{G}$ if $\mathcal{H}$ along with the operation · obeys the axioms above.

It can be seen from the definitions above that vector spaces are a particular kind of group, with the commutative operation $+$. Thus the above definitions and any theorems about groups are applicable to the Hilbert spaces we work with in quantum mechanics. We will be taking $+$ as our group operation in the remainder of this paper, denoting its inverse by $-$ as is conventional. We will also need the following definitions:

Definition 3: Suppose $\mathcal{G}$ is a group, $\mathcal{H}$ is a subgroup of $\mathcal{G}$, and a is an element of $\mathcal{G}$. We define the *coset of $\mathcal{H}$ in $\mathcal{G}$ with respect to a* to be the set:

$$a + \mathcal{H} = \{a + h \mid h \text{ is an element of } \mathcal{H}\}$$

Definition 4: Suppose $\mathcal{C}$ is a subspace of some larger vector space $\mathcal{V}$. We define $\mathcal{C}^{\perp}$ to be the *orthogonal space* to $\mathcal{C}$, that is, the subspace of all vectors orthogonal to the subspace $\mathcal{C}$:

$$\mathcal{C}^{\perp} = \{v \text{ in } \mathcal{V} \mid v \cdot x = 0 \text{ for every x in } \mathcal{C}\}$$

When V is some Hilbert space and $\mathcal{C}$ is a code in $\mathcal{V}$ then we call $\mathcal{C}^{\perp}$ the code *dual* to $\mathcal{C}$. If $\mathcal{C}$ has generator matrix G and parity check matrix H, then $\mathcal{C}^{\perp}$ has generator matrix H^T and parity check matrix G^T. Furthermore, if the dimension of $\mathcal{V}$ is n and the dimension of $\mathcal{C}$ is k then the dimension of $\mathcal{C}^{\perp}$ is $n - k$.

We state the following theorem without proof. The proof of this theorem can be found in [5].

Theorem 1 (Lagrange's Theorem): Let $\mathcal{G}$ be a group and let $\mathcal{H}$ be a subgroup of $\mathcal{G}$. Let $|\mathcal{G}|$ and $|\mathcal{H}|$ denote the number of elements in $\mathcal{G}$ and $\mathcal{H}$ respectively. If $|\mathcal{G}|$ is finite and $[\mathcal{G} : \mathcal{H}]$ denotes the number of unique left cosets of $\mathcal{H}$ in $\mathcal{G}$ then the following equality holds:

$$|\mathcal{G}| = [\mathcal{G} : \mathcal{H}]|\mathcal{H}|$$

It can be shown that the number of left cosets is equal to the number of right cosets, so the above equation holds for right cosets as well. We call $[\mathcal{G} : \mathcal{H}]$ the *index of $\mathcal{H}$ in $\mathcal{G}$*. We will also use the following theorems:

Theorem 2: Suppose $\mathcal{G}$ is a group and $\mathcal{H}$ is a subgroup of $\mathcal{G}$. Suppose a and b are elements of $\mathcal{G}$. Then $b - a$ is an element of $\mathcal{H}$ if and only if $a + \mathcal{H} = b + \mathcal{H}$.

Proof: Suppose that $a + \mathcal{H} = b + \mathcal{H}$, then each element of $a + \mathcal{H}$ is equal to some element of $b + \mathcal{H}$. This implies that for some h and h' in $\mathcal{H}$ we must have that $a + h' = b + h$ and thus $b - a = h' - h$. Since $\mathcal{H}$ is a subgroup $h' - h$ is an element of $\mathcal{H}$, so $b - a$ is an element of $\mathcal{H}$.

Conversely suppose that $b - a = h'$ for some element h of $\mathcal{H}$. Then $b = a + h$ so by associativity:

$$
\begin{aligned}
b + \mathcal{H} &= \{b + h \mid h \text{ is an element of } \mathcal{H}\} \\
&= \{a + h' + h \mid h \text{ is an element of } \mathcal{H}\} \\
&= \{a \cdot h'' \mid h'' \text{ is an element of } \mathcal{H}\} \\
&= a + \mathcal{H}
\end{aligned}
$$

$\square$

Theorem 3 Suppose $\mathcal{G}$ is a group and $\mathcal{H}$ is a subgroup of $\mathcal{G}$. Suppose a and b are elements of $\mathcal{G}$. Then a and b belong to different cosets, that is $a + \mathcal{H} \neq b + \mathcal{H}$, if and only if the cosets $a + \mathcal{H}$ and $b + \mathcal{H}$ do not share any elements in common.

Proof: For ease we prove the contrapositive statements, which are logically equivalent. Suppose $a + \mathcal{H}$ and $b + \mathcal{H}$ share an element in common, then by definition 3 there must exist elements h and h' of $\mathcal{H}$ such that $a + h' = b + h$. By Theorem 2 it then follows that $a + \mathcal{H} = b + \mathcal{H}$.

Conversely, suppose that $a + \mathcal{H} = b + \mathcal{H}$, then clearly they share every element in common.

$\square$

2. The CSS Procedure

We can now construct the CSS codes. The following discussion is based on the derivation from [3]. Suppose $\mathcal{C}_1$ is a $[n, k_1]$ classical code, that is, $\mathcal{C}_1$ is a k_1-dimensional subspace of n-dimensional Hilbert space. Suppose $\mathcal{C}_2$ is a $[n, k_2]$ classical code such that $\mathcal{C}_2 \subset \mathcal{C}_1$. Furthermore, suppose $\mathcal{C}_1$ and $\mathcal{C}_2^\perp$ correct up to t errors. Define for each element x of $\mathcal{C}_1$:

$$
|x + \mathcal{C}_2\rangle \equiv \frac{1}{\sqrt{|\mathcal{C}_2|}} \sum_{y \in \mathcal{C}_2} |x + y\rangle \tag{25}
$$

The set of vectors $|x + \mathcal{C}_2\rangle$ define the *CSS code of $\mathcal{C}_1$ over $\mathcal{C}_2$*, $\mathrm{CSS}(\mathcal{C}_1, \mathcal{C}_2)$. Note that the elements of the sum (24) are exactly the elements of the coset $x + \mathcal{C}_2$.

Now, notice that if x' is an element of $\mathcal{C}_1$ such that $x' - x$ is an element of $\mathcal{C}_2$, then it follows from Theorem 2 that $x + \mathcal{C}_2 = x' + \mathcal{C}_2$ and thus the states $|x + \mathcal{C}_2\rangle$ and $|x' + \mathcal{C}_2\rangle$ are equal. Furthermore, note that if x and x' belong to *different* cosets then it follows from Theorem 3 that $x + \mathcal{C}_2 \neq x' + \mathcal{C}_2$. This implies that if x and x' are in different cosets then $|x + \mathcal{C}_2\rangle$ and $|x' + \mathcal{C}_2\rangle$ are orthogonal to each other. By Lagrange's Theorem there are,

$$
\frac{|\mathcal{C}_1|}{|\mathcal{C}_2|} = \frac{2^{k_1}}{2^{k_2}} = 2^{k_1 - k_2} \tag{26}
$$

cosets of $\mathcal{C}_2$ with respect to $\mathcal{C}_1$ and thus Eq. (25) defines $2^{k_1 - k_2}$ orthonormal vectors. These vectors define a $2^{k_1 - k_2}$-dimensional space so the CSS code $\mathrm{CSS}(\mathcal{C}_1, \mathcal{C}_2)$ is a $[n, k_1 - k_2]$ quantum code.

We now demonstrate how the error correction procedure works. Suppose that our original state is $|x + \mathcal{C}_2\rangle$ and this state undergoes an error. We can describe the bit flip error and the phase flip error respectively by the n-dimensional bit vectors e_1 and e_2[vii]. For example, if the nth bit of the code underwent a bit flip the nth entry of e_1 would be a 1. We can write erroneous state as:

$$
\frac{1}{\sqrt{|\mathcal{C}_2|}} \sum_{y \in \mathcal{C}_2} (-1)^{(x+y) \cdot e_2} |x + y + e_1\rangle \tag{27}
$$

Here $\cdot$ denotes the usual vector dot product, modulo 2. We can attach a "blank" extra qubit to this state, called an *ancilla*,

$$
\frac{1}{\sqrt{|\mathcal{C}_2|}} \sum_{y \in \mathcal{C}_2} (-1)^{(x+y) \cdot e_2} |x + y + e_1\rangle |0\rangle \tag{28}
$$

and then apply a quantum operation to this joint state such that:

$$
\begin{aligned}
|x + y + e_1\rangle |0\rangle &\to |x + y + e_1\rangle |H_1(x + y + e_1)\rangle \tag{29} \\
&= |x + y + e_1\rangle |H_1 e_1\rangle
\end{aligned}
$$

Here H_1 is the parity check matrix for the code $\mathcal{C}_1$, and thus since $x + y$ is an element of $\mathcal{C}_1$ it follows that $H_1(x+y) = 0$. After applying this operation on the state from Eq. (28) we end up with the state:

$$
\frac{1}{\sqrt{|\mathcal{C}_2|}} \sum_{y \in \mathcal{C}_2} (-1)^{(x+y) \cdot e_2} |x + y + e_1\rangle |H_1 e_1\rangle \tag{30}
$$

Thus when we measure the ancilla qubit we will retrieve the vector He_1. Since the classical code $\mathcal{C}_1$ can correct up to t errors then as long as less than t bit flip errors occurred the vector $H_1 e_1$ will determine exactly on which qubits the errors occured. We can apply σ_x to the erroneous qubits to eliminate all the bit flip errors. This yields the state:

————

[vii] Recall that the phase flip noise operation on a single qubit is described by the action of σ_z. The dot product $(x + y) \cdot e_2$ counts the number of times that a $|1\rangle$ in the qubit string $|x + y\rangle$ gets acted on by a σ_z noise operator, that is the number of single qubit phase flips that occur due to the noise.

$$\frac{1}{\sqrt{|\mathcal{C}_2|}} \sum_{y \in \mathcal{C}_2} (-1)^{(x+y)\cdot e_2} |x+y\rangle \tag{31}$$

Note that we have discarded the ancilla after measuring it. It remains to correct the phase flip error e_2. In order to accomplish this we introduce the operator known as the *Hadamard gate*. This operator acts on a single qubit, and is defined by the following equations:

$$F|0\rangle = |+\rangle, \; F|1\rangle = |-\rangle, \; F^2 = \mathbb{1} \tag{32}$$

Applying F to every qubit in state (30) and redefining dummy variables we get the state:

$$\frac{1}{\sqrt{2^n|\mathcal{C}_2|}} \sum_{z \in \mathcal{C}_1} \sum_{y \in \mathcal{C}_2} (-1)^{(x+y)\cdot z} |z+e_2\rangle \tag{33}$$

Now, consider the dot product $y \cdot z$. Since y is an element of $\mathcal{C}_2$ then if z is in $\mathcal{C}_2^\perp$ we have that $y \cdot z = 0$ so:

$$\sum_{y \in \mathcal{C}_2} (-1)^{y\cdot z} = \sum_{y \in \mathcal{C}_2} 1 = |\mathcal{C}_2|, \text{ if } z \in \mathcal{C}_2^\perp \tag{34}$$

On the other hand if z is an element of $\mathcal{C}_2$ then for each y such that $y \cdot z = 0$ there exists a y' such that $y' \cdot z = 1$ so when we sum over all y we find that:

$$\sum_{y \in \mathcal{C}_2} (-1)^{y\cdot z} = 0, \text{ if } z \notin \mathcal{C}_2^\perp \tag{35}$$

The vector space $\mathcal{C}_1$ is the direct sum of $\mathcal{C}_2$ and $\mathcal{C}_2^\perp$ so combining Eqs. (34) and (35) with Eq. (33) we can write the latter as,

$$\frac{1}{\sqrt{2^n/|\mathcal{C}_2|}} \sum_{z \in \mathcal{C}_2^\perp} (-1)^{x\cdot z} |z+e_2\rangle \tag{36}$$

and thus we have returned to the case of the bit flip error we encountered in Eq. (27). Using the same procedure we used in that case, with the parity check matrix H_2 for the classical code $\mathcal{C}_2^\perp$ instead of H_1 we can eliminate this bit flip to arrive at the state:

$$\frac{1}{\sqrt{2^n/|\mathcal{C}_2|}} \sum_{z \in \mathcal{C}_2^\perp} (-1)^{x\cdot z} |z\rangle \tag{37}$$

Inverting the effect of the Hadamard operations by applying them once more we finally arrive at the state:

$$\frac{1}{\sqrt{|\mathcal{C}_2|}} \sum_{y \in \mathcal{C}_2} |x+y\rangle \tag{38}$$

Thus we have returned to the original encoded state. We can see that the CSS procedure works in two steps: First it corrects qubit bit flip errors by exploiting the bit flip correction properties of the classical code $\mathcal{C}_1$. It then uses the Hadamard operation to traslate the remaining phase flip errors into bit flip errors, and uses the bit flip correction properties of the classical code $\mathcal{C}_2^\perp$ to correct these errors. Since both $\mathcal{C}_1$ and $\mathcal{C}_2^\perp$ can correct up to t errors, $\text{CSS}(\mathcal{C}_1, \mathcal{C}_2)$ can correct t qubit errors.

VI. DISCUSSION

We have introduced the formalism for describing quantum noise and its effects, and we have showed that classical linear error correcting codes can be used to create quantum error correction codes. The CSS codes can be used to prove interesting bounds of the number of encoding qubits necessary in order to tolerate a particular number of errors. Furthermore, since we know good classical error correction codes exist, the CSS procedure shows that good *quantum* error correction codes also exist.

The 9-qubit code and the CSS codes we have introduced are a subset of a class of codes called *stabilizer codes*. These codes are derived from a very powerful formalism called the *stabilizer formalism*, which can be used to show that some quantum information operations can be simulated efficiently (i.e. in polynomial time) on a classical computer. We encourage the curious reader to refer to section 10.5 of [3] to learn more about this formalism. For those interested in even further reading about quantum error correction, [3] provides a thourough list of important literature on the subject in section 10.6.

In our discussion of error correction we did not consider the possibility that the application of the very operations we used to detect and correct noise might itself induce some noise. This is in fact something that we generally expect to occur in physical systems. Although this does pose an extra complication, it can be shown that if the noise induced by these operations is below a certain threshold then quantum computation to a desireable degree of precision is achievable. We state this result by saying that quantum computation can be made *fault tolerant*. For some discussion on this subject please refer to [3].

[1] S. Lin and W. Ryan, *Channel Codes: Classical and Modern.* Cambridge University Press, New York (2009).

[2] A. W. Harrow, *8.06 Spring 2014 Lecture Notes: 1. Entanglement, density matrices and decoherence.* https://stellar.mit.edu/S/course/8/sp14/8.06/materials.html (2014).

[3] I. Chuang and M. Nielsen, *Quantum Computation and Quantum Information* Cambridge University Press, New York (2010).

[4] P. W. Shor, Phys. Rev. A **52**, 2493 (1995).

[5] M. Artin, *Algebra.* Pearson, Boston (2011).

The Problems with Relativistic Quantum Mechanics

Kevin Burdge

MIT Department of Physics
(Dated: May 2, 2014)

In this discussion we investigate the problems that arise in considering relativistic quantum mechanical systems. These problems are investigated in the context of the Schrodinger equation, Klein-Gordon equation, and Dirac Equation. We also present a resolution to the issues discussed by investigating the second quantization of the above equations.

I. INTRODUCTION

A. Overview

This discussion will open with a brief overview of essential concepts in special relativity and quantum mechanics. After developing these concepts, it delves into the problems with integrating special relativity into the Schrodinger equation. We proceed by developing the problems with the Klein-Gordon Equation, Dirac Equation, Scattering, and continue on to the general tensions between quantum mechanics and relativity present in all of these equations. Finally, the paper concludes with a brief introduction to the second quantization, and describes how quantum field theory successfully integrates special relativity into its framework.

B. Special Relativity and Spacetime

In 1905, Albert Einstein developed a theory known as special relativity which unifies space and time.When Einstein developed the theory of special relativity, he based it on two fundamental postulates: That the laws of physics are a constant to observers in any inertial frame of reference, and that all inertial observers measure the speed of light to be the same velocity, independent of their frame. Out of these two postulates, Einstein developed a mathematical framework for spacetime called an event space. This event space contains a metric to measure the distance between these events. This event space takes the form of a flat four dimensional space known as Minkowski space. In Minkowski space, the metric for measuring the distance between two events takes the form of:

$$ds^2 = -(cdt)^2 + dx^2 + dy^2 + dz^2 \qquad (1)$$

Examining the above equation, one can see the measure of distance between events, ds, contains the normal spatial seperation between two points in three space, $dx^2 + dy^2 + dz^2$. However, Einstein also incorporated the dimension of time into his metric, but with a minus sign and an overall factor of c, the speed of light. Thus, the speed of light serves as a fundamental constant in the form of a velocity, that relates space and time. In our discussion, the significance of Einstein's theory lies in its observation that space and time are fundamentally the

same thing; they are both just ways of measuring the distance between two events.

C. Quantum Mechanics

In the early 1900s, experiments such as the Photoelectric Effect and Double-Slit experiment nessecitated the development of a new framework to describe particles. Thus, quantum mechanics was born in an effort to understand phenomenon such as the wave-particle duality exhibited by particles such as electrons and photons. By describing a particle with a mathematical object known as a wavefunction, physicists created an entirely new non-classical framework for defining particles. The wave-function describes the probabilistic state of a system, giving us only probabilities of finding a particle at a particular place, or having a particlar momentum. In fact, quantum mechanics postulates limits on our knowledge of a system in the form of the Heisenberg uncertainty principle. It which arises from the fact that certain observables in quantum mechanics, such as position and momemtum, fail to commute.

Quantum mechanics differs from the mathematical framework of classical mechanics in its use of operators. Rather than functioning as a paramater like in classical mechanics, position in quantum mechanics takes the form of an operator in the form of an infinite dimensional matrix in a Hilbert space. The act of determining the position of a particle in quantum mechanics involves acting the position operator, $\hat{x}$, on the wavefunction, which can always be expressed as a superposition of position eigenfunctions. Acting the operator on the wavefunction ψ, changes ψ, causing it to "collapse" into a position eigenstate. Thus, if one subsequently measures the position by acting the operator again, one will consistently obtain the same position eigenvalue, ignoring decoherence.

II. THE SCHRODINGER EQUATION

Schrodinger's equation can be understood from the postulation that particles can be described by a wavefunction $\psi(x,t) = \sum_{n=0}^{\infty} C_n e^{i(k_n x - \omega_n t)}$, where the particle's energy is given by $\hbar\omega$ and its momentum given by $\hbar k$. In order to produce these eigenvalues, we construct an

energy operator, $\hat{E} = -i\frac{\partial}{\partial t}$, and similarly, a momentum operator $\hat{p} = i\frac{\partial}{\partial x}$. Using the fact from classical mechanics that the Hamiltonian of a system, which gives its energy, is given by the kinetic energy $\frac{p^2}{2m}$ plus its potential energy V, we obtain the Schrodinger equation by promoting the classical parameters for momentum and energy into operators:

$$i\hbar \frac{\partial \psi(x,t)}{\partial t} = -\frac{\hbar^2}{2m}\frac{\partial^2 \psi(x,t)}{\partial x^2} + V(x)\psi(x,t) \qquad (2)$$

The above equation forms the core of much of what has been accomplished in quantum mechanics, and successfully describes many significant systems such as the hydrogen atom with great precision.

A. Some Problems with the Relativistic Schrodinger Equation

Now we can finally investigate some of the conflicts with relativity and quantum mechanics as seen in the Schrodinger equation. The Schrodinger equation is manifestly non-relativistic for a few reasons. Just looking at the equation, its most glaring violation lies in the fact that it is clearly not Lorentz-invariant. When boosting to a new frame in relativity, coordinates in spacetime are transformed by applying lorentz transformations to the spatial and time coordinates in the system. The Schrodinger equation takes a single derivative in time, but two derivatives in space. This unequal treatement of space and time means that the physics of the Schrodinger equation changes as one changes frames, as only one Lorentz transformation acts on the time derivative half of the Schrodinger equation, but two act on the spatial derivative portion. This violates a fundamental posulate of special relativity, that the physical laws of a system are indepedent of the frame of reference it is viewed in.

III. THE KLEIN-GORDON EQUATION

An answer to the glaring lack of Lorentz invariance in the Schrodinger equation was later postulated in the form of the Klein-Gordon Equation. The Klein-Gordon equation takes full advantage of the relativistic dispersion relation for particles, and observes that the quantity $p^\mu p_\mu = -m^2 c^2$ is a Lorentz scalar, and thus Lorentz invariant. Defined by this relation, the free Klein-Gordon equation reads:

$$\frac{1}{c^2}\frac{\partial^2 \psi(x,t)}{\partial t^2} - \nabla^2 \psi(x,t) + \frac{m^2 c^2}{\hbar^2}\psi(x,t) = 0 \qquad (3)$$

The above equation solves the Schrodinger equation's unequal orders of spatial and temporal derivatives, and uses a completely relativistic dispersion relation. [5]

A. Problems with the Klein-Gordon Equation

Even though the Klein-Gordon equation solves some of the most glaring problems of the Schrodinger equation in a relativistic context, it also carries some non-physical results. Let us investigate this by deriving the probability current in the Klein-Gordon equation. To begin, let us look at the definition of probability density in the Schrodinger equation, $\rho = |\psi|^2$.

We define the probability current as the gradient of the probability density, or:

$$\vec{J} = \frac{\nabla(\psi\psi^*)}{2mi} = \frac{\psi^*\nabla\psi - \psi\nabla\psi^*}{2mi} \qquad (4)$$

Taking a time derivative of the probability density, we obtain:

$$\partial_t \rho = \psi\partial_t\psi^* + \psi^*\partial_t\psi \qquad (5)$$

Which, when combined with the definition of $\partial_t\psi$ from the Schrodinger equation, yields:

$$\partial_t \rho = \frac{i}{2m}\nabla(\psi^*\nabla\psi - \psi\nabla\psi^*) = -\nabla\vec{J} \qquad (6)$$

Where in the last line, $\vec{J}$ is the probability current[2].

Using this same technique, we again define the probability current:

$$\vec{J} = \frac{\psi^*\nabla\psi - \psi\nabla\psi^*}{2mi} \qquad (7)$$

In order to keep a consistent definition of current, we must now redefine our probability density ρ as:

$$\rho = \frac{i}{2m}(\psi^*\partial_t\psi - \psi\partial_t\psi^*) \qquad (8)$$

Which is the natural definiton of a probability density in the second-order Klein-Gordon equation[2], as one can see by proceeding to take its time deritative to obtain a probability current:

$$\partial_t \rho = \frac{i}{2m}(\psi^*\partial_t^2\psi - \psi\partial_t^2\psi^*) \qquad (9)$$

$$= \frac{i}{2m}(\psi^*\nabla^2\psi - \psi\nabla^2\psi^*) = -\nabla\vec{J} \qquad (10)$$

The problem with this expression lies in the fact that $\rho = \frac{i}{2m}(\psi^*\partial_t\psi - \psi\partial_t\psi^*)$, fails to be a positive definite quantity, and thus is not a physical probability density[2].

B. Solutions to the Klein-Gordon Equation

Another problem with the Klein-Gordon equation lies in its solutions. We define a free particle using a wavefuntion of the form:

$$\psi(x) = Ne^{i(kx - \omega t)} \tag{11}$$

Which is more concisely expressed in terms of four-vectors as:

$$\psi(x) = Ne^{ik_\mu x^\mu} \tag{12}$$

Using the Klein-Gordon equation, the solutions for the energies of these particles, k^0, are[5]:

$$k^0 = \pm\sqrt{k^2 + \frac{m^2c^2}{\hbar^2}} \tag{13}$$

The problem with these solutions is that one set is not only negative, but unbounded below. This possibility represents an unphysical result, as all particles would rapidly decay to the infinitely negative energy state. Later in the discussion of the Dirac equation, there will be further elaboration on the problematic nature of these negative energy solutions.

IV. THE DIRAC EQUATION

After the failure of the Klein-Gordon equation to be completely physical because of its negative energy solutions and non positive-definite probability current, Dirac set out to create another quantum mechanical equation which would be fully relativistic and resolve these issues. Dirac's equation differs from the Klein Gordon equation in a few important ways. Below is the Dirac equation[1]:

$$i\hbar\gamma^\mu \partial_\mu \psi - mc\psi = 0 \tag{14}$$

Most importantly, the Dirac equation is first order in both spatial derivatives and time derivatives. This, like the Klein-Gordon equation, achieves an equal treatment of space and time in the order of their derivatives. However, in order to accomplish this form, Dirac had to replace the wavefunction ψ, with a more complicated mathematical object–a spinor. Moreover, the γ^u term is a tensor of 4x4 matrices whose entries contain combinations of the Pauli matrices and the 2x2 identity.

A. Probability Current and Solutions of the Dirac Equation

Like for the Schrodinger and Klein-Gordon equations, we can derive a probability current in the Dirac equation. We take

$$\bar{\psi} = \psi^*\gamma^0 \tag{15}$$

And take the conjugate of the Dirac equation, which gives us:

$$-i\hbar\gamma^\mu \partial_\mu \bar{\psi} - mc\bar{\psi} = 0 \tag{16}$$

Adding the Dirac equation and its conjugate, the mass terms cancel, and we are left with:

$$\partial_\mu(\bar{\psi}\gamma^u\psi) = 0 \tag{17}$$

Since for a probability current we want conservation, or $\partial_\mu j^\mu = 0$.[1] Thus, by this definition, our probability current is:

$$j^\mu = \bar{\psi}\gamma^u\psi \tag{18}$$

This probability current is an improvement on the probability current in the Klein-Gordon equation, as its zereoth component, j^0 can always be taken to be positive definite. However, the solutions of the Dirac equation for the energy of a free particle yield:

$$E = \pm\sqrt{p^2c^2 + m^2c^4} \tag{19}$$

Thus, we are plagued with the same sea of negative energy solutions as the Klein-Gordon equation. Dirac attempted to reconcile this by observing that his equation describes only fermionic particles, and that because of the Pauli-exclusion principle all of the negative energy solutions are saturated with fermions, and could thus create a stable vacuum[1]. However, this explanation fails to account for bosonic particles such as photons existing in the vacuum. Eventually, it was recognized that the negative energy solutions in the Dirac equation could be eliminated by quantizing it in a new way, and imposing anti-commutation relations between its operators. However, when one does this, while only positive energy solutions are recovered, one sacrifices the positivity of the probability current, j^0. An approach to solving this problem quantum field theory (which this paper will not discuss), is to recognize j^0 not as a quantum mechanical probability density, but rather a charge $Q = \int d^3xj^0$, where the new negative charge can be associated with an antiparticle[4].

V. AN UNPHYSICAL SCATTERING

All of the previously discussed examples of problems with relativistic quantum mechanics have focused on ill defined probability densities, negative energy solutions,

etc. The following is an example of an unphysical result arising out of a scattering problem using the Klein-Gordon equation:

Suppose we have a step function potential $V(x)$ which is 0 for $x < 0$ and is V_0 for $x > 0$. Now let us consider a particle scattering off of this potential, with a relativistic energy $E >> mc^2$.[6] Solving this scattering problem using the Klein-Gordon equation, we find the reflection rate R:

$$R = \left| \frac{(E^2 - m^2c^4)^{1/2} \mp ((E - V_0)^2 - m^2c^4)^{1/2}}{(E^2 - m^2c^4)^{1/2} \pm ((E - V_0)^2 - m^2c^4)^{1/2}} \right|^2 \quad (20)$$

And of course, the transmission rate $T = 1 - R$. Taking V_0 to be small compared to the energy of the particle, the transmission rate approaches 1. For a potential V_0 that satisfies the constraint $E - mc^2 < V_0 < E + mc^2$, we get full reflection, and no transmission. However, the trouble occurs if we consider a strong potential, where $V_0 > E + mc^2$. For example, say we take $V_0 = E + 5mc^2$. If we then take the set of solutions to R with the plus sign on top, and the negative on the bottom, we get a solution for R that looks like the following:

$$R = \left| \frac{(E^2 - m^2c^4)^{1/2} + ((E - E - 5mc^2)^2 - m^2c^4)^{1/2}}{(E^2 - m^2c^4)^{1/2} - ((E - E - 5mc^2)^2 - m^2c^4)^{1/2}} \right|^2 \quad (21)$$

After some cancellation, we end up with:

$$R = \left| \frac{(E^2 - m^2c^4)^{1/2} + (24)^{1/2}mc^2}{(E^2 - m^2c^4)^{1/2} - (24)^{1/2}mc^2} \right|^2 \quad (22)$$

Redefining $(E^2 - m^2c^4)^{1/2}$ as k, and $(24)^{1/2}mc^2$ as q, our solution takes the form:

$$R = \left| \frac{k + q}{k - q} \right|^2 \quad (23)$$

Where k and q are both positive quantities. This equation illustrates that our reflection coefficient can exceed 1 in the limit of a relativistic energy $E > mc^2$ and a strong potential $V_0 > E + mc^2$. This clearly represents a problem, as it is inconsistent with the definition of probability to have a reflection coefficient greater than 1. One can treat this solution as physically representing an anti-particle. Essentially, for a strong enough field, anti-particle particle creation can occur, and the creation of the anti-particle accounts for the reflection exceeding 1, and the negative transmission. Effectively, a hole is transmitted, which is the equivalent of negative transmission. [7]

VI. FUNDAMENTAL TENSIONS BETWEEN QUANTUM MECHANICS AND SPECIAL RELATIVITY

The failure of quantum mechanics to integrate special relativity is a consequence of some universal problems in the mathematical framework of quantum mechanics. Solving the Schrodinger equation for the wavefunction, one finds that its time evolution is governed by the unitary operator:

$$U(t) = e^{\frac{-iHt}{\hbar}} \quad (24)$$

This time evolution operator tells us the way the wavefunction evolves naturally given that we know its Hamiltonian. An important thing to observe about this operator, is that it uses time, t, as a parameter governing its evolution. This use of t reveals a problem at the heart of quantum mechanics. Time is a parameter, but position, $\hat{x}$, is an operator. These are two fundamentally different mathematical objects. Thus, the efforts to balance the order of time and spacial derivatives in the Klein-Gordon and Dirac equations cannot balance space and time, as space and time are treated as different mathematical objects.

Another tension between quantum mechanics and relativity comes from their radically different interpretation of the nature of time and events in the universe. Relativity uses events as the fundamental objects that build the universe–which consists of space-time. Quantum mechanics on the other hand chooses to make the wavefunction–a mathematical object describing a particle–its fundamental object of study. The tension between these views is a consequence of what they say about how physics works. A relativistic universe is a fully deterministic one. The space-time manifold contains all events, and our perception of time merely reflects a path we take through the manifold of events. Alternatively, quantum mechanics tells us that the universe follows a less deterministic set of rules, and places a fundamental limit on how much we can deterministically know about it through the uncertainty principle. Even though the time evolution of the wavefunction is deterministic, the information the wavefunction gives us is inherently probabilistic. A symmetry problem manifests itself because of these two different interpretations. Relativitiy treats time like the spacial dimensions, and is completely consistent in a world where time is reversed. Quantum mechanics on the other hand relies on time running only in one direction. In our direction of time, quantum mechanics tells us that when an event occurs and we make a measurement, that a wavefunction collapses into an eigenstate. However, running time backwards, we see something completely different, where the same event causes the once localized wavefunction to delocalize.

VII.   THE SOLUTION

Today, we have a theory in physics that unifies the observations that lead us to form quantum mechanics, and the theory of special relativity. This theory is Relativistic Quantum Field Theory. What quantum field theory does to resolve the problems between quantum mechanics and special relativity is something called the second quantization[**?**]. Take the Klein-Gordon equation for instance. In quantum mechanics, the Klein-Gordon equation reads:

$$\frac{1}{c^2}\frac{\partial^2 \psi(x,t)}{\partial t^2} - \nabla^2 \psi(x,t) + \frac{m^2 c^2}{\hbar^2}\psi(x,t) = 0 \qquad (25)$$

What the second quantization does, is it throws away $\psi(x,t)$, the wavefunction, and replaces it with $\hat{\phi}(x,t)$, a field operator dependent on space-time. The new Klein-Gordon equation thus reads:

$$\frac{1}{c^2}\frac{\partial^2 \hat{\phi}(x,t)}{\partial t^2} - \nabla^2 \hat{\phi}(x,t) + \frac{m^2 c^2}{\hbar^2}\hat{\phi}(x,t) = 0 \qquad (26)$$

$\hat{\phi}(x,t)$ is a fundamentally different object than the wavefunction $\psi(x,t)$.[1] It is a field operator. In our case let us consider it to be a scalar field. This field permeates all of space and time, and takes some value at each space-time coordinate. Space and time are now both parameters, and give a value to this field operator. The beauty of this field lies in it not only treating both space and time as parameters, but that it respects the speed of light through something known as the principle of locality[1]. Basically, the value of the field at two coordinates seperated by space-like distances must commute with each other. In addition to resolving issues with relativity, the field also explains some facts taken for granted in quantum mechanics, such as the idea of indistinguishable particles. What the field tells us, is that it is but one object, and what we call particles are just excitations of the field. Thus, two photons of the same frequency and polarization are indistinguishable, as they are both just completely equivalent excitations of the electromagnetic field. It makes as much sense to try and distiniguish two equivalent electric fields as to try and distiniguish two electrons, or photons, or any other indistinguishable particle.

[1] Steven Weinberg, *The Quantum Theory of Fields*. Cambridge University Press, Cambridge, 2013.
[2] Hong Liu, Spring 2014 8.323 P-Set 2, Problem 2
[3] Hsin-Chia Cheng, *A Bried Introduction to Relativistic Quantum Mechanics*. U.C. Davis
[4] Professor Hong Liu, April 7th, 2013 MIT
[5] http://www.phy.ohiou.edu/~elster/lectures/advqm_3.pdf
[6] Leonid Levitov, Spring 2012 8.322 P-Set 11 Problem 4
[7] Trung Van Phan, Solution to Spring 2012 8.322 P-Set 11 Problem 4
[8] The second quantization involves a procedure of several steps, one of which involves defining canonical commutation relations between the field operators in order to define the new field theory. See Peskin and Schroeder's text on Quantum Field Theory for a nice example of this procedure.

Semiclassical Quantization Methods

Amyas Chew
(Dated: May 2, 2014)

The correspondence principle requires that the predictions of quantum mechanics ultimately reduce to those of classical mechanics, in the limit of macroscopic systems. Now the behavior of quantum systems is already sufficiently described by the Schrodinger equation; however, by appealing to its expected classical behavior in the macroscopic limit, one can take advantage of the correspondence principle to calculate some properties of the system, in particular its energy spectrum. This paper seeks to explore a couple of important semiclassical approximation schemes that can be used to determine the energy states of a system, and demonstrates their applications to some familiar systems.

I. INTRODUCTION

What it often means to understand the behavior of a physical system is to have a model that allows one to accurately make predictions about the state of the system at a future time, given an initial state. In quantum systems, the state of the system comes in the form of a wavefunction $\psi(\mathbf{x}, t)$, whose behavior is modelled (at least in nonrelativistic situations) by the Scrödinger equation. Now the linearity of the Schrödinger equation in the state ψ is an extremely important feature, because it allows one to find a general solution by breaking the problem into easily solvable parts, solving each of these individually, then combining these solutions to obtain the overall solution. In practice, this is performed simply by solving for the eigensystem of the time-independent Schödinger equation, from which one can obtain the overall behavior from a given initial state as a sum of the (easily obtainable) time evolved values of its components in the eigenbasis.

In fact, even knowledge of just the eigenvalues alone provides plenty of useful information. The eigenvalues to the time-independent Schrödinger equation are the energy values of states that are almost stationary, evolving only an overall phase over time. Knowledge of the energy spectrum would allow one to make a variety of predictions about phenomena like the emission spectra, electrical conductivity and chemical properties of substances. Often, the energy eigenvalues are found by invoking the boundary conditions of a system, without having to solve for the corresponding eigenstates beforehand. This makes the process of solving for just the eigenvalues alone a key approach to analyzing quantum systems.

However, the straightforward procedure we have described for obtaining solutions from the eigensystem does not come for free; one must still pay for overcoming the complexity of solving for the behavior of quantum systems, except this time in finding the eigensystem itself. This can generally be very difficult for most quantum systems, especially those with multiple particles or a complicated Hamiltonian. Nevertheless, there are approximation techniques that can help one obtain a close estimate of the eigenvalue spectrum. If there are sufficient particles, one could use a stochastic approach [9] to obtain a

statistical description of their properties. If the Hamiltonian is different from that of a solvable system only by a slight correction, then perturbative methods could be used to find the eigensystem of the former in terms of corrections to that of the latter [6].

In this paper, we explore a class of approximation methods that apply to a different regime: relatively high energies and momenta. At the limit where typical energies overwhelm the energy eigenvalue spacings, and the de Broglie wavelengths of particles become very much smaller than the characteristic spatial dimensions of the system, the behavior of the system approaches that of localized classical particles with a continuous energy spectrum, as the correspondence principle requires. This allows one to motivate some useful assumptions, based on a classical intuition, that simplify the process of calculating[1] the eigensystem.

We divide these various quantization methods into two categories: the first consists of those that involve imposing constraints on the action or wavefunction of the system, according to the boundary conditions, that allow only specific orbits to be supported. The second consists of those that do not directly find the energy eigenvalues, but instead calculate the density of such energy states at a given energy level.

II. CONSTRAINT QUANTIZATION

The methods in this category involve the identification of energy values for which a solution to the Schrödinger equation, that also satisfies the boundary conditions, exists. In many cases, this is done while attempting to solve directly for the wavefunction. The classic example of a one-dimensional infinite square well has discrete energy levels that can be found by imposing the condition of a zero wavefunction at the endpoints. This required that

---

[1] We refer to these methods of determining the energy eigenvalue spectrum of a system as quantization methods, although they are really just part of a broader transition to a quantum description of the system.

the generic sinusoidal form of the wavefunction be found first. For other cases, solving for the generic form for the wavefunction might be too difficult to do analytically. Instead, a semiclassical approximation may be employed to obtain a simplified expression for the wavefunction, and the constraints are imposed as before.

Sometimes, one could further invoke the semiclassical approximation by considering that the eigenstate solutions would simulate periodic classical orbits, each with a defined action over a period. The boundary conditions can be translated into a constraint on the action, which one can impose directly to solve for the energy eigenvalues without having to find the wavefunctions first. The antiquated Bohr-Sommerfeld quantization of old quantum theory (where the action is simply assumed to be in multiples of $2\pi\hbar$) is one such method [2], but will not be discussed here because the WKB quantization serves as a more rigorous and adequately motivated generalization in its place.

A.   Semiclassical Approximation

The limit to classical energies and momenta is mathematically equivalent to taking the limit of $\hbar \to 0$, since $\hbar$ characterizes the energy level spacing and the de Broglie wavelengths of particles in a system. At the latter limit, the de Broglie wavelength $\lambda \sim \frac{\hbar}{p}$ becomes much smaller than the length scale over which the potential varies. This means that we may make the following ansatz that the wavefunction always retains a functional dependence locally like that of a plane wave travelling in the direction of the classical trajectory. This is of the form

$$\psi(\mathbf{x}, t) = A(\mathbf{x}, t) \exp\left(\frac{i}{\hbar} S(\mathbf{x}, t)\right) \qquad (1)$$

for phase $S(\mathbf{x}, t)$ and slowly varying amplitude $A(\mathbf{x}, t)$, both real valued. This is known as the Wentzel-Kramers-Brillouin (WKB) ansatz. Applying the Schrödinger equation for a potential $V(\mathbf{x})$,

$$i\hbar \frac{\partial}{\partial t} \psi(\mathbf{x}, t) = \left(-\frac{\hbar^2}{2m} \nabla^2 + V(\mathbf{x})\right) \psi(\mathbf{x}, t) \qquad (2)$$

and separating the real and imaginary parts, we eventually obtain the following coupled differential equations,

$$\frac{\partial S}{\partial t} + \frac{(\nabla S)^2}{2m} + \left(V - \frac{\hbar^2}{2m} \frac{\nabla^2 A}{A}\right) = 0 \qquad (3a)$$

$$\frac{\partial A^2}{\partial t} + \nabla \cdot \left(A^2 \left(\frac{1}{m} \nabla S\right)\right) = 0 \qquad (3b)$$

Eq (3a) is essentially a classical Hamilton-Jacobi equation where

- the Hamilton principle function is S, and

- the Hamiltonian is $H_{\text{eff}}(\mathbf{x}, \mathbf{p}) = \frac{\mathbf{p}^2}{2m} + V_{\text{eff}}(\mathbf{x}, t)$

where V_{eff} is V with an additional $-\frac{\hbar^2}{2m} \frac{\nabla^2 A}{A}$ correction known as the Bohmian or quantum potential. The $\nabla^2 A$ in the latter is small by our semiclassical assumption that A varies slowly, so we may neglect this correction altogether and solve the Hamilton-Jacobi equation for $H = \frac{\mathbf{p}^2}{2m} + V(\mathbf{x})$ as would classically be done. This is "classical" part of the name "semiclassical".

Since the phase $S(\mathbf{x}, t)$ is identified as the Hamilton principle function, we can identify $\mathbf{p} = \nabla S$ as the momentum. Then

$$\frac{dS(\mathbf{x}, t)}{dt} = \frac{\partial S(\mathbf{x}, t)}{\partial t} + \dot{\mathbf{x}} \cdot \nabla S(\mathbf{x}, t)$$
$$= -H(\mathbf{x}, \mathbf{p}) + \dot{\mathbf{x}} \cdot \mathbf{p} = L(\mathbf{x}, \dot{\mathbf{x}}) \qquad (4)$$

is the Lagrangian, so we can identify S as the action $\int L \, dt$.

B.   Density Flow

We now turn our attention to eq (3b), which one might notice to be in the form of a continuity equation for a flow with "density" A^2 and "velocity field" $\frac{1}{m} \nabla S$. If we interpret A as a probability amplitude density and $\frac{1}{m} \nabla S$ as a velocity field, then indeed, A^2 would be a probability density, while $A^2 \left(\frac{1}{m} \nabla S\right)$ would be a probability current. Since this flow is incompressible, the enclosed probability in a region V_0 at time $t = 0$ is conserved as the region flows over a time t into a new region V, or

$$\int_{V_0} A(\mathbf{x}_0, 0)^2 \, d^n x_0 = \int_V A(\mathbf{x}, t)^2 \, d^n x$$
$$= \int_{V_0} A(\mathbf{x}, t)^2 \det\left(\mathbf{J}(\mathbf{x}, \mathbf{x}_0, t)\right) \, d^n x_0 \quad (5)$$

where n is the number of spatial dimensions and $\mathbf{J}(\mathbf{x}, \mathbf{x}_0, t)$ is the Jacobian matrix with (i, j)-th element $\frac{\partial x_i(\mathbf{x}_0, t)}{\partial (x_0)_j}$, encoding information about the classical trajectory $\mathbf{x}(\mathbf{x}_0, t)$ following the velocity field $\frac{1}{m} \nabla S$ from each initial point $\mathbf{x}_0$. Since the equation holds for any V_0, we may conclude that

$$A(\mathbf{x}, t) = \frac{1}{\sqrt{\det\left(\mathbf{J}(\mathbf{x}, \mathbf{x}_0, t)\right)}} A(\mathbf{x}_0, 0) \qquad (6)$$

Now in many systems, for a given energy there may be regions where the potential rises above this value. These regions are classically forbidden, so the classical trajectories will have turning points at their boundaries. This introduces a few issues:

- A collection of neighboring trajectories forms a manifold embedded in space. When the manifold encounters the boundary of a classically forbidden region, the trajectories turn away, leading to a "fold" in the manifold. This changes

the orientation of the manifold, which effectively leads to a sign change in the Jacobian determinant $\det\left(\mathbf{J}(\mathbf{x}, \mathbf{x}_0, t)\right)$.

- The turning of a classical trajectory, possibly back over itself, would produce points associated with multiple velocities depending on how far along the trajectory the particle has gone. The $\frac{1}{m}\nabla S$ ceases to be a (single-valued) velocity field.

To account for these issues, a few modifications have to be made to the solution in eq (6). Firstly, it is helpful to show the sign change of the Jacobian determinant explicitly, by introducing an extra phase $\exp\left(-\frac{i\pi}{2}\nu(\mathbf{x}_0, t)\right)$, where $\nu(\mathbf{x}_0, t)$ is the Maslov index, or the number of folds (and thus sign changes to the Jacobian determinant) throughout the trajectory from the initial point $\mathbf{x}_0$.

Secondly, for each point $\mathbf{x}$ and time t, there may be multiple initial points $\mathbf{x}_0$ that have trajectories leading from them to $\mathbf{x}$ in time t. The contributions from all these amplitudes superpose to form the overall amplitude A, so we must sum over all these contributions. This gives us

$$A(\mathbf{x}, t) = \sum_k \frac{\exp\left(-\frac{i\pi}{2}\nu\left(\mathbf{x}, \mathbf{x}_0^{(k)}, t\right)\right)}{\sqrt{\left|\det\left(\mathbf{J}\left(\mathbf{x}, \mathbf{x}_0^{(k)}, t\right)\right)\right|}} A\left(\mathbf{x}_0^{(k)}, 0\right) \quad (7)$$

where k indexes all initial points $\mathbf{x}_0^{(k)}$ that have a classical trajectory to $\mathbf{x}$ in time t.

C. WKB Approximation in 1D

The classical trajectories for a multidimensional system are in general very difficult to compute, so to illustrate the application of the methods discussed, we focus our study on one-dimensional systems. We first solve the Hamiltonian-Jacobi equations that we obtained earlier at eq (3a). If the Hamiltonian is not explicitly time-dependent, we may separate out time-dependence in the Hamilton-Jacobi equation by letting

$$S(x, t) = W(x) - Et \quad (8)$$

for some constant E, which turns out to be the energy. Then by the discussed approximation of eqn (3a) neglecting the Bohmian correction,

$$E = -\frac{\partial S}{\partial t} = \frac{1}{2m}\left(\frac{\partial S}{\partial x}\right)^2 + V$$

$$\implies p(x) = \frac{\partial S}{\partial x} = \sqrt{2m(E - V(x))} \quad (9)$$

so we can solve for

$$S(x, t) = \int_{x_0}^x p(x')\, dx' - Et$$

$$= \int_{x_0}^x \sqrt{2m(E - V(x'))}\, dx' - Et \quad (10)$$

Given that the velocity field is $\frac{1}{m}\frac{\partial S}{\partial x} = \frac{p(x)}{m}$, one can show that the Jacobian determinant is $\frac{\partial x}{\partial x_0} = \frac{p(x)}{p(x_0)}$, so combining eqs (1), (7) and (10), one obtains the overall wavefunction for an energy eigenstate

$$\psi(x, t) = \sum_k A_0^{(k)} \sqrt{\left|\frac{p\left(x_0^{(k)}\right)}{p(x)}\right|}$$

$$\times \exp\left(i\Phi^{(k)}(x) - \frac{i\pi}{2}\nu^{(k)}(x, t) - \frac{iEt}{\hbar}\right) \quad (11)$$

where we have used the abbreviations $A_0^{(k)} = A\left(x_0^{(k)}, 0\right)$, $\Phi^{(k)}(x) = \frac{1}{\hbar}\int_{x_0^{(k)}}^x p(x')\, dx'$, and $\nu^{(k)}(x, t) = \nu\left(x, x_0^{(k)}, t\right)$. As intended, this approximates the behavior of a classical trajectory, which for bound states in one dimension can only be that of a particle bouncing back and forth. By invoking the periodicity condition of the wavefunction over one cycle of the trajectory, one obtains

$$\frac{i}{\hbar}\oint p(x')\, dx' - \frac{i\pi\nu_c}{2} = 2in\pi$$

where ν_c is the Maslov index over a cycle, so the action over a cycle is constrained to be

$$I = \oint p(x')\, dx' = \left(2n + \frac{\nu_c}{2}\right)\pi\hbar \quad (12)$$

1. Example: 1D harmonic oscillator

The one-dimensional harmonic oscillator with Hamiltonian $H = \frac{p^2}{2m} + \frac{1}{2}m\omega^2 x^2$ is a simple example of a system where trajectories are bound by $\nu_c = 2$ classical turning points. Letting $x_0 = \sqrt{\frac{2E}{m\omega^2}}$, and invoking the constraint in eq (12) on the action,

$$I = \oint p(x)\, dx = 4m\omega \int_0^{x_0} \sqrt{x_0^2 - x^2}\, dx$$

$$= \pi m\omega x_0^2 = \frac{2\pi E}{\omega} = (2n + 1)\pi\hbar$$

$$\implies E = \left(n + \frac{1}{2}\right)\hbar\omega$$

which is the exact solution. In effect, each classical turning point contributes to a $\frac{\pi}{4}$ phase shift, which is as expected from a calculation using the Airy function solutions of approximately linear potentials to derive connection formulas across a smooth turning point [6].

III. DENSITY QUANTIZATION

The next category of quantization methods do not provide an expression of the energy eigenvalues of a system in terms of an index, but instead the distribution of the

energy spectrum in the energy representation. This is still useful since the semiclassical approximation applies in situations where the energies are already much greater than the energy level separation, so the energy level density is a more practical way to encode information about the energy spectrum of the system.

We first begin by an overview of how the energy level density may in principle be obtained without any approximations, by finding the trace of a Green's function. The semiclassical approximation may then be invoked and the procedure repeated to obtain an expression of the energy level density with the approximation built into it. It turns out that the expression depends just on the classical periodic orbits of the system, so knowledge of the classical behavior of the system can actually be used to predict its quantum properties.

A. Preliminaries

Consider a system with time-independent nondegenerate Hamiltonian $\hat{H}$, and let $\{|n\rangle\}$ be its complete, orthonormal eigenbasis. This means that $\hat{H}|n\rangle = E_n|n\rangle$ for each n, where $\langle n|m\rangle = \delta_{nm}$, and $\sum_n |n\rangle\langle n| = \mathbf{1}$. In general the time evolution of any wavefunction is controlled by the Schrödinger equation

$$i\hbar\partial_t |\psi(t)\rangle = \hat{H}|\psi(t)\rangle, \qquad (13)$$

so it can then be expressed in terms of its initial state $|\psi(0)\rangle$ as

$$
\begin{aligned}
|\psi(t)\rangle &= \exp\left(-\frac{i\hat{H}t}{\hbar}\right)\left(\sum_n |n\rangle\langle n|\right)|\psi(0)\rangle \\
&= \left(\sum_n \exp\left(-\frac{iE_n t}{\hbar}\right)|n\rangle\langle n|\right)|\psi(0)\rangle \\
&= \hat{U}(t)|\psi(0)\rangle
\end{aligned}
\qquad (14)
$$

for time evolution operator $\hat{U}(t)$ on the second line in parentheses. Taking its Fourier transform over $t \geq 0$ into the energy representation, we obtain (for $E \in \mathbb{R}$)

$$
\begin{aligned}
\hat{G}(E) &= -\frac{i}{\hbar}\int_0^\infty \hat{U}(t)\exp\left(\frac{iEt}{\hbar}\right)dt \\
&= \sum_n |n\rangle\langle n|\int_0^\infty -\frac{i}{\hbar}\exp\left(\frac{i(E-E_n)t}{\hbar}\right)dt
\end{aligned}
$$

This is not a generally convergent integral, but we can evaluate it in the upper half of the complex plane, obtaining at $\tilde{E} = E + i\epsilon$ (with $0 < \epsilon \in \mathbb{R}$),

$$
\begin{aligned}
\hat{G}(\tilde{E}) &= \sum_n |n\rangle\langle n|\left[-\frac{\exp\left(i(E-E_n+i\epsilon)t/\hbar\right)}{E-E_n+i\epsilon}\right]_0^\infty \\
&= \sum_n \frac{|n\rangle\langle n|}{E-E_n+i\epsilon}
\end{aligned}
\qquad (15)
$$

which is known as the Green's function for the operator $\tilde{E} - \hat{H}$, because

$$\left(\tilde{E}-\hat{H}\right)\hat{G}(\tilde{E}) = \sum_n \frac{(\tilde{E}-E_n)|n\rangle}{\tilde{E}-E_n}\langle n| = \mathbf{1} \qquad (16)$$

Now we note the fact that

$$
\begin{aligned}
\lim_{\epsilon\to 0^+}\int_{x_1}^{x_2}\frac{dx}{x-x'+i\epsilon} &= \frac{1}{2}\oint_\Gamma \frac{dz}{z-x'} \\
&= -\pi i\int_{x_1}^{x_2}\delta(x-x')\,dx
\end{aligned}
$$

for any $x_1, x_2 \in \mathbb{R}$, where Γ is a rectangle in the complex plane cutting the real axis upwards at x_1 and downwards at x_2. Using this, we can find the density of energy eigenstates, expressed as

$$
\begin{aligned}
\mathcal{D}(E) &= \sum_n \delta(E-E_n) = \frac{i}{\pi}\lim_{\epsilon\to 0^+}\left(\sum_n \frac{1}{E-E_n+i\epsilon}\right) \\
&= \frac{i}{\pi}\lim_{\epsilon\to 0^+}\left(\operatorname{tr}\hat{G}(E+i\epsilon)\right)
\end{aligned}
\qquad (17)
$$

in terms of the trace of the Green's function, since $\operatorname{tr}(|n\rangle\langle n|) = 1$ for each n.

B. Semiclassical Approximation

Consider the following matrix element of the time evolution operator in the position eigenbasis

$$
\begin{aligned}
K(\mathbf{x},\mathbf{x}_1,t) &= \langle\mathbf{x}|\hat{U}(t)|\mathbf{x}_1\rangle \\
&= \sum_n \exp\left(-\frac{iE_n t}{\hbar}\right)\psi_n(\mathbf{x},0)\psi_n^*(\mathbf{x}_1,0)
\end{aligned}
\qquad (18)
$$

where $\psi_n(\mathbf{x},t)$ is the wavefunction of the nth eigenstate. This can be interpreted as the probability amplitude density that a particle localized at an initial position $\mathbf{x}_1$ could travel in time t to the current location $\mathbf{x}$, and is referred to as the quantum mechanical *propagator*, because the position eigenstates form a complete basis, so the wavefunction after time t of any state with initial wavefunction $\psi(\mathbf{x}_1,0)$ is

$$\psi(\mathbf{x},t) = \int K(\mathbf{x},\mathbf{x}_1,t)\psi(\mathbf{x}_1,0)\,d^n x_1 \qquad (19)$$

in analogy to eq (14). The derivation of $\mathcal{D}(E)$ in the previous section could have been expressed in terms of the propagator rather than the time evolution operator, if we had simply written each equation in terms of their matrix elements in the position eigenbasis (or equivalently, written the states as wavefunctions $\psi(\mathbf{x},t)$ rather than as kets $|\psi\rangle$).

Now we note that since $i\hbar\partial_t\hat{U}(t) = \hat{H}\hat{U}(t)$,

$$i\hbar\frac{\partial}{\partial t}K(\mathbf{x},\mathbf{x}_1,t) = \langle\mathbf{x}|\,i\hbar\partial_t U(t)\,|\mathbf{x}_1\rangle = \langle\mathbf{x}|\,\hat{H}U(t)\,|\mathbf{x}_1\rangle$$
$$= \left(-\frac{\hbar^2}{2m}\nabla_x^2 + V(\mathbf{x})\right)K(\mathbf{x},\mathbf{x}_1,t)$$

and so $K(\mathbf{x},\mathbf{x}_1,t)$ satisfies the Schrödinger equation as well. But this means that we may apply the semiclassical approximation via a similar technique as before, expressing the propagator as

$$K_s(\mathbf{x},\mathbf{x}_1,t) = A(\mathbf{x},\mathbf{x}_1,t)\exp\left(\frac{i}{\hbar}S(\mathbf{x},\mathbf{x}_1,t)\right). \quad (20)$$

However, we must first be careful to distinguish the position variable $\mathbf{x}_1$ of the initial wavefunction $\psi(\mathbf{x}_1,0)$ that the propagator integrates over all space in eq (19), from the initial position $\mathbf{x}_0^{(k)}$ of each classical trajectory that is summed over in eq (7). When applying the results of eq (7) here, one must keep in mind that the sum over classical trajectories is no longer a sum over their initial positions $\mathbf{x}_0^{(k)}$, since we are considering only trajectories that begin at $\mathbf{x}_1$. Instead, it is now a sum over their initial momenta $\mathbf{p}_0^{(k)}$.

Hence, the Jacobian matrix in eq (7) has to be replaced by $\mathbf{J}_p(\mathbf{x},\mathbf{x}_1,\mathbf{p}_0,t)$ with (i,j)-th element $\frac{\partial x_i(\mathbf{x}_1,\mathbf{p}_0,t)}{\partial(p_0)_j}$. The propagator is then

$$K_s(\mathbf{x},\mathbf{x}_1,t) =$$
$$\sum_k A_0^{(k)}\frac{\exp\left(\frac{i}{\hbar}S(\mathbf{x},\mathbf{x}_1,t) - \frac{i\pi}{2}\nu^{(k)}(\mathbf{x},\mathbf{x}_1,t)\right)}{\sqrt{\left|\det\left(\mathbf{J}_p\left(\mathbf{x},\mathbf{x}_1,\mathbf{p}_0^{(k)},t\right)\right)\right|}} \quad (21)$$

where we use the abbreviations $A_0^{(k)} = A^{(k)}(\mathbf{x},\mathbf{x}_1,0)$ and $\nu^{(k)}(\mathbf{x},\mathbf{x}_1,t) = \nu\left(\mathbf{x},\mathbf{x}_1,\mathbf{p}_0^{(k)},t\right)$.

Now for very short intervals of time where $t\to 0$, one can regard the velocity field as uniform so

$$\frac{\mathbf{p}}{m} = \frac{1}{m}\nabla_x S \approx \frac{\mathbf{x}-\mathbf{x}_1}{t} \implies S(\mathbf{x},\mathbf{x}_1,t) \approx \frac{m(\mathbf{x}-\mathbf{x}_1)^2}{2t}$$

and

$$\mathbf{p}_1 \approx \nabla_{x_1}\left(\frac{\mathbf{x}-\mathbf{x}_1}{t}\right) = -\nabla_x\left(\frac{\mathbf{x}-\mathbf{x}_1}{t}\right) \approx -\mathbf{p}$$
$$\implies \frac{\partial x_i}{\partial(p_1)_j} = -\frac{\partial x_i}{\partial p_j} = -\frac{t}{m}\delta_{ij}.$$

We may also assume in the limit $t\to 0$ that there is only a single trajectory to consider, since the chance of trajectories overlapping in a fold should vanish. Then for n spatial dimensions,

$$K_s(\mathbf{x},\mathbf{x}_0,t) \to \frac{A(\mathbf{x},\mathbf{x}_0,0)}{\sqrt{\left|\left(-\frac{t}{m}\right)^n\right|}}\exp\left(\frac{im(\mathbf{x}-\mathbf{x}_0)^2}{2\hbar t}\right) \quad (22)$$

which is the form of a gaussian with width $\sigma^2 = -\frac{\hbar t}{im}$. In this limit, the time evolution operator $\hat{U}(t)\to 1$ so the propagator should approximate $\langle\mathbf{x}|\mathbf{x}_1\rangle = \delta(\mathbf{x}-\mathbf{x}_1)$. This means that we must normalize the propagator, by setting the constant

$$A(\mathbf{x},\mathbf{x}_0,0) = \left(\frac{1}{2\pi i\hbar}\right)^{\frac{n}{2}}$$

so that

$$K_s(\mathbf{x},\mathbf{x}_1,t) =$$
$$\sum_k\left(\frac{1}{2\pi i\hbar}\right)^{\frac{n}{2}}\frac{\exp\left(\frac{i}{\hbar}S(\mathbf{x},\mathbf{x}_1,t) - \frac{i\pi}{2}\nu^{(k)}(\mathbf{x},\mathbf{x}_1,t)\right)}{\sqrt{\left|\det\left(\mathbf{J}_p\left(\mathbf{x},\mathbf{x}_1,\mathbf{p}_0^{(k)},t\right)\right)\right|}}. \quad (23)$$

This is known as the semiclassical or Van-Vleck propagator. If one has knowledge about the classical trajectories permitted by the system, then one could use this to make predictions about the time evolution of any given wavefunction via eq (19).

The process of obtaining a Green's function for the Van-Vleck propagator and then computing a formula for its trace is rather involved, and will not be explored in this paper. However, the key ideas can already be seen through the analogous steps for the exact case. The final Gutzwiller trace formula, from which the density of states $\mathcal{D}(E)$ can be obtained via eq (17), is expressed in terms of a sum over the classical periodic orbits of the system, as has been encountered numerous times above.

Interestingly, there are alternative ways of deriving the trace formula. Gutzwiller himself first used the Feynman integral formulation [8], and there have been proofs of it using coherent states [10].

IV.   DISCUSSION

We have explored two main approaches in implementing a semiclassical approximation in the process of solving for the energy eigenvalues of a quantum system. The methods which provide constraints on the action provide the conceptual simplicity that was found in the rough quantization methods of old quantum theory, where one could still be rather successful in making predictions about the spectra in systems like the hydrogen atom, with very simple calculations.

On the other hand, the density quantization methods take much more work to derive, but they provide an important insight into the link between the quantum and classical realms. By expressing the quantum energy levels of a system in terms of its classical orbits, they provide a heuristic way to understand the behavior of a quantum system without having to first persist through the tedium of solving the Schrödinger equation directly. This means

that our classical intuitions are not worthless after all, we just need to be careful about how we apply them.

The methods described above do not provide a description for a completely general physical system, because we have made many assumptions like non-degeneracy or integrability of the classical trajectories. There are modifications [2] to these methods that improve their generality, including even some that make a connection with the zeros of the Riemann zeta function. Nevertheless, it must also be noted that even though the semiclassical approximation methods presented here may give the impression of "simplifying" quantum systems by a reduction to classical problems, the complexity in studying quantum systems does not just go away, because the problem of solving for classical trajectories can be an extremely difficult one by itself, especially in systems that display chaotic behavior.

In practice, semiclassical methods still serve as one of a range of types of approximation tools that can be used in solving otherwise intractable quantum systems. As with any tool, it is up to the user's discernment on the right situation to use it.

[1] M. Lübcke, *Gutzwiller Trace Formula and Applications* (University of Uppsala, 2001).

[2] M. Brack and R. Bhaduri, "Semiclassical Physics" (Addison-Wesley, 1997).

[3] P. Cvitanovic *et al*, "Classical and Quantum Chaos", v9.2.3 (2002).

[4] H.J. Stöckmann, "Quantum Chaos: An Introduction" (Cambridge University Press 1999).

[5] F. Haake, "Quantum Signatures of Chaos" (3rd edition, Springer, Heidelberg 2010).

[6] D.J. Griffiths, "Introduction to Quantum Mechanics" (Prentice Hall Inc, NJ 1995).

[7] H. Goldstein *et al*, "Classical Mechanics" (3rd edition, Addison Wesley, 2001).

[8] M.C. Gutzwiller, Journal of Mathematical Phyics **12**, 343 (1971).

[9] C.H. Lewenkopf and H.A. Weidenmüller, Annals of Physics **212**, 53 (1991).

[10] M. Combescure *et al*, Communications in Mathematical Physics **202** 463 (1999).

Pseudospin in Graphene

Sang Hyun Choi

MIT Department of Physics, 77 Massachusetts Ave., Cambridge, MA 02139

(Dated: May 2, 2014)

Graphene is a one atom thick monolayer of graphite and is an important research topic in the field of condensed matter physics. The carbons in graphene form sp^2 hybridized bonds, which lead to a hexagonal honeycomb lattice structure. The honeycomb lattice structure contains two sublattice structures, which give rise to an additional spin-like degree of freedom, pseudospin. Because of pseudospin, the energy-momentum relation for graphene is linear, which is characteristic of relativistic systems. We see that charge carriers in graphene indeed behave like massless relativistic particles. As an example of relativistic quantum phenomena, we discuss Klein tunneling in graphene.

I. INTRODUCTION

Graphene is a monolayer of graphite with a two-dimensional (2D) honeycomb lattice. For a long time, physicists believed that 2D crystal structures did not exist because it would be thermodynamically unstable [1][2]. Graphene was thought to be only a theoretical material. However, in 2004, graphene was experimentally proven to stably exist and since then, many physicists and engineers have done research on interesting properties of this material [3]. Many interesting properties of graphene are due to its honeycomb structure. This structure gives rise to the linear relation between energy and momentum, as in relativistic systems [4]. In this paper, we will explore the structure of graphene in more detail and derive its Dirac-like Hamiltonian and energy-momentum dispersion relation. We will show how graphene's structure gives rise to one of its unusual properties, pseudospin. As an example of the consequences of pseudospin, we then discuss Klein tunneling.

II. STRUCTURE OF GRAPHENE

A. Chemical Structure

Carbons in graphene form sp^2 hybridization between one s orbital and two p orbitals, which leads to the formation of a trigonal planar structure [5]. This generates a hexagonal honeycomb structure as a whole as shown in Figure 1. The remaining p orbital, which we label as p_z, is perpendicular to the plane formed by the sp^2 bonds. While the electrons forming sp^2 bonds are bound to keep the hexagonal structure, those in the p_z orbital are relatively free to move around and form π band with neighboring carbon atoms [5]. It is the electrons in the p_z orbital that lead to overlapping of orbitals and electron hopping.

B. Sublattice Structure

As we discussed, the crystal structure of graphene forms repetitions of hexagons. In crystalline solids, the periodically repeated identical groups of atoms are called bases, and the set of points attached to the basis is called the lattice [6]. Thus, graphene has a honeycomb lattice structure.
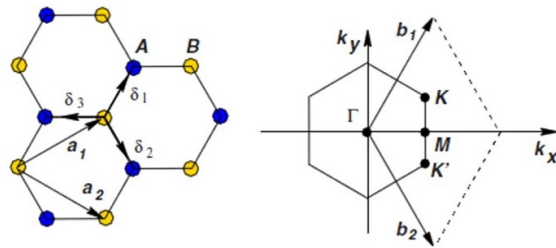
FIG. 1: The honeycomb lattice of graphene (left) and its first Brillouin zone (right). Blue and yellow color in the left figure indicate the two different sublattices, labeled as A and B. In the Brillouin zone, the vertices of the hexagon are named K and K' points alternatively, and the center of the hexagon is called Γ point. This figure is taken from Castro Neto et al. (2009) [5].

The honeycomb lattice structure has two different bases. We indicate a relative coordinate from each starting yellow or blue point with a two-dimensional vector (x, y). All yellow points are connected to their nearest neighbors in the $(-1, 0)$, $(1/2, \sqrt{3}/2)$ and $(1/2, -\sqrt{3}/2)$ directions while all blue points are connected to their nearest neighbors in the $(1, 0)$, $(-1/2, \sqrt{3}/2)$ and $(-1/2, -\sqrt{3}/2)$ directions. Therefore, the yellow points are indistinguishable from each other, but they are distinguishable from blue points. In other words, translating the system between yellow points will not change the system. Whereas translating from a yellow point to a blue point will change the system because how the points are connected to the neighbors is different. We can visualize two distinct lattice structures within a bigger structure; yellow vertices of the hexagons are said to form a sublattice structure and blue vertices form another sublattice structure. As indicated in Figure 1, we refer to the sublattice of blue points as sublattice A and the sublattice of yellow points as sublattice B.

A primitive unit cell is defined as the smallest unit that fills up the space without overlapping the neighbor-

ing primitive unit cells and without any voids [7]. The primitive unit cell of graphene contains one lattice point from sublattice A and one from sublattice B. Therefore, electronic states in graphene have components belonging to two sublattices. An index indicating sublattices A and B becomes necessary. This index, or an additional degree of freedom, is analogous to the spin up and spin down index and is therefore referred to as pseudospin [4], which we will discuss in more detail in Section III.

C. The Reciprocal Lattice

We have thusfar examined the structure of graphene in real space. It is often more useful to represent the structure in momentum space, or k-space, because this leads to the derivation of the energy-momentum relation. The transformation from real space to k-space is through the Fourier transform [6].

The reciprocal lattice is a counterpart of the lattice in real space, or the direct lattice. It is a set of wave vectors that satisfy the mathematical relation $e^{i\vec{K}\cdot(\vec{r}+\vec{R})} = e^{i\vec{K}\cdot\vec{r}}$, where $\vec{K}$ are wave vectors in the reciprocal lattice, $\vec{r}$ is any position in real space and $\vec{R}$ is a point in the direct lattice [7]. A lattice is spanned by primitive vectors. From the relation between the reciprocal and direct lattices, primitive vectors that span the reciprocal lattice are calculated from those that span the direct lattice. In Figure 1, $\vec{b_i}$ is the primitive vector for the reciprocal lattice while $\vec{a_i}$ is the primitive vector for the direct lattice. Linear combination of primitive vectors forms the lattice vector and the reciprocal lattice vector.

The Wigner-Seitz primitive cell of a lattice point is the region of space that is closer to that point than to any other lattice point [7]. One can get Wigner-Seitz cell by bisecting the lines connecting the point in which we are interested with its nearest neighbors. The first Brillouin zone (BZ) is defined as the Wigner-Seitz primitive cell of the reciprocal lattice. There are higher-order Brillouin zones, but we need only the first for our purpose. As shown in Figure 1, BZ of a hexagonal lattice is also hexagonal. Since sublattice A and sublattice B are not equivalent, K point and K' point in BZ are not equivalent for the same reason and thus labeled separately. K and K' points are also called Dirac points for the reason that will be discussed in Section III.

III. DIRAC-LIKE HAMILTONIAN

We will now derive pseudospin more rigorously by using the tight-binding approximation for graphene. The tight-binding method used in this section follows steps from McCann (2012) [8] and Castro Neto et al. (2009) [5].

A. Bloch's Theorem

In solids like graphene, electrons are under a periodic potential, which can be expressed as $U(\vec{r} + \vec{R}) = U(\vec{r})$. Bloch's theorem states that the eigenstates of such a system can be chosen to have a form $\psi_{n,\vec{k}}(\vec{r}) = e^{i\vec{k}\cdot\vec{r}}u_{n,\vec{k}}(\vec{r})$, where $u_{n,\vec{k}}(\vec{r} + \vec{R}) = u_{n,\vec{k}}(\vec{r})$ and the eigenstates are labeled by both energy level n and wave vector $\vec{k}$ [7]. This implies that

$$\psi_{n,\vec{k}}(\vec{r} + \vec{R}) = e^{i\vec{k}\cdot\vec{r}}\psi_{n,\vec{k}}(\vec{r}) \tag{1}$$

$\psi_{n,\vec{k}}(\vec{r})$ is called a Bloch function or a Bloch wave. We assume that eigenstates of graphene have this form.

B. The Tight-binding Approximation

When atoms are closely packed together, their atomic orbital overlaps and the energy levels are affected by the overlap. Therefore, corrections to the Hamiltonian are needed, and the tight-binding method is one widely used approximation. The wave function is approximated as the superposition of wave functions of isolated atoms. As its name suggests, the tight-binding approximation is used for a tightly bound system of atoms in a solid where interaction between the states is limited to nearby atoms. Therefore, the resulting wave function is similar to that of an isolated atom [7]. Here the periodic potential is approximated as the potential energy between the nucleus of a fixed atom of the solid and an incoming electron.

Since we are dealing with a periodic potential, by Bloch's theorem, Bloch functions are used as the eigenstates. Then the wave function is expressed as the superposition of such eigenstates. Each entry of the Hamiltonian represents the transition or 'hopping' of electrons from one lattice point to another. The diagonal entries of the Hamiltonian show the hopping within the same sublattice while the off-diagonal entries show the hopping between different sublattices. By using the tight-binding approximation, we will derive the form of Hamiltonian of graphene and verify the energy dispersion relation.

C. The Tight-binding Approximation for Graphene

By Bloch's theorem, the wave function ψ_A at sublattice A can be expressed as

$$\psi_A = \frac{1}{\sqrt{N}} \sum_{i=1}^{N} e^{i\vec{k}\cdot\vec{R}_{A,i}} \phi_A(\vec{r} - \vec{R}_{A,i}) \tag{2}$$

where $\vec{r}$ is the position, $\vec{R}_{A,i}$ is the position of the orbital in sublattice A of the ith unit cell, and $\vec{k}$ is the wave vector. This system is assumed to have N unit cells. The wave function at sublattice B is identical to Eq 2

except that the index of sublattice is B instead of A. Here, as mentioned earlier, electrons that are likely to interact with neighboring electrons are in the $2p_z$ orbital. Therefore, we consider only this orbital.

The diagonal entry of the Hamiltonian $H_{AA} = \langle \psi_A | H | \psi_A \rangle$ is expressed as

$$H_{AA} = \frac{1}{N} \sum_{i=1}^{N} \sum_{j=1}^{N} e^{i\vec{k} \cdot (\vec{R}_{A,j} - \vec{R}_{A,i})}$$
$$\times \left\langle \phi_A(\vec{r} - \vec{R}_{A,i}) \middle| H \middle| \phi_A(\vec{r} - \vec{R}_{A,j}) \right\rangle \quad (3)$$

H_{BB} can also be expressed in the same way. We can assume that the dominant term is when $i = j$ since it is difficult to hop to a far lattice point, for example from a yellow vertex to another yellow vertex in Figure 1 [8]. Then Eq 3 is simplified to have only i as the index of summation. Defining $\epsilon \equiv \left\langle \phi_A(\vec{r} - \vec{R}_{A,i}) \middle| H \middle| \phi_A(\vec{r} - \vec{R}_{A,i}) \right\rangle$, we find $H_{AA} \approx \epsilon$, which is independent of lattice points. This result was predictable since the lattice points within the same sublattice are indistinguishable from each other. Moreover, $H_{AA} = H_{BB}$ since the structure of sublattice B is the same as the structure of sublattice A, except that it is rotated [8].

In a similar way, the off-diagonal term of the Hamiltonian is obtained. The off-diagonal term describes the hopping between the two different sublattices such as from sublattice A to sublattice B. Replacing $\vec{R}_{A,j}$ with $\vec{R}_{B,j}$ and $|\phi_A\rangle$ with $|\phi_B\rangle$ in Eq 3 gives the expression for the off-diagonal entry H_{AB}. In this case, the expression is simplified as j goes from 1 to 3, instead of from 1 to N since it is highly unlikely to observe hopping of an electron to a point farther than its nearest neighbors, and there are three nearest neighbors to each point, as shown in Figure 1. We define $-t \equiv \left\langle \phi_A(\vec{r} - \vec{R}_{A,i}) \middle| H \middle| \phi_B(\vec{r} - \vec{R}_{B,j}) \right\rangle$, where $t > 0$. The evaluated value is defined as $-t$ since the potential energy is negative and thus the whole integral is negative. Also, the phase difference $\vec{R}_{B,j} - \vec{R}_{A,i}$ in the expression for the off-diagonal entry of Hamiltonian indicates the vector from each point to its neighbor, which is δ_j in Figure 1 where $j = 1, 2, 3$. Then the off-diagonal term is simplified as $H_{AB} \approx -\frac{t}{N} \sum_{i=1}^{N} \sum_{j=1}^{3} e^{i\vec{k} \cdot \vec{\delta}_j}$.

By defining $f(\vec{k}) \equiv \sum_{j=1}^{3} e^{i\vec{k} \cdot \vec{\delta}_j}$, it is further simplified as $H_{AB} \approx -tf(\vec{k})$. From Figure 1, we know that

$$\vec{\delta_1} = \frac{a}{2}(1, \sqrt{3}), \ \vec{\delta_2} = \frac{a}{2}(1, -\sqrt{3}), \ \vec{\delta_3} = -a(1, 0) \quad (4)$$

setting the lattice point as the origin, where a is the carbon-carbon distance, or the distance between two connected yellow and blue points in Figure 1. By substituting Eq 4 to the definition of $f(\vec{k})$, we get the value of $f(\vec{k})$ and thus H_{AB} and H_{BA}.

Collecting the diagonal terms and the off-diagonal terms, the Hamiltonian of the system is expressed as

$$H = \begin{pmatrix} \epsilon & -tf(\vec{k}) \\ -tf^*(\vec{k}) & \epsilon \end{pmatrix} \quad (5)$$

Solving the eigenvalue problem for Eq 5 gives the energies

$$E_\pm = \epsilon \pm t|f(\vec{k})| \quad (6)$$

Figure 2 is the plot of Eq 6 as a function of $\vec{k}$. The diagonal terms of Hamiltonian are taken to be zero since they are constant. As there are two values of energies (Eq 6), the plot shows two layers of energies. This range of energies where electron orbitals can exist is called a band structure. The conduction band is the upper energy in the band structure, and the valence band is the lower energy [6]. The distance between the conduction band and the valence band is called a gap, and metals usually have a nonzero gap between the bands. However, as shown in Figure 2, the band structure of graphene does not have a gap.

This plot has actually taken into account the hopping to not only the nearest neighbors but also the next nearest neighbors [5]. However, near the point where two bands meet, which is called the Dirac point, our approximation of only considering the hopping to the nearest neighbors is valid, and this is the regime where we are interested in.
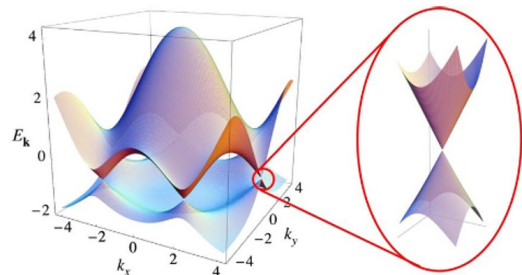
FIG. 2: The band structure of graphene. It is gapless and conical near the Dirac points. This figure is taken from Castro Neto et al. (2009) [5].

Note that as shown in the zoomed figure in Figure 2, near the Dirac point, the band structure is conical. This reflects the linear dispersion relation between energy and momentum, which is discussed more in the next section.

D.   Energy at the vicinity of K point

As shown in Figure 3, two bands of graphene meet at K points and K' points of BZ of graphene. The position of K and K' points in k-space are

$$\vec{K} = (\frac{2\pi}{3a}, \frac{2\pi}{3\sqrt{3}a}), \ \ \vec{K'} = (\frac{2\pi}{3a}, -\frac{2\pi}{3\sqrt{3}a}) \quad (7)$$

Using the definition of $f(\vec{k})$ and Eq 4, we can check that $|f(\vec{K})| = 0$. Thus both $E_\pm(\vec{K}) = \epsilon = 0$ as expected in Figure 2.

If $\vec{k} \neq \vec{K}$, but $\vec{k} \approx \vec{K}$, then $\vec{k} = \vec{K} + \vec{q}$ where $|\vec{q}| \ll |\vec{K}|$. We rewrite our expression in terms of $\vec{q}$, so $f(\vec{q}) \approx -\frac{3a}{2}(q_x - iq_y)$. Thus the Hamiltonian for hopping
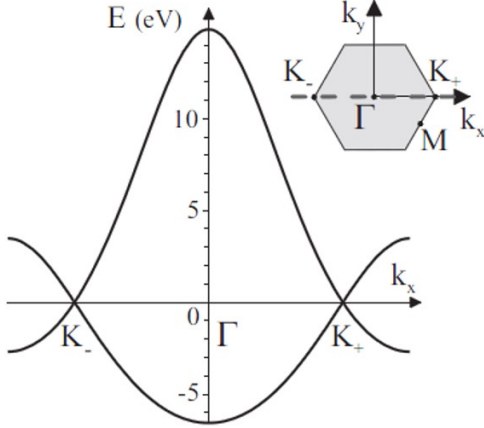
FIG. 3: The band structure and Brillouin zone of graphene. Two bands meet at K and K' points, or Dirac points. This figure is taken from McCann (2012) [8].

between different sublattices becomes

$$H = \hbar v_F \begin{pmatrix} 0 & q_x - iq_y \\ q_x + iq_y & 0 \end{pmatrix} = \hbar v_F \vec{\sigma} \cdot \vec{q} \quad (8)$$

where $v_F = 3at/2\hbar$ and $\vec{\sigma}$ are the 2D Pauli matrices (σ_x, σ_y). v_F is Fermi velocity, which is the velocity associated with Fermi energy, the highest energy electrons can occupy in the solid at 0 K. In our case, v_F does not depend on the value of k and its numerical value is $v_F \approx c/300$, where c is speed of light [4].

The Hamiltonian in Eq 8 is a Dirac-like Hamiltonian, which is the 2D Dirac equation with Fermi velocity v_F instead of speed of light c [4]. The Dirac equation deals with relativistic quantum systems so its Hamiltonian is different from the Hamiltonian usually used in the Schrödinger equation [9] [10]. A particle traveling in graphene is called a quasiparticle, not an electron, because its complex interaction with neighbors makes it behave as if it were a different particle with different mass. The Dirac-like Hamiltonian from Eq 8 implies that quasiparticles in graphene behave as massless relativistic particles or massless Dirac fermions [11].

The relation $H\psi = E\psi$ gives the following results

$$E_\pm(\vec{q}) = \pm\hbar v_F|\vec{q}|, \quad \psi_{\pm,\vec{K}}(\vec{q}) = \frac{1}{\sqrt{2}} \begin{pmatrix} e^{-i\theta_{\vec{q}}/2} \\ \pm e^{i\theta_{\vec{q}}/2} \end{pmatrix} \quad (9)$$

where $\pm$ refers to the conduction band and the valence band respectively, and the phase refers to the polar angle

of momentum in k-space, $\theta_{\vec{q}} = \arctan(q_x/q_y)$ [5]. The wave function around the K' point is also derived in the same way and the result is the complex conjugate of Eq 9. The linear dispersion relation shown in Eq 9, as opposed to the usual parabolic dispersion in metals, also shows that the quasiparticles in graphene are relativistic. This is from the equation for energy in relativity $E = \sqrt{p^2c^2 + m^2c^4}$ [12]. When $m = 0$, it becomes $E = pc$ where $p = \hbar k$ for quantum particles. This implies the linear dispersion relation in a relativistic system.

Here we have already derived pseudospin. Pauli matrices in Hamiltonian are usually related to spin states. However, $\vec{\sigma}$ in Eq 8 refers to pseudospin, not the real spin that we are familiar with [4]. More explicitly, the wavefunction $\psi_{\pm,\vec{K}}$ in Eq 9 is two-dimensional and looks similar to spin states, but this is not spin since ψ is the superposition of Bloch functions (Eq 2). The state ψ gives the relative amplitude between the Bloch wave in sublattice A and sublattice B. This additional degree of freedom indicating the relative amplitude between the sublattices is pseudospin [8]. For example, pseudospin 'up' state describes that all the electron density is located in sublattice A while pseudospin 'down' state describes that all the electron density is located in sublattice B.

IV. KLEIN TUNNELING

Pseudospin gives rise to the relativistic properties of quasiparticles in graphene. Therefore, it shows unusual behaviors that are not observed in other materials and enables physicists to set up experiments to explicitly observe physical phenomena that have been only theoretically discussed like Klein tunneling, or the Klein paradox.

The Klein paradox refers to the counterintuitive relativistic process in which an incoming electron penetrates an energy barrier higher than its rest energy with the probability of transmission (T) nearly being one [13]. As the energy barrier gets bigger and approaches to infinity, T approaches to one. This is counterintuitive because nonrelativistic quantum mechanics predicts that T decreases exponentially as the energy barrier increases [14].

The setup that was used in Klein's original paper was a step function with $V(x) = V$ for $x > 0$ and $V(x) = 0$ for $x < 0$ [13] [15]. By using the Dirac equation, it has been found

$$T = \frac{4k}{(1+k)^2}, \quad k = \sqrt{\frac{(V - E + m)(E + m)}{(V - E - m)(E - m)}} \quad (10)$$

where E is energy of the incoming particle, V is the potential barrier and m is the rest energy [15]. Here one can see that as $V \to \infty$, $T \to 1$. Klein paradox still holds in a finite square barrier. Although the exact formula for T is different, the tendency of $T \to 1$ as $V \to \infty$ still holds [15].

Let's see the Klein paradox observed in graphene. Figure 4 shows the setup of the problem. The potential is

a square finite barrier which does not depend on y for simplicity, and $V(x) = V_0$ at $0 < x < D$ and $V(x) = 0$ elsewhere. The calculation for this section involves the
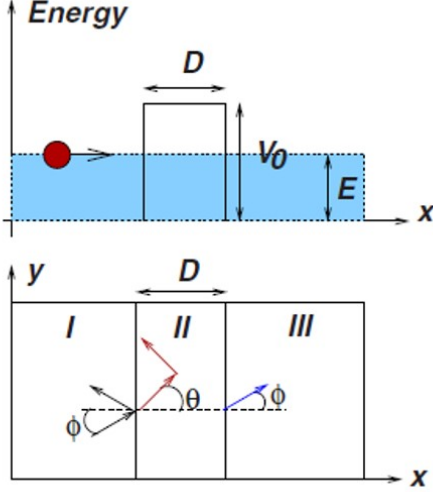
FIG. 4: Schematic of Klein tunneling. The upper figure shows energy as a function of x while the lower figure is the view on xy-plane. ϕ is the incident angle and θ is the refraction angle of the wave. This figure is taken from Castro Neto et al. (2009) [11].

Dirac equation and relativistic quantum physics. For our purpose, the results from Katsnelson et al.(2006) [11] and Castro Neto et al.(2009) [5] are cited.

In region I of Figure 4, the wave function has an incoming wave and a reflected wave. Therefore, we can write the wave function as

$$\psi_1(\vec{r}) = \frac{1}{\sqrt{2}}\begin{pmatrix} 1 \\ se^{i\phi} \end{pmatrix} e^{i(k_x x + k_y y)}$$
$$+ \frac{r}{\sqrt{2}}\begin{pmatrix} 1 \\ se^{i(\pi-\phi)} \end{pmatrix} e^{i(-k_x x + k_y y)} \qquad (11)$$

where $\phi = \arctan(k_y/k_x)$. In region II, the wave function is

$$\psi_2(\vec{r}) = \frac{a}{\sqrt{2}}\begin{pmatrix} 1 \\ s'e^{i\theta} \end{pmatrix} e^{i(q_x x + k_y y)}$$
$$+ \frac{b}{\sqrt{2}}\begin{pmatrix} 1 \\ s'e^{i(\pi-\theta)} \end{pmatrix} e^{i(-q_x x + k_y y)} \qquad (12)$$

where $\theta = \arctan(k_y/q_x)$ and q_x satisfies $V_0 - E = \hbar v_F \sqrt{q_x^2 + k_y^2}$. In region III, there is only a transmitted wave, so

$$\psi_3(\vec{r}) = \frac{t}{\sqrt{2}}\begin{pmatrix} 1 \\ se^{i\phi} \end{pmatrix} e^{i(k_x x + k_y y)} \qquad (13)$$

Here, $s = \mathrm{sgn}(E)$ and $s' = \mathrm{sgn}(E - V_0)$ [5]. Boundary conditions are $\psi_1(x = 0, y) = \psi_2(x = 0, y)$ and

$\psi_2(x = D, y) = \psi_3(x = D, y)$ since wave functions have to be continuous [14]. The coefficients r, a, b, t are obtained with this boundary conditions. Unlike the non-relativistic case, the derivative of wave functions are not matched up [5].

The probability of transmission is obtained by $T = |t|^2 = 1 - |r|^2$. We are interested in the case of large energy barrier. Taking $|V_0| \gg |E|$ gives

$$T = \frac{\cos^2 \phi}{1 - \cos^2 q_x D \sin^2 \phi} \qquad (14)$$

According to Eq 14, $T = 1$ when $q_x D = \pi n$ where $n = 0, \pm 1, \dots$. This condition is called the resonance conditions [11]. More remarkably, $T = 1$ when $\phi = 0$, which is directly related to the Klein paradox. The reason for the perfect transparency at normal incidence is the conservation of pseudospin [11]. Let's see how this conservation works.
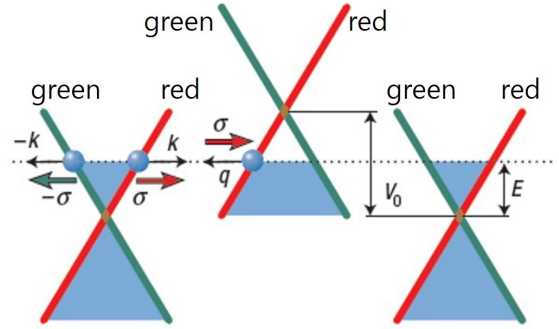
FIG. 5: The band structure of graphene showing the origin of the linear spectrum. The red and green curves are each associated with sublattices A and B. This figure is taken from Katsnelson et al. (2006) [11].

Electrons in the conduction band are electrons as usual. However, when Fermi energy is below the Dirac point, and thus the valence band has a void of an electron, we can think the absense of an electron as a positively charged particle. This quasiparticle is called a hole [6]. Note that holes are not positrons; they are not antiparticles. But it is often more convenient to deal with holes than electrons.

Let's look at the red curve in Figure 5. Electrons and holes in the same branch, which is the red curve in this case, have pseudospin σ (Eq 5) in the same direction because they originate from the same sublattice. As shown in Figure 5, electrons in the conduction band are propagating in the positive direction, or the outward direction from the cone, while holes in the valence band are propagating in the negative direction, or the inward direction to the cone. This shows that the direction of σ is parallel to the momentum of electrons while antiparallel to the momentum of holes, which gives rise to chirality [11]. Chirality is formally a projection of $\vec{\sigma}$ on the direction of propagation $\vec{k}$ [4].

Because of the conservation of pseudospin, charge carriers from the red branch do not get scattered into the green branch. Due to chirality, electrons which were originally moving to the right are scattered as either right-moving electrons or left-moving holes, but not as left-moving electrons nor right-moving holes. Matching the boundary conditions for directions of σ inside and outside the energy barrier gives $T = 1$, which is the result of Klein tunneling [11]. Klein tunneling in graphene was experimentally observed in 2008 [16].

V. CONCLUSION

Graphene is an unusual 2D material because charge carriers in graphene behave like massless relativistic particles. This property originates from the honeycomb structure of graphene, which contains two sublattice structures. This gives an additional degree of freedom called pseudospin. It gives rise to the linear dispersion relation between energy and momentum near the Dirac point, which is characteristic of a relativitistic system. This means that graphene is expected to show relativistic phenomena like Klein tunneling. Indeed, when a charge carrier is normally incident on a large energy barrier, the probability of transmission is 1, resulting in perfect tunneling. In conclusion, graphene is an exciting subject that will bring both interesting theoretical models and experimental observations for the study of relativistic quantum physics.

[1] R.E. Peierls, Ann. I. H. Poincare **5**, 177 (1935).
[2] L.D. Landau, Phys. Z. Sowjetunion **11**, 26 (1937).
[3] K.S. Novoselov et al., Science **306**, 666 (2004).
[4] A.K. Geim and K.S. Novoselov, Nature Materials **6**, 183 (2007).
[5] A.H. Castro Neto et al., Rev. Mod. Phys. **81**, 109 (2009).
[6] C. Kittel, *Introduction to Solid State Physics* (John Wiley & Sons, Inc., 2005).
[7] N.W. Ashcroft and N.D. Mermin, *Solid State Physics* (Cengage Learning, 1976).
[8] E. McCann, *Graphene Nanoelectronics: Metrology, Synthesis, Properties and Applications* (Springer Verlag, 2012).
[9] P.A.M. Dirac, Proc. Roy. Soc. **117**, 612 (1928).
[10] R. Shankar, *Principles of Quantum Mechanics* (Plenum Press, New York, 1988).
[11] M.I. Katsnelson, K.S. Novoselov and A.K. Geim, Nature Phys **2**, 620 (2006).
[12] A.P. French, *Special Relativity* (W.W. Norton & Company, 1968).
[13] O. Klein, Z. Phys **53**, 157 (1929).
[14] D. J. Griffiths, *Introduction to quantum mechanics* (Pearson Prentice Hall, 2005).
[15] A. Calogeracos and N. Dombey, Contemp. Phys. **40**, 313 (1999).
[16] A. F. Young and P. Kim, Nature Phys **5**, 222 (2009).

Forces from the Vacuum: The Casimir Effect

Jordan S. Cotler

Department of Physics, 77 Massachusetts Ave., Cambridge, MA 02139-4307

(Dated: May 2, 2014)

The quantization of fields leads to the presence of physical forces from the vacuum in a variety of circumstances. These phenomena are collectively known as the "Casimir effect." We provide semi-classical intuition for the Casimir effect, and then derive the vacuum forces between two parallel conducting plates using quantum field theory. During the calculation, we use analytic continuations to tame the infinities that arise, and provide the necessary background in complex analysis. The discussion concludes with a derivation of Casimir forces in a uniform gravitational field.

I. INTRODUCTION

It is counter-intuitive to think that "empty space" has non-zero energy. Surprisingly, quantum field theory predicts that empty space has divergent energy density at *every point in spacetime.* It is tempting to ignore the divergent term in the energy density calculation by writing it off as non-physical, but doing so is not without consequence. In fact, boundary conditions on regions of empty space can yield differently divergent energy densities and it is valid to reason about the relative difference between two divergent densities.

In 1948, Hendrik Casimir showed that in certain instances, the difference between two divergent energy densities is finite, which generates forces from the vacuum [1,2]. The eponymous Casimir effect was first observed in 1997 [3], and its theoretical and experimental implications continue to be an active field of research. In this paper, we will explore several instantiations of the Casimir effect which range from semi-classical analysis to quantum field theory in curved spacetime.

II. CASIMIR EFFECT FOR A LOADED STRING

We begin with a semi-classical derivation of the Casimir effect in a loaded one-dimensional string. This derivation is based on the argument of [4]. The derivation will provide intuition for the essence of Casimir's argument because it will not be obscured by the mathematical machinery required for dealing with quantum field theory. Consider a massless string of length L, clamped at both ends, with N equally-spaced point masses of mass m. The masses divide the string into $N + 1$ equal segments of length $L/(N + 1)$. We will further assume that the string is under uniform tension T, and is constrained to move in one transverse direction.

For the moment, consider N to be large, but finite. Thus, it is reasonable to consider the average linear mass density of the string, which we will write as $\mu = Nm/L$. Note that in the continuum limit as $N \to \infty$ and $m \to 0$ in such a manner that Nm approaches some finite constant, μ becomes exactly the linear mass density of the string. In this limit, transverse waves on the string will propagate with velocity $v = \sqrt{T/\mu}$. For convenience, we will utilize the variables μ and v in the discrete case.

Our string with N masses has N vibrational modes with frequencies

$$\omega_k = \frac{2v}{d} \sin\left(\frac{k\pi}{2N+1}\right) \tag{1}$$

for $k = 1, ..., N$. Treating each vibrational mode as a quantum harmonic oscillator, the quantum-mechanical ground state energy of our system is

$$E_{gs} = \sum_{k=1}^{N} \hbar\omega_k = \text{Im}\left[\frac{2v\hbar}{d}\sum_{k=1}^{N}\left(\exp\left(\frac{i\pi}{2N+1}\right)\right)^k\right] \tag{2}$$

Noting that the sum in Eq. (2) is a geometric series, we can evaluate it explicitly to get

$$E_{gs} = \frac{\hbar v}{2d}\left(\cot\left(\frac{4d}{2L}\right) - 1\right) \tag{3}$$

In the continuum limit as $N \to \infty$, $m \to 0$ and thus $d = L/(N+1) \to 0$, we find that

$$E_{gs} = \hbar v\left[\frac{2L}{\pi d^2} - \frac{1}{2d} - \frac{\pi}{24L}\right] + \mathcal{O}(d^2) \tag{4}$$

which diverges as $\sim 1/d^2$. This divergence is expected since we are summing over the non-zero ground state energies of infinitely many quantum harmonic oscillators. We can think of E_{gs} as a function of the length of the rope, and so we will denote it by $E_{gs}(L)$. If we clamp our rope of length L so that it is divided into two segments of length a and $L - a$ respectively, since the clamp imposes a fixed boundary condition we find that the new ground state energy is $E_{gs}(a) + E_{gs}(L-a)$ which is just the sum of the ground state energies of each of the two segments. Note that $E_{gs}(a)$ and $E_{gs}(L-a)$ both diverge to $+\infty$, and likewise so does their sum. Explicitly, we have that the sum of $E_{gs}(a)$ and $E_{gs}(L-a)$ is

$$\hbar v\left[\frac{2L}{\pi d^2} - \frac{1}{d} - \frac{\pi}{24}\left(\frac{1}{a} + \frac{1}{L-a}\right)\right] + \mathcal{O}(d^2) \tag{5}$$

Let us denote Eq. (5) by $E_{tot}(a)$ which we treat as a function of a since a can be varied as the clamp is moved.

We have not computed the ground state ψ of our clamped string, but we know from quantum mechanics

that $\langle H \rangle_\psi = \langle T \rangle_\psi + \langle U \rangle_\psi$ where H is the hamiltonian of the system, T is the kinetic energy operator, and U is the potential energy operator. Since ψ is an eigenstate of H, we have that $\langle H \rangle_\psi = E_{gs}(a)$. Additionally, since the ground state of a single quantum harmonic oscillator has zero expectation for its kinetic energy, by the linearity of expectation $\langle T \rangle_\psi = 0$ and thus $\langle U \rangle_\psi = E_{gs}(a)$. Therefore, the expected force experienced by the system in its ground state by varying the parameter a is $\langle F \rangle_\psi = -\frac{\partial}{\partial a} \langle U \rangle_\psi = -\frac{\partial}{\partial a} E_{gs}(a)$, and so utilizing Eq. (5) we obtain

$$\langle F \rangle_\psi = -\frac{\hbar v \pi}{24 a^2} \tag{6}$$

which is non-zero. The above result is finite since it is independent of d. Therefore, the string will experience an expected longitudinal force of $-\hbar v \pi / 24 a^2$ if the clamp is at position a. We see that the different energies of the ground states of the two segments of the string have generated a Casimir force. As pointed out in [4], for a string the propagation velocity v can be at most on the order of the speed of sound, and so the Casimir force is way too small to measure in any practical way since $\hbar$ is very small. When we repeat this calculation for electromagnetic waves, the analog of v will be the speed of light, and the corresponding Casimir force is large enough to be measurable.

Before proceeding to the quantum field theory case, we make a brief mathematical digression. You might think that it seems reckless to treat the divergent terms in Eq. (5) as "infinite constants" so that they vanish when we take the derivative with respect to a. However, the problem is more subtle, since we could have first taken the derivative with respect to a in the discrete approximation, and then taken the limit to the continuum approximation. Therefore, the real question is whether the derivative of a limit is the limit of a derivative. Formally, one is allowed to make such an interchange only if the limit of the ground state energy converges uniformly, which in our case it does not since Eq. (5) is divergent.

Since there is no mathematically rigorous way in which Eq. (5) can be differentiated with respect to a, we can instead *define* its derivative with respect to a as the continuum limit of the expected force experienced by the ground state of the discrete system. This definition is not useful for mathematicians because it does not aid in formal proofs, but it is useful for physicists, being physically well-motivated in our present context. In particular, perfectly continuous strings do not exist in our physical world and likewise continuum descriptions of nature such as quantum field theories do not hold at arbitrarily small length scales.

We will experience an analogous but more difficult mathematical dilemma when we utilize quantum field theory to do a similar calculation of Casimir forces. In the next section, we devlop the mathematical machinery to resolve this dilemma.

III. MATHEMATICAL INTERLUDE

In the calculation of the Casimir force between two conducting plates, we are going to encounter divergent sums and integrals which are hard to make sense of. Therefore, we briefly develop the mathematical apparatus necessary to deal with these divergences. As a motivating example, consider the power series

$$f(x) = \sum_{n=0}^\infty x^n \tag{7}$$

which converges to $1/(1-x)$ on $[0,1)$. Let us inquire what it means to evaluate $f(x)$ at $x = 2$. We will get the sum $\sum_{n=0}^\infty 2^n$ which diverges. But what if we wanted to *assign* a value to $f(2)$ that is finite? One idea is to consider the formula $1/(1-x)$ which is only equal to $f(x)$ for x in $[0,1)$, and then *define* $f(2) = 1/(1-2) = -1$. This procedure is perfectly reasonable, and works as long as $x \neq 1$. However, it seems very arbitrary, because it does not appear that there is anything preventing someone from defining $f(2) = 10$ or $f(2) = -\pi$.

Nevertheless, there is a surprising fact: the only reasonable value to assign $f(2)$ is -1. This fact is by no means obvious, but in this section we will show it is correct. In general, we will be able to show that many divergent sums and integrals can be assigned an essentially *unique* finite value, which will be useful in future calculations.

The required tool is complex analysis. The derivative of a complex function $f(z)$ is defined by

$$f'(z) := \lim_{\epsilon \to 0} \frac{f(z + \epsilon) - f(z)}{\epsilon} \tag{8}$$

for complex ϵ. Alternatively, we can write this as

$$f'(x + iy) = \lim_{(\epsilon_1, \epsilon_2) \to (0,0)} \frac{f(x + iy + \epsilon_1 + i\epsilon_2) - f(x + iy)}{\epsilon_1 + i\epsilon_2} \tag{9}$$

which is just a standard multivariable limit. The limit may not exist in which case the derivative does not exist, but for our purposes we will assume that all of the complex functions we encounter are differentiable.

One of the most remarkable facts about complex functions is *if a complex function is once differentiable, then it is infinitely differentiable*. Let us sketch a proof of this fact. First, let C_r be a circle of radius r in the complex plane centered around some point a and parameterized counter-clockwise. Consider the following contour integral:

$$\oint_{C_r} \frac{1}{z - a} \, dz \tag{10}$$

Changing variables by letting $z = re^{i\theta} + a$, the above integral becomes

$$\int_0^{2\pi} \frac{1}{re^{i\theta}} ire^{i\theta} \, d\theta = 2\pi i \tag{11}$$

and thus

$$\frac{1}{2\pi i} \oint_{C_r} \frac{1}{z-a}\, dz = 1 \qquad (12)$$

Now, if $f(z)$ is a complex differentiable function, then for some small real number $\epsilon > 0$, we have

$$\frac{1}{2\pi i} \oint_{C_\epsilon} \frac{f(z)}{z-a}\, dz = \frac{1}{2\pi i} \oint_{C_\epsilon} \left[\frac{f(z)-f(a)}{z-a} + \frac{f(a)}{z-a} \right] dz \qquad (13)$$

$$= \frac{1}{2\pi i} \oint_{C_\epsilon} \frac{f(z)-f(a)}{z-a}\, dz + f(a) \qquad (14)$$

$$\approx \frac{1}{2\pi i} \oint_{C_\epsilon} f'(a)\, dz + f(a) \qquad (15)$$

$$\approx \frac{1}{2\pi i}(2\pi\epsilon) f'(a) + f(a) \qquad (16)$$

$$\longrightarrow 0 + f(a) \text{ as } \epsilon \to 0 \qquad (17)$$

Therefore

$$f(a) = \lim_{\epsilon \to 0} \frac{1}{2\pi i} \oint_{C_\epsilon} \frac{f(z)}{z-a}\, dz \qquad (18)$$

which holds if f is differentiable. If we differentiate both sides of Eq. (18) n times with respect to a we find that

$$f^{(n)}(a) = \lim_{\epsilon \to 0} \frac{n!}{2\pi i} \oint_{C_\epsilon} \frac{f(z)}{(z-a)^{n+1}}\, dz \qquad (19)$$

which likewise holds if f is differentiable. Thus, if f is differentiable, it is infinitely differentiable as we claimed.

There is actually an even stronger statement that we can prove: *if a complex function is once differentiable, then it is analytic, meaning that it can be written as a power series.* The argument is as follows [5]:

$$f(z) = \lim_{\epsilon \to 0} \frac{1}{2\pi i} \oint_{C_\epsilon} \frac{f(w)}{w-z}\, dw \qquad (20)$$

$$= \lim_{\epsilon \to 0} \frac{1}{2\pi i} \oint_{C_\epsilon} \frac{f(w)}{(w-a)-(z-a)}\, dw \qquad (21)$$

$$= \lim_{\epsilon \to 0} \frac{1}{2\pi i} \oint_{C_\epsilon} \frac{1}{w-a} \cdot \frac{1}{1 - \frac{z-a}{w-a}}\, dw \qquad (22)$$

$$= \lim_{\epsilon \to 0} \frac{1}{2\pi i} \oint_{C_\epsilon} \frac{1}{w-a} \cdot \sum_{n=0}^{\infty} \left(\frac{z-a}{w-a} \right)^n dw \qquad (23)$$

$$= \sum_{n=0}^{\infty} \frac{1}{n!}(z-a)^n \left[\lim_{\epsilon \to 0} \frac{n!}{2\pi i} \oint_{C_\epsilon} \frac{f(w)}{(w-a)^{n+1}}\, dw \right] \qquad (24)$$

$$= \sum_{n=0}^{\infty} \frac{1}{n!} f^{(n)}(a)(z-a)^n \qquad (25)$$

The upshot of all of our work thus far is that we can now discuss *analytic continuation*. Let us reconsider the function f from Eq. (7), but this time we define it over the complex numbers so that $f(z) = \sum_{n=0}^{\infty} z^n$. Since

f can be expressed as a power series for $|z| < 1$, it is analytic for $|z| < 1$. If we want to extend $f(z)$ so that it is defined for $|z| > 1$, then we want to find an analytic function F that agrees with $f(z)$ on $|z| < 1$, but that is also defined for $|z| > 1$, such as at $z = 2$. One analytic function that does the job is $1/(1-z)$ which agrees with $f(z)$ if $|z| < 1$ and is also defined for $|z| > 1$. Note that $1/(1-z)$ is analytic for $|z| < 1$ and $|z| > 1$ since it is once differential for $|z| < 1$ and $|z| > 1$, which is a sufficient condition. We can now ask if there are any other analytic functions which agree with $f(z)$ if $|z| < 1$ and which are also defined for $|z| > 1$. The answer is actually no, and $1/(1-z)$ is the unique analytic function that satisfies the necessary conditions. We call this function the *analytic extension* of $f(z)$.

The general statement is this: *if a complex function f is analytic on some region U of the complex plane and has an analytic extension F to the entire complex plane such that F agrees with f on U, then F is the unique extension* [5]. To prove this, say that F_1 and F_2 are both analytic extensions of f. Then $F_1 - F_2$ is zero on U, along with all of its derivatives. This implies that the power series expansions of F_1 and F_2 are the same, and thus they are the same function.

From this point forward, if we encounter a divergent integral or sum which depends an a complex parameter, we will evaluate its corresponding unique analytic extension in the hope that we will get a finite answer. It is an interesting question as to why the laws of nature should abide by analytic extensions. In other words, why do we expect our mathematical trickery to yield physically correct answers? One compelling reason is that since analytic extensions are unique, if nature is going to provide us with a non-divergent observable, then analytic extensions appear to be the only possibility. A more heuristic approach is to let experiments tell us if analytic extensions are justified in our calculations. Interestingly, the answer is yes in many circumstances, including for the calculations in the following section.

IV.   CASIMIR FORCES BETWEEN NEUTRAL CONDUCTING PLATES

We will derive the Casimir force between two neutral conducting plates, based on the derivations in [6,7,8,9]. So consider two identical perfectly conducting parallel plates, each with surface area S which we take to be very large. Furthermore, say that the two plates are a distance a apart, and are in vacuum. From classical electromagnetism, we know that the component of the electric field parallel to the plates must disappear on the boundary of each plate, and that the component of the magnetic field orthogonal to the plates also disappears on the boundary of each plate.

With these boundary conditions in mind, we can treat the electromagnetic field between the plates as infinitely many quantum harmonic oscillators with frequencies

$\omega_{\mathbf{k}} = c|\mathbf{k}|$. To satisfy the boundary conditions, we must have that $\mathbf{k} = (k_1, k_2, \pi n/a) = (\mathbf{k}_\perp, \pi n/a)$ where n is an integer and $\mathbf{k}_\perp$ is an element of $\mathbb{R}^2$. Therefore, the frequencies take the form

$$\omega_{\mathbf{k}_\perp, n} = c\sqrt{k_1^2 + k_2^2 + \left(\frac{\pi n}{a}\right)^2} \qquad (26)$$

Noting that each mode corresponds to a quantum harmonic oscillator with ground state energy $\frac{1}{2}\hbar\omega_{\mathbf{k}_\perp, n}$, we can determine the ground state energy of the vacuum between the plates as a function of a by

$$E_{gs}(a) = \frac{\hbar}{2} \iint_{\mathbb{R}^2} \frac{dk_1 dk_2}{(2\pi)^2} \left(\sum_{n=-\infty}^{\infty} \omega_{\mathbf{k}_\perp, n}\right) S \qquad (27)$$

Let us rewrite this integral in the form

$$E_{gs}(a, \delta) = \frac{\hbar}{2} \iint_{\mathbb{R}^2} \frac{dk_1 dk_2}{(2\pi)^2} \left(\sum_{n=-\infty}^{\infty} \omega_{\mathbf{k}_\perp, n}^{1-2\delta}\right) S \qquad (28)$$

where by construction $\lim_{\delta \to 0} E_{gs}(a, \delta) = E_{gs}(a)$ for a complex variable δ. Now we change variables twice, switching to polar coordinates (r, ϕ) by letting $r^2 = k_1^2 + k_2^2$ and then integrating out over ϕ, followed by letting $y = ar/n\pi$. The end result is

$$E_{gs}(a, \delta) = \frac{\hbar c}{2\pi} \int_0^\infty dy\, y(y^2+1)^{\frac{1}{2}-\delta} \left(\sum_{n=1}^{\infty} \left(\frac{n\pi}{a}\right)^{3-2\delta}\right) S \qquad (29)$$

Evaluating the integral, we find that

$$\int_0^\infty dy\, y(y^2+1)^{\frac{1}{2}-\delta} = -\frac{1}{2} \int_0^\infty du\, (u+1)^{\frac{1}{2}-\delta} \qquad (30)$$

$$= -\frac{1}{2}\left(\frac{1}{3/2-\delta}\right) \qquad (31)$$

which is defined only if the real part of δ is greater than $3/2$. The reason is that the integral in Eq. (30) only converges if $\mathrm{Re}(\delta) > 3/2$. However, letting Eq. (31) be the analytic extension of the integral, we can justify evaluating the integral in the limit $\delta \to 0$ by evaluating the extension at $\delta = 0$. Factoring out constants, Eq. (29) becomes

$$E_{gs}(a, \delta) = -S\frac{\hbar c\pi^2}{6a^3} \sum_{n=1}^{\infty} \frac{1}{n^{2\delta-3}} \qquad (32)$$

which we rewrite as

$$E_{gs}(a, \delta) = -S\frac{\hbar c\pi^2}{6a^3} \zeta(2\delta - 3) \qquad (33)$$

where we have introduced the Riemann zeta function $\zeta(s)$ which is defined by $\zeta(s) = \sum_{n=1}^{\infty} \frac{1}{n^s}$. Since $\zeta(s)$ has a unique analytic extension to $s = -3$ where $\zeta(-3) = \frac{1}{120}$, we can take the limit of Eq. (33) as $\delta \to 0$ to obtain

$$E_{gs}(a) = -S\frac{\hbar c\pi^2}{720a^3} \qquad (34)$$

The Casimir force is thus $-\partial E_{gs}(a)/\partial a$, and dividing this by the surface area S of the plates, we find that the Casimir pressure is

$$P_{cas} = -\frac{\hbar c\pi^2}{240a^4} \qquad (35)$$

To obtain a pressure on the order of micropascals, the distance a between the plates needs to be on the order of micrometers. Fortunately, it is possible to measure pressures on this scale.

In the last twenty years, there have been numerous experimental realizations of the Casimir effect between conducting bodies. The earliest conclusive results were obtained by Lamoreaux in 1997, in which he examined the Casimir pressure between a conducting sphere and plate using a sophisticated torsion pendulum [3]. Lamoreaux used a sphere and a plate instead of two parallel plates to simplify the task of alignment. In particular, it is much easier to make a plate lie nearly tangential to a sphere than to align two parallel plates with high precision. Since a sphere has non-zero curvature, the formula for the Casimir pressure in Eq. (35) must be modified by a multiplicative factor of $2\pi R$ where R is the radius of the sphere. With separations on the order of micrometers, Lamoreaux measured pressures that agree with the theory to within five percent [3].

Soon after Lamoreaux's experiment, Mohideen and Roy performed a more precise variation using an atomic force microscope to measure the force between a conducting sphere and plate with separations on the order of tenths of micrometers [10]. Their measured forces agree with the theory to within one percent [10]. Despite the relative ease of the sphere and plate setup, the parallel plate setup was ultimately instantiated by Bressi et. al. [11]. With separations on the order of micrometers, they were able to measure Casimir forces that agree with the theory to within fifteen percent [11].

There is current interest in the physics community in performing measurements of the Casimir effect with more complex boundary conditions because such measurements provide a unique probe of the quantum vacuum [9]. Additionally, recent provocative work attempts to use measurements of the Casimir effect to constrain the possibilities for extra dimensions of spacetime [9].

V. CASIMIR FORCES IN A UNIFORM GRAVITATIONAL FIELD

The unification of quantum field theory with general relativity is an old and difficult program. While there is no complete theory of quantum gravity, we can still perform quantum field theoretic calculations in curved spacetime, where we treat the gravitational field as classical. Consider a gravitational field with metric tensor $g_{\mu\nu}$ which defines the infinitesimal distance element $ds^2 = g_{\mu\nu}dx^\mu dx^\nu$. We will now derive the redshift of a

photon in a gravitational field [12,13]. For our analysis, we will use the $\eta_{\mu\nu} = \text{diag}(-1, 1, 1, 1)$ sign convention.

Say we have a clock which ticks every Δt seconds in the absence of gravity. In our gravitational field, the space-time interval between ticks satisfies

$$c\,\Delta t = (-g_{\mu\nu} dx^\mu dx^\nu)^{\frac{1}{2}} \qquad (36)$$

Taking the inverse of both sides, multiplying by dt and rearranging terms, we find that if the clock has 4-velocity dx^μ/dt then

$$c\,dt = \Delta t \left(-g_{\mu\nu} \frac{dx^\mu}{dt} \frac{dx^\nu}{dt}\right)^{-\frac{1}{2}} \qquad (37)$$

where dt is the time between ticks of the clock. If the clock is at rest, then $dx^\mu/dt = (c, 0, 0, 0)$ and so Eq. (36) reduces to

$$dt = \Delta t (-g_{00})^{-\frac{1}{2}} \qquad (38)$$

On Earth, our local gravitational field is best described by the weak field metric

$$g_{\mu\nu} = \begin{pmatrix} -(1 + 2gz/c^2) & 0 & 0 & 0 \\ 0 & 1 & 0 & 0 \\ 0 & 0 & 1 & 0 \\ 0 & 0 & 0 & 1 \end{pmatrix} \qquad (39)$$

where $g \approx 9.8\,m/s^2$ is the average gravitational acceleration at sea level and the coordinate z is the height above the ground. Note that the metric in Eq. (39) is not time dependent which will simplify our argument.

Now, consider an atom at rest at $z = 0$ which emits a photon of frequency ν_1 in the positive z-direction due to an atomic transition. Also, say that we are on a crane exactly above the atom at $z = a$. Since our gravitational field is time-independent, the crest of a wave from the electromagnetic radiation will take the same amount of time to reach us no matter when we perform the experiment. Therefore, the amount of time that we observe *between* crests of the electromagnetic radiation is

$$dt_1 = \Delta t \left(-g_{00}(z = 0)\right)^{-\frac{1}{2}} \qquad (40)$$

where Δt is the time between crests in the absence of gravity. However, if we observed the same atomic transition from an identical atom at the top of our crane, then we would measure the time between the crests of the electromagnetic radiation to be

$$dt_2 = \Delta t \left(-g_{00}(z = a)\right)^{-\frac{1}{2}} \qquad (41)$$

Taking the ratio of Eq.'s (40) and (41), we find that the ratio between the angular frequency of the photon emitted from the atom in the crane and the angular frequency of the photon emitted from the atom on the ground is

$$\frac{\omega_{ground}}{\omega_{crane}} = \left(\frac{g_{00}(z = 0)}{g_{00}(z = a)}\right)^{\frac{1}{2}} = \frac{1}{(1 + 2ga/c^2)^{\frac{1}{2}}} \qquad (42)$$

We see from the above equation that the photon from the ground was redshifted as it climbed the gravitational potential. In other words, if the initial frequency of the photon when emitted from the ground is ω_{ground}, then the frequency of the photon at height z tales the form $\omega_{ground}(1 + gz/c^2)$ to first order in z. Therefore, if the photon emitted from the ground has a uniform probability of being anywhere in the region $0 \le z \le a$, we can say that to first order in a it has an *average* angular frequency

$$\omega_{avg} = \frac{1}{a} \int_0^a \omega_0 \left(1 + \frac{gz}{c^2}\right) dz = \left(1 + \frac{ga}{2c^2}\right) \omega_0 \qquad (43)$$

Let us recall our two identical perfectly conducting parallel plates in vacuum. We will impose the weak field metric on the vacuum, place one of the plates in the $z = 0$ plane, and the other plate parallel in the $z = a$ plane. If there was no gravitational field, then as in Section IV, we could integrate and sum over all of the photon modes between the plates, treating each one as a quantum harmonic oscillator with frequency of the form $\omega_{\mathbf{k}_\perp, n} = c\sqrt{k_1^2 + k_2^2 + (\pi n/a)^2}$ as in Eq. (26). But in the gravitational field, the story is slightly different. Inspired by Eq. (43), we should treat each photon mode as a quantum harmonic oscillator with average frequency approximately of the form

$$\omega_{\mathbf{k}_\perp, n, avg} = \left(1 + \frac{ga}{2c^2}\right) c \sqrt{k_1^2 + k_2^2 + \left(\frac{\pi n}{a}\right)^2} \qquad (44)$$

Since we have just changed the form of our frequencies by a constant factor from the non-gravitational case, the calculation is identical to the one in Section IV, but with an overall factor of $(1 + ga/2c^2)$. Thus, we find that for the weak field metric, the Casimir energy between our parallel plates is approximately

$$E_{gs, grav} = -\left(1 + \frac{ga}{2c^2}\right) S \frac{\hbar c \pi^2}{720 a^3} \qquad (45)$$

and the Casimir pressure is approximately

$$P_{cas, grav} = -\frac{g}{2c^2} \frac{\hbar^2 c \pi^2}{720 a^3} - \left(1 + \frac{ga}{2c^2}\right) \frac{\hbar c \pi^2}{240 a^4} \qquad (46)$$

which are the analogs of Eq.'s (34) and (35). While our calculation agrees with other theoretical calculations [14], we do not yet know if it agrees with experiment. To understand how difficult it is to observe this effect experimentally, we calculate the percent difference between $P_{cas, grav}$ in Eq. (46) and P_{cas} in Eq. (35) to get

$$\frac{|P_{cas} - P_{cas, grav}|}{P_{cas}} = a \frac{2g}{3c^2} \approx a \cdot (7.27 \cdot 10^{-17}\, m^{-1}) \quad (47)$$

Therefore, for any reasonable a, the effect will be impossible to measure with current technology. Nonetheless, our result predicts that the Casimir energy is different in curved spacetime, which is a far-reaching theoretical result. If instead we had chosen a more intricate geometry

for our spacetime, the result implies that an experimenter would measure different values for the Casimir energy depending on where he is in spacetime. This complication is one of the central themes of quantum field theory in curved spacetime, and in general makes calculations very difficult.

VI. CONCLUSION

The Casimir effect exemplifies the counter-intuitive nature of the quantum vacuum, and the divergences in its calculation emphasize the necessity for a more mathematically rigorous theory of quantum fields. In the mean time, techniques like analytic continuation suffice to provide what so far have been experimentally correct results. The calculation of the Casimir effect in curved spacetimes hints at the beauty and complexity of quantum gravity. A deeper understanding of the interplay between the quantum vacuum energy and the curvature of spacetime is a step in the right direction towards resolving the greatest unsolved problem in physics.

[1] H.B.G. Casimir, Proc. Kon. Nederl. Akad. Wet. **51** (1948) 793.

[2] H.B.G. Casimir, D. Polder, Phys. Rev. **73** (1948) 360.

[3] Lamoreaux, S. K. "Demonstration of the Casimir Force in the 0.6 to 6 m Range." Physical Review Letters 78.1 (1997): 5-8. Print.

[4] Cooke, J. H. (1998). "Casimir force on a loaded string." *American Journal of Physics* **66** (7): 569-561.

[5] Saff, E. B., and Snider, A.D. *Fundamentals of Complex Analysis with Applications to Engineering and Science.* Upper Saddle River, NJ: Prentice Hall, 2003. Print.

[6] Schwartz, Matthew Dean. *Quantum Field Theory and the Standard Model.* Cambridge UP, 2013. Print.

[7] Zee, A. *Quantum Field Theory in a Nutshell.* Princeton, NJ: Princeton UP, 2003. Print.

[8] Huang, Kerson. *Quantum Field Theory: From Operators to Path Integrals.* New York: Wiley, 1998. Print.

[9] Bordag, Michael, Umar Mohideen, and Vladimir M. Mostepanenko. "New developments in the Casimir effect." Physics reports 353.1 (2001): 1-205.

[10] Mohideen, U., and Anushree Roy. "Precision Measurement of the Casimir Force from 0.1 to 0.9 μm." *Physical Review Letters* 81.21 (1998): 4549-552. Print.

[11] Bressi, G., G. Carugno, R. Onofrio, and G. Ruoso. "Measurement of the Casimir Force between Parallel Metallic Surfaces." *Physical Review Letters* 88.4 (2002):

[12] Carroll, Sean M. *Spacetime and Geometry: An Introduction to General Relativity.* San Francisco: Addison Wesley, 2004. Print.

[13] Weinberg, Steven. Gravitation and Cosmology: Principles and Applications of the General Theory of Relativity. New York: Wiley, 1972. Print.

[14] Nazari, B., and M. Nouri-Zonoz. "Casimir Effect in a Weak Gravitational Field and the Spacetime Index of Refraction," 2010.

Atoms in an external magnetic field: energy levels and magnetic trapping states

Tamara Dordevic

Department of Physics, MIT

(Dated: May 2, 2014)

In this paper we present a derivation of the energy level splittings in an external magnetic field. The results for the energy level splittings are presented in the form of a Breit-Rabi diagram, using Rb^{87} $S_{1/2}$ manifold of states. Using the Breit-Rabi diagram, we show how to decide which states can be captured in a magnetic trap, and which trap strength should be chosen for particular transitions to be magnetic field independent.

I. INTRODUCTION

Quantum physics was initially developed in order to better explain the structure and behavior of atoms, and atoms still remain its central focus because they display a variety of different quantum phenomena. A central question in the atomic physics is precise determination of the atomic energy levels and their dependence on the external effects. The goal of this paper is to examine the behavior of energy levels of atoms in an external magnetic field. While this problem may seem rudimentary, it reveals many interesting aspects of quantum physics, particularly the solutions to non-diagonal Hamiltonians. The presented results have many interesting experimental applications, some of which will be explored in this paper.

The exploration of atomic energy levels begins with solving the Schrodinger equation in the Coulomb potential, $V(r) = -\frac{e^2}{r}$. The well-known solutions reveal the quantization of energy levels which defer with respect to their main quantum number n, but are degenerate with respect to the orbital quantum number L, spin quantum number S, as well as their projections on the quantization axis, L_z and S_z. If we modify the Coulomb potential so that it includes higher order contributions, some of these degeneracies are broken. In order to understand the effects of magnetic field, we need to first discuss the relevant correction terms to the Coulomb Hamiltonian (the fine and hyperfine structure) and how they relate to the choice of basis for eigenstates in a magnetic field.

II. CORRECTIONS TO COULOMB HAMILTONIAN

A. Choice of basis

In order to determine energy eigenstates of the Coulomb Hamiltonian H_0 and additional terms, we need to simultaneously diagonalize them. This problem can be solved by a suitable choice of basis which contains a complete set of commuting observables (CSCO)[7]. The problem of finding a CSCO usually reduces to an angular momenta addition problem, as it will be described in the following example.

Assume we have two different angular momenta, $\vec{J}$ and $\vec{K}$, which commute with H_0. That means that the CSCO for this problem contains H_0, K^2, J^2, J_z and K_z. If we now introduce a coupling term proportional to $\vec{J} \cdot \vec{K}$, the new term does not commute with the initial CSCO since $\vec{J} \cdot \vec{K} = J_x K_x + J_y K_y + J_z K_z$ and $[J_x K_x, J_z] = [J_x, J_z] \neq 0$. Therefore, in order to make a new CSCO which will account for all the terms in the Hamiltonian, we need to reparametrize the Hamiltonian. We do this by introducing a new angular momentum operator, $\vec{F} = \vec{J} + \vec{K}$. If we square both sides of this expression, we get $F^2 = J^2 + K^2 + 2\vec{J} \cdot \vec{K}$, from where we can express the new term in the Hamiltonian as $\frac{F^2 - J^2 - K^2}{2}$. Therefore, the new CSCO should include the operator F^2. However, since $[F^2, J_z] \neq 0$ and $[F^2, K_z] \neq 0$, we have to exclude J_z and F_z from CSCO. In order to complete the CSCO, we then add $F_z = J_z + K_z$ to it. Therefore, the new CSCO for H_0 alongside with a coupling term is CSCO = $\{H, K^2, J^2, F^2, F_z\}$.

B. Fine structure

The first correction to the Coulomb potential is the fine structure correction, which includes several contributions. These are the relativistic second order contribution to the electron kinetic energy, spin-orbit coupling and the so-called Darwin term, which describes the changes to the Coulomb potential due to the fluctuations in the electron position [3]. The spin-orbit coupling comes from the fact that electrons have intrinsic angular momenta or spins, which tend to align with the external magnetic field. From the electron frame of reference, the protons are moving around them and thus creating a magnetic field due to their charge. Therefore, the electronic spins will interact with that field, and the interaction Hamiltonian is proportional to the term $\vec{L} \cdot \vec{S}$, where $\vec{L}$ is the electron orbital angular momentum and $\vec{S}$ its spin angular momentum. If we define the total electron angular momentum as $\vec{J} = \vec{L} + \vec{S}$, the total fine structure correction splits the energy levels with different values of J (the convention used throughout this paper is that an angular momentum operator $\vec{X}$ has an associated eigenvalue X such that $X^2 |X, m_X\rangle = \hbar^2 X(X+1) |X, m_X\rangle$). If we use the spectroscopic notation for electron energy levels, L_J, the fine structure interaction would split the

first excited state of an alkali atom into $S_{1/2}$, $P_{1/2}$ and $P_{3/2}$. From the previous discussion about the CSCO, it is clear that the CSCO for the Coulomb potential alongside with fine structure should be CSCO(FS) = $\{H + H_{fs}, L^2, S^2, J^2, J_z\}$.

C. Hyperfine structure

While the fine structure takes into account the electronic spin and motion, the hypefine correction takes into account the internal structure of the nucleus, namely its multipole moments (there are also corrections due to the nuclear finite mass and volume called the "mass shift" and the "volume shift", but we will not consider them in this paper)[1, 2]. Permanent nuclear multipole moments are defined as non-zero expectation values of multipole operators in the nuclear energy eigenstates [3]. For example, permanent magnetic dipole moment of a nucleus in its ground state $|\Psi_{gs}\rangle$ is non-zero if $\langle\Psi_{gs}|\vec{\mu}|\Psi_{gs}\rangle \neq 0$. Multipole moments can in general be marked by their order l (e.g. $l = 0$ monopole, $l = 1$ dipole). The nuclear multipole moments of order l come from the nuclear angular momentum, and are proportional to spherical harmonics $Y_{l,m}$ [3]. The allowed permanent nuclear multipole moments with the nuclear angular momentum I obey the following selection rules:

- $l \leq 2I$

- electric multipoles can have even values of l

- magnetic multipoles can have odd values of l

The last two rules come from parity considerations - an electric monopole l has a parity $(-1)^l$, and thus only when $(-1)^l = 1$ the monopole has a non-vanishing expectation value in an eigenstate. The opposite is true for magnetic monopoles l - their parity is $(-1)^{l+1}$, so only the odd values of l produce non-vanishing expectation values.

Therefore, the nuclei are allowed to have odd electric dipole moments (monopole, quadrupole etc) and even magnetic dipole moments (dipole, octopole etc). The electric monopole is the dominant term which is accounted for in the Coulomb interaction. The next dominant term is the magnetic dipole moment, which we will consider in this paper.

The magnetic dipole moment of a nucleus can be expressed as

$$\vec{\mu}_I = g_I \mu_B \frac{m_e}{M} \frac{\vec{I}}{\hbar} \tag{1}$$

where μ_B is the Bohr magneton, m_e electron mass, M mass of the nucleus, g_I the nuclear gyromagnetic ratio and $\vec{I}$ the nuclear spin [3]. From here we can see that the nuclear dipole moment is about 2000 times smaller than the electric dipole moments due to the mass ratio in the expression.

The nuclear magnetic moment couples to the magnetic field produced by the electrons at the core through the Hamiltonian $H_{HFS} = -\mu_I \cdot B_J$. Since the magnetic field B_J is proportional to the total angular momentum of the electron, $\vec{J}$, we can rewrite the hyperfine Hamiltonian as:

$$H_{HFS} = \frac{C}{\hbar^2} \vec{I} \cdot \vec{J} \tag{2}$$

where C is the hyperfine coupling constant which absorbed the constants from B_J and μ_I [1, 2]. If we define the total atomic angular momentum to be $\vec{F} = \vec{I} + \vec{J}$, H_{HFS} can be rewritten as:

$$H_{HFS} = \frac{C}{2\hbar^2}(F^2 - I^2 - J^2) \tag{3}$$

Therefore, for a given I and J the hyperfine structure splits the energy levels with different values of quantum number F. The CSCO for the hyperfine structure added to the fine structure and Coulomb potential is CSCO(HFS) = $\{H + H_{fs} + H_{hfs}, L^2, S^2, J^2, I^2, F^2, F_z\}$.

D. External magnetic field

If we put an atom in an external magnetic field $\vec{B}$, the total atomic magnetic moment will couple to the external field as

$$H_B = -\vec{\mu} \cdot \vec{B} = -(\vec{\mu}_J + \vec{\mu}_I) \cdot \vec{B} \tag{4}$$

Since $\mu_J = g_J \mu_B \frac{\vec{J}}{\hbar}$, μ_I is given by the equation 1 and $g_I \neq g_J$, we cannot in general express H_B in terms of $\vec{F}$. Therefore, the CSCO for H_B is CSCO(H_B) = $\{H + H_{fs} + H_B, L^2, S^2, J^2, I^2, I_z, J_z\}$.

In order to estimate the energy levels of an atom in an external magnetic field, we need to include energy contributions coming from H_{HFS} and H_B. The magnitude of contribution from H_B depends on the strength of magnetic field, B, so for low values of B, energy contribution from H_{HFS} is dominant and thus cannot be neglected. Moreover, the energy contribution from H_B can be divided into the nuclear spin contribution, $-\mu_I B$, and the electron contribution, $-\mu_J B$. The electron contribution is around 2000 times bigger than the nuclear spin contribution due to the proton-electron mass ratio (as explained in the section II.C). Based on the relative magnitudes of contributions of H_{HFS} and parts of H_B, we can divide the problem of finding energy levels into three regimes [3]:

1. **Weak field:** Weak field regime is defined as the range of values of B for which $H_{HFS} \gg H_B$, or in terms of energy

$$\frac{C}{2}(F(F+1) - I(I+1) - J(J+1)) \gg$$
$$\mu_B B(g_J J_z - g_I I_z) \tag{5}$$

We therefore treat the weak field regime in the CSCO(HFS).

2. **Intermediate field:** Intermediate field regime corresponds to values of B for which electron contribution of H_B is bigger than the H_{HFS}, but the nuclear spin contribution is still negligible. This translates into energy condition:

$$\mu_B B g_J J_z > \frac{C}{2}(F(F+1) - I(I+1) - J(J+1)) \gg$$
$$\mu_B B g_I I_z$$
$$(6)$$

Since the most dominant contribution comes from H_B, we treat this regime in CSCO(H_B).

3. **Strong field:** Strong field regime is defined as the range of values of B for which both parts of H_B are much bigger than H_{HFS}, which translates into an energy condition opposite from the one presented in equation 5. We treat the strong field regime in the CSCO(H_B), same as the intermediate field regime.

Since L, S, J and I are suitable quantum numbers for all the regimes, we will exclude them from the notation of the energy eigenstates with the underlying assumptions that they are known.

III. WEAK FIELD LIMIT

As already explained, in the weak field limit the suitable CSCO is CSCO(HFS). We can then rewrite the Hamiltonian $H'_w = H_{HFS} + H_B$ as

$$H'_w = \frac{C}{2\hbar^2}(F^2 - I^2 - J^2) + g_F \mu_B \frac{\vec{F}}{\hbar} \cdot \vec{B} \qquad (7)$$

where g_F is the composite Lande g factor derived in the following subsection. The derivation of the Lande g_F factor assumes that our total Hamiltonian is diagonal in the F basis, an approximation which we use in the weak field limit. If we assume that $\vec{B} = B\vec{e_z}$, we can rewrite the H'_w as

$$H'_w = \frac{C}{2\hbar^2}(F^2 - I^2 - J^2) + g_F \mu_B \frac{F_z}{\hbar} B$$

The shift of the energy eigenvalues due to H'_w can be found as $\Delta E_w = \langle F, F_z | H'_w | F, F_z \rangle$, or

$$\Delta E_w = \frac{C}{2}(F(F+1) - I(I+1) - J(J+1)) + g_F \mu_B F_z B \quad (8)$$

A. Lande g factors

In general, the magnetic moment $\vec{\mu}_X$ is proportional to $\vec{X}$ with the constant of proportionality

$$\frac{\vec{\mu}_X}{\vec{X}} = \frac{\mu_B g_X}{\hbar} \qquad (9)$$

where μ_B is the Bohr magneton and g_X is the Landè g factor associated with the angular momentum $\vec{X}$ [2]. Therefore, the g factor should encode dependence of the Hamiltonian, and therefore energy splittings, on different quantum numbers relevant to the problem. For electrons, the g_L factor for orbital angular momentum equals 1, whereas the g_S factor for spin angular momentum equals 2. The g factors for coupled angular momenta can be found by combining the coupling contributions. However, in combining the contributions we assume that the Hamiltonian is diagonal in the basis of quantum numbers we use.

1. Spin $\vec{S}$ and orbital $\vec{L}$ angular momenta

If we are considering both the spin and the orbital angular momentum of an electron, we can write the total magnetic moment using the formula 9 as:

$$\vec{\mu} = \frac{\mu_B}{\hbar}(g_L \vec{L} + g_S \vec{S}) \qquad (10)$$

Our goal is to express $\vec{\mu}$ in terms of only one angular momentum and its associated g factor. Since $g_L \neq g_S$, we cannot factor them out from the equation 10 and express only in terms of $\vec{J}$. Therefore, we have to add them as vectors, keeping in mind that both $\vec{L}$ and $\vec{S}$ have an orthogonal and a colinear component to $\vec{J}$. This addition is graphically described in the figure 1. Since both $\vec{L}$, $\vec{S}$ and therefore $\vec{J}$ precess around the magnetic field, the motion of $\vec{L}$ and $\vec{S}$ can be split into a component that precesses around $\vec{J}$ and a component that is colinear with $\vec{J}$. The contribution of the precessing component averages out to zero [2], so to get $\vec{J}$, we should take the projections of $\vec{L}$ and $\vec{S}$ onto it:

$$\vec{\mu}_J = \frac{\mu_B}{\hbar}(g_L L \cos(\alpha) + g_S S \cos(\beta)) \qquad (11)$$

The angles α and β can be obtained from the figure 1 using the law of cosine as $\cos(\alpha) = \frac{J^2 + L^2 - S^2}{2|J||L|}$ and $\cos(\beta) = \frac{J^2 + S^2 - L^2}{2|J||S|}$. Substituting these expressions into the equation 11, using that $g_J = \frac{\mu_J \hbar}{\mu_B |J|}$, and noting that the eigenvalues of a general angular momentum operator X^2 are $\hbar^2 X(X+1)$, we can write g_J as:

$$g_J = 1 + \frac{J(J+1) + S(S+1) - L(L+1)}{2J(J+1)} \qquad (12)$$

where in this notation J, S and L are quantum numbers associated with operators $\vec{J}$, $\vec{S}$ and $\vec{L}$.

2. Nuclear $\vec{I}$, spin $\vec{S}$ and orbital $\vec{L}$ angular momenta

In the case when we do not want to neglect nuclear angular momentum $\vec{I}$ and the Hamiltonian describing the
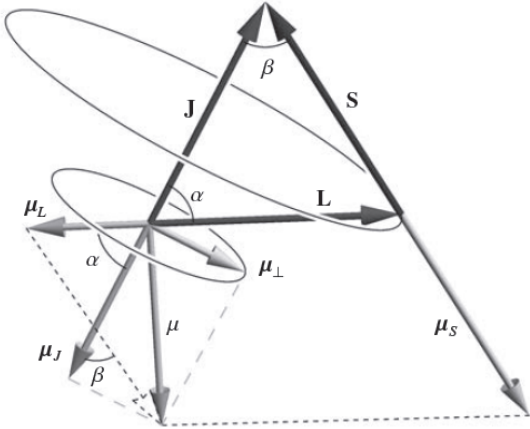
FIG. 1: Addition of $\vec{L}$ and $\vec{S}$. The precessing components perpendicular to $\vec{J}$ average out to zero, whereas the colinear components contribute in proportion to $\cos(\alpha)$ and $\cos(\beta)$. Adapted from [2]

system depends on it, we can define a new total angular momentum of the system to be $\vec{F} = \vec{J} + \vec{I}$. The process of deriving g_F is completely analogous to the process of obtaining g_J described before if we substitute $\vec{L}$ and $\vec{S}$ with $\vec{J}$ and $\vec{I}$. The equation 11 now becomes

$$\vec{\mu}_F = \frac{\mu_B}{\hbar}(g_J J \cos(\alpha') + g_I I \cos(\beta'))$$

We can make a simplification here by noting that the nuclear magnetic moment μ_I is much smaller than μ_J as a consequence of formula 1, so we can neglect the second term. The expression for g_F simplifies then to

$$g_F = g_J \frac{F^2 + J^2 - I^2}{2F^2}$$

After we substitute squares of angular momenta operators with their eigenvalues, we can rewrite g_F as

$$g_F = g_J \frac{F(F+1) + J(J+1) - I(I+1)}{2F(F+1)} \qquad (13)$$

where g_J is given by equation 12.

Since this paper will use Rb^{87} $S_{1/2}$ level to exemplify the dependence of the energy level splitting on the external magnetic field, it is useful to calculate the possible values of g_J and g_F for this state. Since the nuclear spin of Rb^{87} is $I = 3/2$, and $S = 1/2$ for electrons in general, we can narrow down the possible values of the quantum numbers F, J and L to those in the table I. The possible values of J (and analogously F) can be found from the angular momentum addition rule, $|L - S| \le J \le |L + S|$ [7].

I	L	$\|L - \frac{1}{2}\| \le J \le \|L + \frac{1}{2}\|$	g_J	$\|J - I\| \le F \le \|J + I\|$	g_F
$\frac{3}{2}$	0	$\frac{1}{2}$	2	1	$-\frac{1}{2}$
				2	$\frac{1}{2}$

TABLE I: The g factors for $I = 3/2$ ground state.

IV. INTERMEDIATE AND STRONG FIELD LIMIT

According to the previous definitions, the energy contribution of H_B dominates over the contribution of H_{HFS} in both the intermediate and the strong field limit. Since both the electron and the nuclear spin part of H_B have $CSCO(H_B)$, we will treat the strong and intermediate regime together in this basis. In that case, the equation 7 is no longer valid since the g_F factor cannot be defined. The suitable eigenbasis becomes the uncoupled basis, $|I_z, J_z\rangle$ [3]. Due to the angular momentum addition rule, these quantum numbers are related as $F_z = I_z + J_z$. The Hamiltonian in the uncoupled basis becomes

$$H'_s = \frac{C}{\hbar^2}\vec{I} \cdot \vec{J} + \frac{\mu_B}{\hbar}(g_J \vec{J} - g_I \vec{I}) \cdot \vec{B} \qquad (14)$$

If we again assume that $\vec{B} = B\vec{e_z}$, we can rewrite the Hamiltonian as

$$H'_s = \frac{C}{\hbar^2}\vec{I} \cdot \vec{J} + \frac{\mu_B}{\hbar}B(g_J J_z - g_I I_z)$$

The Hamiltonian H'_s cannot be further simplified and therefore cannot be diagonalized in the $|I_z, J_z\rangle$ basis due to the coupled term $\vec{I} \cdot \vec{J}$. For arbitrary I and J, we would have to find the eigenvalues of the non-diagonal Hamiltonian by evaluating $\langle I_z, J_z| H'_s |I_z, J_z\rangle$. The second term in the equation 14 is diagonal in this basis and therefore its evaluation is straight-forward. In order to evaluate the first term, we have to express $\vec{I} \cdot \vec{J}$ in terms of the raising and lowering operators $I_\pm$ and $J_\pm$. That can be done in the following way:

$$\vec{I} \cdot \vec{J} = \frac{1}{2}(I_+ J_- + I_- J_+) + I_z J_z \qquad (15)$$

However, even after evaluating the matrix elements of H'_s, we cannot always analytically find the eigenvalues of an $N \times N$ matrix. In order to show an example of an analytic derivation of the eigenvalues of H'_s, in this paper we will further explore $S_{1/2}$ level of Rb^{87} which has $I = 3/2$. The goal of this calculation is to express the energy eigenvalues of H'_s as a function of magnetic field strength and quantum number F_z, which is a suitable parameter since it appears in the weak field limit as well. We define a dimensionless magnetic field strength parameter $\delta = \frac{(g_I + g_J)\mu_B B}{2C}$. Assuming F_z is known, we can express $I_z = F_z - J_z$. Since J_z has two possible values of $\pm 1/2$, the eigenbasis for the Rb^{87} ground state then becomes two-dimensional, with eigenvectors $\left|F_z - \frac{1}{2}, \frac{1}{2}\right\rangle$ and $\left|F_z + \frac{1}{2}, -\frac{1}{2}\right\rangle$ [4].

...

We can solve for the eigenvalues of a two-by-two matrix representing H'_s using any of the standard algorithms. The result of this calculation, with $I = 3/2$, is

$$\Delta E_\pm = -\frac{C}{4} - g_I \mu_B F_z B \pm C\sqrt{\delta^2 + \delta F_z + 1} \qquad (16)$$

The equation 16 is known as the Breit-Rabi equation for the energy level shifts of $I = 3/2$ $S_{1/2}$ atomic energy state in an external magnetic filed [6]. It is expressed in terms of a dimensionless parameter δ which characterizes the magnetic field strength.

In order to check for the consistency of results in the weak and strong field limits, we can set $B = 0$ and calculate the energy eigenvalues in both cases. Using formula 16 for the strong field limit, and setting $B = \delta = 0$, we get $\Delta E \in (-\frac{5}{4}C, \frac{3}{4}C)$. On the other hand, the energy separation in the weak field limit with $B = 0$ and $F \in (1, 2)$ as given by formula 8 is $\Delta E \in (-\frac{5}{4}C, \frac{3}{4}C)$, which reproduces the zero field result of the strong field expression.

A. Breit-Rabi diagrams

Using equation 16 for strong and intermediate magnetic field, and equation 8 for weak magnetic field, we can plot the behavior of the energy levels of Rb^{87} $S_{1/2}$ at different values of B. The energy level diagram corresponding to the dependence of the energy splitting on the magnetic field magnitude which uses the Breit-Rabi formula is known as the Breit-Rabi diagram [3].

First thing to note for a Breit-Rabi diagram is that a line which corresponds to an energy level does not correspond to a well-defined energy eigenstate in either the $|F, F_z\rangle$ or the $|I_z, J_z\rangle$ basis. For weak magnetic fields, the energy eigenstates are well approximated by the basis $|F, F_z\rangle$, but this is still an approximation since we are assuming that the H_B term in the Hamiltonian is diagonal in this basis. Furthermore, since the Hamiltonian H'_s is not diagonal in the $|I_z, J_z\rangle$ basis, its eigenstates are in general a linear combination of the basis states, whose coefficients change with B. Therefore, the eigenstates are continuously mixing between the coupled and the uncoupled basis as we increase B.

Some of the key features of the Breit-Rabi diagram for Rb^{87} $S_{1/2}$ shown in the figure 2 are:

- **Weak magnetic field:** Since the energy splittings are now described by the formula 8, we can see that holding J and I fixed, energies will split according to different values of F and $g_F F_z$. According to the table I, the allowed values of F are 1 and 2, so we expect two groups of splitting, with $F = 1$ group below the $F = 2$ group. Within the group $F = 1$, $g_F = -1/2$ so the levels with positive F_z will be below the levels with negative F_z. We therefore get the ordering: $|2, 1\rangle < |2, 0\rangle < |2, -1\rangle$. In the $F = 2$ group, $g_F = 1/2$ so the ordering will be reversed: $|2, -2\rangle < |2, -1\rangle < |2, 0\rangle < |2, 1\rangle < |2, 2\rangle$.
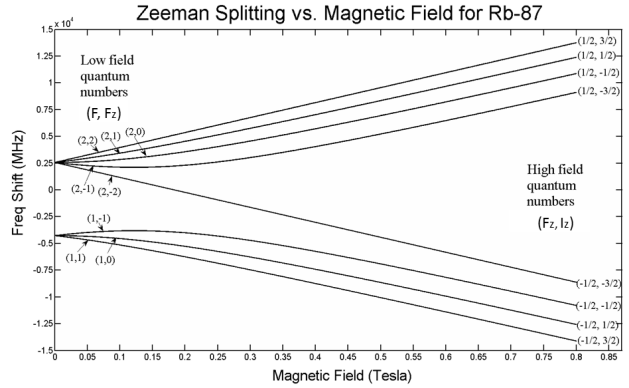
FIG. 2: Breit-Rabi diagram for Rb^{87} $S_{1/2}$, adapted from [5]. The energy splitting between different eigenstates is expressed in terms of frequency, using the formula $E = h\nu$.

- **Intermediate magnetic field:** According to the previous definitions, the energy contribution of nuclear spin is still negligible in the intermediate field regime. The Hamiltonian then has dominant contributions on the order of $g_J \mu_B J_z B + C I_z J_z$. The eigenstate ordering is still divided into two groups of lines, as shown in the figure 2, with the eigenstates with $J_z = 1/2$ being in the upper group, while the ones with $J_z = -1/2$ in the lower group. Within the J_z groups, I_z ordering goes from highest($3/2$) having the highest energy to lowest ($-3/2$) having the lowest energy in the upper group. In the lower group, the ordering of I_z values is reversed due to the sign change in multiplication with $-1/2$.

- **Strong magnetic field:** In the strong magnetic field regime, even nuclear spin energy contributes more to the energy splittings than the hyperfine interaction. The main contributions to the Hamiltonian are then on the order of $g_J \mu_B J_z B - g_I \mu_B I_z B$. The groups of lines are still split according to J_z as in the intermediate magnetic field, but the ordering of I_z is now reversed: $I_z = -3/2$ is the highest energy state in the upper group while $I_z = 3/2$ is the lower energy state in the lower group etc.

V. FIRST ORDER FIELD-INDEPENDENT TRANSITIONS AND TRAPPABLE STATES

According to the previous discussion, we can conclude that different atomic energy eigenstates have different energy values when they are in an external magnetic field. Conversely, if an electron makes a transition from one energy level to another while in a magnetic field, the atom

will gain or lose energy by a different amount than it would without an external field. This effect is exploited for trapping neutral atoms in a magnetic field by preparing them in the states whose energy is an increasing function of the magnetic field [2–4]. Since atoms, as everything else in nature, tend to minimized their energy, they will stay confined in the part of the space where the magnetic field is lower.

On the other hand, if we would do experiments on atoms trapped in this way, we would not want them to change their energy abruptly since then they would fall out from the trap. Therefore, if we would do a precision measurement of a resonant frequency of one of the transitions in a trapped atom, we should choose one which is as little dependent on the magnetic field as possible. These transitions are called first order field-independent transitions since their dependence of the energy change ΔE on the external field parameter δ is of the order $O(\delta^2)$ [4]. We will now apply the aforementioned criteria to determine which field independent trappable atomic states we can choose from the $S_{1/2}$ Rubidium manifold previously explored.

In order to magnetically trap an atomic state, as already mentioned, its energy has to be an increasing function of the magnetic field. By looking at the figure 2, we can see that the only state in the $F = 1$ group which has such property is $|1, -1\rangle$ for weak fields (it slopes down for stronger fields). If we consider the electric dipole selection rule that $\Delta F_z = 0, \pm 1$ for a single photon transition, the allowed transitions from this state are to $|2, 0\rangle$, $|2, -1\rangle$ and $|2, -2\rangle$. The states $|2, -1\rangle$ and $|2, -2\rangle$ have, however, a decreasing energy with magnetic field, so they cannot be trapped. The only remaining transition is from $|1, -1\rangle$ to $|2, 0\rangle$

We now want to see which field strength we need in order to have a first-order magnetic field independent transition between these two states. We will express the energy of that transition using the formula 16 and substituting the appropriate values for F_z and I. The normalized energy difference, $\frac{E(|2,0\rangle) - E(|1,-1\rangle)}{2C}$ is equal to

$$
\begin{aligned}
\frac{E(|2,0\rangle) - E(|1,-1\rangle)}{2C} = \\
-2\delta \frac{g_I}{g_I + g_J} + \frac{1}{2}(\sqrt{\delta^2 + 1} + \sqrt{\delta^2 - \delta + 1})
\end{aligned} \tag{17}
$$

Since we are in the weak field regime, δ is very small and we can therefore expand the previous expression to the

second order in δ. The transition energy then simplifies to

$$
\frac{E(|2,0\rangle) - E(|1,-1\rangle)}{2C} = -2\delta \frac{g_I}{g_I + g_J} + 1 - \frac{\delta}{4} + \frac{7\delta^2}{16}
$$

Since the requirement for the desired transition is that the transition energy is insensitive to the first order in B and therefore δ, we take the first derivative of the previous expression and set it to zero to determine the optimal value of δ:

$$
\frac{1}{2C} \frac{\partial(E(|2,0\rangle) - E(|1,-1\rangle))}{\partial \delta} = -2\frac{g_I}{g_I + g_J} - \frac{1}{4} + \frac{7}{4}\delta = 0
$$

from where we get

$$
\delta = \frac{1}{7} + \frac{8}{7} \frac{g_I}{g_I + g_J}
$$

Therefore, using the derived results for the energy splittings in the magnetic field, we can decide which states could be trapped magnetically, and we can derive the value of the magnetic field needed for making the transitions between them field insensitive.

VI. CONCLUSION

In this paper we presented a derivation of the energy level splittings in the external magnetic field, taking into consideration the fine and hyperfine atomic structure. The main challenge in the derivation was how to treat different parts of Hamiltonian which cannot be diagonalized simultaneously. That challenge was overcome by considering the relative importance of different terms in the Hamiltonian, and choosing to work in the basis of the dominant terms. In the case of the external magnetic field, this results in mixing of the states with different quantum numbers at different values of magnetic fields. In order to visualize how the energies of the quantum states change with the changing field, we introduced the Breit-Rabi diagrams, and showed their properties on the example of Rb^{87} $S_{1/2}$ state. Finally, we showed how the energy level diagrams can be used to deduce which states can be captured in a magnetic trap, and which trap strength should be chosen in order to make selected electronic transitions first order field-insensitive.

[1] M. Auzinsh, D. Budker, S. Rochester, *Optically Polarized Atoms: Understanding Light-atom Interactions*, Oxford: Oxford University Press (2010)
[2] C.J. Foot, *Atomic physics*, Oxford : Oxford University Press (2005)
[3] *MIT Atomic Physics Wiki*, cua-admin.mit.edu/apwiki/ wiki/Main_Page
[4] I. Chuang, *Solutions to Problem set 3 of 8.421 Spring*

2014, MIT (2014)
[5] *Breit-Rabi diagram of Rubidium 87*, http://commons. wikimedia.org/wiki/File:Breit-rabi-Zeeman.png
[6] G. Breit and I.I. Rabi, *Measurement of Nuclear Spin*, Phys.Rev, 38, 2082 (1931)
[7] B. Zwiebach, *8.05 Course Notes*, MIT (2013)

An Exploration of Quantum Walks

Steven B. Fine[*]

MIT Department of Physics
(Dated: May 2, 2014)

The concept of a quantum walk is introduced and is motivated by the classical problem of a random walk. Two specific examples of quantum walks, one between two glued binary trees and another to calculate the output of a NAND tree are discussed along with the universality of quantum walks and their presence in nature.

1. INTRODUCTION

1.1. Graph Fomalism

In the field of classical computation, one of the most fundamental abstract data types is a graph. Graphs are defined by a set of vertices, and a set of edges, where the edges connect the vertices. For the purposes of this paper I will be discussing undirected graphs. In an undirected graph, edges do not have a specified direction.
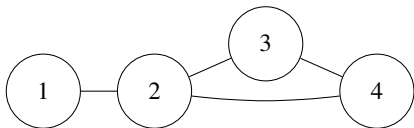
FIG. 1: A simple undirected graph

Figure 1 illustrates a very simple undirected graph. The vertices that define this graph are $V = \{1, 2, 3, 4\}$, and the edges are given by a set of unordered pairs connecting the vertices as shown: $E = \{\{1, 2\}, \{2, 3\}, \{2, 4\}, \{3, 4\}\}$.

An alternate representation of a graph is given by an adjacency matrix. Two vertices are said to be adjacent if they are connected by an edge. An adjacency matrix is a $v \times v$ matrix where v is the number of vertices. The matrix element $A_{ij} = 1$ if the vertices are connected by an edge, and 0 otherwise. The adjacency matrix of the graph in Figure 1 is given by the following matrix:

$$A = \begin{bmatrix} 0 & 1 & 0 & 0 \\ 1 & 0 & 1 & 1 \\ 0 & 1 & 0 & 1 \\ 0 & 1 & 1 & 0 \end{bmatrix}$$

Its important to note that the matrix is symmetric. This reflects the undirected nature of the graph because if there is an edge connecting vertices i and j, then there is an edge connecting vertices j and i.

_____

[*]Electronic address: sfine@mit.edu

1.2. The Quantum Analog of Random Walks

One common application of a graph is a random walk. In a random walk an agent starts at a specific vertex and has a certain probability of moving to any given adjacent vertex at the next time step. After a certain amount of time, the possible locations of the agent will be represented by a probability distribution over the vertices of the graph.

In analogy to the classical random walk, we can construct a quantum walk. For the purposes of this paper I will discuss continuous-time quantum walks, where time is treated as a continuous variable (as opposed to discrete time quantum walks). We will define the Hilbert space of our continuous-time quantum walk to be $\mathcal{H} = \text{span}\{|v\rangle\} \, \forall \, v \in V$, where we previously defined V to be the set of vertices in the graph. Each vertex $v \in V$ defines a basis state which we will refer to as $|v\rangle$. The Hamiltonian of a particular graph is given by the negative of the adjacency matrix: $H = -A$. [1] This is justified because the off diagonal terms of the Hamiltonian represent the coupling between states. Therefore, in the Hamiltonian when you have $\langle i| H |j\rangle = -1$, there must be an edge connecting vertex i and vertex j.

In order to determine the time evolution of our quantum walk, we need to solve the Schrödinger equation, given by:

$$i\frac{\partial |\Psi\rangle}{\partial t} = H |\Psi\rangle \tag{1}$$

For most systems, since our graph is not changing in time, the solution to the Schrödinger equation is given by:

$$|\Psi(t)\rangle = e^{-iHt} |\Psi(t = 0)\rangle \tag{2}$$

2. QUANTUM WALK ON GLUED BINARY TREES

2.1. An Exponential Speedup Over Random Walks

Quantum walks are an interesting topic of study because some quantum walks exhibit highly different behavior from their classical counterparts. In this section

I will discuss the traversal of two binary trees that are said to be "glued" together (Shown in Figure 2). This graph shows two trees that each have depth 4, but we can imagine them being of arbitrary depth.

Consider the classical problem. An agent starts at the vertex on the left and wants to end up at the vertex on its right. However, at each position, the agent has an equal probability of moving to any adjacent vertex. During the first time step, the agent will move either to the left or the right, but no matter which way it goes, it will get closer to the destination. During every future time step, as long as the agent is in the left half of the tree, there are two vertices it can move to that will bring it closer to its destination, and one vertex that brings it farther away. This means that the agent always has a probability of $2/3$ of moving forwards and a probability of $1/3$ of moving backwards.
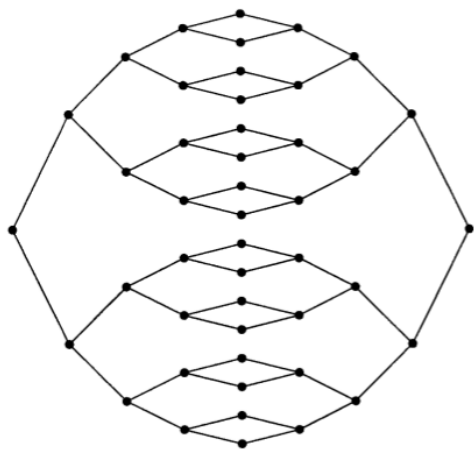
FIG. 2: Binary Trees "Glued" Together (Taken From [3])

The problem arises when the agent makes its way to the right half of the tree. Because the right binary tree is identical, but reversed, the agent now has a higher probability of moving back towards the middle of the tree, than to its destination. Therefore, the probability of reaching its destination after any number of steps is smaller than $\frac{1}{2^n}$, where n is the depth of each tree. [2]

In the quantum analog, if an agent were to traverse this graph such that its behavior is defined by a quantum walk, there is an exponential speedup in the traversal time of the agent. The reason for the quantum mechanical speedup is due to a symmetry in the graph that restricts the evolution to a lower dimensional subspace of the Hilbert space defined by our graph. We will define the set of states,

$$|\text{col j}\rangle = \frac{1}{\sqrt{N_j}} \sum_{\alpha \in \text{col j}} |\alpha\rangle \qquad (3)$$

where each $|\text{col j}\rangle$ represents all the nodes that are of equal depth in the graph. The original Hilbert space was a $2^{n+1}+2^n-2$-dimensional space, where n is the depth of each tree. The new space consists of $2n-1$ basis states. [2] The key feature of these states is that applying the Hamiltonian to any individual state $|\text{col j}\rangle$, puts the system in a uniform superposition of its neighboring states $|\text{col j-1}\rangle$, $|\text{col j+1}\rangle$, which can be seen in Equation 4.

$$H |\text{col j}\rangle \propto -|\text{col j-1}\rangle - |\text{col j+1}\rangle \qquad (4)$$

Considering our graph in terms of the column states that we have constructed, the quantum walk on this graph can be reduced to a much simpler problem. The action of the Hamiltonian on our states $|\text{col j}\rangle$ is identical to the action of the Hamiltonian of a finite line graph (Figure 3) on the basis states $|v\rangle$, where v are the vertices of the finite line graph.
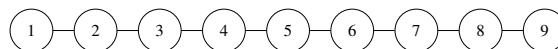
FIG. 3: Finite Line Graph

Given the transformation to this new problem, there is a substantial probability of measuring that an agent that started at the leftmost vertex is at the rightmost vertex after a time on order n. [2] This is exponentially faster than the classical time.

2.2. A Slowdown Compared To Random Walks

The traversal of the graph using the quantum walk formalism is exponentially faster than the classical random walk. However, in order to restrict our problem to the Hilbert space given by $\mathcal{H} = \text{span}\{|\text{col j}\rangle\}$ and achieve the exponential speedup, we must have started in one of the $|\text{col j}\rangle$ states. But what if our agent started at a different node? Would we see the same exponential speedup over the random walk?

It has been shown that if the agent starts at the topmost vertex of the glued binary tree as depicted in Figure 2, the probability of reaching the bottom vertex is actually much smaller than for a classical random walk. [4]

3. A QUANTUM WALK ON A NAND TREE

The next application of quantum walks that I will discuss is the efficient evaluation of a NAND tree. I follow the treatment by Farhi et al. [5] A NAND gate is a device that takes in two classical bits as input and returns one classical bit as output: it outputs 0 if both inputs are 1, and 1 otherwise. We define a NAND tree to be a binary tree where each leaf (top vertex) is given an input of a 0 or 1. We can recursively define the output of each sub-NAND tree to be the NAND gate computation of the output of its two input NAND trees. We will say

that the output of a leaf is the initial input to that leaf. This can be seen in Figure 4. The goal of this problem is to determine the output of the tree.
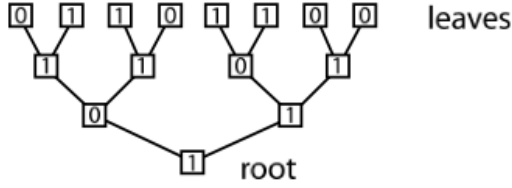
FIG. 4: A Sample NAND Tree (Taken From [5])

Classically, the brute force method of solving this problem is to fill in the NAND tree, one vertex at a time, which takes O(N) if there are N leaves, because there are 2N-1 vertices in the tree. There is a probabilistic algorithm that is O(N$^{.753}$) [6], but using the quantum walk walk formalism the output of a NAND tree can be calculated in O($\sqrt{N}$).

The basic setup is to take the binary tree that is the same shape as the NAND tree, and connect it to a long runway of vertices that connects to the root node of the tree. The inputs of the NAND tree are set to 1 if there is an additional vertex that is connected to that leaf. If the additional vertex is not connected to the leaf, then that leaf will behave as a 0. The graph that represents the the NAND tree in Figure 4 is shown in Figure 5. The output of the NAND tree can be determined by sending in a wave packet from the left. If the packet transmits to the right side of the tree, the output of the tree can be shown to be a 1, otherwise it is a 0.
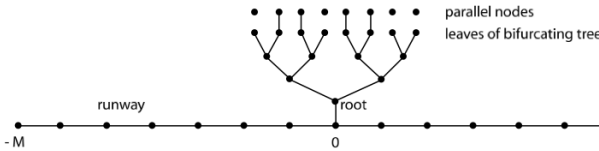
FIG. 5: A Sample NAND Graph For a Quantum Walk (Taken From [5])

The first thing to realize is that while on the runway applying the Hamiltonian to a state $|r\rangle$, where r is the position on the runway, puts the state into a superposition of the neighboring states,

$$H |r\rangle = - |r+1\rangle - |r-1\rangle \qquad (5)$$

Therefore, in the position basis the energy eigenstates are of the form $e^{+ir\theta}$ and $e^{-ir\theta}$ which we will call $\langle r| E\rangle$. Applying the Hamiltonian to the $e^{+ir\theta}$, which refers to a wave moving to the right gives,

$$He^{ir\theta} = -e^{i(1+r)\theta} - e^{i(-1+r)\theta} = -2\cos\theta e^{ir\theta} \qquad (6)$$

The $e^{-ir\theta}$ state has the same eigenvalue, which refers to a left moving wave. Since our initial wave is a right moving wave our state is of the form,

$$\langle r| E\rangle = \begin{cases} e^{ir\theta} + R(E)e^{-ir\theta} & : r \le 0 \\ T(E)e^{ir\theta} & : r \ge 0 \end{cases}$$

where $1 + R(E) = T(E)$ by plugging in to $r = 0$. Applying the Hamiltonian to $|r = 0\rangle$,

$$H |r = 0\rangle = - |r = -1\rangle - |r = 1\rangle - |root\rangle \qquad (7)$$

where $|root\rangle$ is the root of the NAND tree. Taking the inner product with $|E\rangle$ gives,

$$T(E) = \frac{2i\sin\theta}{2i\sin\theta + y(E)} \qquad (8)$$

where $y(E) = \frac{\langle root| E\rangle}{\langle r=0| E\rangle}$.

The remainder of the discussion is to show that $y(0) = 0$ if the NAND tree evaluates to 1, and $y(0) = -\infty$ if the NAND tree evaluates to 0. A wave packet with $E = 0$ cannot be constructed precisely, but in [5] they show that you can build a wave packet that is close enough to $E = 0$, so that $T(E)$ is very close to $T(0)$. Here we will assume that the wave packet has a near 0 energy, but positive.

Other than the root vertex and the leaves of the NAND tree, all vertices are surrounded by exactly three other vertices, 1 parent and 2 children, as shown in Figure 6.
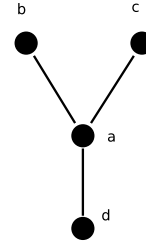
FIG. 6: The Vertices Surrounding a Local Vertex (a)

Applying the Hamiltonian to the vertex a, puts the system in the state,

$$Ea = -b - c - d \qquad (9)$$

This can be rewritten as,

$$Y = \frac{-1}{E + Y' + Y''} \qquad (10)$$

where $Y = \frac{a}{d}$, $Y' = \frac{b}{a}$, $Y'' = \frac{c}{a}$. In this setup, y(E) is equal to Y in the case where (a) is equal to $|root\rangle$ and (d) is equal to $|r = 0\rangle$.
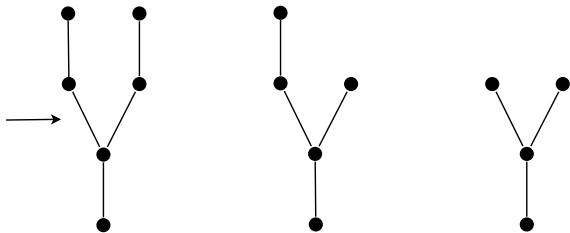
FIG. 7: The Possible Inputs To The NAND Tree

At the leaves of the NAND tree there are 3 possible inputs as shown in Figure 7. Calculating the value of Y at the level of the arrow on the left you find that if the leaf does not have the extra connection $Y = -\frac{1}{E}$, and if it has the extra connection, $Y = \frac{E}{1-E^2}$. This can be found by applying the Hamiltonian to the different nodes in the tree. Plugging in for E = 0 gives that when the leaf of the NAND tree was designated a 1 by the extra connection, we have that $Y = 0$, otherwise $Y = -\infty$. This yields precisely the NAND gate. Looking at the recursion relationship in equation 12, we can see that $Y = 0$ if either Y' or Y'' are -∞, and $Y = -\infty$ only if $Y' = Y'' = 0$. This is a NAND gate where $Y = 0$ corresponds to a 1, and $Y = -\infty$ corresponds to a 0. Therefore, if the output of the NAND tree is a 1, $y(0) = 0$, and if the output of the NAND tree is a 0, $y(0) = -\infty$. This means that if we measure the wave at positive r, then the NAND tree outputs a 1, because the transmission amplitude, $T(0)$ was roughly equal to 1. If we don't measure the wave, then the NAND tree outputs

a 0, because the $T(0) \approx 0$. In Farhi et al. [5] they show that the wave starting with $E \approx 0$ takes $O(\sqrt{N})$ time to either propagate to the right side or get reflected.

4. DISCUSSION

In this paper I have introduced the concept of a quantum walk motivated from the classical random walk. I would like to expand a little on broader applications of quantum walks. First there are a lot of resources that discuss the theoretical possibility that mechanism of energy transport in photosynthesis is a quantum walk. [7] When a photosynthetic cell absorbs a photon it produces an exciton that must travel to the reaction center of the cell. There is a much higher efficiency of energy absorption than would be expected from any classical model, and can be predicted by models that resemble quantum walks. Additionally, it has been shown that a generalized quantum walk is universal for any quantum computation. [8] The presence of quantum walks in nature, and their universality make them a particularly interesting topic of study.

Acknowledgments

[1] . E. Farhi, S. Gutmann, Quantum computation and decision trees. *Physical Review* A, 58:915-928, 1998.

[2] . A. Childs, E. Farhi, S. Gutmann, An example of the difference between quantum and classical random walks. *Journal of Quantum Information Processing*, 1:35, 2002.

[3] . A. M. Childs, R. Cleve, E. Deotto, E. Farhi, S. Gutmann, D. A. Spielman, Exonential Algorithmic Speedup by a Quantum Walk.

[4] . O. Mülken, and A. Blumen, Slow transport by continuous time quantum walks. *Physical Review* E 71, 016101 2005.

[5] . E. Farhi, J. Goldstone, S. Gutmann, A Quantum Algo-

rithm for the Hamiltonian NAND Tree.

[6] . P. Hoyer and R. Spalek, Lower Bounds on Quantum Query Complexity. Bulletin of the EATCS, 87, (2005); quant-ph/0509153.

[7] . M. Mohseni, P. Rebentrost, S. Lloyd, and A. Aspuru-Guzik. Environment-assisted quantum walks in photosynthetic energy transfer. *The Journal of Chemical Physics*, 129, 174106 (2008)

[8] . Andrew M. Childs, Universal Computation by Quantum Walk

Computing Physics: Quantum Cellular Automata

Goodwin Gibbins
University of Cambridge - MIT
(Dated: May 2, 2014)

This report outlines the logical progression from the desire to simulate physics with computers through cellular automata, computability, Turing machines, quantum-dot cellular automata, quantum Turing machines and finally quantum cellular automata. Modeling large-scale quantum mechanical systems in the natural world will require an increase in localized parallel computing power which quantum cellular automata seem, at first glance, to be ideal candidates for. However, as this paper introduces, the concept of universality in computing systems means that the theoretical computing constraints which apply to Turing machines apply to cellular automata too, although the spatial distribution of the computing may be more physical or efficient. Quantum computing can provide advances in efficiency due to the possibility of simultaneous exploration of multiple entangled states, but the limits of unitary time evolution constrain the types of quantum computers which can be explored.

I. INTRODUCTION

There are are two major approaches to simulating physics: building a model system which replicates the original by obeying the same physical rules (analogue) or programming a computer to estimate the properties of the system at discrete intervals following certain laws (digital) [1]. This paper will explore the second of those two options, specifically as applied to quantum mechanical computing systems. For a treatment of the first option, see A. Ireland's report in this volume.

In his formative 1981 lecture titled *Simulating Physics with Computers*, Richard Feynman introduces two physically-motivated goals for simulation of the natural world [1]. The first is that the algorithms which the computer carries out should be local: updates to a part of the system being modeled should be made based on the state of nearby regions only. This condition reflects the natural world under the limitations of the speed of light, but is not mirrored in the archetypical universal computer, the Turing machine. Instead, it suggests exploration of a computational system based on *cellular automata*, which will be explored at length in this paper.

Feynman's second condition is that the size of the model should be proportional to the space-time volume of the system, so that the model can be scaled up comfortably with the size of the system. Consider, for example, N numbered boxes each containing one of Schrödinger's famous cats. Classically, the system can be described by N bits, a 1 if the cat inside the nth box is alive and a 0 if it is dead. If the size of the system were doubled, $2N$ bits would be needed and Feynman's condition would be unproblematic. However, in a quantum mechanical situation, classical variables cannot describe the system as succinctly. Not only could a 'cat' be in a superposition of alive or dead states within the box, the system could be in an *entangled state* where the aliveness of each cat depends on the state the measured for the other cats. When recorded classically, the model would then have to keep track of 2^N complex numbers for N cats and $(2^N)^2$ if the number of boxes were doubled, defying Feynman's

condition. Recording the system in quantum bits, *qubits*, which singly can be in a superposition of state 0 and 1 or which as a group can be in an entangled state, is the natural computing extension which makes models of the quantum world tractable.

In this report we will explore computing systems which have the potential to fulfill both of these conditions. Starting from a theoretical discussion of classical Cellular Automata (CA) in Section II and the theory of computability in Section III, we explore a brief example of a quantum mechanical system used to implement a classical CA (Sec IV). In Section V we then introduce Quantum Turing Machines (QTM) and discuss the difficulties in combining the concepts of QTM and CA into Quantum Cellular Automata (QCA). Specifically we examine the case of 1D Partitioned Watrous Quantum Cellular Automata (1d-QCA) in Section VI.

II. CLASSICAL CELLULAR AUTOMATA

Following the notation in Ref. [2], a classical deterministic cellular automata consists of a lattice of cells (L) each of which takes a state in the finite set Σ. Every cell is updated simultaneously at discrete time intervals according to some transition function or *rule* $f : \Sigma^{\mathcal{N}} \to \Sigma$ where $\mathcal{N}$ defines the finite local neighborhood which each lattice point evolution can depend on. The state at each time point is some $C_t \in \Sigma^L$ which is absolutely determined by the starting configuration C_0.

The simplest cellular automata are one-dimensional periodic arrays, $L = 1, 2, 3....n$ with neighborhoods restricted to the current cell and the adjacent cell on either side. There are therefore 2^3 possible triplet configurations of 1 (black) and 0 (white) in the input space of f and two choices of output for each input, leading to $2^{2^3} = 256$ possible rules, one of which is shown in Figure 1. As time proceeds, each new configuration of the 1D lattice is printed on subsequent lines, showing the emergence of large and complicated patterns from a simple starting seed.

80
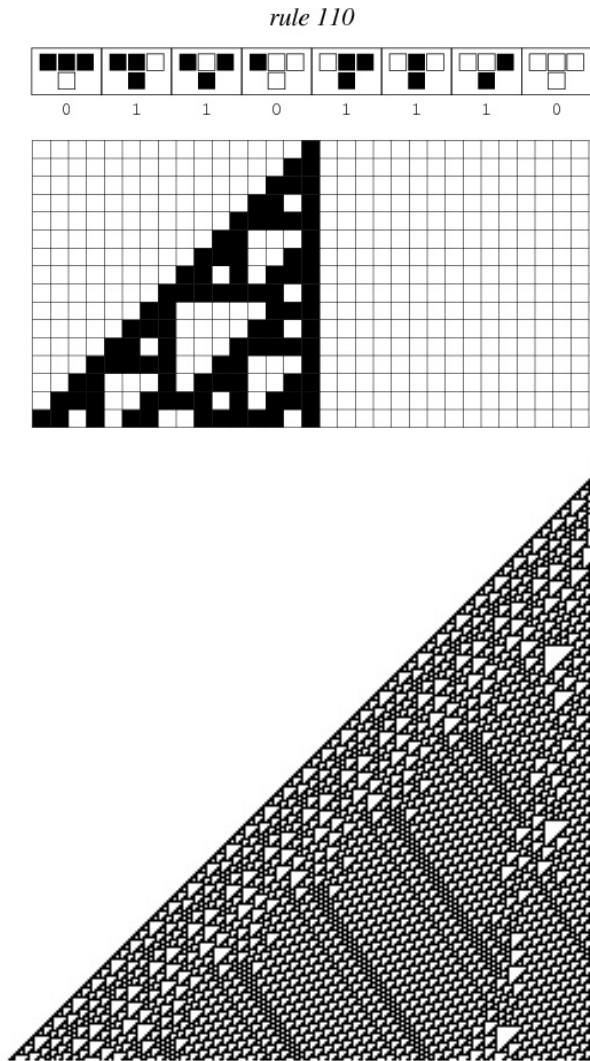
rule 110

FIG. 1: An example of an elementary cellular automata identified as Rule 110 due to the binary interpretation of the program (the row of numbers above). In the figures, a pattern is grown starting from a single black cell. The vertical direction shows discrete time steps on two different scales. Even from this simple starting configuration, large scale structures emerge which can interact and propagate through time, providing the basis for the construction of universal computers based on this rule [3]. (Figure from [4])

This complexity is representative of the exciting potential of cellular automata. Although they are built from simple update rules (like Hamiltonians in the physical world), the interaction of many adjacent cells demonstrably leads to complex behavior (like life in the physical world). These complex rules are also the most computationally rich ones as the large scale structures which emerge can interact with each other, annihilating or changing in prototypes of NOT or OR gates [5]. It can be shown that some cellular automata, such as the Rule 110 above, are capable of computations as complex as any computer can perform (See Ref. [3] for details).

III.   COMPUTABILITY

Proving that the computing capabilities of two systems are equivalent requires demonstration that each is capable of running a simulation of the other. In *computability theory*, the common benchmark for comparison is the *Turing Machine* (TM), which also provides a definition of what it means for a problem to be *computable*.

Developed in 1936 by Alan Turing, the Turing machine is a purely theoretical device designed to provide a framework for answering the question of which types of problems are solvable by computers [6]. A TM consists of a semi-infinite tape with spaces in which characters from a finite alphabet can be recorded and replaced. The read/write head of the machine is found at any time step over a certain space on the tape, although the absolute position is not recorded. However, the machine can keep track of another variable in the form of its state (as in 'state of mind'), which must be drawn from a finite set including a 'halt' state to be entered once a problem has been solved. The program is then a set of rules for updating the machine's internal state, replacing the character on the tape and moving the reader left or right depending on the current state of the machine and the character read on the current square of tape. A problem is then defined to be *computable* if there exists a Turing machine which will eventually solve any instance of the problem and halt.

Church's Thesis establishes that all computer systems are limited by the bound of computability. Specifically, there exist non-computable problems that no computer can solve, such as the *halting problem*. To understand this, suppose contrarily that there existed a machine, $\mathbf{H}$, that could compute whether or not any Turing Machine T would ever halt when presented with a problem, S. Now consider another machine $\tilde{\mathbf{H}}$ which is defined such that it runs $\mathbf{H}(T, S)$ and halts if and only if $\mathbf{H}(T, S)$ returns 'does not halt', i.e. T running S does not ever halt. The contradiction occurs when considering running $\tilde{\mathbf{H}}$ on itself: if it (the outer version of $\tilde{\mathbf{H}}$) halts, it implies that the inner version does not halt and vice versa. If you arrange the machines so that they are both acting on a string which represent themselves, this contradiction is unresolvable and the halting problem has to be declared *non-computable* [7]. This logic is similar to the diagonalization approach to proving the uncountably infinite nature of the real numbers [7] or, more directly, to the statement 'this sentence is false' [8].

Quantum computers are not thought to be able to provide ways to compute non-computable problems, but they are known to provide improvements in efficiency when solving other problems. A program is *efficient* if, given any instance of a problem which can be specified

with n characters, it runs in *polynomial time*: $t \propto n^a$ for some constant a. Problems which can be solved by an efficient program are contained within the class P, which is contrasted with the class of NP (Nondeterministic Polynomial-Time) problems, which can be checked but not (we think) solved in polynomial time. In the early 1970s, the theory of "NP-completeness" showed that many of the NP problems are equivalently difficult to each other; that is, given an algorithm that would solve one, another could be solved in similar time. Examples of NP-complete problems include finding the largest subset of people who know each other in a group (the clique problem) or deciding whether a certain map can be colored with only three colors. Quantum computers have not provided a method for solving NP-complete problems efficiently, but they do give improvements on lesser non-P problems, such as the factoring algorithm provided by Shor [8]. The limit on the efficiency improvements quantum computers might provide is an open question which we will not seek to address further here.

IV.   QUANTUM DOT CELLULAR AUTOMATA

At present, cellular automata computing systems are almost exclusively being modeled on conventional computers and not being used as computation tools in their own right. However, circuits based on the classical cellular automata but built out of quantum components are currently being investigated for new generation small computing systems. In modern computers, bits are encoded in current switches in a circuit which are probed by sending voltages into the circuit. This means that the size of the system is ultimately limited by the statistical fluctuations on the order of a charge quanta and requires a constant power supply as the current flows to ground [9]. The quantum-dot cellular automata (QDCA) discussed here are a system for encoding classical bits in the bistable ground states of quantum dot arrangements. Note that although these QDCA are both 'quantum' and 'cellular automata', they are deterministic computational systems and so not 'quantum computers' in the technical sense.

A quantum dot is a small finite well potential in which individual units of charge can be confined at discrete energy levels. Since the essential behavior of quantum dots relies only on the small size and electric properties of electrons, they can be constructed in many systems: in small metal regions in an insulating matrix, in areas of molecules which can accept electrons without reacting and in wells drawn by current-carrying wires onto semiconductors [9]. Recall the form of the energy levels in an infinite square well potential [10]:

$$E_{n_x n_y n_z} = \frac{\hbar^2 \pi^2}{2m} \left(\frac{n_x^2 + n_y^2 + n_z^2}{a^2} \right)$$

where E is the energy, n_x, n_y, n_z index the energy levels in the x, y, z directions, m is the mass of the electron

and a is the size of the potential well. By reducing a the energy of the ground state of the well can be increased. Although, by the Pauli exclusion principle, up to two electrons can fill the ground state energy level, Coulomb forces introduce an interaction term into the Hamiltonian which increases the energy penalty for adding a second electron to the same dot. By ensuring that the chemical potential of the surroundings is sufficiently low, it is possible to ensure that each well will have an expectation number of electrons between 0 and 1.

A second well placed spatially close to the first will be accessible to the electron via *tunneling*, which can be tuned by the manufacturer by changing the spacing or the height of the potential step between wells. This allows a configuration of nearby quantum dots to update itself to find the distribution of electrons which minimizes energy without external prompting.
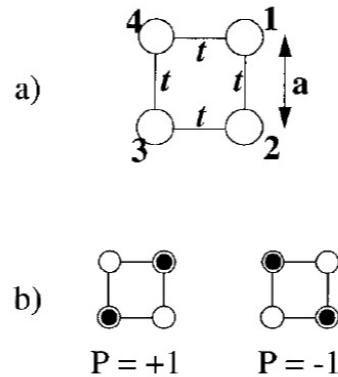
FIG. 2: A diagram of the simple four-dot cell used in QDCA. In (a) each site, 1-4, represents an identical 3D finite well potential with barriers between that can be tunneled through. When two electrons (shaded black) are added to the system there will be two degenerate ground states as shown in (b) due to the electrostatic repulsion between electrons. Alone, a single cell will adopt a superposition of both ground states, but if driven by an external electrostatic potential (such as an adjacent cell) one configuration will be favored, allowing each cell to behave like a classical bit. In this model, electrons may not tunnel out of the four-dot cell. (Image from Ref. [11])

Quantum dot cellular automata present a possible way to use this fact to build fast, low energy computing gates. The basic unit cell consists of four quantum dots, arranged in a square in two dimensions (see Figure 2, a) and containing two electrons. The tunneling barrier between adjacent cells is large enough that the electrons cannot escape and so they localize into dots across the diagonal from each other to reduce electrostatic energy, as in Figure 2 (b). Without external interactions, the stable configuration will be a superposition $P = 1$ and $P = -1$, but when two such cells are placed next to each other, the electrostatic repulsive term will act between the cells, resolving the degeneracy in favor of the

bistable diagonal configuration causing the cell to adopt a determined polarization corresponding to a classical bit.
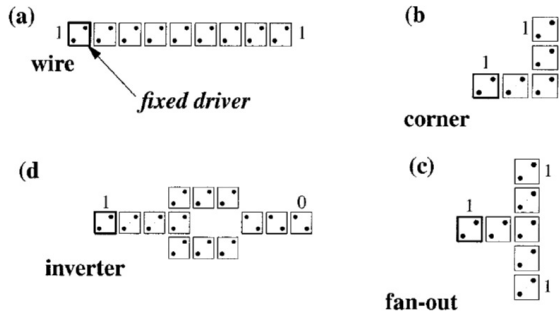
FIG. 3: Four possible components which can be built out of adjacent quantum dot cells interacting through Coulomb interactions. (Image from Ref. [11])

With only nearest-neighbor cell interactions and 2D spatial organization, many logical components can be built, as displayed in Figure 3. These components can then be put together to construct at Turing-complete computer, as capable as the theoretical Turing computer discussed above.

Although the quantum dot cellular automata relies heavily on quantum mechanical features of the system, it does not allow superpositions of states in each bit - the electrons are localized in a specific ground state parallel to the adjacent cell state. To create a true quantum cellular automata, we require the ability to have superpositions of multiple quantum states which in turn requires careful redefining of quantum cellular automata.

V. QUANTUM TURING MACHINE

Like the classical TM discussed above, Quantum Turing Machines (QTM) are the central theoretical model in quantum computation. Following the notation in Ref. [12], a machine M can be described by a quintuple (K, Σ, μ, k, A) where K is the finite set of states the machine can adopt, Σ is the *tape alphabet* which represents the possible states each square on an infinite tape can be in (including a blank state), μ is the *local transition function* which dictates the updates carried out at each time step, k is the *acceptance tape square*, an integer indicating the current position of the machine, and $A \subseteq \Sigma$ is the set of *accepting symbols*.

Each *configuration* of the machine is then uniquely described by a triple (k, h, c), with $k \in K$ indicating the current state of the machine, $h \in \mathbb{Z}$ the location of the tape head and $c : \mathbb{Z} \to \Sigma$ the contents of each cell on the tape. The model requires that there be only a finite number of non-blank squares on the tape in any configuration so that the set of all possible configurations is

countably infinite. While it is running, a quantum Turing machine will be in a *superposition* of some finite subset of these states with complex *amplitude* determined by μ. The set of possible configurations is akin to the set $\{|\uparrow\uparrow\rangle, |\uparrow\downarrow\rangle, |\downarrow\uparrow\rangle, |\downarrow\downarrow\rangle\}$ in the case of two entangled spin-1/2 particles.

The program which the QTM executes is written into the definition of the local transition function μ which is a map

$$\mu : K \times \Sigma \times K \times \Sigma \times (L, R) \longrightarrow \mathbb{C}$$

which gives a complex amplitude $\mu(k, s, k', s', d)$ for the transition of the machine from internal state k and current tape state s to internal state k', tape state s' with the head moving left or right. In contrast to the classical Turing machine, rather than giving a deterministic program for updating the tape, internal state and position, all possible changes are explored in parallel with different amplitudes. The probability of measuring the machine in some final state will depend on the sum of the amplitudes for all possible paths from the initial state to this final state. A challenge for successful QTM algorithms is to make the probability of measuring the 'correct' final state as close to 1 as possible without losing the benefit of being in a superposition of multiple states in the middle of the computation [12].

The essential condition for a well-formed quantum Turing machine is that the probability be conserved, that is that the sum of the squares of the complex amplitudes associated with each possible configuration of the machine be one at every time step. This puts limits on the types of local transition functions μ which are allowed, which can be found in Ref. [12].

VI. QUANTUM CELLULAR AUTOMATA

Unlike cellular automata, Turing machines and even quantum Turing machines, there is not currently a strict definition of the ideal n-dimensional quantum cellular automata (QCA). Over the past 20 years, many different models have been suggested which have been rejected or improved upon to make behavior more physical or more representative of classical cellular automata. In this section, we will explore the simplest universal quantum cellular automata, the Partitioned Watrous QCA, though many of the lessons carry forward to other models. For a detailed outline of types of QCA, see Reference [2].

Much of the framework for a QCA is similar to that of a QTM, except that there are no universal states and at each time step every square is updated simultaneously, as opposed to just the one at the read/write head. Formally [12], a (non partitioned) Watrous quantum cellular automata M is defined by a quadruple (Q, δ, k, A) where Q is the finite set of states each cell can take (including a *quiescent state*, ϵ) and δ is the *local transition function*, similar to μ above. The variable k indexes a certain cell to be the *acceptance cell* and a configuration in which

that cell contains an element of $A \subseteq Q$ is in an accepting configuration. The cellular automata is run on an infinite 1D lattice of cells with a neighborhood consisting of the nearest neighbor on either side.

The algorithm for a cellular automata is encoded both in the initial configuration and the update function δ. So that there is only amplitude in a finite number of configurations of the machine at any time and the overall state is normalizable, the number of non-quiescent states in the starting configuration must be finite and the update rule must keep entirely quiescent neighborhoods quiescent. In general, δ can then be any map

$$\delta : Q^4 \longrightarrow \mathbb{C}$$

(which satisfies the quiescence condition) such that the neighborhood (q_1, q_2, q_3) maps the central square to q with amplitude $\delta(q_1, q_2, q_3, q)$. As in the case of the quantum Turing machine, the machine evolves through many configurations simultaneously by being in a superposition of multiple configurations at every time after the starting time, ideally reducing to one dominant configuration before measurement occurs, destroying the superposition.

As with the QTM, quantum cellular automata is only *well formed* if the time-evolution rule is unitary, that is if probability is conserved. Although there are only a countably infinite number of normalized configurations, characterizing maps E_M between these states in terms of update functions δ is non trivial in the non-partitioned case, and so an arbitrary machine can not necessarily be proven to be well formed.

The partitioned Watrous cellular automata simplifies the conditions on δ for a well-formed machine. Just as in the non-partitioned case, a machine M is described as (Q, δ, k, a), except that each cell is subdivided into three parts:

$$Q = Q_l \times Q_m \times Q_r$$

such that $|Q| = |Q_l||Q_c||Q_r|$. The update rule again depends on the current cell q_2 and the two cells on either side q_1 and q_3, but through a more complicated update rule:

$$\delta(q_1, q_2, q_3) = \lambda((l(q_3), m(q_2), r(q_1)), q)$$

where $\lambda : Q \times Q \longrightarrow \mathbb{C}$ maps one set of three subcells to another with some complex probability amplitude. The effect of this update rule is the composition of a rearrangement of subcells between neighboring cells σ and the update λ applied to the new configuration. A diagram of the rearrangement process applied to a configuration a can be found in Figure 4.

It can be shown (see Ref. [12]) that a machine M is a well-formed 1D partitioned quantum cellular automata (1d-QCA) if and only if Λ, the $|Q| \times |Q|$ matrix with elements $\Lambda_{ij} = \lambda(q_i, q_j)$ is unitary. This makes intuitive sense since the well formed condition is that probability be conserved which would be expected to be reflected
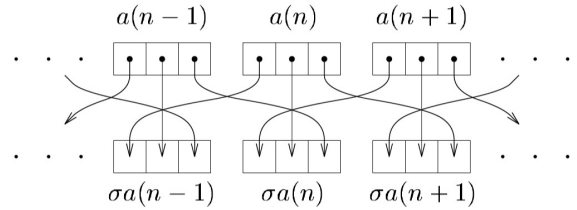
FIG. 4: A diagram of the first step of the Partitioned Watrous QCA update in which the right subsection of one cell becomes the right cell of the cell to its right and the left section of that cell becomes the left section of the cell to its left. This step is followed by an update to each newly defined cell via λ to define a full QCA time step. (Figure from Ref. [12])

in the update rule in some form. Armed with this simple condition, it becomes possible to explicitly define a $M \in 1d - QCA$ which will simulate an arbitrary quantum Turing machine with constant slow-down and a quantum Turing machine which simulates a $1d - QCA$ with linear slow down [12], proving that these 1D portioned Watrous cellular automata are universal.

VII.   CONCLUSIONS

Classical cellular automata provide a potentially powerful computing system with locality which mirrors the physical world, but extending their definitions to the quantum realm is not straight-forward. There is much room for further development exploring and enumerating new ways to design a theoretical quantum cellular automata computing system which is consistent with the requirements established by Feynman in 1981. Although progress is being made quickly, the final goal of usable quantum cellular automata computers is still a long way off.

To understand the potential power of CA and QCA as computational systems, the classical and quantum Turing machines must also be discussed. Although the computing strategies in cellular automata and Turing machines are starkly different, they are capable of simulating each other and therefore are in many ways the same computer. However, returning to Feynman's 1981 ministrations, there is something deeply elegant, if not computationally valuable, to carrying out calculations in a spatially distributed local computational system like QCA.

VIII.   ACKNOWLEDGEMENTS

[1] R. P. Feynman, "Simulating physics with computers," *International journal of theoretical physics*, vol. 21, no. 6, pp. 467–488, 1982.

[2] K. Wiesner, "Quantum Cellular Automata," in *Encyclopedia of Complexity and Systems Science*, pp. 7154–7164, New York, NY: Springer New York, 2009.

[3] M. Cook, "Universality in elementary cellular automata," *Complex Systems*, 2004.

[4] E. W. Weisstein, "Rule 110," *Wolfram MathWorld*.

[5] M. Mitchell, "Computation in cellular automata: A selected review," *Nonstandard Computation*, pp. 95–140, 1996.

[6] S. Wolfram, *A New Kind of Science*. Wolfram Media Inc, Jan. 2002.

[7] R. Geroch, *Perspectives in Computation*. University of Chicago Press, Oct. 2009.

[8] S. Aaronson, "The Limits of Quantum Computers," 2008.

[9] C. S. Lent, "The Concept of Quantum-Dot Cellular Automata," in *Quantum Cellular Automata* (M. Macucci, ed.), pp. 1–15, London: Imperial College Press, 2006.

[10] D. J. Griffiths, *Introduction to Quantum Mechanics*. Pearson College Division, 1995.

[11] G. L. Snider, A. O. Orlov, I. Amlani, X. Zuo, G. H. Bernstein, C. S. Lent, J. L. Merz, and W. Porod, "Quantum-dot cellular automata: Review and recent experiments," *Journal of Applied Physics*, vol. 85, no. 8, pp. 4283–4285, 1999.

[12] J. Watrous, "On one-dimensional quantum cellular automata," pp. 528–537, 1995.

Formalism and Applications of the Path Integral Approach to Quantum Mechanics

Luis Carlos Gil

MIT Department of Physics, 77 Massachusetts Ave., Cambridge, MA 02139-4307

(Dated: May 2, 2014)

The path integral approach provides an alternate description of how particles "decide" to move in space and time. In the Schrödinger formulation of quantum mechanics, the approach looks for eigenstate solutions of the Hamiltonian operator describing a particular system. The time-dependent Schrödinger equation then provides a means for calculating the time evolution of the system as time-evolving superpositions of these states. If we imagine the wavefunction solutions in position space, the equation describes the direction and infinitesimal distance a particle transits in an infinitesimal amount of time. In the path integral approach, we will see that the equations of motion are arrived at via a "global" (i.e. integral) process rather than a infinitesimal (i.e. differential) one. The particle in a sense explores all possible paths before deciding which particular path to take. This exploration is encoded into the path integral equations of the formalism that determine the propagator of the wavefunction and thus all the probabilistic information for a particle. In this paper, I demonstrate the mathematics and applications of this approach.

I. INTRODUCTION

The goal of this paper is to demonstrate to the reader the use and usefulness of the Feynman formulation of quantum mechanics. The first half of the paper covers the formalism of the approach. I will discuss how path integral techniques generalize from the least action principles of Lagrangian mechanics. The mathematics of path integrals will then be described both heuristically and systematically. Then, in the second half, the applications section, I will motivate the use of this formulation by describing how one may directly compute the expression for the unitary propagator, $U(t)$, for problems with a certain class of potentials. Finally, with the power of the path integral formulation at hand, I wish to explore the solution to problem of finding the propagator for the harmonic oscillator potential.

II. FORMALISM

A. Principle of Least Action

Let us imagine a closed physical system of N particles with generalized positions $q_1, q_2, ..., q_N$ and their corresponding velocities $\dot{q}_1, \dot{q}_2, ..., \dot{q}_N$. In classical systems, we know that, given a set of initial conditions $\{q_i(t = 0), \dot{q}_i(t = 0)\}$, the particles will travel along a unique set of paths that satisfies the constraints of the system. For each possible system, there is a function $\mathcal{L}\{q_i, \dot{q}_i, t\}$ called the "Lagrangian" of the system, which characterizes its physical properties and introduces its constraints. The Lagrangian is defined as the difference in the kinetic and potential energy of the system,

$$\mathcal{L} = K - V , \tag{1}$$

which are themselves, in general, functions of position, momentum, and time.

We obtain the classical equations of motion for a system by extremizing the "action" of the system. The action S is defined as

$$S = \int_{t_1}^{t_2} \mathcal{L}\{q_i, \dot{q}_i, t\} \, dt, \tag{2}$$

where $[t_1, t_2]$ is the time interval over which the system has evolved. The action is minimized when $\mathcal{L}$ satisfies the set of Euler-Lagrange equations:

$$\frac{d}{dt}\left(\frac{\partial \mathcal{L}}{\partial \dot{q}_i}\right) - \frac{\partial \mathcal{L}}{\partial q_i} = 0 \qquad (i = 1, 2, ..., N). \tag{3}$$

After solving these N partial differential equations and applying the 2N initial conditions, the classical problem is fully solved. Thus, we find the equations of motion for a system by requiring that the actual particle trajectories produce the least action of all possible trajectories.

B. Generalization to Quantum Mechanics

It turns out that when $\hbar \neq 0$, deriving the equations of motion for a quantum mechanical particle is not as straightforward as solving the Euler-Lagrange equations for a given $\mathcal{L}$. Instead, we would like to find a unitary function U, which evolves the wavefunction with respect to time while preserving its normalization. In the language of the Schrödinger formulation, this is the propagator, in which the matrix elements $\langle q_b, t_b | \hat{U} | q_a, t_a \rangle$ give the probability that the state originally in $|q_a\rangle$ at time t_a will be found in the new state $|q_b\rangle$ at time t_b. However, in the path integral approach we want to treat q and $\dot{q}$ as variables, and not infinite vectors interrelated by infinite matrices representing linear operators. Therefore, the propagator (now only a function of variables) will ultimately give us, for our choice of $(q_b, t_b; q_a, t_a)$, the transmission amplitude (and thereby the probability) for these transitions.

The necessity for an approach differing from the simple Euler-Lagrange equations is best seen when we consider the behavior of light waves and the generalization of this behavior to massive particles (after all quantum mechanics is based on the understanding that matter is exhibits both wave-like and particle-like characteristics). In the two-slit experiment, it is understood that in order to get the proper interference relationship at the detector, one must add up the amplitude of the planes waves $\psi_n = \exp(i\omega_n t)$, i.e. one must use superposition. We must do the same for massive particles if we are to believe in the tenants of quantum mechanics. We can imagine increasing the number of slits to a large value, N. We must then add up all the contributions from each slit in such a case. In the limit of an infinite number of slits, $N \to \infty$, we arrive at an infinite sum of plane waves. This represents the case of a particle propagating in free space. In this case, we see that we will need to compute the sum of an infinite number of plane waves if we want to determine the position of a particle in time.

What should represent the phase of the particle in this plane wave picture is not immediately straightforward. However, we know that the action of a particle plays a fundamental role in how nature decides the trajectory of particles as we saw with the Principle of Least Action. It so happens that the units of action (Energy·Time) are identical to the fundamental constant $\hbar$ of the quantum world. Using the ratio of the action to $\hbar$ as an ansatz for our mysterious particle phase factor, we'll see that this approach gives us a picture of quantum mechanics equivalent to the one devised by Schrödinger.

Choosing to follow the Feynman approach, the story of how a particle goes from one point to another is drastically different. Here, the particle explores all possible paths between two endpoints. In doing so, the particle picks up a certain phase factor that evolves with position and time in each trajectory. If one takes the sum of all phase factors for each trajectory, a combination of constructive and destructive interference occurs and the path which adds most constructively has a higher probability of being the actual trajectory the system will take. In the case of light propagation, the frequency, $\omega = E/\hbar$, determines the where and when the interference will occur. For massive particles, we construct our phase factor not directly using any particular ω of the particle, but the action of the particle in the system divided by $\hbar$. We claim that

$$U(q, t; q_0, t_0) = A \; \Sigma_{\text{all paths}} e^{iS[q(t)]/\hbar}, \tag{4}$$

where $A \in \mathcal{C}$ is a normalization factor.

Here, the action is the argument of the phase factor and the sum over all paths refers to a path integral from $[t_0, q_0]$ to $[t, q]$, meaning we must integrate the phase contributions of *every* path that may possibly link the two endpoints. The exact mathematics of this will be introduced shortly. It should be noted, however, that this procedure for finding the propagator serves to simplify only a certain class of potentials. Other potentials will prove just as difficult in either the Schrödinger or path integral approach. Fortunately, the class of potentials that are simplified turn out to be of great use.

C. The Heuristic Approach to Evaluating the Path Integral of the Free Particle

We now turn our attention to the evaluation of the enigmatic right-hand side of equation (4) in the case of a free particle. Instead of delving directly into a mathematical description of this path integral, we will take a heuristic approach which will better highlight the inherent physics as well as give a more intuitive description of the path integral itself.
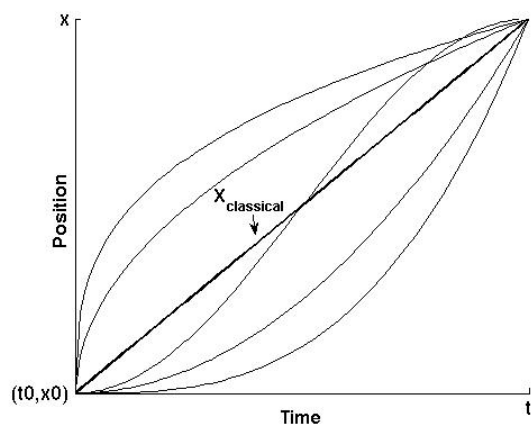
FIG. 1: Discrete set of paths connecting $[t_0, x_0]$ to $[t, x]$ including the classical Newtonian path

We choose to work in cartesian coordinates and we make the first simplification that instead of a continuum of paths connecting $[t_0, x_0]$ to $[t, x]$ there exists only a discrete set as shown in figure 1. Each path $x_i(t)$, where i ranges from 0 to N, contributes an amount $Z_i = e^{iS[x_i(t)/\hbar]}$ to the summation.

Since each path contributes a different phase in the summation, paths that exist far away from the classical path will tend to destructively interfere with each other on average. Even though the classical path x_{cl} contributes just as much to the summation as the other paths, the fact that the action is stationary for this path ($S = 0$) means that it will not be washed out by the destructive interference with other paths. Paths that differ greatly from the classical straight line trajectory in figure 1 will have kinetic energy terms in the action that differ from the stationary value of the classical path. These terms integrate to produce large values of S and rapidly oscillating phase factors that will tend to cancel out paths with similar deviations from the classical one. Only the phases belonging to paths "close" to the classical path will constructively interfere.

Here, we take "close" to mean paths $x_i(t)$ that produce an action S_i which differs from the classical action $S[x_{cl}(t)] = S_{cl}$ by less than $\hbar\pi$. In this region, the sum of Z_i's become large and is the dominant contribution to the propagator $U(x,t)$. The contributions of paths outside this area are taken to be negligible. Therefore, we may limit our sum to paths within this region of constructive interference.

Our third simplification will be to assume that all Z_i's within the coherent region contribute to the the the sum the same amount as the classical Z_i value: $Z_{cl} = e^{iS_{cl}/\hbar}$. We can therefore write the propagator as

$$U(x,t) = A' \; e^{iS_{cl}/\hbar}, \tag{5}$$

where the new normalization factor A' accounts for the number of paths we have in our region of constructive interference. We will now check that we can reproduce the propagator $U(x,t)$ for a free particle using equation (5).

Straight-line motion defines the path of a classical free particle with constant velocity $v = \frac{x-x_0}{t-t_0}$ such that

$$x'_{cl}(t') = \frac{x-x_0}{t-t_0}(t'-t_0) + x_0 \tag{6}$$

where (t,x) is some point along the trajectory not equal to (t_0, x_0). Since $\mathcal{L} = \frac{1}{2}mv^2$, and $v = \frac{dx}{dt}$, the action of the particle is thus:

$$S_{cl} = \int_{t_0}^{t} \frac{1}{2}m\frac{(x-x_0)^2}{(t-t_0)^2}dt' = \frac{1}{2}m\frac{(x-x_0)^2}{t-t_0}. \tag{7}$$

This leaves us with

$$U(x,t) = A' \exp\left[\frac{im(x-x_0)^2}{2\hbar(t-t_0)}\right], \tag{8}$$

where A' is found by noting that the propagator should become a delta function in the limit $(t,x) \to (t_0, x_0)$. We know that a delta function is the limit of a gaussian as its variance approaches zero and its height approaches infinity. We are thus justified in taking equation (8) to be a gaussian function with variance $\Delta^2 = 2i\hbar(t-t_0)/m$. Proper normalization of the gaussian gives us our expression for $A' = \frac{1}{(\pi\Delta^2)^{1/2}}$. Our final result, taken from analyzing the delta function as a limit of a gaussian, is

$$U(x,t) = \left[\frac{m}{2\pi\hbar i(t-t_0)}\right]^{\frac{1}{2}} \exp\left[\frac{im(x-x_0)^2}{2\hbar(t-t_0)}\right], \tag{9}$$

which is the known answer attained from the Schrödinger formulation. The fact that we were able to find the exact answer in spite of all the simplifications derives from the fact that the free particle potential is a part of the class of potentials who's propagator may be attained by direct computation of the action. We will analyze these potentials in the applications section.

D.   Systematic Approach to Evaluating Path Integrals

The form of the right-hand side of equation (4) in exact mathematical form is actually:

$$U(x,t) = \int_{x_0}^{x} e^{iS[x(t)]/\hbar}\mathcal{D}[x(t)], \tag{10}$$

where $\int_{x_0}^{x}\mathcal{D}[x(t)]$ is the instruction to integrate over all paths connecting x_0 and x in the interval $[t_0, t]$. To perform this integral we first make a finite step approximation to it and then take the limit as the step size goes to zero to arrive at the desired result.

As stated, we make a discrete approximation of all paths $x(t)$ connecting x_0 and x. We break each path into $N+1$ time-steps of length ϵ, where $t_n = t_0 + n\epsilon$, for $n = 0, ..., N$. Thus, the path is broken into points evaluated at each time-step: $x(t_0), x(t_1), ..., x(t_N)$. Each point is interpolated by lines of constant slope: $\frac{dx}{dt} = \left(\frac{x_{n+1}-x_n}{\epsilon}\right)^2$, where $x_n = x(t_n)$. If we consider again the free particle case, the action of the particle is now given by

$$S = \int_{t_0}^{t_N} \frac{1}{2}m\left(\frac{dx}{dt}\right)^2 \, dt = \sum_{n=0}^{N-1} \frac{m}{2}\left(\frac{x_{n+1}-x_n}{\epsilon}\right)^2 \epsilon. \tag{11}$$

If we now take the limit that $N \to \infty$, which implies $\epsilon \to 0$, equation (10) becomes

$$U(x,t) = \lim_{N\to\infty} A \int_{-\infty}^{\infty}\int_{-\infty}^{\infty}\cdots\int_{-\infty}^{\infty} \exp\left[\frac{i}{\hbar}\frac{m}{2} \times \right.$$
$$\left. \sum_{n=0}^{N-1}\frac{(x_{i+1}-x_n)^2}{\epsilon}\right] \times dx_1\cdots dx_{N-1}, \tag{12}$$

where the $N-1$ integrals are evaluated for all space since we are considering a continuum of paths where $x(t)$ may take on any x value at any given point except at the endpoints, which are fixed.

We can simplify the integrand by making the linear substitution $y_i = (\frac{m}{2\hbar\epsilon})^{1/2}x_i$. The constant A is subsequently modified to include the proportionality constant in the substitution $dx_i \to dy_i$, $A \to A' = A(\frac{2\hbar\epsilon}{m})^{(N-1)/2}$. The new expression is

$$U(x,t) = \lim_{N\to\infty} A' \int_{-\infty}^{\infty}\int_{-\infty}^{\infty}\cdots\int_{-\infty}^{\infty}$$
$$\exp\left[-\sum_{n=0}^{N-1}\frac{(y_{i+1}-y_n)^2}{i}\right] \times dy_1\cdots dy_{N-1} \tag{13}$$

This complicated mess of integrals can be simplified by examining the first integration:

$$\int_{-\infty}^{\infty} \exp\left\{-\frac{1}{i}\left[(y_2-y_1)^2 + (y_1-y_0)^2]\right]\right\} dy_1$$
$$= \left(\frac{i\pi}{2}\right)^{1/2} e^{-(y_2-y_0)^2/2i}, \tag{14}$$

which carries over to the next integration

$$\left(\frac{i\pi}{2}\right)^{1/2}\int_{-\infty}^{\infty}e^{-(y_3-y_2)^2/i}\cdot e^{-(y_2-y_0)^2/2i}dy_2$$

$$=\left[\frac{(i\pi)^2}{3}\right]^{1/2}e^{-(y_3-y_0)^2/3i}. \quad (15)$$

If we iterate this $N-1$ times we arrive at

$$\frac{(i\pi)^{(N-1)/2}}{N^{1/2}}e^{(y_N-y_0)^2/Ni}$$

$$=\frac{(i\pi)^{(N-1)/2}}{N^{1/2}}e^{-m(x_N-x_0)^2/2\hbar\epsilon Ni}. \quad (16)$$

We see that the only way that U may be normalized is if A' is unity or, equivalently, if $A=\left[\frac{2\pi\hbar\epsilon I}{m}\right]^{-N/2}\equiv B^{-N}$. Otherwise, the expression would blow up because of the fact that there are constants raised to N, where $N\to\infty$. Finally,

$$U(x_N,t_N)=\left(\frac{m}{2\pi\hbar iN\epsilon}\right)^{1/2}\exp\left[\frac{im(x_N-x_0)^2}{2\hbar N\epsilon}\right], \quad (17)$$

where $N\epsilon\to t_N-t_0$, thus providing the exact result as given by equation (9).

This example has illustrated the exact meaning of the path integral, which is

$$\int\mathcal{D}[x(t)]=\lim_{N\to\infty}\frac{1}{B}\int_{-\infty}^{\infty}\int_{-\infty}^{\infty}\cdots\int_{-\infty}^{\infty}\frac{dx_1}{B}$$

$$\times\frac{dx_2}{B}\cdots\frac{dx_{N-1}}{B}, \quad (18)$$

where each $N-1$ integration has a factor of $1/B$ associated with it and the remaining factor of $1/B$ is attributed to the process as a whole. These factors exist to keep the integration over infinite paths normalizable.

E.   Equivalence to the Schrödinger Picture

As a brief aside, it should be mentioned that, although we built up the path integral approach from a completely different starting point than the one from which the Schrödinger picture begins, the two approaches are mathematically the same at the end of the day. It turns out one may derive the Schrödinger equation from this formalism by solving for the time-evolved wavefunction in the limit of a very small time step. Given a propagator $U(x,t)$ found through the path integral approach, we can time evolve a generic wavefunction from its initial value, $\psi(x,t_0)$, over an arbitrarily small time interval $\Delta t=t-t_0=\epsilon$, while considering second-order variations in space:

$$\psi(x,\epsilon)=\int_{-\infty}^{\infty}U(x,\epsilon)\psi(x',t_0)\,dx'. \quad (19)$$

For a generic potential V and an infinitesimal time slice ϵ, one may easily show that in this limit U is simply

$$U(x,\epsilon)=\left(\frac{m}{2\pi\hbar i\epsilon}\right)^{1/2}\exp\left[\frac{im(x-x')^2}{2\epsilon\hbar}\right]$$

$$\times\exp\left[-\frac{i\epsilon}{\hbar}V\left(\frac{x+x'}{2},0\right)\right]. \quad (20)$$

The second exponential term in the propagator can be taylor expanded to first order in ϵ as $1-\frac{i\epsilon}{\hbar}V(x,0)+\mathcal{O}(\epsilon^2)$. Paths that lie with a coherence range η are considered by taking the second term inside the integral $\psi(x',t_0)$ and representing it as $\psi(x+\eta,t_0)$, where $x'=x+\eta$. Expanding ψ to second order in space we get $\psi(x+\eta,t_0)=\psi(x,t_0)+\eta\frac{\partial\psi}{\partial x}+\frac{\eta^2}{2}\frac{\partial^2\psi}{\partial x^2}$. Plugging this all into equation (19) gives us

$$\psi(x,t_0+\epsilon)=\left(\frac{m}{2\pi\hbar i\epsilon}\right)^{1/2}\int_{-\infty}^{\infty}\exp\left(\frac{im\eta^2}{2\hbar\epsilon}\right)^{-1/2}$$

$$\times\left[\psi(x,t_0)-\frac{i\epsilon}{\hbar}V(x,t_0)\psi(x,t_0)+\eta\frac{\partial\psi}{\partial x}+\frac{\eta^2}{2}\frac{\partial^2\psi}{\partial x^2}\right]d\eta \quad (21)$$

Integrating, subtracting both sides by $\psi(x,t_0)$, and dividing through by ϵ leaves us with the relation

$$\frac{\psi(x,t_0+\epsilon)-\psi(x,t_0)}{\epsilon}=-\frac{i}{\hbar}\left[\frac{-\hbar^2}{2m}\frac{\partial^2}{\partial x^2}+V(x,t_0)\right]\psi(x,t_0)$$

$$(22)$$

In the limit where $\epsilon\to0$, this returns the Schrödinger equation.

III.   APPLICATIONS

Now that we understand what path integration means, we will now see how it applies to systems with non-trivial potentials.

A.   Potentials of the form $V=a+bx+cx^2+d\dot{x}+ex\dot{x}$

Suppose we have a physical system that corresponds to a Lagrangian of the form

$$\mathcal{L}=\frac{1}{2}m\dot{x}^2-a-bx-cx^2-d\dot{x}-ex\dot{x}. \quad (23)$$

We may write every path between x_0 and x in terms of the classical path x_{cl} and departures from it y, such that $x(t')=x_{cl}(t')+y(t')$. After taking a time derivative becomes $\dot{x}(t')=\dot{x}_{cl}(t')+\dot{y}(t')$, where $y(0)=y(t)=0$ such that the endpoints agree. As before, we slice the path into N time-slices such that $x(t'_n)=x_{cl}(t'_i)+y(t'_i)$. Since $x_{cl}(t'_n)$ is constant at any t'_n, $dx_n=dy_n$ holds, and equation (18) simplifies to

$$\int_{x_0}^{x}\mathcal{D}[x(t')]=\int_{0}^{0}\mathcal{D}[y(t')] \quad (24)$$

and equation (10) may be written as

$$U(x, t; x_0, t_0) = \int_0^0 \exp\left\{\frac{i}{\hbar}S[x_{cl}(t') + y(t')]\right\}$$
$$\times \mathcal{D}[y(t')]. \quad (25)$$

If we perform an expansion of the functional S around x_{cl} we get:

$$S[x_{cl} + y] = \int_0^t \mathcal{L}(x_{cl} + y, \dot{x}_{cl} + \dot{y}) \, dt'$$

$$\equiv \int_0^t \mathcal{L}(x_{cl}, \dot{x}_{cl}) + \left(\frac{\partial \mathcal{L}}{\partial x}\big|_{x_{cl}}y + \frac{\partial \mathcal{L}}{\partial \dot{x}}\big|_{x_{cl}}\dot{y}\right) \quad (26)$$

$$+ \frac{1}{2}\left(\frac{\partial^2 \mathcal{L}}{\partial x^2}\big|_{x_{cl}}y^2 + 2\frac{\partial^2 \mathcal{L}}{\partial x \partial \dot{x}}\big|_{x_{cl}}y\dot{y} + \frac{\partial^2 \mathcal{L}}{\partial \dot{x}^2}\big|_{x_{cl}}\dot{y}^2\right) dt'.$$

The expansion is only second order since $\mathcal{L}$ is only quadratic in x and $\dot{x}$. Plugging in our Lagrangian from equation (23) and noticing that the first term in the expansion evaluates to $S[x_{cl}]$, the propagator becomes

$$U(x, t; x_0, t_0) = \exp\left(\frac{iS_{cl}}{\hbar}\right)\int_0^0 \exp\left[\frac{i}{\hbar}\int_{t_0}^t\left(\frac{1}{2}m\dot{y}^2\right.\right.$$
$$\left.\left. - cy^2 - ey\dot{y}\right)dt'\right] \times \mathcal{D}[y(t')]. \quad (27)$$

Note that the outer integral has no dependence on x_{cl} and only depends on t. Thus, the propagator is of the form $U(x, t) = e^{iS_{cl}/\hbar}f(t)$, where $f(t)$ is unknown until the exact system and therefore the Lagrangian is specified. Since it is typically straightforward to find S_{cl}, the heart of the matter is finding $f(t)$ for a given potential. So we now turn our attention to finding $f(t)$ for the harmonic oscillator potential.

B. The Quantum Harmonic Oscillator

The harmonic oscillator potential $V = \frac{1}{2}m\omega^2 x^2$ is ubiquitous in physics since it may be used to approximate an arbitrary potential for a particle near a potential minimum. We notice that its Lagrangian, $\mathcal{L} = \frac{1}{2}m\dot{x}^2 - \frac{m\omega^2}{2}x^2$, is a special case of equation (23), with $a = b = d = e = 0$ and $c = \frac{1}{2}m\omega^2$. The classical action of this system is found by evaluating (2) for a general path $x(t) = A\cos(\omega t) + B\sin(\omega t)$. In order to evaluate the integral, A and B are chosen such that $x(0) = x_1$ and $x(T) = x_2$. After integration, the parameters $x_2 \to x$ and $T \to t$ are allowed to vary, which leaves

$$S_{cl}(x, t) = \frac{m\omega}{2\sin(\omega t)}\left[(x_1^2 + x^2)\cos\omega t - 2x_1 x\right] \quad (28)$$

Plugging in the values of a,b,c,d, and e for the harmonic oscillator potential into equation (27), the function

$f(t)$ becomes:

$$f(t) = \int_0^0 \exp\left[\frac{i}{\hbar}\int_0^t \frac{1}{2}m(\dot{y}^2 - \omega^2 y^2)\right] dt' \, \mathcal{D}[y(t')] \quad (29)$$

To evaluate this expression we first represent the value of the fluctuations of the trajectory $y(t')$ by a Fourier series:

$$y(t') = \sum_n a_n \sin\left(\frac{n\pi t'}{t}\right), \qquad (n = 1, 2, ..., N-1). \quad (30)$$

Substituting this expression into the inner integral of equation (29), the second term evaluates to

$$\frac{-m\omega^2}{2}\int_0^t y(t')^2 dt' = \frac{-m\omega^2}{2}\sum_{n,m}\int_0^t a_n a_m \sin\left(\frac{n\pi t'}{t}\right)$$
$$\times \sin\left(\frac{m\pi t'}{t}\right)dt' = \frac{-m\omega^2 t}{4}\sum_n a_n^2. \quad (31)$$

In the same fashion, the first term evaluates to $\frac{m\pi^2}{4t}\Sigma_n n^2 a_n^2$. Note that the equivalent of integrating over all possible values of $y(t)$ is to integrate over all possible values of a_n, which we now do. Using the finite step approximation like before, the $f(t)$ becomes

$$f(t) = \lim_{N \to \infty} G \int_{-\infty}^{\infty} \cdots \int_{-\infty}^{\infty} \exp\left[\frac{imt}{4\hbar}\right.$$
$$\left.\times \sum_{n=1}^{N-1}\left(\frac{n^2\pi^2}{t^2} - \omega^2\right)a_n^2\right]da_1 \cdots da_{N-1}, \quad (32)$$

where G accounts for the constants produced during the change of variables. The result is the product of decoupled Gaussian integrals, where each integral evaluates to $\left(\frac{4\pi i\hbar}{mt}\right)^{1/2}\left(\frac{t}{n\pi}\right)\left(1 - \left(\frac{\omega t}{n\pi}\right)^2\right)^{-1/2}$. Using the identity $\lim_{N \to \infty} \Pi_{n=1}^{N-1}\left(1 - \left(\frac{\omega t}{n\pi}\right)^2\right) = \frac{\sin(\omega t)}{\omega t}$, the propagator becomes

$$U(x, t; x_0, t_0) = G' \exp\left(\frac{iS_{cl}}{\hbar}\right)\left(\frac{\omega t}{\sin(\omega t)}\right)^{1/2}. \quad (33)$$

We find G' by considering the limit of the propagator as $\omega \to 0$. In this limit, the Lagrangian represents a free particle system since the potential V goes to zero, and thus the propagator will be that for a free particle. Therefore, we find that $G' = \left(\frac{m}{2\pi i\hbar t}\right)^{1/2}$, and the complete expression for the propagator is

$$U(x, t; x_0, t_0) = \left(\frac{m}{2\pi i\hbar t}\right)^{\frac{1}{2}}\left(\frac{\omega t}{\sin(\omega t)}\right)^{\frac{1}{2}}\exp\left(\frac{iS_{cl}}{\hbar}\right). \quad (34)$$

Comparison to the propagator obtained through the Schrödinger formulation shows that the two results agree.

IV. CONCLUSION

The procedure by which we found the propagator of the harmonic oscillator may be applied to a Lagrangian with any value of the coefficient a, b, and c. For e and $f \neq 0$, the procedure involves more advanced mathematical tools, but the end result will be the same: a set of $N - 1$ decoupled Gaussian integrals that evaluate to give an analytic function that, upon squaring, describes the probability of a particle being at a position x at a time t. Potentials that do not fall into this narrow range of possible potentials maybe be approximated by these potentials or treated using perturbation theory.

The ultimate goal of quantum mechanics is to find the probability that an event will take place at a given time. There are two ways to go about this. One may take an approach where differential equations are used to describe the local trajectory a particle and how it evolves over an infinitesimal amount of time. Alternatively, a global approach may be used where a particle explores all possible paths in a finite amount of time and the actual path is determined by consequence of which of these minimizes how much "effort" the particle must put in to travel it. We have shown how the latter approach may be applied to physical systems, and, though it may be mathematically more involved for certain types of problems, it gives us a different way of understanding the reality of how motion plays out in the physical world.

[1] Mechanics, L.D. Landau, Butterworth-Heinemann (1976)
[2] Principles of Quantum Mechanics, R. Shankar, Springer LLC (1994)
[3] Path Integrals and Quantum Mechanics, Feynman and Hibbs, McGraw-Hill (1965)
[4] Mathematics of the Feynman Path Integral, Kolokoltsov, Russian Academy of Science (2001)
[5] The Lagrangian in Quantum Mechanics, Dirac, Physikalische Zeitschrift der Sowjetunion (1933)

The Dirac Equation: Relativistic Electrons and Positrons

Cole Graham

Department of Mathematics, MIT, 77 Massachusetts Ave., Cambridge, MA 02139-4307

(Dated: May 2, 2014)

We develop the Dirac equation for the relativistic electron. We introduce the 4-component wavefunction of the electron, and determine the relativistic probability current. In the non-relativistic limit we derive the magnetic moment of the electron, and find $g_e = 2$. By cosidering negative energy solutions to the Dirac equation, we deduce the existence of the electron antiparticle, the positron.

I. INTRODUCTION

In the most elementary form of quantum mechanics, a particle is described by a scalar wavefunction ψ which extends throughout three-dimensional space, and which satisfies the famous Schrödinger Equation:

$$i\hbar \frac{\partial \psi}{\partial t} = \left[-\frac{\hbar^2}{2m}\nabla^2 + V \right]\psi, \qquad (1)$$

where V is the potential experienced by the particle and m is the particle mass. Erwin Schrödinger published his equation in 1926, and thereby neatly explained numerous quantum effects. In particular, the equation predicts the quantized energy levels of hydrogen, matching the Rydberg formula. Unfortunately, the equation does not exhibit the relativistic corrections to the hydrogen energies. Indeed, the Schrödinger equation is patently non-relativistic, since it treats time and space asymmetrically: the equation is first-order in time and second-order in space. Schrödinger himself was aware of this inadequacy, and only published equation (1) after failing to find a relativistic wave equation consistent with experiment.

In 1928, Paul Dirac resolved the conflict between special relativity and early quantum mechanics with a relativistic wave equation for the electron. To develop the equation, Dirac was forced to abandon a scalar wavefunction for the electron, and instead introduced a 4-component vector wavefunction. This vector wavefunction resolved another outstanding issue in contemporary quantum mechanics: spin. The internal spin of the electron had been postulated by Pauli in 1924, but Dirac first provided a natural mathematical explanation for the extra degree of freedom of the electron. In fact, only two degrees of freedom are necessary to describe spin using the Pauli representation. The 4-component vector required for the Dirac equation therefore has two *extra* degrees of freedom. These extra components led Dirac to predict the existence of a second particle, dual to the electron but with opposite charge [4]. This particle, the positron, was first observed in 1933 [1]. Dirac had combined relativity and quantum mechanics, described the electron spin, and predicted antimatter all in one elegant wave equation.

II. RELATIVISTIC FREE ELECTRONS

We begin by developing the Dirac equation for a free electron, which experiences no potential. In this setting, the Schrödinger equation (1) reduces to

$$i\hbar \frac{\partial \psi}{\partial t} = -\frac{\hbar^2}{2m}\nabla^2 \psi. \qquad (2)$$

As written in (2), Schrödinger's equation is a representation of the classical relation $E = \frac{p^2}{2m}$. In non-relativistic quantum mechanics, E and p are identified with the operators $i\hbar\frac{\partial}{\partial t}$ and $-i\hbar\frac{\partial}{\partial x_i}$, which act on a wavefunction ψ.

To develop a relativistic theory, we must use the relativistic relation: $E = \sqrt{m^2c^4 + p^2c^2}$. To make this energy equation Lorentz-invariant, we form a momentum 4-vector $\mathbf{p}$, whose contravariant components we denote p^μ for $\mu = 0, 1, 2, 3$. The derivative with respect to contravariant coordinates x^μ is *covariant*, so for the spatial coordinates, $p_i = -i\hbar\partial_i$. Hence when we raise the index, $p^i = -i\hbar g^{ij}\partial_j = i\hbar\partial^j$. Finally, we introduce the new variable p^0 corresponding to the operator $i\hbar\partial^0$. As the timelike component in the momentum 4-vector, p^0 must represent energy (divided by c) [5]. We then have the full contravariant momentum:

$$p^\mu = i\hbar\partial^\mu. \qquad (3)$$

Writing the relativistic energy formula as a wave equation, we have

$$p^0 \psi = \sqrt{m^2c^2 + (p^i)^2}\,\psi, \qquad (4)$$

where i is summed over the spatial coordinates $i = 1, 2, 3$. Although (4) is a relativistic equation, it is still not manifestly symmetric between p^0 and p^i. It is entirely unclear how (4) will transform under the Lorentz group. To recover the Lorentz-invariance of relativistic theory, we write the energy formula as $\mathbf{p} \cdot \mathbf{p} = p^\mu p_\mu = m^2c^2$. Then the wave equation (4) becomes

$$(p^\mu p_\mu - m^2c^2)\psi = 0. \qquad (5)$$

Substituting $p^\mu = -i\hbar\partial^\mu$, and using $x_0 = ct$, we obtain the Klein-Gordon equation:

$$\left[\frac{1}{c^2}\frac{\partial^2}{\partial t^2} - \nabla^2 + \frac{m^2c^2}{\hbar^2} \right]\psi = 0. \qquad (6)$$

This equation has finally attained the symmetry required in a Lorentz-invariant theory, since time and space derivatives are both second-order. However, the second-order nature of the Klein-Gordon equation is troubling, as it implies that a state is not fully determined by its initial value $\psi|_{t=0}$ [5] . Rather, to fully specify the evolution of the wavefunction, we must provide both $\psi|_{t=0}$ and $\frac{\partial \psi}{\partial t}|_{t=0}$. The extent of this issue becomes further apparent when we consider the probability distribution arising from (6) [8]. In non-relativistic quantum mechanics, the probability density ρ for a particle is given by $\rho = \psi^*\psi$. This density satisfies the conservation law

$$\frac{\partial \rho}{\partial t} + \nabla \cdot J = 0, \tag{7}$$

where $J = -\frac{i\hbar}{2m}(\psi^*\nabla\psi - \psi\nabla\psi^*)$ is the probability current. To make these equations relativistic, we form the 4-vector current **J** given by $J^\mu = \frac{i\hbar}{2m}(\psi^*\partial^\mu\psi - \psi\partial^\mu\psi^*)$. The Klein-Gordon equation then implies that

$$\partial_\mu J^\mu = 0. \tag{8}$$

The probability density has become the timelike coordinate in a 4-vector:

$$\rho = \frac{1}{c}J^0 = \frac{i\hbar}{2mc^2}\left(\psi^*\frac{\partial\psi}{\partial t} - \psi\frac{\partial\psi^*}{\partial t}\right). \tag{9}$$

However, because $\psi|_{t=0}$ *and* $\frac{\partial \psi}{\partial t}|_{t=0}$ may be freely specified, (9) may be made negative. So ρ cannot be interpreted as a probability distribution. This entirely undermines the physical interpretation of the Schrödinger wavefunction [13].

These issues would be resolved if (6) were made first-order in t. Lorentz symmetry then demands that the equation be first order in p^μ. To attain this goal, we attempt to factor (5) into two terms, each linear in **p**:

$$p^\mu p_\mu - m^2c^2 = (\gamma^\kappa p_\kappa + mc)(\gamma^\lambda p_\lambda - mc). \tag{10}$$

Expanding this product, we see that the coefficients γ^κ must satisfy $p^\mu p_\mu = \gamma^\kappa\gamma^\lambda p_\kappa p_\lambda$. Matching terms, we require

$$\gamma^\kappa\gamma^\lambda + \gamma^\lambda\gamma^\kappa = 2g^{\kappa\lambda}. \tag{11}$$

That is, $(\gamma^0)^2 = 1$, $(\gamma^i)^2 = -1$, and $\gamma^\kappa\gamma^\lambda + \gamma^\lambda\gamma^\kappa = 0$ when $\kappa \neq \lambda$ [8]. These equations cannot be satisfied for any complex numbers. Dirac brilliantly realized that the equation (11) could be satisfied if each γ^μ is a *matrix*. The requirement of 4 independent anticommuting matrices cannot be satisfied by 2×2 matrices, for there are only 3 independent Pauli matrices [3]. In fact, the matrices γ^μ must be at least 4×4 in size to satisfy (11). This in turn demands that ψ have 4 components. Hence a relativistic formulation of quantum mechanics demands that electrons be described by 4-component wavefunctions, not the simple scalar wavefunctions found in the Schrödinger equation. There are a variety of 4×4 matrix

representations of γ^μ which satisfy the relations (11). We choose the convention of Bjorken and Drell [2]. In block form, the matrices are

$$\gamma^0 = \begin{pmatrix} 1 & 0 \\ 0 & -1 \end{pmatrix}, \quad \gamma^i = \begin{pmatrix} 0 & \sigma^i \\ -\sigma^i & 0 \end{pmatrix}, \tag{12}$$

where σ^i denotes the 2×2 Pauli matrix. Having established a representation for γ^μ, we select one factor from (10) as our wave equation. Which factor is a matter of convention—we use the standard choice of

$$\gamma^\mu p_\mu - mc = 0. \tag{13}$$

If we represent p_μ by the operator $i\hbar\partial_\mu$, we obtain the Dirac equation for the wavefunction of a free electron [8]:

$$i\hbar\gamma^\mu\partial_\mu\psi - mc\psi = 0. \tag{14}$$

To understand the relativistic behavior of the Dirac equation, we consider how ψ transforms under the Lorentz group. Notably, although ψ has 4-components, it is *not* a 4-vector. Rather, if we perform a boost in the x^i-direction by speed v, the transformation $\psi \mapsto \psi'$ is given by $\psi' = S\psi$, where S is a 4×4 matrix. In block form,

$$S = \begin{pmatrix} a_+ & a_-\sigma^i \\ a_-\sigma^i & a_+ \end{pmatrix}, \tag{15}$$

where $a_\pm = \pm\sqrt{\frac{1}{2}(\gamma \pm 1)}$ and $\gamma = \left(1 - \frac{v^2}{c^2}\right)^{-1/2}$. We omit the derivation of (15); it is outlined in [8]. The transformation matrix S is clearly not the usual Lorentz boost matrix used to transform a 4-vector. More generally, any Lorentz transformation Λ acts on ψ as multiplication by some matrix $S(\Lambda)$. However, $S(\Lambda)$ is not the matrix describing the transformation of 4-vectors.

A. Probability Density

In contrast to the Klein-Gordon equation, the wavefunction in (14) corresponds to a probability distribution. Since ψ has 4 components, we form $\rho = \psi^\dagger\psi$. Again we expect a relativistic conservation law of the form (8). So ρ should be the timelike component of a 4-vector probability current **J**. In particular, ρ is not Lorentz invariant [14]. To find J^μ in terms of ψ, we define the Dirac adjoint:

$$\overline{\psi} = \psi^\dagger\gamma^0. \tag{16}$$

Although it appears somewhat arbitrary, $\overline{\psi}$ is chosen to reestablish the Lorentz invariance absent in $\psi^\dagger\psi$. We do not show it here, but $S^\dagger\gamma^0 S = \gamma^0$ [8]. Indeed, this relation holds for any $S(\Lambda)$ corresponding to an arbitrary Lorentz transformation. We then have

$$\overline{\psi}'\psi' = (\psi')^\dagger\gamma^0\psi' = \psi^\dagger S^\dagger\gamma^0 S\psi = \psi^\dagger\gamma^0\psi = \overline{\psi}\psi. \tag{17}$$

Hence $\overline{\psi}\psi$ is a Lorentz-invariant scalar, unlike $\psi^\dagger\psi$. Because $(\gamma^0)^2 = 1$, we may write

$$\rho = \psi^\dagger\psi = \psi^\dagger\gamma^0\gamma^0\psi = \overline{\psi}\gamma^0\psi. \qquad (18)$$

This formulation suggests the following definition of the 4-vector **J**:

$$J^\mu = \overline{\psi}\gamma^\mu\psi. \qquad (19)$$

The fact that (19) describes the contravariant components of a 4-vector is not as trivial as the notation suggests. Indeed, γ^μ are *not* the contravariant component of a 4-vector. The Dirac matrices are fixed mathematical objects independent of physical coordinate transformations. In (19), the terms changed under a Lorentz transformation are $\overline{\psi}$ and ψ. Nevertheless, it is straightforward to verify that $\overline{\psi}$ and ψ transform in precisely the right way to make **J** a 4-vector. For instance, if we consider a boost in the x^1 direction, the J^0 and J^1 components will mix appropriately, while J^2 and J^3 will be unchanged. These calculations reveal the power of the notation for γ^μ and $\overline{\psi}$. γ^μ are not contravariant components, and $\overline{\psi}$ is not the usual Hermitian conjugate. Nevertheless, $\overline{\psi}\psi$ is a Lorentz scalar, and $\overline{\psi}\gamma^\mu\psi$ are the contravariant components of a Lorentz 4-vector [8].

We can now show that **J** satisfies the continuity equation (8) required of probability current. This procedure is nearly identical to that used to derive (7) from the Scrödinger equation. We first write the Dirac equation for the Dirac adjoint. We take the Hermitian conjugate of (14), and right multiply by γ^0:

$$\psi^\dagger(-i\hbar(\gamma^\mu)^\dagger\overleftarrow{\partial}_\mu - mc)\gamma^0 = 0, \qquad (20)$$

where the left arrow in $\overleftarrow{\partial}_\mu$ indicates that the derivative acts on the left. Now, $(\gamma^0)^\dagger\gamma^0 = \gamma^0\gamma^0$, while $(\gamma^i)^\dagger\gamma^0 = -\gamma^i\gamma^0 = \gamma^0\gamma^i$. So $(\gamma^\mu)^\dagger\gamma^0 = \gamma^0\gamma^\mu$. Hence the γ^0 term on the right moves through the operators in the middle, yielding

$$\overline{\psi}(-i\hbar\gamma^\mu\overleftarrow{\partial}_\mu - mc) = 0. \qquad (21)$$

In the bra-ket formalism, (14) is the Dirac equation for kets, and (21) is the equation for bras. To obtain a scalar equation, we multiply (14) on the left by $\overline{\psi}$, and (21) on the right by ψ. These operations yield:

$$i\hbar\overline{\psi}\gamma^\mu\overrightarrow{\partial}_\mu\psi - mc\overline{\psi}\psi = 0,$$
$$-i\hbar\overline{\psi}\gamma^\mu\overleftarrow{\partial}_\mu\psi - mc\overline{\psi}\psi = 0, \qquad (22)$$

where the right arrow in $\overrightarrow{\partial}_\mu$ indicates action on the right. Subtracting the second equation from the first, we have the conservation law:

$$\overline{\psi}\gamma^\mu\overrightarrow{\partial}_\mu\psi + \overline{\psi}\gamma^\mu\overleftarrow{\partial}_\mu\psi = \partial_\mu\left[\overline{\psi}\gamma^\mu\psi\right] = \partial_\mu J^\mu = 0. \qquad (23)$$

The Dirac equation is therefore a Lorentz-compatible wave equation for a 4-component wavefunction ψ, and ψ corresponds to a conserved (non-negative) probability density $\psi^\dagger\psi = J^0$. In this sense, the wavefunction in the Dirac equation has the same physical interpretation as that in the Schrödinger equation.

III. ELECTROMAGNETIC POTENTIALS

We turn now to the Dirac equation for an electron moving in an electromagnetic potential. In relativity, the electric scalar potential ϕ and the magnetic vector potential $\vec{A}$ are assembled into a single 4-vector **A**, where $A^\mu = \left(\frac{\phi}{c}, \vec{A}\right)$. We adapt the Hamiltonian for a free particle to an electromagnetic potential by replacing **p** by the canonical momentum $\mathbf{p} - q\mathbf{A}$ (in SI units) [12]. This leads us to perform the same substitution in the Dirac equation, with $q = -e$. Hence we have

$$\gamma^\mu\left(i\hbar\partial_\mu + eA_\mu\right)\psi - mc\psi = 0. \qquad (24)$$

An equation describing the interaction between an electron and a magnetic field should reveal the internal spin of the electron. In fact, the usual Hamiltonian for an electron in a magnetic field may be recovered from (24) in the non-relativistic limit. To see this, we fix a reference frame, and consider the low velocity limit, in which $\left(\frac{v}{c}\right)^2 \ll 1$. To isolate the effect of the magnetic field alone, we take $\phi = 0$. Changing from the operator form to the momentum form of the Dirac equation, we have

$$\gamma^\mu(p_\mu + eA_\mu)\psi - mc\psi = 0. \qquad (25)$$

In our fixed reference frame, $p_\mu = \left(\frac{E}{c}, -\vec{p}\right)$ and $A_\mu = (0, -\vec{A})$. Let $\vec{\pi} = \vec{p} + e\vec{A}$ denote the canonical momentum. Using the block forms of γ^μ and multiplying by c, the Dirac equation becomes

$$\begin{pmatrix} E - mc^2 & -c\vec{\pi}\cdot\vec{\sigma} \\ c\vec{\pi}\cdot\vec{\sigma} & -E - mc^2 \end{pmatrix}\psi = 0. \qquad (26)$$

We now consider the first pair and second pair of components of ψ separately. Let

$$\psi = \begin{pmatrix} \Theta \\ \Xi \end{pmatrix}, \qquad (27)$$

where Θ and Ξ are 2-component vectors. In this decomposition, (26) separates into two equations [12]:

$$(mc^2 - E)\Theta + c\vec{\sigma}\cdot\vec{\pi}\,\Xi = 0 \qquad (28)$$
$$(mc^2 + E)\Xi - c\vec{\sigma}\cdot\vec{\pi}\,\Theta = 0. \qquad (29)$$

Now, in the low velocity limit, $E \approx E_S + mc^2$, where E_S is the energy in the Schrödinger equation, and $E_S \ll mc^2$. With this approximation, (29) reduces to

$$\Xi = \frac{\vec{\sigma}\cdot\vec{\pi}}{2mc}\Theta. \qquad (30)$$

Note that $\|\Xi\| \propto \frac{v}{c}\|\Theta\|$, so for low velocities, the term Ξ is suppressed in ψ. Now, substituting (30) into (28), we obtain the Pauli equation:

$$E_S\Theta = c\vec{\sigma}\cdot\vec{\pi}\,\Xi = \frac{(\vec{\sigma}\cdot\vec{\pi})(\vec{\sigma}\cdot\vec{\pi})}{2m}\Theta. \qquad (31)$$

We now recall the Pauli matrix formula:

$$(\vec{\sigma} \cdot \vec{\pi})(\vec{\sigma} \cdot \vec{\pi}) = \vec{\pi} \cdot \vec{\pi} + i\vec{\sigma} \cdot (\vec{\pi} \times \vec{\pi}). \qquad (32)$$

Because $\vec{p}$ and $\vec{A}$ need not commute, we cannot simply write $\vec{\pi} \times \vec{\pi} = 0$. Instead,

$$\vec{\pi} \times \vec{\pi} = \vec{p} \times e\vec{A} + e\vec{A} \times \vec{p} = -i\hbar e[\vec{\nabla} \times \vec{A} + \vec{A} \times \vec{\nabla}]. \quad (33)$$

To simplify this operator, we consider its action on a scalar function φ:

$$\begin{aligned}[\vec{\nabla} \times \vec{A} + \vec{A} \times \vec{\nabla}]\varphi &= \vec{\nabla} \times (\vec{A}\varphi) + \vec{A} \times (\vec{\nabla}\varphi) \\ &= (\vec{\nabla} \times \vec{A})\varphi + (\vec{\nabla}\varphi) \times \vec{A} + \vec{A} \times (\vec{\nabla}\varphi) \\ &= \vec{B}\varphi. \qquad (34)\end{aligned}$$

Therefore $\vec{\pi} \times \vec{\pi} = -i\hbar e\vec{B}$. With this, we write (31) in full [3, 5, 12]:

$$E_S\Theta = \left[\frac{(\vec{p} + e\vec{A})^2}{2m} + \frac{e\hbar}{2m}\vec{\sigma} \cdot \vec{B} \right] \Theta. \qquad (35)$$

The first term on the right hand side of (35) is the usual kinetic term in the Schrödinger equation. The second term corresponds to the magnetic moment of the electron. If we substitute $\vec{S} = \frac{\hbar}{2}\vec{\sigma}$ and $\mu_B = \frac{e\hbar}{2m}$, we have

$$E_S\Theta = \left[\frac{(\vec{p} + e\vec{A})^2}{2m} + 2\mu_B \frac{\vec{S}}{\hbar} \cdot \vec{B} \right] \Theta. \qquad (36)$$

The factor of 2 in the spin term is the g-factor for the electron. The Dirac equation therefore naturally exhibits the internal spin of the electron, and (almost) correctly calculates $g_e = 2$. According to (36), Θ incorporates the spin of the electron. As a 2-component wavefunction, Θ effectively belongs in the tensor product of position space with the 2-state spin space. In this formulation, the components of Θ may be identified as the wavefunctions of the spin up and down components of the electron. An arbitrary Θ is a superposition of the up and down wavefunctions.

The electron spin had been observed and described before the publication of the Dirac equation [7, 10]. However, Dirac was the first to provide a mathematical framework in which spin emerged naturally as part of the fundamental theory. In this perspective, particle spin is a consequence of the merger of relativity and quantum mechanics.

IV. THE POSITRON

Let us now return to the case of a free electron, so that $A^\mu = 0$. In the rest frame of the electron, $p^\mu = 0$, and the Dirac equation (26) reduces to

$$\begin{pmatrix} E - mc^2 & 0 \\ 0 & -E - mc^2 \end{pmatrix} \psi = 0. \qquad (37)$$

This equation will have a normalizable solution ψ precisely when $E = \pm mc^2$. In the previous section we followed non-quantum relativity, and assigned a rest energy $E = +mc^2$ to the electron. However, the decoupled equation (37) suggests that there is no physical reason to prefer the positive energy solution to the negative energy solution [12]. In the non-quantum theory, this sign ambiguity has no physical significance. When considering a (massive) particle, we are free to let the energy be mc^2 in the rest frame [15]. All changes in classical variables are continuous, so the energy cannot discontinuously jump to negative values. A particle with positive rest energy invariably has positive energy, so the negative energy solutions may be ignored as mathematical curiosities. This simplification is impossible in quantum mechanics [3, 4]. Quantum mechanics admits discontinuous changes in energy: an electron initially in a positive energy state may, through some perturbation of the electromagnetic field, decay to a negative energy state.

In the low-velocity limit for negative energy solutions, E_S is negative, and $E \approx E_S - mc^2$. With this substitution, the roles of Θ and Ξ are reversed in (30) and (31). At low velocities, the term Θ is suppressed in ψ, and Ξ becomes the spin of a negative energy electron. This observation finally establishes the physical significance of the 4 components of ψ. In the low velocity limit, two components form the spin state of a positive energy electron, and 2 components form the spin of a negative energy electron. Of course at higher velocities the components cannot be neatly separated in this manner, but the need for 4 components is still clear. The 2-component wavefunction describing a spin-$\frac{1}{2}$ particle is called a spinor. The 4-component ψ is a composite of 2 spinors, and is called a Dirac spinor, or a bispinor [8].

At first glance, negative energy electron states constitute a serious problem with the Dirac equation [3]. If there are infinitely many negative energy states available for the electron, the positive energy states should be unstable, liable to decay to a high-velocity negative energy state. Evidently, physical electrons are observed to be stable. Dirac suggested that the negative energy states are in fact almost entirely occupied. Then the Pauli exclusion principle prevents positive energy electrons from decaying [4]. This model, now called the Dirac sea, requires the vacuum to be populated by infinitely dense yet unobservable negative energy electrons. In the absolute vacuum, all negative energy states are occupied, while all positive energy states are empty. Deviations from this configuration can take two forms. A positive energy state might be occupied, which would appear as a standard electron. Alternatively, a negative energy state might be unoccupied. Such a vacancy would imply the absence of a negative energy, negatively charged particle. In any physical observation, this absence would manifest itself as a positive energy *positively charged* particle. The electron "hole" would have the same mass as the electron. This particle was predicted by Dirac in 1929, and observed in 1933 [1, 4].

Such a hole is now called a positron, the antiparticle of the electron. In this perspective, a Dirac spinor is a composite wavefunction formed from the spinor of an electron and the spinor of a positron. Familiar behaviors of antiparticles can be neatly explained by the Dirac sea model. When a positron and an electron meet, the positive energy electron state may decay to fill the negative energy vacancy. This decay erases both the electron and the positron from observable existence, and emits a burst of radiation equal in energy to the sum of the energies of the electron and positron [4]. This process is particle-antiparticle annihilation. In the reverse process, a perturbing field may induce a negative energy electron to spontaneously jump to a positive energy state. Energy is absorbed from the perturbing electromagnetic field, and an electron-positron pair is created. This process is particle-antiparticle pair production.

Although this model is effective for fermions, it cannot explain the antiparticles of bosons, which do not obey the Pauli exclusion principle. An alternate explanation for antiparticles was proposed by Feynman in 1949 [6]. In Feynman's model, first suggested by Stückelberg, negative energy electrons travel backwards in time. For observers moving forward in time, the particles appear to have positive energy and positive charge [12].

V.   MODERN DEVELOPMENTS

Despite the explanatory and predictive power of the Dirac equation, it is not the final word in physics. The equation accurately describes all corrections to the hydrogen spectrum down to hyperfine splitting [12]. However, still finer perturbations to the hydrogen spectrum are observed. Most prominently, the Lamb shift is not explained by the relativistic quantum mechanics of the Dirac equation. Instead, these finer perturbations are effects of quantum field theory [8]. The magnetic moment of the electron also exhibits QFT effects. While the Dirac equation predicts $g_e = 2$, as in (36), field theory interactions cause g_e to deviate slightly from 2. In a modern measurement [9]:

$$g_e = 2.002319304(36).$$

QFT does not, however, simply jettison the Dirac equation. Instead the equation is adapted to describe particle fields. This Dirac field equation governs fermionic fields. In the field theory formulation, electrons and positrons are field states governed by creation and annihilation operators[11].

Although the QFT interpretation of electron-positron production has replaced the Dirac sea model, the model is not obsolete. It is currently used to describe the behavior of electrons and electron holes in the solid state physics of metals and semiconductors. In semiconductors the ground state can consist of a sea of electrons occupying low energy states, separated from higher level states by an energy band gap. When the semiconductor is excited, an electron is promoted across the band gap, yielding a negatively charged electron in the conduction band and a positively charged hole in the valence band.

[1] C. D. Anderson. The positive electron. *Phys. Rev.*, 43:36–365, 1933.

[2] J. D. Bjorken and S. D. Drell. *Relativistic Quantum Mechanics*. McGraw-Hill, 1964.

[3] P. A. M. Dirac. The quantum theory of the electron. *Proc. R. Soc. Lond.*, 117(778):610–624, 1928.

[4] P. A. M. Dirac. A theory of electrons and protons. *Proc. R. Soc. Lond.*, 126(801):36–365, 1929.

[5] P. A. M. Dirac. *The Principles of Quantum Mechanics*. Oxford Science Publications, 4th edition, 1958.

[6] R. P. Feynman. The theory of positrons. *Phys. Rev.*, 76:749–759, Sep 1949.

[7] W. Gerlach and O. Stern. Das magnetische moment des silberatoms. *Zeitschrift fr Physik*, 9(1):353–355, 1922.

[8] D. Griffiths. *Introduction to Elementary Particles*. Wiley-VCH, 2nd edition, 2008.

[9] D. Hanneke, S. Fogwell Hoogerheide, and G. Gabrielse. Cavity control of a single-electron quantum cyclotron: Measuring the electron magnetic moment. *Phys. Rev. A*, 83:52–122, May 2011.

[10] J. Pauli, W. Zur quantenmechanik des magnetischen elektrons. *Zeitschrift fr Physik*, 43(9-10):601–623, 1927.

[11] M. E. Peskin and D. V. Schroeder. *An Introduction to Quantum Field Theory*. Westview Press, 1995.

[12] R. Shankar. *Principles of Quantum Mechanics*. Springer, 2nd edition, 1994.

[13] Although the Klein-Gordon equation does not describe spin-$\frac{1}{2}$ particles, it can be applied to spin-0 particles. Then $\rho = \psi^*\psi$ becomes a charge density, which is allowed to assume negative values.

[14] The fact that ρ is not a Lorentz-invariant scalar field is expected. In non-quantum relativity, charge density is not a scalar, but rather transforms like the timelike component of the current density 4-vector.

[15] The Dirac equation also applies to massless particles. Substituting $m = 0$ reduces the equation to $\gamma^\mu \partial_\mu \psi = 0$, the Weyl equation. This equation describes (hypothetical) massless spin-$\frac{1}{2}$ particles.

Isospin and the Approximate SU(2) Symmetry of the Strong Nuclear Force

Owen J. Gray

Massachusetts Institute of Technology, MA 02142

(Dated: May 2, 2014)

We discuss isospin and the approximate computation of the matrix elements for example strong interactions and decays.

I. INTRODUCTION

A particle can be in once of several spin states, which, along with its electric charge, determines how it interacts with the electromagnetic force. While it may be counterintuitive, it is perfectly valid to call each of those states a different particle: e.g. there is an upelectron and a downelectron and they are identical in every aspect except for their spin. An electron with an indeterminate spin is thus a superposition of upelectron and downelectron, just as some particles are in a superposition of photon and electron-positron pair or a superposition of electron neutrino and muon neutrino. As the electron is a spin-1/2 particle, there are two types of electron: the upelectron and downelectron, which have $\hat{z}$ spin 1/2 and -1/2, respectively.

The interaction of a particle with the electromagnetic force is determined solely by its electric charge and spin. To a first order approximation and considering only the first generation of particles, a particle's interaction with the strong nuclear force is determined solely by its color charge and its isospin (though conservation laws remain in force). Color confinement prevents the direct observation of particles with color charge, so this paper will focus on isospin.

Just as the upelectron and downelectron can be considered to be different states of the electron, the proton and neutron can be considered different states of the isospin-1/2 "nucleon" particle with $\hat{z}$ isospin 1/2 and -1/2, respectively. Because this approximation is only an approximation, the two states of the nucleon have different masses, decay modes, and interactions with other forces.

However, we know that the nucleons are composed of quarks, with the proton begin composed of two up and one down quarks and the neutron being composed of one up and two down quarks. This seems to clash with the preceding claims.

For the first part of this paper, we will consider only the first-generation quarks: the up quark and down quark.

Quarks are (as far as we know) fundamental subatomic particles with isospin 1/2. Baryons (including protons and neutrons) are composed of three quarks, and mesons are composed of a quark and an antiquark (tetra quarks composed of two quarks and two antiquarks exist, but will not be discussed in this paper). Protons and Neutrons are both composed only of first-generation quarks, which can be in the up $|u\rangle$ state or the down $|d\rangle$ state. In analogy with spin angular momentum, we choose a direction along which to project the isospin to generate the projection isospin I_3 such that the up quark has I_3 1/2 and the down -1/2). This means that the set of baryons composed of first-generation quarks is in the isospin space generated by $2\otimes2\otimes2=(2\otimes2)\otimes2=(3\oplus1)\otimes2=3\otimes2\oplus1\otimes2=4\oplus2\oplus2$. The order-4 group is the delta baryons, a set of four isospin-3/2 particles which have the four I_3 states 3/2, 1/2, -1/2, and -3/2. The next two doublets describe states composed of a down and two up quarks or an up and two down quarks. However, the order-two lie group consisting of bound states describing an up and two down quarks only contains a single particle, as the following nonrigorous argument will demonstrate. The derivation of the wavefunction for the proton may also be performed through a rigorous method, but such a derivation is complicated enough that it is beyond the scope of this paper and requires a substantial amount of quantum field theory, unlike the symmetry argument which follows. Any particle consisting of a bound state of three quarks must be an eigenstate of the operator which permutes the identities of the individual quarks. Thus, all allowed states must have an equal contribution from $|uud\rangle$ and $|udu\rangle$, so for brevity all states will be shown aggregated by number of down quarks. However, this disallows the creation of a singlet state, so there can be no difference between the Δ^+ baryon and the proton (both being $|uud\rangle$), which does not agree with experiment. "The quarks are indistinguishable" does not match experiment, so the quarks must be in some way distinguishable.

The first property that quarks have which comes to mind is color- it seems plausible that the quarks inside a proton are distinguished by their color, and that this allows the existence of a singlet state. A proton is color neutral, so it is plausible to suppose that the a proton could be something like $\frac{1}{\sqrt{3}}(|(ru)(bu)(gd)\rangle+|(ru)(gu)(bd)\rangle)-|(bu)(gu)(rd)\rangle\rangle$, with (ru) representing a red up quark. However, transforming red to blue, blue to green, and green to red must not change the state- this color symmetry is an explicit SU(3) symmetry of the strong force. This requires that the proton state transform under a unitary transformation in color space as if it were a pure state, so the hadron wave function must be the product of a color term and a non-color term.

Quarks do have another property which allows them to be distinguished- spin. It may be obvious in retrospect that the proton has something odd going on inside with spin, because protons are spin-1/2 yet they are composed of three spin 1/2 particles. We began this paper with an

analogy between isospin and spin- so the same problems we are having in constructing isospin-1/2 nucleons out of three indistinguishable isospin-1/2 quarks would also occur in constructing spin-1/2 particles out of three indistinguishable spin-1/2 particles. In addition, the nucleon is spin-1/2 and there is no observed isospin-1/2 spin-3/2 particle, so there must be some kind of coupling between isospin and spin. It is thus logical to try to construct a state which is spin-1/2 and isospin-1/2 out of three first generation quarks by entangling the quarks' spin states with their isospin states. Consider first a spin-up proton. The two possibilities are that the down quark is spin down and the up quarks are spin-up or that the down quark is spin-up and the up quarks have opposite spins. We now have $|p\uparrow\rangle = \frac{1}{\sqrt{(A^2+B^2)}}(A|u\uparrow u\uparrow d\downarrow\rangle + B|u\uparrow u\downarrow d\uparrow\rangle)$.
Undoing the symmetry contraction we did above, we get

$$|p\uparrow\rangle = \frac{1}{\sqrt{6}\sqrt{A^2+B^2}}(A|u\uparrow u\uparrow d\downarrow\rangle + A|u\uparrow d\downarrow u\uparrow\rangle + A|d\downarrow u\uparrow u\uparrow\rangle)$$
$$+B|u\uparrow u\downarrow d\uparrow\rangle + B|u\uparrow d\uparrow u\downarrow\rangle + B|d\uparrow u\uparrow u\downarrow\rangle)$$
$$+B|u\downarrow u\uparrow d\uparrow\rangle + B|u\downarrow d\uparrow u\uparrow\rangle + B|d\uparrow u\downarrow u\uparrow\rangle)$$

It is necessary to note that $\langle u\uparrow u\uparrow d\downarrow|u\uparrow u\uparrow d\downarrow\rangle = 1/2$ on average- there are two orthogonal states with the representation $|u\uparrow u\uparrow d\downarrow\rangle$, so on average the inner product is 1/2 Symmetry would seem to suggest that each of these states must be equally probable, and thus $A = 2Be^{i\theta}$. If the proton and the Δ^+ baryon are to be distinct particles, the dot product of $|p\rangle$ and

$$|\Delta^+\uparrow\rangle = |uud\rangle \otimes |\uparrow\uparrow\downarrow\rangle = \frac{1}{\sqrt{12}}(2|u\uparrow u\uparrow d\downarrow\rangle + 2|u\uparrow d\downarrow u\uparrow\rangle + 2|d\downarrow u\uparrow u\uparrow\rangle)$$
$$+|u\uparrow u\downarrow d\uparrow\rangle + |u\uparrow d\uparrow u\downarrow\rangle + |d\uparrow u\uparrow u\downarrow\rangle)$$
$$+|u\downarrow u\uparrow d\uparrow\rangle + |u\downarrow d\uparrow u\uparrow\rangle + |d\uparrow u\downarrow u\uparrow\rangle)$$

must be zero. This dot product is $(A+2B)/\sqrt{(2)}$, so we have A=-2B and $|p\uparrow\rangle = \frac{1}{\sqrt{3}}(2|u\uparrow u\uparrow d\downarrow\rangle - |u\uparrow u\downarrow d\uparrow\rangle)$

We find experimentally that the projection isospin can be calculated using the Gell-Mann-Nishijima formula $I_3 = Q - \frac{1}{2}(A+S)$ where Q is charge, A is baryon number, and S is strangeness (which will be unimportant (zero) until the later part of the paper where SU(3) is discussed). For example, consider the delta baryons. They have isospins 3/2, 1/2, -1/2, and -3/2. They are baryons, so they have baryon number 1. Being composed of first-generation quarks, they have strangeness zero. This implies that they have electric charges 2, 1, 0, and -1, respectively. They are typically denoted $\Delta^{++}, \Delta^+, \Delta^0, \Delta^-$.

While it is possible for matter and antimatter to annihilate and create energy, this does not happen instantaneously- if the matter and antimatter together have momentum, mass, electric charge, isospin, or something else that is conserved the annihilation will result in the creation of particles that carry away that conserved quantity, which adds an energy barrier to the annihilation and increases the particle pair's half-life. Parity inversion (the mapping between a particle and its antiparticle) does not affect isospin, though it inverts electric charge, thus the antiup quark $\bar{u}$ has electric charge

-2/3 and projection isospin 1/2. Due to color confinement, all quarks and antiquarks appear in bound states consisting of three-quark or three-antiquark triplets and quark-antiquark pairs. The first-generation hadrons are the nucleons, the antinucleons, the deltas, the antideltas, the pions, and presumably several tetraquarks. Pions are mesons, particles consisting of a quark and an antiquark. They should thus be in 2⊗2=3⊕1. However, mesons are far less massive and interact far less readily than baryons, because the mass-energy of a baryon is thousands of times that of its components quarks due to the highly energetic internal gluon field. Consisting only of a quark-antiquark pair, mesons have much less energetic internal gluon fields, zero baryon number, and zero strangeness. They thus decay very readily through non-strong-force interactions; and thus dividing the zero-charge pion into the isospin-1 and isospin-0 superpositions is not useful. The useful distinction is the division by electric charge, because electric charge (unlike isospin) is conserved in electroweak decays. This results in there being three types of mesons rather than four: a positively charged meson, a negatively charged meson, and a neutral meson that is some superposition of $|1,0\rangle$ and $|0,0\rangle$, or in a different basis some superposition of $|d\bar{d}\rangle$ and $|u\bar{u}\rangle$.

II. DELTA-DELTA INTERACTIONS

In considering interactions and decays mediated by the strong force, we need only represent particles by their representations in isospin space; i.e. a proton p = $\left|\frac{1}{2}\frac{1}{2}\right\rangle$. The probability of a specific decay is proportional to the square of the absolute value of the expression $\langle\Psi_f|A(i,f)|\Psi_i\rangle$ where $|\Psi_i\rangle$ and $|\Psi_f\rangle$ are the initial and final states respectively of the system in isospin space and $A(i,f)$ is an isospin operator which is a function of the initial and final total isospins. However, conservation of isospin demands that the initial and final total isospins must be identical, or that $A(i,f)=0$ if $\vec{i}\neq\vec{f}$, or (because isospin vectors are two-dimensional) if $(I_i\neq I_f$ or $I3_i\neq I3_f)$. In addition, because the choice of a direction along which to compute the projection isospin is unphysical, $A(i,f)$ and $\langle\Psi_f|A(i,f)|\Psi_i\rangle$ (which is observable and physical) cannot depend on, and thus must depend only on $I_f=I_i$. We thus denote $A(i,f)$ as $A(I)$. Let $p_I=|\langle I,I3_f|A(I)|I,I3_i\rangle|$. We know that the interaction probabilities are proportional to p_I^2.

As an example, consider the interactions between mesons and baryons of the first generation. We have six categories of interaction: pion-pion, nucleon-nucleon, delta-delta, delta-pion, delta-nucleon, and pion-nucleon. The first two are largely uninteresting. The third serves as a rarely-analyzed illustrative example for calculation (though is not physically significant due to the short lifetimes of the delta baryons and the difficulty in detecting an interaction between two deltas), while analyses of the last three may be easily found in other media. The al-

lowed delta-delta interactions are:

difficult to perform the inner products to find that

$a)\Delta^{++}+\Delta^{++}\Rightarrow\Delta^{++}+\Delta^{++}$ $b)\Delta^{++}+\Delta^{+}\Rightarrow\Delta^{++}+\Delta^{+}$

$c)\Delta^{++}+\Delta^{0}\Rightarrow\Delta^{++}+\Delta^{0}$ $d)\Delta^{++}+\Delta^{0}\Rightarrow\Delta^{+}+\Delta^{+}$

$e)\Delta^{++}+\Delta^{-}\Rightarrow\Delta^{++}+\Delta^{-}$ $f)\Delta^{++}+\Delta^{-}\Rightarrow\Delta^{+}+\Delta^{0}$

$g)\Delta^{+}+\Delta^{+}\Rightarrow\Delta^{+}+\Delta^{+}$ $h)\Delta^{+}+\Delta^{+}\Rightarrow\Delta^{++}+\Delta^{0}$

$i)\Delta^{+}+\Delta^{0}\Rightarrow\Delta^{+}+\Delta^{0}$ $j)\Delta^{+}+\Delta^{0}\Rightarrow\Delta^{++}+\Delta^{-}$

$k)\Delta^{+}+\Delta^{-}\Rightarrow\Delta^{+}+\Delta^{-}$ $l)\Delta^{+}+\Delta^{-}\Rightarrow\Delta^{0}+\Delta^{0}$

$m)\Delta^{0}+\Delta^{0}\Rightarrow\Delta^{0}+\Delta^{0}$ $n)\Delta^{0}+\Delta^{0}\Rightarrow\Delta^{+}+\Delta^{-}$

$o)\Delta^{0}+\Delta^{-}\Rightarrow\Delta^{0}+\Delta^{-}$ $p)\Delta^{-}+\Delta^{-}\Rightarrow\Delta^{-}+\Delta^{-}$

$$p_b= \frac{1}{2}p_3+\frac{1}{2}p_2$$

$$p_c= \frac{1}{5}p_3+\frac{1}{2}p_2+\frac{3}{10}p_1$$

$$p_e= \frac{1}{20}p_3+\frac{1}{4}p_2+\frac{9}{20}p_1+\frac{1}{4}p_0$$

$$p_g= \frac{3}{5}p_3+\frac{2}{5}p_1$$

$$p_i= \frac{9}{20}p_3+\frac{1}{4}p_2+\frac{1}{20}p_1+\frac{1}{4}p_0$$

$$p_k= \frac{1}{5}p_3+\frac{1}{2}p_2+\frac{3}{10}p_1$$

$$p_m= \frac{1}{20}p_3+\frac{1}{4}p_2+\frac{9}{20}p_1+\frac{1}{4}p_0$$

$$p_o= \frac{1}{2}p_3+\frac{1}{2}p_2$$

$$p_d= \frac{\sqrt{3}}{5}p_3-\frac{\sqrt{3}}{5}p_1$$

$$p_f= \frac{3}{20}p_3+\frac{1}{4}p_2-\frac{3}{20}p_1-\frac{1}{4}p_0$$

$$p_h= p_d$$

$$p_j= p_f$$

$$p_l= \frac{\sqrt{3}}{5}p_3-\frac{\sqrt{3}}{5}p_1$$

$$p_n= p_l$$

To begin the analysis, use the Clebsch-Gordon coefficients to compute the isospin vectors for each pair of particles:

$$\Delta^{++}+\Delta^{++}:\left|\frac{3}{2}\frac{3}{2}\right\rangle\left|\frac{3}{2}\frac{3}{2}\right\rangle=|33\rangle$$

$$\Delta^{++}+\Delta^{+}:\left|\frac{3}{2}\frac{3}{2}\right\rangle\left|\frac{3}{2}\frac{1}{2}\right\rangle=\sqrt{\frac{1}{2}}|32\rangle+\sqrt{\frac{1}{2}}|22\rangle$$

$$\Delta^{++}+\Delta^{0}:\left|\frac{3}{2}\frac{3}{2}\right\rangle\left|\frac{3}{2}-\frac{1}{2}\right\rangle=\sqrt{\frac{1}{5}}|31\rangle+\sqrt{\frac{1}{2}}|21\rangle+\sqrt{\frac{3}{10}}|11\rangle$$

$$\Delta^{++}+\Delta^{-}:\left|\frac{3}{2}\frac{3}{2}\right\rangle\left|\frac{3}{2}-\frac{3}{2}\right\rangle=\sqrt{\frac{1}{20}}|30\rangle+\sqrt{\frac{1}{4}}|20\rangle+\sqrt{\frac{9}{20}}|10\rangle+\sqrt{\frac{1}{4}}|00\rangle$$

$$\Delta^{+}+\Delta^{+}:\left|\frac{3}{2}\frac{1}{2}\right\rangle\left|\frac{3}{2}\frac{1}{2}\right\rangle=\sqrt{\frac{3}{5}}|31\rangle-\sqrt{\frac{2}{5}}|11\rangle$$

$$\Delta^{+}+\Delta^{0}:\left|\frac{3}{2}\frac{1}{2}\right\rangle\left|\frac{3}{2}-\frac{1}{2}\right\rangle=\sqrt{\frac{9}{20}}|30\rangle+\sqrt{\frac{1}{4}}|20\rangle-\sqrt{\frac{1}{20}}|10\rangle-\sqrt{\frac{1}{4}}|00\rangle$$

$$\Delta^{+}+\Delta^{-}:\left|\frac{3}{2}\frac{1}{2}\right\rangle\left|\frac{3}{2}-\frac{3}{2}\right\rangle=\sqrt{\frac{1}{5}}|3-1\rangle-\sqrt{\frac{1}{2}}|2-1\rangle+\sqrt{\frac{3}{10}}|1-1\rangle$$

$$\Delta^{0}+\Delta^{0}:\left|\frac{3}{2}-\frac{1}{2}\right\rangle\left|\frac{3}{2}-\frac{1}{2}\right\rangle=\sqrt{\frac{3}{5}}|3-1\rangle-\sqrt{\frac{2}{5}}|1-1\rangle$$

$$\Delta^{0}+\Delta^{-}:\left|\frac{3}{2}-\frac{1}{2}\right\rangle\left|\frac{3}{2}-\frac{3}{2}\right\rangle=-\sqrt{\frac{1}{2}}|3-2\rangle+\sqrt{\frac{1}{2}}|2-2\rangle$$

$$\Delta^{-}+\Delta^{-}:\left|\frac{3}{2}-\frac{3}{2}\right\rangle\left|\frac{3}{2}-\frac{3}{2}\right\rangle=|3-3\rangle$$

It is immediately evident that $p_a=p_p=p_3$. It is also not

III. DELTA BARYON DECAYS

As an example of strong decays, we consider the strong decay of the first-generation hadrons. A delta baryon can decay to a pion and a nucleon or a pion and a delta, a pion can decay into two pions, and a nucleon can decay into a nucleon and a pion. The latter three are disallowed because the products have greater energy than the reactants, so we consider the first: the decay of a delta into a pion and a nucleon. The decays which conserve isospin are:

$$a)\Delta^{++}\Rightarrow\pi^{+}+N^{+}$$

$$b)\Delta^{+}\Rightarrow\pi^{+}+N^{0}$$

$$c)\Delta^{+}\Rightarrow\pi^{0}+N^{+}$$

$$d)\Delta^{0}\Rightarrow\pi^{0}+N^{0}$$

$$e)\Delta^{0}\Rightarrow\pi^{-}+N^{+}$$

$$f)\Delta^{-}\Rightarrow\pi^{-}+N^{0}$$

Computing Clebsch-Gordon coefficients:

$$\pi^+ + N^+ : |11\rangle + \left|\frac{1}{2}\frac{1}{2}\right\rangle \qquad = \left|\frac{3}{2}\frac{3}{2}\right\rangle$$

$$\pi^+ + N^0 : |11\rangle + \left|\frac{1}{2}-\frac{1}{2}\right\rangle \qquad = \sqrt{\frac{1}{3}}\left|\frac{3}{2}\frac{1}{2}\right\rangle + \sqrt{\frac{2}{3}}\left|\frac{1}{2}\frac{1}{2}\right\rangle$$

$$\pi^0 + N^+ : |10\rangle + \left|\frac{1}{2}\frac{1}{2}\right\rangle \qquad = \sqrt{\frac{2}{3}}\left|\frac{3}{2}\frac{1}{2}\right\rangle - \sqrt{\frac{1}{3}}\left|\frac{1}{2}\frac{1}{2}\right\rangle$$

$$\pi^0 + N^0 : |10\rangle + \left|\frac{1}{2}-\frac{1}{2}\right\rangle \qquad = -\sqrt{\frac{2}{3}}\left|\frac{3}{2}-\frac{1}{2}\right\rangle - \sqrt{\frac{1}{3}}\left|\frac{1}{2}-\frac{1}{2}\right\rangle$$

$$\pi^- + N^+ : |1-1\rangle + \left|\frac{1}{2}\frac{1}{2}\right\rangle \qquad = -\sqrt{\frac{1}{3}}\left|\frac{3}{2}\frac{1}{2}\right\rangle + \sqrt{\frac{2}{3}}\left|\frac{1}{2}\frac{1}{2}\right\rangle$$

$$\pi^- + N^- : |1-1\rangle + \left|\frac{1}{2}-\frac{1}{2}\right\rangle \quad = \left|\frac{3}{2}-\frac{3}{2}\right\rangle$$

We thus have

$$p_a = p_f = p_{\frac{3}{2}}$$

$$p_b = \sqrt{\frac{1}{3}}p_{\frac{1}{2}}$$

$$p_c = \sqrt{\frac{2}{3}}p_{\frac{1}{2}}$$

$$p_d = -\sqrt{\frac{2}{3}}p_{\frac{1}{2}}$$

$$p_e = -\sqrt{\frac{1}{3}}p_{\frac{1}{2}}$$

Without even knowing the values of the matrix elements, we now know that the Δ^+ baryon is twice as likely to decay into a proton and a neutral pion than into a neutron and a positive pion, that the decays rates of Δ^{++} and Δ^- baryons are equal, and that the decay rates of Δ^+ and Δ^0 baryons are equal. It turns out that theory also predicts $p_{\frac{3}{2}} = p_{\frac{1}{2}}$ so all the delta baryon decay rates should be the same, which is observed experimentally.

IV.   SUMMARY

Beginning by arguing that it is valid to treat spin-up and spin-down electrons as different types of particles, we draw the analogy to treating the proton and neutron as isospin-up and isospin-down states of the nucleon. Using this inexact symmetry, we calculate states for combinations of delta baryons, pions, and nucleons. From even the basic analysis in this paper, it is clear that nontrivial and nonobvious results such as the relative probabilities for the decay modes of the Δ^+ and Δ^0 baryons can be obtained from simple calculations using isospin, even though isospin symmetry is inexact. By improving the approximation by adding additional terms, it is possible to construct a relatively-high-accuracy model of many strong force processes.

[1] D. J. Griffiths. Introduction to Elementary Particles. Wiley-VCH, 2008.
[2] K. S. Krane, Introductory Nuclear Physics. Wiley, 1987.
[3] Xiangdong Ji, Lecture notes on UMD class Physics 741. Accessible at http://www.physics.umd.edu/courses/Phys741/xji/lecture_notes.htm.

Two interacting fermions in a Double-Well Potential: the building block of the Fermi-Hubbard Model

Elmer Guardado-Sanchez

MIT Department of Physics, 77 Massachusetts Ave., Cambridge, MA 02139-4307

(Dated: May 2, 2014)

This paper discusses the ground state corresponding to two distinguishable fermions inside a Double-Well Potential using WKB and the Fermi-Hubbard Model. Given the nature of the particles, there will be preferred accommodations inside the potential depending on the strength of the interaction between them. The two most interesting states are those where the particles want to be in the same well (attraction) and when the preference is to be in different wells (repulsion). The latter is specially interesting because it defines a Mott-insulating state. This potential is a very interesting tool to understand how the Fermi-Hubbard Model works in its most diluted form.

I. INTRODUCTION

In 1963, John Hubbard proposed a very simple Hamiltonian to describe the behavior of electrons inside a periodic potential at low temperatures; this Hamiltonian is now known as the Fermi-Hubbard model [1]. This model is used to describe an ensemble of fermions inside a periodic potential when only the lowest energy levels are being filled. However its general solutions have not been found yet. In an attempt to experimentally find a solution, ultracold Fermi-gases have been studied inside optical lattices to gain a better understanding of the model [2, 5, 7].

As often done in physics, in order to solve a hard problem it is necessary to look first at its most simple form. In the case of a lattice potential, this will be the Double-Well Potential. This potential is in essence a one-dimensional, double-site lattice and thus its most basic states can be treated with the Fermi-Hubbard Model. In this paper, I will demonstrate the complete solution for the case of having two distinguishable fermions (one $|\uparrow\rangle$ and one $|\downarrow\rangle$) interacting inside a Double-Well Potential using the Fermi-Hubbard model in order to gain insight into the behavior of fermions in lattice potentials.

II. THEORY

A. WKB in a Double-Well Potential

First, I solve for the ground state and the first excited state to better visualize the possible basis for the Fermi-Hubbard Model. By applying the WKB method as in Problem 8.15 of Griffiths [9, p. 348] it is possible to find a numerically exact solution for the Double-Well Potential as shown in [6].

Having a Double-well Potential that is symmetrical about the y axis; I take into account just the well for positive values of x. At a specific energy E, there are two crossings with the potential of unknown form for the moment; this divides the well into three different regions. This is shown in Figure 1. By applying the WKB approximation, it is then possible to express the eigenfunction at energy E as:

$$|\Psi\rangle = \begin{cases} \frac{A}{\sqrt{|p(x)|}}e^{|P(x_2,x)|} & x > x_2 \\ \frac{2A}{\sqrt{p(x)}}\sin\left(-P(x,x_2)\right) + \frac{\pi}{4} & x_1 < x < x_2 \\ \frac{A}{\sqrt{|p(x)|}}\left(2\cos\theta e^{-|P(x,x_1)|} + \sin\theta e^{|P(x,x_1)|}\right) & 0 < x < x_1 \end{cases}$$

(1)

where $p(x) = \sqrt{2m(E - V(x))}$, $P(a,b) = -\frac{1}{\hbar}\int_a^b p(x)dx$, A is a normalization constant, and $\theta = \frac{1}{\hbar}\int_{x_1}^{x_2} p(x)dx$.
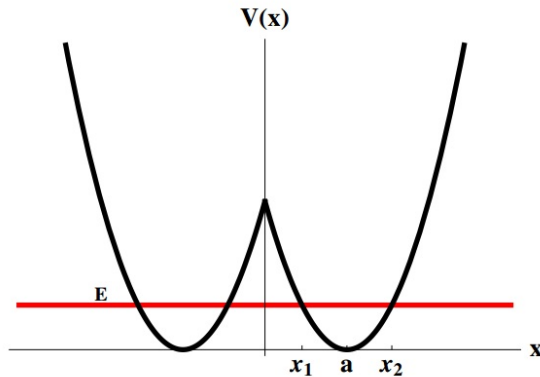
FIG. 1: Sample Double-Well Potential showing a potential eigenvalue and the crossings of it with the potential itself. Adapted from [10]

This is only half of the solution and it is known that in a symetric potentia,l there can only be symmetric or anti-symmetric solutions with respect to the central barrier. Therefore, there are two sets of boundary conditions: for symmetric solutions $\frac{\partial}{\partial x}|\Psi(0)\rangle = 0$; and for anti-symmetric solutions $|\Psi(0)\rangle = 0$. These conditions take me to the final condition:

$$\tan\theta = \pm 2e^{-|P(-x_1,x_1)|} = \pm 2e^{\phi}$$

(2)

The regime where the Fermi-Hubbard Model applies is that for which the temperature is low enough that the maximum energy level is way smaller to the wall between

the wells. Thus, $e^\phi \gg 1$ and there is a final condition on the eigenstates:

$$\theta = \left(n + \frac{1}{2}\right)\pi \mp e^{-\phi} \qquad (3)$$

For the rest of the paper, I will use only the lowest possible energies of atoms in the potential and therefore only the solutions for $n = 0$ are taken into account. The symmetric (even) solution will be the ground state of this basis $|0\rangle$ and the anti-symmetric (odd) solution the first excited state $|1\rangle$. An example of these states' forms is shown in Figure 2 for two different types of Double-Well Potential.
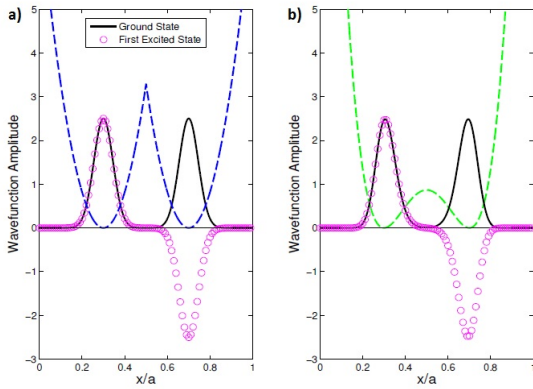
FIG. 2: Exact numerical solutions of the two lowest states a Double-Well Potential. a) has the form $V(x) = \frac{V_{max}}{b^2}\left(|x - \frac{a}{2}| - b\right)^2$. b) has the form $\frac{V_{max}}{b^4}\left((x - \frac{a}{2})^2 - b^2\right)^2$. Adapted from [6]

Figure 2 serves only to show a visual representation of the two lowest energy solutions in a Double-Well Potential in order to better understand the change of basis used in the solution of the Fermi-Hubbard Model.

Knowing the solution in the eigenbasis $\{|0\rangle, |1\rangle\}$ I define a different eigenbasis that is more useful for the rest of the analysis: $\{|L\rangle, |R\rangle\}$. This last eigenbasis corresponds to the particle being on the left $|L\rangle$ or the right $|R\rangle$ well and its relationship to the WKB solutions is:

$$\begin{aligned} |L\rangle &= \tfrac{1}{\sqrt{2}}(|0\rangle + |1\rangle) \\ |R\rangle &= \tfrac{1}{\sqrt{2}}(|0\rangle - |1\rangle) \end{aligned} \qquad (4)$$

The basis $\{|0\rangle, |1\rangle\}$ is not used in the rest of the analysis and its derivation is done just to show where the basis comes from.

B.   Hamiltonian of two atoms in a potential

When treating two particles instead of just one, there has to be the addition of a term equal to the interaction

between them. Defining the Hamiltonian of only one particle to be $H_0(x)$, we can define the Hamiltonian of the two-particle system as:

$$H(x_1, x_2) = H_0(x_1) + H_0(x_2) + UV(|x_1 - x_2|) \qquad (5)$$

where U determines the strength and nature of the interaction between the particles and $V(|x_1 - x_2|)$ is a potential depending on their relative distance, which is often regarded as a delta function due to particles being of negligible size. The eigenstates of this Hamiltonian will be superpositions of entangled states of the individual particles.

C.   The Fermi-Hubbard Model and Phase Diagram

1.   Hamiltonian

As mentioned before, the Fermi-Hubbard Model defines the behavior of fermions inside a lattice potential. It is composed of two major parts: a tunneling term and an interaction term. Its general form is[8]:

$$\hat{H}_{FH} = -J \sum_{\sigma=\{\uparrow,\downarrow\}} \sum_{\langle i,j \rangle} \hat{c}_{i\sigma}^\dagger \hat{c}_{j\sigma} + U \sum_i \hat{n}_{i\uparrow}\hat{n}_{i\downarrow} \qquad (6)$$

where J is the tunneling factor, U is the interaction factor, $\hat{c}$ is the creation operator, $\hat{c}^\dagger$ is the annihilation operator, and $\hat{n} = \hat{c}^\dagger\hat{c}$ is the number operator. The summation over i and j represents the sum over the possible lattice sites. It is very important to note that here, the creation and annihilation operator refer to the second quantization and therefore their action is actually creating or annihilating a particle from the lattice site they are acting on.

There is an intuitive way to understand the Hamiltonian. The tunneling term is understood as the energy lost as a particle tunnels from one site to the another (annihilation in one site and creation in other site). The interaction factor is the energy due to particles interacting in the same single site (number of particles in each site).

2.   Phase Diagram

With the Hamiltonian form of the Fermi-Hubbard Model, it is theoretically possible to tune both the tunneling and interactions of particles to find different phases by defining values of J and U. Experimentally, the tunneling would be modified by changing the strength of the walls in the lattice potential by modifying the power of the laser used. The interaction would be modified using a Feshback resonance; this is basically a resonance where the scattering length has an asymptotic behavior at a value that depends on an offset of the energy levels. The offset of the energy levels can be achieved with a tunable magnetic field for particles with spin.

FIG. 3: Phase Diagram of the Fermi-Hubbard Model in a 3D lattice. The abbreviations are: Bose-Einstein Condensate (BEC), Bardeen-Cooper-Schrieffer (BCS), and antiferromagnetic phase (AFM). Adapted from [8]

A full Phase Diagram for a 3D lattice is found in Figure 3. As mentioned before, it is possible to tune the scattering length experimentally. This allows to tune the interaction between particles from a strongly attractive interaction to a strongly repulsive interaction. The Phase Diagram also shows the dependence on the Temperature as it defines which states will be most probable to be occupied.

In the cases with attractive interaction, the fermions behave like a superfluid, which is the same as a superconductor (e.g. electrons in metal). The attraction first creates Cooper pairs (bosons by sum of spin) in the BCS regime (Bardeen-Cooper-Schrieffer) and with more attraction these pairs create a Bose-Einstein Condensate (BEC). At higher temperatures not all particles will form Cooper pairs so they cannot break full degeneracy and thus they cannot act as a BEC.

In the cases of a repulsive interaction, the fermions start separating by spin in a checkerboard manner (alternating); therefore the net spin is zero. This alignment of the fermions in the lattice is known as antiferromagnetism (AFM). When the repulsion is high and the temperature rises, the Mott Insulator phase appears. This phase is very similar to AFM but shows a variety of unexplained properties that make it a very interesting area of reasearch in Condensed Matter Physics and Ultra-Cold Atoms [7]. This paper shows the transition of the ground state to the Mott-Insulating phase when the interaction is strongly repulsive.

III. MODEL DESCRIPTION

As mentioned above, this paper expects to show how the building block of the Fermi-Hubbard Model behaves. The model for that building block is that of a Double-

Well Potential with arbitrary form, which is perfectly symmetric about its central barrier. A second condition is that only the lowest states are being occupied as it would be at very low temperatures. The third and final condition is that the strength of the barrier is big compared to the energy levels that are being occupied.

In the model, there is one $|\uparrow\rangle$ fermion and one $|\downarrow\rangle$ fermion interacting. The eigenbasis that these two fermions are described by is the one from Equation 4. The full basis to describe both fermions in the potential is that of the possible entangled states ($|\uparrow\downarrow\rangle$). The basis of states $\{|LL\rangle, |LR\rangle, |RL\rangle, |RR\rangle\}$ is the one which I use for the reduced form of the Fermi-Hubbard model in the Double-Well Potential.

IV. SOLVING OF THE FERMI-HUBBARD MODEL

A. Matrix form and Eigenstates

In the Double-Well Potential, the Fermi-Hubbard Hamiltonian from Equation 6 gets reduced to:

$$\hat{H}_{FH} = -J\left(\hat{c}^\dagger_{L\uparrow}\hat{c}_{R\uparrow} + \hat{c}^\dagger_{L\downarrow}\hat{c}_{R\downarrow} + \hat{c}^\dagger_{R\uparrow}\hat{c}_{L\uparrow} + \hat{c}^\dagger_{R\downarrow}\hat{c}_{L\downarrow}\right) + U\left(\hat{n}_{L\downarrow}\hat{n}_{L\uparrow} + \hat{n}_{R\downarrow}\hat{n}_{R\uparrow}\right)$$

(7)

For the basis $\{|LL\rangle, |LR\rangle, |RL\rangle, |RR\rangle\}$, this Hamiltonian can be represented as a 4×4 matrix of the form:

$$\hat{H}_{FH} = \begin{pmatrix} U & -J & -J & 0 \\ -J & 0 & 0 & -J \\ -J & 0 & 0 & -J \\ 0 & -J & -J & U \end{pmatrix}$$

(8)

From this matrix I solve for the eigenstates and eigenvalues to get:

$$|\Psi_1\rangle = \frac{1}{\sqrt{2}}(|RL\rangle - |LR\rangle); E_1 = 0$$

$$|\Psi_2\rangle = \frac{1}{\sqrt{2}}(|RR\rangle - |LL\rangle); E_2 = U$$

$$|\Psi_{3,4}\rangle \propto |LL\rangle + |RR\rangle$$

$$+ \left(\frac{U}{4J} \mp \sqrt{1 + \left(\frac{U}{4J}\right)^2}\right)(|LR\rangle + |RL\rangle)$$

$$; E_{3,4} = \frac{1}{2}\left(U \pm \sqrt{(4J)^2 + U^2}\right)$$

B. Tuning the Interaction

With these solutions being the eigenstates of the system, the probability of both particles being in the same well is defined as: $P_i = P(|\Psi_i\rangle = |LL\rangle) + P(|\Psi_i\rangle = |LL\rangle)$, where i denotes the eigenstate. From this relation, it

should be obvious that for eigenstates 1 and 2 we have: $P_1 = 0$ and $P_2 = 1$ since these states are superpositions of different-well and same-well states respectively. In the case of states 3 and 4, I need to first normalize $|\Psi_{3,4}\rangle$ to get the following:

$$P_{3,4} = \frac{1}{1 + \left(\frac{U}{4J} \mp \sqrt{1 + \left(\frac{U}{4J}\right)^2}\right)^2} \qquad (9)$$

Plots of the energy eigenvalues and the probabilities of having double occupancy with respect to the interaction parameter $\frac{U}{4J}$ are shown in Figure 4.
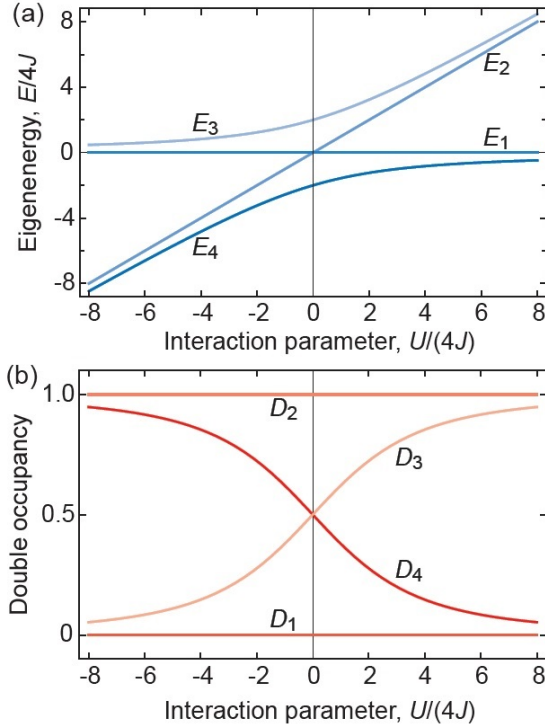

FIG. 4: (a) Energy eigenvalues of the 4 eigenstates for the Hamiltonian in Equation 8 for different interaction strength. (b) Probability of having double occupancy in the Potential, D_i corresponds to the probability value. Adapted from [8]

C.   Transition to a Mott-Insulator

As Figure 4 shows, the state $|\Psi_4\rangle$ is the ground state of the system as the energy is always the lowest for the entire range of interactions. In the limit of very strong attractive interactions ($\frac{U}{J} \ll 0$), the probability of double occupancy goes to 1 as $|\Psi_4\rangle \to \frac{1}{\sqrt{2}}(|LL\rangle + |RR\rangle)$ in the paired/superfluid regime of the Phase Diagram in Figure 3. On the other hand, in the limit of very strong repulsive interactions ($\frac{U}{J} \gg 0$), the probability of double occupancy goes to 0 as $|\Psi_4\rangle \to \frac{1}{\sqrt{2}}(|LR\rangle + |RL\rangle)$ and the two particles effectively transition to a Mott-Insulator state. In this ground state, the particles will always be in different sites of the lattice and the tunneling probability goes to zero.

V.   CONCLUSION

Through the analysis performed above, I was able to effectively solve the ground state for two distinguishable fermions inside a Double-Well Potential. I used the WKB approximations to first describe the states of a single particle in the potential and then applied the Fermi-Hubbard model in its most basic form to solve the system. This toy-model potential is important as it gives important intuition for the yet generally unsolved Fermi-Hubbard Model and its experimental realization [5] marks the beginning of a far better understanding of any fermion on a periodic potential.

Acknowledgments

[1] J. Hubbard. *Electron Correlations in Narrow Energy Bands.* Proc. R. Soc. Lond. A, vol. 276 no. 1365, 238-257, 26 November 1963

[2] G. Zürn, F. Serwane, T. Lompe, A. N. Wenz, M. G. Ries, and S. Jochim. *Fermionization of Two Distinguishable Fermions.* Phys. Rev. Lett. 108, (2012)

[3] S. Franke-Arnold, S.M. Barnett, G. Huyet, and C. Sailliot. *Coherence properties of two trapped particles.* Eur. Phys. J. D 22, 373-383 (2003)

[4] Thomas Busch, Berthold-George Englert, Kazimierz Rzazewski, and Martin Wilkens. *Two Cold Atoms in a Harmonic Trap.* Foundations of Physics, Vol. 28, No. 4 (1998)

[5] S. Murmann, A. Bergschneider, V. Klinkhamer, G. Zürn, T. Lompe, and S. Jochim. *Deterministic Control of two Fermions in a Double Well.* In preparation (2014)

[6] V. Jelic and F. Marsiglio. *The double well potential in quantum mechanics: a simple, numerically exact formu-*

lation. Eur. J. Phys. 33, 1651-1666 (2012)

[7] Markus Greiner, Olaf Mandel, Tilman Esslinger, Theodor W. Hansch, and Immanuel Bloch. *Quantum phase transition from a superfluid to a Mott Insulator in a gas of ultracold atoms.* Nature 415, 39-44 (3 January 2002)

[8] Sebastian Will. *From Atom Optics to Quantum Simulation: Interacting Bosons and Fermions in Three-Dimensional Optical Lattice Potentials.* Dissertation, Johannes Gutenberg University of Mainz. Springer, 2013.

(Publication No. 978-3-642-33632-4)

[9] David J. Griffiths. *Introduction to Quantum Mechanics.* Pearson Education, Inc. 2nd Edition. (2005)

[10] Aram Harrow. *Solutions to Problem set 4 of 8.06 Spring 2014.* Materials for 8.06. (2014)

[11] C. Chin, R. Grimm, P. Julienne, and E. Tiesinga. *Feshbach resonances in ultracold gases.* Rev. Mod. Phys. 82, 2, 1225-1286. (2010)

Baby steps towards Quantum Statistical Mechanics: A solution to a One Dimensional Chain of Interacting Spins

Diptarka Hait

Departments of Chemistry and Physics, 77 Massachusetts Ave., Cambridge, MA 02139-4307
(Dated: May 2, 2014)

Systems with inter-particle interactions often exhibit complex behavior that cannot readily be explained. Herein we model a system of interacting N $s = \frac{1}{2}$ particles in the presence of an external magnetic field, and analytically solve it using operator techniques. The obtained eigenenergies are employed to get a partition function, which is then used to predict the values of thermodynamic observables. Finally, an interesting hypothetical material is considered, and the model is used to predict its properties.

I. INTRODUCTION

To date, neither Quantum nor Classical Physics has been able to provide an exact analytic solution to the general N body problem (N $\geq$ 3) and yet there is a need to explain macroscopic phenomena that involve particle numbers of the order of 10^{23}. This has led to a proliferation of somewhat unrealistic approximate models like the ideal gas, where inter-particle interactions are completely ignored. Though these simplified models are often reasonable first approximations for many phenomena, they completely fail to describe behavior where inter-particle forces play a significant role, such as in phase transitions.

Facing this problem while studying the paramagnetic to ferromagnetic transition, E. Ising came up with his own model of particle interaction in 1925 [1]. He represented each atom as a $s = \frac{1}{2}$ particle and proposed that the potential energy of the interaction between particles i and j is $-J\vec{S}_i \cdot \vec{S}_j$ if they are nearest neighbors and 0 otherwise. He then used statistical mechanics to solve the case of a 1D chain of N $s = \frac{1}{2}$ particles [1], and was able to predict the behavior of linear magnetic chains. However, Ising's model had two great flaws: it approached the purely quantum phenomenon of spin from an essentially classical perspective and it did not account for any anisotropy.

The Heisenberg model was developed to be a quantum mechanical generalization of the Ising model that incorporated anisotropy. This took much longer to solve, with exact solutions only being published by Lieb et.al. in 1961[2] and Katsura in 1962 [3]. However, both had ultimately found the complete Heisenberg model to be too difficult to tackle, and had instead attacked a physically relevant special case called the XY model, where interactions along one direction are neglected.

This paper intends to introduce the reader to Quantum Statistical Mechanics, by using the approach of Lieb et.al. and Katsura to solve the simplest model of interacting particles in Quantum mechanics. In Sec. II, we will present the notation employed in this paper and discuss the exact mathematical form of the Heisenberg and XY models. In Sec. III, we will convert the spin operators into a more tractable form by using a set of unitary transformations called the Jordan Wigner trans-

formations. In Sec. IV, we will partition the Hamiltonian into two orthogonal subspaces, and discuss how it simplifies the problem. In Sec. V, we will explicitly solve for the eigenvalues in one subspace by means of a Fourier Transform and a linear transform called the Boguliubov transform. In Sec. VI, we will use the eigenenergies so generated to calculate the partition function, which will be employed to calculate thermodynamic quantities for some particular cases of the problem, and check consistency with earlier models (such as the Ising). We use the thermodynamic data to examine properties of an unusual material of with both ferro-magnetic and antiferromagnetic coupling in Sec. VII. We conclude in Sec. VIII by discussing the significance of the solutions to the XY model.

II. PRELIMINARY DISCUSSIONS

A. Heisenberg model and Notation

The Heisenberg model incorporates anisotropy by proposing that the interaction between nearest neighbors i and j is $-J_x S_i^x S_j^x - J_y S_i^y S_j^y - J_z S_i^z S_j^z$, instead of the $-J\vec{S}_i \cdot \vec{S}_j$ used by Ising. Though it is possible to immediately write down the Heisenberg Hamiltonian in terms of the operators $\hat{S}^{\{x,y,z\}}$, we choose to first introduce some unconventional notation for convenience.

The motivation is simple: we are going to deal with a system of N $s = \frac{1}{2}$ particles, whose state space consists of tensor products over N individual-particle subspaces. The individual states are of the form $|1\rangle \otimes |2\rangle \otimes \ldots |N\rangle$, where $|i\rangle = c_1 |+\rangle + c_2 |-\rangle$ denotes the spin-state of the ith particle. The terms of the Hamiltonian are also are tensor products over N subspaces, like $\hat{S}_x \otimes \hat{S}_x \otimes I \otimes \ldots I$. Tensor products are generally cumbersome, and therefore we choose to use the simplified, condensed notation that is described beneath.

We will represent a term like $\underbrace{I \otimes I \otimes \ldots}_{i-1 \text{ times}} \otimes S_x \otimes S_x \otimes \underbrace{I \otimes \ldots I}_{N-i-1 \text{ times}}$ as $S_i^x S_{i+1}^x$, which says that S_x operator is acting on the ith and the $i + 1^{\text{th}}$ particle, while Identity

operators cause no change and are ignored. We generalize this notation to account for any number of spin operators (or Pauli matrices or any linear combinations thereof) acting on any number of particles, with the subscript of each operator depicting the particle it acts on.

It is to be kept in mind however, that this condensed notation is not extended to *any* operator $\hat{O}$, though we can define operators $\hat{O}_i$ in terms of these condensed forms (with the implicit understanding that it is a tensor product and need not act on particle i alone). For example:
$$\hat{F}_i \equiv \sigma_i^x \sigma_{i+1}^x \sigma_{i+2}^z = \underbrace{I \otimes I \dots}_{i-1 \text{ times}} \otimes \sigma_x \otimes \sigma_x \otimes \sigma_z \otimes \underbrace{I \otimes \dots I}_{N-i-2 \text{ times}}$$

Having discarded the explicit tensor product notation, we are now prepared to describe the Hamiltonian for the system. There is a chain of N $s = \frac{1}{2}$ particles in the presence of an external magnetic field $\vec{B} = B\hat{z}$. Interparticle interactions are assumed to obey the Heisenberg model, giving the Hamiltonian:

$$H = -\sum_{i=1}^{N}(J_x \hat{S}_i^x \hat{S}_{i+1}^x + J_y \hat{S}_i^y \hat{S}_{i+1}^y + J_z \hat{S}_i^z \hat{S}_{i+1}^z + M\hat{S}_i^z) \tag{1}$$

$$\hat{\vec{S}}_{N+1} = \hat{\vec{S}}_1 \text{ (Periodic boundary condition)} \tag{2}$$

$$M = \frac{gBq}{2m} \text{ (q=charge, m=mass, g=Lande factor)} \tag{3}$$

J_i are coupling constants (possibly unequal) that give a measure of spin-spin interaction.

Here we are using periodic boundary condition (2) to simplify a great deal of mathematics later. This condition is not unphysical as the periodic case converges to the non-periodic in the limit of large N (which is what we are interested in), as particles in the middle of the chain will be essentially isolated from the boundary. Ising himself had required these conditions to solve his model [1].

Also, this paper will use Pauli matrices instead of spin operators, and so the Hamiltonian is converted to:

$$H = -\sum_{i=1}^{N}(j_x \sigma_i^x \sigma_{i+1}^x + j_y \sigma_i^y \sigma_{i+1}^y + j_z \sigma_i^z \sigma_{i+1}^z + h\sigma_i^z) \tag{4}$$

$$j_k = J_k \frac{\hbar^2}{4} \ (k \in \{x, y, z\}), \qquad h = \frac{\hbar}{2}M = \frac{\hbar gBq}{4m} \tag{5}$$

B. The XY Model

The XY model is a special case of the Heisenberg model where $j_z = 0$. Therefore:

$$H = -\sum_{i=1}^{N}(j_x \sigma_i^x \sigma_{i+1}^x + j_y \sigma_i^y \sigma_{i+1}^y + h\sigma_i^z) \tag{6}$$

This is the model which we will solve in this paper, as the general Heisenberg model is too complex to tackle.

For most physical purposes though, it is sufficient to only consider interactions transverse to the applied field (here along the z direction), and so the XY model proves adequate.

III. THE JORDAN-WIGNER TRANSFORMATION

The first step in the process of diagonalizing the Hamiltonian is to convert the Pauli matrices into the more useful form of ladder operators. In 1928, P. Jordan and E. Wigner [4] had published a beautiful technique for achieving this, and it is their approach that we will use.

We begin by defining the operators $\hat{a}$ and $\hat{a}^\dagger$:

$$\hat{a} \equiv \begin{pmatrix} 0 & 1 \\ 0 & 0 \end{pmatrix} \iff \hat{a}^\dagger \equiv \begin{pmatrix} 0 & 0 \\ 1 & 0 \end{pmatrix} \tag{7}$$

It thereby follows that:

$$\sigma_i^x = \hat{a}_i + \hat{a}_i^\dagger \tag{8}$$
$$\sigma_i^y = i(\hat{a}_i^\dagger - \hat{a}_i) \tag{9}$$
$$\sigma_i^z = 1 - 2\hat{a}^\dagger_i \hat{a}_i \tag{10}$$

$\hat{a}_i$ and $\hat{a}_i^\dagger$ are linear combinations of σ_i^x and σ_i^y and thus only act on particle i. Therefore, we are allowed to use the condensed notation in Sec. II for $\{\hat{a}_i\}$ as well.

$\{\hat{a}_i\}$ and $\{\hat{a}_i^\dagger\}$ look like the harmonic oscillator ladder operators but:

$$[\hat{a}, \hat{a^\dagger}] = \begin{pmatrix} 1 & 0 \\ 0 & -1 \end{pmatrix} = \sigma^z \neq I \tag{11}$$

That was not unexpected, as we are dealing with fermions ($s = \frac{1}{2}$) and fermionic ladder operators obey the anti-commutation relations (not commutation like that of bosonic operators):

$$\{\hat{A}, \hat{B}\} = \hat{A}\hat{B} + \hat{B}\hat{A} = 1 \iff \hat{A} = \hat{B}^\dagger \tag{12}$$

$$\{\hat{A}, \hat{B}\} = 0 \qquad \text{(otherwise)} \tag{13}$$

The problem is that $\{\hat{a}_i\}$ do not satisfy (13). Within the same subspace it does hold, $\{\hat{a}_i, \hat{a}_i\} = \{\hat{a}_i^\dagger, \hat{a}_i^\dagger\} = 0$ but not when we are working over different subspaces. $i \neq j \iff \{\hat{a}_i, \hat{a}_j\} \neq 0$ since $\hat{a}_i \hat{a}_j = \hat{a}_j \hat{a}_i \neq 0$. Therefore, Jordan and Wigner used a unitary transformation to construct new operators that obey both (12) and (13).

In order to achieve that, we first need to define the operator:

$$\hat{n} \equiv \hat{a}^\dagger \hat{a} = \begin{pmatrix} 0 & 0 \\ 0 & 1 \end{pmatrix}. \tag{14}$$

It is evident that $|+\rangle$ and $|-\rangle$ are eigenvectors of $\hat{n}$, with eigenvalues 0 and 1 respectively. We also see that:

$$e^{i\pi\hat{n}} = I + i\pi\hat{n} - \frac{1}{2}(\pi\hat{n})^2 \dots$$
$$= I + \hat{n}(-1 + \cos\pi + i\sin\pi) \text{ (as } (\hat{n})^2 = \hat{n})$$
$$= \sigma^z \tag{15}$$

We can now define the sign function:

$$\hat{\nu}_i = \prod_{j=1}^{i-1} \sigma_j^z = e^{i\pi \sum_{j=1}^{i-1} \hat{n}_j} \qquad (16)$$

as $\{\hat{n}_j\}$ act on different particles and hence commute.

It is clear that the eigenvalues of $\hat{\nu}_i$ are ± 1. It also has the useful properties:

$$\hat{\nu}_i^\dagger = \hat{\nu}_i \qquad (17)$$

$$\hat{\nu}_i^\dagger \hat{\nu}_i = (\hat{\nu}_i)^2 = I \qquad (18)$$

$$[\hat{\nu}_i, \hat{a}_i] = [\hat{\nu}_i, \hat{a}_i^\dagger] = 0 \qquad (19)$$

The last property stems from the fact that $\hat{a}_i$ acts on the ith subspace while $\hat{\nu}_i$ acts on the preceding $i-1^{th}$ subspaces, making them independent.

We can then use $\hat{\nu}_i$ to do an unitary transform of $\hat{a}_i$ and $\hat{a}_i^\dagger$ to define $\hat{c}_i$ and $\hat{c}_i^\dagger$:

$$\hat{c}_i^\dagger \equiv \hat{\nu}_i \hat{a}_i^\dagger = e^{i\pi \sum_{j=1}^{i-1} \hat{n}_j} \hat{a}_i^\dagger = e^{i\pi \sum_{j=1}^{i-1} \hat{a}_j^\dagger \hat{a}_j} \hat{a}_i^\dagger \qquad (20)$$

$$\hat{c}_i \equiv \hat{a}_i \hat{\nu}_i = \hat{a}_i e^{i\pi \sum_{j=1}^{i-1} \hat{n}_j} = \hat{a}_i e^{i\pi \sum_{j=1}^{i-1} \hat{a}_j^\dagger \hat{a}_j} \qquad (21)$$

It immediately follows that $\hat{c}_i^\dagger \hat{c}_i = \hat{n}_i$ and therefore we can multiply (20) and (21) by $\hat{\nu}_i$ from left and right respectively to get:

$$\hat{a}_i^\dagger = \hat{\nu}_i \hat{c}_i^\dagger = e^{i\pi \sum_{j=1}^{i-1} \hat{n}_j} \hat{c}_i^\dagger = e^{i\pi \sum_{j=1}^{i-1} \hat{c}_j^\dagger \hat{c}_j} \hat{c}_i^\dagger \qquad (22)$$

$$\hat{a}_i = \hat{c}_i \hat{\nu}_i = \hat{a}_i = \hat{c}_i e^{i\pi \sum_{j=1}^{i-1} \hat{n}_j} = \hat{c}_i e^{i\pi \sum_{j=1}^{i-1} \hat{c}_j^\dagger \hat{c}_j} \qquad (23)$$

This is a significant as $\{\hat{a}_i\}$ were single particle operators which only acted on a single subspace, while $\{\hat{c}_i\}$ are multiparticle operators which act on the first i subspaces and therefore their algebra is not as simple as that of $\{\hat{a}_i\}$. We take advantage of this to calculate:

$$\{\hat{c}_i, \hat{c}_i^\dagger\} = \hat{a}_i \hat{\nu}_i \hat{\nu}_i \hat{a}_i^\dagger + \hat{\nu}_i \hat{a}_i^\dagger \hat{a}_i \hat{\nu}_i$$
$$= \hat{a}_i \hat{a}_i^\dagger + \hat{a}_i^\dagger \hat{a}_i \text{ (using (18), (19))} \qquad (24)$$
$$= I,$$

and similarly:

$$\{\hat{c}_i, \hat{c}_j\} = \{\hat{c}_i^\dagger, \hat{c}_j^\dagger\} = 0 \qquad (25)$$

$$\{\hat{c}_i, \hat{c}_j^\dagger\} = 0 \iff j \neq i \qquad (26)$$

making $\hat{c}_i$ a purely fermionic ladder operator ((12), (13)).

It is also straightforward to show that:

$$\hat{c}_i^\dagger \hat{c}_{i+1}^\dagger = \hat{\nu}_i \hat{a}_i^\dagger \hat{\nu}_{i+1} \hat{a}_{i+1}^\dagger$$
$$= \hat{\nu}_i \hat{a}_i^\dagger \hat{\nu}_i \sigma_i^z \hat{a}_{i+1}^\dagger \text{ (from (16))}$$
$$= (\hat{\nu}_i)^2 \hat{a}_i^\dagger \hat{a}_{i+1}^\dagger \text{ } (\hat{a}_i^\dagger \sigma_i^z = \hat{a}_i^\dagger\text{-from (7))} \qquad (27)$$
$$= \hat{a}_i^\dagger \hat{a}_{i+1}^\dagger \text{ (from (18))}$$

And similarly

$$\hat{c}_i^\dagger \hat{c}_{i+1} = \hat{a}_i^\dagger \hat{a}_{i+1} \qquad (28)$$

$$\hat{c}_{i+1}^\dagger \hat{c}_i = \hat{a}_{i+1}^\dagger \hat{a}_i = \hat{a}_i \hat{a}_{i+1}^\dagger \text{ } (\{\hat{a}_i\} \text{ commutes)} \qquad (29)$$

$$\hat{c}_i \hat{c}_{i+1} = -\hat{a}_i \hat{a}_{i+1} \text{ } (\hat{a}_i \sigma_i^z = -\hat{a}_i) \qquad (30)$$

The periodic boundary condition (2) causes the boundary behavior to be slightly different.

$$\hat{a}_N^\dagger \hat{a}_{N+1}^\dagger = \hat{a}_N^\dagger \hat{a}_1^\dagger \quad \text{(using(2))}$$
$$= \hat{\nu}_N \hat{c}_N^\dagger \hat{c}_1^\dagger \text{ (from (22), } \nu_1 = I)$$
$$= -\hat{\nu}_N \hat{c}_1^\dagger \hat{c}_N^\dagger \text{ (from (25))} \qquad (31)$$

Similarly:

$$\hat{a}_N \hat{a}_{N+1} = -\hat{\nu}_N \hat{c}_1 \hat{c}_N \qquad (32)$$

$$\hat{a}_N \hat{a}_{N+1}^\dagger = -\hat{\nu}_N \hat{c}_1 \hat{c}_N^\dagger \qquad (33)$$

$$\hat{a}_N^\dagger \hat{a}_{N+1} = -\hat{\nu}_N \hat{c}_1^\dagger \hat{c}_N \qquad (34)$$

IV.   PARTITION OF THE HAMILTONIAN

Armed with the Jordan Wigner Transformations, we are now ready to try to simplify the XY model Hamiltonian, in the fashion shown by Katsura [3]. From (8)-(10), (27)-(30) and (31)-(34), we get:

$$H = -\sum_{i=1}^{N}(j_x \sigma_i^x \sigma_{i+1}^x + j_y \sigma_i^y \sigma_{i+1}^y + h\sigma_i^z)$$

$$= -\sum_{i=1}^{N-1} \left[(j_x + j_y)(\hat{c}_i^\dagger \hat{c}_{i+1} + \hat{c}_{i+1}^\dagger \hat{c}_i) + (j_x - j_y)(\hat{c}_i^\dagger \hat{c}_{i+1}^\dagger \right.$$
$$\left. - \hat{c}_i \hat{c}_{i+1}) \right] + \hat{\nu}_N \left[(j_x + j_y)(\hat{c}_1^\dagger \hat{c}_N + \hat{c}_1 \hat{c}_N^\dagger) \right. \quad (35)$$
$$\left. + (j_x - j_y)(\hat{c}_1^\dagger \hat{c}_N^\dagger + \hat{c}_1 \hat{c}_N) \right] - h\sum_{i=1}^{N}(1 - 2\hat{c}_i^\dagger \hat{c}_i)$$

This looks rather complicated, especially on account of the $\hat{\nu}_N$ containing boundary terms.

Fortunately, we can manipulate these terms to eliminate $\hat{\nu}_N$, which is aided by the fact that $\hat{\nu}$ is simply a sign-function. We find that:

$$(\hat{\nu}_N)(1 \pm \hat{\nu}_N) = \pm(1 \pm \hat{\nu}_N) \text{ (using (18))} \qquad (36)$$

(36) can be used to define projection operators $\frac{1 \pm \hat{\nu}_N}{2}$, which have the following properties:

$$\frac{1 + \hat{\nu}_N}{2} + \frac{1 - \hat{\nu}_N}{2} = 1 \text{ (Complete)} \tag{37}$$

$$\left(\frac{1 + \hat{\nu}_N}{2}\right)\left(\frac{1 - \hat{\nu}_N}{2}\right) = 0 \text{ (Orthogonal)} \tag{38}$$

$$\left(\frac{1 \pm \hat{\nu}_N}{2}\right)^2 = \frac{1 \pm \hat{\nu}_N}{2} \text{ (Property of projection)} \tag{39}$$

We can then define H^+ by:

$$(1 + \hat{\nu}_N)H$$

$$= -(1 + \hat{\nu}_N) \sum_{i=1}^{N-1} \left[(j_x + j_y)\hat{c}_i^\dagger \hat{c}_{i+1} \dots\right] + (1 + \hat{\nu}_N)(\hat{\nu}_N)$$

$$\left[(j_x + j_y)\hat{c}_1^\dagger \hat{c}_N \dots\right] - (1 + \hat{\nu}_N)h \sum_{i=1}^{N}(1 - 2\hat{c}_i^\dagger \hat{c}_i)$$

$$= (1 + \hat{\nu}_N)\left[- \sum_{i=1}^{N-1}(j_x + j_y)\hat{c}_i^\dagger \hat{c}_{i+1} \dots + (j_x + j_y)\hat{c}_1^\dagger \hat{c}_N \dots \right.$$

$$\left. - h \sum_{i=1}^{N}(1 - 2\hat{c}_i^\dagger \hat{c}_i)\right] (\hat{\nu}_N(1 + \hat{\nu}_N) = (1 + \hat{\nu}_N) \text{from}(36))$$

$$= (1 + \hat{\nu}_N)H^+ \tag{40}$$

Similarly, we define H^- by:

$$(1 - \hat{\nu}_N)H = (1 - \hat{\nu}_N)H^-, \tag{41}$$

where $H^\pm$ are given by (from (36), (40), (41)):

$$H^\pm = - \sum_{i=1}^{N-1} \left[(j_x + j_y)(\hat{c}_i^\dagger \hat{c}_{i+1} + \hat{c}_{i+1}^\dagger \hat{c}_i) + (j_x - j_y)\right.$$

$$\left. (\hat{c}_i^\dagger \hat{c}_{i+1}^\dagger - \hat{c}_i \hat{c}_{i+1})\right] \pm \left[(j_x + j_y)(\hat{c}_1^\dagger \hat{c}_N + \hat{c}_1 \hat{c}_N^\dagger)\right.$$

$$\left. + (j_x - j_y)(\hat{c}_1^\dagger \hat{c}_N^\dagger + \hat{c}_1 \hat{c}_N)\right] - h \sum_{i=1}^{N}(1 - 2\hat{c}_i^\dagger \hat{c}_i) \tag{42}$$

Therefore, (40) and (41) allow us to split the Hamiltonian into two orthogonal subspaces:

$$H = \frac{1 + \hat{\nu}_N}{2}H + \frac{1 - \hat{\nu}_N}{2}H = \frac{1 + \hat{\nu}_N}{2}H^+ + \frac{1 - \hat{\nu}_N}{2}H^- \tag{43}$$

$\hat{\nu}_N$ has eigenvalues ± 1 and therefore only one of the partitions of the Hamiltonian matter for any given case.

H^+ and H^- are easier to solve than H as the $\hat{\nu}_N$ term has been eliminated. We simply need to choose solutions with $\hat{\nu}_N = 1$ out of the solutions of H^+ (there must be an even number of spins pointing down, (16)). Similarly, an odd number of spins need to point down for a solution from the space of H^- to be acceptable. We simply need to combine the acceptable solutions from both subspaces.

V. DIAGONALIZING THE PARTITIONS

H^+ and H^- are not yet diagonalized, and a Fourier transform, followed by a simple linear transform called the Boguliubov transform, is required to complete the task. We will only explicitly solve H^+, as H^- can be solved in a similar fashion.

For the Fourier transform, we first define A_k and $A_k^\dagger$ to be the following:

$$A_k = \frac{1}{\sqrt{N}} \sum_{l=1}^{N} c_l e^{-i\pi(\frac{kl}{N} - \frac{1}{4})} \iff A_k^\dagger = \frac{1}{\sqrt{N}} \sum_{l=1}^{N} c_l^\dagger e^{i\pi(\frac{kl}{N} - \frac{1}{4})} \tag{44}$$

Therefore,

$$A_{2k-1}^\dagger A_{2k-1} = \frac{1}{N} \sum_{l=1}^{N} \sum_{m=1}^{N} c_l^\dagger c_m e^{i\pi \frac{(2k-1)(l-m)}{N}} \tag{45}$$

and thus,

$$\sum_{k=1}^{N} \left(e^{-i\pi \frac{2k-1}{N}} A_{2k-1}^\dagger A_{2k-1}\right)$$

$$= \frac{1}{N} \sum_{l=1}^{N} \sum_{m=1}^{N} c_l^\dagger c_m \sum_{k=1}^{N} e^{i\pi \frac{(2k-1)(l-m-1)}{N}}$$

$$= \frac{1}{N} \sum_{l=1}^{N} \sum_{m=1}^{N} c_l^\dagger c_m \left(\frac{e^{2i\pi \frac{(l-m-1)}{N}}(1 - e^{2i\pi(l-m-1)})}{1 - e^{2i\pi \frac{(l-m-1)}{N}}}\right) \tag{46}$$

We obtain (46) by summing the geometric series over k. It is evident $l - m - 1$ is an integer, and therefore, $e^{2i\pi(l-m-1)} = 1$.

Only the terms where the denominator goes to zero (and hence prevents us from using the formula for summing geometric series) can have non-zero contributions. l and m are both constrained between 1 and N, and so $-N \le l - m - 1 \le N - 2$. However, $e^{2i\pi \frac{(l-m-1)}{N}} = 1 \iff \frac{l-m-1}{N} \in Z$. Therefore, $l = m + 1$ or $l = m + 1 - N$. Since l and m are individually constrained between 1 and N, $l = m + 1, m \in \{1, 2, \dots N - 1\}$ and $l = 1, m = N$ are the only cases where the geometric series does not sum to 0. Therefore,

$$\sum_{k=1}^{N} \left(e^{-i\pi \frac{2k-1}{N}} A_{2k-1}^\dagger A_{2k-1}\right)$$

$$= \frac{1}{N} \left(\sum_{l=1}^{N-1} c_l^\dagger c_{l-1} \sum_{k=1}^{N} e^0 + c_1^\dagger c_N \sum_{k=1}^{N} e^{i\pi}\right)$$

$$= \sum_{l=1}^{N-1} c_l^\dagger c_{l-1} - \hat{c}_N^\dagger \hat{c}_1 \tag{47}$$

Which is a term in the Hamiltonian H^+. Even more importantly, the opposite sign of the boundary term is

beautifully accounted for by the algebra. We finally see why it was important to impose periodic boundary conditions, as the Fourier transform would have failed otherwise.

Proceeding similarly with other terms, H^+ reduces to:

$$H^+ = -2 \sum_{k=1}^{N/2} \left[(-(j_x + j_y) \cos \frac{(2k-1)\pi}{N} + h)(A_{2k-1}^\dagger A_{2k-1} \right.$$

$$+ A_{-2k+1} A_{-2k+1}^\dagger) + (j_x - j_y) \sin \frac{(2k-1)\pi}{N}$$

$$\left. (A_{2k-1}^\dagger A_{-2k+1}^\dagger + A_{2k-1} A_{-2k+1}) - h \right] \qquad (48)$$

This may look exceedingly complicated, but in reality we are almost done. Already we can see creation-annihilation pairs over a single index. To eliminate the pesky cross terms, we define the Boguliubov Transformation to be [5] [3]:

Let $A_k = u_k \beta_k + v_k \beta_k^\dagger$, with u_k and v_k such that:

$$u_k^2 + v_k^2 = 1, \ \ u_k = u_{-k} \ \& \ v_k = -v_{-k} \qquad (49)$$

and the coefficients of $\beta_k^\dagger \beta_{-k}^\dagger + \beta_k \beta_{-k}$ in H^+ vanish. The final Hamiltonian then looks like:

$$H^+ = 2 \sum_{k=1}^{N/2} \left(\left[j_x^2 + j_y^2 + 2j_x j_y \cos \left(\frac{2(2k-1)\pi}{N} \right) \right. \right.$$

$$\left. - 2h(j_x + j_y) \cos \left(\frac{(2k-1)\pi}{N} \right) + h^2 \right]^{1/2}$$

$$\left. (\beta_k^\dagger \beta_k + \beta_{-k}^\dagger \beta_{-k} - 1) \right) \qquad (50)$$

and we are done. The Hamiltonian has been converted to a sum of fermionic creation and annihilation operators after much effort, and thus has been diagonalized. The Boguliubov transformation ensures that $\{\beta_k\}$ are anti-commutating Fermionic ladder operators, and thus eigenvalues of $\beta_k^\dagger \beta_k \in \{0, 1\}$. Therefore, $(\beta_k^\dagger \beta_k + \beta_{-k}^\dagger \beta_{-k} - 1)$ has eigenvalues $1 + 1 - 1 = 1, 0 + 0 - 1 = -1, 1 + 0 - 1 = 0 + 1 - 1 = 0$ (0 is doubly degenerate)[3].

The energy eigenvalues are:

$$\sum_{k=1}^{N/2-1} 2s_k \left[j_x^2 + j_y^2 + 2j_x j_y \cos \left(\frac{2(2k-1)\pi}{N} \right) - 2h(j_x + j_y) \right.$$

$$\left. \cos \left(\frac{(2k-1)\pi}{N} \right) + h^2 \right]^{1/2}, \{s_k\} \in \{-1, 0, 1\} \qquad (51)$$

Similarly solving H^-, we find the eigenvalues to be:

$$\sum_{k=1}^{N/2-1} 2s_k \left[j_x^2 + j_y^2 + 2j_x j_y \cos \left(\frac{4k\pi}{N} \right) - 2h(j_x + j_y) \right.$$

$$\left. \cos \left(\frac{2k\pi}{N} \right) + h^2 \right]^{1/2}, \{s_k\} \in \{-1, 0, 1\} \qquad (52)$$

$\{s_k\}$ indicates which of the Boguliubov eigenvalues are used for each k. $s_k = 0$ is doubly degenerate in both (51) and (52), while $s_k = \pm 1$ are singly degenerate.

VI. PARTITION FUNCTION

We have done a lot of calculations and now it is time to use Statistical mechanics to connect this quantum result with the macroscopic world. We first find the partition function Z, from which useful thermodynamic information can be extracted.

As we tend to the continuum limit (large N), the difference between the eigenvalues of H^+ and H^- fades. The selection rule of (43) demands that we only take some specific eigenvalues out of both subspaces, but since the values essentially become identical anyways, we can get away with picking half of the values from the combined space. Furthermore, we can simply ignore H^+ and pick only H^- eigenvalues, as values become effectively identical. This allows us to define $\omega_k = \frac{2k\pi}{N}$ (k spans all integers from 0 to $\frac{N}{2}$). Then, allowed energies of every k mode are approximately $2s_k [j_x^2 + j_y^2 + 2j_x j_y \cos(2\omega_k) - 2h(j_x + j_y) \cos(\omega_k) + h^2]^{1/2}$, ω_k ranges from 0 (k=0) to $\pi (k = \frac{N}{2})$.

We can now calculate the partition function Z to be:

$$Z = \sum e^{-\beta E} \qquad \left(\beta = \frac{1}{k_b T} \right) \qquad (53)$$

$$= \sum e^{-2\beta s_k [j_x^2 + j_y^2 + 2j_x j_y \cos(2\omega_k) - 2h(j_x + j_y) \cos(\omega_k) + h^2]^{1/2}}$$

$$= \prod_{\text{all } \omega_k} (\sum e^{-2s_k \beta [j_x^2 + j_y^2 + 2j_x j_y \cos(2\omega_k) \dots]}$$

$$= \prod_{\text{all } \omega_k} (4 \cosh^2 (\beta [j_x^2 + j_y^2 + 2j_x j_y \cos(2\omega_k)$$

$$- 2h(j_x + j_y) \cos(\omega_k) + h^2]^{1/2})), \qquad (54)$$

$$\ln Z = 2 \sum_{\text{all } \omega_k} \ln(2 \cosh(\beta [j_x^2 + j_y^2 + 2j_x j_y \cos(2\omega_k)$$

$$- 2h(j_x + j_y) \cos(\omega_k) + h^2]^{1/2})) \qquad (55)$$

as s_k=0 is doubly degenerate.

In the continuum limit, the sum can be replaced by an integral, leaving:

$$\ln Z = 2 \frac{N}{2\pi} \int_0^\pi d\omega \ln(2 \cosh(\beta [j_x^2 + j_y^2 + 2j_x j_y \cos(2\omega)$$

$$- 2h(j_x + j_y) \cos(\omega) + h^2]^{1/2})) \qquad (56)$$

The factor of $\frac{N}{2\pi}$ comes from the change of variables $\omega = \frac{2k\pi}{N}$, as we were summing over all k previously.

We can now switch over to Classical Thermodynamics to get:

$$E = -\frac{\partial \ln(Z)}{\partial \beta} = -\frac{N}{\pi} \int_0^\pi d\omega \ g(\omega) \tanh(\beta g(\omega)) \quad (57)$$

$$g(\omega) = [j_x^2 + j_y^2 + 2j_x j_y \cos 2\omega - 2h(j_x + j_y) \cos \omega + h^2]^{1/2}$$

The energy scales extensively ($\propto N$), as expected for macroscopic systems.

Let us now look at some previously solved cases to see if our solution is consistent with them. For the particular case of the Ising Model of spin interaction, $j_y = 0$ [3] and using (57) gives:

$$E = -\frac{N}{\pi} \int_0^\pi d\omega \ u(\omega) \tanh(\beta u(\omega)) \quad (58)$$

$$(u(\omega) = [j_x^2 - 2h j_x \cos \omega + h^2]^{1/2})$$

This integral is not analytically solvable, but one last assumption brings us to a quantity we can actually calculate, the case of the zero-field ($h = 0$):

$$E = -\frac{N}{\pi} \int_0^\pi d\omega j_x \tanh(\beta j_x) = -N j_x \tanh(\beta j_x) \quad (59)$$

Which is exactly the same as the result obtained by classical methods [6],[1]. The specific heat is:

$$C_h = N k_b (\beta j_x \operatorname{sech} \beta j_x)^2 \quad (60)$$

which again matches up with the classical result [6].

Furthermore, we can explore the case of non-interacting spins ($j_x = j_y = 0$) and find:

$$E = -\frac{N}{\pi} \int_0^\pi d\omega h \tanh(\beta h) = -N h \tanh(\beta h) \quad (61)$$

which again matches up with the classical result [6].

VII. THE FERRO-ANTIFERROMAGNETIC (FAF) MATERIAL

Now, slightly more confident about the accuracy of our model, we explore the special case where $j = j_x = -j_y > 0$, where there is ferromagnetic coupling in the x direction and antiferromagnetic coupling in the y (henceforth to be referred as FAF).With 0 external field:

$$E = -\frac{N}{\pi} \int_0^\pi d\omega \ 2j \sin \frac{\omega}{2} \tanh \left(2\beta j \sin \frac{\omega}{2}\right) \quad (62)$$

This is not analytic, but salient features of the system can be seen. Firstly, the energy unchanged if we flip the sign of j, as the system does not care if our definitions of x and y axes are exchanged. The integrand is positive in the domain over which we are integrating, making the energy negative. The negative energy immediately tells us that the ferromagnetic coupling wins

over the anti-ferromagnetic. This can be contrasted with the classical case, where it would be wrongly thought the antiferromagnetic coupling and ferromagnetic coupling exactly cancel each other. In fact, even at high temperatures ($\beta \to 0$), we get an energy of $-2\beta j^2$, which tells the asymptotic rate of decay of energy with rising Temperature (Figure 1).
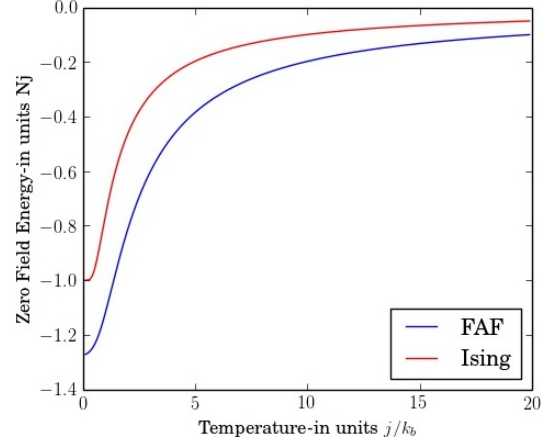

FIG. 1. Comparison between FAF coupling and Ising model with change in T (same j for both). Even at high temperatures, they have different asymptotic rate of decay.

Encouraged by this, we proceeded to numerically integrate (62) to compare how the FAF system compares with the Ising, with change in temperature. The results have been plotted in Figure 1. At low temperatures the FAF model has energy-per-particle $-\frac{4}{\pi} j_x$, which is less than the Ising value of $-j_x$. This is indeed rather surprising, that *destabilizing* y interaction actually stabilizes the system more than the case of no y interaction. This is a consequence of the quantum-mechanical behavior of the system, which could not be inferred from any classical model.

Numerical evaluations can also tell us what happens when the field is non-zero. Figure 2 depicts a graph comparing how the energy of the FAF material, and the classical Ising material vary with field strength. The main takeaway are the slopes, which suggests that the susceptibility is greater for the FAF than the Ising, another counterintuitive result. FAF material therefore has greater potential as magnets than what the word anti-ferromagnetic might suggest.

Finally, we numerically evaluated zero-field specific heat capacity at different temperatures, and a plot has been given in Figure 3. The sharply peaked shape is characteristic of systems like the XY model, which have a finite number of energy levels.
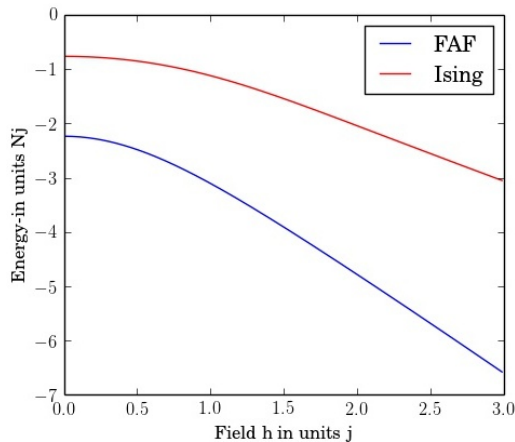
FIG. 2. Comparison between FAF coupling and Ising model with change in field h (same j). $\beta = j$ for this example.
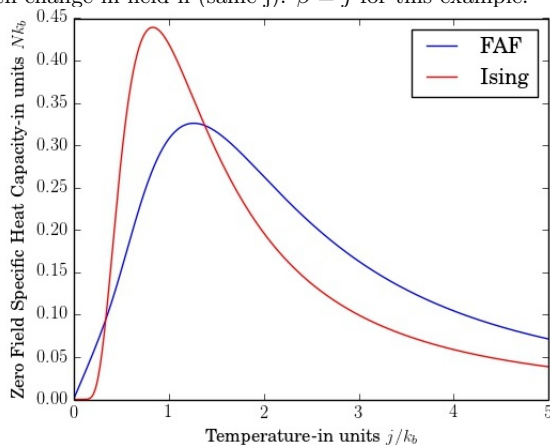

FIG. 3. Specific heat of FAF and Ising models (same j) at different Temperatures.

VIII. CONCLUSIONS

A solution to the general 1D XY model has been presented here, which is an immensely important theoretical result in its own right. Even though this model (like the 1D Ising model) does not account for phase transition on the account of there being only one path for spins to communicate, it conveys other important results. The mathematical framework developed here can be used to solve for the 2D system [2], where it does predict phase transitions and even the qualitative features of this solution help predict what we might find in 2D and 3D systems. Additionally, there has been considerable research attention given to development of linear chains of 'molecular' magnets [7]. The XY model can be used to predict behavior of such systems, making the 1D system useful in its own right. Even though very few of the integrals are analytic, numerical evaluation is far less computationally expensive than approximate methods like variational wavefunction fitting, showing the importance of the exact solution. This model is also robust enough to explain the effects of a time-varying external magnetic field [8]-which highlights its use in trying to predict the dynamics of magnetic systems.

Uses aside, an analytic solution to a system of interacting spins is valuable in its own right as a theoretical result. Though this is a highly simplified system, it represents the first step towards proper Quantum Statistical Mechanics, where we take interactions into account while trying to predict system behavior. It is hoped that the reader appreciates the mathematical complexity behind solving even such a simple system of interacting particles, but at the same time appreciates the elegance with which Lieb et.al. and Katsura had solved this problem in an era before personal computers.

[1] E. Ising, Zeitschrift fr Physik **31**, 253 (1925), ISSN 0044-3328, URL http://dx.doi.org/10.1007/BF02980577.

[2] E. Lieb, T. Schultz, and D. Mattis, Annals of Physics **16**, 407 (1961), ISSN 0003-4916, URL http://www.sciencedirect.com/science/article/pii/0003491661901154.

[3] S. Katsura, Phys. Rev. **127**, 1508 (1962), URL http://link.aps.org/doi/10.1103/PhysRev.127.1508.

[4] P. Jordan and E. Wigner, Zeitschrift fr Physik **47**, 631 (1928), ISSN 0044-3328, URL http://dx.doi.org/10.1007/BF01331938.

[5] N. Boguliubov, J. Phys. (USSR) **11**, 23 (1947).

[6] J. England, 8.08 Lecture notes (2014).

[7] A. Caneschi, D. Gatteschi, N. Lalioti, C. Sangregorio, R. Sessoli, G. Venturi, A. Vindigni, A. Rettori, M. G. Pini, and M. A. Novak, Angewandte Chemie International Edition **40**, 1760 (2001), ISSN 1521-3773, URL http://dx.doi.org/10.1002/1521-3773(20010504)40:9<1760::AID-ANIE17600>3.0.CO;2-U.

[8] J. Dziarmaga, Phys. Rev. Lett. **95**, 245701 (2005), URL http://link.aps.org/doi/10.1103/PhysRevLett.95.245701.

How Do Stars Shine?
A WKB Analysis of Stellar Nuclear Fusion

Anna Y. Ho
8.06 Spring 2014
(Dated: May 2, 2014)

A star generates energy through nuclear fusion. The particular fusion pathway depends on its age and mass, but most stars spend the majority of their lifetimes fusing hydrogen nuclei to form helium. This process cannot be understood without quantum mechanics, because in order to fuse, two nuclei need to become close enough ($\approx 1\,\mathrm{fm}$) for the strong force to take hold. Classically, two nuclei inside a stellar core do not have the energy to overcome the Coulomb potential barrier separating them, and thus cannot fuse. In this paper, we use the WKB approximation to estimate the tunneling rate for a sun-like star, calculate the temperature-dependence of the rate, and discuss the physical implications of this relationship. In particular, we use the temperature-dependence to show that lower-mass stars like our sun have convectively stable cores, whereas more massive stars ($M > 1.5 M_\odot$) have convectively unstable cores.

I. OVERVIEW

In Section II, we begin with an introduction to stellar structure and nuclear fusion, and show that our understanding of how stars shine was revolutionized by the advent of quantum mechanics. In Section III, we use a technique from quantum mechanics - the WKB approximation - to derive an estimate for the fusion reaction rate in stellar cores and its power-law dependence on temperature, and use this to explain why massive stars have convective cores and low-mass stars have radiative cores.

II. AN INTRODUCTION TO STELLAR STRUCTURE AND NUCLEAR FUSION

A. Before Quantum Mechanics

Since the universe became cool enough for protons and electrons to combine into atoms, hydrogen has been the most abundant element in the universe. Interstellar clouds of gas and dust are thus primarily comprised of hydrogen, and when these clouds collapse to form stars, the resulting stars are primarily comprised of hydrogen.

Before the advent of quantum mechanics in the 1920s, astronomers had measured the age and elemental composition of the sun but could only speculate about the nature of its internal energy source. Based on age measurements, they could infer that stars like our sun radiate energy ("shine") for billions of years while remaining stable, and understood that there must be an energy source intrinsic to the star. Suggestions included gravitational energy, atomic disintegration, and the mutual neutralization of positive and negative electric charges, but none of these hypotheses could properly account for all the observables; in particular, when the age of the Sun was accurately measured, the theory of gravitational energy was ruled out simply because it could not support such a long lifespan [1].

In 1920, Sir Arthur Eddington argued that subatomic processes must be the source of this energy, and pointed out that "the assemblage of four hydrogen nuclei and two electrons to form the helium atom" would provide the appropriate amount of energy to balance the energy radiated away by the star. However, he acknowledged, "we should say that the assemblage...was impossible if we did not know that it had occurred." [2].

Eddington's impossibility was a classical impossibility. In order to fuse, nuclei need to be close enough for the strong nuclear force to dominate the Coulomb barrier. The particle energies in a typical stellar core are on the order of a keV, which is 1000 times smaller than what would be needed to overcome the Coulomb potential barrier and enter the regime of the strong force [9]. Thus, without quantum mechanics, stellar nuclear fusion was impossible.

B. With Quantum Mechanics

Less than a decade after Eddington's 1920 paper, quantum mechanics had revolutionized astronomy and George Gamow demonstrated that nuclei could in fact tunnel through the Coulomb barrier and get close enough ($\approx 1\,\mathrm{fm}$) to fuse [7]. The process is still statistically unlikely, but the vast number of collisions within stars still results in a significant reaction rate. We now know that the core of a star is the site of these thermonuclear reactions, that most stars spent their lives fusing hydrogen nuclei to form helium, and that these nuclear reactions balance the star's energy radiation until the hydrogen supply is exhausted. High-mass stars ($M > 8 M_\odot$) undergo additional stages of fusion that form heavier elements such as iron, calcium, and magnesium: these elements are ultimately distributed to the rest of the universe when the star explodes in a supernova. However, lower-mass stars like our Sun stop at helium, radiate away their remaining energy, and become inert [4].

Thus, an understanding of quantum mechanics - in particular, quantum tunneling - is critical to understanding the life cycles of stars and where the heavy elements

in our universe come from.

III.   THE REACTION RATE OF STELLAR NUCLEAR FUSION

The tools of quantum mechanics allow us to calculate the probability that two nuclei will fuse when they collide: as a function of their relative velocity, this is called the reaction cross section σ. We perform this calculation using the WKB approximation, then take the average over the cross section velocity distribution to derive the reactivity $< \sigma v >$. From this, we calculate the reaction rate. We will see that the reaction rate R has a power-law dependence on temperature T. In other words, $R \propto T^\nu$. We will show that the index ν of this power-law relationship depends on the temperature inside the core of the star.

A.   Calculating the Reaction Cross Section

The cross section of a nuclear reaction σ is a measure of the probability that two nuclei will fuse when they collide, and is defined by the following equation:

$$\sigma(E) = P_t(E) \frac{S(E)}{E} \tag{1}$$

This is evaluated in the particles' center-of-mass frame. E is the energy of their relative motion in this frame. $P_t(E)$ is the probability of tunneling across the Coulomb barrier. $S(E)$ is the probability of fusion itself given the details of the nuclear reaction and has been precisely experimentally measured for a wide range of systems. It peaks sharply in a narrow energy range, so it is reasonable to take its value as a given for a particular energy. Finally, the extra E^{-1} dependence is due to the finite "size" of each particle involved in the collision. For intuition: the cross section of a particle should be proportional to its "area" which (approximating the particle as a sphere) is proportional to λ^2. In stellar core temperatures, we are dealing with a non-relativistic limit. In this limit, the de Broglie wavelength is $\frac{h}{\sqrt{2mE}}$, and thus $\lambda^2 \propto E^{-1}$ [8–10].

Next, we calculate $P_t(E)$. The Coulomb barrier is represented by the following potential:

$$V_c(r) = \frac{Z_1 Z_2 e^2}{r} \tag{2}$$

where Z_1 and Z_2 are the atomic numbers of each colliding particle respectively, e is the electric charge, and r is the distance between the particles.

Clearly, the barrier is lower for smaller Z: this is another reason why stars spend the majority of their lifetimes burning hydrogen rather than heavier elements.

In the center-of-mass frame, μ is the reduced mass

$$\mu = \frac{m_1 m_2}{m_1 + m_2} \tag{3}$$

and v_∞ is the relative velocity of the two particles in the limit in which they are too far apart to affect each other. Thus the pre-fused state has an energy E defined as follows:

$$E = \frac{1}{2} m v_\infty^2 \tag{4}$$

With these definitions, we can write the Schrodinger equation that governs this system:

$$\frac{\hbar^2}{2\mu} \bigtriangledown^2 \psi + [E - V_c(r)]\psi = 0 \tag{5}$$

Note that here r is the radial coordinate, defined from the center of a spherical potential, and thus takes on values from 0 to ∞.

With the approximation that there is no relative angular momentum between the two atoms, Equation (5) simplifies to

$$\frac{\hbar^2}{2\mu} \frac{1}{r^2} \frac{\partial}{\partial r}(r^2 \frac{\partial \psi}{\partial r}) + [E - V_c(r)]\psi = 0 \tag{6}$$

To simplify this equation further, we define $\chi = r\psi$:

$$\frac{\hbar^2}{2\mu} \frac{\partial^2 \chi}{\partial r^2} + [E - V_c(r)]\chi = 0 \tag{7}$$

The setup can be visualized through Figure 1.

For a nucleus arriving from the right with energy E, we would like to calculate the probability that it will tunnel from A ($r = r_e$) to B ($r = r_0$) through the classically forbidden region. Equation (7) is non-linear so we will estimate the tunneling rate using the WKB approximation. For a more thorough discussion of this approximation, see [11]. Briefly, the WKB approximation is valid in the limit that the potential is slowly-varying (in this case, that the barrier is tall and wide). In this limit, the wavefunction assumes the general form $\chi(r) = e^{\frac{i\kappa(r)}{\hbar}}$. The approximation consists of plugging this general form into Equation (7) then expanding in a power series in $\hbar$ and taking the leading and first-order terms. Intuitively, in the limit that $\hbar \to 0$, the de Broglie wavelength also tends to zero and thus any potential is relatively slowly-varying.

The WKB approximation states that the transmission coefficient P_t is described by the following equation:
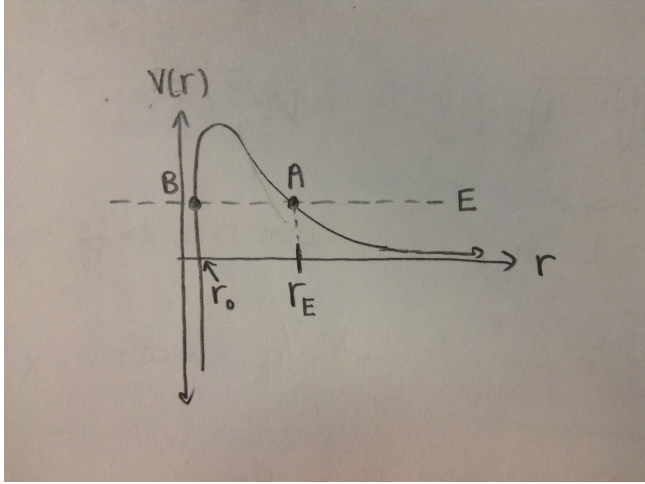
$$P_t \approx e^\phi \tag{8}$$

where

FIG. 1: Setup of the problem. A nucleus enters from the right with energy E, and would classically rebound from the barrier at A. Quantum mechanically, there is some probability that the nucleus will tunnel from $r = r_e$ to $r = r_0$ and "exit" the barrier at point B.

$$\phi = -\frac{2}{\hbar} \int_{r_0}^{r_e} \kappa(r')dr' \qquad (9)$$

and $\kappa(r)$ is defined as follows:

$$\kappa(r) = \sqrt{2m(V(r) - E)} \qquad (10)$$

E can be written in terms of r_e and $V(r)$ can be written in terms of a general r. Thus, ϕ can be rewritten:

$$\phi = -\frac{2}{\hbar}\sqrt{\frac{2\mu Z_1 Z_2 e^2}{r_E}} \int_{r_0}^{r_e} dr \sqrt{\frac{r_e}{r} - 1} \qquad (11)$$

We make the substitution $x = \frac{r}{r_e}$:

$$\phi = -\frac{2}{\hbar}r_e\sqrt{2\mu E} \int_{r_0/r_e}^{1} dx \sqrt{\frac{1}{x} - 1} \qquad (12)$$

The result is approximately:

$$\phi = -\frac{2}{\hbar}\frac{\pi}{2}\frac{Z_1 Z_2 e^2}{E}\sqrt{2\mu E} \qquad (13)$$

Thus, we have calculated an approximate transmission probability: the probability that two nuclei will get close together to fuse.

$$P_t \approx e^{-\pi \frac{Z_1 Z_2 e^2}{\hbar}\sqrt{\frac{2\mu}{E}}} \qquad (14)$$

Pluging this value into the nuclear cross-section:

$$\sigma(E) = \frac{S(E)}{E}e^{-\pi \frac{Z_1 Z_2 e^2}{\hbar}\sqrt{\frac{2\mu}{E}}} \qquad (15)$$

B. Calculating the Thermonuclear Reaction Rate using the Reaction Cross-Section

For reactant number densities n_1 and n_2, cross-section σ, and relative velocity v, the thermonuclear reaction rate is defined as follows:

$$R = n_1 n_2 < \sigma v > \qquad (16)$$

$< \sigma v >$ is called the reactivity. It is the average over the velocity distribution that characterizes the cross section.

In stellar cores, the relative velocities of nuclei obey a Maxwellian thermal distribution. Mathematically, the distribution is:

$$< \sigma v >= (\frac{8}{\pi\mu})^{1/2}\frac{1}{(kT)^{3/2}}\int_0^\infty Ee^{-E/kT}\sigma(E)dE \quad (17)$$

In the previous section, we calculated $\sigma(E)$ and found it to be

$$\sigma(E) = \frac{S(E)}{E}e^{-\sqrt{\frac{\tilde{E}}{E}}} \qquad (18)$$

where

$$\tilde{E} \equiv 2\mu(\pi\frac{Z_1 Z_2 e^2}{\hbar})^2 \qquad (19)$$

We plug that into Equation 17 to get

$$< \sigma v >= (\frac{8}{\pi\mu})^{1/2}\frac{1}{(kT)^{3/2}}\int_0^\infty S(E)e^{-\sqrt{\frac{\tilde{E}}{E}}-\frac{E}{kT}} dE \quad (20)$$

The integral is dominated by the exponential. So, it is convenient to define $f(E)$ as

$$f(E) = \sqrt{\frac{\tilde{E}}{E}} + \frac{E}{kT} \qquad (21)$$

and seek to find the value E_0 of E that will maximize $f(E)$. Solving for $f'(E_0) = 0$ and expanding $f(E)$ around the minimum $E = E_0$ we get

$$< \sigma v >\approx (\frac{8}{\pi\mu(kT)^3})^{1/2}(\frac{2\pi}{f''(E_0)})^{1/2}e^{-f(E_0)}S(E_0) \quad (22)$$

At this point, we essentially have the reaction rate. The final rate value R is simply Equation (22) multiplied by the product of the number densities of the participating nuclei.

C.   Temperature Dependence

We now use Equation (22) to determine the power-law index ν of the rate's dependence on temperature T. Assume the following form, where the rate of reaction R is proportional to $<\sigma v>$:

$$R \propto <\sigma v> \propto T^{\nu} \tag{23}$$

Solving for the power-law index:

$$\nu = \frac{dln(<\sigma v>)}{dln(T)} \tag{24}$$

To calculate the power law temperature dependence, we use Equation (22) to calculate $\frac{dlnR}{dlnT}$. This gives

$$ln <\sigma v> = -\frac{2}{3}lnT + (\frac{C}{4kT})^{1/3} \tag{25}$$

where C is a measurable constant. Solving for the power-law index,

$$\nu = -\frac{2}{3} + \frac{\tilde{C}}{4kT}^{1/3} \tag{26}$$

where $\tilde{C}$ is another measurable constant.

There are two different pathways predominantly responsible for the fusion of hydrogen into helium in stellar cores. For low-mass stars such as our Sun ($M < M_{\odot}$) the primary pathway is called the proton-proton (pp) chain. For higher-mass stars ($M > M_{\odot}$) the primary pathway is called the carbon-nitrogen-oxygen (CNO) cycle.

For the pp chain, the bottleneck reaction is the following:

$$p + p \rightarrow d + e^{+} + \nu_e \tag{27}$$
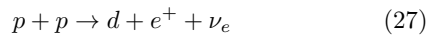
For this reaction, the constant $\tilde{C}$ has been experimentally measured to be roughly 493 keV. Typical stellar cores in stars of this mass range have temperature $T = 1.6 \times 10^7$ K. Thus the power law dependence is $\nu = 3.8$ [9].

For the CNO cycle, the bottleneck reaction is

$$^{14}N + p \rightarrow ^{15}O + \gamma \tag{28}$$

A similar calculation gives $\nu = 16.7$ [9].

Clearly, the temperature dependence of the CNO cycle is significantly steeper than that of the pp-chain. For more advanced stages of burning, the dependence becomes even steeper: for helium burning, it is roughly $\nu = 40$ [9].

We can use these temperature dependences to understand stellar structure and radiation mechanisms. Stars like our sun have radiative cores, which means that they dissipate energy primarily through radiation rather than convection. Massive stars, though - those which fuse helium through the CNO cycle - generate energy in a very small central region where the temperature peaks. Energy generation falls off much more steeply with radius than it does in lower-mass stars. To maintain equilibrium, the star must channel energy away from its core very efficiently. Simple photon diffusion - radiation - is insufficient. These stars rely on convection to carry away hot plasma [9, 10].

IV.   CONCLUSION

Stellar structure and stellar energy balance cannot be understood without quantum mechanics. In fact, without quantum mechanics, stars could not generate enough energy to replenish the supply that is radiated away. With the simple model of two nucleons tunneling through a barrier to fuse, we can draw conclusions about how stars of different mass ranges maintain thermal equilibrium.

[1] H.N. Russell, "On the Sources of Stellar Energy," Pub. Ast. Soc. Pacific, August (1919).

[2] A.S. Eddington, "The Internal Constitution of the Stars," Observatory 43, 353 (1920).

[3] H. A. Bethe, "Energy production in Stars," Phys. Rev. 55, 436 (1939).

[4] F. W. Aston, "The Mass-Spectra of Chemical Elements," Philosophical Magazine and Journal of Science, 39, 611-625 (1920).

[5] Ryan, Sean, and Andrew J. Norton. Stellar evolution and nucleosynthesis. Cambridge: Cambridge University Press, 2010.

[6] Karnakov, Boris Mikhailovich, and Vladimir Pavlovich Krainov. "WKB approximation in atomic physics." New

York: Springer, 2013.

[7] Gamow, G. and E. Teller. "The Rate of Selective Thermonuclear Reactions." Phys. Rev. 53, 608 (1938).

[8] E. C. Adelberger et al. "Solar fusion cross sections." Rev. Mod. Phys. 70 (1998).

[9] S. Mao. "Nuclear Fusions." From his lecture notes from the course Physics of Stellar Structure.

[10] J. Knapp. "The physics of fusion in stars." From her lecture notes from the course Stars and Star Formation, as taught at Princeton in Spring 2011.

[11] D.J. Griffiths, *Introduction to Quantum Mechanics, 2nd Ed.* (Pearson Prantice Hall, Upper Saddle River, MA, 2005).

The Supersymmetric Method in Quantum Mechanics

Matt Hodel

Department of Physics, 77 Massachusetts Ave., Cambridge, MA 02139-4307
(Dated: May 2, 2014)

We present the basic formalism of the supersymmetric method in non-relativistic quantum mechanics and apply it to a particular problem of interest. Specifically, the method allows us to use our knowledge of the infinite square well to immediately solve the obstensibly more complicated potential $V(x) \sim \sec^2(x)$. We go on to sketch the relation between the supersymmetric method and the concept of supersymmetry in particle physics.

I. INTRODUCTION

One of the most elegant algebraic solutions to a quantum problem is that of the harmonic oscillator. Indeed, the harmonic oscillator is one of the few systems we know how to solve exactly in the context of non-relativistic quantum mechanics. A common strategy to approach more complicated potentials is to expand them around local minima and treat them as if they were harmonic oscillators. Moreover, the elegance of the algebraic method in the solution, due to Dirac, is of great aesthetic and practical value. We use a similar method to algebraiclly obtain the energy spectrum and eigenstates of the angular momentum Hamiltonian, and the same technique can be used to solve Hydrogen.

The supersymmetric method in quantum mechanics effectively amounts to using the same strategy employed in the algebraic solution to the harmonic oscillator—namely, factoring Hamiltonians into a product of objects that function as creation and annihilation operators—to solve more complicated potentials than the harmonic oscillator.

We will first review the aforementioned algebraic solution to the harmonic oscillator and then introduce the basic structure of the supersymmetric method, drawing analogies to the harmonic oscillator where applicable. We will enumerate the key properties of the method and then work through an illustrative example involving the infinite square well. Finally, we will briefly examine the relation of the supersymmetric method in quantum mechanics to the topic of supersymmetry as it appears in quantum field theory.

II. THE HARMONIC OSCILLATOR

Let us quickly review the results of the harmonic oscillator calculation, since they will be of fundamental importance in understanding the more general factorization method. For a more detailed derivation of the results in this section, refer to Ref. 1. For further reading, refer to Ref. 6, section 2.1 (p.21).

Our Hamiltonian takes the form

$$\mathcal{H} = \frac{P^2}{2m} + \frac{1}{2}m\omega^2 X^2. \tag{1}$$

We can define unitless variables $H, p,$ and x to simplify this equation like so:

$$\mathcal{H} = \hbar\omega H \tag{2}$$
$$P = (2m\hbar\omega)^{1/2}p \tag{3}$$
$$X = \left(\frac{2\hbar}{m\omega}\right)^{1/2} x. \tag{4}$$

Now our "reduced" Hamiltonian is

$$H = p^2 + x^2. \tag{5}$$

We now define the creation and annihilation operates $a^\dagger$ and a, respectively

$$a^\dagger = x - ip \tag{6}$$
$$a = x + ip \tag{7}$$

which satisfy the commutation relation

$$[a, a^\dagger] = 1. \tag{8}$$

We can now rewrite the Hamiltonian as

$$H = a^\dagger a + \frac{1}{2} \tag{9}$$

We define the ground state to be the unique state $|0\rangle$ annihilated by a: $a|0\rangle = 0$. The excited states $|n\rangle$ of the osciallator can be constructed with the creation operator as

$$|n\rangle = \sqrt{\frac{1}{n!}}(a^\dagger)^n|0\rangle \tag{10}$$

with associated energies

$$E_n = n + \frac{1}{2} \tag{11}$$

(note that here E_n is the eigenvalue of H, the "reduced" Hamiltonian, and that the actual energies have an extra factor of $\hbar\omega$. Alternatively, we can think of this as a unit system where $\hbar = \omega = 1$).

Note the utility of the creation and annihilation operators in moving up and down the ladder of states, respectively. The analogues of creation and annihilation operators in the supersymmetric method will play the same

role. Note, too, how the null space of the annihilation operator *defines* the ground state.

In the supersymmetric method, we consider Hamiltonians (Ref. [2]) of the form

$$H = A^\dagger A \tag{12}$$

for some "creation" and "annihilation" operators

$$A^\dagger = -\frac{\mathrm{d}}{\mathrm{d}x} + W(x) \tag{13}$$

$$A = \frac{\mathrm{d}}{\mathrm{d}x} + W(x) \tag{14}$$

where $W(x)$ is assumed to be real and is called the *superpotential*.

Problems of this form are particularly easy to solve given our knowledge of the harmonic oscillator. We can find the ground state of H by simply asserting that it is annihilated by A, and subsequently build up the excited states by repeatedly acting on the ground state with $A^\dagger$. As we will see later, knowledge of such a system will immediately give us the solution to a related system with Hamiltonian $H = AA^\dagger$.

III. GENERAL FORMALISM

Both this section and the next follow the discussion in Ref. 3. The Hamiltonians described in Eqn. 12 are defined in terms of a single variable x, and therefore implicitly assume that our system is one-dimensional. We note, however, that the formalism applies equally well to one-dimensional or three-dimensional problems–in three dimensions the variable x would represent the radial coordinate and would range from 0 to ∞.

We can now explicity construct the two partner Hamiltonians mentioned in the introduction:

$$H^{(1)} = A^\dagger A = -\frac{\mathrm{d}^2}{\mathrm{d}x^2} + W^2(x) - W'(x) \tag{15}$$

$$H^{(2)} = AA^\dagger = -\frac{\mathrm{d}^2}{\mathrm{d}x^2} + W^2(x) + W'(x). \tag{16}$$

Though we will not carry out the explicit calculation, you can convince yourself these equations are correct by acting on an arbitrary function f with each $A^\dagger A$ or $AA^\dagger$. From these expressions we arrive at the potentials

$$V^{(1)} = W^2(x) - W'(x) \tag{17}$$

$$V^{(2)} = W^2(x) + W'(x). \tag{18}$$

A. Key Properties

We now turn our attention to several important properties of the Hamiltonians described above.

1. **All the energies $E_n^{(1)}$ and $E_n^{(2)}$ are non-negative**.

   proof:

   $$\begin{aligned}
   H^{(1)}|\phi_n^{(1)}\rangle &= E_n^{(1)}|\phi_n^{(1)}\rangle \\
   E_n^{(1)} &= \langle\phi_n^{(1)}|H^{(1)}|\phi_n^{(1)}\rangle \\
   &= \langle\phi_n^{(1)}|A^\dagger A|\phi_n^{(1)}\rangle \\
   &= \langle A\phi_n^{(1)}|A\phi_n^{(1)}\rangle \geq 0
   \end{aligned} \tag{19}$$

   where the final inequality follows because the norm of a vector is non-negative. Here $|\phi_n^{(1)}\rangle$ is the n-th energy eigenstate of $H^{(1)}$. The proof for $H^{(2)}$ is identical.

2. **The zero energy eigenstate of $H^{(1)}$ is annihilated by A, and the zero energy eigenstate of $H^{(2)}$ is annihilated by $A^\dagger$**

   Note that neither of the Hamiltonians are guaranteed to have a zero-energy eigenstate by Eqn. (19). However, since we know their spectra are strictly non-negative, *if a zero-energy eigenstate exists*, it is guaranteed to be the ground state.

   This follows from the inequality (19) and the corresponding inequality for $H^{(2)}$. In symbols,

   $$A|\phi_0^{(1)}\rangle = 0 \tag{20}$$

   $$A^\dagger|\phi_0^{(2)}\rangle = 0 \tag{21}$$

3. **The non-zero energy spectrum of $H^{(1)}$ and $H^{(2)}$ are identical.**

   proof: Let $|\phi_n^{(1)}\rangle$ be an eigenstate of $H^{(1)}$ with $E_n^{(1)} \neq 0$.

   $$\begin{aligned}
   H^{(1)}|\phi_n^{(1)}\rangle &= E_n^{(1)}|\phi_n^{(1)}\rangle \\
   A^\dagger A|\phi_n^{(1)}\rangle &= E_n^{(1)}|\phi_n^{(1)}\rangle
   \end{aligned} \tag{22}$$

   Act from the left with A:

   $$\begin{aligned}
   (AA^\dagger)(A|\phi_n^{(1)}\rangle) &= E_n^{(1)}(A|\phi_n^{(1)}\rangle) \\
   = H^{(2)}|\phi_n^{(2)}\rangle &= E_n^{(1)}|\phi_n^{(2)}\rangle
   \end{aligned} \tag{23}$$

   where

   $$|\phi_n^{(2)}\rangle = A|\phi_n^{(1)}\rangle. \tag{24}$$

   Thus every non-zero energy eigenstate of $H^{(1)}$ corresponds to an eigenstate of $H^{(2)}$ with the same energy upon action by A.

   Similarly, if $|\phi_n^{(2)}\rangle$ is an eigenstate of $H^{(2)}$ with $E_n^{(2)} \neq 0$,

   $$\begin{aligned}
   H^{(2)}|\phi_n^{(2)}\rangle &= E_n^{(2)}|\phi_n^{(2)}\rangle \\
   AA^\dagger|\phi_n^{(2)}\rangle &= E_n^{(2)}|\phi_n^{(2)}\rangle
   \end{aligned} \tag{25}$$

Act from the left with $A^\dagger$:

$$
\begin{aligned}
(A^\dagger A)(A^\dagger|\phi_n^{(2)}\rangle) &= E_n^{(2)}(A^\dagger|\phi_n^{(2)}\rangle) \\
&= H^{(1)}|\phi_n^{(1)}\rangle = E_n^{(2)}|\phi_n^{(1)}\rangle
\end{aligned} \tag{26}
$$

where

$$
|\phi_n^{(1)}\rangle = A^\dagger|\phi_n^{(2)}\rangle. \tag{27}
$$

So we get the analogous result that every non-zero energy eigenstate of $H^{(2)}$ corresponds to an eigenstate of $H^{(1)}$ with the same energy upon action by $A^\dagger$.

The only uncertainty we have about the spectra of the partner Hamiltonians at this point is whether they have zero-engergy eigenstates. They cannot both have zero-energy eigenstates because such a state would be annihilated by both A and $A^\dagger$, which, as a quick calculation will confirm, means the state must be zero everywhere.

Thus the possibilities can be enumerated as follows:

1. Neither Hamiltonian has a zero-energy eigenstate. In this case we say the partner Hamiltonians exhibit supersymmetry.

2. Either $H^{(1)}$ or $H^{(2)}$ has an zero-energy eigenstate, but not both. In the case we say supersymmetry has been broken.

IV.   A SIMPLE EXAMPLE: $W(x) = \tan(x)$

We will use the formalism derived above to examine the case when $W(x) = \tan(x)$, restricted to the interval $x = [-\pi/2, \pi/2]$. Though it is not obvious from the start, the appeal of this case derives from the fact that one of the partner Hamiltonians will end up being the infinite square well, which we already know how to solve.

We begin by using Eqn.s (15) and (16) to calculate the Hamiltonians.

$$
W'(x) = \sec^2(x) \tag{28}
$$

$$
\begin{aligned}
H^{(1)} &= -\frac{d^2}{dx^2} + W^2(x) - W'(x) \\
H^{(1)} &= -\frac{d^2}{dx^2} + \tan^2(x) - \sec^2(x) \\
H^{(1)} &= -\frac{d^2}{dx^2} - 1.
\end{aligned} \tag{29}
$$

Where we used the identity $\sec^2(x) - \tan^2(x) = 1$. The resulting potential is simply

$$
V^{(1)} = -1, x \in [-\pi/2, \pi/2] \tag{30}
$$

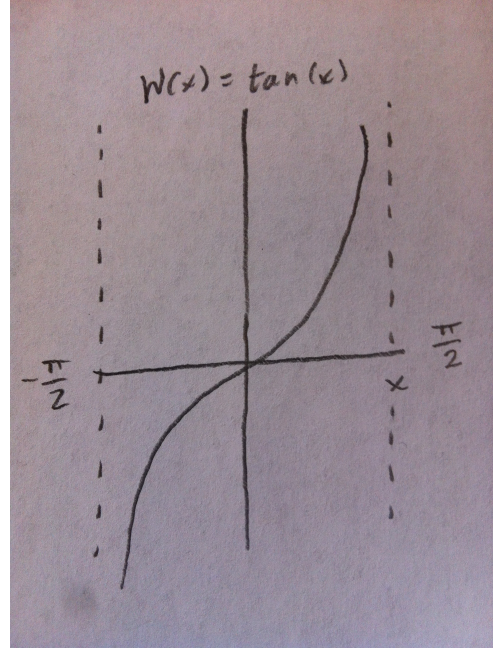with infinite walls at $x = \pm\pi/2$. This is the infinite square well!

FIG. 1: The superpotential $W(x) = \tan(x)$.

Now let's find $H^{(2)}$:

$$
\begin{aligned}
H^{(2)} &= -\frac{d^2}{dx^2} + \tan^2(x) + \sec^2(x) \\
H^{(2)} &= -\frac{d^2}{dx^2} + 2\sec^2(x) - 1,
\end{aligned} \tag{31}
$$

so we conclude
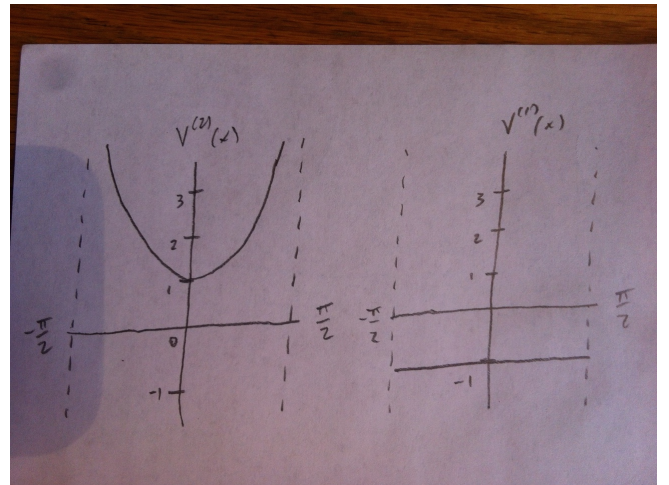
$$
V^{(2)} = -\frac{2}{\cos^2(x)} - 1 \tag{32}
$$

FIG. 2: The partner potentials $V^{(1)}$ and $V^{(2)}$.

We see from inspection that $H^{(2)}$ has no zero-energy eigenstate, since the potential $V^{(2)}$ is everywhere greater than zero.

We now solve explicity for the ground state of $H^{(1)}$ starting from Eqn. (20):

$$A \left| \phi_0^{(1)} \right\rangle = 0$$

$$\frac{\mathrm{d}}{\mathrm{d}x} \phi_0^{(1)} + \tan(x)\phi_0^{(1)} = 0 \tag{33}$$

This differential equation is easily solved via separation of variables.

$$\begin{aligned}
\phi_0^{(1)} &= N \exp\left(-\int_0^x dx', \tan(x')\right) \\
&= Ne^{\ln \cos x} = N \cos x \tag{34}
\end{aligned}$$

For normalization over the interval we need the constant N to be $\sqrt{2/\pi}$.

$$\phi_0^{(1)} = \sqrt{\frac{2}{\pi}} \cos(x) \tag{35}$$

We can now check that the energy is indeed zero.

$$\begin{aligned}
H^{(1)} \phi_0^{(1)} &= (-\frac{\mathrm{d}^2}{\mathrm{d}x^2} - 1)\phi_0^{(1)} \\
&= \sqrt{\frac{2}{\pi}} \cos x - \sqrt{\frac{2}{\pi}} \cos x = 0. \tag{36}
\end{aligned}$$

From our knowledge of the solution to the infinite square well, we can write down the solution for the first excited state:

$$\phi_1^{(1)} = \sqrt{\frac{2}{\pi}} \sin(2x) \tag{37}$$

which vanishes at $\pm\pi/2$. We can now calculate the energy of the state. This time, taking the second derivative of the wavefunction will bring out two factors of 2 from the argument of $\sin(2x)$ from the chain rule, and we see the energy is

$$E_1^{(1)} = 2^2 - 1 = 3. \tag{38}$$

The general solution to the infinite well on the interval $-\pi/2$ to $\pi/2$ is

$$\phi_n^{(1)} = \begin{cases} \sqrt{\frac{2}{\pi}} \cos((n+1)x), & n = 0, 2, 4, \dots \\ \sqrt{\frac{2}{\pi}} \sin((n+1)x), & n = 1, 3, 5, \dots \end{cases} \tag{39}$$

with associated energies

$$E_n^{(1)} = (n+1)^2 - 1, n = 0, 1, 2, \dots \tag{40}$$

Having solved the problem for $H^{(1)}$, we can *immediately* write down the solutions for $H^{(2)}$ by simply acting on them with the A operator, as per Eqn. (24)! Indeed, we find

$$\begin{aligned}
\phi_n^{(2)} &= A\phi_n^{(1)} = (\frac{\mathrm{d}}{\mathrm{d}x} + \tan(x))\phi_n^{(1)} \\
&= (\frac{\mathrm{d}}{\mathrm{d}x} + \tan(x)) \begin{cases} \sqrt{\frac{2}{\pi}} \cos((n+1)x), & n = 2, 4, \dots \\ \sqrt{\frac{2}{\pi}} \sin((n+1)x), & n = 1, 3, 5, \dots \end{cases}
\end{aligned}$$

where we have left out $n = 0$ since we know that $H^{(2)}$ has no zero-energy eigenstate.

Recall, as well, that, with the exception of the ground state energy, the energy spectrum for $H^{(2)}$ is identical to that of $H^{(1)}$. Explicitly, the eigenstates $\left| \phi_n^{(2)} \right\rangle$ of $H^{(2)} = 2\sec^2(x) - 1$ enumerated above have associated energies identical to the inifite square well:

$$E_n^{(2)} = (n+1)^2 - 1, n = 1, 2, \dots \tag{41}$$

Though we will not delve into the details, it is worth noting that a very closely related problem is important in scattering theory because it allows scattering states with zero reflection amplitude. Specifically, if we instead had chosen $W = \tanh(x)$, we would have gotten a partner Hamiltonian with a potential $V(x) \sim \mathrm{sech}^2(x)$. It is quite a happy surprise that we can solve for its bound states with minimal effort using our knowledge of the infinite square well and the supersymmetric methods presented above.

V. RELATION TO SUPERSYMMETRY

The concept of supersymmetry in particle physics says that every fundamental particle has a supersymmetric partner with identical properties except that its spin differs by 1/2. In this way it matches up fermions (particles with half integer spin) with bosons (particles with integer spin). At first sight this idea does not appear to be at all related to the above discussion about superpotentials. The key is to turn our attention to a larger space, in which the partner Hamiltonians $H^{(1)}$ and $H^{(2)}$ apply to subsystems. [6] Specifically, we combine the two Hamiltonians into a "super-Hamiltonian" H as follows:

$$H = \begin{pmatrix} H^{(1)} & 0 \\ 0 & H^{(2)} \end{pmatrix} \tag{42}$$

States of the system take the form

$$\Psi(x) = \begin{pmatrix} \phi(x) \\ \psi(x) \end{pmatrix} \tag{43}$$

Eigenstates of $H^{(1)}$ take the form $\begin{pmatrix} \phi(x) \\ 0 \end{pmatrix}$ and are referred to as "boson" states. Similarly, eigenstates of $H^{(2)}$ take the form $\begin{pmatrix} 0 \\ \psi(x) \end{pmatrix}$ and are referred to as "fermion" states.

We must define a "parity" operator $(-1)^F$, which we will take to simply be the Pauli matrix σ_3:

$$(-1)^F = \begin{pmatrix} 1 & 0 \\ 0 & -1 \end{pmatrix}. \qquad (44)$$

Under this definition, bosons and fermions are eigenstates of the parity operator with eigenvalues 1 and -1, respectively. The label F distinguishes between bosons and fermions. If it is even, the particle is a boson (has eigenvalue 1), and if it is odd, the particle is a fermion (has eigenvalue -1).

$$(-1)^F |b\rangle = |b\rangle \qquad (45)$$
$$(-1)^F |f\rangle = -|f\rangle \qquad (46)$$

We then define an antihermitian supersymmetry operator Q (sometimes referred to as the "super-charge"):

$$Q = \begin{pmatrix} 0 & A^\dagger \\ -A & 0 \end{pmatrix} \qquad (47)$$

which will send bosons to fermions and fermions to bosons. We see this explicitly as follows:

$$Q \begin{pmatrix} \phi \\ 0 \end{pmatrix} = \begin{pmatrix} 0 & A^\dagger \\ -A & 0 \end{pmatrix} \begin{pmatrix} \phi \\ 0 \end{pmatrix}$$
$$= \begin{pmatrix} 0 \\ -A\phi \end{pmatrix} \qquad (48)$$
$$Q \begin{pmatrix} 0 \\ \psi \end{pmatrix} = \begin{pmatrix} 0 & A^\dagger \\ -A & 0 \end{pmatrix} \begin{pmatrix} 0 \\ \psi \end{pmatrix}$$
$$= \begin{pmatrix} A^\dagger \psi \\ 0 \end{pmatrix} \qquad (49)$$

This result is a consequence of the fact that $(-1)^F$ and Q anti-commute:

$$\{(-1)^F, Q\} = \{\sigma_3, Q\} = 0. \qquad (50)$$

A quick calculation confirms this property:

$$\sigma_3 Q = \begin{pmatrix} 1 & 0 \\ 0 & -1 \end{pmatrix} \begin{pmatrix} 0 & A^\dagger \\ -A & 0 \end{pmatrix}$$
$$= \begin{pmatrix} 0 & A^\dagger \\ A & 0 \end{pmatrix}$$
$$Q\sigma_3 = \begin{pmatrix} 0 & A^\dagger \\ -A & 0 \end{pmatrix} \begin{pmatrix} 1 & 0 \\ 0 & -1 \end{pmatrix}$$
$$= \begin{pmatrix} 0 & -A^\dagger \\ -A & 0 \end{pmatrix}$$
$$= -\sigma_3 Q \qquad (51)$$

Armed with this knowledge, we see

$$(-1)^F (Q|\psi\rangle) = -Q(-1)^F |\psi\rangle = -(-1)^{F_\psi}(Q|\psi\rangle). \qquad (52)$$

Here $(-1)^{F_\psi}$ represents the parity of the state $|\psi\rangle$–its $(-1)^F$ eigenvalue. The conclusion we have drawn is that the state $Q|\psi\rangle$ has the *opposite* parity as the state $|\psi\rangle$. The supersymmetry operator Q turns bosons into fermions, and fermions into bosons, as desired.

We now ask what is the square of the supersymmetry operator, Q^2.

$$QQ = \begin{pmatrix} 0 & A^\dagger \\ -A & 0 \end{pmatrix} \begin{pmatrix} 0 & A^\dagger \\ -A & 0 \end{pmatrix}$$
$$= \begin{pmatrix} -A^\dagger A & 0 \\ 0 & -AA^\dagger \end{pmatrix}$$
$$= -H$$

We find that Q^2 is simply minus the total Hamiltonian of the system! Recall, also, that the adjoint of Q is simply minus itself. In summary,

$$Q^2 = -H \qquad (53)$$
$$Q^\dagger = -Q. \qquad (54)$$

Though it is beyond the level of our discussion, it is worth noting that these operators form a closed super-algebra called the Witten superalgebra, defined by the following properties [4].

$$[Q, H] = [Q^\dagger] = 0 \qquad (55)$$
$$\{Q, Q^\dagger\} = 2H. \qquad (56)$$

Here $\{A, B\} = AB + BA$ is the anti-commutator of A and B.

We can now see clearly the positivity of the spectrum:

$$\langle \Psi| H |\Psi\rangle = -\langle \Psi| QQ |\Psi\rangle$$
$$= \langle \Psi| Q^\dagger Q |\Psi\rangle$$
$$= \langle Q\Psi|Q\Psi\rangle \geq 0. \qquad (57)$$

We can also demonstrate that ground states with zero energy are invariant under supersymmetry transformations. We know that, for such a zero-energy eigenstate $|\Psi_0\rangle$,

$$Q|\Psi_0\rangle = 0$$
$$\begin{pmatrix} 0 & A^\dagger \\ -A & 0 \end{pmatrix} \begin{pmatrix} \phi \\ \psi \end{pmatrix} = 0$$
$$\implies A^\dagger \psi = 0 \qquad (58)$$
$$A\phi = 0 \qquad (59)$$

Eqn.s (58) and (59) are just the familiar conditions for ground states that appear in Eqn.s (20) and (21).

Supersymmetry transformations are generated by a unitary operator $U = e^{\epsilon Q}$ (recall Q is antihermitian). A ground state $|\Psi_0\rangle$ is invariant under the action of such an operator:

$$U \left| \Psi_0 \right\rangle = e^{\epsilon Q} \left| \Psi \right\rangle$$
$$= (I + \epsilon Q + \frac{1}{2}(\epsilon Q)^2 + \dots) \left| \Psi_0 \right\rangle$$
$$= \left| \Psi \right\rangle . \tag{60}$$

Colloquially, we say that "ground states are supersymmetric." For intuition, one can keep in mind, for example, plane wave states $\psi \sim \mathcal{N} e^{ikx}$, which are invariant under translations

$$T(x_0)\psi = \mathcal{N} e^{ik(x+x_0)}$$
$$= \mathcal{N} e^{ikx_0} e^{ikx}$$
$$= \mathcal{N}' e^{ikx} \tag{61}$$

where $\mathcal{N}'$ is the same normalizing constant up to a overall phase. We say that these plane wave states have *translational symmetry*.

Ground states of Hamiltonians in supersymmetric problems[7] are invariant under a different kind of transformation–a supersymmetric transformation–and thus we say they are *supersymmetric*.

For further reading regarding supersymmetry refer to the excellent discussion in Ref. 6.

VI. CONCLUSIONS

The above discussion was meant to provide a introduction to the subject of the supersymmetric method in quantum mechanics and its relation to supersymmetry.

Due to their importance in the formulation of the supersymmetric method and their utility as a guide to our intuition in our study of supersymmetry, we briefly recounted the main results of Dirac's algebraic solution to the harmonic oscillator potential. We later encountered ladders of states akin to the spectrum of the harmonic oscillator in the formulation of the supersymmetric method.

The formalism of the supersymmetric method in quantum mechanics was the main topic of our discussion. We sketched derivations of the most important results

in the subject, which we summarize here. We considered two *partner Hamiltonians* $H^{(1)}$ and $H^{(2)}$, related by a *super-potential* $W(x)$. We went on to show that both Hamiltonians necessarily had strictly non-negative spectra, which were identical up to the possibility of a single lower energy state in one of the two spectra. Moreover, we demonstrated that the zero-energy eigenstates of $H^{(1)}$ and $H^{(2)}$ were annihilated by A and $A^\dagger$, respectively (if they existed!).

We explicitly ran through one very simple application of the method to the problem of the infinite square well, and–somewhat surprisingly–we learned with minimal effort about the eigenstates and energy spectrum of the potential $V(x) \sim \sec^2(x)$. A closely related problem tells us about the potential $V(x) \sim \text{sech}^2(x)$, which shows up in investigations of one-dimensional scattering problems that have no reflections. There are many other applications of the supersymmetric method in quantum mechanics that we neglect to discuss in this paper; for example, when one of the partner Hamiltonians is that of the hydrogen atom, similarly powerful results are found, although the mathematics are somewhat more tedious.

We learned about the significance of supersymmetry in quantum field theory. The subject centers around three operators: the super-charge Q, its adjoint $Q^\dagger$, and the super-Hamiltonian H. These operators form a closed superalgebra called the Witten superalgebra. The parity operator $(-1)^F$ also plays an important part in the theory, particularly in relating bosons (fermions) to their fermionic (bosonic) super-partners.

[1] P.A.M. Dirac, *The Principles of Quantum Mechanics, 4th Ed.* (Oxford University Press 2011) Chapter 34, page 136.
[2] We are working in units where $\hbar/2m = 1$.
[3] B. Zwiebach, 8.05 Lecture Notes, Cambridge, MA, 2011
[4] Adolfo del Campo, Supersymmetric Quantum Mechanics, Basque Country University, Spain, 2005
[5] For a full treatment of the infinite well, see, for example, D.J. Griffiths, *Introduction to Quantum Mechanics, 2nd Ed.* (Pearson Prentice hall, Upper Saddle River, MA,

2005) page 30.
[6] F. Cooper, A. Khare, U. Sukhatme: Supersymmetry in Quantum Mechanics, World Scientific, Singapore, 2001.
[7] Since we can find a super-partner Hamiltonian for any given Hamiltonian H, this language is somewhat redundant. All problems can be formulated as supersymmetric problems; there are no restrictions on H.

Simulating Quantum Systems

A.T. Ireland

aireland@mit.edu

Department of Physics, M.I.T., Cambridge, MA

(Dated: May 2, 2014)

Studying systems of many quantum particles has great relevance to many current areas of research, but even today's most powerful supercomputers are unable to simulate quantum systems with more than around 30 atoms. Simulating quantum systems in other ways has therefore recently become a field of great importance. Here we explore the current state of the field of quantum simulation, and discuss what can be achieved in the future. Two examples of recent experiments are analysed, chosen with the goal of capturing the key ideas of how one system can simulate another. The first example is a simulation of a phase transition in an Ising chain of spins, using a tilted optical lattice. The second shows how artificial gauge potentials can be simulated in condensates of neutral atoms. Achieving controllable, scalable simulations of these types could lead to dramatic advances in our understanding of quantum magnetism, superconductivity, and other poorly understood phenomena.

I. INTRODUCTION

The need for quantum simulators stems from the intractability of modelling some types of quantum systems with classical computers. The field has grown rapidly in the last decade, after being first proposed by Feynman in his 1982 talk [1]. The field has grown rapidly in the last decade, and is already very broad, with simulators making use of systems ranging from photons in a cavity to quantum dots [2]. In this paper we focus on gases of cold atoms, which have led to the some of the most successful demonstrations of quantum simulation to date.

Some of the hardest problems in quantum mechanics to solve using classical computation are those involving many interacting particles. To understand the problem with simulating such systems, consider how a classical computer stores data: sequences of 1s and 0s encoded in the states of transistors. The states of a quantum system of many bodies are described by their wavefunctions, which are in a vector space whose size grows exponentially with the size of the system: for example, for a system of spin particles, for each particle put in, the number of states will double. Hence for a system of N spin $-\frac{1}{2}$ particles, we would need 2^N numbers, corresponding to the coefficients of each of the basis states, to fully describe the state of the system. Furthermore, to calculate the time evolution of the quantum system, we would have to exponentiate the Hamiltonian, which is a $2^N \times 2^N$ matrix. Therefore, simulating a general quantum system is described as an 'intractable' problem for classical computers, and the amount of computation power required for simulating any more than 20-30 particles is well beyond the reach of todays classical computers, and of those in the foreseeable future[3].

The subject is intimately linked with the development of the quantum computer; Feynman conjectured that we might use a Universal Quantum Computer for solving problems in quantum mechanics, as such a machine would not suffer from the classical problem exponential growth in computation time with increasing number of degrees of freedom. Whereas a classical bit is either 0 or 1, a quantum bit can be a superposition of the two, and so one can directly map a spin$-\frac{1}{2}$ system with, say, 40 particles onto just 40 quantum bits. A quantum computer is therefore ideal for simulating systems of interacting quantum particles. In addition, whilst decoherence of the states of the quantum computer leads to errors in calculations such as factorizing large numbers, it has been suggested that it could in fact be beneficial when using the computer for simulation[3]. Decoherence in a real quantum system is effected by characteristics of the environment such as temperature, pressure, density, and electric field strength. If the dependence of the quibits of a quantum computer on these parameters is the same as that of the system it is being used to simulate, then by simply re-scaling the 'Bloch Parameters', such as the decoherence times T_1 and T_2, to match those of the real system, we can transform the seemingly detrimental effect of decoherence into an improvement of the simulation.

The universal quantum computer envisaged by Feynman is referred to as a digital quantum simulator. Such a simulator breaks down the time evolution of the system into discrete time-steps, just as a classical computer would do, and performs computations using programmable algorithms. This approach is beyond our current capability: we are not yet able to control an array of quantum bits reliably enough to perform this many calculations without error. A more promising approach, therefore, may be to use analogue quantum simulators. These are used only for the specific systems for which they were designed, and imitate that system directly rather than performing calculations or running algorithms to simulate it. In the same way as an Orrery mimics the motion of the planets in the solar system, quantum simulators can reveal much about the basic behaviour of the system they represent (just as the Orrery can show the relative motions of the planets), but are able to get around the problems that might be faced in studying the system directly. These simulators are systems of quantum particles which have the capability to be initialized into a known state, and then evolved with an artificial Hamiltonian with parameters that can be varied by the experimenter.

Implementing these simulators therefore requires that the experimenter have a large degree of control over the system, often with the capability to address the states of individual particles. Quantum simulators will soon allow us to both test the predictions of existing models, and to generate new, unpredicted results that could not have been classically simulated.

The remainder of this paper describes examples of analogue quantum simulation. The systems presented here were chosen because they demonstrate the key ideas behind simulation in the context of two very different problems. In Sec. II we explore the use of an optical lattice to simulate a chain of quantum spins in a phase transition. In Sec. III we demonstrate how the adiabatic evolution of the 'dressed states' of the Jaynes-Cummings Hamiltonian (for example, that of an atom-light interaction) can lead to a geometric phase which can simulate gauge potentials in a system of neutral atoms.

II. ANTIFERROMAGNETIC SPIN CHAINS SIMULATED USING AN OPTICAL LATTICE

One example of a system specifically designed to simulate another is the case of a one dimensional Ising model of a chain of spins simulated by cold atoms in an optical lattice, as carried out by Simon et al (2011). The Ising chain of spins is at the heart of the field of quantum magnetism, which is currently an area of great relevance in condensed matter physics, with implications for high-temperature superconductors, spintronic devices and many more. However, simulating even a short chain of quantum spins on a classical computer is complex, because of entanglement between the spins.

The Ising model is a simplistic model of a system of interacting spins in a lattice, based on the assumption that the spins only interact with their nearest neighbours. For particles with both a spatial and a spin component of their wavefunction, there is a different energy associated with neighbouring spins being aligned or anti-aligned: this is called the exchange energy, J. If the spin is in an external magnetic field, then this will also contribute to the energy. We can therefore write the Hamiltonian as a sum over the exchange interactions with nearest neighbours plus the total energy of the applied field with the spins in the lattice:

$$H(s_i) = -J \sum_{n.n} s_i s_j - h \sum_i s_i, \qquad (1)$$

where h represents the effect of the external field. Note that in this simple model the spins cannot point in any direction – they must be either aligned or anti-aligned with the field. Because of the simplicity of the Ising model it is found that many other quite different physical systems may map onto it with a suitable choice of the parameters J and h. The experiment described in this section makes use of the isomorphism between the Ising model for a 1D

spin chain, and that of a one dimensional lattice of spinless bosons, mapping spin to lattice site occupancy. The justification for the mapping that forms the basis for this experiment is an advanced proof, and is treated in [5].

For an Ising chain of spins at zero temperature when the external field dominates, the spins will align in the direction of the applied field, behaving like a paramagnet. However, as the interaction between neighbouring spins becomes the dominant term, antiferromagnetism is exhibited. The set-up used by Simon et al., described as a 'tilted lattice', consisted of ^{87}Rb atoms suspended in an optical lattice designed such that the energy of each lattice site decreases across the lattice in one direction, as shown in Fig. 1. This tilting is achieved by applying a magnetic field gradient across the lattice. In a Bose-Einstein gas of ^{87}Rb atoms, the Van der Waals interaction is observed to result in a repulsive force, which translates to a positive energy of interaction, U, when two atoms are in the same lattice site. The 'tilt' of the lattice, E, is simply the difference in energy between adjacent lattice sites. Unlike atoms in a crystal, which can lose or gain energy with ease, those suspended in an optical lattice have no means of giving up excess energy. The consequence of this is that tunnelling to an adjacent lattice site with a lower energy is not possible except when E is tuned to be close to U: this way, the energy an atom loses by tunnelling to a new site further down the slope of the lattice is offset by its interaction with the atom that already occupies the new site. The experiment therefore involved gradually increasing E to simulate the changing strength of an applied magnetic field: as the tilt E approaches U, each atom becomes free to tunnel to its neighbour, which is equivalent to the spins in the simulated chain switching from aligned to anti-aligned — the phase transition occurs at E = U. As E goes past U, tunnelling is once again energetically forbidden.
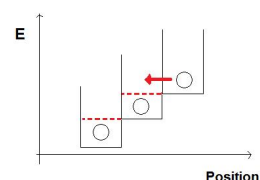
FIG. 1: A schematic representation of three lattice sites when E = U. The dotted red lines indicate the effective energy of the site when taking into account the interaction energy, U, between ^{87}Rb atoms. As the atoms cannot lose or gain energy, tunnelling can only occur when E = U.

The cloud of atoms was then imaged by a microscope sensitive to the parity of the site occupation number, with the result that lattice sites containing either two atoms or no atoms show up dark, and those containing a single atom appear bright[4]. The dark regions are therefore those in which the phase transition to the antiferromagnetic regime has occurred.

In this section we studied an example of simulation
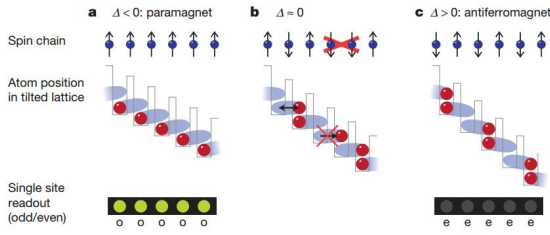
FIG. 2: The mapping between spins and lattice occupancy that forms the basis of the simulation set up by Simon et al. Here $\Delta = E - U$, the difference in energy between the lattice tilt and the interaction energy of two atoms on the same site. Figure reproduced from [4]
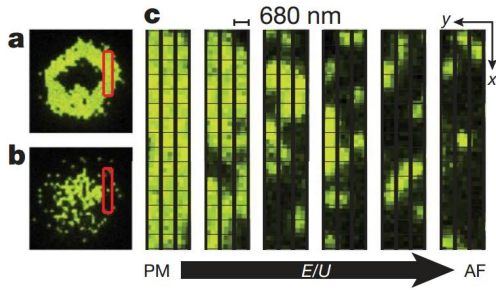
FIG. 3: **(a)** Images of the cloud of atoms as the system is swept through the phase transition by changing the tilt of the lattice, E. Figure **a** shows a snapshot of the whole system whilst in the paramagnetic phase. Figure **b** shows a second snapshot, taken in the antiferromagnetic phase. Figure **c** shows several snapshots of rows of atoms taken at different times throughout the transition. Figure reproduced from [4]

based on the mapping of the behavior of a lattice site filling model onto an Ising model. In the next section, we explore a simulation based on a different mathematical similarity: the close relation of Berry's phase to the mathematics of a quantum particle in a magnetic field.

III. ADIABATIC EVOLUTION OF A TWO STATE ATOM

To see how an atom interacting with light can lead to artificial magnetic fields, we start with a simplified example which captures the essential physics: a single two-state atom in a light field. The following calculation provides an outline of how the geometric phase, acquired by the atom as a result of its adiabatic movement through the light field, can enable us to write the Schrödinger equation for the atom in a form identical to that of a charged particle moving in a magnetic field. The two states of the atom are denoted $|g\rangle$, for the ground state, and $|e\rangle$, for the excited state. To derive the final result, we first need to find the basis states of the atom-

light interaction, known as 'dressed states'. These are the eigenstates of the Jaynes-Cummings Hamiltonian, which is denoted by H_{total} and describes the whole atom-light system:

$$H_{total} = H_{atom} + H_{light} + H_{int} \qquad (2)$$

H_{int} is the term that describes the interaction, and is given by

$$H_{int} = \frac{\hbar\Omega}{2}(|e\rangle\langle g|\,\hat{a}e^{-i(\omega-\omega_a)t} - |g\rangle\langle e|\,\hat{a}^\dagger e^{i(\omega-\omega_a)t}). \quad (3)$$

Ω is the Rabi frequency of the system, ω_a is the frequency corresponding to the transition in the atom, and ω is the frequency of the incident light.

H_{atom} and H_{light} are given by

$$H_{atom} = \frac{\hbar\omega_a}{2}(|e\rangle\langle e| - |g\rangle\langle g|) \qquad (4)$$

$$H_{light} = \hbar\omega\hat{a}^\dagger\hat{a} \qquad (5)$$

Using basis vectors $|n+1, g\rangle$ and $|n, e\rangle$, where $|n\rangle$ is the nth eigenstate of $\hat{a}^\dagger\hat{a}$ (corresponding to the state of the light field), we can express the total Hamiltonian for the atom-light interaction as a matrix U (calculation omitted):

$$\hat{U} = \frac{\hbar\Omega}{2}\begin{bmatrix} \cos\theta & e^{-i\phi}\sin\theta \\ e^{i\phi}\sin\theta & -\cos\theta \end{bmatrix}. \qquad (6)$$

θ and ϕ are functions of the parameters of the system and, importantly, can be spatially varied by the experimenter. The eigenstates of the coupling matrix U are the 'dressed states' we need to derive the result. They are found to be

$$|\chi_1\rangle = \begin{bmatrix} \cos\frac{\theta}{2} \\ e^{i\phi}\sin\frac{\theta}{2} \end{bmatrix}, \quad |\chi_2\rangle = \begin{bmatrix} -e^{-i\phi}\sin\frac{\theta}{2} \\ \cos\frac{\theta}{2} \end{bmatrix}. \qquad (7)$$

Now if we allow this atom to move in a potential V, where V has no effect on the internal state of the atom, the Hamiltonian becomes

$$H = \frac{\hat{p}^2}{2m} + \hat{V} + \hat{U} \qquad (8)$$

We are now ready to explore the adiabatic evolution of the atom, as the parameters of the system are tuned slowly by the experimenter. As $|\chi_1\rangle$ and $|\chi_2\rangle$ are eigenstates of U, solving the time dependent Schrödinger equation is as simple as calculating the action of $\hat{p}^2$ on the general wavefunction. This wavefunction must have both a spatially and temporally varying component $\psi_j(\vec{r}, t)$, and a component relating to the state of the atom and its interaction with the light field, which we have shown to be represented by the $|\chi_j\rangle$. It is important to note that the $|\chi_j\rangle$ have $\vec{r}$ dependence, as the parameters of the light

field, described by θ and ϕ, are not constant in space. From here on we will highlight this position dependence of the dressed states by writing them as $|\chi_j(\vec{r})\rangle$.

$$|\Psi\rangle = \sum_{j=1}^{2} \psi_j(\vec{r},t) |\chi_j(\vec{r})\rangle \qquad (9)$$

In the following steps we apply the Schrödinger equation only to the dressed state component of the overall wavefunction, with the goal of writing the equation in terms of $\psi(\vec{r},t)$ only. We first apply $\hat{p} = -i\hbar\vec{\nabla}$, which gives

$$\hat{p}|\Psi\rangle = \sum_{j=1}^{2} (-i\hbar\left|\vec{\nabla}\chi_j(\vec{r})\right\rangle + |\chi_j(\vec{r})\rangle\,\hat{p})\psi_j(\vec{r},t). \qquad (10)$$

Inserting a complete set of states:

$$\hat{p}|\Psi\rangle = \sum_{j,k=1}^{2} [(-A_{k,j} + \delta_{k,j}\hat{p})\psi_j(\vec{r},t)]\,|\chi_k(\vec{r})\rangle, \qquad (11)$$

where

$$A_{k,j} = i\hbar\left\langle\chi_k(\vec{r})|\vec{\nabla}\chi_j(\vec{r})\right\rangle. \qquad (12)$$

To calculate the action of $\hat{p}^2$, we apply $\hat{p}$ once more. What at first looks to be a tricky calculation is simplified by noting that we can use the product rule just as when operating $\hat{p}$ for the first time, but replacing ψ_j with the expression $[(-A_{k,j} + \delta_{k,j}\hat{p})\psi_j(\vec{r},t)]$. Therefore, after inserting a complete set of states $|\chi_l(\vec{r})\rangle$, we obtain

$$\hat{p}^2|\Psi\rangle = \sum_{j,k,l=1}^{2} [(-A_{l,k}+\delta_{l,k}\hat{p})(-A_{k,j}+\delta_{k,j}\hat{p})\psi_j(\vec{r},t)]\,|\chi_l(\vec{r})\rangle. \qquad (13)$$

If we now assert that the atom was prepared in state $|\chi_1\rangle$, and we ensure that it moves adiabatically, then we can set any terms involving $\psi_2(\vec{r},t)$ equal to 0 in the adiabatic approximation. Expanding the brackets, contracting over k and setting j equal to 1 gives:

$$\hat{p}^2|\Psi\rangle = \sum_{l=1}^{2}[(\delta_{l,1}\hat{p}^2 + A_{l,1}^2 - A_{l,1}\hat{p} - \hat{p}A_{l,1})\psi_1(\vec{r},t)]\,|\chi_l(\vec{r})\rangle. \qquad (14)$$

Finally, writing the Schrödinger equation for $|\Psi\rangle = \psi_1(\vec{r},t)|\chi_1(\vec{r})\rangle$ and right-multiplying by $\langle\chi_1(\vec{r})|$ gives us an equation which looks just like that of a particle moving in a B field[7]:

$$i\hbar\frac{\partial\psi_1(\vec{r},t)}{\partial t} = [\frac{(\hat{p} - A_{1,1})^2}{2m} + A_{2,1}^2 + \frac{\hbar\Omega}{2} + \hat{V}]\psi_1(\vec{r},t) \qquad (15)$$

$$= [\frac{(\hat{p} - A)^2}{2m} + W + \frac{\hbar\Omega}{2} + \hat{V}]\psi_1(\vec{r},t) \qquad (16)$$

The terms A and W play the role of the gauge potentials of real magnetic and electric fields respectively. Using the dressed eigenstates, we calculate

$$A = i\hbar\langle\chi_1|\nabla\chi_1\rangle \qquad (17)$$

$$= \frac{\hbar}{2}(\cos\theta - 1)\nabla\phi. \qquad (18)$$

and $\qquad\qquad\qquad\qquad\qquad\qquad\qquad$ (19)

$$W = |A_{2,1}|^2 = \frac{\hbar^2}{2m}|\langle\chi_2|\nabla\chi_1\rangle|^2 \qquad (20)$$

$$= \frac{\hbar^2}{8m}[(\nabla\theta)^2 + \sin^2\theta(\nabla\phi)^2] \qquad (21)$$

It is now apparent that A here is closely related to Berry's phase $\gamma = \oint i\left\langle\chi_1(\vec{r})|\vec{\nabla}\chi_1(\vec{r})\right\rangle \cdot d\vec{R}$[8]. Hence the similarity between Berry's phase and magnetic flux, which is no more than a mathematical curiosity, can be put to use in simulating the effects of a magnetic field. These 'psuedopotentials' have arisen as a result of the interaction of the internal states of the atom with a light field that varies in space, which gives them the property of being purely geometric (depending only on θ and ϕ, quantities that vary in space only). They share this property with the real gauge fields of the magnetic and scalar potential in a system of charged particles. We have therefore shown that a system of neutral atoms can be used to simulate systems of charged particles.

The physics described here was demonstrated by Lin et al.[6], using a Bose-Einstein condensate of ^{87}Rb atoms, irradiated with laser light in such a way that θ and ϕ were spatially varying. When superfluids of charged particles are exposed to a real B field, a vortex lattice is produced as the fluid expels magnetic flux everywhere except at the centre of vortices, where thin lines of flux are able to pass through. Importantly, the formation of a vortex lattice was observed in the set-up with an artificial B field applied using the technique described above.
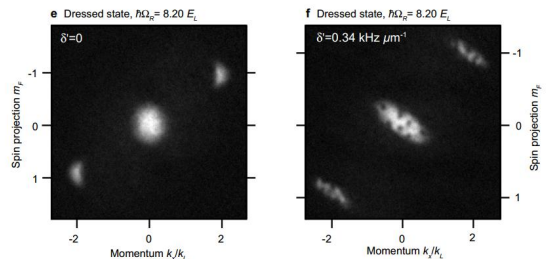

FIG. 4: **(a)** Image of the cloud of ^{87}Rb in the experiment by Lin et al. On the left, there is no spatial variation in θ and ϕ. On the right, spatial variation is introduced and the vortices indicative of an artificial B field can be seen. Figure reproduced from [6].

IV.   DISCUSSION

We have explored two different examples of quantum simulators. The first was a simulation of a 1D Ising chain of quantum spins, simulated by a site-filling interaction in an optical lattice of ^{87}Rb atoms. This experiment was intended as a proof of principle; the results it produced could have been simulated on a classical computer, because of the short length of the spin chains involved. It does however represent an important step on the way to achieving a better understanding of quantum magnetism, as further experiments using the same novel technique may simulate more complex systems that would otherwise be out of reach. The second simulation relied on the geometric phase for a two-state atom moving in a spatially varying light field. We showed how a Hamiltonian of this form can be rearranged to take the form of the Hamiltonian of a system involving the magnetic vector potential, and thereby showed that such a set-up could be used to simulate a magnetic field in a system of neutral atoms. The results of the experiment by Lin et al show the effects of this simulation, which take the form of a vortex lattice in a Bose-Einstein condensate of ^{87}Rb atoms. Having the ability to simulate charged particles using neutral atoms in a condensate could in the future allow us to simulate electrons moving in a solid. Both of these experiments demonstrate the potential that the field of quantum simulation has to make significant progress towards closing the current gaps in our knowledge about many quantum mechanical systems. Although the universal quantum computer is still a long way off, novel analogue simulation techniques such as those detailed in this paper promise to make significant progress on many important problems in the interim.

[1] R.P. Feynman, *Simulating physics with computers*, International Journal of Theoretical Physics **21** (1982), 467–488

[2] A. Aspuru-Guzik et al, *Photonic simulators*, Nature Physics **8** 2012, 285–291

[3] S. Lloyd, *Universal Quantum Simulators*, Science **273**, 1996 1073–1078

[4] J. Simon et al., *Quantum simulation of antiferromagnetic spin chains in an optical lattice*, Nature **472** (2011), 307–312

[5] S. Sachdev et al., *Mott insulators in strong electric fields*, Physical Review B **66** (2002), 075128

[6] Y.J. Lin et al., *Synthetic magnetic fields for ultracold neutral atoms*, Nature **462** (2009), 628–632

[7] J. Dalibard et al., *Colloquium: Artificial gauge potentials for neutral atoms*, Reviews of Modern Physics **83** (2011), 1523–1543

[8] M.V. Berry, *Quantal phase factors accompanying adiabatic changes*, Proceedings of the Royal Society **392** (1984), 45–57

A Brief Discussion on the Casimir Effect

Yijun Jiang[*]

MIT Department of Physics

(Dated: May 2, 2014)

When two perfectly conducting plates are placed in vacuum, an attractive force will occur due to the existence of vacuum energy. This phenomenon, known as the Casimir effect, shows that vacuum energy has measurable consequences, and it has been confirmed by experiments. In this paper, the Casimir effect is derived through various ways including Euler-Maclaurin formula, zeta regularization and radiation pressure approach. The procedure of regularization as well as its physical meanings are discussed, and some experimental results are briefly introduced.

I. INTRODUCTION

Quantum field theory states that all fundamental fields are quantized at every point in space. Quantization of the electromagnetic field requires that it must behave like a harmonic oscillator. This analogy implies that the energy of the electromagnetic field is $(n+\frac{1}{2})\hbar\omega$ for a vibrational mode of frequency ω, where n is a non-negative integer. Therefore, even in vacuum, where the number eigenvalue n is zero, there is still a nonzero ground state energy $\frac{1}{2}\hbar\omega$ for each possible vibrational mode. The total energy $\sum \frac{1}{2}\hbar\omega$ is known as the vacuum energy, where the sum runs over all possible frequencies.

When this vacuum energy was first known to physicists, it was often treated as a background term and ignored in calculations. In 1940, when Dutch physicist H. Casimir consulted N. Bohr about his research on Van der Waals force between two polarizable molecules and between a molecule and a metal plate [1], the suggestion from Bohr was to consider the effects of vacuum energy. Casimir then discovered an attractive force between two perfectly conducting parallel plates [2], which directly originates from the existence of vacuum energy. This result, known as the Casimir effect, shows that vacuum energy has measurable consequences, and this was later confirmed by experiments [3][4]. The Casimir effect can be further generated from perfectly conducting plates to various other boundary conditions [8].

The basic idea of the Casimir effect is, when materials are placed in vacuum, they will interact with the electromagnetic field. The boundary conditions select out only the eigen-modes of electromagnetic vibration. Therefore the total vacuum energy is altered. Typically this energy changes from a continuous integral over all frequencies to a discrete summation of eigen-frequencies. Both these two energies diverge, but their difference is usually a finite value, which can be calculated by a procedure known as regularization. In this article, the simplest version of the Casimir effect, namely the double plates problem, is considered. Euler-Maclaurin regularization and zeta function regularization are discussed. This effect is also derived in the viewpoint of pressure difference from radiation on both sides of the plates. Further discussions are made on the equivalence of different regularizations as well as the physical views on regularization. Finally, some experimental results and applications are mentioned.

II. THE DOUBLE PLATES PROBLEM

A. Physical Picture

Let us consider the scenario described by Casimir himself [2]. We have a cubic cavity of volume L^3 bounded by perfectly conducting walls. A perfectly conducting plate is placed inside this box, parallel to one pair of the walls (say, $z=0$ and $z=L$). Suppose L is sufficiently large, so that we can let the plate be far away from both $z=0$ and $z=L$. Under this configuration, the boundaries are so distant from each other that they hardly affect the vibrational modes of the electromagnetic field in vacuum. Let us call this case I, with the corresponding vacuum energy $E^I = \sum_i \frac{1}{2}\hbar\omega_i^I$. We then consider case II, where the plate in the box is moved to $z=a \ll L$. Then the plate and the $z=0$ wall are close enough to affect the possible modes between them. In this case, the vacuum energy can be written as $E^{II} = \sum_i \frac{1}{2}\hbar\omega_i^{II}$. The energy difference in these two cases depends on the distance a, which results in a force between the two close plates. This is the physical picture of the Casimir effect.

B. Vibrational Modes & Zero Point Energy

Classically, it is not hard to calculate the electric field between the plates. The parallel components of the electric field must vanish at the boundaries.

$$\mathbf{E_x} = E_x \cos k_x x \sin k_y y \sin k_z z e^{-i\omega t}$$
$$\mathbf{E_y} = E_y \sin k_x x \cos k_y y \sin k_z z e^{-i\omega t}$$
$$\mathbf{E_z} = E_z \sin k_x x \sin k_y y \cos k_z z e^{-i\omega t}$$

where in case II, $k_x = \frac{\pi}{L}n_x$, $k_y = \frac{\pi}{L}n_y$, $k_z = \frac{\pi}{a}n_z$, and $\omega = \omega_{n_x,n_y,n_z} = c\sqrt{k_x^2+k_y^2+k_z^2}$, with $n_x, n_y, n_z =$

[*]Electronic address: yjjiang@mit.edu

$0, 1, 2, \cdots$. And in case I, we just use L to replace a in k_z. $\nabla \cdot \mathbf{E} = 0$ gives

$$k_x E_x + k_y E_y + k_z E_z = 0$$

Therefore, when k_x, k_y, k_z are fixed, there are generally two linear independent solutions for E_x, E_y, E_z, corresponding to two independent polarizations. But when one of k_x, k_y, k_z is zero, there will be only one polarization left. For k_x and k_y, this is not important, for L is so large that we can treat them as continuous variables, and use integrals to replace discrete summations. But for k_z in case $\mathbb{II}$, as we will see, this subtle difference in polarization degrees of freedom does matter.

The vacuum energy in case $\mathbb{II}$ can be written as

$$E^{\mathbb{II}} = \frac{\pi\hbar c}{2L}\int_0^\infty\!\!\int_0^\infty\left(\sqrt{n_x^2 + n_y^2} + 2\sum_{n_z=1}^\infty\sqrt{n_x^2 + n_y^2 + n_z^2\frac{L^2}{a^2}}\right)\mathrm{d}n_x\mathrm{d}n_y$$

We can introduce polar coordinates in n_x, n_y plane to simplify the integral. Let $n_x = r\cos\theta$ and $n_y = r\sin\theta$,

$$E^{\mathbb{II}} = \frac{\pi^2\hbar c}{2L}\sum_{n_z=0}^\infty{}'\int_0^\infty r\sqrt{r^2 + n_z^2\frac{L^2}{a^2}}\,\mathrm{d}r \qquad (1)$$

where $\sum'$ means that the term with $n_z = 0$ should have a $\frac{1}{2}$ coefficient.

In case I, the summation over n_z (or k_z) becomes an integral. Replacing a by L, we get the total vacuum energy inside the box,

$$E^I_{\mathrm{tot}} = \frac{\pi^2\hbar c}{2L}\int_0^\infty \mathrm{d}n_z\int_0^\infty r\sqrt{r^2 + n_z^2}\,\mathrm{d}r$$

The energy in the region between $z = a$ and $z = L$ can be considered the same for the two cases since $L \gg a$. So the difference comes merely from the thin layer between $z = 0$ and $z = a$. A factor $\frac{a}{L}$ is introduced to get the energy in this region.

$$E^I = \frac{\pi^2\hbar ca}{2L^2}\int_0^\infty \mathrm{d}n_z\int_0^\infty r\sqrt{r^2 + n_z^2}\,\mathrm{d}r \qquad (2)$$

And the energy difference is given by

$$\Delta E = E^{\mathbb{II}} - E^I$$

It is obvious that neither E^I nor $E^{\mathbb{II}}$ converges. However, their difference is a finite value and can be calculated.

C. Dealing with Infinities

One useful method to deal with divergency is regularization. The idea is to introduce a regulator with a tunable parameter that forces the summation or integral to converge. The correct physics is recovered then by taking the limit of the tunable parameter and making

the regulator disappear. This is commonly used in quantum field theory. Its physical meanings will be discussed later.

There are different kinds of regularizations. Here, the original regularization used by Casimir is applied [2]. Let us first rewrite Equation (1) and (2) as:

$$E^{\mathbb{II}} = \frac{\pi^2\hbar c}{2L}\sum_{n_z=0}^\infty{}'\int_{n_z\frac{L}{a}}^\infty w^2\mathrm{d}w \qquad (3)$$

$$E^I = \frac{\pi^2\hbar c}{2L}\int_0^\infty \mathrm{d}n_z\int_{n_z\frac{L}{a}}^\infty w^2\mathrm{d}w \qquad (4)$$

where n_z is replaced by $\frac{L}{a}n_z$ in E^I, and $w = \sqrt{n_z^2\frac{L^2}{a^2} + r^2}$. We introduce a general regulator $f(\varepsilon w)$ that has the property $f(0) = 1$ and $f(x)$ decays to 0 faster than x^{-3} as $x \to \infty$. This regularization can be removed afterwards simply by taking $\varepsilon \to 0$. The summand or integrand in Equation (3) or (4) is now:

$$F(n_z) = \int_{n_z\frac{L}{a}}^\infty w^2 f(\varepsilon w)\mathrm{d}w$$

Then it is easy to get

$$F^{(k)}(\infty) = 0 \qquad\qquad\qquad (k \geq 0)$$

$$F^{(k)}(0) = -(k-1)(k-2)\varepsilon^{k-3}\left(\frac{L}{a}\right)^k f^{(k-3)}(0) \quad (k > 0)$$
$$(5)$$

Use the Euler-Maclaurin formula, which relates the difference of the summation and the corresponding integral of a function to its derivatives on the boundaries:

$$\sum_{i=m}^n F(i) = \int_m^n F(x)\mathrm{d}x + \frac{1}{2}(F(n) + F(m)) +$$
$$\sum_{k=1}^p \frac{B_{2k}}{(2k)!}\left(F^{(2k-1)}(n) - F^{(2k-1)}(m)\right) + R_p$$
$$(6)$$

where B_n are the Bernoulli numbers, $B_0 = 1$, $B_1 = -\frac{1}{2}$, $B_2 = \frac{1}{6}$, $B_3 = 0$, $B_4 = -\frac{1}{30}$, $\cdots$, and R_p is the error term that vanishes when p is infinitely large. A mathematically friendly proof of this formula was given by T. M. Apostol [9]. Take the limit $p \to \infty$, $n \to \infty$ and let $m = 0$, and notice that the $\frac{1}{2}F(0)$ term changes the summation $\sum$ into $\sum'$:

$$\sum_{i=0}^\infty{}'F(n_z) - \int_0^\infty F(n_z)\mathrm{d}n_z = -\sum_{k=1}^\infty\frac{B_{2k}}{(2k)!}F^{(2k-1)}(0)$$
$$= -\frac{1}{12}F'(0) + \frac{1}{720}F'''(0) + \cdots$$

The higher derivatives $F^{(k)}(0)$ are on the order of $O(\varepsilon^{k-3})$. When $k > 3$, they will vanish as we finally

take $\varepsilon \to 0$. $F'(0)$ also vanishes by Equation (5). The only nonzero term left is $F'''(0) = -2\frac{L^3}{a^3}f(0) = -\frac{2L^3}{a^3}$.

Finally, we obtain

$$\Delta E = \frac{\pi^2 \hbar c F'''(0)}{1440L} = -\frac{\pi^2 \hbar c L^2}{720 a^3} \qquad (7)$$

D. The Casimir Force

The energy difference depends on the distance a between the two plates. This results in a nonzero pressure

$$P(a) = -\frac{1}{L^2}\frac{\partial \Delta E(a)}{\partial a} = -\frac{\pi^2 \hbar c}{240 a^4}$$

This is the formula for the Casimir force. We see that L drops out. This makes sense, for L is the size of our auxiliary box, which should not appear in the final result. The minus sign shows that it is attractive. Notice that this force decays quickly by a^{-4}.

Plugging in numerical values, we get

$$P(a) \approx 0.013 \frac{1}{a^4} \quad \text{dyn/cm}^2 = 1.3 \times 10^{-3} \frac{1}{a^4} \quad \text{Pa}$$

where a is measured in microns. If the two plates are one microns apart, the inward pressure is about 1.3×10^{-8} atm. This small order of magnitude makes the effect hard to be observed. However, this effect can be of importance below the micron scale. For example, future very-large-scale integration designers may have to take the Casimir force into account.

III. ZETA REGULARIZATION

Besides the method described above, there are various other ways of regularization that pulls out a finite value from infinities, among which I find the zeta function regularization especially interesting.

A. Zeta Function

The Riemann zeta function is defined as

$$\zeta(s) = \sum_{n=1}^{\infty} n^{-s} \qquad (8)$$

This sum converges when $\text{Re}(s) > 1$. But its analytic continuation extends to the whole complex plane except the single pole $s = 1$ (where the residue is 1), by the reflection formula

$$\zeta(s) = 2^s \pi^{s-1} \sin\left(\frac{\pi s}{2}\right)\Gamma(1-s)\zeta(1-s) \qquad (9)$$

A more understandable way to say it is, our zeta function is now defined by Equation (8) when $\text{Re}(s) > 1$, and

by Equation (9) when $\text{Re}(s) < 1$. For more details on the zeta function, see [10]

Some special values of $\zeta(s)$ are listed below

$$\zeta(-n) = -\frac{B_{n+1}}{n+1} \qquad (n > 0)$$

$$\zeta(2n) = \frac{(-1)^{n+1}B_{2n}(2\pi)^{2n}}{2(2n)!} \qquad (n \geq 0)$$

where B_n are the Bernoulli numbers.

B. Calculating Divergent Series

When an infinite series does not converge, we cannot speak of its sum in the sense of the limit of its partial sums. However, it makes sense to define a summation method that assigns a value to the series. This value is usually called the sum of the series when the summation method is well-defined, that is to say, compatible with the usual sum when applied to a convergent series.

The zeta function defines such a summation method that assigns a value to a series of the type $\sum n^s$. For example, it assigns value $\zeta(0) = -\frac{1}{2}$ to the infinite sum $S = 1+1+1+\cdots$, and $\zeta(-1) = -\frac{1}{12}$ to $S = 1+2+3+\cdots$.

C. Zeta Regularization

Now let us go back to the Casimir effect. Define a regulator $f(x;s) = x^{-s/2}$ $(s > 3)$, which satisfies $f(x;0) = 1$ and $f(\infty;s) = 0$. Let $x = r^2 + n_z^2 \frac{L^2}{a^2}$ and put this regulator into the expression of $E^{I\!I}$ in Equation (1):

$$E^{I\!I} = \frac{\pi^2 \hbar c}{2L}\sum_{n_z=1}^{\infty}\int_0^{\infty} r\left(r^2 + n_z^2\frac{L^2}{a^2}\right)^{(1-s)/2} \mathrm{d}r \qquad (10)$$

$$= \frac{\pi^2 \hbar c}{2L}\sum_{n_z=1}^{\infty}\frac{1}{s-3}\left(n_z\frac{L}{a}\right)^{3-s}$$

$$= \frac{\pi^2 \hbar c L^{2-s}}{2(s-3)a^{3-s}}\zeta(s-3) \qquad (11)$$

Notice that we do not take into account the single polarization when $k_z = 0$. This will be discussed later.

When we define the regulator, we set $s > 3$ in order to make the integral (10) finite. When $s < 3$, the idea of analytic continuation still allows us to write the result in the form of Equation (11).

Take the limit $s \to 0$ to remove the regulator:

$$E^{I\!I} = -\frac{\pi^2 \hbar c L^2}{6a^3}\zeta(-3) = -\frac{\pi^2 \hbar c L^2}{720 a^3}$$

This result is identical to ΔE in Equation (7). A finite value appears without subtracting from $E^{I\!I}$ the vacuum energy of free space.

Zeta regularization never involves such a subtraction. It pulls out a finite number directly from a divergent sum.

The way to understand this is, there is a finite value left when an infinite background is excluded from the series. And zeta function defines the sum of the divergent series to be exactly this finite value left.

The single polarization at $k_z = 0$ plays an important role in those regularizations where subtraction of two "regulated infinities" are involved. To be specific, it cancels out the term that blows up as regulation is taken away after subtraction. Since zeta regularization does not have this problem, it makes sense not to add $k_z = 0$. Again, this should be explained as, being a summation method, zeta regularization has already excluded all the divergence by defining a new sum.

Looking back at the Euler-Maclaurin approach discussed in the previous section, we can also regard Equation (6) as a summation method of divergent series, defined by

$$\sum_{i=1}^{\infty}{}^{\mathcal{R}} F(i) := -\frac{1}{2}F(0) - \sum_{k=1}^{\infty} \frac{B_{2k}}{(2k)!} F^{(2k-1)}(0)$$

This method, here denoted by a $\mathcal{R}$ symbol, is known as the Ramanujan summation. Using this definition, we can assign $E^{I\!I}$ a finite value, without having to worry about E^{I}. Ramanujan summation can also derive things like $1 + 1 + 1 + \cdots = -\frac{1}{2}$ and $1 + 2 + 3 + \cdots = -\frac{1}{12}$. But generally, different summation methods may assign different values to the same series.

D.   Why Does Zeta Regularization Work

We use the zeta function to assign a finite value to a divergent series. It is astonishing that this value has physical meanings. Terence Tao discussed this in his blog [11]. I will briefly re-state it here.

Let us consider a pure mathematical question first. The series

$$S = \sum_{n=1}^{\infty} (-1)^{n-1} = 1 - 1 + 1 - 1 + \cdots$$

diverges, since its partial sum

$$S_N = \sum_{n=1}^{N} (-1)^{n-1} = \frac{1}{2} + \frac{1}{2}(-1)^{N-1}$$

jumps between -1 and 1. The discontinuity of the partial sum sequence is troublesome, for we cannot stop at some N to get an approximation of S. The solution is to introduce a cutoff function $\eta(x)$, which equals 1 at the origin and vanishes when $x \geq 1$. Suppose N is odd, we can write

$$\sum_{n=1}^{N} (-1)^{n-1} \eta\left(\frac{n}{N}\right)$$

$$= \frac{1}{2}\eta\left(\frac{1}{N}\right) + \sum_{m=1}^{\frac{N-1}{2}} \frac{1}{2}\eta\left(\frac{2m-1}{N}\right) - \eta\left(\frac{2m}{N}\right) + \frac{1}{2}\eta\left(\frac{2m+1}{N}\right)$$

There should be another $\frac{1}{2}\eta(1)$ term, but $\eta(1) = 0$ so it does not show up. If $\eta(x)$ is twice continuously differentiable, it can be Taylor expanded:

$$\sum_{n=1}^{N} (-1)^{n-1} \eta\left(\frac{n}{N}\right) = \frac{1}{2}\eta(0) + \frac{1}{2}\eta'(0)\frac{1}{N} + O\left(N^{-2}\right) +$$

$$\sum_{m=1}^{\frac{N-1}{2}} \frac{1}{N^2}\eta''(0) + \sum_{m=1}^{\frac{N-1}{2}} O\left(N^{-3}\right)$$

$$= \frac{1}{2} + O\left(N^{-1}\right)$$

Let $N \to \infty$, we can take the constant leading term $\frac{1}{2}$ as the value of the sum S.

Similarly, we can apply the cutoff function to the zeta-typed sum $\sum n^s$. The value assigned by the zeta function is exactly the constant term of the asymptotic expansion of the smoothed sum. The mathematical statements can be found in Tao's blog [11].

Now we go back to physics. We write $E^{I\!I} = (E^{I\!I} - E^{I}) + E^{I} = \Delta E + E^{I}$. ΔE can be regarded as the constant leading term, and E^{I} is then the rest part of the expansion. Only the leading term ΔE has physical meanings and the zeta regularization exactly picks it out. This explains why the value assigned by the zeta function gives the correct physics.

IV.   THE RADIATION PRESSURE APPROACH

Another derivation of the Casimir effect is the difference in radiation pressure inside and outside the plates [12]. Suppose a plane wave with energy density E bounces off a board elastically at incident angle θ. It is not hard to see that the radiation pressure exerted on the board is

$$P = 2E \cos^2 \theta$$

Between the two Casimir plates, the energy density for a monochromatic wave is $E(\omega) = \frac{\hbar\omega}{2aL^2}$. Summing up all possible wave modes, and use integration to replace summation in x and y direction, we get the pressure on

the inner side of the parallel plates:

$$P^{\text{in}} = \frac{\hbar c}{aL^2} \sum_{k_z}{}' \int_0^\infty \frac{L}{\pi} \mathrm{d}k_x \int_0^\infty \frac{L}{\pi} \mathrm{d}k_y \frac{k_z^2}{\sqrt{k_x^2 + k_y^2 + k_z^2}}$$

$$= \frac{\hbar c}{a^3} \sum_{n_z=0}^\infty \int_0^\infty \mathrm{d}k_x \int_0^\infty \mathrm{d}k_y \frac{n_z^2}{\sqrt{k_x^2 + k_y^2 + n_z^2 \frac{\pi^2}{a^2}}}$$

$$= \frac{\pi \hbar c}{4a^3} \sum_{n_z=0}^\infty \int_0^\infty \frac{n_z^2}{\sqrt{u + n_z^2 \frac{\pi^2}{a^2}}} \mathrm{d}u$$

$$= \frac{\pi^2 \hbar c}{4a^4} \sum_{n_z=0}^\infty \int_0^\infty \frac{n_z^2}{\sqrt{v + n_z^2}} \mathrm{d}v$$

$$= \frac{\pi^2 \hbar c}{2a^4} \sum_{n_z=0}^\infty n_z^2 \int_{n_z}^\infty \mathrm{d}w$$

where I made a series of variable substitutions: $u = k_x^2 + k_y^2$, $v = \frac{a^2}{\pi^2} u$ and $w = \sqrt{v + n_z^2}$. $\sum'$ is replaced by $\sum$ since the term with $k_z = 0$ equals zero.

The pressure on the outer side of the plates is similarly derived by turning summation into integration over n_z:

$$P^{\text{out}} = \frac{\pi^2 \hbar c}{2a^4} \int_0^\infty n_z^2 \mathrm{d}n_z \int_{n_z}^\infty \mathrm{d}w$$

The a dependence of the outer pressure seems confusing, since the radiation outside the plates does not feel the typical length scale a. In fact, since the vacuum energy diverges, it makes no sense to speak of the outer pressure alone. The only thing that has physical meanings is the pressure difference. If we regard P^{in} as the "infinite part" of P^{out}, it is then natural to use the inner distance a as a length scale of the outer pressure.

The finite pressure difference can be calculated using various regularization methods. For example, we can introduce a regulator $e^{-\varepsilon w}$ and use Euler-Maclaurin formula. Let $F(x) = x^2 \int_x^\infty e^{-\varepsilon x} dx = \frac{1}{\varepsilon} x^2 e^{-\varepsilon x}$. It is easy to get $F(0) = 0$, $F'(0) = 0$ and $F'''(0) = -6$.

$$P^{\text{in}} - P^{\text{out}} = \lim_{\varepsilon \to 0} \frac{\pi^2 \hbar c}{2a^4} \left(\sum_{n_z=0}^\infty{}' F(n_z) - \int_0^\infty F(n_z) \mathrm{d}n_z \right)$$

$$= \lim_{\varepsilon \to 0} \frac{\pi^2 \hbar c}{2a^4} \left(-\frac{1}{12} F'(0) + \frac{1}{720} F'''(0) + O(\varepsilon^2) \right)$$

$$= -\frac{\pi^2 \hbar c}{240 a^4}$$

The negative sign means the pressure outside the plates is larger. The value of the net inward pressure is identical to the calculation based on vacuum energy.

We can see some correlations between the vacuum energy approach and the radiation approach to the Casimir effect. The pressure can be thought of as being exerted by reflection of "virtual photons", which can be understood as fluctuations of vacuum energy due to the time-energy uncertainty principle.

V. DISCUSSIONS ON REGULARIZATION

A. Equivalence of Different Regularizations

So far, several different regularization methods are discussed. It is a surprising fact that they all lead to the same result. The Casimir effect seems to be independent of how the regulator suppresses the infinity. However, this is generally not true, for there exist regulators that fail to produce the correct result. A good regulator must satisfy certain conditions, which are discussed in [5] and [6].

B. Physical Views on Regularization

Regularization is not just a mathematical trick. It makes sense physically. In the derivation of the Casimir effect, divergence occurs because the frequencies that are summed over reach infinity (thus, it is called ultraviolet divergence). However, arbitrarily high frequencies bring about physical problems. One thing to notice is that the electrons inside the conducting plates cannot follow those very fast oscillating modes. Thus the boundary condition fails, and the plates become transparent. In other words, there is a frequency range out of which new physics appear and our theory breaks down.

To solve this problem, we can introduce a finite cutoff Λ to replace the infinite upper limit. Mathematical implementation of this cutoff is exactly the regulator that kills the high frequencies. The divergent sum or integral now becomes a finite but cutoff-dependent value. As is discussed in A. Zee's textbook [7], Λ should be regarded as a parameter that characterizes "the threshold of our ignorance". Indeed, we know nothing about the physics beyond Λ, and we do not know what value Λ itself is, either. But it is fine for us to be ignorant about these if we can remove Λ in the end.

The final result must be physically measurable. However, the vacuum energy itself is not such a quantity. It is the energy difference that should appear in the answer. This subtraction process is known as renormalization. By doing this, Λ cancels out, and we are left with a cutoff-independent energy difference. The cancellation of Λ is related to the fact that electromagnetism is a renormalizable theory [7].

VI. EXPERIMENTAL RESULTS

The Casimir effect is so weak that measurement is not an easy job. One of the first experimental tests was made by M. J. Sparnaay in 1958 [3]. In his experiment, Sparnaay designed a delicate lever system that converted the distance between two parallel plates into capacitance, which was much easier to measure. His result did not show contradiction against Casimir's prediction, but had an effective uncertainty of about 100%.

A much more accurate measurement was performed by S. K. Lamoureaux in 1997 [4], whose experiment involved a carefully designed electromechanical system based on a torsion pendulum. His results agreed with the theory by 5%.

VII.   CONCLUSIONS

The Casimir effect is an astonishing result of the quantization of electromagnetic field and the existence of vacuum energy. It shows that vacuum energy is not just a background that can be ignored or some auxiliary concepts in theories, but something that is concrete and can be experimentally observed. Results from labs further confirmed the "reality" of vacuum energy. However, other explanations to the Casimir effect do exist [13].

The Casimir effect has many potential applications. In 2001, H. B. Chan designed a nonlinear Casimir oscillator, which showed the possibility to use the Casimir effect to detect some microscopic structures [14]. Recent progress made by J. Zou *et al* demonstrated a possible way to harness vacuum energy from the Casimir effect [15].

[1] H. B. G. Casimir, D. Polder, Phys. Rev. **73**, 360 (1948).
[2] H. B. G. Casimir, Koninkl. Ned. Adak. Wetenschap. Proc. **51**, 793 (1948).
[3] M. J. Sparnaay, Physica (Utrecht) **24**, 751 (1958).
[4] S. K. Lamoreaux, Phys. Rev. Lett. **78**, 5 (1997).
[5] S. Brzezowski, Acta Physica Polonica, **12**, 295 (1981).
[6] S. Brzezowski, Acta Physica Polonica, **16**, 799 (1985).
[7] A. Zee, Quantum Mechanics in a Nutshell (2nd Edition).
[8] See, for example, K. A. Milton *et al*, J. Phys. A: Math. Theor. **45**, 374006 (2012).
[9] T. M. Apostol, Amer. Math. Monthly **106**, 409 (1999).
[10] NIST Digital Library of Mathematical Functions http://dlmf.nist.gov/.
[11] Blog of Terence Tao http://terrytao.wordpress.com/2010/04/10/.
[12] P. W. Milonni, R. J. Cook, M. E. Goggin, Phys. Rev. A, **38**, 1621 (1988).
[13] R. L. Jaffe, Phys. Rev. D, **72**, 021301 (2005).
[14] H. B. Chan, *et al*, Phys. Rev. Lett. **87**, 211801 (2001).
[15] J. Zou, *et al*, Nat. Commun. **4**, 1845 (2013).

Quantum Chemistry and the Hartree-Fock Method

Jonathan S. Jove

MIT Department of Physics, 77 Massachusetts Ave., Cambridge, MA 02139-4307

(Dated: May 2, 2014)

The Hartree-Fock method forms the theoretical foundation for all of modern quantum chemistry, specifically the theory of atomic and molecular orbitals. It provides a convenient approximate computational framework to determine the orbitals of individual electrons in multi-electron systems such as atoms, ions, and molecules. From these orbitals, a variety of other interesting quantities such as ionization energies and the total system energy can be calculated. In this paper, we will develop the theory of the Hartree-Fock method and apply it numerically to the helium atom.

I. INTRODUCTION

With the development of quantum theory came a great interest in the theoretical study of the spectra of atoms. While the hydrogen atom proved to be a tractable problem, with the energy of the nth level proportional to $1/n^2$, the multi-electron atoms presented great challenges. Even today there are no known exact analytic solutions to even the simplest multi-electron atom, helium. Many scientists resorted to ad hoc methods, such as the introduction of additional empirical parameters which were fit to known data. This approach has the obvious disadvantage that it does not make new predictions.

The Hartree-Fock method was developed as an ab initio technique for the study of multi-electron systems, such as atoms and molecules. It will be shown later in this paper that this method is in fact a mean field theory of independent particles. In practice, this means that each electron moves independently within the average potential that it experiences from the other electrons. The Hartree-Fock method is sometimes, especially in the older literature, referred to as the self-consistent field theory [1, 2]. The reason for this is that an initial configuration of the electrons within orbitals is assumed, and then more accurate orbitals are found using iterative optimization. At the end of the process, each electron is in the lowest energy state that it can occupy within the mean field of the other electrons. This implies that the field is self-consistent.

A. History

The development of the Hartree-Fock method occurred almost immediately following the discovery of the quantum theory. In 1928, the English physicist Douglas Hartree was working on a series of articles regarding the wave mechanics of particles in a non-Coulomb central field. In this work, Hartree first developed the basic theory for his eponymous method. He made a variety of approximations in order to reduce the problem of a particle in a non-Coulomb central field to an approximate problem which was more tractable. Although Hartree had been motivated by the prospects of an ab initio method

free of empirical parameters, many physicists of the time did not see or understand the theoretical basis for his method and viewed it as just another ad hoc approach.

Within months, the American physicist John Slater published an article discussing the validity of the approximations by Hartree. His goal was to develop a strong foundation upon which the self-consistent field theory could be built. What he found was that some of the approximations made by Hartree introduced error that could not be neglected. For example, Hartree assumed that all electron orbitals are spherical but this is clearly not a good approximation for some electrons of heavy elements. After fixing these mistakes, Hartree's method still did not agree well with experiment.

The reason for this disagreement was found independently by Slater and a Soviet physicist, Vladimir Fock, in 1930. They realized that the assumption made in Hartree's theory that a wave function could be written as a product of orbitals implied that all electrons were symmetric under exchange, while in reality it is known that electrons with the same spin are anti-symmetric under exchange. They proposed instead a trial wave function in which every electron was anti-symmetric under exchange with every other electron. This trial wave function, known as a Slater determinant, can be used in place of the Hartree product in Hartree's theory. This improved approach is known as the Hartree-Fock method.

B. Overview

In what follows the theory of the Hartree-Fock Method will first be developed thoroughly, and further approximations will be introduced which aid computational work within the Hartree-Fock framework. Then several applications will be explored including the helium atom.

II. THE THEORY OF THE HARTREE-FOCK METHOD

A. The Hartree-Fock Equation

The derivation of the Hartree-Fock equation begins from the non-relativistic time independent multi-electron

Schrödinger equation with N electrons and M nuclei. Let $\hbar$ denote the reduced Planck constant, m denote the electron mass, and e the electron charge. The position of electron i will be given as $\mathbf{r}_i$, and the position of nucleus j will be given as $\mathbf{R}_j$. The position of the nuclei are assumed to be fixed and will be treated as a parameter. This assumption that the position of the nuclei will be treated as a parameter when solving the multi-electron Schrödinger equation is known as the Born-Oppenheimer approximation and represents an indispensable simplification in quantum chemical calculations. In order to write this equation in a succinct form, one- and two-electron operators will be introduced. The one-electron operator is defined as

$$h_i = \frac{-\hbar^2}{2m}\nabla_i^2 - e^2\sum_{j=1}^{M}\frac{Z_j}{|\mathbf{R}_j - \mathbf{r}_i|} \tag{1}$$

where the first term is the kinetic energy of electron i, and the second term is the Coulomb interaction of electron i with each nucleus. Here we let Z_j be the atomic number of nucleus j. The two-electron operator is defined as

$$k_{i,j} = \frac{e^2}{|\mathbf{r}_i - \mathbf{r}_j|}. \tag{2}$$

and determines the energy of electron i from its interaction with electron j. We also introduce the potential energy from interactions between nuclei, which is given by

$$V = e^2\sum_{i=1}^{M}\sum_{j=i+1}^{M}\frac{Z_iZ_j}{|\mathbf{R}_i - \mathbf{R}_j|}. \tag{3}$$

Then it is clear that the non-relativistic time independent multi-electron Schrödinger equation can be written as

$$\left[\sum_{i=1}^{N}h_i + \sum_{i=1}^{N}\sum_{j=i+1}^{N}k_{i,j} + V\right]|\Psi\rangle = E|\Psi\rangle \tag{4}$$

where it should be noted that while the nuclear positions do not appear explicitly in the equation when written in this form, both the energy eigenvalues E and the energy eigenstates Ψ do depend on the nuclear positions.

All that has been done up to this point is to express the Hamiltonian for the multi-electron system in a convenient form. Still, it is well known that this problem is intractable so an approximation must be employed. Following in the footsteps of Slater and Fock, it is assumed that the wave function is a single fully antisymmetric function of individual spin orbitals, where the spin orbital for electron i, denoted by $|i\rangle$, is a function of the position and spin of electron i only. This fully antisymmetric function is known as a Slater determinant and can be written as a sum over permutations

$$|\Psi\rangle = \frac{1}{\sqrt{N!}}\sum_{\sigma\in S_N}\text{sgn}(\sigma)\bigotimes_{i=1}^{N}|\sigma(i)\rangle \tag{5}$$

where the sign of a permutation is $\text{sgn}(\sigma) = (-1)^n$ with n the number of transpositions, and $\sigma(i)$ denotes the element in the ith position of σ. It is assumed without loss of generality that the spin orbitals are orthonormal. Although the spin is not written explicitly, it is important to remember that it must be included in the calculation of inner products. For example, given an operator A which acts on only the spatial components of the wave function and two spin orbitals $|1\rangle$ and $|2\rangle$, then

$$\langle 1|\,A\,|2\rangle = \langle\phi_1|\,A\,|\phi_2\rangle\,\langle s_1|s_2\rangle$$

where ϕ_1, ϕ_2 are the spatial components of the spin orbitals and s_1, s_2 are the spin components of the spin orbitals. This result will be critical in the analysis to follow.

With this approximate wave function Ψ, the variational principle can now be employed to find the Hartree-Fock energy as

$$E_{HF} = \frac{\langle\Psi|\,H\,|\Psi\rangle}{\langle\Psi|\Psi\rangle}$$

$$= \sum_{\alpha,\beta\in S_N}\text{sgn}(\alpha)\text{sgn}(\beta)\left(\bigotimes_{i=1}^{N}\langle\alpha(i)|\right)H\left(\bigotimes_{j=1}^{N}|\beta(j)\rangle\right)$$

and it is known that $E \leq E_{HF}$ from the variational bound [3]. The above expression however is not very useful or easy to work with, and so the goal is to simplify it. Note that H is simply a linear combination of the one- and two-electron operators. Therefore, we can simplify the expression for E_{HF} by simplifying inner products involving the individual operators.

Let us begin with the one-electron operator h_i. It is apparent that h_i acts only on the spatial components of electron i. Then

$$\left(\bigotimes_{i=1}^{N}\langle\alpha(i)|\right)h_l\left(\bigotimes_{j=1}^{N}|\beta(j)\rangle\right)$$

$$= \left(\prod_{i\neq l}^{N}\langle\alpha(i)|\beta(j)\rangle\right)\langle\beta(l)|\,h_l\,|\alpha(l)\rangle$$

$$= \begin{cases}\langle\alpha(l)|\,h_l\,|\alpha(l)\rangle & : \alpha(i) = \beta(i)\,\forall i \\ 0 & : \text{otherwise}\end{cases}$$

where the first equality follows from the properties of tensor products. The second equality follows from the fact that the spin orbitals are orthonormal, so the product would be zero if $\alpha(i) \neq \beta(i)$ for some $i \neq l$. But then since α and β are permutations which agree at all indices but one, they must be the same permutation.

We now turn our attention to the two-electron operator $k_{i,j}$. It is again apparent that $k_{i,j}$ acts only on the spatial

components of electrons i and j. Then

$$\left(\bigotimes_{i=1}^{N}\langle\alpha(i)|\right)k_{l,m}\left(\bigotimes_{j=1}^{N}|\beta(j)\rangle\right)$$

$$=\left(\prod_{i\neq l,m}^{N}\langle\alpha(i)|\beta(j)\rangle\right)\langle\alpha(l)\alpha(m)|\,k_{l,m}\,|\beta(l)\beta(m)\rangle$$

$$=\begin{cases}\langle\alpha(l)\alpha(m)|\,k_{l,m}\,|\beta(l)\beta(m)\rangle & :\ \alpha(i)=\beta(i)\,\forall i\neq l,m\\ 0 & :\ \text{otherwise}\end{cases}$$

where the first equality follows from the properties of tensor products. The second equality follows from the fact that the spin orbitals are orthonormal, so the product would be zero if $\alpha(i)\neq\beta(i)$ for some $i\neq l,m$. But then since α and β are permutations which agree at all indices but two, the two permutations must either be the same or have one relative transposition.

These two identities lead to a remarkable simplification of the expression for the Hartree-Fock energy. By simply expanding H and substituting the previous two results concerning h_i and $k_{i,j}$ into the expression for the Hartree-Fock energy, it is found that

$$E_{HF}=V+\sum_{i=1}^{N}\langle i|\,h_1\,|i\rangle$$

$$+\frac{1}{2}\sum_{i=1}^{N}\sum_{j\neq i}^{N}\left[\langle ij|\,k_{1,2}\,|ij\rangle-\langle ii|\,k_{1,2}\,|jj\rangle\right].\quad(6)$$

It is important to note here that we have transitioned from the notation h_l to h_1 and from $k_{l,m}$ to $k_{1,2}$. We are able to do this because of the fact that electrons are indistinguishable. This implies that whether we discuss spin orbital $|i\rangle$ described by $\mathbf{x}_i$ or spin orbital $|i\rangle$ described by $\mathbf{x}_1$ is entirely irrelevant.

The contributions to this energy cannot all be explained classically. The first term V can easily be traced back to the energy which results from the Coulomb repulsion between distinct nuclei. Each term of the form $\langle i|\,h_1\,|i\rangle$ is the contribution to the energy from the kinetic energy of electron i and its Coulomb interaction with the nuclei. Each term of the form $\langle ii|\,k_{1,2}\,|jj\rangle$ is the energy contribution from the Coulomb interaction between electrons i and j. However, the terms of the form $\langle ij|\,k_{1,2}\,|ij\rangle$ are not classical in nature. These terms are a result of the anti-symmetry under exchange of electrons with the same spin, and as such it is said that these terms correspond to the exchange interaction.

It is worth noticing that when $i=j$, the Coulomb interaction involving electrons i and j is equal to the exchange interaction involving electrons i and j. This is a purely mathematical statement as it is well known that an electron does not experience Coulomb or exchange interactions with itself. Still, this mathematical result

allows one to write

$$E_{HF}=V+\sum_{i=1}^{N}\langle i|\,h_1\,|i\rangle$$

$$+\frac{1}{2}\sum_{i,j=1}^{N}\left(\langle ij|\,k_{1,2}\,|ij\rangle-\langle ij|\,k_{1,2}\,|ji\rangle\right)\quad(7)$$

where the restriction that $j\neq i$ has been removed because the Coulomb and exchange interactions cancel when $i=j$.

The reason the variational principle was employed was that it would allow us to find good electron orbitals by minimizing the Hartree-Fock energy. The goal then is to minimize this energy with respect to any possible variation in each χ_i. However, the equations derived above are valid only if the spin orbitals are orthonormal. Therefore, we apply the technique of Lagrange multipliers to ensure that the spin orbitals remain orthonormal through the optimization procedure. To this end we introduce the functional

$$\mathcal{L}=E_{HF}-\sum_{i=1}^{N}\sum_{j=1}^{N}\epsilon_{i,j}(\langle i|j\rangle-\delta_{i,j})\quad(8)$$

with Lagrange multipliers $\epsilon_{i,j}$. It follows that the functional derivative of $\mathcal{L}$ with respect to $|i\rangle$ must be 0 for each i. Evaluating each of these functional derivatives is merely a mathematical exercise, and as such we state the result without proof. Then if f denotes the arbitrary test function, it is found

$$0=\langle f|\,h_1\,|i\rangle-\sum_{j=1}^{N}\epsilon_{i,j}\,\langle f|j\rangle$$

$$+\sum_{j=1}^{N}(\langle fj|\,k_{1,2}\,|ij\rangle-\langle fj|\,k_{1,2}\,|j\chi_i\rangle)\quad(9)$$

for each i. Now applying the fundamental lemma of calculus of variations leads to the integro-differential equation

$$(h_1+\mathcal{J}-\mathcal{K})\,|i(\mathbf{x_1})\rangle=\sum_{j=1}^{N}\epsilon_{i,j}\,|j(\mathbf{x_1})\rangle\quad(10)$$

where $\mathcal{J}$ is the Coulomb operator defined by

$$\mathcal{J}\,|i(\mathbf{x_1})\rangle=|i(\mathbf{x_1})\rangle\sum_{j=1}^{N}\langle j(\mathbf{x_2})|\,k_{1,2}\,|j(\mathbf{x_2})\rangle\quad(11)$$

and $\mathcal{K}$ is the exchange operator defined by

$$\mathcal{K}\,|i(\mathbf{x_1})\rangle=|j(\mathbf{x_1})\rangle\sum_{j=1}^{N}\langle j(\mathbf{x_2})|\,k_{1,2}\,|i(\mathbf{x_2})\rangle.\quad(12)$$

We then define the Fock operator for electron i as

$$\mathcal{F}_i=h_i+\mathcal{J}-\mathcal{K}\quad(13)$$

so the integro-differential equation for the spin orbitals can be written as

$$\mathcal{F}_1 \left|i(\mathbf{x}_1)\right\rangle = \sum_{j=1}^{N} \epsilon_{i,j} \left|j(\mathbf{x}_1)\right\rangle. \tag{14}$$

It should be noted that the Fock operator is Hermitian. This can be seen because any linear combination of Hermitian operators is also Hermitian. As it is apparent by inspection that h_i is Hermitian, it remains to be shown that $\mathcal{J}$, and $\mathcal{K}$ are Hermitian. But it is similarly apparent that $k_{i,j}$ is Hermitian as it is a simple function of the coordinates. Then

$$\left\langle i\right| \mathcal{J} \left|j\right\rangle = \sum_{k=1}^{N} \left\langle ik\right| k_{1,2} \left|jk\right\rangle$$
$$= \sum_{k=1}^{N} \left\langle jk\right| k_{1,2} \left|ik\right\rangle$$
$$= \left\langle j\right| \mathcal{J} \left|i\right\rangle$$

where the second equality follows from the Hermiticity of $k_{i,j}$. Similarly,

$$\left\langle i\right| \mathcal{K} \left|j\right\rangle = \sum_{k=1}^{N} \left\langle ik\right| k_{1,2} \left|kj\right\rangle$$
$$= \sum_{k=1}^{N} \left\langle kj\right| k_{1,2} \left|ik\right\rangle$$
$$= \left\langle j\right| \mathcal{K} \left|i\right\rangle$$

which completes the argument.

At this point, the $\epsilon_{i,j}$ are still undetermined coefficients. It is easy to see then that the $\epsilon_{i,j}$ are simply the matrix elements of the Fock operator in the spin orbital basis. Then we write

$$\epsilon_{i,j} = \left\langle j\right| \mathcal{F}_1 \left|i\right\rangle \tag{15}$$

and note that the set of integro-differential equations for the spin orbitals is now

$$\mathcal{F}\chi = \chi\epsilon \tag{16}$$

where $\mathcal{F}$ is a vector of Fock operators, χ is a row vector of spin orbitals, and ϵ is the matrix of Lagrange multipliers. But due to the Hermiticity of the Fock operators, ϵ is Hermitian and it admits a representation of the form $\epsilon = U\epsilon'U^\dagger$ where ϵ' is a diagonal matrix and U is a unitary matrix. Then

$$\mathcal{F}\chi = \chi U\epsilon'U^\dagger \tag{17}$$

which can alternatively be written as

$$\mathcal{F}\chi U = \chi U\epsilon'. \tag{18}$$

Finally we define $\chi' = \chi U$ and note that this basis of spin orbitals is orthogonal. Therefore it is just as good

of a choice of spin orbitals as our initial spin orbitals. An important remark is that the Fock operators always send a spin orbital to a linear combination of other spin orbitals, so the ϵ matrix is unchanged under a unitary transformation of the spin orbitals. Then we forget about our initial basis, omit the primes in our notation, and find that

$$\mathcal{F}_1 \left|i\right\rangle = \epsilon_i \left|i\right\rangle \tag{19}$$

This is known as the canonical Hartree-Fock equation [4, 5], and the ϵ_i denotes the energy of orbital i.

It is here that it finally becomes apparent that the Hartree-Fock method is a mean field theory of independent particles. The Fock operator is a linear combination of the Coulomb operator and exchange operator. These operators represent the average potential generated by all of the other electrons from the Coulomb and exchange interactions, respectively. But none of the instantaneous positions of electrons appear explicitly in this expression. Therefore the assumption that the multi-electron wavefunction can be represented as a single Slater determinant leads inevitably to the result that each electron approximately experiences the average potential generated by the other electrons.

While the Hartree-Fock equation appears to be an eigenvalue problem, it is actually a highly nonlinear relationship between the spin orbitals. This can be seen by observing that the Fock operators depend on the spin orbitals, which implies that the solution to the equation is a complicated function of itself. Therefore the equation is normally solved iteratively by guessing spin orbitals and then solving for the resulting spin orbitals until they approach a stationary solution. It is for this reason that the Hartree-Fock equation is known as the self-consistent field theory. When the solution ceases to change, the potentials generated by the spin orbitals are consistent with the potentials that they experience.

B. The Hartree-Fock-Roothaan Equation

As noted at the end of the previous section, the Hartree-Fock equation is a nonlinear equation for the spin orbitals. Unfortunately, the very compact notation for the equation obscures the fact that it is actually a nonlinear integro-differential equation. The prospect of solving such an equation, even with great computer assistance, is extremely daunting. Therefore, the Dutch physicist Roothaan in 1951 made an additional approximation which made the method better adapted to use on computers. His approximation was simply to consider a finite basis of functions for the spin orbitals [6]. This allows one to transform the nonlinear integro-differential equation into a nonlinear matrix equation which is much more tractable.

The derivation of the Hartree-Fock-Roothaan equation resumes where we ended in the previous section. It is

assumed that a spin orbital can be written as a sum of K basis states such as

$$|i\rangle = \sum_{j=1}^{K} C_{j,i} |\tilde{\chi}_j\rangle. \tag{20}$$

Then the Hartree-Fock equation for such a state can be written as

$$\mathcal{F}_1 \sum_{j=1}^{K} C_{j,i} |\tilde{\chi}_j\rangle = \epsilon_i \sum_{j=1}^{K} C_{j,i} |\tilde{\chi}_j\rangle. \tag{21}$$

Taking the inner product of this equation with each $\tilde{\chi}_k$ yields

$$\sum_{j=1}^{K} C_{j,i} \langle \tilde{\chi}_k | \mathcal{F}_i |\tilde{\chi}_j\rangle = \epsilon_i \sum_{j=1}^{K} C_{j,i} \langle \tilde{\chi}_k | \tilde{\chi}_j\rangle. \tag{22}$$

After expanding the Fock operator and applying linearity, it is found that

$$\sum_{j=1}^{K} C_{j,i} \langle \tilde{\chi}_k | (h_1 + \mathcal{J} - \mathcal{K}) |\tilde{\chi}_j\rangle = \epsilon_i \sum_{j=1}^{K} C_{j,i} \langle \tilde{\chi}_k | \tilde{\chi}_j\rangle. \tag{23}$$

However, at this point it must be recalled that $\mathcal{J}$ and $\mathcal{K}$ are themselves functions of the spin orbitals. Therefore they can also be expanded in terms of the basis functions. Then we consider

$$\langle \tilde{\chi}_k | \mathcal{J} |\tilde{\chi}_j\rangle = \sum_{n=1}^{N} \sum_{l,m=1}^{K} C_{l,n}^* C_{m,n} \langle \tilde{\chi}_k \tilde{\chi}_l | k_{1,2} |\tilde{\chi}_j \tilde{\chi}_m\rangle$$

where the first equality follows from expanding each spin orbital in terms of the basis functions. We similarly find that

$$\langle \tilde{\chi}_k | \mathcal{K} |\tilde{\chi}_j\rangle = \sum_{n=1}^{N} \sum_{l,m=1}^{K} C_{l,n}^* C_{m,n} \langle \tilde{\chi}_k \tilde{\chi}_l | k_{1,2} |\tilde{\chi}_m \tilde{\chi}_j\rangle$$

by using the same approach as was used for $\mathcal{J}$. Substituting these two results into (23) leads to the matrix equation

$$FC = SC\epsilon \tag{24}$$

where F is the Fock matrix whose elements are

$$F_{i,j} = \langle \tilde{\chi}_i | h_1 |\tilde{\chi}_i\rangle$$
$$+ \sum_{l,m=1}^{K} (CC^\dagger)_{l,m} (\langle \tilde{\chi}_i \tilde{\chi}_l | k_{1,2} |\tilde{\chi}_j \tilde{\chi}_m\rangle - \langle \tilde{\chi}_i \tilde{\chi}_l | k_{1,2} |\tilde{\chi}_m \tilde{\chi}_j\rangle)$$

and S is the overlap matrix whose elements are

$$S_{i,j} = \langle \tilde{\chi}_i | \tilde{\chi}_j\rangle.$$

This matrix equation is known as the Hartree-Fock-Roothaan equation [4–6] and is used for finding approximate numerical solutions to the Hartree-Fock equation.

C. Results of the Hartree-Fock Method

The first important step to making the Hartree-Fock method more intuitive is to determine the Hartree-Fock energy of the atomic or molecular system from the orbital energies. Beginning from the Hartree-Fock equation, it is known that

$$\mathcal{F}_1 |i\rangle = \epsilon_i |i\rangle$$

which, after taking the inner product with $\langle i|$, implies that

$$\epsilon_i = \langle i| \mathcal{F}_1 |i\rangle$$
$$= \langle i| h_1 |i\rangle + \langle i| \mathcal{J} |i\rangle - \langle i| \mathcal{K} |i\rangle. \tag{25}$$

An expression for the Hartree-Fock energy was given in (6) and can be expressed more compactly using the Coulomb and exchange operators as

$$E_{HF} = V + \sum_{i=1}^{N} \left[\langle i| h_i |i\rangle + \frac{1}{2} \langle i| (\mathcal{J} - \mathcal{K}) |i\rangle \right]$$
$$= V + \sum_{i=1}^{N} \epsilon_i - \frac{1}{2} \sum_{i=1}^{N} \langle i| (\mathcal{J} - \mathcal{K}) |i\rangle \tag{26}$$

where the second equality follows from direct substitution. This shows that adding the energies of the occupied orbitals does not lead to the correct ground state energy for the system. This is to be expected, as the energy of each electron already contains contributions from the average potential of each other electron. Then adding the orbital energies directly should lead to a double counting of both Coulomb and exchange energies. It is apparent that the above formula rectifies this double counting issue.

But if the orbital energies do not directly correspond to the ground state energy, then one might wonder what they are. This question was answered elegantly by Tjalling Koopmans, a Dutch-American mathematician and economist who briefly studied theoretical physics. Koopmans' theorem, which we will subsequently prove, states that the orbital energies are the ionization energies of the system in the approximation that the orbitals of the ion are identical to those of the neutral system. This is sometimes referred to as the frozen orbital approximation [4].

Let $E_{HF}(N)$ denote the Hartree-Fock energy when there are N electrons occupying orbitals. Suppose that an electron is to be removed from orbital k. Then in the frozen orbital approximation, the ionization energy is given by

$$I = E_{HF}(N-1) - E_{HF}(N)$$

which can be readily written as

$$I = \sum_{i \neq k}^{N} \langle i| h_1 |i\rangle - \sum_{i=1}^{N} \langle i| h_1 |i\rangle$$

$$+ \frac{1}{2} \sum_{i \neq k}^{N} \sum_{j \neq k}^{N} [\langle ij| k_{1,2} |ij\rangle - \langle ii| k_{1,2} |jj\rangle]$$

$$- \frac{1}{2} \sum_{i=1}^{N} \sum_{j=1}^{N} [\langle j| k_{1,2} |ij\rangle - \langle ii| k_{1,2} |jj\rangle]$$

by using (6). But many terms in this complicated expression cancel, leaving

$$I = - \langle k| h_1 |k\rangle$$

$$- \sum_{i \neq k}^{N} [\langle ik| k_{1,2} |ik\rangle - \langle ii| k_{1,2} |kk\rangle].$$

Noting again that the Coulomb and exchange terms cancel when $i = k$, this expression can be converted to one involving the Coulomb and exchange operators as

$$I = - \langle k| h_1 |k\rangle - \langle k| \mathcal{J} |k\rangle + \langle k| \mathcal{K} |k\rangle$$

$$= -\epsilon_k \tag{27}$$

which completes the proof of Koopmans' theorem.

This is a powerful result that provides a lot of intuition about which spin orbitals are occupied in an atomic or molecular system. Specifically, by applying Koopmans' theorem, one can see that the system would lose energy if an electron transitioned from a spin orbital with higher orbital energy to one with lower orbital energy. Therefore it is expected that, in the ground state of the system, the electrons will always occupy the lowest energy orbitals. This is a very intuitive result, and it is a relief that orbital energy does indeed satisfy our expectation of energy minimization.

III. APPLICATIONS OF THE HARTREE-FOCK METHOD

The Hartree-Fock method is a computational tool. For that reason, no discussion of it would be complete without a simulation. The purpose of this will be to test some of the predictions of the Hartree-Fock method and compare them to accepted experimental values.

It should be noted at this point that most implementations of the Hartree-Fock method employ the Hartree-Fock-Roothaan equation. This has been done in our implementation as well. Furthermore, most implementations use Gaussian functions as the basis function for the spatial components of their spin orbitals. This is done to enable fast computation of one- and two-electron integrals. We chose instead to use the basis of hydrogen type orbitals, as their physical interpretation is more natural. To be specific, the hydrogen type orbitals are the orbitals of a single electron around a nucleus of known atomic number.
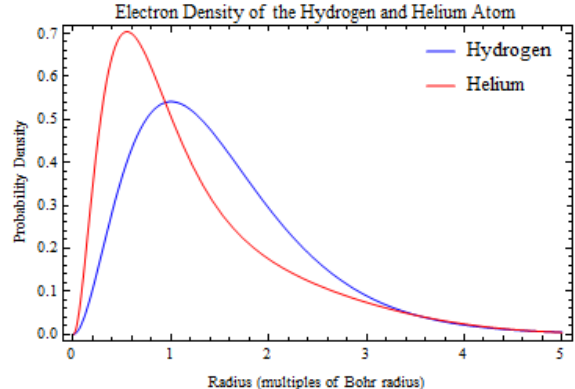

FIG. 1: The electron density of the helium atom as a function of radius in units of the Bohr radius.

A. Helium Atom

Let $|n, l, m, s\rangle$ denote an energy eigenstate of the helium ion He^+. Then we choose the basis functions for this model of the helium atom to be $|1, 0, 0, s\rangle$, $|2, 0, 0, s\rangle$, and $|3, 0, 0, s\rangle$ where $s = \pm\frac{1}{2}$. For notational convenience, we let $+$ denote $s = \frac{1}{2}$ and $-$ denote $s = -\frac{1}{2}$. These states were chosen for the basis functions because when the helium atom is ionized, the energy eigenstates of the remaining electron are the basis functions. This provides us with a natural system in which one can explore Koopmans' theorem and the frozen orbital approximation.

We began with the initial assumption that the orbitals of He were the orbitals of He^+. From this ansatz, the Hartree-Fock-Roothaan equation was solved iteratively using standard numerical methods for integration and linear algebra. It was found that the ground state of helium is approximately

$$|\Phi\rangle = (.93 |1, 0, 0, +\rangle - .36 |2, 0, 0, +\rangle - .10 |3, 0, 0, +\rangle)$$
$$\otimes (.93 |1, 0, 0, -\rangle - .36 |2, 0, 0, -\rangle - .10 |3, 0, 0, -\rangle).$$

By applying (26), it was determined that this state corresponds to a ground state energy of approximately $E_0 = -76.43$ eV. The accepted value of the ground state energy is about $E_0 = -79.00$ eV [7], which means that the Hartree-Fock-Roothaan method with only three basis functions achieves a relative error of only 3.3%. This relative error could be significantly reduced by increasing the size of the set of basis functions.

The first ionization energy of helium was then found, by applying Koopmans' theorem, to be $I_1 = 24.44$ eV. The accepted value of this quantity is about $I_1 = 24.59$ eV [7] which means that relative error of the Hartree-Fock-Roothaan method with only three basis functions is only 0.56%. This is a great success of the theory, and it is generally true that the ionization energies predicted by the Hartee-Fock method agree well with experiment. It is interesting that the prediction is accurate even though the remaining electron should be

in its true spatial orbital, the $|1, 0, 0\rangle$ spatial state, about 86% of the time in the frozen orbital approximation.

IV. CONCLUSION

The Hartree-Fock method is a powerful ab initio tool to make predictions about atomic and molecular systems. It makes good predictions about the ground state energy of a system and can accurately approximate the ionization energy for electrons in different orbitals. The method also makes it possible to accurately determine the shapes of orbitals and the electron density which can be used to predict chemical and electrical properties. Furthermore, all of this can be done efficiently with the Hartree-Fock-Roothaan equation when working in a particular basis of functions such as the atom-centered Gaussian functions.

Despite these advantages of the Hartree-Fock method, it is an approximate method. It sometimes fails by underestimating the electron correlation. This leads to errors in the energy of the system, which can present a significant problem when considering certain molecular systems. For example, in molecules which are extremely unstable due to very low bond energies between certain atoms, the Hartree-Fock method may predict that these systems actually do not form.

In these cases, it is necessary to turn to even more powerful methods. These methods, built upon the Hartree-Fock method, are appropriately called post Hartree-Fock methods. One popular method is known as Møller-Plesset perturbation theory. It adds more electron correlation to the Hartree-Fock method by introducing it as a perturbation. There are many other techniques which are used to enhance the Hartree-Fock method and they present a rich area for further study.

[1] D. R. Hartree, *The wave mechanics of an atom with a non-coulomb central field. part ii. some results and discussion.*
[2] J. C. Slater, *The self consistent field and the structure of atoms.*
[3] D. J. Griffiths, *Introduction to Quantum Mechanics* (Prentice Hall, Upper Saddle River, NJ, 2005).
[4] D. B. Cook, *Handbook of Computational Quantum Chemistry* (Dover, Mineola, NY, 2005).
[5] D. B. Cook, A. Szabo, and N. S. Ostlund, *Modern Quantum Chemistry: Introduction to Advanced Electronic Structure* (Dover, Mineola, NY, 1996).
[6] C. C. J. Roothaan, *New developments in molecular orbital theory.*
[7] A. Kramida, Yu. Ralchenko, J. Reader, and NIST ASD Team, NIST Atomic Spectra Database (ver. 5.1), [Online]. Available: `http://physics.nist.gov/asd` [2014, April 18]. National Institute of Standards and Technology, Gaithersburg, MD. (2013).
[8] C. C. J. Roothaan, *A study of two-center integrals useful in calculations on molecular structure.*

Optical Properties of Lateral Quantum Dots

Alex Kiefer

(Dated: May 2, 2014)

We provide a derivation of the eigenenergies for a single-particle quantum dot implemented as a thin sample of a III/V compound between two barriers, using the radial Schrödinger equation. The response of the QD to infrared radiation and allowed energy transitions are analyzed. Then we will describe a multiple-particle QD with a sample interaction potential. Raising and lowering operators are used to factorize the Hamiltonian and decompose it into center of mass and relative modes. Finally, we demonstrate that the optical response is independent of the particle number.

I. INTRODUCTION

Advances in nanofabrication techniques have revealed a myriad of structures with valuable electronic properties and powerful applications. By arranging semiconductors and metals in clever arrangments, we can trap particles in nanometer-sized pockets. This was first done with the quantum well, a two-dimensional electron gas suspended between two semiconductor barriers. It wasn't long until the quantum wire (1-D) and quantum dot (0-D) were developed as well. Quantum dots (QDs) have been dubbed "artificial atoms" because they have properties similar to an atomic nucleus but on a much larger scale.

There are various ways to design a QD and sometimes QDs appear spontaneously as a byproduct of other processes. In this paper we will deal with the lateral QD, a small conducting "island" of free electrons tens of nm wide and a few nm tall. Fabrication begins with two large semiconductor slabs separated by a quantum well made of a III-V compound such as GaAs. A polymer mask is applied everywhere on the top surface except the desired location of the QD, like a photographic negative. The whole top surface is etched with an ion beam, which erodes the outer annulus and leaves behind only a cylinder (see Fig. 1). The small disk of GaAs left behind is the quantum dot, with the electrons confined in all spatial dimensions. Although there's no way to measure the potential experienced by the electrons, it has often been modeled as a quadratic potential with good agreement with experimental results. [9]

Much research is focused on the application of QDs as photodetectors. As we will show, QDs are excellent at absorbing light in a narrow frequency band. They can be used in digital cameras, with different sized QDs used to measure the incident light in different visible bands. In astronmy, the QD can be tuned so its optical resonance matches the phenomenon we wish to observe – for example, the chemical reactions that accompany a red giant's transition to a white dwarf.

II. SINGLE ELECTRON

Here we will compute the energy eigenvalues for a QD in a lateral confinement $V(r, \phi) = \frac{1}{2} m \omega_0 r^2$ and a magnetic field orthogonal to the plane of the quantum well.
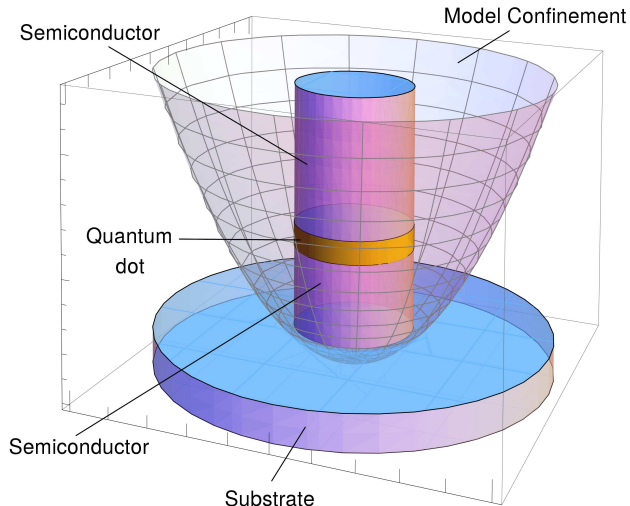
FIG. 1: A lateral quantum dot and the potential well used to model the confinement.

The potential is modeled as a harmonic oscillator with strength ω_0; this strength is inversely related to the size of the QD, since a smaller disk binds the electrons more tightly. The actual value of ω_0 that gives the most accurate predictions depends on the material used for the QD. The magnetic field and magnetic potential are

$$\mathbf{B} = B\hat{\mathbf{z}} = \nabla \times \mathbf{A} = \left(\frac{A_\phi}{r} + \frac{\partial A_\phi}{\partial r} - \frac{1}{r} \frac{\partial A_r}{\partial \phi} \right) \hat{\mathbf{z}}$$

$$\Rightarrow \mathbf{A} = \frac{B}{2} r \hat{\boldsymbol{\phi}} \tag{1}$$

The Hamiltonian with a magnetic potential $\mathbf{A}$ in two dimensions can be derived from the Euler-Lagrange Equation. Denoting the electron mass by m, electron charge by e, the result is

$$\mathcal{H} = \frac{1}{2m}\left(\mathbf{p} + \frac{e}{c}\mathbf{A}\right)^2 + \frac{1}{2}m\omega_0^2 r^2 \tag{2}$$

$$= \frac{p^2}{2m} + \frac{e}{2mc}\left(\mathbf{p}\cdot\mathbf{A} + \mathbf{A}\cdot\mathbf{p}\right) + \frac{e^2}{2mc^2}A^2 + \frac{1}{2}m\omega_0^2 r^2$$

$$= -\frac{\hbar^2}{2m}\nabla^2 - i\frac{e\hbar}{2mc}\left(\nabla\cdot\mathbf{A} + \mathbf{A}\cdot\nabla\right)$$
$$+ \frac{e^2}{2mc^2}A^2 + \frac{1}{2}m\omega_0^2 r^2 \tag{3}$$

The notation might be misleading; we must be careful to treat both $\nabla\cdot\mathbf{A}$ and $\mathbf{A}\cdot\nabla$ as operators acting on the wavefunction ($\nabla\cdot\mathbf{A}$ is not a scalar). Since the electron is constrained to two dimensions, $\psi = \psi(r,\phi)$. The Laplacian and gradient have the following forms in polar coordinates:

$$\nabla^2 = \frac{\partial^2}{\partial r^2} + \frac{1}{r}\frac{\partial}{\partial r} + \frac{1}{r^2}\frac{\partial^2}{\partial\phi^2}$$

$$\nabla = \hat{\mathbf{r}}\frac{\partial}{\partial r} + \hat{\phi}\frac{1}{r}\frac{\partial}{\partial\phi}$$

$$\text{so,}\ \ \nabla\cdot\mathbf{A}(\psi) = \frac{1}{r}\frac{\partial}{\partial\phi}(A_\phi\psi) = \frac{B}{2}\frac{\partial\psi}{\partial\phi}$$

$$\mathbf{A}\cdot\nabla(\psi) = A_\phi\frac{1}{r}\frac{\partial}{\partial\phi} = \frac{B}{2}\frac{\partial\psi}{\partial\phi}$$

Substituting these into (3) and noting that $A^2 = \frac{1}{4}B^2 r^2$, we obtain for the time-independent Schrödinger equation,

$$-\frac{\hbar^2}{2m}\left(\frac{\partial^2\psi}{\partial r^2} + \frac{1}{r}\frac{\partial\psi}{\partial r} + \frac{1}{r^2}\frac{\partial^2\psi}{\partial\phi^2}\right) - i\frac{eB\hbar}{2mc}\frac{\partial\psi}{\partial\phi}$$
$$+ \left(\left(\frac{e^2 B^2}{8mc^2} + \frac{1}{2}m\omega_0^2\right)r^2 - E\right)\psi = 0 \tag{4}$$

Now, assuming ψ is separable into functions of r and ϕ, we express it as $\psi(r,\phi) = R(r)\Phi(\phi)$. It must also be periodic in ϕ, so we may choose basis states

$$\psi(r,\phi) = R(r)e^{i\ell\phi} \tag{5}$$

where ℓ is the azimuthal quantum number. Defining the cyclotron frequency $\omega_c = eB/mc$, we substitute (5) into (4) to get

$$\frac{\hbar^2}{2m}\left(\frac{d^2R}{dr^2} + \frac{1}{r}\frac{dR}{dr} - \frac{\ell^2}{r^2}R\right) - \frac{1}{2}\hbar\omega_c\ell R$$
$$+ \left[E - \frac{1}{2}m\left(\omega_0^2 + \left(\frac{\omega_c}{2}\right)^2\right)r^2\right]R = 0 \tag{6}$$

Now we introduce the dimensionless variable u and frequency Ω:

$$u = \frac{m\Omega}{\hbar}r^2 \tag{7}$$

$$\Omega = \sqrt{\omega_0^2 + \left(\frac{\omega_c}{2}\right)^2} \tag{8}$$

so (6) becomes

$$\frac{\hbar^2}{2m}\left(\left(\frac{du}{dr}\right)^2\frac{d^2R}{du^2} + \left(\frac{d^2u}{dr^2} + \frac{1}{r}\frac{du}{dr}\right)\frac{dR}{du} - \frac{m\Omega\ell^2}{\hbar}\frac{R}{u}\right)$$
$$+ \left(E - \frac{1}{2}m\Omega^2 r^2 - \frac{1}{2}\hbar\omega_c\ell\right)R$$

$$= \hbar\Omega\left(u\frac{d^2R}{du^2} + \frac{dR}{du} - \frac{\ell^2}{4u}R\right)$$
$$+ \left(\frac{E}{2} - \frac{1}{4}\hbar\Omega u - \frac{1}{4}\hbar\omega_c\ell\right)R = 0$$

Letting $\beta = \frac{E}{2\hbar\Omega} - \frac{\omega_c\ell}{4\Omega}$, this simplifies to the radial equation

$$u\frac{d^2R}{du^2} + \frac{dR}{du} + \left(\beta - \frac{u}{4} - \frac{\ell^2}{4u}\right)R = 0$$

This equation can be solved analytically, but the proof is obscure and not very illustrative, so we will simply quote the results. [3] The allowed eigenenergies for which this equation has a solution are

$$E_{n\ell} = (2n + 1 + |\ell|)\hbar\Omega - \frac{1}{2}\ell\hbar\omega_c \tag{9}$$

where n is the radial quantum number, analogous to that of the hydrogen atom. These are graphed in Fig. 2. When $B = 0$, the energies form the familiar ladder with a spacing of $\hbar\omega_0$ and degeneracy increasing by 1 with each step. When B is large, $\omega_c \gg \omega_0$, and the energies bunch together into nearly degenerate clusters separated by $\hbar\omega_c$, independent of the QD size. This means that with a strong enough B field, we can override the QD's natural energy levels. But as ω_0 increases, a larger B is required to observe the clustering, so smaller QDs are more resistant to this magnetic collapsing of energies.

III. OPTICAL EXCITATION

In order to examine the efficacy of QDs as photodetectors, suppose we have an electromagnetic wave of frequency $\omega = 2\pi c/\lambda$ incident on the QD from the previous section. We assume that the wavelength is much longer than the size of the QD and we can safely ignore the spatially varying part of the wave. This is known as the far infrared regime (FIR). Under this condition, the electric field is described by $\mathbf{E} = E_0\mathbf{d}e^{i\omega t}$, where $\mathbf{d}$ is
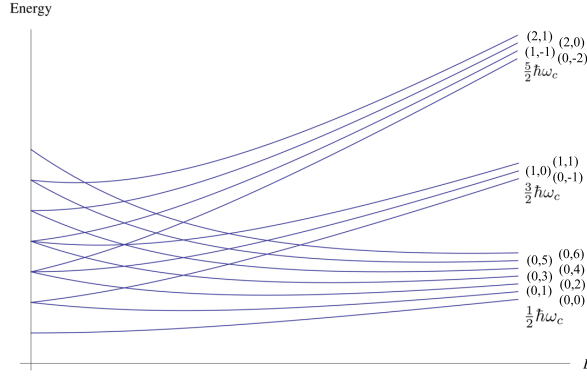
FIG. 2: Eigenenergies as a function of magnetic field for several values of (n, ℓ).

the polarization vector. This adds a perturbation to the Hamiltonian, which we model with the dipole operator,

$$\delta\mathcal{H} = e\mathbf{E} \cdot \mathbf{r} = eE_0 e^{i\omega t}\mathbf{d} \cdot \mathbf{r} \tag{10}$$

$$\mathbf{d} \cdot \mathbf{r} = c_1\hat{x} + c_2\hat{y} = c_+ re^{i\phi} + c_- re^{-i\phi} \tag{11}$$

We can apply first-order perturbation theory to calculate the probability amplitude of light causing a state transition, using (5)

$$A(n'\ell', n\ell) = \langle \psi_{n'\ell'}| \, \delta\mathcal{H} \, |\psi_{n\ell}\rangle$$
$$= eE_0 \left\langle R_{n'}(r)e^{i\ell'\phi} \middle| c_\pm re^{\pm i\phi} \middle| R_n(r)e^{i\ell\phi}\right\rangle$$
$$\propto \int_0^{2\pi} e^{i(\ell-\ell'\pm 1)\phi}\,\mathrm{d}\phi \int_0^\infty R_{n'}^*(r)R_n(r)r^2\,\mathrm{d}r \propto \delta_{\ell-\ell'\pm 1}$$

The radial integral is beyond the scope of this paper, but its value is 0 unless $\ell = 0$ or $n' = n$. [4] Thus, the only allowed transitions are those with $\Delta n = 0$ and $\Delta \ell = \pm 1$. Substituting into (9), the allowed transition energies are then

$$\Delta E = \hbar\Omega \pm \frac{1}{2}\hbar\omega_c \tag{12}$$

If the incident light is near either frequency, an electron will absorb the incident photon and undergo a state transition with the same change in energy. The detection is implemented by attaching electrodes to the QD, so that the state transition shows up as a change in voltage across the electrodes.

IV.   MULTIPLE INTERACTING ELECTRONS

The analysis becomes much trickier when we consider more than one electron, so a typical approach is to diagonalize the Hamiltonian numerically. Here I will analyze

an interaction model which can actually be solved analytically, due to Johnson and Payne. [10] We will use this model to examine the optical response and compare it to the single-electron QD. Let us model the interaction potential between electrons labeled i and j as

$$V(\mathbf{r}_i, \mathbf{r}_j) = V_0 - \frac{1}{2}m\alpha^2|\mathbf{r}_i - \mathbf{r}_j|^2 \tag{13}$$

where α has units of frequency. The QD contains N interacting electrons at locations $\{\mathbf{r}_i\}$. The maximum interaction potential is when two electrons are in the same spot $(\mathbf{r}_i = \mathbf{r}_j)$, as expected for identically charged particles. Neglecting spin, the Hamiltonian is

$$\mathcal{H} = \frac{1}{2m}\sum_{i=1}^N \left(\mathbf{p}_i + \frac{e}{c}\mathbf{A}_i\right)^2$$
$$+ \left\{\frac{1}{2}m\omega_0^2\sum_{i=1}^N |\mathbf{r}_i|^2 + \sum_{i<j} V(\mathbf{r}_i, \mathbf{r}_j)\right\}$$
$$= \frac{1}{2m}\sum_i \mathbf{p}_i^2 + \frac{e}{2mc}\sum_i \mathbf{A}_i\cdot\mathbf{p}_i + \frac{e^2}{2mc^2}\sum_i A_i^2 + V_{eff}$$
$$= \frac{1}{2m}\sum_i \mathbf{p}_i^2 + \frac{eB}{2mc}\sum_i L_{i,z} + \frac{e^2B^2}{8mc^2}\sum_i |\mathbf{r}_i|^2 + V_{eff}$$
$$\mathcal{H} = \frac{1}{2m}\sum_i \mathbf{p}_i^2 + \frac{\omega_c}{2}\sum_i L_{i,z} + \frac{1}{2}m\Omega^2\sum_i |\mathbf{r}_i|^2$$
$$+ \sum_{i<j}\left(V_0 - \frac{1}{2}m\alpha^2|\mathbf{r}_i - \mathbf{r}_j|^2\right) \tag{14}$$

with ω_c and Ω defined in eqs. (1) and (3), and the angular momentum operator $L_{i,z} = x_i p_{i,y} - y_i p_{i,x}$. To simplify this, we will adopt a new coordinate system based on center of mass and relative coordinates between particles i and j.

$$\text{C.M. Position: } \mathbf{R} = X\hat{\mathbf{x}} + Y\hat{\mathbf{y}} = \frac{1}{N}\sum_i \mathbf{r}_i \tag{15}$$

$$\text{C.M. Momentum: } \mathbf{P} = P_X\hat{\mathbf{x}} + P_Y\hat{\mathbf{y}} = \sum_i \mathbf{p}_i \tag{16}$$

$$\text{Relative position: } \mathbf{r}_{ij} = x_{ij}\hat{\mathbf{x}} + y_{ij}\hat{\mathbf{y}} = \mathbf{r}_i - \mathbf{r}_j \tag{17}$$

$$\text{Relative momenutm: } \mathbf{p}_{ij} = p_{ij,x}\hat{\mathbf{x}} + p_{ij,y}\hat{\mathbf{y}} = \mathbf{p}_i - \mathbf{p}_j \tag{18}$$

Now we make an analogy to the harmonic oscillator by introducing center-of-mass and relative raising (+) and lowering (−) operators:[1]

―――――

[1] Compare these to the canonical raising and lowering operators for the harmonic oscillator:

$$\hat{a}^\pm = \sqrt{\frac{m\omega}{2\hbar}}\left(\hat{x} \pm \frac{i\hat{p}}{m\omega}\right)$$

$$A^{\pm} = \sqrt{\frac{Nm\Omega}{4\hbar}}\left((X \mp iY) \mp \frac{i}{Nm\Omega}(P_X \mp iP_Y)\right) \quad (19)$$

$$B^{\pm} = \sqrt{\frac{Nm\Omega}{4\hbar}}\left((X \pm iY) \mp \frac{i}{Nm\Omega}(P_X \pm iP_Y)\right) \quad (20)$$

$$a_{ij}^{\pm} = \sqrt{\frac{m\Omega_0}{4\hbar}}\left((x_{ij} \mp iy_{ij}) \mp \frac{i}{m\Omega_0}(p_{ij,x} \mp ip_{ij,y})\right) \quad (21)$$

$$b_{ij}^{\pm} = \sqrt{\frac{m\Omega_0}{4\hbar}}\left((x_{ij} \pm iy_{ij}) \mp \frac{i}{m\Omega_0}(p_{ij,x} \pm ip_{ij,y})\right) \quad (22)$$

where $\Omega_0^2 = \Omega^2 - N\alpha^2$. In order to carry out this factorization, we must have $\Omega > \sqrt{N}\alpha$. Intuitively, as more electrons are added to the QD, the combined strength of the potential well and magnetic field must increase in order to override the inter-particle repulsion. We can gain some insight by investigating the commutators:

$$[X, P_X] = [Y, P_Y] = i\hbar \quad (23)$$
$$[x_{ij}, p_{kl,x}] = [y_{ij}, p_{kl,y}] = i\hbar(\delta_{ik} + \delta_{jl} - \delta_{il} - \delta_{jk}) \quad (24)$$

All the other commutators between $\mathbf{R}$, $\mathbf{P}$, $\mathbf{r}_{ij}$ and $\mathbf{p}_{ij}$ are zero. For the raising and lowering commutators, a straightforward computation using (23) and (24) shows that

$$[A^-, A^+] = [B^-, B^+] = 1 \quad (25)$$
$$[a_{ij}^-, a_{kl}^+] = [b_{ij}^-, b_{kl}^+] = \delta_{ik} + \delta_{jl} - \delta_{il} - \delta_{jk} \quad (26)$$

and all other commutators are zero. Since (25) matches the H.O. commutator ($[\hat{a}, \hat{a}^\dagger] = 1$), we anticipate that the energies for the center of mass modes will form a similar ladder structure to the H.O. However, (26) does not have such a simple interpretation; the relative modes affect the energies in a more convoluted way. Using this factorization, the Hamiltonian can be decomposed into center of mass and relative components:

$$\mathcal{H} = \mathcal{H}_{C.M.} + \mathcal{H}_{rel} \quad (27)$$

$$\mathcal{H}_{C.M.} = \left(\hbar\Omega - \frac{\hbar\omega_c}{2}\right)A^+A^- + \left(\hbar\Omega + \frac{\hbar\omega_c}{2}\right)B^+B^- + \hbar\Omega \quad (28)$$

$$\mathcal{H}_{rel} = \frac{1}{N}\left(\hbar\Omega_0 - \frac{1}{2}\hbar\omega_c\right)\sum_{i<j} a_{ij}^+a_{ij}^- +$$
$$\frac{1}{N}\left(\hbar\Omega_0 + \frac{\hbar\omega_c}{2}\right)\sum_{i<j} b_{ij}^+b_{ij}^- + (N-1)\hbar\Omega_0 + \frac{N(N-1)}{2}V_0 \quad (29)$$

To show that (27) is equivalent to (14), we begin by expanding the operator products, applying (23) and (24):[2]

———————

[2] Note the similarity to the canonical number operator, $\hat{N} = \hat{a}^\dagger \hat{a}$.

$$A^+A^- = \frac{Nm\Omega}{4\hbar}|\mathbf{R}|^2 + \frac{1}{4\hbar Nm\Omega}\mathbf{P}^2 - \frac{1}{2\hbar}(XP_Y - YP_X) - \frac{1}{2} \quad (30)$$

$$a_{ij}^+a_{ij}^- = \frac{m\Omega_0}{4\hbar}|\mathbf{r}_{ij}|^2 + \frac{1}{4\hbar m\Omega_0}\mathbf{p}_{ij}^2 - \frac{1}{2\hbar}(x_{ij}p_{ij,y} - y_{ij}p_{ij,x}) - 1 \quad (31)$$

B^+B^- and $b_{ij}^+b_{ij}^-$ are identical except for a sign change in the third term. Substituting these into (28) and (29) gives

$$\mathcal{H}_{C.M.} = \frac{1}{2}Nm\Omega^2|\mathbf{R}|^2 + \frac{1}{2Nm}\mathbf{P}^2 + \frac{\omega_c}{2}(XP_Y - YP_X) \quad (32)$$

$$\mathcal{H}_{rel} = \frac{m\Omega_0^2}{2N}\sum_{i<j}|\mathbf{r}_{ij}|^2 + \frac{1}{2Nm}\sum_{i<j}\mathbf{p}_{ij}^2 + \frac{\omega_c}{2N}\sum_{i<j}(x_{ij}p_{ij,y} - y_{ij}p_{ij,x}) + \frac{N(N-1)}{2}V_0$$

$$\mathcal{H}_{rel} = \frac{m\Omega^2}{2N}\sum_{i<j}|\mathbf{r}_{ij}|^2 - \frac{1}{2}m\alpha^2\sum_{i<j}|\mathbf{r}_{ij}|^2 + \frac{1}{2Nm}\sum_{i<j}\mathbf{p}_{ij}^2 + \frac{\omega_c}{2N}\sum_{i<j}(x_{ij}p_{ij,y} - y_{ij}p_{ij,x}) + \frac{N(N-1)}{2}V_0 \quad (33)$$

Matching up the C.M. and relative terms between (32) and (33) and substituting in (15) – (18), we recover all the terms in the original Hamiltonian (14):

$$\frac{1}{2}Nm\Omega^2|\mathbf{R}|^2 + \frac{m\Omega^2}{2N}\sum_{i<j}|\mathbf{r}_{ij}|^2 = \frac{1}{2}m\Omega^2\sum_i|\mathbf{r}_i|^2$$

$$\frac{1}{2Nm}\mathbf{P}^2 + \frac{1}{2Nm}\sum_{i<j}\mathbf{p}_{ij}^2 = \frac{1}{2m}\sum_i\mathbf{p}_i^2$$

$$\frac{\omega_c}{2}(XP_Y - YP_X) + \frac{\omega_c}{2N}\sum_{i<j}(x_{ij}p_{ij,y} - y_{ij}p_{ij,x}) = \frac{\omega_c}{2}\sum_i L_{i,z}$$

$$\frac{N(N-1)}{2}V_0 = \sum_{i<j}V_0$$

$$-\frac{1}{2}m\alpha^2\sum_{i<j}|\mathbf{r}_{ij}|^2 = -\frac{1}{2}m\alpha^2\sum_{i<j}|\mathbf{r}_i - \mathbf{r}_j|^2$$

Summing all the R.H.S. terms above yields (14), so the Hamiltonian in (27) is valid. This interpretation of the Hamiltonian is well suited for describing the optical properties of the multiple-electron QD. As in Section 3, suppose there is radiation incident on the QD, so the perturbation due to the electromagnetic field is

$$\delta\mathcal{H} = e\sum_j \mathbf{E}\cdot\mathbf{r}_j e^{-i\omega t} = e\mathbf{E}\cdot\Big(\sum_j \mathbf{r}_j\Big)e^{-i\omega t}$$

$$\delta\mathcal{H} = Q\mathbf{E}\cdot\mathbf{R}e^{-i\omega t} \tag{34}$$

where $Q = Ne$. Surprisingly, $\delta\mathcal{H}$ influences only the center of mass mode, so the interaction between electrons has no effect on the optical transitions of the QD! It turns out the transition energies are the same as the single particle case (12). To show this, we express (32) as

$$\mathcal{H}_{C.M.} = \frac{1}{2M}(\mathbf{P} + \frac{Q}{c}\mathbf{A}')^2 + \frac{1}{2}M\omega_0^2|\mathbf{R}|^2 \tag{35}$$

where $\mathbf{A}' = \frac{1}{2}B(-X\hat{\mathbf{y}} + Y\hat{\mathbf{x}})$ and $M = Nm$. This is similar to (2), but we have replaced the operators with their center of mass versions. Because $[\mathcal{H}_{C.M.}, \mathcal{H}_{rel}] = 0$, there is no coupling between the C.M. and relative modes. ω_c has not changed since $e/m = Q/M$, so the eigenvalues are still given by (9). Therefore the optical transition energies are given by (12) regardless of the number of electrons in the QD.

V.　DISCUSSION

We began with one electron in parabolic confinement and magnetic field orthogonal to the plane, and found that the energies can be specified by the radial and azimuthal quantum numbers, similar to the hydrogen atom.

It's peculiar that this atom-like dependence is exhibited in a system that is orders of magnitude larger. A convenenient feature of the energies is that the level spacing can be controlled simply by altering the size of the dot. This tunes the optical resonace as well, since the transition energies are closely linked to the level spacing. This makes QDs very appealing for photodetection applications in fields such as astronomy, biomedical imaging and spectroscopy where the light's frequency indicates the strength of a process we would like to measure.

Although the multiple-electron QD is much more complex, it bears some striking resemblances to the one-electron QD. The energies in the center of mass mode form two ladders with spacing determined by the QD's size and applied magnetic field. In the ideal case, the optical transition frequencies do not depend on the number of particles. This is convenient for photodetection applications, since we don't have to worry about leakage current into or out of the dot. For very large particle numbers or large QDs, the model breaks down as it behaves more like a plasma. However, the model has been verified within experimental error for up to 210 electrons by Sikorski and Demel et al, using Fourier transform spectroscopy to measure how much light the QD absorbed at a given frequency.[6, 13]

VI.　ACKNOWLEDGEMENTS

[1] R. C. Ashoori, H. L. Stormer, J. S. Weiner, L. N. Pfeiffer, K. W. Baldwin, and K. W. West. N-electron ground state energies of a quantum dot in magnetic field. *Phys. Rev. Lett.*, 71(4), 1993.

[2] D.V. Averin and K.K. Likharev. Coulomb blockade of single-electron tunneling, and coherent oscillations in small tunnel junctions. *Journal of Low Temperature Physics*, 62(3), 1986.

[3] T. Chakraborty. *Quantum Dots: A survey of the properties of artificial atoms*. Elsevier, 1999.

[4] R.B. Dingle. Some magnetic properties of metals iii. diamagnetic resonance. *Proc. Roy. Soc. A*, 38(212), 1952.

[5] L.P. Kouwenhoven et al. Single electron charging effects in semiconductor quantum dots. *Z. Phys. B - Condensed Matter*, 85, 1991.

[6] T. Demel et al. *Phys. Rev. Lett.*, page 788.

[7] F. Geerinckx, F.M. Peeters, and J.T. Devreese. *J. Appl. Phys.*, 3435(68), 1990.

[8] F. Henneberger, S. Schmitt-Rink, and E.O. Göbel, editors. *Optics of Semiconductor Nanostructures*. Akademie Verlag, 1993.

[9] L. Jacak, P. Hawrylak, and A. Wojs. *Quantum Dots*. Springer, 1998.

[10] N.F. Johnson and M.C. Payne. Exactly solvable model of interacting particles in a quantum dot. *Phys. Rev. Lett.*, 67(9):1157–1160, 1991.

[11] J. Kolehmainen, S.M. Reimann, M. Koskinen, and M. Manninen. Magnetic interaction between coupled quantum dots. *Eur. Phys. J. B*, 13, 2000.

[12] D. Pfannkuche and R.R. Gerhardts. Theory of quantum dot helium. *Physica B*, 189:6–15, 1993.

[13] Ch. Sikorski and U. Merkt. *Phys. Rev. Lett.*, page 2164.

Magnetic Field Sensing via Ramsey Interferometry in Diamond

Derek M. Kita

MIT Department of Physics,
MIT Department of Materials Science and Engineering,
77 Massachusetts Ave., Cambridge, MA 02139-4307
(Dated: May 2, 2014)

Magnetic field sensing with high-precision has attracted multidisciplinary interest and is feasible in solid-state quantum systems such as diamond nitrogen-vacancy centers. In particular, diamond nitrogen-vacancy (NV) centers are systems that have gained attention for their ease of manipulation and long-coherence times. This paper presents a method for sensing magnetic fields with very high resolution by performing Ramsey interferometry on NV centers between two spin-1 sublevels that form an effective spin-1/2 system. A protocol for performing the Ramsey interferometry is presented and the final state expectation values are shown to be proportional to the external magnetic field applied to the NV center. Attention is given to dephasing processes and how they impact the measured values of the magnetic field. Precise reconstruction of time-dependent fields is demonstrated with controlled sequences of π-pulses that act as digital filters.

I. INTRODUCTION

Magnetic field sensing is a topic of growing interest across the fields of biology, chemistry, materials science, and physics. Applications are multidisciplinary and range from sensing action-potentials in neurons to studying magnetic phenomena in new superconducting materials [1] [2].

To perform accurate magnetometry, it is possible to manipulate the spin degrees of freedom of a solid state defect site. These defects are promising sensors because they provide unparalleled measurement sensitivity, are robust solid-state systems, and typically have energy levels addressable via optical and microwave frequency light [3]. In particular, the nitrogen-vacancy (NV) center in diamond is a popular topic of recent research in nanoscale magnetometry [4] [5].

The diamond NV center consists of a substitutional nitrogen atom on a carbon site next to a carbon vacancy in a diamond lattice [6]. The associated energy structure may be seen in Figure 1. A magnetic field measurement can be performed with an interferometry procedure between two of the triplet spin energy levels ($m_s = +1, 0$ or $m_s = -1, 0$) in one of the manifolds separated by orbital angular momentum. The energy levels are Zeeman shifted by a local magnetic field, which will result in a post-interferometry population difference between the two energy levels.

A. Background

The method of measuring the magnetic field is an extension of Ramsey's original experiments with separated oscillating fields [7]. First, the diamond NV center spins are prepared in a low energy spin state ($m_s = 0$) and subjected to a strong magnetic field along the axis of the nitrogen-vacancy bond (the z-axis) [8]. The "separated oscillating fields" are successive applications of a rotating magnetic field with frequency tuned to the
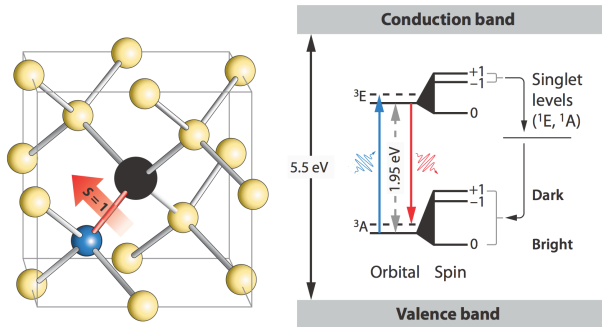
FIG. 1. Image on the left depicts a nitrogen-vacancy (NV) center in a diamond lattice with a red arrow denoting the axis of the localized spin-1 system. Right hand image depicts the NV center energy structure with ground (^{3}A) and excited (^{3}E) orbital levels with each of their $m_s = \pm1, 0$ sublevels. Images from Dobrovistky, et al [3].

Larmor frequency. This generates a transition between the $m_s = 0$ and $m_s = +1$ energy levels (shown in Figure 1) and takes the system to a 50:50 superposition of $m_s = 0, +1$ states. The spins are rotated by $\pi/2$ in the Bloch-sphere picture, so this procedure will be referred to as a "$\pi/2$-pulse" (likewise, an oscillating field that rotates spins by π will be referred to as a "π-pulse"). After this the spins precess about the z-axis and accumulate a phase proportional to the strength of the local magnetic field. At some time $\tau_{\text{precession}}$ after the first $\pi/2$-pulse a second $\pi/2$-pulse is applied. This rotates the spins into a state in which the $m_s = +1, 0$ expectation values correspond to the magnetic field strength along the z-axis. The resulting state expectation values from this process form "Ramsey Fringes", shown in Figure 2 [9]. During the time between the two $\pi/2$-pulses, inhomogeneities in the magnetic field will dephase neighboring spins. Lastly, time-dependent magnetic fields may be measured via application of a sequence of π-pulses during the "precession period" between the two $\pi/2$-pulses.
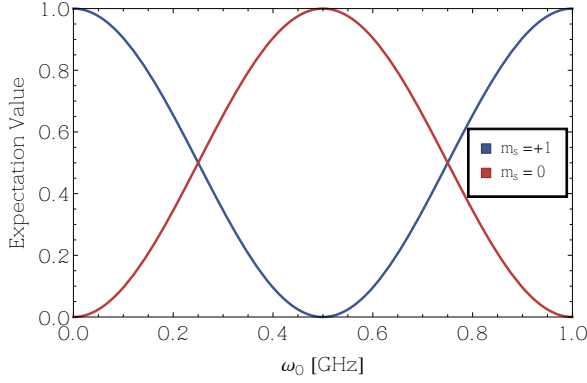
FIG. 2. Characteristic "Ramsey fringes", or expectation values of $m_s = +1, 0$ spin states, after a $\pi/2$-pulse, spin precession for time $\tau_{\text{precession}} = 2\pi$ ns, and then a final $\pi/2$-pulse. The spins are initially prepared each in the $m_s = 0$ state and the frequency ω_0 corresponds to the strength of the local magnetic field.

II. ENERGY LEVELS

Within the large, 5.5 eV bandgap of diamond [6], the NV center's energy levels are divided into orbital ground states and orbital excited states. The orbital ground states are denoted the ^{3}A states and the orbital excited states are denoted the ^{3}E states. Transitions between manifolds with different orbital angular momentum are optically addressable with a green laser, allowing for easy manipulation of the NV centers [10]. The states are further divided into three distinct spin-1 sub-levels ($m_s = -1, 0, +1$) addressable by microwave frequency light [3]. In the following sections, the interferometry is performed between two states in the spin-1 manifold and contributions of orbital angular momentum will be neglected from the Hamiltonian.

A. Hamiltonian

Studying the relevant components of the diamond NV center Hamiltonian will provide an accurate model of the system's dynamics. Without the influence of external fields, the Hamiltonian takes the form

$$H = \Delta S_z^2 - \gamma_e B_z S_z - \sum_n \gamma_N \vec{B} \cdot \vec{g}_n(|S_z|) \cdot \vec{I}_n$$
$$+ \text{(Hyperfine interaction)} + \text{(Crystal-field splitting)}$$
$$+ \text{(Dipolar interaction between nuclei)}$$
$$\tag{1}$$

where γ_e is the gyromagnetic ratio, the zero-field splitting (first term) $\Delta = 2.87$GHz, and the second/third terms correspond to the Zeeman interactions for the electron and nuclei, respectively [11]. To simplify the analysis, the nuclear Zeeman interaction and the last three terms will be taken as small perturbations of a base Hamiltonian H_0 such that

$$H_0 = \Delta S_z^2 - \gamma_e B_z S_z \tag{2}$$

where S_z is the spin-1 spin operator.

The interest of this paper is on electron spin dynamics between two sub levels ($m_s = +1, 0$), so it will be assumed that transitions to the $m_s = -1$ level are off-resonant and negligible. The Hamiltonian in this 2×2 basis is

$$H_0 = \begin{pmatrix} \Delta\hbar^2 - B_z\gamma_e\hbar & 0 \\ 0 & 0 \end{pmatrix} = H_S + \text{(constant)} \tag{3}$$

and since constant energy shifts do not affect the dynamics of the system, the Hamiltonian to be studied, H_S, corresponds to a spin-1/2 system

$$H_S = (\Delta\hbar - B_z\gamma_e)S_z$$
$$= \frac{\hbar}{2} \begin{pmatrix} \Delta\hbar - B_z\gamma_e & 0 \\ 0 & B_z\gamma_e - \Delta\hbar \end{pmatrix} \tag{4}$$

where S_z is now the 2×2 spin-1/2 operator and the constant term from Equation 3 is omitted.

III. THE SPIN-RAMSEY INTERFEROMETER

A general method of performing interferometry using the diamond spin-1/2 system is presented and may be readily adapted to other spin-1/2 systems. Spin-Ramsey interferometry follows the method of separated oscillatory fields and is traditionally used to sense a time-independent, or DC magnetic field [7]. Later sections will address applications of Ramsey interferometry in diamond for time-independent field sensing, dephasing from inhomogeneities in the magnetic field, and the use of π-pulses to sense time-dependent magnetic fields.

A. Oscillating Fields

When the diamond system is subjected to an oscillating magnetic field

$$B(t) = B_{xy}(\cos(\omega t)\hat{x} + \sin(\omega t)\hat{y}) \tag{5}$$

where B_{xy} is the magnitude of the field and ω the angular frequency, the Hamiltonian takes the form

$$H(t) = -\omega_0 S_z + \gamma_e B_{xy}(\cos(\omega t)S_x + \sin(\omega t)S_y) \tag{6}$$

where $\omega_0 = B_z\gamma_e - \Delta\hbar$. We will consider a system that is initially prepared in the $m_s = 0$ state such that the density operator $\rho(t)$ takes the form

$$\rho(0) = \begin{pmatrix} 0 & 0 \\ 0 & 1 \end{pmatrix} \tag{7}$$

This problem may be solved exactly by moving to the frame that rotates with frequency ω. This transformation results in a new rotated Hamiltonian H_R,

$$H_R = (\omega - \omega_0)S_z - \gamma_e B_{xy} S_x \tag{8}$$

which is commonly seen in the analysis of nuclear magnetic resonance [12]. Assuming that $\omega = \omega_0$, the spins will rotate about the x-axis in the rotated frame and the density operator will evolve according to

$$\rho(t) = U^\dagger(t) U_R(t) \rho(0) U_R^\dagger(t) U(t) \tag{9}$$

where $U(t)$ is a unitary transformation into the frame rotating with frequency ω_0 about the $\hat{z}$-axis and $U_R(t)$ is the resulting time-evolution operator for the Hamiltonian H_R.

$$U(t) = \exp\left(\frac{i\omega_0 t S_z}{\hbar}\right) \tag{10a}$$

$$U_R(t) = \exp\left(\frac{i\gamma_e B_{xy} t S_x}{\hbar}\right) \tag{10b}$$

To account for multiple applications of the oscillating field separated by a finite amount of time, it is necessary to develop time evolution operators for a field that has been on for some previous time t_i. From Equation 9, we know the time evolution is

$$
\begin{aligned}
U^\dagger(t_i + t) U_R(t_i + t)|\psi(0)\rangle &= U^\dagger(t_i + t) U_R(t) U_R(t_i)|\psi(0)\rangle \\
&= U^\dagger(t_i + t) U_R(t) U(t_i) U^\dagger(t_i) U_R(t_i)|\psi(0)\rangle \\
&= U^\dagger(t_i + t) U_R(t) U(t_i)|\psi(t_i)\rangle \\
&= U_{\text{osc}}(t_i, t)|\psi(t_i)\rangle
\end{aligned}
\tag{11}
$$

The above equation has the following interpretation: $|\psi(t_i)\rangle$ is the state immediately before the oscillating field is turned back on and $U^\dagger(t + t_i) U_R(t) U(t_i)$ describes the time evolution given that the field has been on for a time t_i and the state is in a frame with some previously accumulated phase.

B. Preparation of the spin-mixture via $\pi/2$-pulse

To prepare the initial system in a 50:50 superposition of $m_s = +1, 0$ states, we begin with $\rho(0)$ completely in the $m_s = 0$ state (Equation 7). Now, a resonant oscillating field is applied for a time

$$\tau_{\pi/2} = \frac{\pi}{2 B_{xy} \gamma_e} \tag{12}$$

such that the final state is

$$
\begin{aligned}
\rho(\tau_{\pi/2}) &= U^\dagger(\tau_{\pi/2}) U_R(\tau_{\pi/2}) \rho(0) U_R^\dagger(\tau_{\pi/2}) U(\tau_{\pi/2}) \\
&= \begin{pmatrix} \frac{1}{2} & \frac{i}{2} e^{\frac{i\pi\omega_0}{2 B_{xy} \gamma_e}} \\ -\frac{i}{2} e^{-\frac{i\pi\omega_0}{2 B_{xy}\gamma_e}} & \frac{1}{2} \end{pmatrix}
\end{aligned}
\tag{13}
$$

It is immediately clear that a 50:50 spin-mixture is formed from the expectation values, or diagonal elements, of the above density matrix.

C. Phase accumulation

After the first $\pi/2$-pulse, the oscillating magnetic field is turned off. For a time τ the diamond NV center spins will be subjected to the Hamiltonian in Equation 4. Since these spins point in the $x - y$ plane of the Bloch sphere, they precess about the z-axis with angular frequency $\omega_0 = \Delta\hbar - B_z\gamma_e$. The corresponding time evolution operator is

$$U_S = \exp\left(-\frac{iH_S \tau}{\hbar}\right) \tag{14}$$

The state of the system after time $t_2 = \tau_{\pi/2} + \tau$ is therefore given by

$$
\begin{aligned}
\rho(t_2) &= U_S(\tau) \rho(\tau_{\pi/2}) U_S^\dagger(\tau) \\
&= \begin{pmatrix} \frac{1}{2} & \frac{i}{2} e^{\frac{i\omega_0(\pi + 2 B_{xy}\gamma_e \tau)}{2 B_{xy}\gamma_e}} \\ -\frac{i}{2} e^{-\frac{i\omega_0(\pi + 2 B_{xy}\gamma_e \tau)}{2 B_{xy}\gamma_e}} & \frac{1}{2} \end{pmatrix}
\end{aligned}
\tag{15}
$$

where the phases picked up by the diagonal elements of $\rho(t_2)$ are proportional to the strength of the local magnetic field and the expectation values remain unchanged.

D. The second $\pi/2$-pulse

A second application of the oscillating field, or $\pi/2$-pulse, will result in a system in the state $m_s = +1$ with unit probability if the precession time

$$\tau = \frac{2n\pi}{\omega_0} \tag{16}$$

or the state $m_s = 0$ with unit probability if

$$\tau = \frac{2n\pi}{\omega_0} + \frac{\pi}{2} \tag{17}$$

where in both cases $n \in \mathbb{Z}$. The resulting state of our ensemble $\rho(t_3)$ (where $t_3 = t_2 + \tau_{\pi/2}$) is obtained via the procedure outlined in Equation 11 on the state $\rho(t_2)$ with $t_i = t = \tau_{\pi/2}$

$$
\begin{aligned}
\rho(t_3) &= U_{\text{osc}}(\tau_{\pi/2}, \tau_{\pi/2}) \rho(t_2) U_{\text{osc}}^\dagger(\tau_{\pi/2}, \tau_{\pi/2}) \\
&= \begin{pmatrix} \cos^2(\frac{\tau\omega_0}{2}) & -\frac{1}{2}\sin(\tau\omega_0) e^{\frac{i\pi\omega_0}{B_{xy}\gamma_e}} \\ -\frac{1}{2}\sin(\tau\omega_0) e^{-\frac{i\pi\omega_0}{B_{xy}\gamma_e}} & \sin^2(\frac{\tau\omega_0}{2}) \end{pmatrix}
\end{aligned}
\tag{18}
$$

After this procedure, the final expectation values of the $m_s = +1, 0$ states have a cosine and sine squared dependence on the strength of the magnetic field, as shown in Figure 2.

IV. EXPERIMENTAL PROTOCOL

A. State preparation

To begin, the system must be initialized in the $m_s = 0$ state of the ^{3}A manifold via optical pumping. To do this,
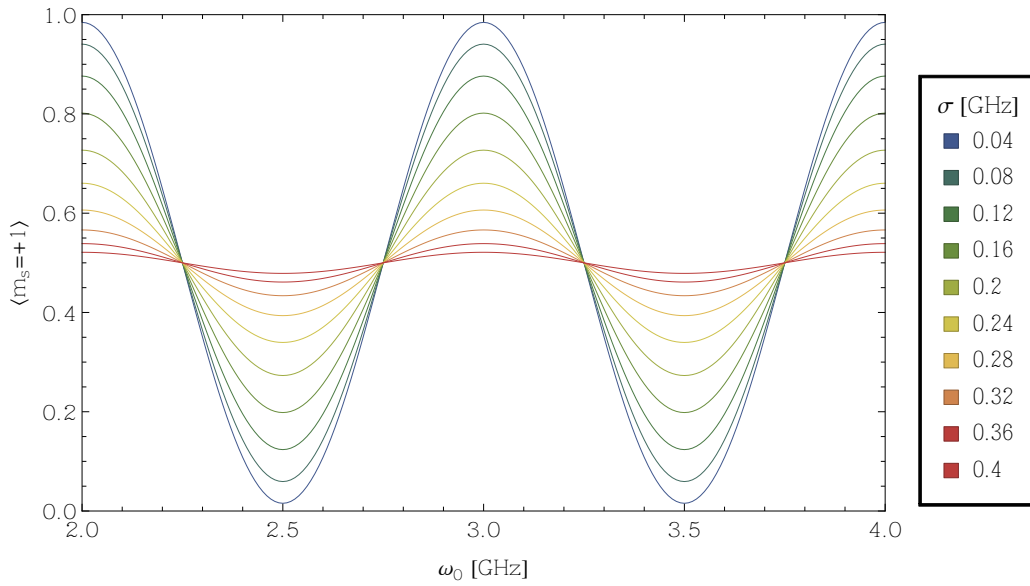
FIG. 3. Ramsey interferometry measurement of the average magnetic field in the presence of local magnetic field fluctuations with variances on the range $\sigma \in [0.04, 0.4]$ GHz and a precession time $\tau_2 = 2\pi$ ns. The precession frequency relates to the magnetic field via $\omega_0 = B_z \gamma_e - \Delta \hbar$. From the diagram, increasing magnetic field variations reduce the amplitude of the expectation value resulting in miscalculations of the average value of a time-independent (static) magnetic field ω_0.

the diamond NV centers are illuminated with a green laser of energy ~ 2 eV ($\lambda = 532$ nm) such that the NV centers are excited to the ^{3}E orbital levels [13]. During this process, the $m_s = 0$ spins undergo continuous excitation and spontaneous emission cycles. The $m_s = \pm 1$ spins also experience spontaneous emission, but are far more likely to decay through multiple singlet states (as shown in Figure 1) that slowly repopulate the $m_s = 0, \pm 1$ states equally [14]. After $\approx 5\ \mu s$ of optical pumping, the system becomes $70 - 90\%$ spin-polarized in the $m_s = 0$ ^{3}A ground state [3]. At this point the system is prepared for the Ramsey interferometry measurement sequence.

B.   Ramsey Oscillating Fields

Two coils along the x- and y-axis create an oscillating magnetic field. After state preparation, the oscillating field is applied for a time $\tau_{\pi/2}$. Then, the spins are allowed to precess at a rate proportional to the strength of the magnetic field. Finally, a second application of the oscillating field prepares the system for measurement. If a time-dependent field measurement is to occur, a sequence of π-pulses will be applied during the precession time period, as will be shown in Section VI.

C.   Measurement

To measure the final states after the Ramsey interferometry protocol, the diamond NV centers are illuminated

with a 532 nm green laser for $\approx 5\mu s$ [14]. The $m_s = 0$ ^{3}A states will transition to the $m_s = 0$ ^{3}E state and spontaneously decay, emitting detectable light in the visible range. The $m_s = +1$ ^{3}A state will transition to the $m_s = +1$ ^{3}E state and then decay through long lived non-radiative spin-singlet channels [13]. Detection of the fluorescence will thus correspond to the final expectation value of the $m_s = 0$ state. Since the expectation value of the final state oscillates as a function of the DC magnetic field, the range of magnetic fields detectable by the measurement is ultimately limited to a single period of oscillation.

V.   DEPHASING OF SPINS

In reality, an ensemble of NV centers will be distributed across a finite region of space and each will experience a slightly different magnetic field strength. As such, the probability of the magnetic field being a strength B for a particular spin may be approximated as a Gaussian distribution

$$p(B) = \frac{1}{\sigma\sqrt{2\pi}} e^{-\frac{(\omega(B)-\omega_0)^2}{2\sigma^2}} \tag{19}$$

where $\omega(B) = \gamma_e B - \Delta \hbar$, ω_0 is the average precession frequency, and σ is the variance of the frequency distribution. For simplicity, it will be assumed that the $\pi/2$-pulses are perfectly resonant with each NV center and the spins will perfectly rotate into the $x - y$ plane. The magnetic field fluctuations will then contribute to dephasing
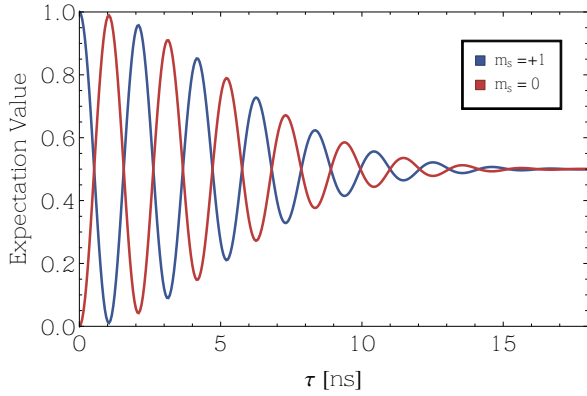
FIG. 4. Expectation values of the $m_s = +1, 0$ states after a time τ of precession between $\pi/2$-pulses in an inhomogeneous magnetic field. In this figure, $\omega_0 = 3$ GHz and the variance $\sigma = 0.2$GHz.

during the spin-precession period ($t_1 < t < t_2$). To account for this, the new density operator after time t_3 may be expressed as

$$\rho(t_3)_{\text{dephased}} = \int_{-\infty}^{\infty} dB p(B)\rho(t_3) \qquad (20)$$

and thus the $m_s = 0, +1$ expectation values become

$$\langle +1 \rangle = \frac{1}{\sigma\sqrt{2\pi}} \int_{-\infty}^{\infty} dB \cos^2\left(\frac{\tau\omega(B)}{2}\right) e^{-\frac{(\omega(B)-\omega_0)^2}{2\sigma^2}} \quad (21a)$$

$$\langle 0 \rangle = \frac{1}{\sigma\sqrt{2\pi}} \int_{-\infty}^{\infty} dB \sin^2\left(\frac{\tau\omega(B)}{2}\right) e^{-\frac{(\omega(B)-\omega_0)^2}{2\sigma^2}} \quad (21b)$$

The resulting Ramsey fringes decrease in intensity as the variance in the local magnetic fields increases, as shown in Figure 3. Additionally, as the time of precession increases the expectation values of the magnetic field will each decrease to 0.5, as shown in Figure 4.

VI. TIME-DEPENDENT FIELD SENSING

The Ramsey interferometer serves as a useful tool for sensing time-independent magnetic fields. However, it is also possible to retrieve useful information about the magnetic field's time dependence by the application of π-pulses to the diamond spins during the precession period [15].

To understand this, lets consider the action of the U_S time evolution operator during spin precession when the magnetic field (and thus the Hamiltonian) is a function of time,

$$U_S(t_i, t_f) = \exp\left(-\frac{i}{\hbar}\int_{t_i}^{t_f} dt H_S(t)\right) = e^{i\phi(t_i,t_f)} \quad (22)$$

where t_i and t_f are the initial and final times during spin-precession. If we start out with an ensemble of spins in the $x-y$ plane, the density operator at some time t_2 later in a time-dependent field is now

$$\rho(t_2) = U_S(t_1, t_2)\rho(\tau_{\pi/2})U_S^\dagger(t_1, t_2) \qquad (23)$$

$$= \begin{pmatrix} \frac{1}{2} & \frac{i}{2}e^{2i\phi(t_1,t_2)+i\frac{\pi\omega_0}{2B_{xy}\gamma_e}} \\ -\frac{i}{2}e^{-2i\phi(t_1,t_2)-i\frac{\pi\omega_0}{2B_{xy}\gamma_e}} & \frac{1}{2} \end{pmatrix}$$

Comparing $\rho(t_2)$ and $\rho(\tau_{\pi/2})$ from Equation 13, it is clear that the action of U_S adds a phase proportional to $\phi(t_1, t_2) = \phi_{12}$ to the diagonal elements of the density operator. Now, consider a π-pulse applied at time t_2 and then another subsequent period of spin-precession. The π-pulse transforms the system to

$$\rho(t_3) = U_{\text{osc}}(\tau_{\pi/2}, \tau_\pi)\rho(t_2)U_{\text{osc}}^\dagger(\tau_{\pi/2}, \tau_\pi)$$

$$= \begin{pmatrix} \frac{1}{2} & -\frac{i}{2}e^{-2i\phi_{12}+\frac{3i\pi\omega_0}{2B_{xy}\gamma_e}} \\ \frac{i}{2}e^{2i\phi_{12}-\frac{3i\pi\omega_0}{2B_{xy}\gamma_e}} & \frac{1}{2} \end{pmatrix} \quad (24)$$

Here we notice something very interesting. The sign of the phase $\phi(t_1, t_2)$ accumulated during the first spin-precession is reversed! If we let the spin precess for another period of time until t_4, the state will gain another phase $\phi(t_3, t_4) = \phi_{34}$ with an *opposite* sign from the first phase ϕ_{12}. More explicitly,

$$\rho(t_4) = U_S(t_3, t_4)\rho(t_3)U_S^\dagger(t_3, t_4) \qquad (25)$$

$$= \begin{pmatrix} \frac{1}{2} & -\frac{i}{2}e^{-2i(\phi_{12}-\phi_{34})+\frac{3i\pi\omega_0}{2B_{xy}\gamma_e}} \\ \frac{i}{2}e^{2i(\phi_{12}-\phi_{34})-\frac{3i\pi\omega_0}{2B_{xy}\gamma_e}} & \frac{1}{2} \end{pmatrix}$$

From the above expression, we can see immediately that when the precession times are equal and the field is time-*independent*, $\phi_{12} - \phi_{34} = 0$. However, for a time-dependent field that oscillates with frequency ω_0, these two will not necessarily be equal. A final $\pi/2$-pulse will result in the following population differences:

$$\begin{aligned} \langle m_s = +1 \rangle &= \sin^2(\phi_{12} - \phi_{34}) \\ \langle m_s = 0 \rangle &= \cos^2(\phi_{12} - \phi_{34}) \end{aligned} \qquad (26)$$

This measurement gives us information about the time-dependence of the magnetic field before and after the π-pulse [16]. In fact, it is possible to write the total phase ϕ accumulated during precession as the original phase (Equation 22) multiplied by a square-function $f(t)$ that takes one of the two values ± 1 and changes with each π-pulse. This assumes that the time needed to apply the π-pulse is much less than the precession times. The phase is then

$$\phi = -\frac{1}{\hbar}\int_0^T f(t')H_S(t')dt' \qquad (27)$$

where T is the total time between initial and final $\pi/2$-pulses.

Since $f(t)$ measures the difference between phases accumulated before and after π-pulses, the π-pulses may be
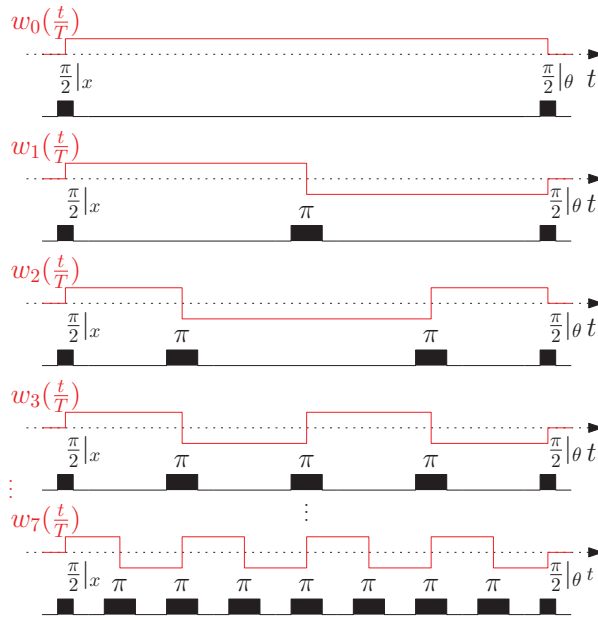
FIG. 5. Interferometry protocols in which $f(t)$ from Equation 27 is equal to the first few Walsh functions $\omega_n(\frac{t}{T})$ where T is the acquisition time, or total time the spins are spent precessing between the $\pi/2$-pulses. A π-pulse corresponds to a changing sign of $f(t)$. Image from Magesan, et al [17].

interpreted as digital filters [17]. There exists a complete set of orthogonal square waves, or "Walsh functions", that may be used to describe the protocol function $f(t)$ in an analogous fashion to Fourier decomposition [17]. The first of these Walsh functions are shown in Figure 5. Any time-dependent function, such as $b(t)$, may be rewritten as a sum of these Walsh functions

$$b(t) = \sum_{n=0}^{\infty} \left(\int_0^T \omega_n(t')b(t')dt' \right) \omega_n(t) \equiv \sum_{n=0}^{\infty} c_n \omega_n(t)$$
(28)

and coefficients c_n corresponding to the overlap between the Walsh function and our magnetic field over a time period T. This is precisely the phase we pick up when we choose a protocol $f(t) = \omega_n(t)$. For example, an interferometry protocol where $f(t) = \omega_1(t)$ corresponds to a single π-pulse halfway into the precession period. The measurement of the $m_s = +1, 0$ states will be proportional to the phases picked up before and after this π-pulse, and thus proportional to the component of $b(t)$ along $\omega_1(t)$. A similar protocol performed for higher-order Walsh functions will provide higher-order coefficients and allow for a more accurate reconstruction of the time-dependent magnetic field.

VII.   CONCLUSION

Nitrogen-vacancy centers in diamond are stable quantum systems that may be carefully manipulated to provide valuable information about local magnetic fields. The energy structure of these defects allows for careful manipulation with both optical and microwave frequencies of light, while specific decay channels enable easy optical pumping of the $m_s = 0$ ground state. Coupling the spins in the $m_s = 0$ state to one of the other ground state energy levels (such as $m_s = +1$) is possible with successive applications of resonant oscillating fields. Final spin populations in either the $m_s = 0$ or $+1$ state is read out by illuminating the sample with green light and exciting the spins to the corresponding ^3E orbital states. The $m_s = +1$ ^3E states will decay non-radiatively, while the $m_s = 0$ ^3E states decay radiatively, resulting in detectable fluorescence.

The Ramsey interferometer consists of an ensemble of spins, initially prepared in this lower energy spin-1/2 state, that are subject to an oscillating magnetic field that rotates the spins $90°$ into the $x-y$ plane of the Bloch sphere. From here, the spins acquire a phase that is proportional to the strength of the magnetic field. During this precession time, π-pulses may be applied to detect time-dependent properties of the magnetic field. Without π-pulses, a standard interferometry measurement can detect the absolute value of a time-independent magnetic field. Local fluctuations of the magnetic field result in dephasing of the spins that take the ensemble to a mixed state with equal $m_s = 0$ and $+1$ expectation values.

Applications of π-pulses during the precession period have been shown to act as digital filters. The fluorescence measured after a protocol with n π-pulses is proportional to the coefficient of the nth Walsh function. Multiple measurements that correspond to different orthonormal Walsh functions allow for the piecewise reconstruction of time-dependent magnetic fields.

[1] A. Waxman, Y. Schlussel, D. Groswasser, V. M. Acosta, L. S. Bouchard, D. Budker, and R. Folman, Physical Review B **89** (2014).

[2] L. Pham, D. L. Sage, P. L. Stanwix, T. K. Yeung, D. Glenn, A. Trifonov, P. Cappellaro, P. R. Hemmer, M. D. Lukin, H. Park, A. Yacoby, and R. L. Walsworth, New Journal of Physics **13** (2011).

[3] V. V. Dobrovitski, G. D. Fuchs, A. L. Falk, C. Santori, and D. D. Awschalom, in *Annual Review of Condensed Matter Physics*, Annual Review of Condensed Matter Physics, Vol. 4, edited by J. Langer (2013) pp. 23–50.

[4] M. HJ, K. M, S. MH, R. CT, O. K, A. DD, and R. D, Science **339**, 557 (2013).

[5] W. JR, K. WF, V. JB, J. A, B. BB, V. de Walle CG, and A. DD, Proceedings of the National Academy of Sciences of the United States of America **107**, 8513 (2010).

[6] C. Kittel, *Introduction to Solid State Physics*, 8th ed. (Wiley, 2004).

[7] N. Ramsey, Physical Review **78**, 695 (1950).

[8] P. Kehayias, M. Doherty, D. English, R. Fischer, A. Jarmola, K. Jensen, N. Leefer, P. Hemmer, N. B. Manson, and D. Budker, Physical Review B **88** (2013).

[9] N. LD, D. DI, and G. TF, Physical Review A **45**, 4734 (1992).

[10] L. A, B. SW, R. DA, R. SC, S. J, and F. E, Physical Review B **53** (1996).

[11] J. Maze Rios, "Quantum manipulation of nitrogen-vacancy centers in diamond: from basic properties to applications," (2010).

[12] B. Zwiebach, "Two-state systems: Nuclear magnetic resonance," (2013), 8.05 Course Notes.

[13] A. VM, J. A, B. E, and B. D, Physical Review B **82** (2010).

[14] H. F and B. G, Physical Review B **86** (2012).

[15] L. Hall, J. Cole, C. Hill, and L. Hollenberg, Physical Review Letters **103** (2009).

[16] A. Cooper, E. Magesan, H. Yum, and P. Cappellaro, Nature Communications **5** (2014).

[17] E. Magesan, A. Cooper, H. Yum, and P. Cappellaro, Physical Review A **88** (2013).

Supersymmetric Quantum Mechanics

Reed LaFleche
(Dated: May 2, 2014)

We introduce the factorization methods known as Supersymmetric Quantum Mechanics for generating different Hamiltonians with similar spectra. After stating the general procedure, we show that any Hamiltonian which takes the form of an otherwise free nonrelativistic scalar moving in the presence of a potential energy can be embedded in a larger Hamiltonian which exhibits supersymmetry, and motivate the terminology. Afterwards, we develop the method of shape invariance which is used to solve certain Hamiltonians that exist in one spatial dimension, and show how it is used in the case of the Hydrogen atom.

I. INTRODUCTION

A Supersymmetric Quantum Mechanical system is defined by the existence of operators $\hat{Q}_i, i \in \{1,...N\}$ (in this paper $N = 2$ always) satisfying:

$$[\hat{Q}_i, \hat{H}] = 0$$
$$\{\hat{Q}_i, \hat{Q}_j\} = \delta_{ij}\hat{H}, \tag{1}$$

where $\hat{H}$ is the Hamiltonian. Supersymmetric Quantum Mechanics was first introduced by Edward Witten in [1] (from which the above definition is taken) as part of an attempt to understand supersymmetry breaking in Quantum Field Theory. In that paper, he used a two dimensional supersymmetric Hamiltonian, and discussed conditions for supersymmetry to be broken.

Supersymmetric Quantum Mechanics has since been studied for its own sake, i.e. as a quantum mechanical theory rather than as a simplified model for a supersymmetric quantum field theory. It has been found that using the methods of Supersymmetric Quantum Mechanics, it is possible to solve certain problems algebraically rather than analytically. It is possible to start from a single Hamiltonian $\hat{H}_1$ and generate an infinite sequence $\{\hat{H}_i\}$ with nearly identical energy spectra. Given the eigenfunctions of $\hat{H}_1$, it is possible to construct operators which subsequently yield the eigenfunctions of the $\hat{H}_i$'s. Thus the problem of solving the infinite set of Hamiltonians is reduced to that of solving a single Hamiltonian and constructing the required operators (which latter can be done mechanically).

If the $\{\hat{H}_i\}$ are all in some way similar (a definition which can be made rigorous), then $\hat{H}_1$ is known as shape invariant, and can be solved algebraically. Thus Supersymmetric Quantum Mechanics allows us to define the class of shape invariant Hamiltonians, which includes many known solvable Hamiltonians such as the radial equation for the Coulomb problem, the Harmonic Oscillator, and many potentials involving trigonometric and hyperbolic functions. Examples can be found in [2], [3].

In this paper, we will set up the formalism of Supersymmetric Quantum Mechanics and shape invariance and show how it is used for the Hydrogen atom. In Section II Part A we begin to set up the formalism. In Section II Part B we develop ideas from Part 1 further, show

that any Hamiltonian of the form $-\frac{\hbar^2}{2m}\nabla^2 + V$ can be embedded inside a Hamiltonian which obeys supersymmetry, and discuss the relation between Supersymmetric Quantum Mechanics and the supersymmetries proposed in Quantum Field Theory. In section III we define shape invariance. In section IV we apply shape invariance to develop a framework to solve the hydrogen atom algebraically.

In what follows we use the convention that $\hbar = 1$, and use Einstein summation over repeated indices unless otherwise stated.

II. GENERAL FRAMEWORK

A. Factorization of the Hamiltonian

Let $\hat{H}$ be a nondegenerate Hamiltonian with ground state energy E_0. Consider the Hamiltonian $\hat{H}_0 = \hat{H} - E_0$. This Hamiltonian has ground state energy 0, and is thus positive semidefinite. It may thus be factored as $\hat{H}_0 = \hat{A}^\dagger \hat{A}$. It is natural to consider the pair:

$$\hat{H}_0 = \hat{A}^\dagger \hat{A}$$
$$\hat{H}_1 = \hat{A}\hat{A}^\dagger \tag{2}$$

which are both positive semidefinite by construction. We have the identities $\hat{A}\hat{H}_0 = \hat{H}_1\hat{A}$, $\hat{A}^\dagger\hat{H}_1 = \hat{H}_0\hat{A}^\dagger$. These allow us to relate the eigenstates and eigenvalues of $\hat{H}_0, \hat{H}_1$. In particular,

$$\hat{H}_0 |\psi_n\rangle = E_n |\psi_n\rangle \rightarrow \hat{H}_1 \hat{A} |\psi_n\rangle = E_n \hat{A} |\psi_n\rangle$$
$$\hat{H}_1 |\phi_n\rangle = E_n |\phi_n\rangle \rightarrow \hat{H}_0 \hat{A}^\dagger |\phi_n\rangle = E_n \hat{A}^\dagger |\phi_n\rangle \tag{3}$$

We may be more explicit if $\hat{H}$ has the form $-\frac{1}{2m}\partial_x^2 + V(x)$. If the ground state is $\psi_0(x)$, then:

$$-\frac{1}{2m}\partial_x^2 + (\psi_0(x))^{-1}(\frac{1}{2m}\partial_x^2\psi_0(x)) = -\frac{1}{2m}\partial_x^2 + V(x) - E_0$$
$$= \hat{H}_0$$

This implies that if $\hat{A} = \frac{1}{\sqrt{2m}}\partial_x - \frac{1}{\sqrt{2m}}\partial_x \ln(\psi_0(x))$, then $\hat{A}^\dagger \hat{A} = \hat{H}_0$. The quantity

$$W(x) = -\frac{1}{\sqrt{2m}}\partial_x \ln(\psi_0(x)) \tag{4}$$

is referred to as the superpotential of the Hamiltonian $\hat{H}_0$. We have $\hat{H}_0 = -\frac{1}{2m}\partial_x^2 + (W^2 - \frac{1}{\sqrt{2m}}\partial_x W)$,

$\hat{H}_1 = -\frac{1}{2m}\partial_x^2 + (W^2 + \frac{1}{\sqrt{2m}}\partial_x W)$. We also have that $\hat{A}|\psi_0\rangle = 0$, and by non degeneracy of $\hat{H}_0$, $|\psi_0\rangle$ is unique in this. Further, as $\psi_0(x)$ is normalized, $\lim_{|x|\to\infty}\psi_0(x) = 0$, and no solution of $\hat{A}^\dagger|\phi_n\rangle = 0$ can be normalized, as any such solution will be a multiple of $\psi_0(x)^{-1}$, and so will blow up at infinity. Along with (3), this shows that $\mathrm{Spec}(\hat{H}_1) = \mathrm{Spec}(\hat{H}_0) - \{0\}$, that the operators $\hat{A}, \hat{A}^\dagger$ may be used to move between the two eigenbases, and that $\hat{H}_1$ is also nondegenerate.

We make a few remarks on $W(x)$, and in particular on why $\partial_x \ln(\psi_0(x))$ is a sensible quantity to talk about. $\psi_0(x)$ is real and nonnegative for all x by [4], so $\ln(\psi_0(x))$ is well defined and real at all points save the zeroes of $\psi_0(x)$. As $\psi_0(x)$ is nonnegative, its first derivative must either vanish or be undefined at any zero. Because the Schrödinger equation is second order in spatial derivatives, any point where both $\psi_0(x)$ and its first derivative are 0 must be a singularity for the potential energy—otherwise $\psi_0(x) = 0$ everywhere—and every point where $\partial_x\psi_0(x)$ is undefined must also be a singularity for the potential energy. Thus we see that every singularity of $\ln(\psi_0(x))$ is also a singularity of the potential energy, so singularities of the superpotential can only occur at singularities of the potential energy.

It should be noted that the above factorization process may be repeated indefinitely, taking $\hat{H}_0' = \hat{H}_1 - E_1$, and thus generating Hamiltonians $\hat{H}_2, \hat{H}_3, ...$, where E_1 is the ground state energy of $\hat{H}_1$, or equivalently the energy of the first excited state of $\hat{H}_0$.

In more than one dimension, we may still factor the Hamiltonian as $\hat{A}^\dagger\hat{A}$, or alternatively we may introduce:

$$\hat{A}_i = \frac{1}{\sqrt{2m}}\partial_{x_i} - \frac{1}{\sqrt{2m}}\partial_{x_i}\ln(\psi_0(x)), \qquad (5)$$

which has the properties:

$$
\begin{aligned}
\hat{A}_i^\dagger\hat{A}_i &= \hat{H}_0 \\
[\hat{A}_i, \hat{A}_j] &= \frac{1}{2m}[\partial_{x_i} - \partial_{x_i}\ln(\psi_0(x)), \partial_{x_j} - \partial_{x_j}\ln(\psi_0(x))] \\
&= \frac{1}{2m}(\partial_{x_j}\partial_{x_i} - \partial_{x_i}\partial_{x_j})\ln(\psi_0(x)) \\
&= 0 \\
[\hat{A}_i^\dagger, \hat{A}_j^\dagger] &= [\hat{A}_i, \hat{A}_j] = 0 \\
[\hat{A}_i, \hat{A}_j^\dagger] &= \frac{1}{2m}[\partial_{x_i} - \partial_{x_i}\ln(\psi_0(x)), -\partial_{x_j} - \partial_{x_j}\ln(\psi_0(x))] \\
&= \frac{1}{2m}(-\partial_{x_i}\partial_{x_j} - \partial_{x_i}\partial_{x_j})\ln(\psi_0(x)) \\
&= -\frac{1}{m}\partial_{x_i}\partial_{x_j}\ln(\psi_0(x))
\end{aligned}
$$

$$(6)$$

B. The Superhamiltonian and Supercharges

Thus far we have yet to construct a system satisfying (1). We do so now, in the process generalizing the factorization methods to any number of spatial dimensions. We follow a procedure given in [5].

We introduce operators $\hat{b}_i$, where i runs over the dimensions of space. We impose upon these the relations

$$
\begin{aligned}
\{\hat{b}_i, \hat{b}_j\} = \{\hat{b}_i^\dagger, \hat{b}_j^\dagger\} &= 0, \\
\{\hat{b}_i, \hat{b}_j^\dagger\} &= \delta_{ij},
\end{aligned}
\qquad (7)
$$

where $\{\cdot, \cdot\}$ is the anticommutator, and additionally require the $\hat{b}$'s to be constant throughout space, so $[A_i, b_j] = [A_i^\dagger, b_j] = [A_i, b_j^\dagger] = [A_i^\dagger, b_j^\dagger] = 0$, for the $\hat{A}_i$'s defined in (5). We then construct the operators

$$
\begin{aligned}
\hat{Q} &= \hat{A}_i\hat{b}_i^\dagger, \\
\hat{Q}^\dagger &= \hat{A}_i^\dagger\hat{b}_i,
\end{aligned}
\qquad (8)
$$

We then can define the supersymmetric Hamiltonian $\boldsymbol{\hat{H}}$ by:

$$
\begin{aligned}
\boldsymbol{\hat{H}} &= \{\hat{Q}, \hat{Q}^\dagger\} \\
&= \{\hat{A}_i\hat{b}_i^\dagger, \hat{A}_j^\dagger\hat{b}_j\} \\
&= \hat{A}_i\hat{A}_j^\dagger\hat{b}_i^\dagger\hat{b}_j + \hat{A}_j^\dagger\hat{A}_i\hat{b}_j\hat{b}_i^\dagger \\
&= \hat{A}_i^\dagger\hat{A}_i + \hat{b}_i^\dagger\hat{b}_j[\hat{A}_i, \hat{A}_j^\dagger] \\
&= -\frac{1}{2m}\nabla^2 + V(x) - \frac{1}{m}\hat{b}_i^\dagger\hat{b}_j\partial_i\partial_j ln(\psi_0(x)),
\end{aligned}
\qquad (9)
$$

By (7), the third line of (6), we have $\hat{Q}^2 = (\hat{Q}^\dagger)^2 = 0$. We form Hermitian operators:

$$
\begin{aligned}
\hat{Q}_1 &= \frac{\hat{Q} + \hat{Q}^\dagger}{\sqrt{2}} \\
\hat{Q}_2 &= \frac{\hat{Q} - \hat{Q}^\dagger}{i\sqrt{2}},
\end{aligned}
\qquad (10)
$$

known as the supercharges. It is easy to check that the supercharges satisfy (1), with $\hat{H}$ replaced by $\boldsymbol{\hat{H}}$.

In Quantum Field Theory, particles are described as excitations of a vacuum (ground) state, and ladder operators are introduced which act on the system to create or annihilate particles. The ladder operators for fermions obey relations which are similar to (7), while those for bosons obey commutation relations similar to those of the harmonic oscillator:

$$
\begin{aligned}
[\hat{a}_i, \hat{a}_j] = [\hat{a}_i^\dagger, \hat{a}_j^\dagger] &= 0, \\
[\hat{a}_i, \hat{a}_j^\dagger] &= \delta_{ij},
\end{aligned}
\qquad (11)
$$

We thus introduce the 'Number of Fermions' operator in analogy with the number operator of the harmonic oscillator:

$$\hat{N} = \hat{b}_i^\dagger\hat{b}_i, \qquad (12)$$

We will now give a set of identities, which have various implications to be discussed afterwards:

$$[\hat{N}, \hat{b}_i^\dagger] = \hat{b}_i^\dagger$$
$$[\hat{N}, \hat{b}_i] = -\hat{b}_i$$
$$[\hat{Q}, \hat{\boldsymbol{H}}] = [\hat{Q}, \{\hat{Q}, \hat{Q}^\dagger\}]$$
$$= \hat{Q}^2\hat{Q}^\dagger + \hat{Q}\hat{Q}^\dagger\hat{Q} - \hat{Q}\hat{Q}^\dagger\hat{Q} - \hat{Q}^\dagger\hat{Q}^2$$
$$= [\hat{Q}^2, \hat{Q}^\dagger]$$
$$= 0$$
$$[\hat{Q}^\dagger, \hat{\boldsymbol{H}}] = [\hat{Q}, \hat{\boldsymbol{H}}] = [\hat{Q}_i, \hat{\boldsymbol{H}}] = [\hat{N}, \hat{\boldsymbol{H}}] = 0,$$
$$[\hat{N}, \hat{Q}] = \hat{Q},$$
$$[\hat{N}, \hat{Q}^\dagger] = -\hat{Q}^\dagger$$
$$[\hat{N}, \hat{Q}_1] = i\hat{Q}_2$$
$$[\hat{N}, \hat{Q}_2] = -i\hat{Q}_1$$

$$(13)$$

Thus $\hat{Q}_i, \hat{N}$ are conserved, and $\hat{Q}, \hat{Q}^\dagger$ change the number of fermions by one without changing the energy. We may simultaneously diagonalize $\hat{\boldsymbol{H}}$ and $\hat{N}$. A state with $\langle\psi|\hat{N}|\psi\rangle = 0$ has $(\hat{b}_i|\psi\rangle)^\dagger(\hat{b}_i|\psi\rangle) = 0$, so $\hat{b}_i|\psi\rangle = 0$ for all i. It follows that $\hat{\boldsymbol{H}}|\psi\rangle = (-\frac{1}{2m}\nabla^2 + V(x))|\psi\rangle$, so we recover our original Hamiltonian in the $\hat{N} = 0$ subspace.

We construct a Hilbert space by applying the operators $\hat{b}_i, \hat{b}_i^\dagger$ to $N = 0$ states. The eigenvalues of $\hat{N}$ may be determined by starting with the $N = 0$ states $|\psi\rangle$, and noting that as these are annihilated by the $\hat{b}_i$'s (previous paragraph), there is no $N = -1$ state. By the first two lines of (13), each $b_i^\dagger$ we apply raises N by 1. The anti-commutation relations in (7) give us the Pauli Exclusion Principle: no state may have 2 or more fermions of type i for any i. As there are n types of fermions, the Pauli Exclusion Principle tells us that the possible eigenvalues of $\hat{N}$ are the integers between 0 and n.

Thus simultaneously diagonalizing $\hat{H}$ and $\hat{N}$ we have $n + 1$ different Hamiltonians $\{\hat{H}_0, ...\hat{H}_n\}$, each with a different potential, but with the eigenstates related by $\hat{Q}, \hat{Q}^\dagger$. A basis for the $N = l$ states may be formed by starting with a basis for the $N = 0$ states and applying all possible combinations of l $b_i^\dagger$'s with no repetition. There are $\binom{n}{l}$ ways to do this, so we conclude that the Hamiltonian on the $N = l$ subspace is in the form of an $\binom{n}{l}$ dimensional square matrix.

Note that if $n = 1$, we have, by (9):

$$\hat{\boldsymbol{H}} = \{\hat{A}^\dagger\hat{b}, \hat{A}\hat{b}^\dagger\}$$
$$= \hat{A}^\dagger\hat{A}\hat{b}\hat{b}^\dagger + \hat{A}\hat{A}^\dagger\hat{b}^\dagger\hat{b}$$
$$= \hat{H}_0(1 - \hat{N}) + \hat{H}_1\hat{N},$$

and so the $\hat{H}_0, \hat{H}_1$ thus obtained agree with those defined in (2).

The name 'Supersymmetric Quantum Mechanics' can be motivated by considering the case of a harmonic oscillator, where $\hat{A}_i = \hat{a}_i$, satisfying (11). By (9), (11), we

see that $\hat{\boldsymbol{H}} = \hat{a}_i^\dagger\hat{a}_i + \hat{b}_i^\dagger\hat{b}_i$, which is simply a system of n bosons and n fermions. The operator $\hat{Q}^\dagger = \hat{a}_i^\dagger\hat{b}_i$ will create a type i boson and annihilate a type i fermion for each i, and $\hat{Q}$ will do the opposite. The supercharges defined in (1), (10) are Hermitian and conserved. Thus they generate symmetries of the system. Because the supercharges are linear combinations of $\hat{Q}, \hat{Q}^\dagger$, we see that the symmetries generated will replace bosons of type i with fermions of type i, and vice versa. In Quantum Field Theory, such a symmetry is known as a supersymmetry, and thus the name Supersymmetric Quantum Mechanics.

III.   SHAPE INVARIANCE

The above may be used to solve certain types of potentials in one spatial dimension known as shape invariant, using methods first introduced in [5]. For these, the potentials of $\hat{H}_0, \hat{H}_1$ are in some way similar. To be precise, we assume that we have a class of Hamiltonians $\hat{H}(\vec{a})$ depending on some set of parameters $\vec{a} \in S$ for some set S. If upon constructing the superhamiltonian $\hat{\boldsymbol{H}}(\vec{a})$ we find that there are functions $f : S \to S, R : S \to \mathbb{R}$ such that

$$\hat{H}_1(\vec{a}) = \hat{H}_0(f(\vec{a})) + R(\vec{a}), \qquad (14)$$

we say that the potential energy function for $\hat{H}$, or alternatively $\hat{H}$ itself, is shape invariant.

If $\hat{H}$ is shape invariant, then the discussion after (13) tells us that the operators $\hat{Q}, \hat{Q}^\dagger$ relate the energies and eigenfunctions of $\hat{H}_0, \hat{H}_1$. If $|\psi_{k+1}(\vec{a})\rangle$ is the kth excited state of $\hat{H}(\vec{a})$, then:

$$\hat{Q}(\vec{a})|\psi_{k+1}(\vec{a})\rangle = \hat{b}^\dagger|\psi_k(f(\vec{a}))\rangle$$
$$|\psi_{k+1}(\vec{a})\rangle = \hat{Q}^\dagger(\vec{a})\hat{b}^\dagger|\psi_k(f(\vec{a}))\rangle, \qquad (15)$$

up to normalization constants. $|\psi_{k+1}(\vec{a})\rangle, \hat{b}^\dagger|\psi_k(f(\vec{a}))\rangle$ are eigenstates of $\hat{\boldsymbol{H}}(\vec{a})$ with the same eigenvalue, so:

$$\hat{\boldsymbol{H}}(\vec{a})|\psi_{k+1}(\vec{a})\rangle = \hat{H}_0(\vec{a})|\psi_{k+1}(\vec{a})\rangle$$
$$\hat{\boldsymbol{H}}(\vec{a})\hat{b}^\dagger|\psi_k(f(\vec{a}))\rangle = \hat{b}^\dagger\hat{H}_1(\vec{a})|\psi_k(f(\vec{a}))\rangle$$
$$= \hat{b}^\dagger(\hat{H}_0(f(\vec{a})) + R(\vec{a}))|\psi_k(f(\vec{a}))\rangle$$
$$E_{k+1}(\vec{a}) = E_k(f(\vec{a})) + R(\vec{a})$$

We may repeat the above, finding the superhamiltonian $\hat{\boldsymbol{H}}(f(\vec{a}))$, which gives us the energy of the states of $\hat{H}_0(f(\vec{a}))$ in terms of the energies of the states of $\hat{H}_0(f(f(\vec{a})))$, and so on until we have the energies of the kth state of $\hat{H}_0(\vec{a})$ for all natural numbers k. By construction, $\hat{H}_0(\vec{a})$ has ground state energy 0, and so the general formula will be $E_k(\vec{a}) = \sum_{j=0}^{k-1} R(f^j(\vec{a}))$. If we

want the energies of $\hat{H}(\vec{a}) = \hat{H}_0(\vec{a}) + E_0(\vec{a})$, we simply add $E_0(\vec{a})$ to get:

$$E_k(\vec{a}) = E_0(\vec{a}) + \sum_{j=0}^{k-1} R(f^j(\vec{a})), \qquad (16)$$

where $f^j(\vec{a})$ is the result of applying the function f to $\vec{a}$ j times.

Considering (15), note that $\hat{Q}^\dagger(\vec{a})\hat{b}^\dagger = \hat{A}^\dagger(\vec{a})\hat{b}\hat{b}^\dagger = \hat{A}^\dagger(1 - \hat{N})$, and $\hat{N}|\psi_{k+1}\rangle = 0$ by construction. Thus we have $|\psi_{k+1}(\vec{a})\rangle = \hat{A}^\dagger(\vec{a})|\psi_k(f(\vec{a}))\rangle$, up to normalization.

The above also applies for a general non-degenerate Hamiltonian (i.e. not necessarily of the form $-\frac{1}{2m}\nabla^2 + V$): if we can write $\hat{H}_0(\vec{a}) = \hat{A}^\dagger(\vec{a})\hat{A}(\vec{a})$, and $\hat{H}_1(\vec{a}) = \hat{A}(\vec{a})\hat{A}^\dagger(\vec{a}) = \hat{H}_0(f(\vec{a})) + R(\vec{a})$, then $\hat{H}_0$ is shape invariant, and we can use this fact to iteratively solve for the spectrum and eigenstates of $\hat{H}_0$.

IV. THE HYDROGEN ATOM

The radial equation for the Coulomb problem gives an example of a shape invariant potential in 1 spatial dimension. The equation is [6]:

$$\begin{aligned}\hat{H}(l) &= -\frac{1}{2m}\partial_r^2 + \left(\frac{1}{2m}\frac{l(l+1)}{r^2} - \frac{e^2}{4\pi\epsilon_0}\frac{1}{r}\right)\\&= -\frac{1}{2m}\partial_r^2 + \frac{1}{2m}\left(\frac{l(l+1)}{r^2} - \frac{2}{a}\frac{1}{r}\right),\end{aligned} \qquad (17)$$

where $a = \frac{4\pi\epsilon_0}{me^2}$ is the Bohr radius. To analyze this, note that the ground state wavefunction satisfies $\psi_0(r) \propto r^l e^{-r/(l+1)a}$, $u_0(r) = r\psi_0(r) \propto r^{l+1}e^{-r/(l+1)a}$, so by (4), the superpotential is

$$\begin{aligned}W(r) &= -\frac{1}{\sqrt{2m}}\partial_r \ln\left(r^{l+1}e^{-r/(l+1)a}\right)\\&= \frac{1}{\sqrt{2m}}\left(\frac{1}{(l+1)a} - \frac{l+1}{r}\right)\end{aligned}$$

This gives

$$\begin{aligned}\hat{A} &= \frac{1}{\sqrt{2m}}\partial_r + \frac{1}{\sqrt{2m}}\left(\frac{1}{(l+1)a} - \frac{l+1}{r}\right)\\\hat{A}^\dagger &= -\frac{1}{\sqrt{2m}}\partial_r + \frac{1}{\sqrt{2m}}\left(\frac{1}{(l+1)a} - \frac{l+1}{r}\right)\\\hat{H}_1(l) &= \hat{A}^\dagger\hat{A}\\&= -\frac{1}{2m}\partial_r^2 + \frac{1}{2m}\left(\frac{l(l+1)}{r^2} - \frac{2}{a}\frac{1}{r} + \frac{1}{(l+1)^2a^2}\right)\\&= \hat{H}(l) + \frac{1}{2m(l+1)^2a^2}\\\hat{H}_2(l) &= \hat{A}\hat{A}^\dagger\\&= -\frac{1}{2m}\partial_r^2 + \frac{1}{2m}\left(\frac{(l+1)(l+2)}{r^2} - \frac{2}{a}\frac{1}{r} + \frac{1}{(l+1)^2a^2}\right)\\&= \hat{H}(l+1) + \frac{1}{2m(l+1)^2a^2}\\&= \hat{H}_1(l+1) + \frac{1}{2ma^2}\left(\frac{1}{(l+1)^2} - \frac{1}{(l+2)^2}\right)\end{aligned} \qquad (18)$$

Alternatively, we could have derived the above by noting the form of $\hat{H}$ and guessing a superpotential W which is some low degree polynomial function of $\frac{1}{r}$. We see that (14) holds if we choose

$$f(l) = l+1, \; R(l) = \frac{1}{2ma^2}\left(\frac{1}{(l+1)^2} - \frac{1}{(l+2)^2}\right) \quad (19)$$

$\hat{H}(l) - E_0(l) = \hat{H}_0(l) = \hat{H}(l) + \frac{1}{2m(l+1)^2a^2}$, so it follows that the ground state has $E_0(l) = -\frac{1}{2m(l+1)^2a^2}$. By (16), (19), we have:

$$\begin{aligned}E_k(l) =&\, E_0(l) + \sum_{j=0}^{k-1} R(l+j)\\=& -\frac{1}{2m(l+1)^2a^2}\\&+ \sum_{j=0}^{k-1}\frac{1}{2ma^2}\left(\frac{1}{(l+j+1)^2} - \frac{1}{(l+j+2)^2}\right)\\=& -\frac{1}{2m(l+k)^2a^2},\end{aligned} \qquad (20)$$

which is indeed the correct result.

For the wavefunctions, we use the second line of (18) along with (19) to get:

$$\begin{aligned}|u_{k+1}(l)\rangle &= \hat{A}^\dagger(l)|u_k(l+1)\rangle\\&= \left(-\frac{1}{\sqrt{2m}}\partial_r + \frac{1}{\sqrt{2m}}\left(\frac{1}{(l+1)a} - \frac{l+1}{r}\right)\right)|u_k(l+1)\rangle\\&\propto \left(-\partial_r + \left(\frac{1}{(l+1)a} - \frac{l+1}{r}\right)\right)|u_k(l+1)\rangle\end{aligned} \qquad (21)$$

This gives:

$$u_0(r,l) \propto r^{l+1} e^{-r/(l+1)a}$$

$$u_1(r,l) \propto \left(-\partial_r + \left(\frac{1}{(l+1)a} - \frac{l+1}{r} \right) \right) r^{l+2} e^{-r/(l+2)a}$$

$$= \left(-\partial_r + \left(\frac{1}{(l+1)a} - \frac{l+1}{r} \right) \right) r^{l+2} e^{-r/(l+2)a}$$

$$= (2l+3) \cdot \left(\frac{1}{(l+1)(l+2)} \frac{r}{a} - 1 \right) r^{l+1} e^{-r/(l+2)a}$$

$$\propto \left(\frac{1}{(l+1)(l+2)} \frac{r}{a} - 1 \right) r^{l+1} e^{-r/(l+2)a}$$

$$(22)$$

and so on. Thus we see that we are able, using Supersymmetric Quantum Mechanics, to solve for the eigenstates of the radial equation of the hydrogen atom simply by applying the operator $\hat{A}^\dagger(l)$.

V. CONCLUSION

We have shown that given a Hamiltonian with a ground state, we may shift it by some constant to obtain a Hamiltonian with ground state energy 0. Further, we may factor this latter as $\hat{A}^\dagger \hat{A}$, and by considering the new Hamiltonian $\hat{A}\hat{A}^\dagger$ and iterating, we may obtain a sequence of Hamiltonians with similar spectra. Given a Hamiltonian $\hat{H} = -\frac{1}{2m}\nabla^2 + V$ in n dimensions with ground state $\psi_0(x)$, we may construct fermionic creation and annihilation operators $\{\hat{b}_i, \hat{b}_i^\dagger\}|_{i \in \{1, \ldots n\}}$, operators $\{\hat{A}_i = \frac{1}{\sqrt{2m}}\partial_{x_i} - \frac{1}{\sqrt{2m}}\partial_{x_i} \ln(\psi_0(x))\}|_{i \in \{1, \ldots n\}}$, and finally an operator $\hat{Q} = \hat{A}_i \hat{b}_i^\dagger$ such that $\boldsymbol{\hat{H}} = \{\hat{Q}, \hat{Q}^\dagger\}$ is a Hamiltonian acting on a Hilbert Space with n different types of fermions. We have shown that $\boldsymbol{\hat{H}}$ reduces to $\hat{H}$ plus a constant for states containing 0 fermions, and that hermitian operators formed from $\hat{Q}, \hat{Q}^\dagger$ generate symmetries of $\boldsymbol{\hat{H}}$ which may be interpreted for a harmonic oscillator as supersymmetries - i.e. as changing bosons into fermions and vice versa.

We have defined shape invariance: that if a set of Hamiltonians $\{\hat{H}(\vec{a})\}$ is indexed by a parameter $\vec{a}$, and if $\hat{A}(\vec{a})\hat{A}^\dagger(\vec{a}) = \hat{A}^\dagger(f(\vec{a}))\hat{A}(f(\vec{a})) + R(\vec{a})$ for functions f, R, then $\hat{H}(\vec{a}) = \hat{A}^\dagger(\vec{a})\hat{A}(\vec{a})$ is shape invariant. Shape invariance allows us to use the operators $\hat{A}^\dagger(\vec{a})$ to solve for the spectrum and eigenfunctions of $\hat{H}(\vec{a})$. The spectrum is $E_k(\vec{a}) = E_0(\vec{a}) + \sum_{j=0}^{k-1} R(f^j(\vec{a}))$. Finally, we have applied this to the hydrogen atom, obtaining algebraically the correct energies and wavefunctions, and showing in a particular example the usefulness of the methods of Supersymmetric Quantum Mechanics.

[1] E. Witten, Nucl. Phys. B185 (1981) 513.
[2] R. Dutt, A. Khare, and U. Sukhatme. Am. J. Phys. 56 (1988) 163.
[3] B. Chakrabarti, Pranama. 70 (2008) 41.
[4] J. Muir-Petit, A. Pollis, and F. Mazzanti, Am. J. Phys. 70 (2002) 808.
[5] O. Castaños, J.C. D'Olivo, S. Hojman, and L.F. Urrutia, Phys. Lett. B174 (1986) 307.
[6] L. E. Gendenshtein, JETP. Lett. 38 (1983) 356.
[7] D. Griffiths, *Introduction to Quantum Mechanics, 2nd Ed.* Pearson Prentice Hall, Upper Saddle River, NJ, 2005. Page 145.
[8] J. Maluck, *An Introduction to Supersymmetric Quantum Mechanics and Shape Invariant Potentials.* (Capstone Thesis, Amsterdam University College: Netherlands, 2013).-used as a starting point to gain familiarity and find other sources.

A Quantum Statistical Description of White Dwarf Stars

Michael D. La Viola
8.06: Quantum Mechanics III
(Dated: May 4, 2014)

Most stars end their lives as white dwarf stars. These dwarfs typically have mass comparable to the mass of the Sun, and volume comparable to the volume of Earth. In this stage the stars have terminated their thermonuclear reactions, yet they do not experience gravitational collapse. These stars provided support to quantum theory, since electron degeneracy pressure, a quantum mechanical effect, is the only known phenomenon capable of supporting their existence. In this paper we develop key principles of quantum mechanics in order to derive electron degeneracy pressure and apply it to characterize the interior of white dwarf stars. We then use it provide an estimation for the upper bound of the mass of white dwarf stars, known as the Chandrasekhar limit. Finally, we qualitatively synthesize current knowledge on the fate of white dwarfs, which will either cool down and crystallize, or explode as type Ia supernovae.

I. INTRODUCTION

In the early 19th century, F.W. Bessel used the technique of stellar parallax to measure the distance from the Earth to Sirius, the brightest star in the night sky. During this experiment, Bessel found that the star deviated slightly from its expected path, and from that point on decided to follow the star's movements. After years of documenting the star's position, in 1844 Bessel deducted that Sirius was actually a binary system, but that his telescope was not strong enough to detect Sirius' companion star.

In 1862, Alvan Graham Clark, son of a lensmaker, used a large refractor telescope and was the first to be able to visualize Sirius' companion star, Sirius B. By analyzing their binary orbit, he found that Sirius B had a mass of $\sim 1.0 M_\odot$. A little over 50 years later, in 1915, Walter Adams surprisingly discovered that Sirius B was a hot, blue-white star, with a surface temperature of approximately 27,000 K, and a radius comparable to Earth's radius [1]. The other astronomers at the time refused to believe his results, arguing that it was impossible to have a star with the Sun's mass and Earth's volume. It was only with the advent of quantum mechanics that the enigma was resolved.

In this paper we will develop the foundations of Fermi-Dirac statistics in order to derive electron degeneracy pressure. This outward pressure is what allows the star to not collapse on itself due to its inward gravitational pressure. We will also see that there is an upper bound to the amount of mass a white dwarf star can possess, before the star ignites and blows itself apart. Finally, we will qualitatively describe the ultimate fate of the star, which we will see can either cool down and die peacefully, or end with a bang. Let us know describe the basis of quantum mechanics, the Heisenberg uncertainty principle and Pauli's exclusion principle.

II. THEORETICAL FRAMEWORK

A. Heisenberg uncertainty & Pauli exclusion principles

1. Heisenberg uncertainty principle

Heisenberg's uncertainty relations constitute one of the most ground-breaking discoveries of early quantum mechanics. In classical mechanics, measurement of any dynamical variable of a particle will yield well-defined values. In quantum mechanics, instead, the outcome of measurement has a probability distribution with an expectation value and an uncertainty. In particular, Heisenberg discovered that two measureable conjugate properties (such as position and momentum) cannot be simultaneously known to an arbitrary degree of precision. The complete derivation of the uncertainty relation, using the Hermiticity of the operators and the Schwartz inequality, can be found in Shankar [5]. If we consider two Hermitian operators, Ω and Λ, with the commutation relation $[\Omega, \Lambda] = i\Gamma$, then it can be shown [5] that Γ is also Hermitian. Defining the uncertainty of the operators to be $\Delta\Omega = \sqrt{\langle\Omega^2\rangle - \langle\Omega\rangle^2}$ and $\Delta\Lambda = \sqrt{\langle\Lambda^2\rangle - \langle\Lambda\rangle^2}$, where the bra-ket notation is used for the expectation value about a normalized wavefunction $|\Psi\rangle$, then it can be shown[5] that the uncertainties obey the relationship:

$$(\Delta\Omega)^2(\Delta\Lambda)^2 \geq \frac{1}{4}\langle\Psi|\left\{(\Omega-\langle\Omega\rangle),(\Lambda-\langle\Lambda\rangle)\right\}|\Psi\rangle^2 + \frac{1}{4}\langle\Psi|\Gamma|\Psi\rangle^2 \tag{1}$$

where $\{A, B\}$ is the anticommutator of the operators. Mathematically, the uncertainty principle states that there is a lower bound to the product of the conjugate operators' uncertainties. In the specific case of position and momentum, which is the case of interest for later derivations in this paper, $\Gamma = \hbar$, and since the first term is always positive definite, the following inequality must hold

$$(\Delta x)^2(\Delta p_x)^2 \geq \frac{\hbar^2}{4} \tag{2}$$

$$(\Delta x)(\Delta p_x) \geq \frac{\hbar}{2} \tag{3}$$

Another key concept that arose in early quantum mechanics was Pauli's exclusion principle. From Heisenberg's principle, we know that we cannot describe a particle in position-momentum phase space with a point, because its position and momentum cannot both be known with certainty. Therefore, phase space is not a continuum, but it is "quantized" in cells, which correspond to states, of area $\Delta x \Delta p_x \sim \mathcal{O}(h)$[2]. Pauli's exclusion principle states that no more than one fermion with a given spin orientation can occupy a given state in phase space[2]. Since electrons and protons are fermions of spin 1/2, and have two possible spin orientations, no more than two particles can occupy a given state (i.e. cell), and they must have opposite spin. On the other hand particles that obey Einstein-Boson statistics, called bosons, do not follow Pauli's exclusion principle, and there is no limit to how many bosons can occupy a given state.
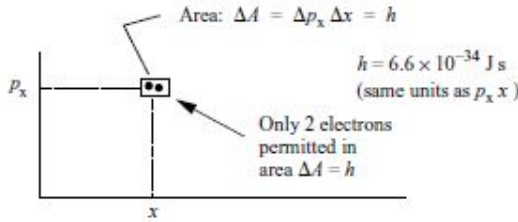

FIG. 1: The cell in phase space has area equal to Planck's constant, and cannot contain more than two electrons, of opposite spins. Figure adapted from [2].

The same argument can be extended to 3-D space, which corresponds to 6-D phase space, by stating that only two fermions, of opposite spin, can occupy the same state of volume h^3 in phase space.

B. Fermi-Dirac statistics

1. Antisimmetry of fermions

This section is not essential for the rest of our analysis, however it is interesting to see how two different sets of statistics arise from considering the effects of interchanging two identical particles in an N-body system. Let us consider such a system, and describe with q_i all the coordinates of the ith particle. The time-independent Schrödinger equation tells us that energy eigenstates obey the following relation

$$\mathcal{H}\Psi_n(q_1,\ldots,q_N) = E_n\Psi_n(q_1,\ldots,q_N) \qquad (4)$$

Let us define $\mathcal{P}_{ij}$ as a "parity operator"[3], such that it simply interchanges the positions of two of the identical particles, q_i and q_j. Applying it a second time would simply return the system the initial system, i.e.

$$\mathcal{P}_{ij}^2\Psi_n = \Psi_n \qquad (5)$$

The eigenvalue of this equation is (+1), so the eigenvalues of the operator $\mathcal{P}_{ij}$ can be +1 or -1[3]. This implies that the eigenstates Ψ_n can either be symmetric or antisymmetric under the interchange of two of particles. Using relativistic quantum field theory, specifically the Dirac equation, it is possible to show that the eigenfunctions with eigenvalue +1 correspond to particles with integer spin, which obey Bose statistics, while those with eigenvalue -1 correspond to half-integer spin particles, which obey Fermi statistics [3].

2. Fermi momentum and energy

A key difference between Fermi particles and Bose particles is that Fermi particles obey Pauli's exclusion principle, while Bose particles do not. If we consider a gas with N particles, Pauli's exclusion principle constrains the system such that no two identical particles can have the same set of 4 quantum numbers.

Let us consider an energy level ϵ_i, with g_i degenerate states. Let n_i ($n_i < g_i$) be the number of fermions of spin 1/2 occupying these states. Since only one fermion can occupy each degenerate state, the number of possible ways that the system can be configured is

$$W_i = \frac{g_i(g_i-1)\ldots(g_i-n_i+1)}{n_i!}$$
$$= \frac{g_i!}{(g_i-n_i)!n_i!}$$

where the $n_i!$ in the denominator accounts for the overcounting due to the particles being identical, a correction known as Botzmann counting [4]. If we consider all the energy levels of the system, we obtain that the total number of ways of configuring the gas is

$$W_F\{n_i\} = \prod_i \frac{g_i!}{(g_i-n_i)!n_i!} \qquad (6)$$

Now, in accordance with thermodynamics, we can define the entropy of the system as $S = k_B \ln(W)$[4]. The state with the largest number of microstates will be the most probable configuration of the system. We can find this configuration by maximizing entropy. Using Stirling's approximation [7],

$$S = k_B \ln \prod_i \frac{g_i!}{(g_i-n_i)!n_i!}$$
$$\simeq k_B \sum_i [g_i \ln g_i - (g_i-n_i)\ln(g_i-n_i) - n_i \ln n_i]$$

Using Lagrange multipliers to maximize S while satisfying the constraints $\sum_i n_i = N$ and $\sum_i n_i\epsilon_i = E$, we obtain[4]

$$n_i = \frac{g_i}{e^{\alpha+\beta\epsilon_i}+1} \qquad (7)$$

To match the known thermodynamic results[1], we can identify β as $1/k_B T$ and $\alpha = -\mu/k_B T$. Hence

$$n_i = \frac{g_i}{e^{(\epsilon_i - \mu)/k_B T} + 1} \tag{8}$$

Since a particle's energy is related to its momentum ($\epsilon_i = p_i^2/2m$), states in the same location with the same energy occupy the same volume in space-momentum phase space. By Pauli's exclusion principle we found that at most two spin 1/2 fermions can occupy the same state in phase space, which has volume h^3. Therefore, the degeneracy for a given energy level ϵ_i is

$$g_i = \frac{\#\text{states}}{\text{phase space volume}} \tag{9}$$
$$= \frac{2}{h^3} \tag{10}$$

We can now write the number density of particles occupying the states of energy ϵ_i as

$$n_i = \frac{2}{h^3} \frac{1}{e^{(\epsilon_i - \mu)/k_B T} + 1} \tag{11}$$

As we decrease the temperature of the system to $T \to 0$, the particles lose their thermal energy and occupy the lowest available energy state. In the limit, all the low energy states will be occupied, and none of the high energy states will be. The maximum energy of the occupied states is known as the Fermi energy, ϵ_F, and all the other particles have energy $E \le \epsilon_F$. At T=0 the Fermi energy is equal to the chemical potential, μ, and, renaming the particles' energy ϵ_i with E, the energy distribution function of the system can be written as,

$$f(E) = \frac{1}{e^{[(E - \epsilon_F)/k_B T]} + 1} \tag{12}$$

and it is equal to 1 if $E < \epsilon_F$ and 0 if $E > \epsilon_F$ [4]. At T=0, the gas is said to be completely degenerate. If $T > 0$, then the distribution will smooth out to include some energies above the Fermi energy, because some particles will have enough thermal energy to jump to higher states. This is captured in figure II. Recall that n_i, as expressed in (11), is the number density of particles occupying a given volume of position-momentum phase volume. We can integrate over the momentum component to obtain the number density of all the particles with a given position. If the gas is completely degenerate there is an upper bound to the momentum. Since all the particles have energy $E \le \epsilon_F$, and energy is related to momentum (in the non-relativistic limit) by $E = p^2/2m$, all the particles will have momentum $p \le p_F = \sqrt{2m\epsilon_F}$, where p_F is known as the Fermi momentum. Therefore integrating over momentum and using the fact that $f(E) = 1$ for $E < \epsilon_F$:

$$n = \int n_i d^3\vec{p} \tag{13}$$
$$= \frac{2}{h^3} \int \frac{1}{e^{[(E - \epsilon_F)/k_B T]} + 1} d^3\vec{p} \tag{14}$$
$$= \frac{2}{h^3} \int_0^{p_F} 4\pi p^2 dp \tag{15}$$
$$= \frac{8\pi}{3h^3} p_F^3 \tag{16}$$
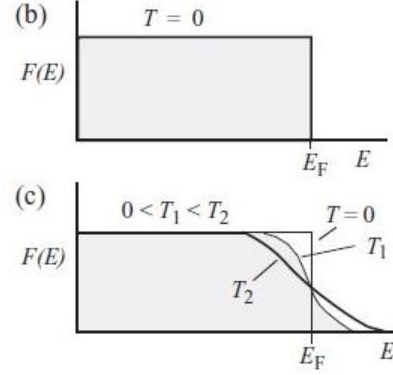
FIG. 2: The Fermi distribution function for a completely degenerate gas, in comparison with the distribution for a gas with $T > 0$. Here the notation $F(E)$ is used in place of $f(E)$ Figure adapted from [2].

$$\to p_F = \left(\frac{3h^3}{8\pi} n\right)^{1/3} = \frac{h}{2}\left(\frac{3n}{\pi}\right)^{1/3} \tag{17}$$

We have derived the expression for the Fermi momentum of a gas, as a function of its number density. In the non-relativistic limit, the Fermi energy is related to the momentum by $\epsilon_F = \frac{p_F^2}{2m}$. Plugging in the expression above and using the fact that $h = 2\pi\hbar$, we obtain

$$\epsilon_F = \frac{1}{2m}\frac{h^2}{4}\left(\frac{3n}{\pi}\right)^{2/3} \tag{18}$$
$$= \frac{\hbar^2}{2m}\left(3\pi^2 n\right)^{2/3} \tag{19}$$

Equipped with this relationship, we can find a condition for which, even when $T > 0$, complete degeneracy is a good approximation to describe the system. In particular, the approximation can be used if the thermal energy of the system is lower than its Fermi energy, because that would imply that the majority of the electrons will not have sufficient thermal energy to jump from a state with $E \le \epsilon_F$ to a state of energy $E > \epsilon_F$. Using Eqn.(19)

$$E_{\text{Thermal}} < \epsilon_F \tag{20}$$
$$\frac{3}{2}kT < \frac{\hbar^2}{2m_e}\left[3\pi^2 n\right]^{2/3} \tag{21}$$

In practice, it is more useful to use the mass density of the system instead of its number density. Let us therefore relate the number density to the mass density of the system, ρ, as carried out in [1]:

$$n = \left(\frac{\#electrons}{nucleon}\right)\left(\frac{\#nucleons}{volume}\right) = \left(\frac{Z}{A}\right)\frac{\rho}{m_H} \tag{22}$$

where Z, A, m_H are, respectively, the number of protons and nucleons, and the mass of a hydrogen atom. Therefore, the condition for degeneracy can be written as

$$\frac{3}{2}kT < \frac{\hbar^2}{2m_e}\left[3\pi^2\left(\frac{Z}{A}\right)\frac{\rho}{m_H}\right]^{2/3} \tag{23}$$

or rearranging

$$\frac{T}{\rho^{2/3}} < \frac{\hbar^2}{3m_e k}\left[\frac{3\pi^2}{m_H}\left(\frac{Z}{A}\right)\right]^{2/3} = 1261\frac{K}{m^2 kg^{2/3}} \qquad (24)$$

Plugging in values for temperature and density for the Sun and the white dwarf Sirius B [1], we obtain that $T/\rho^{2/3}$ for the Sun is equal to $5500 Km^{-2}kg^{-2/3}$, while for Sirius B it equals $37 Km^{-2}kg^{-2/3}$. It is apparent that the condition is not satisfied for the Sun, implying that electron degeneracy is weak in the Sun and can be ignored, while the white dwarf satisfies it and the star can be approximated as completely degenerate.

III.   WHITE DWARF ANATOMY

A.   Electron degeneracy pressure

For 50 years since its discovery, Sirius B puzzled physicists. The star had exhausted its thermonuclear reactions, yet gravitational pressure had not forced it to collapse on itself. The solution to the phenomenon, in fact, required quantum mechanics. As we will see in this section, Fermi statistics lead to a pressure capable of arresting gravitational collapse.

From Eqn.(17) we found that momentum scales as

$$p \sim \hbar n^{1/3} \qquad (25)$$

Using the expression for the number density in Eqn.(22), the momentum is

$$p \sim \hbar\left[\left(\frac{Z}{A}\right)\frac{\rho}{m_H}\right]^{1/3} \qquad (26)$$

The velocity of non-relativistic electrons is related to their momentum by $v = p/m_e$. If we assumed that all the electrons had approximately the same momentum, the pressure of the gas would be[1]

$$P \simeq \frac{1}{3}npv \qquad (27)$$

Plugging in the expressions for n, p, v, we obtain that

$$P \sim \frac{\hbar^2}{m_e}\left[\left(\frac{Z}{A}\right)\frac{\rho}{m_H}\right]^{5/3} \qquad (28)$$

If we substituted ρ with M/R^3 we would get that pressure scales with $\propto R^{-5}$.

If we consider the effect of gravity, hydrostatics tell us that gravitational pressure obeys $dP/dR = -\rho g$. Using dimensional analysis, this tells us that the gravitational pressure at the center of the star scales as

$$\frac{0 - P_c}{R} \simeq -\left(\frac{M}{R^3}\right)\left(\frac{GM}{R^2}\right) \qquad (29)$$

$$P_c \simeq \frac{GM^2}{R^4} \propto R^{-4} \qquad (30)$$

It is the fact the outward electron degeneracy pressure has a steeper dependance on radius than the inward gravitational pressure (R^{-5} vs. R^{-4}) that allows the star to not collapse! In fact, if the star were to shrink, electron degeneracy pressure would increase faster and tend to push the star back out to its equilibrium radius.

B.   Estimation of the Chandrasekhar limit

Electron degeneracy pressure was found to have interesting implications. In 1931, at the young age of 21, Subrahmanyan Chandrasekhar derived that there is an upper bound for the mass of white dwarfs. Here we will find a rough estimate for its value.

The natural next step of the above analysis is to set the two expressions for pressure, Eqn.(28) and Eqn.(30), equal to each other, to find the relationship between the equilibrium radius of the star and its mass.

$$\frac{GM^2}{R^4} \simeq \frac{\hbar^2}{m_e}\left[\left(\frac{Z}{A}\right)\frac{M}{m_H R^3}\right]^{5/3} \qquad (31)$$

which leads to

$$M^{1/3}R \simeq \frac{\hbar^2}{Gm_e}\left[\left(\frac{Z}{A}\right)\frac{1}{m_H}\right]^{5/3} \qquad (32)$$

or, by taking the cube of both sides,

$$\rightarrow MV = \text{constant} \qquad (33)$$

where V is the volume of the star.

This equation tells us something initially counter-intuitive: the more massive the star is the smaller it is [1]! This also means that if a white dwarf were to accrete matter, for example from a companion star if it part of a binary system, it would shrink and get denser. Recall from Eqn.(26) that, using non-relativistic expressions, the velocity of the particles scales positively as $v \propto \rho^{1/3}$. As the star gets denser the particles' momentum increases. This is in accordance with Fermi statistics. Compare with figure III. There is a limit to how dense the star can become before the particles reach relativistic speeds. It turns out that the limiting density is approximately 10^9kg/m^3[1]. For densities above this order of magnitude we need to correct our equations to account for relativitistic effects. In particular, we need to change the energy-momentum expression to be $E_F = [p_F^2 c^2 + m^2 c^4]^{1/2}$. Following the same steps as in sections II.B.2 and in III.A with this modification, we obtain that when the particles reach relativistic speeds, the electron degeneracy pressure scales as [1]

$$P \simeq \hbar c\left[\left(\frac{Z}{A}\right)\frac{M}{m_H R^3}\right]^{4/3} \propto R^{-4} \qquad (34)$$

Eqn. (34) tells us that when the particles achieve relativistic speeds, their electron degeneracy pressure is no
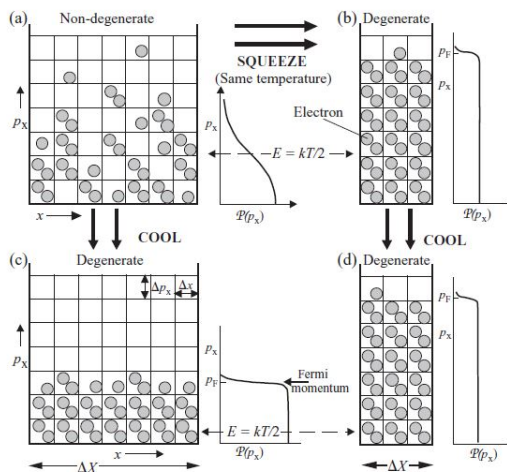
FIG. 3: This graph captures how the momentum of Fermi particles increases as the space they occupy is contracted. There are fewer lower energy states available, so the particles are forced to occupy higher energy and higher momentum states. Figure adapted from [2].

longer steeper than the gravitational pressure. The star is now dynamically unstable [1]. This means that if the star accretes additional mass, shrinks and becomes denser, electron degeneracy pressure will not act as a restorative force, and nothing will be able to stop the gravitational collapse of the star. Once again, we can set the inward gravitational pressure equal to the outward electron degeneracy pressure to gain some insight.

$$\frac{GM^2}{R^4} \simeq \hbar c \left[\left(\frac{Z}{A} \right) \frac{M}{m_H R^3} \right]^{4/3} \tag{35}$$

This time the expression for mass is indipendent of radius, and we obtain (setting $Z/A = 0.5$)

$$M_{Ch} \simeq \left(\frac{\hbar c}{G} \right)^{3/2} \left[\left(\frac{Z}{A} \right) \frac{1}{m_H} \right]^2 \simeq \mathcal{O}(M_\odot) \tag{36}$$

A precise derivation with correct proportionality constants leads to [1]

$$M_{Ch} \simeq 1.44 M_\odot \tag{37}$$

This is known as the *Chandrasekhar limit*, which is the upper bound to the mass a white dwarf can have, if it is to avoid gravitational collapse.

C. Ultimate fate of white dwarfs

Although the white dwarf phase is typically considered as the stage by which point most stars have ended their lives, it is interesting to see what ultimately happens to these stars. As we will see, if a white dwarf does not accrete matter up to the Chandrasekhar limit, it will simply cool off and slowly dissipate its thermal energy. As it cools, the star's carbon and oxygen will eventually crystallize. If on the other hand it gains enough mass to reach the Chandrasekhar limit, it will give way to a spectacular explosion, known as a type Ia supernova.

A satisfying analysis of either of these scenarios requires a detailed description of the structure of the different layers of the star, which is beyond the scope of this paper. In this section we will simply give a qualitative description of the processes.

1. Cooling & crystallization

For the star to cool, energy needs to be transported outward from its interior. In a main-sequence star, photons can typically travel much farther than atoms before losing their energy in a collision. Thus energy is transported from the interior of the star to its surface through radiation. In white dwarfs instead, since most of the low energy states are already occupied, the degenerate electrons cannot lose their energy in a collision and jump to a lower energy state. Therefore the electrons can travel long distances without losing their energy, and are the primary transporters of energy from the interior to the surface of the white dwarfs.

This process is extremely efficient, to the point that, aside from a thin layer around the surface, most of the star is isothermal. Near the surface, density decreases, increasing the quantity $T/\rho^{2/3}$, and by the condition given in Eqn. (24) it reaches a point where the matter can no longer be described as degenerate [1]. Figure IV captures this phenomenon.
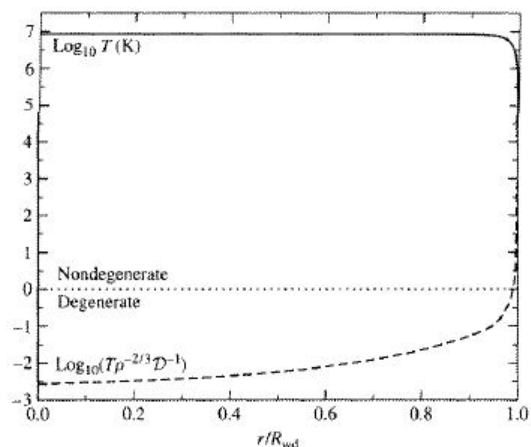

FIG. 4: Temperature and degeracy level in the interior of a white dwarf model. Here $\mathcal{D} = 1261 \frac{K}{m^2 kg^{2/3}}$ as from the condition in Eqn. (24). Figure adapted from [1].

The fact that the interior of the star transitions from degeneracy to non-degeneracy can be used (see [1] for

a derivation) to show that the star's surface luminosity depends on the star's interior temperature according to $L_{Surf} \propto T_c^{7/2}$ [1]. On the other hand, the interior of the star loses thermal energy according to the Stefan-Boltzmann law, in which $L_{Int} \propto T_c^4$. Therefore, the interior of the star cools faster than its surface.

As the star cools, the nuclei begin aligning into a crystalline lattice, since it is the lowest energy system configuration. The nuclei maintain this structure by electrostatic repulsion and vibrate coherently across the lattice. The crystallization process starts at the center, which cools faster, and expands out toward the surface. Eventually, the ultimate fate of the star is to become an "Earth-sized diamond", made of crystallized carbon and oxygen, floating around indefinitely in space [1].

2. *Type Ia supernovae*

Type Ia supernovae are extremely luminous explosions, that have been found to be highly consistent in terms of energy output. Thus they have become one the most widely used "standard candles" adopted by astronomers to determine inter-galactic distances. Given the similarity between all observed type Ia supernovae, physicists believe they must be caused by a fairly uniform mechanism. Additionally, their spectra do not contain hydrogen lines, implying that they must be caused by evolved objects who have already converted their hydrogen to heavier elements [2].

The most widely accepted explanation is that these supernovae are triggered by a white dwarf accreting enough mass to reach the Chandrasekhar limit. This could happen if two white dwarf stars are in binary orbit, with the less massive star disintegrating and combining with the more massive star. As the more massive star nears the Chandrasekhar limit, nuclear reactions re-ignite near its center and blow up the star. This is known as the "double-degenerate model" [1].

The other scenario which could lead to type Ia supernovae is a binary orbit between a main-sequence star and a white dwarf, known as the "single-degenerate model".

The helium accreted by the white dwarf forms a layer above its degenerate carbon-oxygen interior. The helium also becomes degenerate, and when enough helium has accumulated, it explodes in a runaway thermo-nuclear reaction. This explosion, known as a helium flash, only lasts a few seconds but releases a large amount of energy. It also creates a shock wave that propagates inwards throughout the interior of the star. This is thought to trigger ignition of the degenerate carbon and oxygen, and the nuclear reactions ultimately cause the white dwarf to explode in a type Ia supernovae, disintegrating it [1].

IV.   CONCLUSION

In the first part of the paper we described the relevant basic principles of quantum mechanics. We used this foundation to develop Fermi statistics and subsequently electron degeneracy pressure, which is the key phenomenon that sustains white dwarf stars from gravitational collapse. We then derived an estimation of the limiting mass white dwarfs can possess, before electron degeneracy pressure can no longer withstand the inward gravitational pressure. In the final sections of the paper we qualitatively described the ultimate fate of white dwarf stars, in the two scenarios of isolated stars and stars in binary systems.

In future studies we would like to explore current research on type Ia supernovae and analytically develop the processes which are thought to occur. In particular, we are interested in the mechanisms that lead to the ignition of degenerate carbon and oxygen in the white dwarfs' core which cause the stars to explode rather than collapse.

[1] Carroll B.W., Ostlie D.A., "An Introduction to Modern Astrophysics", *Pearson Education, Inc.*, 2007.

[2] Bradt H., "Astrophysics Processes: The Physics of Astronomical Phenomena", *Cambridge University Press*, 2008.

[3] Huang, "N-Body System of Identical Particles".

[4] Griffiths D., "Introduction to Quantum Mechanics", *Pearson Education, Inc.*, 2004.

[5] Shankar R., "Principles of Quantum Mechanics", 1994.

[6] Fointaine, Brassard, Charpinet, Randall, Van Grootel, "An Overview of White Dwarf Stars", *EDP Sciences*, 2013.

[7] Kardar M., "Statistical Physics of Particles", *Cambridge Univ. Press*.

[8] Sakurai J.J., "Modern Quantum Mechanics", *Pearson Education, Inc.*, 2010.

[9] Kawaler S.D., Winget D.E., "White Dwarfs: Fossil Stars", *Sky and Telescope*, August 1987.

[10] Trimble V., "White Dwarfs: The Once and Future Suns", *Sky and Telescope*, October 1986.

[11] D'Antona F., Mazzitelli I., "Cooling of White Dwarfs", *Annual Review of Astronomy and Astrophysics*, 139, 1990.

[12] Salaris M., "The Cooling of CO White Dwarfs: Influence of the Internal Chemical Distribution", *The Astrophysical Journal, 486*, 413, 1997.

CP Violation in Neutral Kaon Oscillations

Jay M. Lawhorn
MIT Department of Physics
(Dated: May 2, 2014)

A two-state formalism for the neutral kaon system is developed, including considerations for neutral meson oscillations and CP violation. I give a brief introduction to the electroweak Lagrangian and the Cabibbo-Kobayashi-Maskawa matrix as they relate to the decay and oscillations of the neutral kaon. I derive the electroweak and CP eigenbases in terms of the strong force eigenbasis by considering the matrix elements of the effective Hamiltonian for the neutral kaon two-state system. I then consider the time evolution of the electroweak eigenstates and discuss indirect and direct CP violating phenomenon in the neutral kaon system.

I. INTRODUCTION

In October 1956, Tsung Dao Lee of Columbia University and Chen Ning Yang of the Institute of Advanced Study at Princeton published a paper [1] that not only opened up an entirely new realm of physics, but also lead to the duo receiving the Nobel prize 14 months later. At the time, all physics was assumed to be invariant under parity transformations, which invert all spatial coordinates. However, while Lee and Yang found that the experimental evidence suggested the strong nuclear force, electromagnetism, and gravity preserved parity symmetry, they found no one had ever investigated parity symmetry in the weak nuclear force. In the same paper, they suggested some simple experiments that could test the effect of parity transformations on weak interactions.

By January 1957, Chien-Shiung Wu of Columbia University showed that the beta decay of cobalt-60 did not preserve parity [2] and another group at Columbia showed that pion and muon decays did not either [3]. This means that the weak interaction somehow makes a distinction between right and left, which went against the prevailing physical intuition at the time.

Symmetries in physics are important because according to Noether's theorem, every symmetry corresponds to a conservation law. By the late 1950's Schwinger, Luders, and Pauli had independently proved that any physical system that is invariant under Lorentz transformations is also invariant under the CPT operator, which takes a particle to its anti-particle under spatial coordinate inversion and time reversal. Physical intuition about handedness aside, physicists also wanted parity symmetry to be true because it is a stronger statement than CPT symmetry - it gives more constraints on the behavior of the system than simply reiterating Lorentz invariance. After parity violation was observed, many physicists still wanted a stronger symmetry. The new proposal was that physical laws are the same for matter and anti-matter under spatial coordinate inversion, known as CP symmetry.

This new symmetry seemed to hold up until 1964, when James Cronin and Val Fitch established that neutral kaons do not conserve CP symmetry in their decays to pions [4]. The observation of CP violation in the weak nuclear force was a very powerful statement about real-

ity. In fact, CP violation led Kobayashi and Maskawa to predict the existence of three new quarks [5] to accompany the already known up, down, and strange quarks in 1973. As modern students of physics will know, the top quark discovery in 1995 rounded out the predicted three generations of quarks, twenty years later!

Clearly CP violation was a powerful physical observation and it is still a rich and active area of research today. In this paper I will present a model for the behavior of neutral kaon systems, including neutral kaon oscillations and CP violating effects. The presented analysis applies equally well to the neutral B^0, B^0_s, and D^0 mesons, but for simplicity I consider only the neutral kaon.

II. KAONS AND THE STANDARD MODEL

A neutral kaon is a meson, or bound state of two quarks, composed of either a down quark and a strange anti-quark (K^0) or a down anti-quark and a strange quark $(\overline{K^0})$. In the Standard Model, kaon decay is mediated by the $W^\pm$ boson, and they commonly decay into pions, which are composed of up and down type-quarks.

For example, the $\overline{K^0}$ in Figure 1 decays into a π^+ and π^- when the kaon's strange quark becomes an up quark by emitting a W^-, which then decays into a down quark and up anti-quark. The down anti-quark from the original $\overline{K^0}$ and the up quark form a π^+, while the down quark and up anti-quark form a π^-.
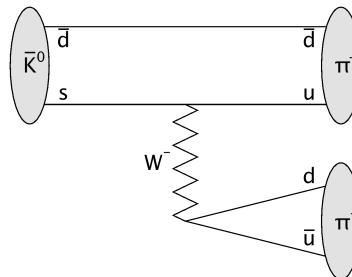

FIG. 1: Kaon decay into two charged pions.

Diagrams like Figure 1 can be interpreted using Feynman rules to relate them to the Standard Model La-

grangian for electroweak interactions. A full discussion of the electroweak force and the Standard Model could easily span several semester courses or books, so I will not go into much detail here. Interested readers can find more information in [6]. The generic Lagrangian for interactions between an anti-up type quark, a down type quark, and a $W^\pm$ boson is given by

$$\mathcal{L}_{W^\pm} = -\frac{g_W}{\sqrt{2}}\overline{u_{Li}}\gamma^\mu \left(V_{\text{CKM}}\right)_{ij} d_{Lj} W_\mu^+ + \text{h.c.} \qquad (1)$$

For our purposes, it is sufficient to note that u_{Li} is the vector (u, c, t) corresponding to the three up-type quarks: up, charm, top; d_{Lj} is the vector (d, s, b) corresponding to the three down-type quarks: down, strange, bottom; and V_{CKM} is the Cabibbo-Kobayashi-Maskawa (CKM) mixing matrix.

The CKM matrix is a 3×3 unitary matrix that is most simply written as

$$V_{\text{CKM}} = \begin{pmatrix} V_{ud} & V_{us} & V_{ub} \\ V_{cd} & V_{cs} & V_{cb} \\ V_{td} & V_{ts} & V_{tb} \end{pmatrix} \qquad (2)$$

where each matrix element corresponds to the strength of the coupling between each set of quarks. The values of the nine matrix elements are determined empirically - there is currently no theoretical model that predicts their values.

In Figure 1, we have two vertices of made up of two quarks and a W^- boson, which leads to an overall probability amplitude proportional to $V_{us}V_{ud}^*$. However, there are also other more complicated diagrams that also contribute to the decay of a kaon into two pions with smaller probability amplitudes involving additional vertices.

An interesting phenomenon in the neutral kaon system is oscillation, where a K^0 becomes a $\overline{K^0}$ or vice versa through a box diagram like the one shown in Figure 2.
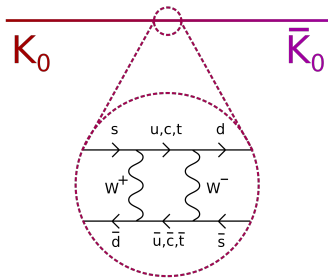

FIG. 2: Kaon oscillation. From [7].

Neutral kaon oscillations occur when the two particles making up the kaon exchange two $W^\pm$ bosons, ending up in the other neutral kaon state. This is possible because electroweak processes, like the emission of a $W^\pm$, do not conserve flavor, unlike strong nuclear processes. Similar phenomenon is also observed in neutrinos.

III.   OPERATORS

Now that we're familiar with our physical system of interest, we need to define our operators and their effects. The two operators of interest, charge conjugation and parity, perform discrete transformations.

The charge conjugation operator, C, transforms a particle into its antiparticle. Since the anti-particle of an anti-particle is simply the particle itself, $C^2 = 1$. I choose to define C such that for a quark q,

$$C|q\rangle = |\overline{q}\rangle, \quad C|\overline{q}\rangle = |q\rangle \qquad (3)$$

where $\overline{q}$ is the anti-quark of the same flavor.

The parity operator, P, inverts all spatial coordinates. As with C, applying P to a system twice returns the system to its original configuration, such that $P^2 = 1$. This means that the eigenvalues of the parity operator can only be -1 or 1. A result from quantum field theory requires that fermionic particles and anti-particles must have opposite parity eigenvalues, but the choice of which eigenvalue is which is arbitrary. Following the convention in Griffiths [6], I define P such that

$$P|q\rangle = |q\rangle, \quad P|\overline{q}\rangle = -|\overline{q}\rangle. \qquad (4)$$

Both C and P are multiplicative, such that

$$P|q\overline{q}\rangle = (P|q\rangle)(P|\overline{q}\rangle) = (+1)(-1)|q\overline{q}\rangle = -|q\overline{q}\rangle. \qquad (5)$$

The CP operator acting on a quark and anti-quark system is thus

$$CP|q\overline{q}\rangle = -|\overline{q}q\rangle. \qquad (6)$$

Neutral kaons, which are composed of two quarks are initially produced as either a K^0 ($d\overline{s}$) or $\overline{K^0}$ ($\overline{d}s$). These two mesons have parity eigenvalue -1, and so acting on a neutral kaon with the CP operator yields

$$CP|K^0\rangle = -|\overline{K^0}\rangle, \quad CP|\overline{K^0}\rangle = -|K^0\rangle. \qquad (7)$$

Clearly, neither neutral kaon is a CP eigenstate. However, two CP eigenstates can be constructed:

$$\begin{aligned} |K_1\rangle &= \frac{1}{\sqrt{2}}(|K^0\rangle - |\overline{K^0}\rangle) \\ |K_2\rangle &= \frac{1}{\sqrt{2}}(|K^0\rangle + |\overline{K^0}\rangle) \end{aligned} \qquad (8)$$

where $|K_1\rangle$ is CP even (eigenvalue $+1$) and $|K_2\rangle$ is CP odd (eigenvalue -1).

The kaon commonly decays into two charged pions $(\pi^+\pi^-)$, two neutral pions $(\pi^0\pi^0)$, or three pions $(\pi^0\pi^0\pi^0$ or $\pi^0\pi^+\pi^-)$. Like the kaon, pions have a parity eigenvalue -1, so a final state with n pions has overall parity $(-1)^n$. The neutral pion is its own anti-particle, and the charged pions are each other's anti-particles such that

$$C|\pi^0\rangle = -|\pi^0\rangle, \quad C|\pi^\pm\rangle = -|\pi^\mp\rangle. \qquad (9)$$

Then under the CP operator the pion final states are,

$$CP|2\pi\rangle = |2\pi\rangle, \ \ CP|3\pi\rangle = -|3\pi\rangle \tag{10}$$

such that the two pion final states are CP even and three pion final states are CP odd. If CP is conserved, the even $|K_1\rangle$ states can only decay to the even two pion final states, while the odd $|K_2\rangle$ states can only decay to three pion final states.

IV. NEUTRAL MESON OSCILLATIONS

Now we develop the neutral kaon system as a two state system, including oscillatory and CP-violating behavior, starting from the weak nuclear force Lagrangian and symmetry considerations. The two state model is valid only when ignoring the various decay final states and for timescales that are much larger than the characteristic timescale of the strong nuclear force. The following discussion follows a number of sources: [6, 8–12].

The neutral meson two-state system is governed by a 2×2 non-Hermitian effective Hamiltonian $\mathcal{H} = M - \frac{i}{2}\Gamma$ where M and Γ are Hermitian such that

$$\begin{pmatrix} \mathcal{H}_{11} & \mathcal{H}_{12} \\ \mathcal{H}_{21} & \mathcal{H}_{22} \end{pmatrix} = \begin{pmatrix} M_{11} & M_{12} \\ M_{21} & M_{22} \end{pmatrix} - \frac{i}{2} \begin{pmatrix} \Gamma_{11} & \Gamma_{12} \\ \Gamma_{21} & \Gamma_{22} \end{pmatrix}. \tag{11}$$

The non-Hermitian character of $\mathcal{H}$ reflects the fact that we are allowing the kaons to decay to states that are not represented in the two state system, thus the probability is not conserved. The matrix M corresponds to mass or propagator terms, while the Γ matrix corresponds to decay terms.

The matrix elements can be approximately evaluated by treating the weak nuclear force as a perturbation to the strong nuclear force eigenstates that the K^0 and $\overline{K^0}$ are produced in, then applying time-independent perturbation theory to second order. We use second order perturbation theory to include oscillations like the one shown in Figure 2. The diagonal matrix elements of M are

$$M_{11} = m_{K^0} + \langle K^0|H_{\text{weak}}|K^0\rangle$$
$$+ \sum \frac{|\langle n|H_{\text{weak}}|K^0\rangle|^2}{(m_{K^0} - m_n)}$$
$$M_{22} = m_{K^0} + \langle \overline{K^0}|H_{\text{weak}}|\overline{K^0}\rangle \tag{12}$$
$$+ \sum \frac{|\langle n|H_{\text{weak}}|\overline{K^0}\rangle|^2}{(m_{K^0} - m_n)}$$

where H_{weak} is the standard model Hamiltonian for the weak nuclear force, and $|n\rangle$ is some intermediate state. These terms represent flavor-preserving oscillations where $K^0 \to K^0$ or $\overline{K^0} \to \overline{K^0}$.

The off-diagonal terms represent flavor-changing oscillations where $K^0 \to \overline{K^0}$ or $\overline{K^0} \to K^0$. Because we require M to be Hermitian, the off-diagonal matrix elements are each other's complex conjugates. The M_{21}

term is given by

$$M_{21} = M_{12}^* = \langle \overline{K^0}|H_{\text{weak}}|K^0\rangle$$
$$+ \sum \frac{\langle \overline{K^0}|H_{\text{weak}}|n\rangle\langle n|H_{\text{weak}}|K^0\rangle}{(m_{K^0} - m_n)}. \tag{13}$$

The matrix Γ has matrix elements

$$\Gamma_{11} = \pi \sum \rho_F |\langle F|H_{\text{weak}}|K^0\rangle|^2$$
$$\Gamma_{22} = \pi \sum \rho_F |\langle F|H_{\text{weak}}|\overline{K^0}\rangle|^2$$
$$\Gamma_{21} = \Gamma_{12}^* = \tag{14}$$
$$\pi \sum \rho_F \langle \overline{K^0}|H_{\text{weak}}|F\rangle\langle F|H_{\text{weak}}|K^0\rangle$$

where $|F\rangle$ is a given final state and ρ_F is the corresponding density matrix for that final state.

By requiring that M and Γ are Hermitian matrices, we find that $\mathcal{H}$ is given by

$$\mathcal{H} = \begin{pmatrix} M_{11} - \frac{i}{2}\Gamma_{11} & M_{21}^* - \frac{i}{2}\Gamma_{21}^* \\ M_{21} - \frac{i}{2}\Gamma_{21} & M_{22} - \frac{i}{2}\Gamma_{22} \end{pmatrix}. \tag{15}$$

We additionally require that the matrix $\mathcal{H}$ be invariant under CPT transformation:

$$(CPT) \begin{pmatrix} M_{11} - \frac{i}{2}\Gamma_{11} & M_{21}^* - \frac{i}{2}\Gamma_{21}^* \\ M_{21} - \frac{i}{2}\Gamma_{21} & M_{22} - \frac{i}{2}\Gamma_{22} \end{pmatrix} (CPT)^{-1}$$
$$= \begin{pmatrix} M_{22} - \frac{i}{2}\Gamma_{22} & M_{21}^* - \frac{i}{2}\Gamma_{21}^* \\ M_{21} - \frac{i}{2}\Gamma_{21} & M_{11} - \frac{i}{2}\Gamma_{11} \end{pmatrix} \tag{16}$$
$$= \begin{pmatrix} M_{11} - \frac{i}{2}\Gamma_{11} & M_{21}^* - \frac{i}{2}\Gamma_{21}^* \\ M_{21} - \frac{i}{2}\Gamma_{21} & M_{22} - \frac{i}{2}\Gamma_{22} \end{pmatrix}$$

and we see that $M_{11} = M_{22} = M$ and $\Gamma_{11} = \Gamma_{22} = \Gamma$. This is the equivalent of requiring that a particle and its anti-particle have the same mass and decay widths.

Now we want to diagonalize this matrix, which requires us to solve the following eigenvalue equation:

$$\begin{pmatrix} M - \frac{i}{2}\Gamma & M_{21}^* - \frac{i}{2}\Gamma_{21}^* \\ M_{21} - \frac{i}{2}\Gamma_{21} & M - \frac{i}{2}\Gamma \end{pmatrix} \begin{pmatrix} K^0 \\ \overline{K^0} \end{pmatrix} = \lambda \begin{pmatrix} K^0 \\ \overline{K^0} \end{pmatrix} \tag{17}$$

where λ is the eigenvalue times the identity matrix.

Solving for the eigenvalues λ, we find that

$$\lambda = (M - \frac{i}{2}\Gamma) \pm \sqrt{(M_{21}^* - \frac{i}{2}\Gamma_{21}^*)(M_{21} - \frac{i}{2}\Gamma_{21})}. \tag{18}$$

To simplify our expression, we define

$$\eta = \sqrt{\frac{M_{21} - \frac{i}{2}\Gamma_{21}}{M_{21}^* - \frac{i}{2}\Gamma_{21}^*}}, \tag{19}$$

which we understand as a measure of CP violation in the system.

The eigenstates of the above equation are given by

$$|K_A\rangle = \frac{1}{\sqrt{1 + |\eta|^2}}(|K^0\rangle - \eta|\overline{K^0}\rangle)$$
$$|K_B\rangle = \frac{1}{\sqrt{1 + |\eta|^2}}(|K^0\rangle + \eta|\overline{K^0}\rangle). \tag{20}$$

Note that if we require exact CP symmetry, $\eta = 1$, and $|K_A\rangle$ and $|K_B\rangle$ are the CP eigenstates discussed above:

$$|K_1\rangle = \frac{1}{2}(|K^0\rangle - |\overline{K^0}\rangle)$$
$$|K_2\rangle = \frac{1}{2}(|K^0\rangle + |\overline{K^0}\rangle). \tag{21}$$

V. MASS EIGENSTATES

In 1955, Murray Gell-Mann and Abraham Pais noted that perhaps the K^0 and $\overline{K^0}$ basis was not the most natural one to use when considering decays of the neutral kaon [13]. K^0 and $\overline{K^0}$ are eigenstates of the strong nuclear force, but kaons decay via the *weak* nuclear force. They suggested instead that perhaps there were two distinct eigenstates of the CP operator, one odd and one even. On the assumption of CP symmetry, the CP even state would have to decay to another CP even state, like two pions, and the CP odd state to something CP odd, like three pions. This would lead to two distinct populations of neutral kaons with separate lifetimes and masses.

The next year, an experiment at the Brookhaven Cosmotron observed two distinct components in a neutral kaon beam [14]. These two components are the actual particles with well-defined lifetimes and masses, not the K^0 and $\overline{K^0}$ created by the strong nuclear force. They were identified by their lifetimes as the K_S (K-short) and K_L (K-long). As it turns out, the lifetimes of the two particles are vastly different, with the K_S lifetime $(0.8954 \pm 0.00004) \times 10^{-10}$, and the K_L lifetime $(511.6 \pm 2.1) \times 10^{-10}$ [15].

Eventually, Cronin and Fitch discovered that the K_L and K_S are not exactly the two CP eigenstates discussed above. To understand the physical system, we instead define

$$|K_S\rangle = \frac{1}{\sqrt{1 + |\epsilon|^2}}(|K_1\rangle + \epsilon|K_2\rangle)$$
$$|K_L\rangle = \frac{1}{\sqrt{1 + |\epsilon|^2}}(|K_2\rangle + \epsilon|K_1\rangle) \tag{22}$$

where $|K_1\rangle$ and $|K_2\rangle$ are the CP eigenstates, and ϵ parameterizes the CP violation in the mass eigenstates.

In terms of the strong eigenstates K_L and K_S are thus

$$|K_L\rangle = \frac{1}{\sqrt{2}\sqrt{1 + |\epsilon|^2}}((1 + \epsilon)|K^0\rangle + (1 - \epsilon)|\overline{K^0}\rangle)$$
$$|K_S\rangle = \frac{1}{\sqrt{2}\sqrt{1 + |\epsilon|^2}}((1 - \epsilon)|K^0\rangle + (1 + \epsilon)|\overline{K^0}\rangle). \tag{23}$$

Upon inspection, we identify the η parameter from Equation 20 as $(1 - \epsilon)/(1 + \epsilon)$ so Equation 23 becomes

$$|K_L\rangle = \frac{1}{\sqrt{1 + |\eta|^2}}(|K^0\rangle + \eta|\overline{K^0}\rangle)$$
$$|K_S\rangle = \frac{1}{\sqrt{1 + |\eta|^2}}(|K^0\rangle - \eta|\overline{K^0}\rangle). \tag{24}$$

Now that we have parameterized these two distinct mass eigenstates K_S and K_L, we turn next to understanding their behavior as a function of time. Consider a beam of kaons that is some mixture of K^0 and $\overline{K^0}$ at time $t = 0$:

$$|\psi(0)\rangle = a(0)|K^0\rangle + b(0)|\overline{K^0}\rangle. \tag{25}$$

The time evolution of this system is governed by the non-Hermitian effective Hamiltonian

$$\mathcal{H}\begin{pmatrix} a \\ b \end{pmatrix} = i\frac{\partial}{\partial t}\begin{pmatrix} a \\ b \end{pmatrix}. \tag{26}$$

Solving Equation 23 for K^0 and $\overline{K^0}$, we can rewrite $|\psi\rangle$ as

$$|\psi(t)\rangle = \sqrt{1 + |\eta|^2}(\frac{a(t)}{2}(|K_L\rangle + |K_S\rangle)$$
$$+ \frac{b(t)}{2\eta}(|K_L\rangle - |K_S\rangle))$$
$$= \sqrt{1 + |\eta|^2}((\frac{a(t)}{2} + \frac{b(t)}{2\eta})|K_L\rangle$$
$$+ (\frac{a(t)}{2} - \frac{b(t)}{2\eta})|K_S\rangle). \tag{27}$$

Now define $a_L(t)$ and $a_S(t)$ such that

$$a_L(t) = a(t) + \frac{b(t)}{\eta}, \quad a_S(t) = a(t) - \frac{b(t)}{\eta}. \tag{28}$$

The time evolution for $a_L(t)$ is then given by

$$i\frac{\partial a_L(t)}{\partial t} = \lambda_+ a_L(t), \tag{29}$$

where λ_+ is the larger eigenvalue from Equation 18. In the same way as the initial formulation of the Hamiltonian, we identify the real part of the eigenvalue as the K_L mass and the imaginary part as the K_L decay rate such that

$$m_L = M + \mathcal{R}e\left(\sqrt{(M_{21}^* - \frac{i}{2}\Gamma_{21}^*)(M_{21} - \frac{i}{2}\Gamma_{21})}\right)$$
$$\Gamma_L = \Gamma - 2\mathcal{I}m\left(\sqrt{(M_{21}^* - \frac{i}{2}\Gamma_{21}^*)(M_{21} - \frac{i}{2}\Gamma_{21})}\right). \tag{30}$$

By the same logic with the smaller eigenvalue from Equation 18,

$$m_S = M - \mathcal{R}e\left(\sqrt{(M_{21}^* - \frac{i}{2}\Gamma_{21}^*)(M_{21} - \frac{i}{2}\Gamma_{21})}\right)$$
$$\Gamma_S = \Gamma + 2\mathcal{I}m\left(\sqrt{(M_{21}^* - \frac{i}{2}\Gamma_{21}^*)(M_{21} - \frac{i}{2}\Gamma_{21})}\right). \tag{31}$$

Now that we have the eigenvalues associated with the K_S and K_L states, we can rewrite the time evolution equation as

$$\begin{pmatrix} m_L - \frac{i}{2}\Gamma_L & 0 \\ 0 & m_2 - \frac{i}{2}\Gamma_S \end{pmatrix}\begin{pmatrix} a_L \\ a_S \end{pmatrix} = i\frac{\partial}{\partial t}\begin{pmatrix} a_L \\ a_S \end{pmatrix}. \tag{32}$$

Finally we find that

$$|\psi(t)\rangle = a_L(0)e^{-im_L t - \Gamma_L t/2}|K_L\rangle$$
$$+ a_S(0)e^{-im_S t - \Gamma_S t/2}|K_S\rangle. \tag{33}$$

This equation contains both an oscillatory term that goes as e^{-imt} as well as an exponentially decaying envelope that goes as $e^{-\Gamma t}$ and as expected, the total probability is not conserved.

VI. CP VIOLATION

We are now prepared to examine the CP violating phenomenon in the neutral kaon system. Combining Equations 22 and 33, we find

$$|\psi(t)\rangle = \frac{1}{\sqrt{1+|\epsilon|^2}}(a_S(0)e^{-im_S t - \Gamma_S t/2}(|K_1\rangle + \epsilon|K_2\rangle)$$
$$+ a_L(0)e^{-im_L t - \Gamma_L t/2}(|K_2\rangle + \epsilon|K_1\rangle)). \tag{34}$$

If we then assume that even two pion final states come from the CP even state, K_1, the decay rate is

$$\Gamma(\psi(t) \to \pi\pi) \propto |\langle K_1|\psi(t)\rangle|^2$$
$$\propto \left(e^{-im_S t - \Gamma_S t/2} + \epsilon e^{-im_L t - \Gamma_L t/2}\right)^2$$
$$= e^{-\Gamma_S t} + |\epsilon|^2 e^{-\Gamma_L t} \tag{35}$$
$$+ 2|\epsilon|\cos(\Delta M t + \phi)e^{-(\Gamma_S + \Gamma_L)t/2},$$

where $\Delta M = M_L - M_S = \mathcal{R}e(\lambda_L - \lambda_S)$ is the mass difference between the two eigenstates and ϕ is an arbitrary phase. This equation contains three separate components to the two pion final state.

The largest component comes from the K_S decays. Next there is the term suppressed by a factor of $|\epsilon|$ representing interference between the K_S and K_L decays. The smallest term is from K_L decays, suppressed by a factor of $|\epsilon|^2$.

After many K_S lifetimes, our kaon beam is almost entirely composed of K_L. Remember that the K_L and K_S states were thought to be precisely the CP eigenstates K_1 and K_2. In that case, $\epsilon = 0$ and the two pion final states should die out with the same decay constant as the K_S component. However, if $\epsilon \neq 0$, there will also be a much longer lived population of two pion final states that falls of with the K_L component of the beam.

It was this long-lived population of CP even two pion final states that Cronin and Fitch observed in 1964 [4] as the first evidence of CP-violation by the weak nuclear force. It is known as indirect CP violation or CP violation in mixing because the effect doesn't involve an actual CP-violating process. Instead it shows that the mass eigenstates, K_L and K_S are not themselves eigenstates of the CP operator, but are both mixtures of CP odd and CP even states.

Cronin and Fitch's original experiment observed 45 ± 10 two pion decays out of 22,700 total decays in a region where the K_S had long since died out. This rate corresponds to a branching ratio of $R = (K_L \to \pi^+\pi^-)/(K_L \to \text{charged}) = (2.0 \pm 0.4) \times 10^{-3}$ and $|\epsilon| \approx 2.3 \times 10^{-3}$ [4].

Current measurements indicate $|\epsilon| = (2.228 \pm 0.0011) \times 10^{-3}$ [10], which is not far off Cronin and Fitch's original result.

There is also a much smaller asymmetry in the decays themselves, known as direct CP violation or CP violation in decay, which can be measured in the ratio between $K^0 \to \pi^0\pi^0$ and $\overline{K^0} \to \pi^0\pi^0$ events. We define

$$\eta_{+-} = \frac{A(K_L \to \pi^+\pi^-)}{A(K_S \to \pi^+\pi^-)} \approx \epsilon + \epsilon'$$
$$\eta_{00} = \frac{A(K_L \to \pi^0\pi^0)}{A(K_S \to \pi^0\pi^0)} \approx \epsilon - 2\epsilon' \tag{36}$$

where ϵ is the previously defined indirect CP violation factor, and ϵ' is the direct CP violation factor.

Direct CP violation was not conclusively observed in the neutral kaon system until the late 1990's by the KTeV experiment at Fermilab and the NA48 experiment at CERN [16]. They measured the observable

$$\frac{\Gamma(K_L \to \pi^+\pi^-)/\Gamma(K_S \to \pi^+\pi^-)}{\Gamma(K_L \to \pi^0\pi^0)/\Gamma(K_S \to \pi^0\pi^0)} = \left|\frac{\eta_{+-}}{\eta_{00}}\right|^2$$
$$\approx 1 + 6\mathcal{R}e(\epsilon'/\epsilon). \tag{37}$$

This can be interpreted as a measure of the relative strength of the direct and indirect CP violating effects. The KTeV experiment measured $\mathcal{R}e(\epsilon'/\epsilon) = (19.2 \pm 2.1) \times 10^{-4}$, indicating that direct CP violation is about ten thousand times less likely than indirect CP violation.

Similar types of CP violation have also been observed in semi-leptonic channels of the neutral kaon, the charged kaons, and the B^0, B_s^0, and D^0 mesons. These CP violating and oscillatory parameters can be used to constrain the values of the CKM matrix, and could potentially show physics beyond the Standard Model as well. It is thought that some yet-to-be-observed CP violation will eventually explain the matter-antimatter asymmetry of our universe. It is an experimentally and theoretically rich topic still being explored today, but this brief introduction to CP violation in the neutral kaon system covers the fundamental observations that established CP violation, as well as a simple model to interpret these phenomenon.

[1] T.D. Lee and C.N. Yang, *Question of Parity Conservation in Weak Interactions*, Phys. Rev. 104, 254 (1956).

[2] C.S. Wu, et al., *Experimental Test of Parity Conservation in Beta Decay*, Phys. Rev. 105, 1413 (1957).

[3] R.L. Garwin, L.M. Lederman, and M. Weinrich, *Observation of the Failure of Conservation of Parity and Charge Conjugation in Meson Decays: the Magnetic Moment of the Free Muon*, Phys. Rev. 105, 1415 (1957).

[4] J.H. Christenson, et al., *Evidence for the 2π Decay of the K_2^0 Meson*, Phys. Rev. Lett. 13, 138 (1964).

[5] M. Kobayashi, T. Maskawa, *CP-Violation in the Renormalizable Theory of Weak Interaction*, Prog. Theor. Phys. 49, 652 (1973).

[6] D. Griffiths, *Introduction to Elementary Particles*, Second Edition, Wiley-VCH (Weinheim, 2010).

[7] Taken from Wikimedia Commons: http://commons.wikimedia.org/wiki/File:Kaon-box-diagram-with-bar.svg

[8] T.D. Lee, and C.S. Wu, *Weak Interactions (Second section) Ch. 9: Decays of Neutral K Mesons*, Annu. Rev. Nucl. Sci. 16, 511 (1966).

[9] M.A. Thomson, *The CKM Matrix and CP Violation*, course notes, 2009.

[10] PDG Collaboration, *CP Violation in the Quark Sector*, Phys. Rev. D86, 010001 (2012).

[11] G. D'Ambrosio and g. Isidori, *CP Violation in Kaon Decays*,

[12] M. Klute *8.811 Lecture Notes*

[13] M. Gell-Mann and A. Pais, *Behavior of Neutral Particles under Charge Conjugation*, Phys. Rev. 97, 1387 (1955).

[14] K. Lande, et al., *Observation of Long-Lived Neutral V Particles*, Phys. Rev. 103, 1901 (1956).

[15] PDG Collaboration, *Review of Particle Physics*, Phys. Rev. D86, 010001 (2012).

[16] KTeV Collaboration, *Precise Measurements of direct CP violation, CPT symmetry, and other parameters in the neutral kaon system*, Phys. Rev. D83, 092001 (2011).

Origins of Spin

Yuri D. Lensky*

MIT Physics Department

(Dated: May 2, 2014)

We derive the the group properties of the Lorentz transform, and from them the Dirac equation, assuming only the relativity principle, a constant speed of light c, that physical laws must be based on observables, and that eigenvalues of Hermitian operators correspond to observables in the formalism of quantum mechanics. Notably, we make no assumptions about the form of our law (we choose the simplest non-trivial one), we do not postulate the relativistic energy-momentum relation $E^2 = p^2 + m^2$, nor do we bring up boosts as anything other than a passing remark. This serves as a demonstration that effects arising from the Dirac equation, the most tractable being particle spin, can be seen as artifacts solely and directly of the principle of relativity. The form of the Dirac equation is also shown to motivate the energy-momentum relationship.

I. INTRODUCTION

Non-relativistic quantum mechanics, although extraordinarily accurate and useful in a wide range of applications, suffers from lack of explanatory power rather quickly. Taking for instance the question of particle spin, why a single particle at rest should have a multiple component wave-function is not explained, and the corrections to the non-relativistic Hamiltonian are phenomenological; although analogies to classical angular momentum exist, they are weak and fail to be quantitatively accurate (i.e. the g-factor for the electron as estimated from that of a spinning charged sphere is a factor of 2 too low).

Dirac originally derived his equation, the standard first-order equation for fermions in quantum field theory, by attempting to factor the quantized Klein-Gordon Hamiltonian $E = \sqrt{p^2 + m^2}$ to retrieve a first-order equation for the energy. Dirac found that his wave-function had to be non-scalar in order for his square root of $p^2 + m^2$ to be valid: the coefficients of p had to have non-trivial commutation and anti-commutation relations.

We attempt to explain the fundamental reasons for the form of the Dirac equation by carefully deriving it from minimal assumptions. We require the relativity principle to motivate Lorentz transformations, and the invariance of the speed of light to provide an abstract but concrete definition of Lorentz transforms. The properties of the Lorentz transformations are derived defining inertial frames only as ones where Newton's first law holds; no reference is made to boosts except to help ground some of the mathematics with familiar concepts, and the detailed form of the 4-vector Lorentz transformations is completely absent. We then motivate the Dirac equation by attempting to construct the invariant law (Hermitian eigenvalue equation) with the fewest possible number of components (i.e. the lowest-dimensional law), defining operators only based on the symmetries of the Lorentz transformations. The simplest first-order equation we can construct this way is the Dirac equation. The form of our equation is used to argue that the energy-momentum relationship is embedded in the Lorentz transformations and their representations in the Dirac equation.

Several conventions used in the paper are worth noting. First, we use units $\hbar = c = 1$. Second, Einstein summation over repeated indices is always implied. Third, two metrics are used depending on the context; for any 4-vectors, the Minkowski metric (introduced in (2)) is used exclusively. For 3-vectors, only the standard identity metric is used. In particular, in expressions involving ϵ_{ijk}, the metric is always the identity metric. The meaning of contraction and the use of the metric is briefly reviewed in the next section. Finally, we refer to the diagonal tensor $\delta^\mu_\nu = \delta_{\mu\nu}$, where the second symbol is the Kronecker delta.

II. SPECIAL RELATIVITY

Although the Lorentz transformations at the heart of special relativity are likely familiar to the reader, the development here emphasizes the group properties of the transformations as arising directly from basic postulates of the theory. The author has not found a similar development elsewhere, so even experienced readers may want to skim this section. Note that despite our convention $\hbar = c = 1$, factors of c will be explicitly written in this section, partly to ease the reader into the convention, and partly because the equations are concise with or without the constant.

Defining an inertial frame as any frame where Newton's first law holds (making inertiality a global property), we assume (in addition to "obvious" facts like the Euclidean nature or dimensionality of free space) the *relativity principle*; that the laws of nature are the same in any inertial frame. Furthermore, we immediately impose a law of nature: the speed of light, c, is constant. We identify "events" in each frame with a time t and location $\vec{x} = x\hat{x} + y\hat{y} + z\hat{z}$, the space of which we call "space-time"; we refer "4-vectors" in this space with a bolded lower-case letter, i.e. $\boldsymbol{x}$. These vectors admit a natural mapping to

* ydl@mit.edu

$\mathbb{R}^4$, with one time-like component and three space-like components. Our convention will be to normalize units by making the time-like component ct and to refer to the components by zero-based numbering, such that $\boldsymbol{x}^0 = ct$ and $\boldsymbol{x}^i = \vec{x} \cdot \hat{x}_i$ for $i = \{1, 2, 3\}$ and where $\hat{x}_i = \{\hat{x}, \hat{y}, \hat{z}\}$. When we represent $\boldsymbol{x}$ as a column vector the ith component corresponds to $\boldsymbol{x}^i$. We call *Lorentz transformations*, or LTs, transformations that take events from one inertial frame to another. For the remainder of this section, all 4-vectors will represent "events".

Our goal is invariance under transformation by LTs; this is analogous to, for example, rotational or spatial translational symmetry, both of which correspond to invariance under specific operators. These operators typically form a set with particular properties, and to study the LTs with the methods we have used to study more familiar symmetries we need to show they have these "group" properties as well. Specifically, a *group* (*with respect to O*) is defined as a set G with an operation $O(\cdot, \cdot) : G \times G \to G$ such that (1) there is an identity element $1 \in G$ such that $O(1, g) = O(g, 1) = g$ for all $g \in G$, (2) for every $g \in G$ there is an inverse element $g^{-1} \in G$ such that $O(g^{-1}, g) = O(g, g^{-1}) = 1$, and (3) the operation O is associative; for $a, b, c \in G$, $O(a, O(b, c)) = O(O(a, b), c)$. After showing the LTs form a group, we will be able to advance our study by characterizing simpler subgroups and building up to a complete understanding of the members of the full group. While we prove the LTs form a group, we leave the proofs that the LT subgroups we define satisfy the group properties to the reader; they are straightforward and concise given the content of this section.

Consider two LTs T_1 and T_2. Once we transform to an inertial frame we may take it equivalent to our original frame by the relativity principle, so LTs defined for one frame are still LTs with respect to the new frame, although in general not to the same frame relative to the original. Then the composition of two LTs, $T_2 T_1$, is a LT. The trivial transformation that takes events to events in the same frame must be the identity transformation, which we call $\mathbb{1}$. For each LT T that takes the original inertial frame A to some inertial frame B, there is a transformation T^{-1} back to A (since both A and B are inertial); by the principle of relativity this transformation must be the inverse of T (otherwise A and B could disagree on the results of physics experiments). Finally, imagine we have four observers situated in inertial frames A, B, C, and D. Since all the frames are inertial there exist transformations $T_{A \to B}, T_{B \to C}$, and $T_{C \to D}$. It is clear that $T_{\beta \to \gamma} T_{\alpha \to \beta} = T_{\alpha \to \gamma}$ (yet again by relativity, for if it were not true observers in α and β would disagree on the results of physics experiments), so $T_{C \to D}(T_{B \to C} T_{A \to B}) = T_{A \to D} = (T_{C \to D} T_{B \to C}) T_{A \to B}$. Thus the set of LTs forms the group $\mathbb{L}$ with respect to composition of LTs.

Any spatial rotation or space-time translation of an inertial frame is trivially inertial (objects obeying Newton's first law will continue to do so), so spatial rotations by angle θ about a space axis $\hat{n}$, $R_{\hat{n}}(\theta)$, and space-time translations by $\boldsymbol{\alpha}$, $\mathbb{T}_\alpha$, are in $\mathbb{L}$. Note that this in combination with the relativity principle implies the homogeneity of space-time and isotropy of space. Consider two frames A and A', and call T the LT from A to A'. By the homogeneity of space-time and the relativity principle we know that $T(\mathbb{T}_\alpha \boldsymbol{x}) - T(\mathbb{T}_\alpha \boldsymbol{y}) = T\boldsymbol{x} - T\boldsymbol{y}$, i.e. there exists a $\mathbb{T}_{\alpha'}$ that does not depend on $\boldsymbol{x}$ such that

$$T(\boldsymbol{x} + \boldsymbol{\alpha}) = T(\mathbb{T}_\alpha \boldsymbol{x}) = \mathbb{T}_{\alpha'} T\boldsymbol{x} = T\boldsymbol{x} + \boldsymbol{\alpha}', \quad (1)$$

where $\mathbb{T}_{\alpha'}$ is translation by some 4-vector in A'. Taking $\boldsymbol{x} = 0$ gives us $\boldsymbol{\alpha}' = T(\boldsymbol{\alpha}) - T(0)$, by substituting for $\boldsymbol{\alpha}'$ in and subtracting $T(0)$ from (1) we can write it in terms of the operator $L = \mathbb{T}_{-T(0)} T$, and we have $L(\boldsymbol{x} + \boldsymbol{\alpha}) = L\boldsymbol{x} + L\boldsymbol{\alpha}$. That L is homogeneous, i.e. $L(\lambda \boldsymbol{x}) = \lambda L\boldsymbol{x}, \lambda \in \mathbb{R}$, comes from its continuity at 0 (this is a well-known and intuitive property of distributive, continuous linear functionals[1]). Then L is a linear LT, and $T = \mathbb{T}_{T(0)} L$. Thus every LT is a composition of a translation and a linear operator. That the LTs without translations form a group (a *subgroup* of $\mathbb{L}$), $\mathbb{LL}$, of linear operators is then clear. They map from and to a real finite-dimensional space (of 4-vectors), and so may be represented by real matrices which we call Λ.

We define the *Minkowski length* in the space of 4-vectors to be $|\boldsymbol{x}|^2 \equiv (\boldsymbol{x}^0)^2 - \sum_{i>0}(\boldsymbol{x}^i)^2$. Suppose $\boldsymbol{\ell}$ denotes the 4-vector corresponding to the end of a light beam emitted from the space-time origin ($t = 0$ and $\vec{x} = 0$). The invariance of the speed of light implies that in *all* frames that are connected only by linear transformations Λ, $|\boldsymbol{\ell}| = 0$ (since linear maps take the origin to the origin). Finally, representing the linear transformations as general 4×4 matrices, carrying out the transformation, and invoking the relativity principle it is straightforward to show that the Minkowski length is preserved by all linear LTs.

We define $g_{\mu\nu} = g^{\mu\nu}$ such that $\boldsymbol{x}^\mu g_{\mu\nu} \boldsymbol{x}^\nu = |\boldsymbol{x}|^2$, and write $\boldsymbol{x}_\mu = g_{\mu\nu} \boldsymbol{x}^\nu$ so that $|\boldsymbol{x}|^2 = \boldsymbol{x}^\mu \boldsymbol{x}_\mu$. The tensor g then admits a natural symmetric matrix representation,

$$g = \begin{pmatrix} 1 & & & \\ & -1 & & \\ & & -1 & \\ & & & -1 \end{pmatrix}, \quad (2)$$

which allows us to concisely state the length-preserving property of elements of $\mathbb{LL}$ in matrix notation:

$$|\Lambda \boldsymbol{x}|^2 = (\Lambda \boldsymbol{x})^T g (\Lambda \boldsymbol{x}) = \boldsymbol{x}^T \Lambda^T g \Lambda \boldsymbol{x} \implies \Lambda^T g \Lambda = g. \quad (3)$$

Both sides of this last relation are symmetric 4×4 matrices, which gives 10 constraint equations on the 16 parameters in Λ. This tells us that at most 6 free parameters plus a 4-vector corresponding to a translation completely specify one inertial frame relative to another. We

---

[1] An outline of the proof proceeds thusly: the proof for positive integer multipliers is trivial. Then prove for negative integers. Then rational numbers. Then since the rational numbers are dense and we have continuity at the origin we are done.

already know spatial rotations consume 3 of those parameters. Consider $d(\Lambda \boldsymbol{x})^i / d(\boldsymbol{x}^0/c), i > 0$. By linearity and homogeneity of space-time this gives three independent constants (in time, $\boldsymbol{x}^0/c$) with units of velocity. These correspond to, in the standard development of special relativity, the three boost directions. This shows that a frame moving with constant velocity relative to another inertial frame is itself inertial, and, more pertinently, that the last equality in (3) may be taken as the *definition* of $\mathbb{LL}$ (since no free parameters remain). We adopt this definition for the remainder of the paper.

Our assumption is that a valid physical theory must be invariant under these transformations, and we proceed to their characterization.

III. LORENTZ GROUP

We are now equipped with a group (and a subgroup) of transformations. A natural next step is to attempt to enumerate the types of objects these transformations can act on, and the particular form the LT takes given the particular object. A clear example given the previous section are event 4-vectors. Another example familiar to those who have studied special relativity are translation-invariant 4-vectors, like the momentum 4-vector, that only transform under the subgroup $\mathbb{LL}$, and the completely Lorentz invariant scalars formed from the Minkowski lengths of these 4-vectors for which the Lorentz transformations are simply the identity. We can approach this enumeration systematically by studying the general properties of $\mathbb{LL}$, then constructing explicit transformations that satisfy these properties, called *representations* of the group, and noting the space they are defined on.

We begin with the properties of a representation we are already familiar with from the previous section; the 4×4 matrix that transforms 4-vectors. The tensor forms of (3) will be useful

$$\Lambda^T g \Lambda = g \implies g_{\beta\eta}\Lambda^\beta_\mu \Lambda^\eta_\nu = g_{\mu\nu} \tag{4}$$

$$\Lambda^T g = g\Lambda^{-1} \implies g_{\beta\nu}\Lambda^\beta_\mu = g_{\mu\beta}(\Lambda^{-1})^\beta_\nu \tag{5}$$

$$\boldsymbol{x}_\mu = g_{\mu\nu}x^\nu \implies (\Lambda\boldsymbol{x})_\mu = g_{\mu\nu}\Lambda^\mu_\beta \boldsymbol{x}^\beta = (\Lambda^{-1})^\nu_\mu x_\nu \tag{6}$$

From (3) we have that $\det\Lambda = \pm 1$ and evaluating the 00 element of (4) we have $|\Lambda^0_0| \geq 1$. We can use this information to further narrow the group we are studying. We take the subgroup with $\det\Lambda = 1$ and $\Lambda^0_0 \geq 1$; the elements we ignore can be trivially recovered from our subgroup by composing with a space-time parity flip (i.e. multiplying by a diagonal matrix consisting solely of ± 1 with determinant -1). The reason we choose this subgroup is that we may now take a continuous path from any element of our subgroup to the identity matrix (this is not possible with $\mathbb{LL}$ since Λ with negative determinant cannot be smoothly taken to a matrix with positive determinant due to the result above); this is the defining property of a *Lie* group.

Many symmetries (all continuous symmetries) are Lie groups; familiar examples are rotations (of which our subgroup is a superset) and spatial translations. Just as rotations are completely specified by their angular momentum (Lie) commutator algebra, the elements and properties of any Lie group are completely specified by an associated Lie algebra. This algebra is itself defined by objects we call *generators*, which may loosely be associated with a complete "basis" for the space of the Lie group; they represent all the linearly independent modifications of the identity that remain in the space of the Lie group. Since a Lie group is defined by smooth connectedness to the identity, we can retrieve any member of a Lie group by composing many such "infinitesimal" changes to the identity[2]. The angular momentum operators, for example, are generators of rotation; we will characterize our subgroup by studying its own generators.

To each free parameter of the transformation there corresponds a generator, so we have 6. Instead of the naive labeling (i.e. a row vector with six entries), we set our parameters so that the 4×4 representation that transforms the 4-vector is generated by the infinitesimal changes to the identity

$$\delta\Lambda^\mu_\nu = \delta^\mu_\nu + \omega^\mu_\nu, \tag{7}$$

where ω^μ_ν is infinitesimal, so we ignore all orders of ω^μ_ν higher than the first, unless the zeroth and first order terms are zero, in which case we take the lowest order non-zero term[3]. Application of (4) to the product of two such operators shows that $\omega_{\mu\nu} = -\omega_{\nu\mu}$; this means $\omega_{\mu\nu}$ defines an anti-symmetric 4×4 matrix, which, as expected, has exactly 6 free parameters. We use this matrix to encode the six parameters of our transformation in a representation-independent way. Although there are only six independent generators corresponding to the six free parameters, it will be convenient to anti-symmetrically label them as well; for generator $G^{\mu\nu}$, $G^{\mu\nu} = -G^{\nu\mu}$ (note there are still only 6 independent generators). These can be used to define the infinitesimal elements of our subgroup (for a similar generator-based analysis for the non-relativistic quantum mechanical operators of momentum, time evolution, and angular momentum see [4]):

$$\delta\Lambda = \mathbb{1} + \frac{i}{2}\omega_{\mu\nu}G^{\mu\nu}. \tag{8}$$

To retrieve the finite transformation in general, we repeatedly apply the infinitesimal one N times with finite

———

[2] *Extremely* non-rigorously (even less than in the main body of the paper), we indicate a "direction" to take the identity with the generators, then "stretch" this quantity in the indicated "direction" by repeatedly composing the perturbation with itself.

[3] This is rigorously justified, but is also intuitive, since we are free to take our infinitesimal term as small as we like.

parameters $\Omega_{\mu\nu}$:

$$\Lambda = \lim_{N \to \infty} \left(\mathbb{1} + \frac{i}{2} \frac{\Omega_{\mu\nu}}{N} G^{\mu\nu} \right)^N \tag{9}$$

$$= \exp\left(\frac{i}{2} \Omega_{\mu\nu} G^{\mu\nu} \right) \tag{10}$$

In this way we are able to generate any element of our subgroup in any representation. Taking

$$(G^{\mu\nu})^\alpha_\beta = i(g^{\nu\alpha}\delta^\mu_\beta - g^{\mu\alpha}\delta^\nu_\beta) \tag{11}$$

for example, reproduces (7), so this is the form of the generator for 4-vectors.

Now that we have an explicit form of a non-trivial (as opposed to, for example, Lorentz scalars where the generators are all 0) generator for a particular representation of our subgroup, we can begin exploring the commutator algebra. It is straightforward to find the basic commutation relation directly from (11):

$$[G^{\mu\nu}, G^{\alpha\beta}] = i(g^{\mu\beta}G^{\alpha\nu} + g^{\mu\alpha}G^{\nu\beta} - g^{\nu\beta}G^{\alpha\mu} - g^{\nu\alpha}G^{\mu\beta}). \tag{12}$$

Any set of generators satisfying (12) will produce valid representations of our subgroup (of LTs).

We now seek new representations. We begin by re-labeling the generators (note that we only combine dependent generators):

$$R^i = \frac{1}{2}\epsilon_{ijk}G^{jk} \tag{13}$$

$$B^i = G^{i0}. \tag{14}$$

We can define (real) 3-vectors $\vec{\zeta}, \vec{\eta}$ from the $\omega_{\mu\nu}$ such that $\Lambda = \exp(-i\vec{\zeta}\cdot R + i\vec{\eta}\cdot B)$ for the same finite element. This relabeling gives a promising new commutator algebra:

$$[R^i, R^j] = i\epsilon_{ijk}R^k \tag{15}$$

$$[R^i, B^j] = i\epsilon_{ijk}B^k \tag{16}$$

$$[B^i, B^j] = -i\epsilon_{ijk}R^k. \tag{17}$$

The first relation is the familiar $SU(2)$[4] algebra of angular momentum; this appears promising, and we can simplify the algebra even more by defining

$$J = \frac{1}{2}(R + iB) \tag{18}$$

$$[J^i, J^j] = i\epsilon_{ijk}J^k \tag{19}$$

$$[(J^\dagger)^i, (J^\dagger)^j] = i\epsilon_{ijk}(J^\dagger)^k \tag{20}$$

$$[(J^\dagger)^i, J^j] = 0. \tag{21}$$

Our Lie algebra is suddenly the commuting algebra of two angular momenta! Note that their commutation is

crucial since it implies that they act on disjoint vector spaces. This means that *any* valid representation for angular momentum can be used to define valid generators, and hence valid representations of (our subgroup of) Lorentz transforms. In particular, we can label the representation by two half-integer or integer[5] total spin eigenvalues corresponding to the two generators, $(j, j^\dagger)$. The form of the finite transformations with these operators is denoted with its own unique symbol

$$\mathscr{L}(\Lambda) \equiv e^{-i((\vec{\zeta}-i\vec{\eta})J \oplus (\vec{\zeta}+i\vec{\eta})J^\dagger)} = e^{-i(\vec{\zeta}-i\vec{\eta})J} \otimes e^{-i(\vec{\zeta}+i\vec{\eta})J^\dagger}. \tag{22}$$

We are now able to comfortably use the well-known algebra of angular momentum to build arbitrary representations of our subgroup. An important note is that although our representation can be based on the unitary operators $SU(n)$, that does not imply the unitarity of the resulting Lorentz transform; for example, the representation $(1/2, 0)$ has $R = J = \vec{\sigma}/2$, but $B = -i\vec{\sigma}/2$. Since B is not Hermitian, the operator in (9) cannot in general be unitary. On the other hand, R will always be Hermitian, and recalling the subgroups of operators that are part of the LTs described in Section II and the commutation relations (15), the association of R with the (Hermitian) generators of rotation in $\mathbb{LL}$ is natural. B is then naturally associated with the remaining directional boosts.

To have a good physical theory (given our assumptions — the possibility of parity violation is discussed in the conclusion) we need to re-expand our subgroup to include parity transforms in our representation. A spatial parity transformation will not affect R since by (15) it is a pseudo-vector, but will invert $B \to -B$. This means that if $j \neq j^\dagger$, the representation $(j, j^\dagger)$ does not contain the spatial parity transform. Fortunately, it is clear from (19) that direct sums of representations are valid as well, so we can patch up our subgroup by making the representation $(j, j^\dagger) \oplus (j^\dagger, j)$. This provides us with a mechanism for generating Lorentz transforms for arbitrarily high (although not arbitrary due to the symmetry imposed by the parity requirement) dimensions.

Finally, we need to treat the non-linear subspace of LT, the space of translations. The treatment here will be brief; the process is almost identical to the translation by a 3-vector done in [4]. We define the translation operator and its infinitesimal form and Hermitian generator P^μ

$$\mathscr{T}(\boldsymbol{\alpha})\psi(\boldsymbol{x}) = \psi(\boldsymbol{x} + \boldsymbol{\alpha}) \tag{23}$$

$$\mathscr{T}(\boldsymbol{\Delta\alpha}) = \mathbb{1} + i\boldsymbol{\Delta\alpha}_u P^\mu \tag{24}$$

It is easy to confirm the infinitesimal form behaves as expected; as the argument goes to zero the operator goes

---

[4] But see the next footnote.

to the identity, composition is addition of translations, translation by the negative is the inverse, and it is unitary (since $(P^\mu)^\dagger = P^\mu$). We generate the finite transformation in the usual way.

From the linearity of Λ, we have $\Lambda^{-1}\mathscr{T}(\mathbf{\Delta\alpha})\Lambda = \mathscr{T}(\Lambda^{-1}\mathbf{\Delta\alpha})$. Substituting (24) to both sides, using (6) on the right, and gathering terms of $\mathbf{\Delta\alpha}_\mu$, we have the transformation law for P^μ,

$$\Lambda^{-1}P^\mu\Lambda = \Lambda^\mu_\nu P^\nu. \tag{25}$$

The focus of this paper is on the physics, so some technical details are glossed over. The mathematically inclined reader may in particular wonder about the reducability of the representations we use; all final representations of the Lorentz transformations we use are irreducible, and the proof is rather trivial. The connectedness of the group we define as the Lorentz transforms is not discussed extensively either, but we are mostly concerned with the subgroup connected to the identity.

IV. DIRAC EQUATION

Now that we have a characterization of a wide range of representations of the LTs, we look to construct a Lorentz-invariant law that describes a wave-function, since any true law must have this property. We assume that this law must be based on an observable quantity, and that eigenvalues of Hermitian operators are observables.

We can begin to "march" up our available representations of the linear LTs to try and find the law requiring the fewest dimensions. Our first representation is $(0,0)$. This is one-dimensional, and corresponds to Lorentz scalars. In this representation the Lorentz transformations are the identity, so they do not convey any information, and the scalars are invariant anyway so this representation is of limited use.

The next valid one is $(1/2,0) \oplus (0,1/2)$. This immediately entails a four-dimensional space (2 for each $1/2$), and we call elements of this space ψ. These elements will transform by $\mathscr{L}(\Lambda)$ as constructed in the $(1/2,0)\oplus(0,1/2)$ representation. We have two Hermitian operators at our disposal with which to write an eigenvalue equation. One is rotation, but the rotational symmetry will be taken care of by making sure that the equation is invariant under the linear LTs; we must enforce this invariance outside of the equation anyway since in this representation $\mathscr{L}(\Lambda)$ is not generally Hermitian. The remaining Hermitian operator is P^μ, and the naive eigenvalue equation is $P^\mu P_\mu \psi = m^2 \psi \implies (P^\mu P_\mu - m^2)\psi = 0$, where $m \in \mathbb{R}$. We can check to see if it is Lorentz invariant (remembering that ψ changes by $\mathscr{L}(\Lambda)$, P^μ by Λ as in (25), and the identity (6)):

$$((\Lambda^{-1})^\nu_\mu P_\nu \Lambda^\mu_\beta P^\beta - m^2)\mathscr{L}(\Lambda)\psi \tag{26}$$

$$= \mathscr{L}(\Lambda)(P_\mu P^\mu - m^2)\psi = 0 \tag{27}$$

which is Lorentz invariant.

This law is not ideal though, since it is quadratic in an operator. Inspired by this law, we propose a simpler one:

$$(\gamma^\mu P_\mu - m)\psi = 0 \tag{28}$$

for some set of four invariant (i.e. scalar) matrices γ. Define $L^{\mu\nu}$ as the Lorentz generators corresponding to the 4-vector transform, given explicitly in (11), and define $S^{\mu\nu}$ as the Lorentz generators that arise from the $(1/2,0) \oplus (0,1/2)$ representation. Note that we can get explicit 4×4 matrices for $S^{\mu\nu}$ quite easily by substituting $J = \vec{\sigma}/2$ and $J^\dagger = 0$ into, sequentially, (18) to find R and B, then (13) and (14), noting the asymmetry in the extra generators, then repeating the process for $J^\dagger = \vec{\sigma}/2$ and $J = 0$, and taking the direct sum of the resulting 2×2 generators.

Suppose then that there exists a set of four 4×4 matrices γ^μ (this method of finding γ^μ due to [7]) such that

$$S^{\mu\nu} = \frac{i}{4}[\gamma^\mu, \gamma^\nu] \tag{29}$$

The following commutation relation can then be directly checked,

$$[\gamma^\mu, S^{\alpha\beta}] = (L^{\alpha\beta})^\mu_\nu \gamma^\nu, \tag{30}$$

and this implies

$$\mathscr{L}(\Lambda)^{-1}\gamma^\mu\mathscr{L}(\Lambda) = \Lambda^\mu_\nu \gamma^\nu. \tag{31}$$

Such matrices do exist; one example is $\gamma^0 = \sigma^3 \otimes \mathbb{1}_2$, $\gamma^j = i\sigma^2 \otimes \sigma^j$. Then taking the Lorentz transform of (28),

$$(\gamma^\mu(\Lambda^{-1})^\nu_\mu P_\nu - m)\mathscr{L}(\Lambda)\psi \tag{32}$$

$$= \mathscr{L}(\Lambda)\mathscr{L}(\Lambda)^{-1}(\gamma^\mu(\Lambda^{-1})^\nu_\mu P_\nu - m)\mathscr{L}(\Lambda)\psi \tag{33}$$

$$= \mathscr{L}(\Lambda)(\mathscr{L}(\Lambda)^{-1}\gamma^\mu\mathscr{L}(\Lambda)(\Lambda^{-1})^\nu_\mu P_\nu - m)\psi \tag{34}$$

$$= \mathscr{L}(\Lambda)(\gamma^\beta\Lambda^\mu_\beta(\Lambda^{-1})^\nu_\mu P_\nu - m)\psi \tag{35}$$

$$= \mathscr{L}(\Lambda)(\gamma^\mu P_\mu - m)\psi = 0 \tag{36}$$

Then (28) is Lorentz invariant (both linearly and generally), and we have our first-order law. This equation, with any suitable choice of γ, is called the Dirac equation.

V. CONCLUSION

The Dirac equation (28) may be re-cast in perhaps a more familiar manner by making the "standard" association between generators of spatial translation and momentum and time translation and energy. Then P^μ becomes the (dual or "raised") four-momentum operator $P^0 = i\partial^0$ (since the standard Schrodinger equation reads $i\partial_t = H$), $P^\mu = -i\partial^\mu$ (since the standard relation is momentum goes as $-i\nabla$). Noting that $P_\mu = i\partial_\mu$, we have

$$(i\gamma^\mu\partial_\mu - m)\psi = 0. \tag{37}$$

Although we assumed nothing about relativistic energy relations or the form of the four-momentum vector in deriving (28), with it now in hand the physical interpretation of the eigenvalue m as the rest energy (or equivalently for particles the rest mass) is quite natural given the $(m, 0)$ form for the rest four-momentum in standard special relativity. Since the equation is invariant under LTs, the association between m and the rest energy is valid in all frames. Again, this is secondary and is being stated only to aid with interpretation; it is perhaps most interesting that this equation could be derived without any reference to the *additional* postulate of special relativity concerning the four-vector and rest energy — all we assume is the relativity principle and an invariant speed of light. Even our operators only arise from the Lorentz transformations.

Even the substitutions of derivatives for the P^μ do not necessarily depend on this assumption; the substitutions for the space-like components of translation are already well-known from non-relativistic quantum mechanics, and the substitution for the time-like can be given the right sign on the basis of its time-like nature as opposed to its postulated relationship to energy. Thus we can "derive" the famous equation of invariance for the four-momentum scalar in special relativity through quantum mechanics. In fact, if we locate ourselves in the rest frame of the field, we get a one-dimensional Schrodinger equation for all the components of the field, and the invariance of the eigenvalue strongly hints at its nature as the rest energy.

From this point forward standard manipulations of the Dirac equation to get corrections like the g-factor of the electron and the phenomenological spinor equations (both of these come from applying an electromagnetic Dirac operator a second time) or the fine structure of the hydrogen atom can be done; many of these are straightforward and outlined in [7].

It is worth noting that the assumptions chosen here are actually too stringent for all of modern quantum theory; parity conservation is violated in several systems, for example neutrinos, whose spin always points opposite their velocity. The lifting of this restriction allows representations in arbitrary dimensions: in particular, instead of being forced to a 4-dimensional equation we may use either the $(1/2, 0)$ or $(0, 1/2)$ representations to act on a space of two-dimensional objects. The equations obtained this way are called the Weyl equations and describe massless spin-1/2 particles.

VI. ACKNOWLEDGMENTS

We would like to thank Trond Andersen for advice on which sections needed more explanation, and Daniel Kolodrubetz for providing general comments on the structure, language, and clarity of the piece. We would also like to thank Prof. Robert Jaffe for reading the paper and pointing out the existence of parity-violating systems. The derivation was largely independent, but the rearrangements of the generators (equations (13), (14), and (18)) of the Lorentz transformations were inspired by Exercise 3.3 in [7].

[1] An outline of the proof proceeds thusly: the proof for positive integer multipliers is trivial. Then prove for negative integers. Then rational numbers. Then since the rational numbers are dense and we have continuity at the origin we are done.
[2] *Extremely* non-rigorously (even less than in the main body of the paper), we indicate a "direction" to take the identity with the generators, then "stretch" this quantity in the indicated "direction" by repeatedly composing the perturbation with itself.
[3] This is rigorously justified, but is also intuitive, since we are free to take our infinitesimal term as small as we like.
[4] J. Sakurai, *Modern Quantum Mechanics*, 2nd ed. (Addison-Wesley, 2011).
[5] But see the next footnote.
[6] The careful reader may object that we are dealing with a real transformation, and so should exclude the half-integer transformations (i.e. we are in $SO(3)$, not $SU(2)$). Fortunately all observables are quadratic in the wave-function so the complexity of $SU(2)$ causes no trouble.
[7] M. E. Peskin and D. V. Schroeder, *An Introduction To Quantum Field Theory (Frontiers in Physics)* (Westview Press, 1995).

A Simplistic Theory of Coherent States

Lanqing Li

MIT Physics Department, 77 Massachusetts Ave., Cambridge, MA 02139

(Dated: May 2, 2014)

We reviewed and developed a theory of the simplest type of coherent states, which are also referred as "field coherent states" in some contexts, based on three fundamental definitions. We examined some of the properties, physical interpretations and applications of the coherent states resulted from the formalism, which are believed to have more profound implications.

I. INTRODUCTION

Coherent state is the specific quantum state of the quantum harmonic oscillator whose dynamics most closely resembles that of a classical harmonic oscillator. The basic concept was first proposed by Erwin Schrödinger in 1926 while searching for solutions of the Schrödinger equation that satisfy the correspondence principle [1]. However, after Schrodinger's discovery, it was not until 1963, when Roy J. Glauber developed a systematic quantum theory of electromagnetism based on this coherent-state formalism that this fruitful field of study got launched. In the past two and a half decades, developments in the field of coherent states and their applications have been blossoming, especially in mathematical physics and quantum optics. In this paper, I will make a brief review of the coherent-state formalism following a systematical approach, by introducing the theoretical basics from a mathematical point of view and then discuss its physical interpretation as a natural bridge for studying the quantum-classical correspondence. A coherent-state representation of laser states will be included as an example of application at the end.

It is worth noting, that the coherent states we will discuss in this paper are also specified as "field coherent states" in some contexts [2], namely the ones with a harmonic-oscillator prototype. But indeed the concept of coherent state have been generalized to all types of physical problems [2]. And in fact, the term "coherent state" was first coined in Glauber's two seminal papers, in which he constructed the eigenstates of the annihilation operator of the harmonic oscillator in order to study the electromagnetic correlation functions, a subject of great importance in quantum optics.

II. THEORY

A. Definition

According to Glauber [3], the field coherent states can be characterized by any one of the three mathematical definitions [2]:

Definition 1: The coherent states $|\alpha\rangle$ are eigenstates of the harmonic-oscillator annihilation operator a,

$$a|\alpha\rangle = \alpha|\alpha\rangle \tag{1}$$

where α is a complex number.

Definition 2: The coherent states $|\alpha\rangle$ can be obtained by applying a displacement operator $D(\alpha)$ on the vacuum state of the harmonic oscillator:

$$|\alpha\rangle = D(\alpha)|0\rangle \tag{2}$$

where the displacement operator $D(\alpha)$ is defined as

$$D(\alpha) = \exp(\alpha a^\dagger - \alpha^* a) \tag{3}$$

which is anti-Hermitian.

Definition 3: The coherent states $|\alpha\rangle$ are quantum states with a minimum-uncertainty relationship,

$$(\Delta p)^2 (\Delta q)^2 = \left(\frac{1}{2}\right)^2 \tag{4}$$

where the dimensionless coordinate and momentum operators $(\hat{q},\hat{p})$ are defined as

$$\hat{q} = \frac{1}{\sqrt{2}}(a + a^\dagger) \tag{5}$$

$$\hat{p} = \frac{1}{i\sqrt{2}}(a - a^\dagger) \tag{6}$$

with

$$(\Delta f)^2 \equiv \langle\alpha|(\hat{f} - \langle\hat{f}\rangle)^2|\alpha\rangle \tag{7}$$

$$\overline{f} \equiv \langle\hat{f}\rangle \equiv \langle\alpha|\hat{f}|\alpha\rangle \tag{8}$$

for any operator $\hat{f}$.

Note that unlike the first two definitions, definition 3 is not a complete description of coherent states, as it does not give unique solutions in Hilbert space. Such non-uniqueness is graphically depicted in Fig 1. For the coherent states we will talk about in this paper (i.e., field coherent states, $(\Delta p)^2 = (\Delta q)^2 = \frac{1}{2}$, which is depicted in (a). Any other choice of Δp and Δq constrained by the third definition, shown in (b), represents an "uncertainty ellipse", which lies in the category of so-called squeezed states.

We will see in the next subsection that how these definitions give rise to formulation of the coherent states under the so-called Fock representation.
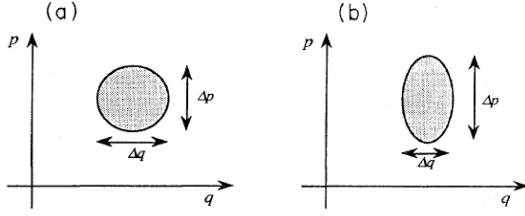
177

B.   Formalism

1.   Quantum Theory of Harmonic Oscillator

Inspired by Schrödinger's original conception, the coherent-state formalism we will discuss in this paper is built on the quantum theory of Harmonic Oscillator. Let's consider the Hamiltonian with an one-dimensional quadratic potential: $\hat{H}(x) = -\frac{\hbar^2}{2m}\frac{\partial^2}{\partial \hat{x}^2} + \frac{1}{2}m\omega^2\hat{x}^2$. By interpreting $-i\hbar\frac{\partial}{\partial \hat{x}}$ as the momentum operator $\hat{p}$ in x direction, we have:

$$\hat{H}(p,x) = \frac{\hat{p}^2}{2m} + \frac{1}{2}m\omega^2\hat{x}^2 \tag{9}$$

Let's define the operator a and its Hermitian conjugate as the following:

$$\hat{a} = \frac{1}{\sqrt{2\hbar m\omega}}(m\omega\hat{x} + i\hat{p}), \quad \hat{a}^\dagger = \frac{1}{\sqrt{2\hbar m\omega}}(m\omega\hat{x} - i\hat{p}) \tag{10}$$

that is,

$$\hat{x} = l_c(\hat{a} + \hat{a}^\dagger), \quad \hat{p} = -ip_c(\hat{a} - \hat{a}^\dagger) \tag{11}$$

where $l_c = \sqrt{\frac{\hbar}{2m\omega}}$, $p_c = \sqrt{\frac{\hbar m\omega}{2}}$ are characteristic length and momentum of the system respectively.

One can easily see that the preceding definitions give rise to an interesting algebra, by observing:

$$\hat{a}\hat{a}^\dagger = \frac{m\omega}{2\hbar}\hat{x}^2 + \frac{1}{2\hbar\omega}\hat{p}^2 + \frac{i}{2\hbar}[\hat{p},\hat{x}] \tag{12}$$

$$\hat{a}^\dagger\hat{a} = \frac{m\omega}{2\hbar}\hat{x}^2 + \frac{1}{2\hbar\omega}\hat{p}^2 - \frac{i}{2\hbar}[\hat{p},\hat{x}] \tag{13}$$

Hence we have

$$[\hat{a},\hat{a}^\dagger] = \hat{a}\hat{a}^\dagger - \hat{a}^\dagger\hat{a}$$
$$= \frac{i}{\hbar}[\hat{p},\hat{x}] = 1 \tag{14}$$

In the last line we used the canonical commutation relation: $[x, p_x] = i\hbar$. Moreover, using $\hat{a}$ and $\hat{a}^\dagger$, the Hamil-

tonian can be written in the following elegant form:

$$\hat{H}(p,x) = \frac{\hat{p}^2}{2m} + \frac{1}{2}m\omega^2\hat{x}^2$$
$$= \hbar\omega(\hat{a}^\dagger\hat{a} + \frac{i}{2\hbar}[\hat{p},\hat{x}])$$
$$= \hbar\omega(\hat{a}^\dagger\hat{a} + \frac{1}{2}) \tag{15}$$

Therefore the eigenstates of the quadratic-potential system are precisely those of the operator $\hat{a}^\dagger\hat{a}$. In order to find a complete set of basis (eigenstates) of the Hilbert space, we observe that:

$$[\hat{a}^\dagger\hat{a}, \hat{a}] = \hat{a}^\dagger[\hat{a},\hat{a}] + [\hat{a}^\dagger,\hat{a}]\hat{a}$$
$$= -\hat{a} \tag{16}$$

for which we used the commutation relation (14). The newly-obtained commutation relation has profound implications. Let's consider one eigenstate $|N\rangle$ of $\hat{a}^\dagger\hat{a}$ with eigenvalue N. Since $\hat{a}^\dagger\hat{a}$ is Hermitian, N must be real and non-negative. Additionally, from (16) we have:

$$[\hat{a}^\dagger\hat{a}, \hat{a}]|N\rangle = (\hat{a}^\dagger\hat{a})\hat{a}|N\rangle - \hat{a}(\hat{a}^\dagger\hat{a})|N\rangle$$
$$= (\hat{a}^\dagger\hat{a})\hat{a}|N\rangle - N\hat{a}|N\rangle$$
$$= -\hat{a}|N\rangle$$
$$\Rightarrow (\hat{a}^\dagger\hat{a})\hat{a}|N\rangle = (N-1)\hat{a}|N\rangle \tag{17}$$

Therefore, $\hat{a}|N\rangle$ is another eigenstate of $\hat{a}^\dagger\hat{a}$ with eigenvalue $N-1$. As Acting the operator $\hat{a}$ on a state $|N\rangle$ simply lowers the index N to $N-1$, $\hat{a}$ is called lowering operator, or alternatively, annihilation operator in context of physics. We can calculate its norm (similar to the absolute value of a c-number) by taking the inner product:

$$|\hat{a}|N\rangle|^2 = \langle N|\hat{a}^\dagger\hat{a}|N\rangle$$
$$= \langle N|(\hat{a}^\dagger\hat{a}|N\rangle)$$
$$= \langle N|N|N\rangle$$
$$= N \tag{18}$$

Hence we have

$$\hat{a}|N\rangle = \sqrt{N}|N-1\rangle \tag{19}$$

Since $\langle N|\hat{a}^\dagger\hat{a}|N\rangle = N \geq 0$. If N is a non-integer, say N_n, we can use $\hat{a}$ to lower the state $|N_n\rangle$ to a non-vanishing (i.e., has nonzero norm) state $|N_0\rangle$ with $0 < N_0 < 1$. However, if we apply $\hat{a}$ on the residual state one more time, from (19):

$$\hat{a}|N_0\rangle = \sqrt{N_0}|N_0-1\rangle \tag{20}$$

That is, we obtain a non-vanishing state with index $N_0 - 1 < 0$, which is forbidden by the hermiticity of $\hat{a}^\dagger\hat{a}$. This is, however, not a problem for integer since $\hat{a}|0\rangle = 0|-1\rangle$ simply vanishes, and by induction, no eigenstates of $\hat{a}^\dagger\hat{a}$ with negative eigenvalue will appear.

Therefore we assert that only $|N\rangle$'s with non-negative integer N exist as eigenstates of $\hat{a}^\dagger \hat{a}$. In fact, it can be proved that these eigenstates form a complete basis of the Hilbert space of the one-dimensional system, thus giving rise to the so-called Fock (number) representation [4].

2. Formulation Under Fock Representation

For the rest of the paper, I will restrict myself to the Fock representation to discuss the coherent-state formalism. For this purpose, we need to first construct the wavefunction of coherent states based on the foregoing three definitions. Since $\{|n\rangle, n \in \mathbb{Z}^*\}$ span the whole Hilbert space, we can write the wavefunction as the following:

$$|\alpha\rangle = \sum_{n=0}^{\infty} \alpha_n |n\rangle \qquad (21)$$

where the coefficient α_n for any n is a complex c-number. Consider the first definition, in which (1) indicates:

$$
\begin{aligned}
\hat{a}|\alpha\rangle &= \begin{cases} \sum_{n=0}^{\infty} \alpha \alpha_n |n\rangle \\ \sum_{n=0}^{\infty} \alpha_n \hat{a} |n\rangle \end{cases} \\
&= \sum_{n=0}^{\infty} \sqrt{n} \alpha_n |n-1\rangle \\
&= \sum_{n=0}^{\infty} \sqrt{n+1} \alpha_{n+1} |n\rangle \\
&\Rightarrow \alpha_{n+1} = \frac{\alpha}{\sqrt{n+1}} \alpha_n \\
&\Rightarrow \alpha_n = \frac{\alpha^n}{\sqrt{n!}} \alpha_0 \qquad (22)
\end{aligned}
$$

where α_0 can be determined up to a free phase factor e^{iS} by the normalization condition:

$$
\begin{aligned}
\langle \alpha | \alpha \rangle = &= \sum_{n_1,n_2=0}^{\infty} \frac{(\alpha^*)^{n_1} \alpha^{n_2}}{\sqrt{n_1! n_2!}} |\alpha_0|^2 \langle n_1 | n_2 \rangle \\
&= \sum_{n=0}^{\infty} \frac{|\alpha|^{2n}}{n!} |\alpha_0|^2 \\
&= e^{|\alpha|^2} |\alpha_0|^2 = 1 \qquad (23)
\end{aligned}
$$

As a result, $|\alpha_0| = e^{-\frac{|\alpha|^2}{2}}$. The normalized wavefunction of coherent states can be therefore expressed as:

$$|\alpha\rangle e^{iS} = e^{-\frac{|\alpha|^2}{2}} \sum_{n=0}^{\infty} \frac{\alpha^n}{\sqrt{n!}} |n\rangle \qquad (24)$$

where the phase factor e^{iS} corresponds to a redundant degree of freedom.

Let's now show how (24) can be obtained from the second definition. The most straightforward way to do

this is to invoke the so-called Baker-Campbell-Hausdorff formula [2], that given any two complex numbers α and α'

$$\exp(\alpha \hat{a}^\dagger - \alpha' \hat{a}) = \exp(\frac{1}{2}\alpha\alpha') \exp(-\alpha' \hat{a}) \exp(\alpha \hat{a}^\dagger) \quad (25)$$

$$= \exp(-\frac{1}{2}\alpha\alpha') \exp(\alpha \hat{a}^\dagger) \exp(-\alpha' \hat{a}) \tag{26}$$

which I will not prove in this paper [for a derivation using the so-called faithful matrix representation method check [5]]. By the second definition:

$$
\begin{aligned}
|\alpha\rangle &= \exp(\alpha \hat{a}^\dagger - \alpha^* \hat{a}) |0\rangle \\
&= \exp(\frac{1}{2}|\alpha|^2) \exp(-\alpha^* \hat{a}) \exp(\alpha \hat{a}^\dagger) |0\rangle \\
&= \exp(\frac{1}{2}|\alpha|^2) \exp(-\alpha^* \hat{a}) \sum_{n=0}^{\infty} \frac{\alpha^n}{\sqrt{n!}} |n\rangle \\
&= \exp(\frac{1}{2}|\alpha|^2 - \alpha^* \alpha) \sum_{n=0}^{\infty} \frac{\alpha^n}{\sqrt{n!}} |n\rangle \\
&= e^{-\frac{|\alpha|^2}{2}} \sum_{n=0}^{\infty} \frac{\alpha^n}{\sqrt{n!}} |n\rangle \qquad (27)
\end{aligned}
$$

as desired.

At last, let's show how the third definition combined with the additional constraint $\Delta p = \Delta q$ lead to the same formula (24). By (5)(6)(7)(8):

$$
\begin{aligned}
(\Delta q)^2 &= \tfrac{1}{2}(\langle \alpha | \hat{a}^2 + \hat{a}\hat{a}^\dagger + \hat{a}^\dagger \hat{a} + (\hat{a}^\dagger)^2 |\alpha\rangle - (\langle \alpha | \hat{a} + \hat{a}^\dagger |\alpha\rangle)^2) \\
&= \tfrac{1}{2}(\overline{\hat{a}^2} + \overline{\hat{a}\hat{a}^\dagger} + \overline{\hat{a}^\dagger \hat{a}} + \overline{(\hat{a}^\dagger)^2} - (\overline{\hat{a}})^2 - (\overline{\hat{a}^\dagger})^2 - 2\overline{\hat{a}}\overline{\hat{a}^\dagger}) \quad (28)
\end{aligned}
$$

$$
\begin{aligned}
(\Delta p)^2 &= \tfrac{1}{2}(\langle \alpha | -\hat{a}^2 + \hat{a}\hat{a}^\dagger + \hat{a}^\dagger \hat{a} - (\hat{a}^\dagger)^2 |\alpha\rangle + (\langle \alpha | \hat{a} - \hat{a}^\dagger |\alpha\rangle)^2) \\
&= \tfrac{1}{2}(-\overline{\hat{a}^2} + \overline{\hat{a}\hat{a}^\dagger} + \overline{\hat{a}^\dagger \hat{a}} - \overline{(\hat{a}^\dagger)^2} + (\overline{\hat{a}})^2 + (\overline{\hat{a}^\dagger})^2 - 2\overline{\hat{a}}\overline{\hat{a}^\dagger}) \quad (29)
\end{aligned}
$$

The constraint that both of them equal $\frac{1}{2}$ indicates that:

$$\overline{\hat{a}^2} + \overline{(\hat{a}^\dagger)^2} - (\overline{\hat{a}})^2 - (\overline{\hat{a}^\dagger})^2 = 0 \qquad (30)$$

$$\overline{\hat{a}\hat{a}^\dagger} + \overline{\hat{a}^\dagger \hat{a}} - 2\overline{\hat{a}^\dagger \hat{a}} = 1 \qquad (31)$$

Recall (16), from which we can rewrite (31) as:

$$\overline{[\hat{a}, \hat{a}^\dagger]} + 2\overline{\hat{a}^\dagger \hat{a}} - 2\overline{\hat{a}}\overline{\hat{a}^\dagger} = 1$$
$$\Rightarrow \overline{\hat{a}^\dagger \hat{a}} = \overline{\hat{a}^\dagger}\overline{\hat{a}} \qquad (32)$$

In order to see it more clearly, let's rewrite (32) as:

$$\langle \alpha | \hat{a}^\dagger \hat{a} |\alpha\rangle = \langle \alpha | \hat{a}^\dagger (\text{a complete basis}) \hat{a} |\alpha\rangle \quad (33)$$
$$= \langle \alpha | \hat{a}^\dagger (|\alpha\rangle \langle \alpha|) \hat{a} |\alpha\rangle \qquad (34)$$

The first line results from the fact that we are free to insert an identity operator inside the braket, which can be expressed as the sum of density matrices of a complete basis $\{|\beta_n\rangle\}$ of the Hilbert space: $I = \sum_n |\beta_n\rangle \langle \beta_n|$, for coherent states, as we will see in equation (36), it

can be represented by an integral over the entire complex plane of α. Comparing (33) and (34), we conclude the state (a vector in the Hilbert space of the system) $\hat{a} \, |\alpha\rangle$ lies in the subspace $|\alpha\rangle \, \langle\alpha|$ (as we will see, due to the *over-completeness* of coherent states, a mathematical rigorous representation of the subspace $|\alpha\rangle \, \langle\alpha|$ should be written as $\frac{1}{2\pi} \int_0^{2\pi} |\alpha\rangle \, \langle\alpha| \, d\phi$, the density matrix ρ for a fixed length of α). In other words, a coherent state $|\alpha\rangle$ is an eigenstate of $\hat{a}$, which leads us back to the first definition, thus gives rise to the same expression (24).

C. Properties

Before we move to discuss the physical interpretation and application of the coherent-state formalism, there are two properties of coherent states to be noted [6]:

(a)*Non-orthogonality*. Given any two coherent states $|\alpha\rangle$ and $|\alpha^{'}\rangle$, we can calculate their inner product:

$$
\begin{aligned}
\left\langle \alpha | \alpha^{'} \right\rangle &= e^{-\frac{1}{2}(|\alpha|^2 + |\alpha^{'}|^2)} \sum_{n_1, n_2 = 0}^{\infty} \frac{(\alpha^*)^{n_1} (\alpha^{'})^{n_2}}{\sqrt{n_1! n_2!}} \langle n_1 | n_2 \rangle \\
&= e^{-\frac{1}{2}(|\alpha|^2 + |\alpha^{'}|^2)} \sum_{n=0}^{\infty} \frac{(\alpha^*)^{n} (\alpha^{'})^{n}}{n!} \\
&= exp[\alpha^* \alpha^{'} - \frac{1}{2}(|\alpha|^2 + |\alpha^{'}|^2)] \\
\Rightarrow \; |\left\langle \alpha | \alpha^{'} \right\rangle|^2 &= exp(-|\alpha - \alpha^{'}|^2) \qquad (35)
\end{aligned}
$$

This shows that the coherent states $|\alpha\rangle$'s are not orthogonal, but normalized.

(b)*Over-completeness*. For the field coherent states, Glauber showed that the resolution of the identity in terms of coherent states is not unique. A common and useful resolution [2] is:

$$
\int |\alpha\rangle \, \frac{d^2\alpha}{\pi} \, \langle\alpha| = I \qquad (36)
$$

Geometrically, this can be viewed as integrating the displacement α over the entire complex plane (two degrees of freedom). Alternatively, if we restrict the α to a circle centered at the origin on the complex plane (allow only an indefinite phase factor as redundant degree of freedom, as we did before), we will obtain a density matrix for a specific value of $|\alpha|$ [7]:

$$
\rho_{|\alpha|} = \frac{1}{2\pi} \int_0^{2\pi} |\alpha\rangle \, \langle\alpha| \, d\phi \qquad (37)
$$

where $\alpha = |\alpha| e^{i\phi}$. We will maintain this convention for the subsequent calculations.

We will make use of this density matrix as a representation of laser states in the application section. Since the coherent states are labeled by a continuous index in a Hilbert space that has a countable basis, they are over-complete.

III. PHYSICAL INTERPRETATION

There are many physical interpretations of coherent states in all kinds of different contexts. For this section, however, we will only focus on the original conception that Schrödinger had in mind when proposing such states. In the absence of external fields, the time evolution of a coherent state is:

$$
\begin{aligned}
|\alpha(t)\rangle &= e^{-iH_0 t/\hbar} \, |\alpha\rangle \\
&= e^{-|\alpha|^2/2} \sum_n \frac{(\alpha e^{-i\omega t})^n}{\sqrt{n!}} \, |n\rangle \\
&= |\alpha e^{-i\omega t}\rangle \qquad (38)
\end{aligned}
$$

In this case, once the system is in a coherent state, it will remain at all times as a coherent state. Recall our previous definitions in (5)(6), according to which we can calculate the expectation values of the position and momentum operators of the harmonic oscillator:

$$
\begin{aligned}
\langle \hat{q}(t) \rangle &= \frac{1}{\sqrt{2}} \, \langle \alpha(t) | \, \hat{a} + \hat{a}^\dagger \, | \alpha(t) \rangle \\
&= \frac{1}{\sqrt{2}} (\alpha e^{-i\omega t} + \alpha^* e^{i\omega t}) \\
&= \sqrt{2} |\alpha| \cos(\omega t - \phi) \qquad (39) \\
\langle \hat{p}(t) \rangle &= \frac{-i}{\sqrt{2}} \, \langle \alpha(t) | \, \hat{a} - \hat{a}^\dagger \, | \alpha(t) \rangle \\
&= \frac{-i}{\sqrt{2}} (\alpha e^{-i\omega t} - \alpha^* e^{i\omega t}) \\
&= -\sqrt{2} |\alpha| \sin(\omega t - \phi) \qquad (40)
\end{aligned}
$$

where again $\phi = \arg(\alpha)$. (39)(40) indicate that if we regard a coherent state as a "particle" (a wave packet in de Broglie's description), then it follows exactly the classical motion of a harmonic oscillator, as it rotates clockwise along a circular orbit with angular frequency ω in phase space. Since from the third definition, it is also a minimum-uncertainty quantum state with $(\Delta p)^2 = (\Delta q)^2 = \frac{1}{2}$, the "wave packet" never spreads. With this unique "localized" nature, at the classical limit ($\hbar \to 0$), such a coherent state will precisely turns into a point-like particle undergoing harmonic oscillation. From this point of view, the coherent-state formalism manifestly provides a natural framework to discuss the quantum-classical correspondence.

IV. APPLICATION

In Glauber's two seminal papers, he used the coherent-state formalism to study the electromagnetic correlation functions, which is of great importance in quantum optics. A more straightforward example of application of this formalism is the coherent-state description of the laser

states, namely again (24):

$$|\alpha\rangle = e^{-\frac{|\alpha|^2}{2}} \sum_{n=0}^{\infty} \frac{\alpha^n}{\sqrt{n!}} |n\rangle \qquad (41)$$

The density matrix of this laser state, resulted from taking a weighted integral over the redundant degree of freedom (37), is given by [7]:

$$
\begin{aligned}
\rho_{laser} &= \frac{1}{2\pi} \int_0^{2\pi} d\phi \, |\alpha\rangle \langle \alpha| \\
&= \frac{e^{-|\alpha|^2}}{2\pi} \int_0^{2\pi} d\phi \sum_{n,m=0}^{\infty} \frac{|\alpha|^{n+m} e^{i\phi(n-m)}}{\sqrt{n!m!}} |n\rangle \langle m| \\
&= e^{-|\alpha|^2} \sum_{n,m=0}^{\infty} \frac{|\alpha|^{n+m} \delta_{n,m}}{\sqrt{n!m!}} |n\rangle \langle m| \\
&= e^{-|\alpha|^2} \sum_{n=0}^{\infty} \frac{|\alpha|^{2n}}{n!} |n\rangle \langle n| \qquad (42)
\end{aligned}
$$

Under the Fock (number) representation, $|n\rangle$ stands for a state of harmonic-oscillator. For a laser state, in particular, the quantum number n corresponds to the photon number in the state. Therefore the average photon number of the laser can be obtained as:

$$
\begin{aligned}
\langle \hat{n} \rangle_{laser} &= tr(\sum_{n=0}^{\infty} n |n\rangle \langle n| \rho_{laser}) \\
&= e^{-|\alpha|^2} \sum_{n=0}^{\infty} \frac{n|\alpha|^{2n}}{n!} \\
&= e^{-|\alpha|^2} \sum_{n=0}^{\infty} |\alpha|^2 \frac{d}{d(|\alpha|^2)} \frac{(|\alpha|^2)^n}{n!} \\
&= e^{-|\alpha|^2} |\alpha|^2 \frac{d}{d(|\alpha|^2)} e^{|\alpha|^2} = |\alpha|^2
\end{aligned}
$$
$$(43)$$

Since the average photon number characterizes the intensity of the laser field, we have $n \propto I \propto |A|^2$, where A is the amplitude of the electromagnetic field. Therefore it is very natural to regard $|\alpha|$, the displacement (recall the second definition) of the coherent state from the vacuum state as the amplitude of the laser. In addition, we can compute the fluctuations in photon number under the same representation:

$$
\begin{aligned}
\langle \hat{n}^2 \rangle_{laser} &= e^{-|\alpha|^2} \sum_{n=0}^{\infty} \frac{n^2 |\alpha|^{2n}}{n!} \\
&= e^{-|\alpha|^2} \sum_{n=0}^{\infty} (|\alpha|^4 \frac{d^2}{d(|\alpha|^2)^2} + |\alpha|^2 \frac{d}{d(|\alpha|^2)}) \frac{(|\alpha|^2)^n}{n!} \\
&= e^{-|\alpha|^2} |\alpha|^2 (|\alpha|^4 \frac{d^2}{d(|\alpha|^2)^2} + |\alpha|^2 \frac{d}{d(|\alpha|^2)}) e^{|\alpha|^2} \\
&= |\alpha|^4 + |\alpha|^2 \qquad (44)
\end{aligned}
$$

hence,

$$\langle \Delta \hat{n}_{laser}^2 \rangle = (|\alpha|^4 + |\alpha|^2) - (|\alpha|^2)^2 = |\alpha|^2 = \langle \hat{n} \rangle_{laser} \quad (45)$$

This shows that the relative fluctuation of photon number in a lase state:

$$\frac{\langle \Delta \hat{n} \rangle_{laser}}{\langle \hat{n} \rangle_{laser}} = \frac{1}{\sqrt{\langle \hat{n} \rangle_{laser}}} \qquad (46)$$

That is, the laser state modeled by a coherent state has a Poissonian nature, which is endowed by the intrinsic structure of coherent-state wavefunction under Fock representation, as shown in (24).

V.   CONCLUSION AND DISCUSSION

Starting from three fundamental definitions, we have presented a systematic review of coherent-state formalism by showing explicitly how the elegant mathematical structure and properties of coherent states arise from the quantum theory of harmonic oscillator under Fock representation (space). The Hilbert-space properties, physical interpretations as a bridge connecting quantum and classical physics, as well as one application as a description of Possionian laser states are also discussed as the mathematical and physical consequences of this formalism. It's inspiring to see even for the simplest "field coherent state", which arose as a primordial conception of Schrödinger immediately after the birth of quantum mechanics, there are so many interesting physics and mathematics underlying. Indeed, the theory of coherent states provides a promising approach to modeling quantum systems as well as studying the correspondence principle (quantum-classical correspondence). However, on the experimental side, a physical realization of the coherent states in a realistic dynamic system is certainly of great experimental importance, and also remains an exciting challenge for the future [2].

[1] Erwin Schrödinger. Der stetige übergang von der mikro- zur makromechanik. *Naturwissenschaften*, 14(28):664–666, 1926.

[2] Wei-Min Zhang, Robert Gilmore, et al. Coherent states: theory and some applications. *Reviews of Modern Physics*, 62(4):867, 1990.

[3] Roy J Glauber. Coherent and incoherent states of the radiation field. *Physical Review*, 131(6):2766, 1963.

[4] Vladimir Fock. Configuration space and dirac's method of quantisation. *Z. Phys.*, 75:622–647, 1932.

[5] Robert Gilmore. *Lie groups, Lie algebras, and some of their applications*. Courier Dover Publications, 2012.

[6] Jean-Pierre Gazeau. *Coherent states in quantum physics*. Wiley, 2009.

[7] Aram W. Harrow. Mit 8.06 - solution 1. Spring, 2014.

Plane Wave Solutions to the Dirac Equation and SU_2 Symmetry

Camilo Cela López

Massachusetts Institute of Technology, 77 Massachusetts Ave., Cambridge, MA 02139-4307

(Dated: May 3, 2014)

I will explain the motivation behind the Dirac equation and derive it. I will work out the solutions to the equation for the case of free particles and we will observe new physical phenomena that arise from the interpretation of the solutions. Finally, I will show that the Dirac equation describes the behavior of spin-1/2 particles by proving that it satisfies the SU_2 symmetry .

I. INTRODUCTION

The Schrödinger equation is a good first approach to develop intuition on the behavior of physical systems. However, there are some extrema in which we find the need to use perturbation theory to analyze the corrections originated by the electron spin, relativistic speeds, and other effects. This is the motivation behind the derivation of an equation with all these corrections already built into it. This is the Dirac equation. The Dirac Equation is a principal postulate for quantum field theory: it is the relativistic version of the Schrödinger equation, which we use to make accurate predictions about the behavior of really small particles (quantum mechanics) that go really fast (relativity). It describes the behavior of all spin-1/2 quantum particles (which will be proved later) subject to an electric potential $\phi(x)$, and a magnetic potential $A(x)$. This includes all fermions that have been experimentally confirmed to exist, which consist of the electron, the muon, and the tauon, their corresponding neutrinos, and all the quarks. The equation emerges, as in the case of the nonrelativistic Schrodinger equation, from the postulates that $H \to i\hbar\partial/\partial t$ and $p \to -i\hbar\partial/\partial x$, but this time the relationship between the kinetic component of H (free Hamiltonian) and p is different, given by Einsteins relativistic equation $E = (p^2c^2 + m^2c^4)^{1/2}$. In order to get rid of the square root we could just apply the Hamiltonian to the state twice. This way we get the Klein-Gordon equation [3]:

$$(H/c)^2 = p^2 + m^2c^2 \to$$
$$-\frac{1}{c^2}\frac{\partial^2}{\partial t^2}|\psi\rangle = (-\frac{\hbar^2}{2m}\frac{\partial^2}{\partial x^2} + m^2c^2))|\psi\rangle.$$

Although useful, this is not the equation we are looking for. This equation describes the behavior of spin-0 particles. The problem with this approach is that we get an equation that is second order in time. This fact is incompatible with the statistical interpretation of ψ [2], that states that the probability density of finding the particle at (x,t) is $|\psi^2|$. To account for this we want a "new Schrödinger equation" that is first order in time, in such a way that the wave function is determined at any later time by the initial conditions.

II. DIRACS IDEA

In order to satisfy the conditions we introduced above we will rewrite this equation with the relativistic covariant-contravariant notation (in which we sum over repeated indexes) as $p^\mu p_\mu - mc^2 = 0$. Diracs strategy to deal with this problem was to factor this equation into a product of two components (a sum and a difference) [2]. Since the first components of the equation are four-vectors there is no immediately obvious way to factor this equation into the two components that we want and still get a nice result.

Mathematical Derivation

One might try to factor the components as

$$(\gamma^\mu p_\mu + mc)(\gamma^\kappa p_\kappa - mc) = 0. \tag{1}$$

But if we choose the gammas to be numbers this approach will not work. The cross terms will not cancel because they are all proportional to the anticommutators of the gammas:

$$p^\lambda p_\lambda - m^2c^2 = \gamma^\mu p_\mu \gamma^\kappa p_\kappa - (\gamma^\mu p_\mu - \gamma^\kappa p_\kappa)mc - m^2c^2$$
$$= \gamma^\mu p_\mu \gamma^\kappa p_\kappa - m^2c^2$$

Since we are considering the case in which the Hamiltonian has no contribution from fields, then all points in space should be equivalent [2], and therefore the Hamiltonian does not have any contributions from the position operators. This means that the γs commute with the momentum operators, and since the momentum operators commute amongst themselves, then, the above equation becomes:

$$p^\lambda p_\lambda = \frac{1}{2}(\gamma^\mu \gamma^\kappa + \gamma^\kappa \gamma^\mu)p_\mu p_\kappa \tag{2}$$

At this point is when Dirac had his idea of letting the gammas be operators, instead of scalars [2]. The anticommutator of two operators can be zero, and this way, expanding the sum we find it is possible to cancel the cross terms. We just need to impose the restriction that

$$(\gamma^0)^2 = 1, \text{ and } (\gamma^\mu)^2 = -1, \text{ for } \mu = 1, 2, 3,$$

and that the different gammas anticommute

$$\{\gamma^\mu, \gamma^\kappa\} = 0.$$

In summary,

$$\{\gamma^\mu, \gamma^\kappa\} = 2g^{\mu\kappa}. \tag{3}$$

The equation above implies that $\gamma^\mu p_\mu + mc = 0$, or that $\gamma^\mu p_\mu - mc = 0$. We will use the second equality (although it can be done either way [3]). Now we can let the resulting operator to act on the state $|\psi\rangle$ to get the Dirac equation:

$$(\gamma^\kappa p_\kappa - mc)|\psi\rangle = 0. \tag{4}$$

The only thing left at this point to get our final equation is the quantum substitution of $p \to i\hbar\partial/\partial x$, where $x^0 = ct, x^1 = x, x^2 = y, x^3 = z$, to start making analytical calculations. Back to the gamma matrices, there are a lot of different choices we could make for the 4 matrices, but it just happens that the smallest matrices that can satisfy the above conditions are 4×4 matrices. It cannot be 2×2 matrices, because that would mean we could add an extra spin matrix to the 3 existing Pauli matrices, and we know that is not possible (because there is no additional traceless Hermitian 2×2 matrix that is linearly independent of the 3 Pauli matrices). These matrices also need to be even dimensional to be able to satisfy the requirement [4]. The standard convention for these are the following [3], expressed in shortened notation:

$$\gamma^0 = \begin{pmatrix} 1 & 0 \\ 0 & -1 \end{pmatrix}$$

$$\gamma^\mu = \begin{pmatrix} 0 & \sigma^\mu \\ -\sigma^\mu & 0 \end{pmatrix} \text{ for } \mu = 1, 2, 3,$$

where 0 and 1 represent the 0 and the identity 2×2 matrices, respectively, and σ^μ are the Pauli matrices. Therefore, $|\psi\rangle$ must be a four component wave function, but we will divide it into two 2×1 components, just as we did with the gamma matrices above. These will be $|\psi_A\rangle$ (corresponding to the two upper components of $|\psi\rangle$), and $|\psi_B\rangle$ (which correspond to the lower components).

III. DIRAC EQUATION

A. Solution of Particles at Rest

The equation can be easily solved when the momentum is set to zero. In this case we can work in the momentum basis, and we can drop the special components of the momentum operator acting on $|\psi\rangle$. We will approach this simple problem first and use the solution to later find out the form of the wave function when the momentum is arbitrary. The equation gets reduced to $\gamma^0 \partial/\partial t|\psi\rangle = -imc/\hbar|\psi\rangle$, which is equivalent to:

$$\begin{pmatrix} 1 & 0 \\ 0 & -1 \end{pmatrix} \frac{\partial}{\partial t}|\psi\rangle = -\frac{imc}{\hbar}|\psi\rangle. \tag{5}$$

The solution is given by the following familiar expressions for the time evolution of the wave function:

$$|\psi_A(t)\rangle = e^{-imc^2t/\hbar}|\psi_A(0)\rangle, \tag{6}$$

$$\text{and } |\psi_B(t)\rangle = e^{imc^2t/\hbar}|\psi_B(0)\rangle. \tag{7}$$

B. Physical Interpretation

It is important to realize that it is only possible to consider the problem of a particle at rest in the absence of any fields because we are using the relativistic formulas to construct this new Schrodinger equation, eq. (5). If we were using the classical formula for the Hamiltonian, then the energy of the particle at rest would be zero instead of its rest mass. Notice, however, that the right hand side of eq. (5) is not zero. This allows us to obtain the two solutions $|\psi_A(t)\rangle$ and $|\psi_B(t)\rangle$ (rather than the non-relativistic 0 solution, which would be the same as saying there is no particle). One of these solutions seems to reflect a state with a negative value for the energy. The prediction that there exist negative energy eigenstates is something new to this theory that needs a physical explanation, because we have never observed a particle with absolute negative energy. Diracs initial interpretation of this strange result was to postulate a field of particles that was everywhere and that filled those negative energy states. Since the Dirac equation describes the behavior of spin-1/2 particles [4], which are fermions, according to the Pauli exclusion principle, when this sea of particles (as it is commonly referred to) is full, it would not allow any other visible particles (particles with positive energy) to occupy these negative energy states. The reason why we cannot throw away these states by claiming that they are not physical, as we used to do in some cases with non-relativistic quantum mechanics, is that we need a complete basis for the space of states. The positive energy eigenstates alone do not provide such a basis [4]. If the quantum field is excited (by a photon with enough energy), then one of the particles in the negative

energy state will jump up to the positive energy state, thus leaving a hole in the sea and kicking a particle from the sea to the "visible space":
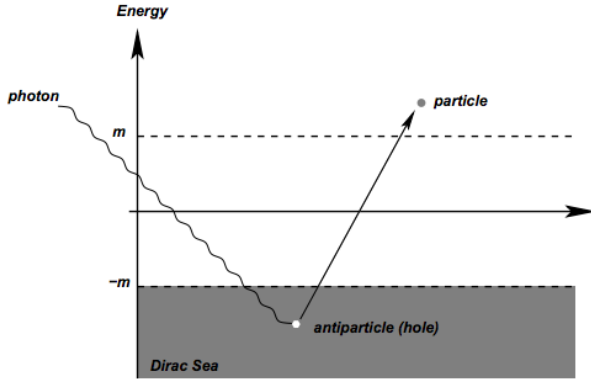

FIG 1. Photon exciting the Dirac fermion sea, creating a particle-antiparticle pair [1].

When there is an empty space, the particle would be able to annihilate with the hole. It behaves the same way as the original particle, but with opposite charge. This hole was initially conjectured by Dirac to be the proton, but he was soon convinced by Oppenheimer that that was not possible, because if that was the case, that would imply that a proton-electron pair would be able to annihilate in the atom, and that would make all matter unstable [?]. This interpretation gives a number of problems, like the fact that if the sea of negative energy particles is infinite, it could always accept more particles, so particles could potentially be swallowed or be created form the vacuum without conserving energy. Nowadays, we interpret the hole in the Dirac sea to be the modern antiparticle. it is a real particle and it still behaves the same way as the original particle but with opposite charge. Thus, a particle-antiparticle pair can be "created" out of the vacuum [1]. This is the context in which the idea of an antiparticle first emerged. The antiparticle corresponding to the electron is the positron, and the positron was finally discovered experimentally by Carl. D. Anderson in 1932.

C. Plane Wave Solutions of the Dirac Equation

As a 4-dimensional vector equation, the solutions to the momentum-less particle in the Dirac equation are given by 4 linearly independent vectors pointing in the axis direction. From the discussion above we get the motivation to interpret what each of these vectors represent. Mathematically speaking, since the two upper components have positive "energy", they correspond to electron states, and similarly, since the two bottom ones have negative "energy", they correspond to positron states. The top state represents spin up, and the bottom one, spin down.

Now we want to find the solutions of particles with momentum, and for this case it is much easier to do the calculation if we start assuming since the beginning that the momentum points in the z-direction (this way the solutions we will get will be automatically eigenstates of S_z, the new z-spin operator). We generalize the old spin matrices to account for the new 4-dimensional vectors. These will be given by:

$$S_i = \begin{pmatrix} \sigma^i & 0 \\ 0 & \sigma^i \end{pmatrix};$$

where the σ^is correspond to the Pauli matrices. The new form of the solutions once we include momentum in the equation should be the following [3]:

$$\psi(r,t) = Ae^{-\frac{i}{\hbar}(Et-p_z z)}u(E,p_z), \qquad (8)$$

where A is a normalization constant, and u is a 4-dimensional vector. We can figure out what the u vector above is by plugging this expression into the Dirac equation. When we do this, we obtain the result

$$\gamma^\mu p_\mu Ae^{-\frac{i}{\hbar}(Et-p_z z)}u(E,p_z) - mcAe^{-\frac{i}{\hbar}(Et-p_z z)}u(E,p_z) = 0,$$

$$\text{or } (\gamma^3 p_z - mc)u(E,p_z) = 0. \qquad (9)$$

This equation can be dealt with the old way (in the position basis), or more easily by transforming the elements into momentum space, in which the momentum operators are scalars. When we do this, eq.(9) is transformed into a familiar algebraic 4×4 matrix eigenvector equation. Taking care of the signs in each of the summation terms, we can calculate the matrix acting on u to be:

$$\gamma^\mu p_\mu - mc = \frac{E}{c}\begin{pmatrix} 1 & 0 \\ 0 & -1 \end{pmatrix} - p_z\begin{pmatrix} 0 & \sigma^z \\ -\sigma^z & 0 \end{pmatrix} - mc\begin{pmatrix} 1 & 0 \\ 0 & 1 \end{pmatrix} \qquad (10)$$

$$= \begin{pmatrix} E/c - mc & p_z\sigma^z \\ -p_z\sigma^z & -E/c - mc \end{pmatrix} \qquad (11)$$

and when we apply it to u we get:

$$\begin{aligned} (E/c - mc)u_A + p_z\sigma^z u_B = 0, \text{ and} \\ -p_z\sigma^z u_A - (E/c + mc)u_B = 0, \end{aligned} \qquad (12)$$

where, once again, u_A and u_B correspond to the upper and lower two components of the 4-dimensional vector u. From these expressions, now we can just pick any choice of u_A (or u_B), and get the resulting energy eigenfunction. The simplest choices for u_A and u_B (namely $(1,0)^t$ and $(0,1)^t$), give the following linearly independent solutions for ψ:

$$\psi_1 = Ae^{-\frac{i}{\hbar}(Et-p_z z)}\begin{pmatrix} 1 \\ 0 \\ \frac{cp_z}{E+mc^2} \\ 0 \end{pmatrix}$$

$$\psi_2 = Ae^{-\frac{i}{\hbar}(Et-p_z z)}\begin{pmatrix} 0 \\ 1 \\ 0 \\ -\frac{cp_z}{E+mc^2} \end{pmatrix}$$

$$\psi_3 = Ae^{-\frac{i}{\hbar}(Et-p_z z)}\begin{pmatrix} \frac{cp_z}{E-mc^2} \\ 0 \\ 1 \\ 0 \end{pmatrix}$$

$$\psi_4 = Ae^{-\frac{i}{\hbar}(Et-p_z z)}\begin{pmatrix} 0 \\ -\frac{cp_z}{E-mc^2} \\ 0 \\ 1 \end{pmatrix},$$

where the normalization constant is given by $A = \sqrt{|E|/c + mc}$ [3].

D. Physical Interpretation

As I mentioned before, these are automatically eigenstates of the spin matrix S_z because they spin is oriented in the z-direction (otherwise these states would correspond to eigenstates of the spin matrix pointing in the direction of motion). This mathematical fact implies that the first two states should be physically interpreted as an electron with spin up and an electron with spin down, respectively. The third and fourth states require a more careful analysis. These would correspond to electrons with a negative energy, but particles cannot have negative energy. This apparent paradox is reinterpreted as these states actually being antiparticles with positive energies. To deal with this problem mathematically we change the form of equation (in which we change the form of u) to:

$$\psi(r,t) = Ae^{\frac{i}{\hbar}(Et-p_z z)}u(-E, -p_z), \qquad (13)$$

and the resulting states are

$$\psi_3 = Ae^{\frac{i}{\hbar}(Et-p_z z)}\begin{pmatrix} \frac{cp_z}{E+mc^2} \\ 0 \\ 1 \\ 0 \end{pmatrix}$$

$$\psi_4 = Ae^{\frac{i}{\hbar}(Et-p_z z)}\begin{pmatrix} 0 \\ -\frac{cp_z}{E+mc^2} \\ 0 \\ 1 \end{pmatrix}.$$

In this situation, we can interpret the last two states as a positron with spin up and positron with spin down. Nevertheless, this is just an ad hoc observation that could very well just obey the math without having much physical meaning behind.

IV. SU_2 **SYMMETRY**

To prove the statements above and, furthermore, that the Dirac equation describes the behavior of spin-1/2 particles, I will show that the theory respects the SU_2 symmetry [5]. In order to do this we need the mathematical concept of representation of a group. The representation of a group is a map used to substitute the elements of a mathematical structure (like a group) by linear transformations [6]. In this case, these linear transformations will be matrices, or the operators acting on our space of states. The group representing the rotation transformations for a spin-1/2 particle in 3 dimensions is SU_2. In general, for a particle of spin-s the representation is given by SU_n with $n = 2s+1$ [5]. This group, SU_2, is given by the set of all 2×2 unitary matrices A with $det(A) = 1$. Unitary matrices, the can be expressed as the exponential of i times a hermitian matrix, or equivalently, an exponential of an antihermitian (2×2) matrix. Since the set of the four matrices composed of the identity and the 3 Pauli matrices span the space of 2 dimensional hermitian matrices, we can express every unitary matrix as the exponential of i times an arbitrary linear combination of these matrices. Nevertheless, we will need to use our new version of the Pauli spin matrices, S_i, defined above. The matrices will have the form $U = e^{-\frac{i}{2}(n^0 I + n^j S_j)}$, but we can actually simplify this further by noticing that the identity commutes with all other matrices. Therefore the matrix above is equal to the same matrix multiplied by a constant factor of length one (a phase). Since this phase can be absorbed into the state whenever we act on it (and this does not change the state) we get the same operator. So all unitary 2×2 matrices can be expressed (up to a phase factor) as

$$U = e^{-\frac{i}{2}n^j S_j},$$

which simplifies to

$$U = I \cos(\frac{|n|}{2}) - i\frac{n^j}{|n|}S_j \sin(\frac{|n|}{2}). \qquad (14)$$

A quick indication to see how the appropriate (SU_2) symmetry is satisfied is to act these operators on the S_z eigenspinors we worked out above. We can see that we get the same states back:

$$U\text{---}\psi_1\rangle = Ae^{-\frac{i}{\hbar}(Et-p_z z)}e^{-\frac{i}{2}n^z S_z}\begin{pmatrix} 1 \\ 0 \\ \frac{cp_z}{E+mc^2} \\ 0 \end{pmatrix}$$

$$= Ae^{-\frac{i}{\hbar}(Et-p_z z)}e^{-\frac{i}{2}n^z}\begin{pmatrix} 1 \\ 0 \\ \frac{cp_z}{E+mc^2} \\ 0 \end{pmatrix}$$

$$= Ae^{-i(\frac{n^z}{2} + \frac{E}{\hbar}t - \frac{p_z}{\hbar}z)} \begin{pmatrix} 1 \\ 0 \\ \frac{cp_z}{E+mc^2} \\ 0 \end{pmatrix} = |\psi_1\rangle,$$

and similarly,

$$U|\psi_2\rangle = -|\psi_2\rangle, U|\psi_3\rangle = |\psi_3\rangle, \text{ and } U|\psi_4\rangle = -|\psi_4\rangle \quad (15)$$

Nevertheless, these are the states in a homogeneous space (in the absence of any fields). Therefore, to formally prove that the symmetry is satisfied we need to verify that Dirac equation itself is invariant under these transformations. The above calculations in eq. (15) will help us in doing this calculation, which will follow directly from the same concept used there (we used eigenspinors). As we learned, the way to transform operators is to act on them from the right with the operator, and from the left with the inverse of the same operator. We also know that the inverse of a unitary matrix U is $U^\dagger$. Therefore, if $|\psi\rangle$ is a state with a given chirality (spin projection onto the momentum direction spin basis), with its spin pointing in the n^j direction (that is, $|\psi\rangle$ is an $n^j S_j$ eigenstate) then we have [5]:

$$(\gamma^\kappa p_\kappa - mc)|\psi\rangle = 0 \rightarrow$$
$$U^\dagger(\gamma^\kappa p_\kappa - mc)U|\psi\rangle = e^{\frac{i}{2}n^j S_j}(\gamma^\kappa p_\kappa - mc)e^{-\frac{i}{2}n^j S_j}|\psi\rangle$$
$$= e^{\frac{i}{2}n^j S_j}(\gamma^\kappa p_\kappa - mc)e^{i\phi}|\psi\rangle$$
$$= e^{i\phi}e^{\frac{i}{2}n^j S_j}(\gamma^\kappa p_\kappa - mc)|\psi\rangle = 0$$

where ϕ is an arbitrary phase imparted to $|\psi\rangle$ by U. We see that using the same concept we used above in eq. (15) we automatically arrive to an expression in which we get an operator acting on the Dirac operator on $|\psi\rangle$, $(\gamma^\kappa p_\kappa - mc)|\psi\rangle$, and this is equal to 0. This calculation additionally shows that a free spin-1/2 particle preserves chirality.

V. DISCUSSION

We have given the arguments and shown the first steps that led to the development of Quantum Field Theory (QFT) at first. Although the facts stated and results showed on this paper are of crucial importance to the theory itself, this is just the foundation of QFT, and a very small sample of the predicting power of this theory. We should also keep in mind that although the predictions of the Dirac equation are in very good agreement with the experiments, they are "not the last word". There are effects that are only discovered once we take an additional step, such as treating the electromagnetic field as an operator. Such an example is given in the formula for the energy spectrum of the Hydrogen atom [4]. The formula for its eigenvalues is much more accurate than the prediction given by the Schrödinger equation, yet it does not account for effects like the Lamb shift, which can be experimentally measured.

[1] Alvarez-Gaume, Luis, and Miguel A. Vazquez-Mozo. "Introductory Lectures on Quantum Field Theory." CERN Yellow Report CERN-2010-001 (n.d.): 4-10. Web. 15 Apr. 2014.

[2] Dirac, Paul A. M. "The Quantum Theory of the Electron." The Royal Society 117.778 (1928): n. pag. Royal Society Publishing. Web. 15 Apr. 2014.

[3] Griffiths, David J. "7." Introduction to Elementary Particles. New York: Wiley, 1987. 213-22. Print.

[4] Shankar, Ramamurti. "The Free -Particle Dirac Equation." Principles of Quantum Mechanics. 2nd ed. New York: Plenum, 1980. 563-75. Print.

[5] Peskin, Michael Edward, and Daniel V. Schroeder. "Lorentz Invariance in Wave Equations/The Dirac Equation." An Introduction to Quantum Field Theory. Reading, MA: Addison-Wesley, 1995. 35-44. Print.

[6] Artin, Michael. "Group Representations." Algebra. 2nd ed. Englewood Cliffs, NJ: Prentice Hall, 1991. N. pag. Print.

[7] Dirac, Paul A.M. "Quantized Singularities In The Electromagnetic Fields." (1931): n. pag. Web.

The Complex Eigenvalue Approach to Calculating Alpha Decay Rates

Nicolas Lopez
*Massachusetts Institute of Technology*
(Dated: May 2, 2014)

It has been well understood that certain unstable nuclei will attempt to reach a more stable state through the emission of an α particle since the initial discovery of α particle emission made by Earnest Rutherford in the late 1800s. However, it was not until shortly after the invention of Quantum Mechanics in the late 1920's that a theoretical model of α particle decay that could accurately predict the wide range of decay times present in many radioactive materials could be developed. In this paper, a general expression for the rate of an α decay process is derived through the use of a cleverly designed nuclear potential function and the WKB approximation methods. The decay rates of known α particle emitters are then calculated using this derived expression, and the results of this calculation are compared to the experimentally observed decay rates. It is found that the calculated decay rates overestimate the experimentally observed decay rates, a fact that can be largely attributed to sole consideration of $\ell = 0$ energy eigenstates in this derivation and the relative simplicity of the nuclear potential function used. Considering $\ell \neq 0$ states and a more sophisticated nuclear potential function will lower the calculated α decay rates into more agreeance with the experimentally observed rates.

I.   INTRODUCTION

A.   A Brief Overview of the Alpha Decay Process

An α particle consists of two protons and two neutrons. It is a doubly ionized Helium atom, thus carrying a $+2$ charge. A typical α decay process can be described through the following reaction:

$$^{A}_{Z}X \rightarrow \, ^{A-4}_{Z-2}X' + \, ^{4}_{2}\alpha \tag{1}$$
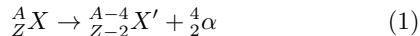
where A and Z are the mass number and atomic number of element X respectively.

Our knowledge of conservation laws allows the development of conditions that govern α decay processes. These conservation laws include the conservation of energy, the conservation of linear momentum, the conservation of charge, the conservation of angular momentum and the conservation of parity. The conservation of energy dictates that the total kinetic energy of the decay products must be equal to the mass deficit of the decay products compared to the initial mass of the mother nucleus. That is to say,

$$Q = (m_X - m_{X'} - m_\alpha)c^2 \tag{2}$$

where Q is the total energy released in the decay process and c is the speed of light in a vacuum, equal to 3×10^8 m/s.

The conservation of linear momentum dictates how this kinetic energy will be distributed between the two decay products, namely

$$E_{X'} = \frac{m_\alpha}{m_\alpha + m_{X'}}Q$$
$$E_\alpha = \frac{m_{X'}}{m_\alpha + m_{X'}}Q \tag{3}$$

The conservation of charge demands that, since an α particle carries a $+2$ charge, the daughter particle must

carry a -2 charge. This fact is generally not considered when analyzing nuclear reactions (which is concerned primarily with the states of the nuclei involved, not with the electrons); however, the charge on the decay products becomes relevant when analyzing how these decay products attenuate through matter. By carrying charge, the interactions between these decay products and matter are dominated by Coulomb interactions. Coulomb interactions occur over larger distances than the interactions due to the nuclear strong force or the nuclear weak force; therefore, charged particles such as these decay products will attenuate less in matter than neutral particles, such as photons or neutrinos, which do not experience Coulomb interactions.

Finally, through the conservation of angular momentum and parity, selection rules can be developed that involve the allowed orbital angular momentum values ℓ for the decay products. Since the alpha particle is spinless, changes in parity between the mother nucleus and the daughter nucleus will determine the ℓ values the α particle is allowed to take. In general, the orbital angular momentum of the alpha particle is restricted such that

$$|\ell_X - \ell_{X'}| \leq \ell_\alpha \leq \ell_X + \ell_{X'} \tag{4}$$

Parity must be conserved as follows:

$$\pi_X = \pi_\alpha \pi'_X \tag{5}$$

where π_i is the parity of nucleus i. Parity can only take values of $+1$ and -1, and in particular, the parity of the α particle can be calculated through the following equation:

$$\pi_\alpha = (-1)^\ell \tag{6}$$

Considering both eqs. 5 and 6, it is clear to see that if the parity of the mother nucleus and the daughter nucleus are the same, then only even values of ℓ_α will be

allowed such that the parity of the overall system is conserved; conversely, if the parity of the daughter nucleus is opposite that of the mother nucleus, only odd values of ℓ_α will be allowed.[1]

B. The Band of Stability as a Model to Predicting the Most Likely Decay Path of a Radionuclide

To briefly describe why unstable atoms exist, and why these unstable atoms tend to approach stability through specific, characteristic decay paths without going into a lot of quantitative detail, it is important to introduce the Band of Stability. The Band of Stability is an experimental result found from plotting the number of protons (Z) versus the number of neutrons (N) contained within a nucleus. In this plot, nuclei that are considered to be stable are found to form a thick band. This band of stable nuclei is often referred to as the Band of Stability, and it serves as a model in an attempt to explain why an unstable nucleus will decay through a decay chain specific to that nucleus type. In order to reach a lower energy state and thus stability, an unstable nuclei will attempt to bring its initial proton-neutron ratio to that of one contained within the band. Thus, the observed decay chain for that nucleus is simply the optimal path through N-Z space to reach the band of stability. In α decay, an equal number of protons and neutrons will be emitted, thus α decay does not change the proton-neutron ratio of an atom; however, it will aid heavier nuclei to approach stability in the region where the band of stability no longer follows the A=Z line. An N-Z plot demonstrating this band of stability is shown in Fig.1.

It should be noted that for the purpose of this derivation the Band of Stability can be considered an empirical result. A more detailed discussion about the nuclear decay process, about what makes a nucleus stable versus unstable or metastable, and about why certain decay paths are favored over the less optimal decay paths, is beyond the scope of the current paper.

II. MODELING AN ALPHA DECAY PROCESS AS A TUNNELING PROBLEM

With the idea of why certain nuclei might undergo an α decay process versus another type of decay process more understood, it is appropriate to return to the initial discussion on the nature of α decay, and more importantly, how an α decay process might be easily modeled for calculations of decay rates and half-lives of a specific radionuclide. A famous derivation, originally designed by physicist George Gamow in 1928, models the α decay process as a tunneling problem in which an α particle, preformed within the nucleus and trapped by an effective nuclear potential well, will at times escape from the potential well into free space. The calculation of the rate of an α decay process is considered to be a two stage
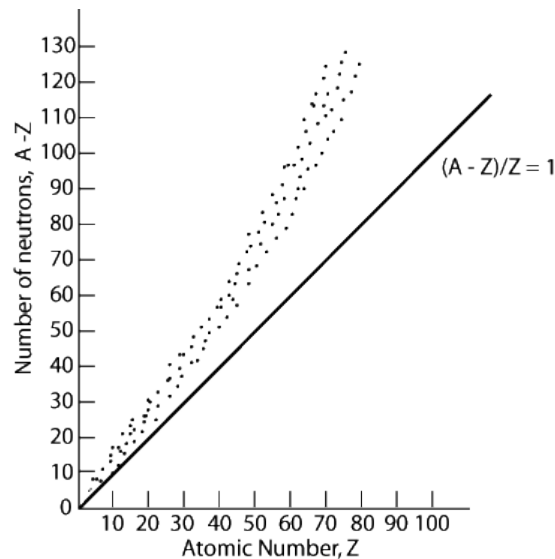
FIG. 1: A plot of the number of neutrons versus the number of protons for the known stable nuclei[2]

calculation: first to calculate the probability that an α particle will form within the nucleus, and second, to then calculate the probability that this newly formed α particle will then transmit through the coulomb barrier and be successfully emitted[1]. For the sake of brevity, this paper will only consider the second part of this two stage process and will assume that the α particle is produced within the nucleus.

A. Approximating the Nuclear Potential as a Finite Square Barrier

The simplest calculation of an α decay rate involves modeling the nuclear potential as a finite barrier of height V_0, shown in Fig.2.
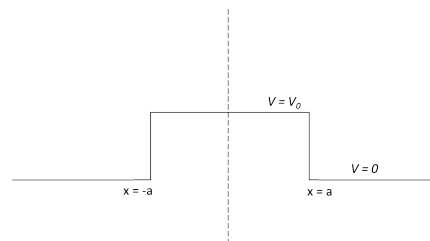
FIG. 2: Modeling the Nuclear Potential as a Finite Barrier

Since the potential is of the form,

$$V(x) = \begin{cases} 0 & |x| > a \\ V_0 & |x| < a \end{cases}$$

We know that the wavefunction will take the general form

$$\psi(x) = \begin{cases} Ae^{ikx} + Be^{-ikx} & -\infty < x < -a \\ Ce^{\kappa x} + De^{-\kappa x} & -a \leq x \leq a \\ Ee^{ikx} + F^{-ikx} & a < x < \infty \end{cases}$$

where k and κ are defined as

$$k = \frac{\sqrt{2mE}}{\hbar}$$

$$\kappa = \frac{\sqrt{2m(V_0 - E)}}{\hbar}$$

where E is the energy of the α particle, and m is the reduced mass of the α particle, mother nucleus system.

In this derivation, we will consider a rightward moving wave, such that A represents the initial amplitude of the wave, B represents the amplitude of the reflected wave, E represents the amplitude of the transmitted wave, and F, which in general represents the initial amplitude of a leftward moving wave, will be set to 0. Additionally, we will assume that the potential barrier is very large and very wide, as will be the case with the energy of an alpha particle compared to the potential barrier it must overcome, such that the coefficient of the growing exponential is very small and negligible. The observant reader will recognize that the unnormalizable momentum eigenfunctions are used as the wavefunction for the region $|x| > a$. A more realistic approach would be to use a moving wavepacket that can be properly normalized; however, for the sake of simplicity, the momentum eigenfunctions will be used instead.

We define the probability of transmission in general as:

$$T = \frac{|t|^2}{|A|^2} \tag{7}$$

where t is the amplitude of the transmitted wave and A is the initial amplitude. Thus for this derivation, our goal is to compute E in terms of A.

Due to the hard walls at $\pm a$, the WKB connection formulae cannot be applied as boundary conditions; however, continuity conditions exist such that the wavefunction and the spatial derivative of the wavefunction must both be continuous at $\pm a$. That is to say:

$$Ae^{-ika} + Be^{ika} = De^{\kappa a}$$
$$Aike^{-ika} - Bike^{ika} = -D\kappa e^{\kappa a}$$
$$De^{-\kappa a} = Ee^{ika}$$
$$-D\kappa e^{-\kappa a} = Eie^{ika} \tag{8}$$

After some manipulation, we find

$$E = \frac{2ike^{-2a(ik+\kappa)}}{ik - \kappa}A \tag{9}$$

and

$$T = \frac{|E|^2}{|A|^2}$$
$$= \frac{4k^2}{\kappa^2 + k^2}e^{-4a\kappa}$$
$$\approx \left(2\frac{k}{\kappa}\right)^2 e^{-2\gamma} \tag{10}$$

where

$$\gamma = \int_{-a}^{a} \kappa \, dx$$

and we used the result that $\kappa \gg k$ from the approximation that the potential barrier be very large. This result can be roughly generalized to state that for a potential barrier with classical turning points a and b

$$T \sim e^{-2\gamma} \tag{11}$$

with γ defined as

$$\gamma = \int_{a}^{b} \kappa(x) \, dx$$
$$= \frac{1}{\hbar}\int_{a}^{b} \sqrt{2m(V(x) - E)} \, dx$$

In our later computation of the transmission probability of an alpha particle, we should expect the relationship given in Eq.11 to be maintained.

B.   The Complex Eigenvalue Approach

The complex eigenvalue approach was originally done by physicist George Gamow in 1928, when he was the first to formulate an expression for the rate of an α decay process that is able to accurately predict the wide range of observed decay rates of in multiple radionuclides[3].

To begin the derivation, we first must construct a potential function that exhibits the same behavior as is present in the atomic nucleus. In general, a nucleus is positively charged, with total charge equal to $+Ze$ where Z is the number of protons and e is the magnitude of the charge of the electron. At large distance, Coulomb's Law tells us that the potential function should behave as if there was a point charge of total charge $+Ze$ located at the origin; we should expect the potential function to scale as $\sim \frac{1}{r}$ as $r \to \infty$. At close range, however, it is obvious that coulomb forces are not dominant; if they were, Z protons in close proximity would not form a low energy state. The nuclear strong force is the dominant interaction at small r, which we can model as a strongly attractive potential well up to an effective nuclear radius R_{eff}. To further simplify this nuclear potential function, we state that at the effective nuclear radius, R_{eff}, there is a sharp discontinuity in the potential function;
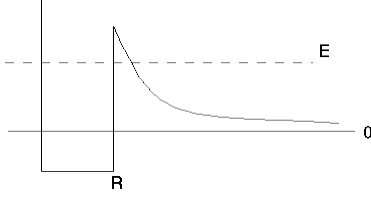
FIG. 3: A More Sophisticated Model of the Nuclear Potential Function[4]

the strong nuclear force abruptly goes to zero and the Coulomb forces immediately take over. The potential function described is shown in Fig.3.

A key assumption in this derivation is that the nuclear potential exhibits spherical symmetry, allowing us to write the potential function strictly as a function of r:

$$V(r) = \begin{cases} -V_0 & r < R_{\text{eff}} \\ \frac{Z'Z_\alpha e^2}{4\pi\epsilon_0 r} & r \geq R_{\text{eff}} \end{cases} \quad (12)$$

The classical turning points are given as R_{eff} and $R_T = \frac{Z'Z_\alpha e^2}{2\pi\epsilon_0 E}$. The wavefunction for this potential can be written as

$$u(r) = N \begin{cases} \sin(k_1 r) & 0 \leq r < R_{\text{eff}} \\ \frac{A}{\sqrt{\kappa(r)}} e^{\int_{R_{eff}}^{r} \kappa(r')\,dr'} \\ \quad + \frac{B}{\sqrt{\kappa(r)}} e^{-\int_{R_{eff}}^{r} \kappa(r')\,dr'} & R_{\text{eff}} \leq r \leq R_T \\ \frac{C}{\sqrt{k_2(r)}} e^{i\int_{R_T}^{r} k_2(r')\,dr'} & r > R_T \end{cases}$$

$$(13)$$

where we have defined

$$k_1 = \sqrt{\frac{2m(E + V_0)}{\hbar^2}}$$

$$\kappa(r) = \sqrt{\frac{2m(V(r) - E)}{\hbar^2}}$$

$$k_2(r) = \sqrt{\frac{2m(E - V(r))}{\hbar^2}} \quad (14)$$

where N is an overall normalization factor, and m is the reduced mass of the α particle - mother particle system

$$m = \frac{m_{X'} m_\alpha}{m_{X'} + m_\alpha}$$

As in the previous derivation, we are not able to use the WKB connection formulae at the hard wall boundary of R_{eff}; however, the second boundary at R_T is not a hard wall, and the WKB connection formulae can be applied to form appropriate boundary conditions. The connection formulae of interest to this derivation are:

$$\frac{A}{\sqrt{\kappa(r)}} e^{\int_r^{R_T} \kappa(r')\,dr'} + \frac{B}{\sqrt{\kappa(r)}} e^{-\int_r^{R_T} \kappa(r')\,dr'} \longleftrightarrow$$
$$\frac{2A}{\sqrt{k_2(r)}} \cos(\int_{R_T}^r k_2(r')\,dr' - \frac{\pi}{4}) - \frac{B}{\sqrt{k_2(r)}} \sin(\int_{R_T}^r k_2(r')\,dr' - \frac{\pi}{4})$$

$$(15)$$

Using the continuity conditions on the wavefunction and its spatial derivative at the hard wall boundary $r = R_{\text{eff}}$, and the WKB connection formulae at the classical turning point $r = R_T$, we can derive the following relationships:

$$\sin(k_1 R_{\text{eff}}) = \frac{1}{\sqrt{\kappa(R_{\text{eff}})}}(A + B)$$

$$k_1 \cos(k_1 R_{\text{eff}}) = \sqrt{\kappa(R_{\text{eff}})}(A - B)$$

$$C = 2Ae^\phi$$

$$C = iBe^\phi \quad (16)$$

with ϕ defined as

$$\phi = \int_{R_{\text{eff}}}^{R_T} \kappa(r')\,dr'$$

It then follows that:

$$A = \frac{\sqrt{\kappa(R_{\text{eff}})}}{2}[\sin(k_1 R_{\text{eff}}) + \frac{k_1}{\kappa(R_{\text{eff}})}\cos(k_1 R_{\text{eff}})]$$

$$B = \frac{\sqrt{\kappa(R_{\text{eff}})}}{2}[\sin(k_1 R_{\text{eff}}) - \frac{k_1}{\kappa(R_{\text{eff}})}\cos(k_1 R_{\text{eff}})]$$

$$A = \frac{i}{2}Be^{-2\phi} \quad (17)$$

These first two relationships can be satisfied for any chosen energy value; however, the third relationship can only be satisfied for specific energy values. The implication of this third relationship is a complex energy eigenvalue, from which this derivation got its name. The imaginary component of the energy eigenvalue is much smaller than the real component such that it can be treated as zero[5]. A common critique of the complex eigenvalue method is that it violates the axiom that hermitian operators yield real eigenvalues, and there are more rigorous derivations one could do, such as summing over all of the possible scattering states, or using a semiclassical path integral. However, the end results from those methods are remarkably similar to the result that will ultimately be obtained through this method[5].

The tunneling probability can be found with Eq.7

$$T = \frac{|C|^2}{k_2(r)}$$

In a nuclear potential, the Coulomb barrier is very large compared to the energy of the emitted α particle, so we can make the approximation that the wavefunction within the region $0 \leq r < R_{\text{eff}}$ is approximately the solution to the infinite well, i.e

$$k_1 R_{\text{eff}} \approx n\pi$$

Additionally, we will evaluate the amplitude of the transmitted wave at large r such that the Coulomb potential

drops to zero. Therefore,

$$
\begin{aligned}
T &= \frac{|C|^2}{k_2(\infty)} \\
&= \frac{|B|^2 e^{-2\phi}}{k_2(\infty)} \\
&\approx \frac{k_1^2}{4\kappa(R_{\text{eff}})k_2(\infty)} e^{-2\phi}
\end{aligned}
\tag{18}
$$

To obtain a decay rate, we must multiply this probability by a frequency. Classically, a particle undergoing simple harmonic motion will have a frequency of oscillation proportional to its velocity.

$$
\begin{aligned}
\frac{1}{2}mv_{\text{max}}^2 &= \frac{1}{2}m\omega^2 x_{\text{max}}^2 \\
v_{\text{max}} &= \omega x_{\text{max}} \\
&= 2\pi f x_{\text{max}}
\end{aligned}
\tag{19}
$$

In treating the α particle as a classical particle oscillating with a known energy, we can relate the final velocity of the α particle to be proportional to a frequency of oscillation that we will use to obtain a decay rate. The final velocity used will be that obtained when evaluating the kinetic energy of the α particle at large r.

$$
\begin{aligned}
v_{\text{max}} &= \sqrt{\frac{2E}{m}} \\
f &= \frac{1}{2\pi x_{\text{max}}}\sqrt{\frac{2E}{m}} \\
&= \frac{1}{2\pi R_{\text{eff}}}\frac{\hbar k_2(\infty)}{m}
\end{aligned}
\tag{20}
$$

Then the rate of decay Γ can be calculated to be

$$
\begin{aligned}
\Gamma &= fT \\
&\approx \frac{1}{2\pi R_{\text{eff}}}\frac{\hbar k_2(\infty)}{m}\frac{k_1^2}{4\kappa(R_{\text{eff}})k_2(\infty)}e^{-2\phi} \\
&\approx \frac{\hbar}{8\pi m R_{\text{eff}}}\frac{k_1^2}{\kappa(R_{\text{eff}})}e^{-2\phi}
\end{aligned}
\tag{21}
$$

To obtain an algebraic expression for the rate of an α decay process through which we can actually calculate values of decay rates, we must now evaluate the expression

$$
\phi = \int_{R_{\text{eff}}}^{R_T} \kappa(r')\,dr'
$$

$$
\begin{aligned}
\int_{R_{\text{eff}}}^{R_T} \kappa(r')\,dr' &= \int_{R_{\text{eff}}}^{R_T} \sqrt{\frac{2m}{\hbar^2}\left(V(r') - E\right)}\,dr' \\
&= \int_{R_{\text{eff}}}^{R_T} \sqrt{\frac{2m}{\hbar^2}\left(\frac{e^2 Z' Z_\alpha}{4\pi\epsilon_0 r'} - E\right)}\,dr' \\
&= \sqrt{\frac{2m}{4\pi\epsilon_0\hbar^2}Z'Z_\alpha e^2}\int_{R_{\text{eff}}}^{R_T} \sqrt{\frac{1}{r'} - \frac{1}{R_T}}\,dr' \\
&= \sqrt{\frac{2m}{4\pi\epsilon_0\hbar^2}Z'Z_\alpha e^2}\int_{R_{\text{eff}}}^{R_T} \sqrt{\frac{1}{r'} - \frac{1}{R_T}}\,dr' \\
&= \sqrt{\frac{2m}{4\pi\epsilon_0\hbar^2}\frac{Z'Z_\alpha e^2}{R_T}}R_T\int_{\frac{R_{\text{eff}}}{R_T}}^{1} \sqrt{\frac{1}{y} - 1}\,dy
\end{aligned}
\tag{22}
$$

where we used the fact that $E = \frac{Z'Z_\alpha e^2}{4\pi\epsilon_0 R_T}$ and defined $y \equiv \frac{r'}{R_T}$. This integral can be solved through a trigonometric substitution, namely, $y \equiv \sin^2(\theta)$. Defining $\theta_1 \equiv \frac{\pi}{2}$ and $\theta_2 \equiv \sin^{-1}\sqrt{\frac{R_{\text{eff}}}{R_T}}$

$$
\begin{aligned}
\int_{\frac{R_{\text{eff}}}{R_T}}^{1} \sqrt{\frac{1}{y} - 1}\,dy &= \int_{\theta_2}^{\theta_1} 2\sin(\theta)\cos(\theta)\sqrt{\frac{1}{\sin^2(\theta)} - 1}\,d\theta \\
&= \int_{\theta_2}^{\theta_1} 2\cos(\theta)\sqrt{1 - \sin^2(\theta)}\,d\theta \\
&= \int_{\theta_2}^{\theta_1} 2\cos^2(\theta)\,d\theta \\
&= \int_{\theta_2}^{\theta_1} 1 + \cos(2\theta)\,d\theta \\
&= \frac{\pi}{2} - \theta_2 - \sin\theta_2\cos\theta_2 \\
&= \cos^{-1}\sqrt{\frac{R_{\text{eff}}}{R_T}} + \sqrt{\frac{R_{\text{eff}}}{R_T}\left(1 - \frac{R_{\text{eff}}}{R_T}\right)}
\end{aligned}
\tag{23}
$$

Thus, the rate of an α decay process can be written as

$$
\Gamma \approx \frac{\hbar}{8\pi m R_{\text{eff}}}\frac{k_1^2}{\kappa(R_{\text{eff}})}e^{-2Z'Z_\alpha\frac{e^2}{4\pi\epsilon_0\hbar c}\sqrt{\frac{2mc^2}{E}}G\left(\sqrt{\frac{R_{\text{eff}}}{R_T}}\right)}
\tag{24}
$$

where we have defined $G(x) \equiv \cos^{-1} x - \sqrt{x(1-x)}$. Table I shows the decay rates of particles known to undergo α decay as calculated from Eq.24 compared to the decay rate data from the National Nuclear Data Center.[6] and the decay rates calculated by John Rasmussen in 1958, who used a nuclear potential derived from α scattering events and considered excited state transitions.[7]

III.   LIMITATIONS IN THE COMPLEX EIGENVALUE APPROACH

To first reiterate the key assumptions made in complex eigenvalue approach to calculating the rate of an α decay

Nuclide	Computed Half-Life	Experimentally Determined Half-Life	Rasmussen (1958)
Uranium-238	1.84×10^8 years	4.47×10^9 years	4.48×10^9 years
Polonium-210	14.5 days	138.3 days	135.42 days
Thorium-220	3.80×10^{-3} sec	9.7×10^{-6} sec	NA
Plutonium-238	51.4 years	87.7 years	89.36 years
Americium-241	78.8 years	437.6 years	NA

TABLE I: The α decay rates of specific radioactive nuclei as computed using the result of this derivation (Eq.24) are compared to the experimentally observed values[6] and the alpha decay rates as calculated by John Rasmussen in 1958[7].

Nuclide	Extreme Cluster Model	Experimentally Determined Values
Uranium-238	1.78×10^{10} years	4.47×10^9 years
Polonium-210	41.7 days	138.3 days
Thorium-220	15 μsec	9.7 μsec
Plutonium-238	111 years	87.7 years
Americium-241	634 years	437.6 years

TABLE II: A table comparing the half-lives of specific α particle emitters calculated through the Extreme Cluster model[8] and the experimentally determined values[6]

process, this derivation relies heavily on the assumption that the nuclear potential function can be characterized by a piecewise function in which there is no overlap between the nuclear strong force and the Coulomb forces of the nuclear protons. In this formation of the potential function, we implicitly considered only the wavefunctions with $\ell_\alpha = 0$, such that the angular term in the Hamiltonian, normally equal to $\frac{\hbar^2 \ell_\alpha(\ell_\alpha+1)}{2mr^2}$, is set to zero. It then should be expected that any decay rates predicted with a model considering only the $\ell_\alpha = 0$ states would be underestimated; any $\ell_\alpha \neq 0$ α particle state will have a positive contribution to the potential function seen in Eq.12, and as such, will have a larger potential barrier and consequently, smaller probability of tunneling into free space. Considering the $\ell_\alpha \neq 0$ states should resolve much of the underestimation in the calculated decay rates, as can be seen in Table I with the decay times calculated by Rasmussen. In Rasmussen's derivation, $\ell_\alpha \neq 0$ states were considered (with the specific values taken by ℓ_α dictated by previous experimental results) along with a 'modified' Gamow potential that included some correction terms based on electron screening. Only even-even nuclei were considered; however, Rasmussen did not calculate a decay time for Thorium-220 as it had yet to be discovered. The results of his derivation, shown in Table I, demonstrate remarkable similarity to the experimentally determined decay times.

Thorium-220 is an interesting case; it was the only radionuclide listed whose half-life was overestimated by this derivation. It may be the case that Thorium-220 is more sensitive to the chosen theoretical model than the other radionuclides. In 1993, Buck, et.al developed a model for α particle decay that relied upon the Extreme Cluster model for α particle formation. Instead of assuming that the α particle is preformed within the nucleus, in the Extreme Cluster model, the mother nucleus is viewed as an α particle orbiting the daughter nucleus. Also, instead of using a piecewise function to represent the nuclear po-

tential, Buck, et.al use a continuous function such that the nuclear potential function is given as:

$$V(r) = V_{\text{N}}(r) + V_{\text{C}}(r) + \frac{\hbar^2}{2m} \frac{(\ell + 1/2)^2}{r^2} \qquad (25)$$

where

$$V_{\text{N}}(r) = -V_0 \frac{1 + \cosh(R_{\text{eff}}/a)}{\cosh(r/a) + \cosh(R_{\text{eff}}/a)}$$

$$V_{\text{C}}(r) = \begin{cases} \frac{Z' Z_\alpha e^2}{r} & \text{for } r \geq R_{\text{eff}} \\ \frac{Z' Z_\alpha e^2}{2R_{\text{eff}}} \left[3 - \left(\frac{r}{R_{\text{eff}}} \right)^2 \right] & \text{for } r \leq R_{\text{eff}} \end{cases}$$

and a is the diffuseness of the α-core system[8]. The half-lives of Uranium-238, Polonium-210, Thorium-220, Plutonium-238 and Americium-241 calculated through this method are shown in Table II.

Much of this derivation relied on the wavefunction only being a function of the radial distance r, which subtly implied that the nuclear potential function exhibited spherical symmetries that allowed for this simplification. In some modern calculations of α decay rates, authors often consider deformed, namely elliptically shaped, nuclei[9]. There are also corrections made to the Gamow nuclear potential such that it is a slightly 'deformed' Gamow nuclear potential in order to more accurately represent the true nature of the coulomb force-strong force interactions, as already discussed with the models proposed by Rasmussen and Buck *et al*. Perhaps the largest approximation made in this derivation is the assumption that the α particle be preformed within the nucleus. As stated before, an α decay process can be well thought of as consisting two distinct stages: the formation of an α particle and the subsequent transmission of that α particle through the coulomb barrier. Neglecting the formation of an α particle neglects a lot of the interesting physics dictating which nuclei are most likely to undergo an α decay process, as well as how quickly an α particle can be 'created' within the nucleus, which will then have an impact on the overall rate of the decay process, as might be the case with Thorium-220.

IV. CONCLUSION

Since the initial observation of α decay processes by Earnest Rutherford in the late 1800's, it was not until after the invention of Quantum Mechanics that George Gamow was able to develop a theoretical model for the process of α decay that was able to accurately predict the wide spectrum of observed decay rates, from the long lived Uranium-238 to the ethereal Thorium-220. In this paper, Gamow's method of using a cleverly designed nuclear potential function and a complex energy eigenvalue to derive the rate of an α decay process was recreated, and the resulting expression was then used to calculate the decay rates of common α particle emitters. In Table I, the half-lives calculated from this theoretical model are compared to experimental values taken from the National

Nuclear Data Center, and to the values produced from a more rigorous theoretical derivation performed by John Rasmussen in 1958. With one notable exception, the experimental values of the α decay times are larger than the calculated decay times, a result that can be attributed to the neglect of $\ell_\alpha \neq 0$ angular momentum states. When considered, the potential barrier for an $\ell_\alpha \neq 0$ final state would be would larger than the potential barrier used in this derivation by a factor of $\frac{\hbar^2 \ell_\alpha(\ell_\alpha+1)}{2mr^2}$; thus, a longer decay time would be calculated. It might be the case that the vast overestimation in the α decay time of Thorium-220 is due to the simplistic model for the nuclear potential function used in the Complex Eigenvalue approach; a more sophisticated model, proposed by Buck *et al*, resolves much of the overestimation in the α decay time of Thorium-220.

[1] Mang, H. J., "Alpha Decay", *Annual Review of Nuclear Science* **14** (1964)
[2] Algebra Lab. "Chemistry Graphs: The Band of Stability." Web. 13 Apr. 2014. http://algebralab.com/practice/practice.aspx?file=Reading_TheBandOfStability.xml
[3] Griffiths, David J. *Introduction to Quantum Mechanics.* Pearson Prentice Hall (2005)
[4] University of Colorado Department of Physics. "Notes 5_37". Web. 13 Apr. 2014. http://www.colorado.edu/
[5] Holstein, Barry, "Understanding Alpha Decay", *American Journal of Physics* **64** (1996)
[6] Brookhaven National Laboratory. "National Nuclear Data Center." 15 Apr. 2014. http://www.nndc.bnl.gov/
[7] Rasmussen, John, "Alpha-Decay Barrier Penetrabilities with an Exponential Nuclear Potential: Even-Even Nuclei", *Physical Review* **113** (1958)
[8] Buck, B. *et al*, "Half-Lives of Favored Alpha Decays from Nuclear Ground States", *Atomic Data and Nuclear Data Tables* **54** (1993)
[9] Garcia, F. *et al*, "Alpha Decay and Nuclear Deformation: The Case for Favoured Alpha Transitions of Even-Even Emitters", *Journal of Physics G: Nuclear and Particle Physics* **26** (2000)
[10] Ferreira, Diogo. "Gamow's Theory of Alpha Decay", **Instituto Superior Tecnico** (2011)

Forbidden transitions and phosphorescence on the example of the Hydrogen atom

Konstantin Martynov

MIT, 77 Massachusetts Ave., Cambridge, MA 02139-4307

(Dated: May 3, 2014)

Luminescence is a very useful phenomenon. Nowadays people make use of it as glow-in-the-dark technology to mark the objects that should be visible in the darkness, such as watch hands, emergency arrows, or children's toys. The intensity is not very strong; with the light bulb turned on the glow is not noticeable. Nowadays scientists have learned how to produce luminescent materials with good features (brightness, lifetime, etc.), but those materials have mostly been found experimentally, because the theory for complex molecules is very complicated. In this paper I will explain the phenomenon of phosphorescence using the model of the hydrogen atom to show time scales for the allowed and forbidden transitions. At the end of the paper it will be discussed about some applications of phosphorescence, its non-linearity and quantitative calculations regarding the intensity of radiation.

I. INTRODUCTION

As a type of luminescence, phosphorescence should be distinguished from the other types of luminescence – fluorescence, chemiluminescence and bioluminescence, because they all have different mechanism of excitation before radiation. Fluorescence happens after excitation by radiation (like in TV tubes) and stops very fast after the radiation is turned off. Chemiluminescence happens after excitation by chemical reaction; a lot of those reactions are not reversible. This problem of irreversibility is solved in living beings and bioluminescence, since they can synthesize the necessary chemicals for it.

Luminescence and phosphorescence demand excitation by external radiation. After the excitation by a photon, an atom may stay in the excited state some time before the spontaneous emission of a photon or transferring of the energy to the other atoms. Sometimes these two processes happen together – the electron makes non-radiative transition to lower energy level and then radiates photon during transition to the ground state; the last one demands intermediate energy levels. That is why the emitted and the absorbed light may have different frequencies. For example, some luminescent materials absorb infrared radiation and emit visible light.

Depending on the lifetime of the excited states, which are dependant on the type of transition (allowed or forbidden), the radiation may have different names. If the re-emission takes $10^{-9} - 10^{-6}$ seconds (allowed transition), it is called fluorescence. With such a short lifetime, to the human eye it looks like an immediate radiation of light. If the re-emission happens from a metastable state it may take $10^{-4} - 10^2$ seconds (forbidden transition). Metastable states are the states with a lifetime that is longer than the one of usual states. In human timescales time those materials may discharge by emitting light for a long amount of time. These long emissions are called phosphorescence. The states are very stable because electrons occupy levels for which the transitions to the ground level are classically forbidden transitions. Because of the forbidden transitions, to calculate the lifetime of metastable states we should use the second-order

time-dependent perturbation theory instead of the first-order. In the next section it is shown what will happen if we apply the first order approximation to the classically forbidden transitions.

Though the emission of a photon with frequency corresponding to the transition is forbidden, the radiation can occur if two or more photons are emitted. Maria Göppert-Mayer was the first person who calculated the multi-photon emissions (1931) [1]. But only after 28 years did Shapiro and Breit [2] calculate the lifetime of the 2S state of a Hydrogen atom with 4 significant figures (0.1216 seconds). They calculated the integrals for the problem using numerical methods and approximations. As it will be shown later, my calculations don't match their answer in the 4th significant digit and are out of their confidence range.

This paper will explain the main ideas of the two-photon emission (or, the second-order perturbation theory) and will provide the reader with the numbers for the time scales of phosphorescence.

In section II the lifetime of some transitions in Hydrogen atom will be calculated using first-order approximations.

All calculations are done in cgs units.

II. APPLICATION OF FIRST-ORDER PERTURBATION THEORY FOR CALCULATION OF THE LIFETIME OF THE TRANSITIONS IN THE HYDROGEN ATOM

In this section I will calculate the lifetime of some transition lifetimes in Hydrogen atom, showing that radiation due to $(2P_{\frac{1}{2}} \rightarrow 1S)$ transition is a fluorescence and $(2S \rightarrow 1S)$ is a forbidden transition.

The spontaneous emission rate is derived in Griffith's textbook [3]:

$$\frac{1}{\tau(|i\rangle \rightarrow |f\rangle)} = A(|i\rangle \rightarrow |f\rangle) = \frac{4\omega_{if}^3 |\langle f| e\vec{r}|i\rangle|^2}{3\hbar c^3}, \quad (1)$$

where $\omega_{if} = (E_i - E_f)/\hbar$ is the angular frequency of

the emitted photon, $\vec{d} = \langle f | e\hat{r} | i \rangle$ is the electron's dipole moment in the atom, $|f\rangle$ and $|i\rangle$ arethe final and initial states, respectively,and τ is defined to be the lifetime of a transition.

The transition rates for transitions $(2S \rightarrow 2P_{\frac{1}{2}})$, $(2S \rightarrow 1S)$ and $(2P_{\frac{1}{2}} \rightarrow 1S)$ will be calculated using this formula. The hydrogen wavefunctions are:

$$\psi_{1S}(r, \theta, \phi) = \frac{1}{\sqrt{\pi} a_0^{\frac{3}{2}}} e^{-\frac{r}{a_0}} \tag{2}$$

$$\psi_{2P_{\frac{1}{2}}}(r, \theta, \phi) = \frac{1}{4\sqrt{2\pi} a_0^{\frac{3}{2}}} \frac{r}{a_0} \exp(-\frac{r}{2a_0}) \cos(\theta) \tag{3}$$

$$\psi_{2S}(r, \theta, \phi) = \frac{1}{4\sqrt{2\pi} a_0^{\frac{3}{2}}} (2 - \frac{r}{a_0}) \exp(-\frac{r}{2a_0}). \tag{4}$$
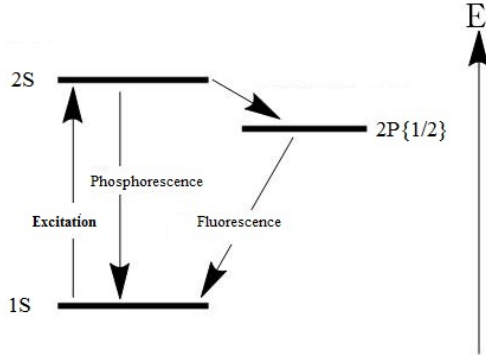
with $a_0 \approx 5.29 * 10^{-9}$ cm being the Bohr radius.

FIG. 1: Transitions in the lower levels of hydrogen atom.

After calculating the integral for the electric dipole moment

$$|\vec{d}| = |\int\limits_0^{2\pi} \mathrm{d}\theta \int\limits_0^{\pi} \mathrm{d}\phi \int\limits_0^{\infty} \mathrm{d}r * r^2 \sin(\theta)\psi^*(|f\rangle)\psi(|i\rangle) \tag{5}$$

$$r(\hat{x}\sin(\theta)\cos(\phi) + \hat{y}\sin(\theta)\sin(\phi) + \hat{z}\cos(\theta))|, \tag{6}$$

and considering that wave-functions are real we obtain the following values for the electric dipole moments

$$|d(2S \rightarrow 2P_{\frac{1}{2}})| = 3a_0 e \tag{7}$$

$$|d(2P_{\frac{1}{2}} \rightarrow 1S)| = \frac{128\sqrt{2}}{243} a_0 e \tag{8}$$

$$|d(2S \rightarrow 1S)| = 0. \tag{9}$$

As seen from the first-order perturbation theory, the rate of $2S \rightarrow 1S$ transition is 0. That is why it is called forbidden transition.

The frequencies are calculated using Planck-Einstein equation $E = \hbar\omega$. The energy difference between 2S and $2P_{\frac{1}{2}}$ is very small and it is called Lamb shift.The energy

difference between $2P_{\frac{1}{2}}$ and 1S is much bigger and may be calculated as an energy difference between levels n=2 and n=1 of the Hydrogen atom, because all next corrections to energy levels are of order $\alpha \approx \frac{1}{137}$.

$$\Delta E(2S \rightarrow 2P_{\frac{1}{2}}) = \Delta E_{Lamb} \approx 4.372 * 10^{-6} eV \tag{10}$$

$$\Delta E(2P_{\frac{1}{2}} \rightarrow 1S) = \frac{3e^2}{8a_0} \approx 10.20 eV. \tag{11}$$

Combining answers we get the lifetime of transitions to be

$$\tau(2S \rightarrow 2P_{\frac{1}{2}}) = \frac{3\hbar^4 c^3}{4\Delta E_{Lamb}^3 e^2 a_0^2} \approx 1.2 * 10^{10} s. \tag{12}$$

$$\tau(2P_{\frac{1}{2}} \rightarrow 1S) = \frac{3^8 a_0 c^3 \hbar^4}{2^8 e^8} \approx 1.6 * 10^{-9} s. \tag{13}$$

From these numbers it can be seen that the transition to the $2P_{\frac{1}{2}}$ state happens with very low probability (lifetime about 480 years.) One may think that the lifetime of $2S \rightarrow 1S$ transition is equal to the sum of $(2S \rightarrow 2P_{\frac{1}{2}})$ and $(2P_{\frac{1}{2}} \rightarrow 1S)$, but that is not true, because there are also possible different two-photon emissions including intermediate imaginary levels. The total probability of the two-photon emissions is higher than $(2S \rightarrow 2P_{\frac{1}{2}})$ transition. That is why the resulting lifetime of the transition is much less than $10^{10} s$. The precise calculations are hard to get because of that continuum spectrum (due to imaginary levels) and because of the effect of the higher P levels [1].

The next section derives the lifetime for 2S state taking into the account the two-photon transitions and neglecting the width of the intermediate states.

III. APPLICATION OF THE SECOND-ORDER PERTURBATION THEORY FOR THE CALCULATION OF 2S STATE'S LIFETIME OF THE 2S STATE OF HYDROGEN ATOM

In this section it will be shown how to calculate the total lifetime of 2S state of Hydrogen atom averaging on all possible two-photon transitions from 2S to 1S states.

The $(2S \rightarrow 1S)$ transition is forbidden, but simultaneous emission of two photons,that obey the following frequences:

$$\omega' + \omega'' = \frac{\Delta E(2S \rightarrow 1S)}{\hbar}, \tag{14}$$

is possible. ω' and ω'' are the frequences of the emitted photons.

The probability of the transition from the initial state $|i\rangle$ to the ground (final) state $|f\rangle$ is given by the second order time dependent perturbation theory

$$P(|i\rangle \to |f\rangle) = |\frac{1}{4\hbar^2} \frac{e^{\omega_{if}-\omega'-\omega''}-1}{\omega_{if}-\omega'-\omega''}$$

$$\sum_k \left[\frac{H_{ik,2}H_{kf,1}}{\omega'-\omega_{kf}} + \frac{H_{ik,1}H_{kf,2}}{\omega''-\omega_{kf}} \right)\right] |^2 \tag{15}$$

where $H_{ab,c} = \langle a| eE_c\hat{e}_c\vec{r}|b\rangle$, e is the electron charge, E_c is the value of an external Electric field in $\hat{e}_c$ direction.

In Shapiot and Breit [2] the lifetime of 2S is derived. The probability of emission of a photon at the frequency range $[\omega', \omega'+d\omega']$, is given by the formula, derived from eq. (15)

$$A(\omega')d\omega' = \frac{8e^4\omega'^3\omega''^3}{\pi h^2 c^6}$$
$$\left\langle \left| \sum_k \left[\frac{\langle i|\vec{r}\hat{e}_1|k\rangle\langle k|\vec{r}\hat{e}_2|f\rangle}{\omega(ik)+\omega''} \right. \right.\right.$$
$$\left.\left.\left. + \frac{\langle i|\vec{r}\hat{e}_2|k\rangle\langle k|\vec{r}\hat{e}_1|f\rangle}{\omega(ik)+\omega'} \right] \right|^2 \right\rangle_{Av} d\omega'. \tag{16}$$

where $\vec{r}$ is the displacement vector of electron, $\hat{e}_1$ and $\hat{e}_2$ are the unit vectors in the directions of the electric intensities of photons ω' and ω''. Summation is done over k - intermediate atomic states. The averaging goes over directions of polarization vectors . The transition rate is calculated using

$$A = \frac{1}{2} \int_0^{\omega_{fi}} A(\omega')d\omega' \tag{17}$$

The facto ofr $\frac{1}{2}$ appears because during the integration each pair of the photons appears twice. While integrating from 0 to $\omega_{2S\to1S}$ we encounter two pairs of photons - $(\omega, \omega_{2S\to1S})$ and $(\omega_{2S\to1S} - \omega, \omega)$, which are, actually, the same pair of photons.

Skipping the calculation and variable change done in [2], we have:

$$A(\eta)d\eta = \frac{2^{23}c\alpha^7}{3^3 a_0\pi}\eta^3(\frac{3}{4}-\eta)^3|M(\eta)+M(\frac{3}{4}-\eta)|^2 d\eta \tag{18}$$

Where

$$\alpha = \frac{e^2}{\hbar c}, \tag{19}$$

is a fine structure constant.

$$\eta = \nu' \frac{2a_0 h}{e^2}, \eta = [0, 0.75] \tag{20}$$

$$M(\eta) = \sum_{m=2}^{\inf} \frac{R(m)}{1-\eta-m^{-2}} + \int_0^\infty \frac{R_c(x)dx}{1-\eta+x^2} \tag{21}$$

$$R(m) = -\frac{1}{2^5 3^3}, (m=2)$$
$$= \frac{m^7(m-1)^{m-2}(m-2)^{m-3}}{(m+1)^{m+2}(m+2)^{m+3}}, (m>2) \tag{22}$$

$$R_c(x) = x(1+x)^{-2}(1+4x^2)^{-3}(1-e^{-\frac{2\pi}{x}})^{-1}$$
$$e^{-\frac{2}{x}(arctanx+arctan2x)}. \tag{23}$$

Behind all these complicated formulas lies a simple idea. There is some probability of emitting two photons with frequences not equal to $\omega_{2S\to2P_{\frac{1}{2}}}$ and $\omega_{2P_{\frac{1}{2}}\to1S}$. Those probabilities are given by eq. (18). Integrating those rates we include all possible probabilities.

In the next section we will calculate the integrals numerically

IV. LIFETIME OF 2S STATE OF HYDROGEN ATOM

The integrals derived in previous section are very complicated. There are two possible ways of solving this problem - approximations to the integrands or numerical integration. Using computer, the latter way is better, because it achieve more precision we only need to lower the step of the integration.

The authors in [2] calculated eq. (17) using numerical methods and approximations. The integral was calculated using Simpson's method for values η at intervals 0.0375 (21 nodes in region $[0, 0.75]$). They got the result

$$A_{2S\to1S} = (8.226 \pm 0.001)s^{-1} \tag{24}$$

The authors do not mention in the paper how they calculated the final error. One of the possible methods of error estimation, knowing the precision of the numerical method, is to use Runge's method [4]. That method is derrived as a correction to the numerical method, but also shows approximate error.

Suppose we have a numerical method of a precision p (Simpson's method has p=3). Then if the integrand has a continuous p^{th} derivative, then there exists C such that

$$I \approx I^p(h) + Ch^p \tag{25}$$

where I is the precise value of the integral,and $I^p(h)$ is value calculated with step h. If the step is small enough, then the constant C is not changing with slightly varying h. Then we may calculate the same integral with step 2h (a different step may be chosen, but step 2h is more convenient, because it doesn't require new calculation of the integrand at new points)

$$I \approx I^p(2h) + C(2h)^p \tag{26}$$

Solving the system of two equations we get

$$I - I^p(h) \approx \frac{I^p(h) - I^p(2h)}{2^p - 1} \tag{27}$$

This method is easy,as it does not even need a new calculation of the integrand. However, strictly speaking, this method sometimes gives lowered error estimation.

To use Simpson's method and estimate its error, I calculated the integrand at the same nodes as the authors

did in [2] precise up to 4th decimal digit in Mathematica.The Simpson's method gave next results:

$$A_{2S \to 1S} \approx (8.228 \pm 0.002)s^{-1}. \qquad (28)$$

To be sure, I calculated this integral in Mathematica numerically with PrecisionGoal of 6 (the effective precise number of digits in the final answer) and accounting for only 1000 elements in eq. (21). The answer was

$$A = 8.230s^{-1} \qquad (29)$$

which is out of range of the original paper's error region. The authors may have not payed a lot of attention to the error estimation.

The lifetime of 2S state was never directly measured [1] and the answer cannot be checked. The experiments on the measurement of the lifetime of 2S state used Electric or Magnetic field, which is described by a different theory. This example was to show the timescales for allowed and forbidden transitions, which in hydrogen vary by 8 orders of magnitude.

Later I will show the calculations concerned with real phosphorescent materials and experimental data.

V. PHOSPHORESCENCE IN COMPLEX MOLECULES

Taking into account the complexity of the calculation for a simple one-electron Hydrogen atom, it is expected that there is no way to precisely calculate the spectrum of complex molecules.

As an example, in Fig. 2 there is a plot of the spectrum of chrysene molecules $C_{18}H_{12}$. It can be seen from the Fig. 2, that the light is re-emitted at lower frequences compared to the absorbed light. It is also typically expected for phosphorescence to have lower frequencies than for fluorescence, because the energy levels at which phosphorescence occur have lower energy than the fluorescence energy levels [5]. In real life collisions between molecules and atoms may occur, which is another way of losing energy. That is why not so many fluids and gases at room temperature have phosphorescence. But the situation changes in crystal structures; those materials may have the ability to re-emmit the light after the crystallization.

Though while talking about phosphorescence we mentioned lifetime, we meant by this the most probable time before radiation. If we suppose the linearity of radiation

$$I \propto -\frac{dN_{excited}}{dt} = \frac{N_{excited}}{\tau}, \qquad (30)$$

then the intensity of radiation has a law similar to the law of radiative decay

$$I = I_0 e^{-\frac{t}{\tau}} \qquad (31)$$
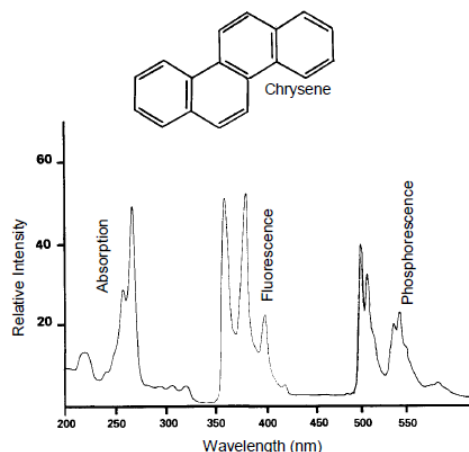
FIG. 2: Relative positions of absorption, fluorescence and phosphorescence bands of chrysene.

where τ is a transition lifetime, I_0 is initial intensity, $N_{excited}$ is the number of excited molecules that depends on time and become smaller due to radiation.

Now let's check whether we can say that the lifetime depends on the intensity of radiation or not.

The 4 values (Intensity, time) taken for material LU-MILUX green N from [6]. For rough estimation we may take first two and last two values and caculate I_0 and τ for them (Fig. 3). If the values are far from each other, then the model is incorrect.
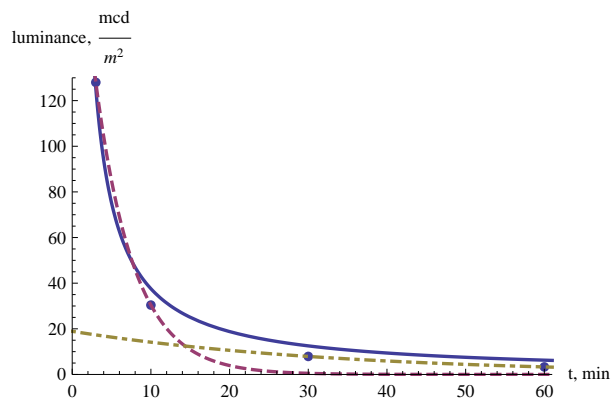
FIG. 3: Approximation of the intensity by first two and last two points. Dashed are exponential approximations, bold is the inverse relation approximation.

For the first two points we have $\tau \approx 4.9$ minutes, for the last two $\tau \approx 34$ minutes. It is a very big difference. Here we can see nonlinearity - the higher the radiation intensity, the lower τ and vice versa.

The experimental graph looks more like inverse dependence rather than the exponential one. Suppose the solution has the common form of $\frac{1}{t}$ dependance.

$$I = \frac{I_0}{1 + \frac{I_0 t}{\beta}}, \qquad (32)$$

where β is some constant. Taking the derrivative and comparing with eq. (31) we have

$$\tau = \frac{\beta}{I} \qquad (33)$$

Which means that in this theory the lifetime is inversely proportional to the intensity.

Though the curve fits experimental points very well, this approximation is precise only in the region [3, 60] minutes, because the integral representing the total emitted energy

$$E \propto \int_0^\infty I \, \mathrm{d}t \qquad (34)$$

does not converge, which means that the source has infinite amount of energy.

VI. CONCLUSION

As seen from the previous section, due to the complexity of the phenomenon, people mostly investigate it from the experimental perspective. Even for Hydrogen atomscientists skipped correction of order $\alpha = \frac{1}{137}$ and interaction between atoms and molecules in materials, but experimentally the numbers may be obtained with higher precision. Real materials are also non-linear, since the rate of change of the excited atoms ($\frac{dN_{excited}}{N_{excited}dt}$) is not a constant , but a function of intensity itself. That is why the decaying of intensity in real materials is not exactly exponential.

[1] W. Ketterle, *Problem Set 10.* (MIT,2010) problem 1.
[2] J. Shapiro and G. Breit, *Metastability of 2s States of Hydrogenic Atoms.* (Yale University, New Haven, 1958).
[3] D. Griffiths, *Introduction to Quantum Mechanics, 2nd Ed.* (Pearson Educcation, Inc., NJ, 2005) formula 9.56, page 356.
[4] V. Verzhbitsky, *Basics of numerical methods, 2nd Ed.* (Higher School, 2002) formula 12.41, page 484.
[5] , *An Introduction to flurescence spectroscopy.* (PerkinElmer, 2000) page 13.
[6] K. Franz et al., *Luminescent Materials.*(Encyclopedia of Industrial Chemistry, Verlag GmbH and Co. KGaA, 2012). table 7, page 617.

A Description of Graphene: From Its Energy Band Structure to Future Applications

Joaquin A. Maury
(Dated: May 2, 2014)

A survey of graphene including band structure derivation and applications.

I. INTRODUCTION

Graphene has the potential to revolutionize the world of modern electronics and physics. It is currently the topic of active research in different fields in science and engineering [1]. The excitement in graphene is generated from its plethora of applications that range from radiofrequency (RF) electronics to effective field transistors, which make graphene an option for post-silicon electronics [2]. Furthermore, because of its unusual electronic spectrum, it improves the performance of experiments on relativistic condensed matter physics without the need of expensive accelerators [3]. This paper will give a survey of graphene and its potential applications in order to explain why it has become such a popular topic of research. In section II, we will derive the energy band structure of graphene. In section III, it will be shown that this band structure has linear Dirac dispersion. This dispersion relation establishes that electrons that propagate through graphene can do so at speeds faster than in any other material at room temperature. Section IV will explain one of the most important applications of graphene, field-effect transistors (FET), and the advances that have been made in order to make this application feasible. This is an important field of research, because FETs are an essential component in modern electronic devices. We will conclude by commenting on the outlook and future of this application.

II. DERIVATION OF THE ENERGY BAND STRUCTURE

It is important for us to understand the derivation of graphene's energy band structure, since it is this feature that gives it unusual properties that will be discussed later in the paper. We will make use of the tight binding model in this derivation. Graphene consists of a thin and flat monolayer of carbon atoms which are arranged in a honeycomb structure. The lattice is shown in Fig 1. We can see that the lattice vectors can be written as:

$$\vec{a}_1 = a_0\sqrt{3}\left(\frac{1}{2}, \frac{\sqrt{3}}{2}\right), \quad \vec{a}_2 = a_0\sqrt{3}\left(-\frac{1}{2}, \frac{\sqrt{3}}{2}\right) \quad (1)$$

in the (x,y) basis and with a_0 representing the neighbor distance, $a_0 = 1.42\text{Å}$. Bloch's theorem states that a wavefunction in a crystal or periodic potential can change under translation only by a phase factor. Using this fact
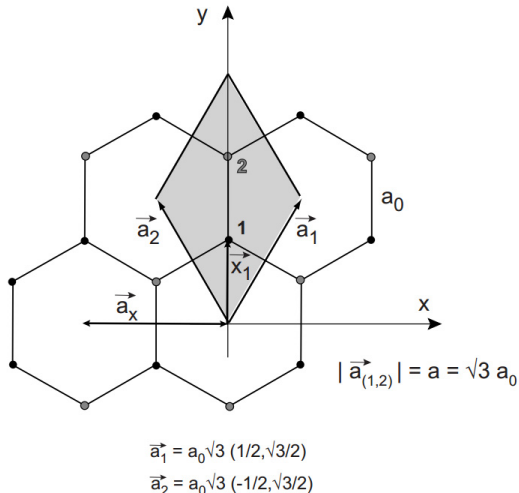
FIG. 1: Lattice of graphene. Carbon atoms are located at each crossings and the lines indicate the chemical bonds, which are derived from sp^2 orbitals. Also shown are the primitive lattice vectors $\vec{a}_{1,2}$ and the unit-cell (shaded). There are two carbon atoms per unit-cell, denoted by 1 and 2 [4].

we can write the wavefunction for this system as:

$$\psi_{\vec{k}} = \sum_{\vec{R} \in G} e^{i\vec{k}\cdot\vec{R}}\phi(\vec{r} - \vec{R}) \quad (2)$$

where G denotes the set of latice vectors and $\vec{R}$ denotes the latice vectors; in our case $\vec{R}$ represents $\vec{a}_1$ and $\vec{a}_2$. $\phi(\vec{r})$ are the atomic wavefunctions. Since we have two atoms per cell, and thus two such functions per cell, we can label them as ϕ_1 and ϕ_2, where 1 and 2 represent the corresponding carbon atoms. As a result, we can write the total wavefunction ϕ as follows:

$$\phi(\vec{r}) = c_1\phi_1(\vec{r}) + c_2\phi_2(\vec{r}) = \sum_n c_n\phi_n \quad (3)$$

The Hamiltonian for a single electron in this atomic potential produced by all the carbon atom is given by:

$$H = \frac{\vec{p}^2}{2m} + \sum_{\vec{R} \in G}\left(V_{atom}(\vec{r} - \vec{r}_1 - \vec{R}) + V_{atom}(\vec{r} - \vec{r}_2 - \vec{R})\right) \quad (4)$$

where $\vec{r}_{1,2}$ represents the position of the two carbon atoms in the unit-cell. If we apply this Hamiltonian to

ϕ_1 we get:

$$H\phi_1 = \epsilon_1\phi_1 + \phi_1 \sum_{\vec{R}\in G} \left(V_a(\vec{r} - \vec{r}_1 - \vec{R}) + V_a(\vec{r} - \vec{r}_2 - \vec{R}) \right)$$
(5)

Here ϵ_1 is the eigenvalue of the kinetic energy. The second part of this equation can be abbreviated as $\Delta U_1\phi_1$. This product is small because ΔU_1 is small in the vicinity of atom 1, and ϕ_1 is small in all places away from location 1. Using this abbreviation, we can re-write the action of the Hamiltonian in a compact way:

$$H\phi_{1,2} = \epsilon_{1,2}\phi_{1,2} + \Delta U_{1,2}\phi_{1,2}$$
(6)

We can further simplify this equation by noting that by symmetry $\epsilon_1 = \epsilon_2$ and that we can set the zeroth energy to any value. If we choose $\epsilon_1 = \epsilon_2 = 0$, Eq. (6) can by simplified as:

$$H\phi_{1,2} = \Delta U_{1,2}\phi_{1,2}$$
(7)

Next, we solve the Schrödinger equation:

$$H\psi_{\vec{k}} = E(\vec{k})\psi_{\vec{k}}$$
(8)

where $\psi_{\vec{k}}$ was defined in Eq. (2). There are two parameters c_1 and c_2, and as a result, two equations are required to solve this system. These are given by by projecting ψ on to the two states ϕ_1 and ϕ_2. By multiplying Eq. (8) by $\langle\phi_j|$, it can be shown that:

$$E(\vec{k})\langle\phi_j|\psi_k\rangle = \langle\phi_j|\Delta U_j|\psi_k\rangle$$
(9)

Calculating the terms $\langle\phi_1|\psi_k\rangle$ and $\langle\phi_2|\psi_k\rangle$, which can be done by assuming that only the nearest-neighbor overlap integrals have to be taking into account and using Eqs. (2) and (3) we obtain:

$$\langle\phi_1|\psi_k\rangle = c_1 + c_2 \left(\int \phi_1^*\phi_2 \, \mathrm{d}^3\vec{r} \right) \left(1 + e^{-i\vec{k}\cdot\vec{a_1}} + e^{-i\vec{k}\cdot\vec{a_2}} \right)$$

$$\langle\phi_2|\psi_k\rangle = c_2 + c_1 \left(\int \phi_2^*\phi_1 \, \mathrm{d}^3\vec{r} \right) \left(1 + e^{i\vec{k}\cdot\vec{a_1}} + e^{i\vec{k}\cdot\vec{a_2}} \right)$$
(10)

Assuming that the overlap integral is real, we can define:

$$\gamma_0 = \int \phi_1^*\phi_2 \, \mathrm{d}^3\vec{r} \in \mathbf{R}$$
(11)

Next, we need to calculate $\langle\phi_j|\Delta U_j|\psi\rangle$. We do this by once again only considering the nearest-neighbor overlap integrals. Additionally, we can use the abreviation:

$$\gamma_1 = \int \phi_1^*\Delta U_1\phi_2 \, \mathrm{d}^3\vec{r} = \int \phi_2^*\Delta U_2\phi_1 \, \mathrm{d}^3\vec{r}$$
(12)

where the second equality holds because changing the index should not matter due to the symmetry of the problem. We get these two equations:

$$\langle\phi_1|\Delta U_1|\psi_k\rangle = c_2\gamma_1 \left(1 + e^{-i\vec{k}\cdot\vec{a_1}} + e^{-i\vec{k}\cdot\vec{a_2}} \right)$$

$$\langle\phi_2|\Delta U_2|\psi_k\rangle = c_1\gamma_1 \left(1 + e^{i\vec{k}\cdot\vec{a_1}} + e^{i\vec{k}\cdot\vec{a_2}} \right)$$
(13)

Combining Eqs. (9), (10), and (13) and using the abbreviation:

$$\alpha(\vec{k}) = 1 + e^{-i\vec{k}\cdot\vec{a_1}} + e^{-i\vec{k}\cdot\vec{a_2}},$$
(14)

the eigenvalue problem can be written as:

$$\begin{pmatrix} E(\vec{k}) & \alpha(\gamma_0 E(\vec{k}) - \gamma_1) \\ \alpha^*(\gamma_0 E(\vec{k}) - \gamma_1) & E(\vec{k}) \end{pmatrix} \begin{pmatrix} c_1 \\ c_2 \end{pmatrix} = \begin{pmatrix} 0 \\ 0 \end{pmatrix}$$
(15)

We solve for $E(\vec{k})$ by taking the determinant of the matrix in Eq. (15) and using the fact that γ_0 is small, since the overall overlap of the atomic wavefunctions is small, we get the simple dispersion relation:

$$E(\vec{k}) = \pm\gamma_1 \left| \alpha(\vec{k}) \right|$$
(16)

Calculating the magnitude of α using Eq. (14) we obtain:

$$E(\vec{k}) = \pm\gamma_1 \sqrt{3 + 2\cos(\vec{k}\cdot\vec{a_1}) + 2\cos(\vec{k}\cdot\vec{a_2}) + 2\cos(\vec{k}\cdot(\vec{a_2} - \vec{a_1}))}$$
(17)

This result can be expressed using the (x, y) components of $\vec{k}$. This yields the formula for the energy band structure of graphene:

$$E(k_x, k_y) = \pm\gamma_1 \sqrt{1 + 4\cos\left(\frac{\sqrt{3}ak_y}{2}\right)\cos\left(\frac{ak_x}{2}\right) + 4\cos^2\left(\frac{ak_x}{2}\right)}$$
(18)

where a is the lattice constant: $a = \sqrt{3}a_0$. This equation gives us the energy band structure of graphene; it is called dispersion relation. We can visualize it in Fig. (2)

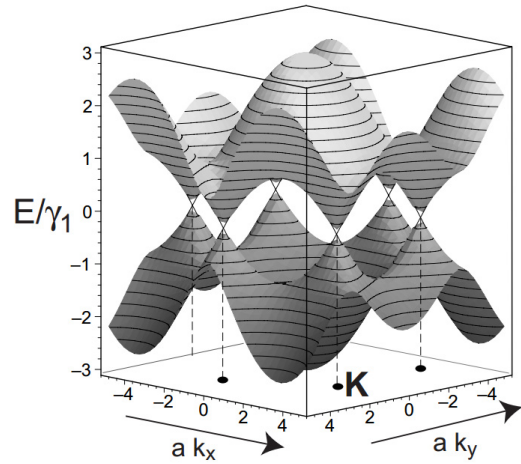FIG. 2: Band structure of graphene [4]

III. LINEARITY OF DISPERSION RELATION

We can see that in Fig. (3) if we zoom in close to the intersection (Dirac points) of the bands that the dispersion relation is linear. We can mathematically formalize this effect by looking at the lattice structure in momentum space. This aforementioned structure is called the Reciprocal Lattice of Graphene, which is the Fourier Transform of Fig. (1).
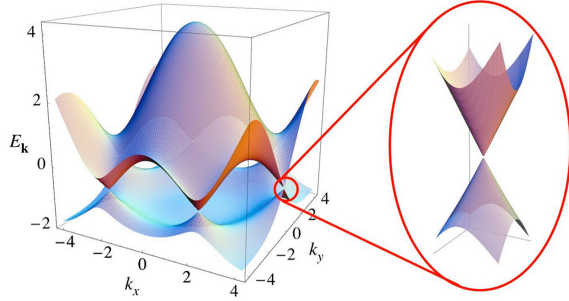

FIG. 3: Band structure of graphene and a zoom-in around the Dirac Points [3].

The primitive lattice vectors in reciprocal lattice space $\vec{b}_1$ and $\vec{b}_2$ are given by:

$$|\vec{b}_{1,2}| = \frac{4\pi}{3a_0} \qquad (19)$$

The 1st Brillouin zone is the unit cell defined in Fig. (1) in reciprocal space. There are six corner points located at the boundary of the Brillouin zone. These points are known as K-points. In Fig. (4) one K-point is shown with its respective wavevector $\vec{K}$ pointing along the x-axis. We can find this K-point by using the geometry of the problem and by plugging it into Eq. (17). We find that:

$$\vec{K} = \frac{4\pi}{3\sqrt{3}a_0}\vec{e}_x \quad \text{and} \quad E(\vec{K}) = 0 \qquad (20)$$

The Fermi-energy is located at the K-points in the energy spectrum. Thus, the low energy properties can be well described by expanding the wavefunctions around $\vec{K}$. We now look at the energy eigenvalue problem in Eq. (15) and write: $\vec{k} = \vec{K} + \vec{q}$ and $E(\vec{k}) = E(\vec{K}) + \epsilon(\vec{q}) = \epsilon(\vec{q})$ since $E(\vec{K}) = 0$. (see Fig (2) and Eq. (20)). Then the new eigenvalue equation is given by:

$$\begin{pmatrix} \epsilon(\vec{q}) & \frac{3\gamma_1 a_0}{2}(q_x + iq_y) \\ \frac{3\gamma_1 a_0}{2}(q_x - iq_y) & \epsilon(\vec{q}) \end{pmatrix} \begin{pmatrix} c_1 \\ c_2 \end{pmatrix} = \begin{pmatrix} 0 \\ 0 \end{pmatrix} \qquad (21)$$

Again taking the determinant of the matrix in Eq. (21), and setting it equal to zero, we obtain the dispersion relation:

$$\epsilon(\vec{q}) = \pm \left(\frac{3\gamma_1 a_0}{2}\right)|\vec{q}| \qquad (22)$$
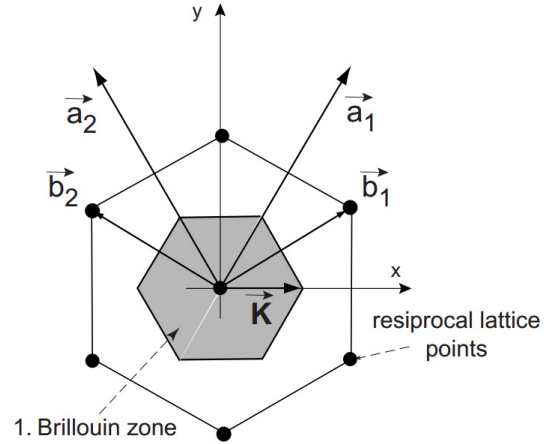
FIG. 4: Reciprocal Lattice of graphene with the 1st Brillouin zone (shaded). $\vec{b}_1$ and $\vec{b}_2$ are the primitive lattice vectors [4].

The velocity of the wavepacket is given by $\vec{v} = \hbar^{-1}\partial E/\partial \vec{q}$. It is also known as the Fermi velocity v_F. Its magnitude in this case is given by:

$$v_F = \frac{3\gamma_1 a_0}{2\hbar} \qquad (23)$$

The parameters are known: $a_0 = 1.42\text{Å}, \gamma_1 = 2.9$ eV, and as a result, $v_F \approx 1\text{x}10^6$ m/s. Using the Fermi velocity v_F we can rewrite Eq. (22) in a very simple form:

$$\epsilon(\vec{q}) = \pm\hbar v_F|\vec{q}| \qquad (24)$$

This energy dispersion in Eq. (24) resembles the energy of ultrarelativistic particles. Thus, we see that the energy dispersion for graphene is linear with group velocity of magnitude close to that of ultrarelativistic particles. This means that electrons can travel at ultrarelativistic speeds in graphene at room temperature. It is this unusual result that inspired applications of graphene to modern electronics. We will discuss this further in the next section.

IV. APPLICATIONS AND THE FUTURE

One of the most famous and talked about applications of graphene is its potential as a replacement for silicon as the main material used to design transistors. We will focus on the Field-effect Transistor (FET) because it's the most successful device concept in electronics and therefore, most of the research on graphene devices has been related to FETs [5].

Most FETs are made out of the semiconductor silicon dioxide. A FET consists of a gate, a channel region connecting source and drain electrodes (Fig. 4). The operation of a typical FET consists of controlling the channel conductivity, and consequently the drain current, by a

voltage, V_{GS}. For high-speed applications, FETs need to respond quickly to variations in V_{GS}. In order to accomplish this, FETs require short gates and fast carriers in the channel. However, FETs with short gates frequently suffer from degraded electrostatics and other short-channel effects [5]. There is a point when the gates reaches a minimum size and Moore's Law will end. This is the reason why the industry is looking for novel materials that can replace silicon. Since graphene has only a one-atom thickness, the possibility of having channels this thin is perhaps its most attractive feature along with the fast-moving electron properties. This would allow us to continue to build smaller transistors, which enables the building of faster microprocessors.
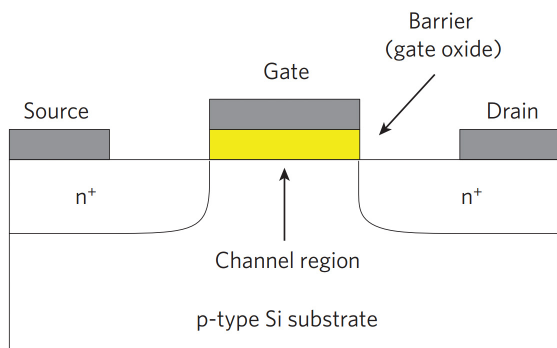

FIG. 5: Cross-section of an n-channel Si MOSFET. When the voltage applied between the source and the gate electrodes exceeds a threshold voltage, V_{Th}, a conducting channnel is formed and a drain current I_D flows. The length of the channel is defined by the length of the gate electrode; the thinkness of the gate-controlled channel region is the depth to which the electronic properties of the semiconductor (p-doped Si in this case) are influenced by the gate [5].

The main feature that graphene lacks in order to replace silicon as the standard material to design FETs is that it is not a semiconductor. As a result, it lacks a bandgap, as it was derived in Section II. Its valence and conducting bands are cone-shaped in most places. Because the bandgap is zero, devices with channels made of large-area graphene cannot be switched on and off, and as a result cannot be used for logic applications like a semiconductor [5]. However, the band structure of graphene can be modified to add bandgaps. This can be done in three ways: by constraining large-area graphene in one dimension to form graphene nanoribbons, by biasing bilayer graphene, or by applying strain to graphene [5].

Graphene nanoribbons are strips of graphene with ultra-thin width (<50 nm). It has been predicted [5] that ideal nanoribbons have a bandgap that is inversely proportional to the width of the nanoribbon. The opening of a bandgap in nanoribbons has been verified experimentally for widths down to about 1nm [5]; theory and experiments both reveal bandgaps above 200 meV for widths below 20 nm. Nonetheless, real nanoribbons have

rough edges and widths that change along their lengths. These edges and width issues destroy the potential to create bandgaps between nanoribbons with different edge geometries [5]. To open a bandgap useful enough for FETs, very narrow nanoribbons with well-defined gaps are needed. This represents a major technological challenge at this moment. Using nanoribbons that have reduced edge roughness creates a larger bandgap. However, as the bandgap increases, the energy band structure becomes parabolic (rather than cone-shaped) (Fig. 6 (ii)). As a result, this tarnishes the electronic properties that make graphene unique.

Bilayer graphene also lacks a bandgap and its energy structure around the K-point also has a parobolic shape. However, when an electric field is applied perpendicular to the bilayer, a bandgap opens and the bands near the K-point take on a "Mexican hat" shape. Theoretical predictions have shown that the size of the bandgap depends on the strength of the electric field [5]. However, even with the bandgap, the cone shape is lost and once again the electronic properties of graphene are compromised. This configuration is shown in Fig. (6 ((iii), (iv))).

Finally, strain is another method to create a bandgap in large-area graphene. The effect of uniaxial strain on the band structure has been simulated. If this is in fact a viable option, opening a gap in this way would require a uniaxial strain exceeding 20%, which would be difficult to achieve in practice. Furthermore, there is not much knowledge about the ways in which other types of strain (biaxial and local) influence the band structure of graphene [5]. Thus, there are a number of techniques for opening a bandgap in graphene, but they are all at this moment some way from being suitable for use in practical applications.

Besides creating a bandgap in graphene, the primary challenges that researchers face at present is to develop other means of improving transistor saturation characteristics, for example developing contacts that block one kind of carrier without degrading the transistor's speed [5]. This challenge will not be discussed further, since it is a subject that mainly involves electrical engineering. Even with these challenges, we must keep in mind that this technology is relatively new and it is impossible to predict whether any of the variations of graphene will actually be able to replace conventional transistors. This promises to generate and motivate research in this field for many years to come.

V. DISCUSSION

Graphene promises to be a fascinating topic of research in the upcoming years. We have derived its energy band structure, the unusual property of graphene, which potentiates its use in solid state physics and modern electronics. We used the tight binding method and Bloch's Theorem along with knowledge of its chemistry struc-
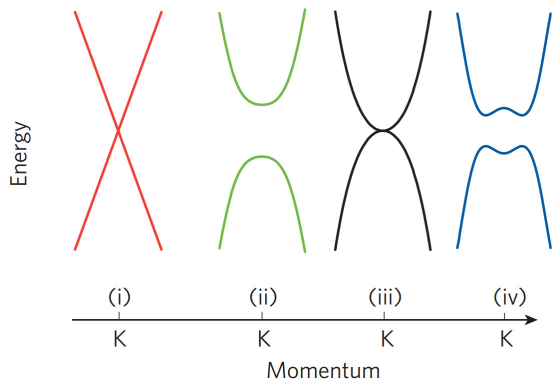
FIG. 6: Band structure around K-point of (i) large area graphene, (ii) graphene nanoribbons, (iii) unbiased bilayer graphene, and (iv) bilayer graphene with an applied electric field. Large-area graphene and unbiased bilayer graphene do not have a bandgap, which makes them less useful for digital electronics [5].

ture to accomplish this derivation. Furthermore, we have shown that the group velocity in graphene is in the order of ultrarelativistic speeds; this leads to large conductivity. In general, large conductivity can also be achieved through the method of superconductivity, but this requires very low temperatures. Graphene's unique energy band structure generates this conductivity effect at room temperature.

From there, we discussed graphene's potential as a Field-Effect Transistor. We emphasized that the main challenge for graphene to substitute silicon as the material for FETs is that it lacks a well-defined bandgap, which is characteristic of semiconductors. There are some methods to create a bandgap, but they are not very efficient so far. As a result, it is hard to predict at this point whether graphene will be the savior of modern electronics as we approach the end of Moore's Law. Nonetheless, we want to remark once again that this material will continue to be a major aspect of modern research in solid state physics and electrical engineering for years to come.

[1] AHC Neto, F Guinea, NMR Peres, and K S Novoselv. The electronic properties of graphene. *Reviews of modern ...*, 2009.

[2] Jeon-Sun Moon and D Kurt Gaskill. Graphene: Its Fundamentals to Future Applications, *IEEE Transactions on Microwave Theory and Techniques*, 2001.

[3] A K Geim and K S Novoselov. The rise of graphene, *Nature Materials*, 2007.

[4] Christian Schoenenberger. Bandstructure of Graphene and Carbon Nanotubes, April 2000

[5] F Schwierz. Graphene transistors. *Nature nanotechnology*, 2010

On The Theory of Superconductivity

Theodore Mouratidis

Center for Theoretical Physics, 77 Massachusetts Ave., Cambridge, MA 02139-4307

(Dated: May 2, 2014)

In this research paper, the foundations of Bardeen Cooper Schrieffer (BCS) theory and the properties of superconductors will be investigated. BCS theory assumes that the attractive Cooper Pair Interaction (weak $e^- - e^-$ bound pair mediated by a phonon interaction) dominates over the repulsive Coulomb force. Cooper's work in 1956 showed that the $e^- - e^-$ paired states can have less energy than the Fermi energy of the material, and thus at adequately low temperatures, these states can form. In order to describe the fundamentals of the BCS theory of superconductivity, the many-body Hamiltonian, consisting of the kinetic energy term, as well as the electron-electron phonon mediated potential energy term, will be utilized. By diagonalizing the Hamiltonian, the BCS ground state and excited states will be found. Furthermore interesting thermodynamic properties of superconductors such as the energy gap and critical temperature, will be investigated, as will the quantum mechanical foundation of the electrodynamic and magnetic properties of superconductors.

I. INTRODUCTION

One of the unsolved problems of solid state physics in the 20th century was that of superconductivity. Below a certain critical temperature for some materials, there are two fascinating effects which occur; namely those of infinite conductivity ($E = 0$), and the Meissner-Oschenfeld effect (very small penetration of the magnetic field into the material such that it falls to zero rapidly). Insights made by Maxwell and Reynolds into the relationship between isotopic mass and the critical temperature T_c, allowed for the conjecture that superconductivity relied on electron phonon interactions, finally leading to Bardeen, Cooper and Schrieffer's discovery of a theory called the Bardeen Cooper Schrieffer (BCS) theory of superconductivity in 1957. BCS theory assumes that the attractive Cooper Pair Interaction dominates over the repulsive Coulomb force. A Cooper pair is a weak $e^- - e^-$ bound pair mediated by a phonon interaction. These $e^- - e^-$ paired states can have less energy than the Fermi energy of the material, and thus at adequately low temperatures, these states can form; this is because thermal energy is not a significant factor at these temperatures. In section II, the Bloch State and the fundamentals underlying electron-phonon interactions will be presented, and in section III the superconducting ground state and excited states will be calculated. In section IV the thermodynamic properties of superconductors will be derived, and in section V, their two most valuable properties, infinite conductivity and an internally expelled magnetic field will be investigated. Finally in sections VI and VII, the characteristics of type I and type II superconductors will be described.

II. THE BLOCH STATE AND ELECTRON-PHONON INTERACTIONS

We will begin the theoretical basis of superconductivity by looking at the Sommerfeld-Bloch individual-particle model. This model assumes each electron moves independently, in a field equivalent to that of all the other electrons in the metal. These electrons occupy individual-particle Bloch states, denoted with wavevector k and spin σ. However, we cannot use these wavefunctions directly to describe superconductivity, as lattice imperfections, and electron-electron and electron phonon interactions result in the Bloch wavefunctions not being exact single-particle eigenstates. If we assume these states have low energies, they can be treated perturbatively, in terms of scattering electrons between single-particle states.

Now let us describe the effect of Cooper pairs. The Coulomb attraction between the electron and the positively charged cores of ions will leave a net positive charge in the vicinity; a paired electron is one with opposite momentum and spin which is attracted by the Coulomb force to this positive charge, thus forming the bound state with the other electron. One electron scatters from a Bloch state with initial wavevector k, to final wavevector $k' = k \pm \kappa$ by exciting an oscillation of the lattice (phonon). Almost immediately, the phonon is absorbed by the other electron, which is then also scattered to a different wavevector. The bound state (the Cooper pair) thus interacts due to phonon exchange, and the overall effective interaction combines phonon-exchange and the Coulomb interaction. The key property for superconductivity is that the overall interaction is attractive for frequencies below the Debaye frequency ω_D. Let us make an argument for this case by considering a Cooper pair interaction at T = 0 K in a Fermi gas, where we will look for a zero momentum wavefunction of the form:

$$\Psi(r_1, r_2) = \sum_k g_k e^{ik \cdot (r_2 - r_1)}(|\uparrow \downarrow\rangle - \langle \downarrow \uparrow|) \quad (1)$$

This is a general expression for a zero momentum, two particle state, and thus the spins are chosen accordingly. Antisymmetry places a constraint on the coefficients $g_k = g_{-k}$. Placing this into the Schrodinger Equation $H\psi = E\psi$, yields the following result [7]:

$$(E - 2\epsilon_k)\, g_k \;=\; \sum_{k' > k_F} V_{kk'}\, g_{k'} \qquad (2)$$

where $V_{kk'} = \frac{1}{Vol} \int_{Vol} d^3r\; V(r) e^{i(k-k')\cdot r}$ and ϵ_k is the Bloch energy of the state. We will make the mean field approximation, which sets the potential equal to an average value over the field, to greatly simplify calculations:

$$V_{kk'} = \begin{cases} -V_0, & \epsilon_F < \epsilon_k < \epsilon_F + \hbar\omega_c \\ 0, & otherwise \end{cases} \qquad (3)$$

The bound on the energy shows that we only consider interactions that are allowed by the metal's frequency range. Here, ϵ_F is the Fermi energy of the metal and ω_c is the cutoff frequency of the metal. This equation therefore becomes:

$$\begin{aligned} \frac{1}{V_0} &= \sum_{k' > k_F} \frac{1}{2\epsilon_k - E} \\ \frac{1}{V_0} &= N_0 \int_{\epsilon_F}^{\epsilon_F + \hbar\omega_c} \frac{d\epsilon}{2\epsilon - E} \\ &= \frac{N_0}{2} \ln\left(\frac{2\epsilon_F - E + 2\hbar\omega_c}{2\epsilon_F - E}\right) \\ 2\epsilon_F - E &= \frac{2\hbar\omega_c}{e^{\frac{2}{N_0 V}} - 1} \approx 2\hbar\omega_c e^{-\frac{2}{N_0 V}} \end{aligned} \qquad (4)$$

This is valid for $N_0 V_0 << 1$ (the weak coupling solution), where N_0 is the number of particles, and finally this shows that the energy of the cooper pair is less than the Fermi energy for the bound state:

$$E \;=\; 2\epsilon_F - 2\hbar\omega_c e^{-\frac{2}{N_0 V}} < 2\epsilon_F \qquad (5)$$

III. SUPERCONDUCTING STATES

In this section, the Hamiltonian for a superconducting system will be introduced. We will transform into a diagonal basis, and find expressions for the coefficients which will help us characterize the ground state. Furthermore, the gap energy between the superconducting ground state and excited states will be quantified.

Due to scattering in the states $|k\uparrow\rangle$ and $|k\downarrow\rangle$ (spin up electron and spin down electron), the Fermi sea becomes unstable, and the ground state is then a superposition of the cooper pairs formed. The problem thus reduces to calculating this ground state and the excited states of a solid state system of fermions interacting via two body potential. The creation and annihilation operators of the Cooper Pairs satisfy the Fermi commutation relations [2]:

$$\left\{ c_{k\sigma},\; c_{k'\sigma'}^\dagger \right\} \;=\; \delta_{kk'} \delta_{\sigma\sigma'}$$

$$(6)$$

where σ is the spin of the electrons. In the previous section we only considered a Hamiltonian for a single Cooper pair. The Hamiltonian for the many-body system can be written as [3]:

$$H_{BCS} = \sum_{k\sigma} \epsilon_k c_{k\sigma}^\dagger c_{k\sigma} + V_{int} \qquad (7)$$

where the interaction potential V_{int} is defined as

$$V_{int} = \frac{1}{N} \sum_{kk'} V_{kk'} c_{k\uparrow}^\dagger c_{-k\downarrow}^\dagger c_{-k',\downarrow} c_{k',\uparrow} \qquad (8)$$

The first term is the kinetic energy of the electrons, and the second is the addition of the phonon mediated interactions into this framework. Before we calculate the ground state, let us notice a few interesting facts about the Hamiltonian. An unusual fact about the H_{BCS} is that it does not conserve the electron number, because it contains terms of the form cc and $c^\dagger c^\dagger$. It is therefore expected that eigenstates of H_{BCS} do not have a sharp electron number, but instead the relative fluctuation is proportional to $N_0^{-1/2}$ [3]. We therefore diagonalize the Hamiltonian, by introducing new fermionic operators in the Bogoliubov basis. The linear transformation is defined as:

$$\begin{aligned} c_{k,\uparrow} &= u_k \gamma_{k,\uparrow} + v_k \gamma_{-k,\downarrow}^\dagger \\ c_{-k,\downarrow}^\dagger &= -v_k^* \gamma_{k,\uparrow} + u_k^* \gamma_{-k,\downarrow}^\dagger \end{aligned} \qquad (9)$$

where the coefficients u_k and v_k will be derived, and the new operators introduced, $\gamma_{k,\uparrow}$ and $\gamma_{-k,\downarrow}^\dagger$, are the lowering operator for the first particle and the raising operator for the second particle, respectively. Each particle in the Cooper pair is known as a quasi-particle. Now we can calculate the Hamiltonian to find expressions for the coefficients u_k and v_k following the derivation in [3]:

$$\begin{aligned} &H_{BCS} \\ &= \sum_k \epsilon_k [(|u_k|^2 - |v_k|^2)(\gamma_{-k,\downarrow}^\dagger \gamma_{-k,\downarrow} + \gamma_{k,\uparrow}^\dagger \gamma_{k,\uparrow}) + 2|v_k|^2 + \\ &\quad 2u_k^* v_k^* \gamma_{k,\uparrow} \gamma_{-k,\downarrow} + 2u_k v_k \gamma_{k,\uparrow}^\dagger \gamma_{-k,\downarrow}^\dagger] + \\ &\sum_k [(\Delta_k u_k v_k^* + \Delta_k^* u_k^* v_k)(\gamma_{-k,\downarrow}^\dagger \gamma_{-k,\downarrow} + \gamma_{k,\uparrow}^\dagger \gamma_{k,\uparrow} - 1) \\ &+ (\Delta_k v_k^{*2} - \Delta_k^* u_k^{*2}) \gamma_{k,\uparrow} \gamma_{-k,\downarrow} + (\Delta_k^* v_k^2 - \Delta_k u_k^2) \gamma_{-k,\downarrow}^\dagger \gamma_{k,\uparrow}^\dagger + \\ &\quad \Delta_k \langle c_{k,\uparrow}^\dagger c_{-k,\downarrow}^\dagger \rangle^*] \quad (10) \end{aligned}$$

where the spins are summed over the spin up and spin down particles, and Δ_k is the gap energy between the ground and excited superconducting states, defined by the equation:

$$\Delta_k = -\frac{1}{N} \sum_{k'} V_{kk'} \left\langle c_{-k',\downarrow} c_{k',\uparrow} \right\rangle \qquad (11)$$

The coefficients are chosen such that the $\gamma\gamma$ and $\gamma^\dagger\gamma^\dagger$ terms vanish because they are not diagonal. This requires:

$$2\epsilon_k u_k^* v_k + \Delta_k^* v_k^2 - \Delta_k (u_k^*)^2 = 0 \qquad (12)$$

and therefore the coefficients u_k and v_k are found to be:

$$u_k^2 = \frac{1}{2}\left(1 + \frac{\epsilon_k}{\sqrt{\epsilon_k^2 + \Delta_k^2}}\right),\ v_k^2 = \frac{1}{2}\left(1 - \frac{\epsilon_k}{\sqrt{\epsilon_k^2 + \Delta_k^2}}\right) \qquad (13)$$

The coefficients u_k and v_k are known as coherence factors; they determine how much of an electrons or a hole is traveling as a quasi particle in the superconductor (in a Cooper pair). u_k^2 and v_k^2 are the probabilities that a pair of states with opposite k and σ are unoccupied and occupied respectively.

In the original basis, the Hamiltonian could be expanded in terms of the gap energy by re-expressing the interaction potential in terms of Δ_k. To express it in terms of the new basis, we will look at the dispersion energy of the quasi-particles defined as $E_k = \sqrt{\epsilon_k^2 + \Delta_k^2}$; these are the resulting excitation energies. By making the assumption that the gap energies of opposite spin states are equal, $|\Delta_{-k}| = |\Delta_k|$, and using the definitions of u_k and v_k, the Hamiltonian in the diagonal basis becomes:

$$H_{BCS} = \sum_k E_k(\gamma_{-k\downarrow}^\dagger \gamma_{-k\downarrow} + \gamma_{k\uparrow}^\dagger \gamma_{k\uparrow}) +$$
$$\sum_k (\epsilon_k - E_k + \Delta_k \langle c_{k\uparrow}^\dagger c_{-k\downarrow}^\dagger \rangle^*) \qquad (14)$$

The first term describes the free fermion excitations above the ground state, with spectrum E_k. The second term is a constant, which will be important in calculating the ground state energy. We will investigate this energy later in this section.

Now let us return to Eqn.(11); this is known as the gap equation. When the expectation value in the equation is calculated, a non-linear integral equation, which can be solved by numerical integration, is obtained [3]:

$$\Delta_k = -\frac{1}{N}\sum_{k'} V_{kk'} \left\langle c_{-k',\downarrow} c_{k',\uparrow} \right\rangle$$
$$\Delta_k = -\frac{1}{N}\sum_{k'} V_{kk'} \frac{\Delta_{k'}}{2\sqrt{\epsilon_{k'}^2 + \Delta_{k'}^2}} \qquad (15)$$

The presence of the potential term $V_{kk'}$ in the gap equation, results from the competition of the phonon attraction and the Coulomb repulsion.

Δ_k is the energy that is required to excite a quasi-particle from the superconducting ground state. Now, let us try and gain some physical intuition about Δ_k, and the relationship between the original operators c, $c^\dagger$ and the

new operators, γ, $\gamma^\dagger$. Originally there were electrons; now the Bogoliubov operators describe quasi-particles. From FIG. 1, we can see that far below the Fermi energy, we have 'hole-like' quasi-particles, and far above the Fermi energy we have electron-like quasi-particles. Near the Fermi energy however, as suggested by Eqn. (9), the quasi-particles are a resonance/mixture of electron-like and hole-like structures. These superpositions describe the pairing correlations present in the BCS state.

Now let us look at the quasi-particle energy dispersion, E_k. The smallest possible excitation is $\Delta E_{min} = 2\Delta_0$, (one per electron) where $\Delta_0 = 2\hbar\omega_D e^{-\frac{1}{N_0 V}}$ (solved by assuming constant Δ_k). It is the energy required to break a pair, and cause the now separated electrons to be excited to a higher energy state in which they are in a Fermi sea (normal metal electron phase), rather than combined as a Cooper pair. Thus electrons can exist separately in a superconducting phase, if they are excited. The BCS ground state is what is known as the pure condensate of Cooper pairs (the only way electrons can exist in the ground state). It can be seen in FIG. 1, that superconductivity raises the spectrum of the quasi-particles by Δ_{k_F}.
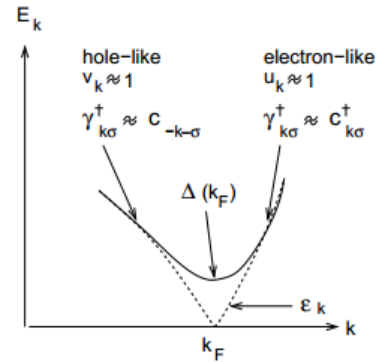
FIG. 1: Variation of Quasi-Particle Energy Dispersion with Wavevector k:
All states are Cooper pairs as $v_k \to 1$. All states are single electron states as $u_k \to 1$. [8]

The foundations of the BCS theory have been laid, so let us now find the ground state. The ground state must take the form [3]:

$$|\Psi_{BCS}\rangle \sim \prod_{k,\sigma} \gamma_{k\sigma} |0\rangle \qquad (16)$$

(where $|0\rangle$ is the vacuum state), as this state is killed by $\gamma_{k\sigma}$ for any σ, because $\gamma_{k\sigma}\gamma_{k\sigma} = 0$. The $|0\rangle$ state is an eigenstate of the original $c_{k,\sigma}$ operator and is killed by it. However, the vacuum is not an eigenstate of the $\gamma_{k\sigma}$ operator, and is not killed by it. But since $\gamma_{k\sigma} |\Psi_{BCS}\rangle = 0$, then $\prod_{k,\sigma} \gamma_{k\sigma} |0\rangle$ is the new vacuum eigenstate of the quasi-particle operators. Thus, in terms of the original

creation and annihilation operators, this ground state is:

$$|\Psi_{BCS}\rangle = \prod_{k,\sigma}(u_k + v_k c_{k,\uparrow}^{\dagger} c_{-k,\downarrow}^{\dagger}) |0\rangle \qquad (17)$$

where u_k and v_k are the calculated complex coefficients. By normalization, it is required $(|u_k|^2 + |v_k|^2) = 1$. Filled states are occupied in pairs such that if $|k\uparrow\rangle$ (spin up electron state) is occupied then so is $|-k\downarrow\rangle$ (spin down electron state). $|\Psi_{BCS}\rangle$ is therefore a linear
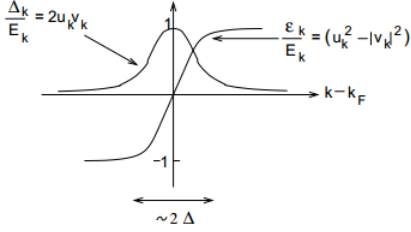
FIG. 2: Variation of Coefficients u_k and v_k:
$u_k = 1$, $v_k = 0$ (positive $k - k_F$) corresponds to no Cooper Pairs. $u_k = 0$, $v_k = 1$ (negative $k-k_F$) corresponds to Cooper Pairs. 2Δ is the energy change of this transition. [8]

combination of empty states, with the probability of no electrons equal to u_k^2, or doubly occupied states (combination of spin up and spin down electrons, $k,\uparrow$ and $-k,\downarrow$), with probability of v_k^2. Therefore looking back at FIG. 1, we can now see that well below the Fermi energy, $v_k = 1$, so all electrons are in Cooper pairs. The fact that we can have $u_k = 1$ shows that ψ_{BCS} is a general expression for not only superconducting states, but also normal states. An interesting observation from FIG. 2 shows that when $v_k^2 = 1$, the BCS ground state becomes $|\Psi_{BCS}\rangle = \prod_{k,\sigma}(c_{k,\uparrow}^{\dagger} c_{-k,\downarrow}^{\dagger}) |0\rangle$, which is the Fermi sea.

It is necessary for the system to reduce the interaction energy, so the net momentum of the Cooper pair is $k_1 + k_2 = 0$, implying that u_k and v_k actually minimize the ground state energy. The ground state energy is calculated to be:

$$\langle \Psi_{BCS} | H | \Psi_{BCS} \rangle$$
$$= \sum_k 2\epsilon_k |v_k|^2 + \frac{1}{N}\sum_{kk'}V_{kk'}v_k^* u_k u_{k'}^* v_{k'}$$
$$= \sum_k (\epsilon_k - \frac{\epsilon_k^2}{E_k}) - \frac{\Delta_k^2}{V} \qquad (18)$$

The normal state at $T = 0$ corresponds to the BCS state with $\Delta_k = 0$ and $E_k = |\epsilon_k|$, so the energy of the normal state is $\sum_{k<k_F} 2\epsilon_k$. We can therefore see that the energy of the superconducting state is less than the energy of the normal state. The difference in energy is known as the condensation energy of the BCS ground state:

$$E_{BCS} - E_{normal} = \frac{-1}{2}N_0 \Delta_0^2 \qquad (19)$$

Now that the ground state has been introduced, we can return to the matter of excited superconducting states. As mentioned previously, since the Hamiltonian is diagonal in the Bogoliubov basis, and the vacuum state of this basis is $|\Psi_{BCS}\rangle$, we can obtain superconducting excited states by acting on this state with the quasi-particle raising operator:

$$\gamma_{k_1\sigma_1}^{\dagger}\gamma_{k_2\sigma_2}^{\dagger}\cdots\gamma_{k_n\sigma_n}^{\dagger} |\psi_{BCS}\rangle \qquad (20)$$

IV.   THERMODYNAMIC PROPERTIES

Arguably the most fundamental of all properties of superconductors is the critical temperature. This is the temperature below which the electrical resistivity drops to zero. We can find T_c using the definition for the gap energy. We will see in this derivation, that by working in the transformed basis, the Fermi distribution will arise in the expectation value of certain combinations of Bogoliubov operators because the quasi-particles are essentially independent fermions. From [1] we have:

$$\langle\gamma_{k'\uparrow}^{\dagger}\gamma_{k'\uparrow}\rangle = f(E_{k'})$$
$$\langle\gamma_{k'\uparrow}^{\dagger}\gamma_{-k'\downarrow}^{\dagger}\rangle = 0$$
$$\langle\gamma_{-k'\downarrow}\gamma_{k'\uparrow}\rangle = 0$$
$$\langle\gamma_{-k'\downarrow}\gamma_{-k'\downarrow}^{\dagger}\rangle = 1 - f(E_{k'}) \qquad (21)$$

where f is the Fermi distribution. Following [1], we begin the derivation of the T_c:

$$\Delta_k = -\frac{1}{N}\sum_{k'}V_{kk'}\left\langle c_{-k',\downarrow}c_{k',\uparrow}\right\rangle$$
$$= -\frac{1}{N}\sum_{k'}V_{kk'}u_{k'}v_{k'}\left(-\left\langle\gamma_{k'\uparrow}^{\dagger}\gamma_{k'\uparrow}\right\rangle + \left\langle\gamma_{-k'\downarrow}\gamma_{-k'\downarrow}^{\dagger}\right\rangle\right)$$
$$= -\frac{1}{N}\sum_{k'}V_{kk'}u_{k'}v_{k'}(1 - 2(f(E_{k'})))$$
$$= -\frac{1}{N}\sum_{k'}V_{kk'}\frac{\Delta_{k'}}{2E_{k'}}\left(\tanh\left(\frac{\beta E_k}{2}\right)\right)$$
$$= \frac{V}{2N}\sum_{k'}\frac{\Delta_{k'}}{E_{k'}}\left(\tanh\left(\frac{\beta E_k}{2}\right)\right) \qquad (22)$$

The critical step from here is to notice that the energy is independent of k in the approximation that the potential is independent of k. Also, at the transition temperature, the energy gap vanishes, and thus the total energy is just that of the Bloch state, ϵ_k. We also define the number of total electrons as N_0.

$$\frac{1}{VN_0} = \int_0^{\hbar\omega_D}\frac{d\epsilon_k}{\epsilon_k}\tanh\left(\frac{\beta_c\epsilon_k}{2}\right)$$
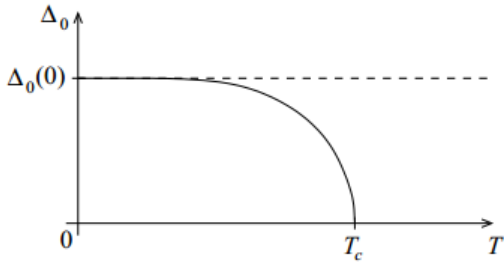$$kT_c = 1.14\hbar\omega_D\exp\left(\frac{-1}{N_0V}\right) \qquad (23)$$

FIG. 3: Energy diagram Δ_0 vs. T:
Minimum required energy to excite a quasiparticle from the ground state increases as T decreases beyond T_c. There is no energy gap above T_c. [1]

In FIG. 3, we see that the gap energy, Δ_0, between the ground and excited superconducting states, will increase rapidly as the temperature drops below T_c. The critical temperature is unsurprisingly equal to the critical temperature of the Cooper instability; the temperature at which the pairs form. For simple elementary superconductors, Eqn. (23) holds, however for unconventional materials, and those with much stronger Cooper coupling, this is not a good approximation.

V. INFINITE CONDUCTIVITY AND THE MEISSNER EFFECT

The two most valuable properties of superconductors are infinite conductivity and the Meissner-Oschenfeld Effect (more commonly known as the Meissner Effect). The Meissner effect describes how and why magnetic fields are actively expelled from superconductors. It is possible to derive these effects from the previous results, but Ginzburg and Landau found a much more direct method to find them. To retain the field within the material, the superconductor will lose free energy, and thus naturally, the most thermodynamically favorable outcome is the expulsion of the field. The Ginzburg-Landau Free energy density for any magnetic field incident on a superconductor is defined as [6]:

$$f = \alpha|\psi\left(\vec{r}\right)|^2 + \frac{\beta}{2}|\psi\left(\vec{r}\right)|^4 + \frac{1}{2m}|\left(-i\hbar\nabla + 2eA\left(\vec{r}\right)\right)\psi\left(\vec{r}\right)|^2$$
$$+ \frac{1}{2\mu_0}(B\left(\vec{r}\right) - B_E\left(\vec{r}\right))^2 \qquad (24)$$

The first two terms are a Taylor series expansion about the phase transition temperature T_c (where $\alpha = \alpha'(T_c - T)$, and α', β are constants), while the third term describes the coupling of the wavefunction to the electromagnetic field, and the final term is the magnetic energy density due to currents within the superconductor ($B\left(\vec{r}\right)$ is the induction field, and $B_E\left(\vec{r}\right)$ is the external field). By observing the $2e$ term which contains the vector potential $A\left(\vec{r}\right)$, it can be inferred that there are two electrons

coupling to the field, as is expected. For the superconducting state, we want to minimize the free energy, such that the state is in the lowest possible energy configuration. By taking the derivative of Eqn.(24) with respect to $\psi^*\left(\vec{r}\right)$ and $A\left(\vec{r}\right)$, two equations are obtained [6]:

$$\frac{1}{2m}(-i\hbar\nabla + 2eA\left(\vec{r}\right))^2\psi\left(\vec{r}\right) + \left(\alpha + \beta|\psi\left(\vec{r}\right)|^2\right)\psi\left(\vec{r}\right) = 0$$
which is the derivative with respect to $\psi^*\left(\vec{r}\right)$

$$(25)$$

$$J_S\left(\vec{r}\right) = \frac{-2e\hbar n_s}{m}\left(\nabla\phi\left(\vec{r}\right) + \frac{2eA\left(\vec{r}\right)}{\hbar}\right)$$
which is the derivative with respect to $A\left(\vec{r}\right)$

$$(26)$$

where $J_S\left(\vec{r}\right)$ is the current density. Equation (25) will be used in section VII to calculate a critical magnetic field.

Here, we have used the de Broglie pilot wave theory postulate that any wavefunction can be written in terms of the probability density ρ and the phase S : $\psi = \sqrt{\rho}e^{\frac{iS}{\hbar}}$. Therefore our wavefunction becomes $\psi = \sqrt{n_s}e^{i\phi(\vec{r})}$, where n_s is the number density of quasi-particles in the superconducting state. Buried within these two equations are the two essential properties of superconductors. Notice that the first equation has the form of the Schrodinger equation without the non linear $|\psi\left(\vec{r}\right)|^2\psi\left(\vec{r}\right)$ term. We therefore expect this wavefunction to behave like a macroscopic wavefunction, however will not satisfy linearity properties including normalization and superposition. Another interesting fact is that without the $A\left(\vec{r}\right)$ term, the equation describing Bose-Einstein condensates arises (Gross-Pitaevski Equation). The second equation defines the quantum mechanical definition of a current. Now, the Meissner effect will be proven. Taking the curl of the current, we obtain:

$$\nabla \times J_S\left(\vec{r}\right) = \frac{-4e^2 n_s}{m}\nabla \times A\left(\vec{r}\right) = \frac{-4e^2 n_s}{m}B\left(\vec{r}\right) \quad (27)$$

Using the fact that $\mu_0\nabla \times J_s\left(\vec{r}\right) = -\nabla^2 B\left(\vec{r}\right) = \frac{-4e^2 n_s\mu_0}{m}B\left(\vec{r}\right)$, the second London equation is obtained, $\nabla^2 B\left(\vec{r}\right) = \frac{B(\vec{r})}{\lambda^2}$, where

$$\lambda = \sqrt{\frac{m}{4\mu_0 e^2 n_s}} \qquad (28)$$

This is the characteristic penetration depth of a superconductor; the depth to which the magnetic field will penetrate. The solution to the second London equation shown above, is:

$$B\left(x\right) = B_0 e^{-\frac{x}{\lambda}} \qquad (29)$$

finally proving that the field in a superconductor exponentially decays rapidly from the wall of the material for temperatures below T_c. Using Fermi statistics, as $T \longrightarrow 0$, and $n_s \longrightarrow n_e/2$, the limit of penetration is purely determined from normal state properties. At T_c, and as $n_s \longrightarrow 0$, λ diverges and the screening of the field breaks down such that the magnetic field can penetrate the superconductor.

To consider the property of zero resistance, gauge transformations must be re-visited. The fields, E and B remain unchanged with the phase transformations $\phi \longrightarrow \phi - \frac{\partial \xi}{\partial t}$, and $A(\vec{r}) \longrightarrow A(\vec{r}) + \nabla \xi$, where ξ is an arbitrary differentiable and single-valued function. Consider the transformation [6], $\phi \longrightarrow \phi - \frac{2e}{\xi}$. Eqn. (24) becomes:

$$\frac{\partial J_S(\vec{r})}{\partial t} = \frac{-2e\hbar n_s}{m}\left(\frac{2e}{\hbar}\nabla\phi(\vec{r}) + \frac{2e}{\hbar}\frac{\partial A(\vec{r})}{\partial t}\right) \quad (30)$$

Since $E(\vec{r}) = -\nabla\phi - \frac{\partial A(\vec{r})}{\partial t}$, then we obtain the first London equation:

$$\frac{\partial J_S(\vec{r})}{\partial t} = \frac{4e^2 n_s}{m}E(\vec{r}) \quad (31)$$

This is an acceleration equation, implying that an electric field $E(\vec{r})$ is needed to kick-start the super-current, but not sustain it. It is simply Newton's second law for quasiparticles, as we know that since the current density is proportional to the current velocity, its derivative is an acceleration. If the electric field drops to zero from some finite value, the acceleration becomes zero, but the quasiparticles will still move at a constant speed. Another way to see the Meissner effect is to notice that the minimum free energy is found when $\nabla\phi(\vec{r}) + \frac{2eA(\vec{r})}{\hbar} = 0$; taking the curl of this equation gives $B = 0$ in the superconductor.

VI. TYPE I AND TYPE II SUPERCONDUCTORS

Type I superconductors are those which only have one superconducting phase below T_c called the Meissner phase, and therefore have one critical magnetic field, H_c, above which superconductivity is destroyed. Type II superconductors have two phases below T_c, and therefore, have two critical magnetic fields. In type two superconductors, once the field is increased beyond H_{c1} (the lower critical field), the Meissner phase transitions to the vortex phase. A vortex lattice forms until H_{c2} (the upper critical field) is reached, beyond which superconductivity is destroyed. Vortices are points in the superconductor where the magnetic field can be non-zero, and they will be investigated in section VII.

To characterize these superconductors, the coherence length must be defined. It is the scale over which the

wavefunction varies [4]:

$$\xi = \sqrt{\frac{\hbar^2}{2m|\alpha|}} \quad (32)$$

From this, the Ginzburg-Landau dimensionless parameter can be defined as $\kappa = \frac{\lambda}{\xi}$. This parameter defines the bound on the two types of superconductors. Type I superconductors have $\kappa < \frac{1}{\sqrt{2}}$, and type II superconductors exist for $\kappa > \frac{1}{\sqrt{2}}$. FIG. 4 and FIG. 5 show the respective critical fields and phases for Type I and Type II superconductors respectively.
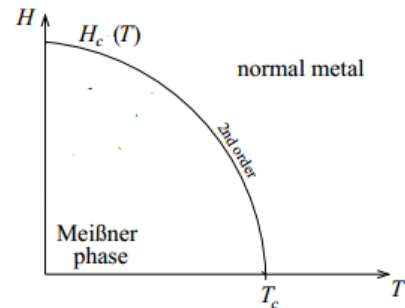
FIG. 4: Type I Superconductor Phase Diagram [7]
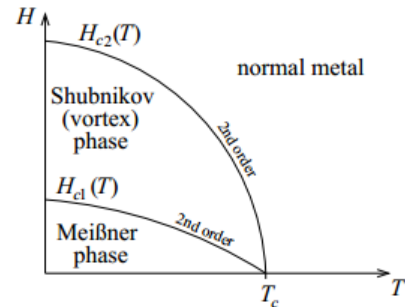
FIG. 5: Type II Superconductor Phase Diagram [7]

VII. CRITICAL MAGNETIC FIELDS, QUANTIZED FLUX AND VORTEX FORMATION

Any small penetration of magnetic flux will occur in a manner such that it minimizes the free energy. For fields greater than a critical field, the superconductivity is destroyed. So not only is there a critical temperature bound, but there is also a maximum magnetic field above which superconductivity is destroyed. Let us derive the critical fields.

For Type I superconductors, the critical magnetic field, H_c, below which exists the Meissner phase and exponen-

tial expulsion of the field, is [4]:

$$H_c = \sqrt{4\pi \frac{\alpha^2}{\beta}} \qquad (33)$$

We will now derive the two critical fields for Type II superconductors, and investigate the very interesting problem of the vortex phase. To do this, flux quantization must be described. Consider a superconducting loop with a magnetic field running through the center. By computing the line integral along a loop within the superconductor, the flux (which is infact just the standard quantized magnetic flux) can be found:

$$\oint \vec{r} \cdot \nabla \phi = 2\pi n = -\oint \vec{r} \cdot \frac{2e}{\hbar} A$$

$$-\frac{2e}{\hbar} \iint \vec{r} \nabla \times \vec{A} = -\frac{2e}{\hbar} \Phi_B$$

$$\Phi_B = -\frac{hn}{2e} \qquad (34)$$

This is a quantized value, but not all type II superconductors are loops of material. The way quantized flux arises in type II superconductors is at points where the wavefunction vanishes, known as quantum vortices. This phenomenon of vortices only arises in type II superconductors.

Let us analyze this mathematically. The minimum amount of flux that can penetrate a type II superconductor is one flux quantum $\phi_0 = \frac{hn}{2e}$. The phase of the wavefunction changes by -2π around the vortex, so in the center, the phase is undefined, implying $\psi = 0$ here. The Ginzburg-Landau equations are solved using the following boundary conditions:

$$\psi(\rho = 0) = 0, \quad |\psi(\rho \to \infty)| = \psi_0, \quad B(\rho \to \infty) = 0 \qquad (35)$$

These must be satisfied as the wavefunction must fall to zero in the vortex and far away, and the field can only exist within the vortex and will exponentially decay within the superconducting material. FIG. 6 shows the numerical solution to the equation.
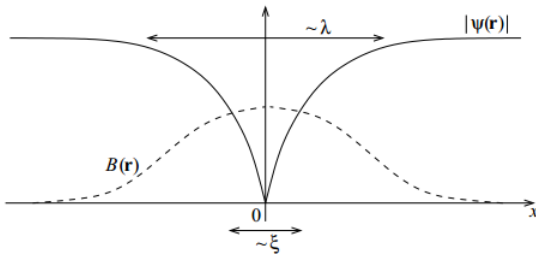

FIG. 6: Wavefunction and Magnetic Field Near a Vortex: Magnetic field exponentially decays away from vortex site, and wavefunction rapidly falls to zero at the site. [5]

The lower critical field H_{c1} occurs when the Gibbs free energy for a superconductor without vortices equals the Gibbs free energy in the presence of a single vortex. To do this we define the free energy per unit length of a vortex line [1]:

$$\epsilon_v = \frac{H_c^2}{8\pi} 4\pi \xi^2 \ln(\kappa) \qquad (36)$$

From this, the condition for H_{c1} is imposed:

$$0 = G_{one\ vortex} - G_{no\ vortex}$$

$$0 = (F_s + L\epsilon_v) - (\frac{1}{4\pi} \int d^3 r H \cdot B + F_s)$$

$$0 = L\epsilon_v - \frac{H_{c1} L \phi_0}{4\pi}$$

$$H_{c1} = \frac{H_c}{\sqrt{2}} \frac{\ln(\kappa)}{\kappa} \qquad (37)$$

where F_s is the free energy density. We have derived the lower critical field.

But type II superconductors can withstand an entire lattice of vortex flux penetration before superconductivity is destroyed. $\frac{B}{\phi_0}$ is the concentration of vortices. We assume the magnetic flux density to be uniform, and valid for $\lambda > l = \sqrt{\frac{\phi_0}{B}}$ (penetration depth is greater than the distance between vortices). To solve the Ginzburg Landau equation for a constant magnetic field $B = B\vec{z}$, the vector potential is chosen to be $A = \vec{y}Hx$. The wavefunction is small in magnitude just below H_{c2}, so the $|\psi(\vec{r})|^2 \psi(\vec{r})$ term can be ignored. By solving Eqn. (25) with the ansatz $\psi(x,y) = e^{ik_y y} r(x)$, where $r(x)$ are arbitrary coefficients, the equation becomes [4]:

$$\frac{1}{2m} \left(\frac{\hbar}{i} \nabla + \frac{2eH}{c} \hat{y}x \right)^2 \psi + \alpha\psi = 0$$

$$\frac{\hbar^2}{2m} \frac{d^2 f}{dx^2} + \frac{1}{2} m\omega_c^2 (x - x_0)^2 f = -\alpha f \qquad (38)$$

This is just the one dimensional shifted Harmonic Oscillator with solutions:

$$\alpha = \hbar\omega_c \left(n + \frac{1}{2} \right), \quad n = 0, 1, 2 \ldots \qquad (39)$$

A solution can only exist if $T \leq T_c$:

$$-\alpha = -\alpha'(T_c - T) = \alpha'(T - T_c) \geq \frac{\hbar\omega_c}{2} = \frac{\hbar e H}{mc} \qquad (40)$$

For superconductivity to occur, $H \leq H_{c2}$. Using the definition of ξ and the relationship between λ and α (for the Type I critical field), the upper critical field can be found if one important assumption is made; since $\xi \sim \frac{1}{\sqrt{T_c - T}}$ close to T_c (by plugging Eqn. (40) into Eqn. (32)), then H_{c2} becomes linear, so this field can be compared to the H_c field for the type I superconductors.

$$H_{c2} = \frac{-mc}{\hbar e} \alpha = \sqrt{2}\kappa H_c \qquad (41)$$

The vortex lattice is a very complex system and is in fact the true reason that objects can levitate and glide without resistance near a superconductor. The phenomenon of an object seemingly floating in space is due to 'vortex pinning', where the magnetic field penetrates the material through the vortices and holds up the object. This is the underlying idea behind all magnetic levitation including that of Maglev trains.

[1] Schrieffer, Robert J. (1999), Theory of Superconductivity (Advanced Books Classics), Perseus Books; Revised Edition.
[2] Bardeen, J., Cooper, N., Schrieffer, R., (1957), Theory of Superconductivity, Physical Review, Volume 108, Number 5, Department of Physics, University of Illinois, Urbana, Illinois.
[3] Carsten, T., (2012), Theory of Superconductivity, Department of Physics, Dresden University of Technology.
[4] Ketterson, J. B., Song, S. N., (1999), Superconductivity, Cambridge University Press, Cambridge University, UK.
[5] Buckel, W., (1991), Superconductivity: Fundamentals and Applications, Wiley Publishing, Germany.
[6] Tinkham, M., (1996), Introduction to Superconductivity:Second Edition, McGraw-Hill, New York.
[7] Superconductivity,(2010), 'http://www.phys.ufl.edu/ pjh/teaching-/phz7427/7427notes/ch5.pdf', University of Florida, Department of Physics
[8] Henley, C., (2009), BCS Theory, 'http://people.ccmr.cornell.edu/ clh/Book-sample/7.3.pdf', Cornell University, Department of Physics

Lieb-Robinson Bounds and Locality in Quantum Systems

Emilio A. Pace

Massachusetts Institute of Technology, 77 Massachusetts Ave., Cambridge, MA 02139-4307

(Dated: April, 2014)

Lieb-Robinson bounds give a limit on the speed at which information can propagate in a quantum many-body system. They have broad applications in quantum information theory, quantum optics and condensed-matter theory. Following Hastings, we prove the bound for time-independent local Hamiltonians on a finite lattice or graph. We then consider implications of the bound for Hamiltonians with a spectral gap, namely exponential correlation decay and the area law for entanglement entropy.

I. INTRODUCTION

An important challenge in quantum many-body physics is characterising the ground state and the expectation values of observables on a large and possibly complex quantum system. Even for simple Hamiltonians, interactions within the system lead to complicated quantum correlations that make diagonalization computationally infeasible [1]. Fortunately, a wide range of many-body systems are local, meaning the interactions between subsystems decay with distance. The correlations between observables on a local system with an energy gap decay exponentially with distance, simplifying the behaviour of the system and making it easier solve [2]. Related to this is the area law for entanglement entropy, which states that the entanglement of a subsystem scales with the area of its boundary, a further simplification of the interactions [3].

The simplicity of local systems and the results mentioned above are a consequence of the Lieb-Robinson bounds [4]. The bounds state that local quantum systems have a "speed limit" that restricts the amount of information that can escape a propagating "light-cone" [13]. We prove the bound for systems with exponentially decaying interactions and show that the bound implies the correlation decay formula for Hamiltonians with an energy gap. We then briefly discuss the open question of area laws for entanglement entropy. The proofs we consider are due to Hastings [4][5][6].

In Section II, we introduce the mathematics and formalism used in the paper. In section III, we introduce two forms of the Lieb-Robinson bound and show that the bound "confines" information within a light-cone. In section IV, we prove the bound for Hamiltonians on a finite graph. In section V, we explore two consequences of the bound, the correlation decay formula and entanglement entropy law.

II. BACKGROUND

We use the Heisenberg picture of time-dependency, with $\mathcal{U}(t)$ denoting the unitary time-evolution oper-ator. Given an operator X, we write $X(t) = \mathcal{U}^\dagger(t) X \mathcal{U}(t)$.

We use the symbol Λ to represent a finite set of points that either forms an *undirected graph* or a *lattice in* $\mathbb{R}^d$. At each of the N *sites* of Λ, we attach a D-dimensional Hilbert space [14]. For example, $\Lambda = \{-N, -N+1, \ldots, N-1, N\}$ with $D = 2$ could represent a linear chain of $2N + 1$ spin-$1/2$ particles. The Hamiltonian is is defined on Hilbert space of the whole system, which is the D^N-dimensional tensor product of the Hilbert spaces associated with each site.

In order to rigorously define locality, we introduce the notion of support on a subset $A \subset \Lambda$. An operator X is *supported on* A if X can be expressed as the tensor product $X = Q \otimes I_{\Lambda \setminus A}$, where $I_{\Lambda \setminus A}$ is the tensor product of the identity on the sites not in A and Q is some operator on the the Hilbert space over the sites of A. Informally, an operator supported on A "only acts on on A." For example, the particles on the length $2N + 1$ spin-$1/2$ chain can be equipped with nearest-neighbour interactions of the form $S_i^z S_{i+1}^z = I_{-N} \otimes \cdots \otimes I_{i-1} \otimes S_i^z \otimes S_{i+1}^z \otimes I_{i+2} \otimes \cdots \otimes I_N$. The operator $S_i^z S_{i+1}^z$ is supported on $\{i, i+1\}$. An important result we use is that if two operators X and Y are supported on *disjoint* sets A and B, i.e. $A \cap B = \emptyset$, then $[X, Y] = 0$.

We will use $d(i, j)$ to denote a metric function that gives the distance between points i and j of Λ. For example, we could use the *Euclidean metric* $d(i, j) = |i - j|$ if i and j represent vectors in $\mathbb{R}^d$. As the Lieb-Robinson bounds involve exponential decay with distance, we want to choose a metric d that assigns a large distance between points of Λ. However, our Hamiltonian has to satisfy the condition given by Equation (2) for the bound to hold, so the distance between points can't be *too* large. When applying the bounds to a particular Hamiltonian, we choose the "largest" convenient metric for which (2) holds.

For any point i and subsets A and B of Λ, we

define the following concepts:

distance between a point and a set: $d(i, B) = \min_{j \in B} d(x, y)$

distance between two sets: $d(A, B) = \min_{i \in A, j \in B} d(i, j)$

diameter of a set: $\text{diam}(A) = \max_{i, j \in A} d(i, j)$

We let $|A|$ denote the *cardinality* of A, the number of points in A.

Finally, we make use of the *operator norm*. For an operator X on our Hilbert space, we define

$$\|X\| = \sup_{\langle\psi|\psi\rangle=1} \sqrt{\langle\psi| X^\dagger X |\psi\rangle}$$

If the reader is not familiar with the supremum (sup), they can think of it as the maximum. The operator norm satisfies the usual axioms of a norm, including the *triangle inequality* $\|X + Y\| \le \|X\| + \|Y\|$ and the *multiplicative property* $\|XY\| = \|X\|\|Y\|$. It can be shown that the norm of a Hermitian operator is the absolute value of its largest eigenvalue [7], which explains how the operator norm represents the "magnitude" of an observable. Notice that for any unitary operator U, $\|U\| = \sup_{\langle\psi|\psi\rangle=1} \sqrt{\langle\psi|\psi\rangle} = 1$, and consequently, $\|UX\| = \|X\|$.

III. THE LIEB-ROBINSON BOUND

A. Local Hamiltonians

We now have the tools we need to define a local Hamiltonian. There are many definitions of locality; we consider Hamiltonians with exponentially decaying interactions. Other versions of the bound exist for other definitions of locality, such as finite-range interactions or sub-exponentially decaying interactions [5].

We can break up any hamiltonian H into *supported components* $\{H_S\}$, where each H_S is supported on some $S \subset \Lambda$, by writing

$$H = \sum_S H_S \qquad (1)$$

Note that there always exists the *trivial decomposition*, $H = H_\Lambda$. We say that H is *local* if there exists *some* decomposition resembling (1) with the property that for every $i \in \Lambda$,

$$\sum_{S \ni i} \|H_S\||S|e^{\mu \, \text{diam}(S)} \le C < \infty \qquad (2)$$

where $S \ni i$ means that the sum is over the subsets from the decomposition (1) that *contain* the point i. μ and C are arbitrary real constants that say *how* local the system

is, i.e. how rapidly the Hamiltonian dies off with the size of each subsystem S. The larger μ is or the smaller C is, the tighter the bound will be. When checking the locality condition for a given Hamiltonian, we want to find a decomposition $\{H_S\}$ that gives the *smallest* value of C/μ. For any Hamiltonian, setting $H = H_\Lambda$, $\mu = 0$ and $C = |\Lambda|$ satisfies the locality condition, but the resulting Lieb-Robinson bound is trivial. Likewise, if we choose $d(i, j) = 0$ for all i, j as our metric, then the locality condition holds for *any* choice of $\mu \in \mathbb{R}$, but the bound is again trivial [4].

B. Theorem and Interpretation

The Lieb-Robinson bound we prove can be stated as follows: if (2) holds for a time-independent Hamiltonian H [15] on a finite lattice or graph Λ and we are given operators X_A and Y_B supported on disjoint sets A and B (i.e. $d(A, B) > 0$) respectively, then

$$\|[X_A(t), Y_B]\| \le 2\|X_A\|\|Y_B\||A|e^{-\mu \, d(A,B)}(e^{2C|t|} - 1) \quad (3)$$

We can reformulate this in terms of the *Lieb-Robinson velocity*, defined as $v_{LR} = 4C/\mu$. Let $l = d(A, B)$. If $|t| \le l/v_{LR}$, (3) implies that

$$\|[X_A(t), Y_B]\| \le 2\|X_A\|\|Y_B\||A|e^{-\mu l}(e^{\mu l/2} - 1)$$
$$\le g(l)\|X_A\|\|Y_B\||A|\frac{v_{LR}|t|}{l} \qquad (4)$$

where $g(l) = l(e^{-\mu l/2} - e^{-\mu l})$ decays exponentially with l. The commutator $\|[X_A(t), Y_B]\|$ is approximately zero if l is sufficiently large and $v_{LR}|t|$ isn't too large. The latter term grows at a rate rate v_{LR}, representing the expansion of the *light-cone*. This terminology comes from the fact that in relativistic quantum mechanics, the commutator of any spacelike separated observables is zero [1]. Otherwise, we could determine if a friend has measured with X_A by measuring with Y_B. Since the Lieb-Robinson bound is a nonrelativistic approximation, the commutator is instead small (but potentially nonzero) outside the light-cone. The larger the commutator, the more information is shared between measurements of X_A and Y_B after time t. So the Lieb-Robinson bound tells us how much information about X_A "escapes" into the region B after time t, at a rate given by the Lieb-Robinson velocity [2].

The following application gives another way of thinking about the system's light-cone. Given an operator X_A supported on A, consider the radius-r region surrounding (and including) A, $B_r(A) = \{i \in \Lambda \text{ with } d(i, A) \le r\}$. The Lieb-Robinson bound allows us to construct an operator $X_A^r(t)$ supported on $B_r(A)$ that approximates $X_A(t)$ when $v_{LR}|t|$ is small [4]. We first define $X_A^r(t)$, then use the Lieb-Robinson bound to prove that it is a

good approximation for $X_A(t)$. Let

$$X_A^r(t) = \int_{\{U \text{ supported on } \Lambda \backslash B_r(A)\}} U X_A(t) U^\dagger dU \qquad (5)$$

The integral in this expression is with respect to the collection of unitary operators on the whole Hilbert space [16]. Integrating over the unitary operators supported on $\Lambda \backslash B_r(A)$ "smears out" the operator $X_A(t)$ outside $B_r(A)$, and is equivalent (up to a constant) to taking the tensor product of the partial trace of $X_A(t)$ over $\Lambda \backslash B_r(A)$ with the identity on $\Lambda \backslash B_r(A)$ [1]. In effect, we throw out any information we have about $X_A(t)$ outside $B_r(A)$, so X_A^r is supported on $B_r(A)$. The following calculation bounds the error in this approximation:

$$\|X_A(t) - X_A^r(t)\| \leq \int \|X_A(t) - U X_A(t) U^\dagger\| dU$$

$$= \int \|U[X_A(t), U^\dagger]\| dU = \int \|[X_A(t), U^\dagger]\| dU$$

If $v_{LR}|t| \leq r$, we can apply the Lieb-Robinson bound given by Equation (4) to the rightmost expression to give

$$\|X_A(t) - X_A^l(t)\| \leq K\|X_A\| |A| g(r) \frac{v_{LR}|t|}{r} \qquad (6)$$

where $K = \int dU$ is a finite constant. $g(r) \approx r e^{-\mu r/2}$, so the approximation is good if r isn't too small. Equation (6) tells us that that $X_A(t)$ interacts negligibly with sites outside a light-cone of radius $r \approx v_{LR}|t|$ around A that propagates with the Lieb-Robinson velocity.

IV. PROVING THE BOUND

Suppose the locality condition (2) holds for H. Write $X = X_A$ and $Y = Y_B$ for the two operators supported on A and B respectively. We can assume without loss of generality that $t \geq 0$, replacing t with $-t$ up until Equation (13) if $t < 0$. Time-independence of H gives $\mathcal{U}(t) = e^{-itH}$. After some manipulation, we will use the locality condition given by Equation (2) to bound the commutator $\|[X(t), Y]\|$.

Step 1. We use the decomposition into supported components, Equation (1), to discard terms in the Hamiltonian that do not contribute strongly to the time-evolution of X. We start by defining

$$\widetilde{H} = \sum_{S:S \cap A \neq \emptyset} H_S$$

Given a component S with $S \cap A = \emptyset$, H_S is the identity on all sites where X is not the identity, so $[H_S, X] = 0$. Therefore, $[H, X] = [\widetilde{H}, X]$. We can use the Baker-Campbell-Hausdorff formula to approximate $X(t) = e^{itH} X e^{-itH}$ with the commutator $it[H, X]$ for

small t. Writing $X(t)$ in terms of the commutator allows us to replace H with $\widetilde{H}$. The following steps will demonstrate this rigorously. The reader may skip to (11) for the result.

The value of t in the term $\|[X(t), Y]\|$ is not necessarily small, so expand in small increments using a telescoping series,

$$\|[X(t), Y]\| - \|[X, Y]\| = \sum_{i=0}^{N-1} \|[X(t_{n+1}), Y]\| - \|[X(t_n), Y]\| \quad (7)$$

where $t_n = tn/N$ and N is any natural number. Notice that for any unitary operator U,

$$\|[U^\dagger X U, Y]\| = \|U^\dagger [X, U Y U^\dagger] U\| = \|[X, U Y U^\dagger]\| \quad (8)$$

Therefore, defining $\epsilon = t/N = t_{n+1} - t_n$,

$$\|[X(t_{n+1}), Y]\| - \|[X(t_n), Y]\| = \|[X(\epsilon), Y(-t_n)]\| - \|[X, Y(-t_n)]\| \quad (9)$$

We use the Baker-Campbell-Hausdorff expansion to linearise $X(\epsilon)$ in terms of ϵ:

$$X(\epsilon) = e^{i\epsilon H} X e^{-i\epsilon H} = X + i\epsilon[H, X] + \mathcal{O}(\epsilon^2)$$

Applying the identity $[H, X] = [\widetilde{H}, X]$ followed by the BCH formula in reverse gives

$$X(\epsilon) = X + i\epsilon[\widetilde{H}, X] + \mathcal{O}(\epsilon^2) = e^{i\epsilon\widetilde{H}} X e^{-i\epsilon\widetilde{H}} + \mathcal{O}(\epsilon^2) \quad (10)$$

Substituting this into Equation (9) and using the triangle inequality to pull the $\mathcal{O}(\epsilon^2)$ terms out of the operator norm gives:

$$\|[X(\epsilon), Y(-t_n)]\| \leq \|[e^{i\epsilon\widetilde{H}} X e^{-i\epsilon\widetilde{H}}, Y(-t_n)]\| + \mathcal{O}(\epsilon^2)$$

By Equation (8),

$$\|[X(\epsilon), Y(-t_n)]\| \leq \|[X, e^{i\epsilon\widetilde{H}} Y(-t_n) e^{-i\epsilon\widetilde{H}}]\| + \mathcal{O}(\epsilon^2)$$

We can linearise this in terms of ϵ by applying the BCH formula again and using the triangle inequality to pull out the $\mathcal{O}(\epsilon^2)$ terms.

$$\|[X(\epsilon), Y(-t_n)]\| \leq \|[X, Y(-t_n) - i\epsilon[\widetilde{H}, Y(-t_n)]]\| + \mathcal{O}(\epsilon^2)$$
$$\leq \|[X, Y(-t_n)]\| + \epsilon\|[X, [\widetilde{H}, Y(-t_n)]]\| + \mathcal{O}(\epsilon^2)$$

The second line follows from the triangle inequality. We use this to bound (9), which represents a term in the telescoping series (7).

$$\|[X(t_{n+1}), Y]\| - \|[X(t_n), Y]\| \leq \epsilon\|[X, [\widetilde{H}, Y(-t_n)]]\| + \mathcal{O}(\epsilon^2)$$

We can use the triangle inequality to simplify the term on the right-hand side:

$$\|[X(t_{n+1}), Y]\| - \|[X(t_n), Y]\| \leq 2\epsilon\|X\| \|[\widetilde{H}, Y(-t_n)]\| + \mathcal{O}(\epsilon^2)$$
$$= 2\epsilon\|X\| \|[\widetilde{H}(t_n), Y]\| + \mathcal{O}(\epsilon^2)$$

This inequality and the fact that $N = \mathcal{O}(1/\epsilon)$ give an estimate of (7) in terms of $\widetilde{H}$,

$$\|[X(t), Y]\| - \|[X, Y]\| \leq 2\|X\| \sum_{i=0}^{N-1} \epsilon \|[\widetilde{H}(t_n), Y]\| + \mathcal{O}(\epsilon) \tag{11}$$

This completes the first step of the proof.

Step 2. We attempt to write Equation (11) in a form that resembles the left-hand side of the locality condition (2), which will allow us to bound $\|[X(t), Y]\|$. The result of this step is Equation (16). Deriving (16) from (11) is an interesting but purely mathematical exercise: we express (11) as an integral, and then repeatedly substitute the integral into itself to get the infinite sum in (16). The reader may skip to Step 3 if they do not wish to see the details.

We first use the definition of $\widetilde{H}$ to expand the right-hand side of (11) in terms of the H_S,

$$\|[X(t), Y]\| - \|[X, Y]\| \leq 2\|X\| \sum_{S:S\cap A\neq\emptyset} \sum_{i=0}^{N-1} \epsilon \|[H_S(t_n), Y]\| + \mathcal{O}(\epsilon) \tag{12}$$

We can simplify this by approximating the inner sum as an integral, provided that the integral of $\|[H_S(t), Y]\|$ exists. Because the whole Hilbert space is D^N-dimensional, $H_S(t) = e^{itH} H_S e^{-itH}$ can be viewed as a $D^N \times D^N$ matrix in some basis, with each entry continuous in t. Therefore, the matrix entries of $[H_S(t), Y]$, which are polynomials in the entries of $H_S(t)$ and Y, are continuous in t. The operator norm $\|[H_S(t), Y]\|$ is (the supremum of) a finite combination of the matrix entries, which is continuous with t, so the operator norm is integrable. Therefore, we can take the limit of (12) as $N \to \infty$, or equivalently $\epsilon \to 0$, to give

$$\|[X(t), Y]\| - \|[X, Y]\| \leq 2\|X\| \sum_{S:S\cap A\neq\emptyset} \int_0^t \|[H_S(s), Y]\| ds$$

Rearranging this and relaxing our assumption $t \geq 0$ gives

$$\frac{\|[X(t), Y]\|}{\|X\|} \leq \frac{\|[X, Y]\|}{\|X\|} + 2 \sum_{S:S\cap A\neq\emptyset} \int_0^{|t|} \|[H_S(s), Y]\| ds \tag{13}$$

We want to get this into a form where we can substitute the integrand back into the expression. To do this, we need to "abstract away" the dependence on X. If $\mathcal{O}_A$ denotes the set of observables supported on A, then $X \in \mathcal{O}_A$. By the definition of the supremum (thinking of it as a maximum if necessary),

$$\frac{\|[X(t), Y]\|}{\|X\|} \leq \sup_{Z \in \mathcal{O}_A} \frac{\|[Z(t), Y]\|}{\|Z\|} \equiv S_Y(A, t)$$

In particular $\|[X(t), Y]\| \leq \|X\| S_Y(A, t)$, so we can always recover a bound on $\|[X(t), Y]\|$ from $S_Y(A, t)$. Taking the supremum of both sides, Equation (13) can be rewritten as

$$S_Y(A, t) \leq S_Y(A, 0) + 2 \sum_{S:S\cap A\neq\emptyset} \|H_S\| \int_0^{|t|} S_Y(S, s) ds \tag{14}$$

Now we can begin the recursive substitution. Recall that Y is supported on B. If $Z \in \mathcal{O}_S$ (e.g. $Z = H_S$) and $S \cap B = \emptyset$, then $[Z, Y] = 0$. $S_Y(S, 0)$ is the supremum of $\|[Z, Y]\|/\|Z\| = 0$ over all such $Z \in \mathcal{O}_S$, so $S_Y(S, 0)$ is zero. That is, $S_Y(S, 0) = 0$ if $S \cap B = \emptyset$. Since we have assumed that $d(A, B) > 0$, A and B are be disjoint, so $S_Y(A, 0) = 0$. Therefore, (14) is equivalent to

$$S_Y(A, t) \leq 2 \sum_{S_1:S_1\cap A\neq\emptyset} \|H_{S_1}\| \int_0^{|t|} S_Y(S_1, s_1) ds_1 \tag{15}$$

The indices on S_1 and s_1 foreshadow the next step. We can use use (14) to bound the $S_Y(S_1, s_1)$ term in the integral by

$$S_Y(S_1, s_1) \leq S_Y(S_1, 0) + 2 \sum_{S_2:S_2\cap S_1\neq\emptyset} \|H_{S_2}\| \int_0^{|s_1|} S_Y(S_2, s_2) ds_2$$

Substituting this in to Equation (15) gives

$$S_Y(A, t) \leq 2 \sum_{S_1:S_1\cap A\neq\emptyset} \|H_{S_1}\| \int_0^{|t|} S_Y(S_1, 0) ds$$

$$+ 2^2 \sum_{S_1:S_1\cap A\neq\emptyset} \|H_{S_1}\| \sum_{S_2:S_2\cap S_1\neq\emptyset} \|H_{S_2}\| \int_0^{|t|} \int_0^{|s_1|} S_Y(S_2, s_2) ds_2 ds_1$$

Notice that we can replace $\int_0^{|t|} S_Y(S_1, 0) ds$ with $|t| S_Y(S_1, 0)$. By the triangle inequality,

$$S_Y(S_1, 0) \leq \sup_{Z \in \mathcal{O}_{S_1}} \frac{2\|Z\|\|Y\|}{\|Z\|} = 2\|Y\|$$

Furthermore, the result $S \cap B = \emptyset \Rightarrow S_Y(S, 0) = 0$ allows us to discard the redundant terms in the sum over $S_1 : S_1 \cap A \neq 0$ by ignoring all S_1 with $S_1 \cap B = \emptyset$. Putting this together gives

$$S_Y(A, t) \leq 2(2|t|)\|Y\| \sum_{S_1:S_1\cap A\neq\emptyset, S_1\cap B\neq\emptyset} \|H_{S_1}\|$$

$$+ 2^2 \sum_{S_1:S_1\cap A\neq\emptyset} \|H_{S_1}\| \sum_{S_2:S_2\cap S_1\neq\emptyset} \|H_{S_2}\| \int_0^{|t|} \int_0^{|s_1|} S_Y(S_2, s_2) ds_2 ds_1$$

We carry out this process recursively, at each step using (14) to bound the $S_Y(S_i, s_i)$ term in the integral, then integrating out the resulting constant term, $S_Y(S_i, 0)$.

This leads to the desired result,

$$\frac{\|[X(t),Y]\|}{\|X\|} \leq S_Y(A,t) \leq 2(2|t|)\|Y\| \sum_{S_1:S_1\cap A\neq\emptyset,\, S_1\cap B\neq\emptyset} \|H_{S_1}\|$$

$$+ 2\frac{(2|t|)^2}{2!}\|Y\| \sum_{S_1:S_1\cap A\neq\emptyset} \|H_{S_1}\| \sum_{S_2:S_2\cap S_1\neq\emptyset,\, S_2\cap B\neq\emptyset} \|H_{S_2}\|$$

$$+ 2\frac{(2|t|)^3}{3!}\|Y\| \sum_{S_1:S_1\cap A\neq\emptyset} \|H_{S_1}\| \sum_{S_2:S_2\cap S_1\neq\emptyset} \|H_{S_2}\| \sum_{S_3:S_3\cap S_2\neq\emptyset,\, S_3\cap B\neq\emptyset} \|H_{S_3}\|$$

$$+ \ldots \quad (16)$$

Step 3. Equation (16) brings us close to the final result. In deriving it, we threw out a number of redundant components of H. This allows us to introduce the exponentials $e^{\mu\,\mathrm{diam}(S_i)}$ to Equation (16), so that the terms in each order of $|t|^n$ resemble the locality condition (2). We then bound the terms individually and evaluate sum over the orders of $|t|^n$, showing that the series (16) converges to the Lieb-Robinson bound given by (3).

If $i \in S_1$ and $S_1 \cap B \neq \emptyset$, pick any point $j \in S_1 \cap B$. From the definitions, $d(i,B) \leq d(i,j) \leq \mathrm{diam}(S_1)$, so $1 \leq e^{-\mu\,d(i,B)}e^{\mu\,\mathrm{diam}(S_1)}$. Using this, the first term in (16) can be bounded by

$$\sum_{S_1:S_1\cap A\neq\emptyset,\, S_1\cap B\neq\emptyset} \|H_{S_1}\| \leq \sum_{i\in A} \sum_{S_1\ni i,\, S_1\cap B\neq\emptyset} \|H_{S_1}\|$$

$$\leq \sum_{i\in A} e^{-\mu\,d(i,B)} \sum_{S_1\ni i} \|H_{S_1}\| e^{\mu\,\mathrm{diam}(S_1)}$$

We now apply the locality condition (2) to bound the order $|t|$ term,

$$2(2|t|)\|Y\| \sum_{S_1:S_1\cap A\neq\emptyset,\, S_1\cap B\neq\emptyset} \|H_{S_1}\| \leq 2(2C|t|)\|Y\| \sum_{i\in A} e^{-\mu\,d(i,B)}$$

Having dealt with the first term of (16), we approach the second term in a similar manner. For any $i,j \in \Lambda$, $d(i,B) \leq d(i,j)+d(j,B)$, so $1 \leq e^{-\mu\,d(i,B)}e^{\mu\,d(i,j)}e^{\mu\,d(j,Y)}$. For $i,j \in S_1$ and $j \in S_2$ with $S_2 \cap Y \neq \emptyset$, this implies that $1 \leq e^{-\mu\,d(i,B)}e^{\mu\,\mathrm{diam}(S_1)}e^{\mu\,\mathrm{diam}(S_2)}$. Therefore,

$$\sum_{S_1:S_1\cap A\neq\emptyset} \|H_{S_1}\| \sum_{S_2:S_2\cap S_1\neq\emptyset,\, S_2\cap B\neq\emptyset} \|H_{S_2}\| \leq \sum_{i\in A} \sum_{S_1\ni i} \sum_{j\in S_1} \|H_{S_1}\| \sum_{S_2\ni j,\, S_2\cap B\neq\emptyset} \|H_{S_2}\|$$

$$\leq \sum_{i\in A} e^{-\mu\,d(i,B)} \sum_{S_1\ni i} \sum_{j\in S_1} \|H_{S_1}\| e^{\mu\,\mathrm{diam}(S_1)} \sum_{S_2\ni j} \|H_{S_2}\| e^{\mu\,\mathrm{diam}(S_2)}$$

$$\leq C \sum_{i\in A} e^{-\mu\,d(i,B)} \sum_{S_1\ni i} \|H_{S_1}\| |S_1| e^{\mu\,\mathrm{diam}(S_1)} \leq C^2 \sum_{i\in A} e^{-\mu\,d(i,Y)}$$

Notice that we applied the locality condition twice in the last line. The second term in (16) is therefore bounded by $2\,(2C|t|)^2/2!\,\|Y\| \sum_{i\in A} e^{-\mu\,d(i,B)}$. Continuing the process of bounding $d(i,B)$ by $\sum_{i=1}^{n} \mathrm{diam}(S_i)$ and applying the locality condition, we can show by induction [17] that the nth term in (16) is bounded above by

$2\,(2C|t|)^n/n!\,\|Y\| \sum_{i\in A} e^{-\mu\,d(i,B)}$. Substituting this into (16) brings us close to the desired result:

$$\frac{\|[X(t),Y]\|}{\|X\|} \leq \sum_{n=1}^{\infty} 2\,(2C|t|)^n/n!\,\|Y\| \sum_{i\in A} e^{-\mu\,d(i,B)}$$

$$= 2\|Y\| \sum_{i\in A} e^{-\mu\,d(i,B)}(e^{2C|t|}-1)$$

For any $i \in A$, $d(i,B) \geq d(A,B)$, so $e^{-\mu\,d(i,B)} \leq e^{-\mu\,d(A,B)}$. Therefore,

$$\|[X(t),Y]\| \leq 2\|X\|\|Y\| \sum_{i\in A} e^{-\mu\,d(i,B)}(e^{2C|t|}-1)$$

$$= 2\|X_A\|\|Y_B\||A|e^{-\mu\,d(A,B)}(e^{2C|t|}-1)$$

proving the Lieb-Robinson bound. The first line of the inequality above is another useful form of the bound.

V. APPLICATIONS TO GAPPED HAMILTONIANS

We now consider two theorems - both consequences of the Lieb-Robinson bound - concerning Hamiltonians with a unique ground state $|\psi_0\rangle$ [18] and an energy difference $\Delta E > 0$ between the ground state energy E_0 and the next-lowest energy, E_1. ΔE is known as the *spectral gap*, and we say that such a Hamiltonian is *gapped*. Our results apply to the ground state of the Hamiltonian, the focus of most quantum many-body physics [4]. The 1D Ising model is a simple example of a gapped and local Hamiltonian on a lattice, and the ground state obeys the correlation decay formula (17) and the area law (see [8]).

A. Correlation Decay

If the Hamiltonian is gapped, we can use Lieb-Robinson bound to show that for any operators X_A and Y_B supported on sets A and B respectively,

$$x\,|\langle\psi_0|\,X_A Y_B\,|\psi_0\rangle - \langle\psi_0|\,X_A\,|\psi_0\rangle\langle\psi_0|\,Y_B\,|\psi_0\rangle|$$

$$\leq K\|X_A\|\|Y_B\|\left(e^{-l\Delta E/2v_{LR}} + \min(|A|,|B|)g(l)\right) \quad (17)$$

for some constant K, where g, l and v_{LR} defined consistently with (4). The term on the left is the quantum correlation of the observables X_A and Y_B analogous to the classical definition of covariance, $\sigma(X,Y) = E[XY] - E[X]E[Y]$. Equation (17) states that the correlations between X_A and Y_B decay exponentially with the distance between their support. The key to deriving the correlation decay formula is to use the Fourier transform to extract the *spatial* bound (17) from the *time-dependent* information decay given by the Lieb-Robinson bound (3) [4]. The proof is somewhat involved, so we provide a rough but detailed sketch.

We assume that $|A| < |B|$, interchanging X and Y if this is not the case, so $\min(|A|,|B|) = |A|$. We first construct Y_B^+, the *positive part* of the operator Y_B. Without loss of generality, we can subtract the ground-state expectation values $\langle Y_A \rangle_{\psi_0}$ and $\langle Y_B \rangle_{\psi_0}$ from Y_A and Y_B respectively to set their ground-state expectation values to zero. The term on the left of (17) now has the simpler form $|\langle X_A Y_B \rangle_{\psi_0}|$. Let $\{|\psi_i\rangle\}$ be an eigenbasis of H with energies $\{E_i\}$ and let $(Y_B)_{ij}$ denote the matrix entry $\langle \psi_i| Y_B |\psi_j\rangle$. With respect to this basis, we can define

$$
(Y_B^+)_{ij} = \begin{cases} (Y_B)_{ij} & (E_i > E_j) \\ (Y_B)_{ij}/2 & (E_i = E_j) \\ 0 & (E_i < E_j) \end{cases}
$$

If there are no degeneracies, this amounts to "continuously" taking the lower-triangular part of the Y_B matrix in the energy eigenbasis. Recall that by assumption, $(Y_B)_{00} = \langle Y_B \rangle_{\psi_0} = 0$. For all $i > 0$, $E_i > E_0$, so $(Y_B^+)_{i0} = (Y_B)_{i0}$ and $(Y_B^+)_{0i} = 0$. Therefore, $Y_B^+ |\psi_0\rangle = Y_B |\psi_0\rangle$ and $\langle \psi_0| Y_B^+ = 0$. This implies that $\langle X_A Y_B \rangle_{\psi_0} = \langle X_A Y_B^+ \rangle_{\psi_0} = \langle [X_A, Y_B^+] \rangle_{\psi_0}$. We bound $\langle [X_A, Y_B^+] \rangle_{\psi_0}$ by approximating Y_B^+ with a more tractable term $\widetilde{Y}_B^+$ and bounding the commutator $[X_A, \widetilde{Y}_B^+]$. We construct $\widetilde{Y}_B^+$ as follows:

$$
\widetilde{Y}_B^+ = \frac{1}{2\pi} \lim_{\epsilon \to 0^+} \int_{-\infty}^{\infty} \mathcal{U}^\dagger(t) Y \mathcal{U}(t) \frac{1}{it + \epsilon} e^{-\frac{t^2 \Delta E^2}{2q}} dt \quad (18)
$$

The energy gap allows us to bound the error term of $\widetilde{Y}_B^+ |\psi_0\rangle$. Using the definition of $\widetilde{Y}_B^+$, we can examine the matrix elements $(Y_B^+ - \widetilde{Y}_B^+)_{i0}$ for $i > 0$:

$$
\left| (Y_B^+ - \widetilde{Y}_B^+)_{i0} \right| = \left| (Y_B)_{i0} \right| \left| 1 - \lim_{\epsilon \to 0^+} \int_{\mathbb{R}} \frac{e^{i(E_i - E_0)t}}{2\pi(it + \epsilon)} e^{-\frac{t^2 \Delta E^2}{2q}} dt \right| \quad (19)
$$

The integral in (19) above is equal to the Fourier transform of $\frac{1}{it+\epsilon} e^{-\frac{t^2 \Delta E^2}{2q}}$, which is the convolution of the Fourier transform of $\frac{1}{it+\epsilon}$ and the Gaussian $e^{-\frac{t^2 \Delta E^2}{2q}}$. In the limit as $\epsilon \to 0^+$, the Fourier transform of $\frac{1}{it+\epsilon}$ approaches a step function [7]. If q is very large, the Fourier transform of $e^{-\frac{t^2 \Delta E^2}{2q}}$ approximates a delta function. The convolution of a delta function with another function preserves the function, so for large q, the integral in (19) approximates a step function in $E_i - E_0$. $E_i > E_0$ for $i > 0$, so this always evaluates to 1, and the term on the right-hand side of (19) is approximately zero.

It is possible to prove that the error in approximating a step function by the integral in (19) is bounded by $K_1 e^{-\frac{q}{2}}$ for some constant K_1 [9]. Therefore, for each $i > 0$, $|(Y_B^+ - \widetilde{Y}_B^+)_{00}| \leq K_1 |(Y_B)_{i0}| e^{-\frac{q}{2}}$. As $(Y_B)_{00} = 0$, $|(Y_B^+ - \widetilde{Y}_B^+)_{00}| = 0$. We can write $|(Y_B^+ - \widetilde{Y}_B^+) |\psi_0\rangle|$ as

$$
\left(\langle \psi_0| (Y_B^+ - \widetilde{Y}_B^+)^\dagger \sum_{i \geq 0} |\psi_i\rangle \langle \psi_i| (Y_B^+ - \widetilde{Y}_B^+) |\psi_0\rangle \right)^{1/2}
$$

Using $(\sum_i x_i^2)^{1/2} \leq \sum_i x_i$, we can pull the sum out to give

$$
|(Y_B^+ - \widetilde{Y}_B^+) |\psi_0\rangle| \leq \sum_{i \geq 1} K_1 |(Y_B)_{i0}| e^{-\frac{q}{2}} \leq K_1 \|Y_B\| e^{-\frac{q}{2}}
$$
$$(20)$$

This shows that for large q, $\widetilde{Y}_B^+$ is a suitable approximation to Y_B^+. We wish to apply this to $\langle X_A Y_B \rangle_{\psi_0} = \langle [X_A, Y_B^+] \rangle_{\psi_0}$. By the triangle inequality,

$$
|\langle [X_A, Y_B^+] \rangle_{\psi_0}| \leq |\langle [X_A, \widetilde{Y}_B^+] \rangle_{\psi_0}| + |\langle [X_A, Y_B^+ - \widetilde{Y}_B^+] \rangle_{\psi_0}|
$$
$$
\leq \|[X_A, \widetilde{Y}_B^+]\| + 2\|X_A\| |(Y_B^+ - \widetilde{Y}_B^+) |\psi_0\rangle|
$$

Substituting in (20) gives

$$
|\langle X_A Y_B \rangle_{\psi_0}| \leq \|[X_A, \widetilde{Y}_B^+]\| + 2K_1 \|X_A\| \|Y_B\| e^{-\frac{q}{2}} \quad (21)
$$

All we need to do now is bound $\|[X_A, \widetilde{Y}_B^+]\|$. Applying the inequality $\|\int X(t)dt\| \leq \int \|X(t)\|dt$ to (18), we can write

$$
\|[X_A, \widetilde{Y}_B^+]\| \leq \frac{1}{2\pi} \lim_{\epsilon \to 0^+} \int_{\mathbb{R}} \|[X_A, Y_B(t)]\| \frac{e^{-\frac{t^2 \Delta E^2}{2q}}}{|it + \epsilon|} dt
$$
$$(22)$$

We can split the integral in (22) into two parts. For $t < l/v_{LR}$, we may apply the Lieb-Robinson bound (4) to the integrand, bounding the section of the integral from $-l/v_{LR}$ to l/v_{LR} by

$$
\frac{g(l)v_{LR}}{2\pi l} \|X_A\| \|Y_B\| |A| \int_{-l/v_{LR}}^{l/v_{LR}} e^{-\frac{t^2 \Delta E^2}{2q}} dt \leq K_3 g(l) \|X_A\| \|Y_B\| |A|
$$

for some constant K_3. For $t \geq l/v_{LR}$, the exponential decay of the gaussian term bounds the rest of the integral by

$$
\frac{1}{2\pi} \int_{t \geq l/v_{LR}} \frac{\|[X_A, Y_B(t)]\|}{|t|} e^{-\frac{t^2 \Delta E^2}{2q}} dt \leq K_2 \|X_A\| \|Y_B\| e^{-\frac{(l\Delta E/v_{LR})^2}{2q}}
$$

for some constant K_2, as the tail-integral $\int_c^\infty e^{-tx}/t \, dt$ is on the order of e^{-cx}. Combining these two bounds gives

$$
\|[X_A, \widetilde{Y}_B^+]\| \leq \|X_A\| \|Y_B\| \left(K_2 e^{-\frac{(l\Delta E/v_{LR})^2}{2q}} + K_3 |A| g(l) \right)
$$

Applying this to (21), we see that $|\langle X_A Y_B \rangle_{\psi_0}|$ is bounded above by

$$
\|X_A\| \|Y_B\| \left(2K_1 e^{-\frac{q}{2}} + K_2 e^{-\frac{(l\Delta E/v_{LR})^2}{2q}} + K_3 |A| g(l) \right) \quad (23)
$$

This holds for arbitrary q, so to get the tightest possible bound, we attempt to minimise (23) by the setting derivative with respect to q to zero,

$$
-K_1 e^{-\frac{q}{2}} + \frac{l\Delta E}{q^2 v_{LR}} e^{-\frac{(l\Delta E/v_{LR})^2}{2q}} = 0
$$

The non-exponential terms don't matter much for large q, so suppose they cancel to one. Then the optimal choice of q is given by equating the exponents, $q/2 = (l\Delta E/v_{LR})^2/2q$, or $q = l\Delta E/v_{LR}$. Letting $K = \max(2K_1 + K_2, K_3)$ for simplicity and substituting in the optimal q shows that (23) gives the desired expression,

$$|\langle X_A Y_B\rangle_{\psi_0}| \leq K\|X_A\|\|Y_B\| \left(e^{-l\Delta E/2v_{LR}} + |A|g(l)\right)$$

B. Area Laws

The quantum complexity of the ground state of a local Hamiltonian is a fundamental aspect of study in quantum information theory [2]. Area laws state that the entanglement entropy of any subsystem of a gapped, local system scales in some manner with the boundary area, rather than with the volume [10]. Area laws have been conjectured in arbitrary dimensions, yet a general proof only exists for 1-dimensional systems [3]. In these systems, the upper bound on the entanglement entropy is a constant that depends on the parameters of the system, increasing with the Lieb-Robinson velocity and decreasing with the energy gap [6].

The intuition for area laws is compelling. The exponential decay of correlations given by Equation (17) suggests that only the sites near the boundary of a region can entangle with points outside. The entanglement of a subsystem should depend on the number of these crossings, which goes as the area of the boundary. However, on small but highly connected graphs known as quantum expanders, the ground state may have exponentially decaying correlations but large entanglement [6], complicating the matter. Even in one dimension, the proof is very involved, certainly beyond the scope of this paper. The reader may consult [3] if they wish to explore the topic in more detail.

VI. DISCUSSION

We have proved two powerful results for local Hamiltonians, namely the Lieb-Robinson bound (3) and the correlation decay theorem (17), and we have examined the area law for entanglement entropy. There are many extensions to consider. Versions of the Lieb-Robinson bound exist for weaker locality conditions, and we ignored time-dependence of the Hamiltonian. The bound can be extended to infinite lattices by first restricting to a bounded subsystem and then taking the uniform limit, if it exists. It can be further generalised to systems with infinite-dimensional Hilbert spaces on each site, as in [11]. Lieb-Robinson bounds imply a number of important and general results in quantum many-body theory that we didn't consider. Examples include a non-relativistic Goldstone theorem, quasi-adiabatic continuation and a generalisation of the Lieb-Schultz-Mattis theorem [4].

[1] B. Nachtergaele and R. Sims, "Much Ado About Something: Why Lieb-Robinson bounds are useful," *ArXiv e-prints*, Feb. 2011.

[2] M. Kliesch, C. Gogolin, and J. Eisert, "Lieb-Robinson bounds and the simulation of time evolution of local observables in lattice systems," *ArXiv e-prints*, June 2013.

[3] F. G. S. L. Brandao and M. Horodecki, "Exponential Decay of Correlations Implies Area Law," *ArXiv e-prints*, June 2012.

[4] M. B. Hastings, "Locality in Quantum Systems," *ArXiv e-prints*, Aug. 2010.

[5] M. Hastings and T. Koma, "Spectral gap and exponential decay of correlations," *Communications in Mathematical Physics*, vol. 265, no. 3, pp. 781–804, 2006.

[6] M. B. Hastings, "An area law for one-dimensional quantum systems," *Journal of Statistical Mechanics: Theory and Experiment*, vol. 8, p. 24, Aug. 2007.

[7] E. Stein and R. Shakarchi, *Functional Analysis: Introduction to Further Topics in Analysis*. Princeton lectures in analysis, Princeton University Press, 2011.

[8] J. Z. Imbrie, "Decay of correlations in the one-dimensional ising model with $j_{ij} = |\ i - j\ |^{-2}$," *Communications in Mathematical Physics*, vol. 85, no. 4, pp. 491–515, 1982.

[9] B. Nachtergaele, Y. Ogata, and R. Sims, "Propagation of correlations in quantum lattice systems," *Journal of statistical physics*, vol. 124, no. 1, pp. 1–13, 2006.

[10] J. Eisert, M. Cramer, and M. B. Plenio, "Colloquium: Area laws for the entanglement entropy," *Reviews of Modern Physics*, vol. 82, pp. 277–306, Jan. 2010.

[11] D. W. Robinson, "Properties of propagation of quantum spin systems," *The Journal of the Australian Mathematical Society. Series B. Applied Mathematics*, vol. 19, pp. 387–399, 12 1976.

[12] E. H. Lieb and D. W. Robinson, "The finite group velocity of quantum spin systems," *Communications in Mathematical Physics*, vol. 28, no. 3, pp. 251–257, 1972.

[13] Some authors refer to the speed limit as the quantum "speed of sound" in the system. We avoid this terminology so we don't get confused with the "light-cone".

[14] It is trivial to incorporate different values of D at each site if we let $D = max_{1 \leq i \leq N}\{D_i\}$.

[15] The proof can be easily extended to time-dependent Hamiltonians, e.g. in [11].

[16] Precisely, it is with respect to the Haar measure dU, which allows us to integrate in a sensible manner over the unitary group.

[17] This is too much work to prove explicitly. See [12] for a rigorous justification.

[18] Ground state degeneracies can be treated, but they are beyond the scope of this paper. See [5] for a general proof of the correlation decay theorem.

The Semiclassical model and the Conductiviy of Metals

Samuel Peana

MIT Physics and Mathematics Departments, 77 Massachusetts Ave., Cambridge, MA 02139-4307

(Dated: May 5, 2014)

In this paper we develop the principles of electron dynamics in metals. This is first done by considering the work of Drude and Sommerfeld who approximated an electron in a metal as a free electron, forming with all of the other electrons a gas. Drude was the first to propose such a model based on the classical description of an electron and Boltzmann statistics for the electron gas. This was then improved upon by Sommerfeld who considered the electron as a wavepacket, and the electrons in a metal as a fermionic gas. Once these models are introduced, the conductivity of a metal is calculated based on the relaxation time approximation for scattering. These models while simple serve as a template for how the conductivity of a metal is calculated once we introduce Bloch's 1928 discovery of Bloch waves which gives the wavefunction of an electron in a periodic lattice. Repeating essentially the same derivation as we conducted for the Drude and Sommerfeld models except that we use the Bloch electrons instead we find the conductivity of metals. This then immediately results in a description of why some materials are conductors and others insulators.

I. INTRODUCTION

The story of the theory of electrical conductivity in metals (electron flow dynamics in metals) is the story of the development of quantum theory. Shortly after J.J. Thompson discovered the electron in 1897 [6] Paul Drude combined the classical electron (a hard charged sphere) and the recently developed statistical theory of gasses, by treating the electrons in a metal as a gas of electrons, to produce the Drude model of electron behaviour in metals in 1900 [4]. This model was a triumph of the nascent quantum mechanical theory that was beginning to arise with the discovery of subatomic particles since it was able to account for many of the properties of metals such as the conductivity, and the Hall effect. This theory while simple and crude even to this day is used to make rough approximations. [1] After this period the development of quantum mechanics began in full force and by 1927 Arnold Sommerfeld took the original energy distribution of the electron energies in the Drude model, the Boltzmann distribution, and replaced it with the Fermi-Dirac energy distribution. In this model much like Drude's model the electrons are treated as free electrons, but the difference being that the electron energies are distributed according to the Fermi-Dirac distribution since by this time the fermionic nature of the electron had been discovered. The result of this modification was that one of the most serious problems with the Drude model was corrected. The specific heat which is dependent on the energy distribution of the electrons was finally corrected by this switch in energy distributions. Despite all of these advances, and triumphs there were still problems with the theory. It had open questions such as: why are only some of the the electrons in metals conducting electrons? Why are electrons able to travel so far without being disturbed by the lattice? These questions among others were answered in 1928 when Felix Bloch discovered the Bloch theorem. This theorem essentially discovered that electrons in a periodic potential due to the effects of constructive interference have a wave function

that is that of a free electron wavefunction modulated by a periodic function with the period of the lattice. Most interestingly this resulting wavefunction is a stationary state of the Hamiltonian, and therefore does not experience any decay over time in this particular potential. Thus our question from before is answered as to why electrons can travel so freely through the metal, it is because the lattice does not cause a degradation of these electron states. Additionally, since our solution is that of a modulated free electron it explains why the crude models of Drude and Sommerfeld were so effective in assuming that the electron was free.

In this paper we shall cover the following topics, with the end goal to see how one can get the conduction of metals from Bloch theorem and Semi-Classical analysis. To reach this objective we shall first take a brief look through the Drude-Sommerfeld model to understand how electric fields can be introduced into a conduction model. This will be done in Section II. Then shall then modify this model by combining it with the Bloch theorem and generate the Semiclassical model in Sections III-IV. This is a model for interactions between the electrons and external electromagnetic fields that treats electrons classically, but the lattice they inhabit quantum mechanically due to Bloch's Theorem. When this framework is complete we shall construct a simple model for electron scattering called the relaxation time approximation in Section V. Since scattering is what causes the finite conductivity in our electron flow this dictates the current in our metal given an external electromagnetic field. Thus with all of these elements in place we will derive the current and resulting conductivity for metals in Section VI for various fields. This is where we will conclude our investigations having derived the conductivity of a metal under the Semi-Classical Theory. These derivations follow heavily after similar work spanning chapters 1, 8, 12, and 13 in the wonderful book by Aschroft and Mermin for the reader who is interested in learning more about various properties of metals beyond just the conduction of metals.[1]

II. THE DRUDE-SOMMERFELD MODELS

Before we move on to Bloch's theorem let us first consider how the theory of electrical conduction works for the Drude-Sommerfeld model or the free electron model as it is often called. This model will serve as a template for how the theory of metal conduction may be carried out when we consider the Bloch theorem. As stated this is a simple model that assumes that electrons are free within the confines of the metal volume. For a piece of metal that is much larger than the de Broglie wavelength of the electron we can approximate the lattice as infinite. This means that the wavefunction of a free electron within the metal may be approximated as a plane wave with some wavevector $\vec{k}$. Thus the wavefunction takes on the form:

$$\psi = e^{i\mathbf{k}\cdot\mathbf{r}} \tag{1}$$

Since electrons are fermionic this means that their energy distribution is described by the Fermi-Dirac distribution which is given by:

$$f(\epsilon) = \frac{1}{e^{(\epsilon-\mu)/k_B T} + 1} \tag{2}$$

Where $f(\epsilon)$ is the probability density that an electron in our metal electron gas has energy ϵ. The μ is the chemical potential, which is the term that governs the drift of electrons in the metal due to electron density differences.[2] While the k_B is the usual Boltzmann constant, and T is the temperature. Now that we have the basic description of a metal at thermal equilibrium, naturally, the next thing to consider is the effect of external electric fields on the electrons inside. What we should notice is that within the metal we can localize the electrons into a minimum uncertainty wavepacket. Therefore, we can use the same classical arguments that Drude used to express conduction assuming that the electrons were classical hard sphere electrons. This is possible due to the Ehrenfest theorem, which for the minimum uncertainty wavepacket (our electrons) can be represented classically.[5] Therefore if we use the classical equations of motion on the minimum uncertainty wavepacket with the average momentum $\mathbf{p} = \hbar\mathbf{k}$ we obtain the following equations of motion:

$$\begin{aligned} \mathbf{v} &= \frac{\hbar\mathbf{k}}{m} \\ \hbar\dot{\mathbf{k}} &= -e(\mathbf{E} + \frac{\mathbf{v}}{c} \times \mathbf{H}) \end{aligned}$$

This description of the electron and its dynamics in the metal are only part of the story. In real metals there are various scattering processes that occur, which lead to the resistances that we observe in real metals. It is not the purpose of this paper to attempt to go through all of these models of scattering within metals. However, we will use the same approximation as Sommerfeld and Drude, the relaxation time approximation. This is a simple approximation in which we assume that if we pick some electron in our metal then it will on average scatter after some time τ which is known as the relaxation time. Our interest is in the conductivity of metals. First lets carefully define the conductivity of metals. This is defined as the following:

$$\mathbf{j} = \sigma\mathbf{E} \tag{3}$$

Where $\mathbf{j}$ is the current density a vector perpendicular to a surface area whose magnitude is given by the number of electrons passing through that area per unit time. The electric field is given by $\mathbf{E}$ and the proportionality between the two of them is given by σ the conductivity. To phrase this in terms of electrons, we note that the current density is given by $j = -ne\mathbf{v}$ in this model. This is because per unit time electrons traveling at speed $\mathbf{v}$ will pass through a perpendicular surface at the rate nv while the $-e$ arises from the charge on the electron. Thus j is exactly the total amount of charge passing through a given surface per unit time. Now, remember that we have scattering effects that we account for by using the τ or the mean relaxation time. This is the mean amount of time that an electron will travel through our metal before colliding with something. Thus since we know that the force from the electric field is given by $-e\mathbf{E}$, classically, then the velocity that an electron puts on before colliding is given by: $\frac{-e\mathbf{E}\tau}{m}$ on average. To tie this back to the wavepacket of the electron, this means that in an electric field $\mathbf{E}$ our wavepackets $\mathbf{k}$ will increase by $\frac{-e\mathbf{E}\tau}{m}$ before it collides again. Notice that after a collision the electrons go in every direction, thus the velocity that is left over after collision does not contribute to the current. This is because on average due to the random direction, the currents cancel out. However, between collisions the velocity is in a definite direction and contributes to the current. Combining this with our definition of j we find the following relationship to be true on average:

$$j = \frac{ne^2\tau}{m}\mathbf{E} \tag{4}$$

Notice this has the same form as our relationship above for conductivity. Therefore for the free electron model we find that the following must be true:

$$\sigma = \frac{ne^2\tau}{m} \tag{5}$$

We shall use the derivation an approximations above as our roadmap to creating the semiclassical model which in addition to taking into account the fermionic nature of electrons, as in the Sommerfeld model, also includes the effects of the periodic lattice on the electron dynamics and metal properties. This occurs through the remarkable result known as Bloch's theorem that Felix Bloch discovered in 1928 [3]

III. BLOCH'S THEOREM

A. Bloch's theorem

Bloch's theorem is a statement about the form of the wavefunction when it is in a periodic potential. Mathematically this is described as the following: If Hamiltonian has the form:

$$\hat{H} = \frac{\hat{p}^2}{2m} + U(\mathbf{r}) \tag{6}$$

Where the potential has the following periodic form:

$$U(\mathbf{r}) = U(\mathbf{r} + \mathbf{R}) \tag{7}$$

Where U is the potential, and $\mathbf{R}$ is a vector such that the function above holds.

Given these constraints Bloch discovered that on such a potential the wavefunction takes on the following form.

$$\psi_{nk}(\vec{r}) = e^{(i\vec{k}*\vec{r})} u_{nk}(\vec{r}) \tag{8}$$

Where the function u_{nk} has the same period as the lattice, IE $u_{nk}(\mathbf{r}) = u_{nk}(\mathbf{r} + \mathbf{R})$ where $\mathbf{R}$ is the vector that is the shift between identical points in between two unit cells in the lattice. These ψ_{nk} are the energy eigenstates of the energy operator on the periodic lattice. This means that they are stationary states over time and are conserved, which is why an electron having the energy ϵ_{nk} will keep this energy unmolested by the lattice. Now since the boundary conditions are identical at the boundary of each unit cell in the lattice this means that we only have to solve the Schrodinger equation over a unit cell to get the solution over the entire lattice. This is because once the Schrodinger equation is solved for one cell the rest of the cells are also resolved due to the periodicity of u_{nk}. This restriction of the space between boundary conditions leads to a restriction in the Fourier space of allowed k values and just like a square well this causes discrete energy levels to occur. These different energy levels lead to the band structure of the metal. This is the essence of Bloch's theorem.

B. Bloch's theorem and Velocity

Given a ψ_{nk}, the number n is the number of the particular energy band that ψ is a member of much like n denotes the particular energy level of an eigenstate in a potential well. However, unlike energy eigenstates at each of these n levels in a simple square wave potential, in the periodic potential there the $\psi_{n\mathbf{k}}$ still depends continuously on k thus we expect that at each n level there will be a range of allowed energies indexed by k. This is where the name energy bands comes from, unlike a single well in a lattice the different energy levels get smeared out because each unit cell contributes an energy level (one for each possible multiple of $\mathbf{R}$), and if there are a large

number of cells we may approximate this dependence as continuous which we have done.

Now, we want to see what the relationship between the velocity and the energy of a particle is in this potential. This is easily found using perturbation theory by noticing that $\epsilon_n(k + \Delta)$ is the energy eigenstate of the energy operator $\hat{H}_{\mathbf{k}+\Delta}$. Therefore, if we expand out $\epsilon_n(\mathbf{k} + \Delta)$ as a power series the first order correction is $\frac{\partial \epsilon_n(\mathbf{k})}{\partial \mathbf{k}}$, then to find this term we take the first order perturbation introduced by Δ into $\hat{H}$. A simple equality results and thus we find the following relationship between v and ϵ:

$$\mathbf{v}_n(\mathbf{k}) = \frac{1}{\hbar} \frac{\partial \epsilon_n(\mathbf{k})}{\partial \mathbf{k}} \tag{9}$$

This result is important to us as we proceed into adding electric and magnetic fields to our model exactly as it was important in the classical models of electron conduction since the velocity is needed for the semiclassical model which we will describe next.

IV. SEMI-CLASSICAL MODEL

A. Limitations of the Drude-Sommerfeld Model

The most important thing to note in both the Drude model and the Sommerfeld model is that the lattice ions are essentially not considered except through the relaxation time and scattering. Only the boundary of our metal is important. Thus the ions in the lattice have no effect on the electron dynamics in the metals outside of scattering. This is a bit of a problem because this type of structure does not give rise to the energy bands that are found in crystals. Without these energy bands the model is not able to differentiate between semiconductors, conductors, and insulators. Thus, our model needs to be improved to take into account the work of Bloch and the energy band structure that arises as a consequence. To do this we will consider the semiclassical model.

B. Semi-Classical Model

Once the Bloch model for the electrons in a lattice was found the question became how can one include electric and magnetic fields into this new model for the electron. It is not as straight forward as the classical model to incorporate these external electromagnetic fields, since one can not just assume that electrons will behave classically. Consider that Bloch electrons are already passing through the lattice in a way that disturbs our classical intuition, since a Bloch electron is able to pass over a lattice without being degraded as would be expected classically. However, one thing to note is that the Sommerfeld model despite its simplifications was able to get many results which indicates that it is not entirely inaccurate. Indeed examining Bloch's theorem closely one

notes that the wave functions of electrons in a periodic lattice are given by the free electron solution $e^{i\mathbf{k}\cdot\mathbf{r}}$ multiplied by a periodic envelop function $u_{n\mathbf{k}}$. This is why Sommerfeld's model which assumed that the electrons could be treated as plane waves was still somewhat accurate, the Bloch electrons are nothing more than modulated plane wave solutions! Now our intention is to derive a model for the electron dynamics in a metal taking into account Bloch's discovery. In order to do this we note that we can construct minimum uncertainty wavepackets out of ψ_{nk} at a fixed n. This is because, given an n we can find a wavefunction solution at any possible $\mathbf{k}$, therefore we may construct our wavepacket. Once again invoking Ehrenfest theorem we shall be able to treat the electrons classically. However, notice that our ψ_{nk} was specified by the lattice throught the inclusion of the lattice as the periodic potential. The effects of this lattice can not be treated classically since the lattice is clearly highly localized spatially. Thus the uncertainty is nowwhere near its minima and so the lattice and its effects can not be treated classically. This is why we can apply the classical uncertainty to the electrons, however, it is also why we must use the Bloch electron wavepacket since this wavepacket takes into account the quantum effects of the lattice quantum mechanically rather than classically yielding the Bloch solutions. This is why the Semiclassical model is an improvement on the Drude-Sommerfeld Models, it includes the quantum mechanical lattice. Since we may treat the Bloch electrons classically this results in equations of motion which are quite similar to the original Drude-Sommerfeld equations of motion.

$$v_n(\mathbf{k}) = \frac{1}{\hbar}\frac{\partial \epsilon_n(\mathbf{k})}{\partial \mathbf{k}}$$

$$\hbar \dot{\mathbf{k}} = -e(\mathbf{E} + \frac{\mathbf{v}_n(\mathbf{k})}{c} \times \mathbf{H})$$

The only difference between this and the classical model is that the forces experienced by the electron are no longer solely given by the classical electromagnetic forces. They are also dictated by the lattice, this is reflected by the usage of the $\mathbf{v}_n$ and the $\hbar\dot{\mathbf{k}}$. These variables inherently contain the interactions between the electron and the lattice due to fact that they both derive from the Schrodinger equation on the lattice, thus the actual reaction of the electron may not be obvious classically. Notice that the energy function is cyclical due to the fact that the only unique $\mathbf{k}$ are bounded by the periodic nature of the solution on the lattice. Thus, if we are near the maximum of this energy and then increase k via the electric field. The electron may actually begin to travel in the opposite direction of the electric field! This is because of the effects of the lattice, a good analogy for this is if we have an electron in a metal box with momentum in the positive direction, now if we increase the electric field and pull it into the wall then the electron can bounce off of the wall and begin traveling in the opposite direction. This type of behaviour occurs also in the lattice leading

to this mysterious behaviour.

V. RELAXATION TIME APPROXIMATION AND ENERGY DISTRIBUTION

A. Relaxation Time Approximation

Notice that once again our model lacks a mechanism for scattering, whats worse is that in this model if the lattice is perfect the electrons will retain any energy inputted via external electromagnetic fields and the current induced will be infinite. Clearly, we need a mechanism for scattering. There are many modes of scattering in metals, some of the most significant are scattering due to the instantaneous thermal deformations in the lattice and permanent defects in the lattice. Both of these factors are leading contributors to scattering in real metals. These are complicated to model, however, for this paper we will once again fall back on the relaxation time approximation similar to that of Drude and Sommerfeld. As we stated before in the Drude-Sommerfeld model the key component of the relaxation time approximation is the relaxation time constant τ. This constant was useful for that model, however, we want to extend it a bit here and allow τ to vary with the energy band of the electron it is associated with n, the position in the lattice $\mathbf{r}$, and finally the wavevector $\mathbf{k}$. Thus our upgraded relaxation time constant becomes $\tau_n(\mathbf{r}, \mathbf{k})$. Since τ_n represents the average time an electron travels without collision. This means that the probability of a collision happening in some time dt is given by $\frac{dt}{\tau_n}$. In addition to this we want our relaxation time model to enforce the thermal equilibrium.

In order to state this mathematically we must recognize that what collisions are doing is changing the energy distribution of the electrons that collide. Lets define the energy distribution function $g_n(\mathbf{r}, \mathbf{k}, t)$ such that $g_n(\mathbf{r}, \mathbf{k}, t)\frac{d\mathbf{r}d\mathbf{k}}{4\pi^3}$ is simply the number of electrons that have the values $\mathbf{r}$, and $\mathbf{k}$ at some time t. Notice that at thermal equilibrium with no external fields this distribution simply becomes the Fermi distribution function as one would expect. However, in the presence of external fields g_n becomes a non-equilibrium distribution function which we will derive by noting that any changes in the distribution function are governed by the collisions which are described by the relaxation time model we gave above. To fufill the requirements that our function goes to the local equilibrium we require the following things from changes in the distribution function. First that our system is memoryless, e.g. after a collision it is not possible to tell what the original energy distribution function was of the electron before the collision. Additionally, if our function is at equilibrium then we want to collisions to maintain that equilibrium. Thus if

$$g_n(\mathbf{r}, \mathbf{k}, t) = g_n^0(\mathbf{r}, \mathbf{k}) = f(\epsilon(\mathbf{k})) = \frac{1}{e^{\epsilon_n(\mathbf{k})-\mu(\mathbf{r}))/k_B T(\mathbf{r})} + 1} \tag{10}$$

,where $T(\mathbf{r})$ is the local temperature at $\mathbf{r}$, the collision will not change the energy distribution function g_n at all. All of these desired properties lead us to the following mathematical statement of how the energy distribution changes over time.

$$dg_n(\mathbf{r}, \mathbf{k}, t) = \frac{dt}{\tau_n(\mathbf{r}, \mathbf{k})} g_n^0(\mathbf{r}, \mathbf{k}) \tag{11}$$

Essentially, at every time interval dt we have the probability $\frac{dt}{\tau_n(\mathbf{r}, \mathbf{k})}$ of the collision returning the non equilibrium solution to the local equilibrium solution at $\mathbf{r}$ and $\mathbf{k}$.

B.   Non-Equilibrium Distribution Function

From the previous section we found that the effect of a collision on the electron distribution function to be

$$dg_n = (\mathbf{r}, \mathbf{k}, t) = \frac{dt}{\tau_n(\mathbf{r}, \mathbf{k})} g_0(\mathbf{r}, \mathbf{k}) \tag{12}$$

If we want to find $g_n(\mathbf{r}, \mathbf{k}, t)$ we must integrate over time. However, this integration is a bit more subtle than just integrating dg_n over time, this is for two reasons. First, notice that because of the external electric field both $\mathbf{r}$ and $\mathbf{k}$ of the electrons in the distribution are changing according to the semi-classical equations given above. Thus, if we want to find the contribution of electrons from a collision at time t' we must look at $dg_n(\mathbf{r}'(t'), \mathbf{k}'(t'), t')$ where $\mathbf{r}'(t) = \mathbf{r}$ and $\mathbf{k}'(t) = \mathbf{k}$ after evolution by the semi-classical equations. Thus the contribution to the change in $g_n(\mathbf{r}, \mathbf{k}, t)$ from these electrons is only counted for the electrons that come from a collision with values $\mathbf{r}'(t')$ and $\mathbf{k}'(t')$ at time t'. However, this is not the full story since between the collision at time t' which has put the electrons on track to contributing to g_n may be disrupted if they experience another collision before time t. Thus, the contribution from electrons at time t' is only counted if there are no intermediary collisions intervening. Thus the percentage of electrons that make it all the way to time t is mitigated by $P(t, t')$, the probability that a collision does not occur between time t' to t. Thus considering these two factors we find that g_n can be written as:

$$g_n(\mathbf{r}, \mathbf{k}, t) = \int_{-\infty}^{t} \frac{dt'}{\tau_n(\mathbf{r}'(t'), \mathbf{k}'(t'))} g_0(\mathbf{r}'(t'), \mathbf{k}'(t')) P(t, t') \tag{13}$$

Let $g_n(\mathbf{r}, \mathbf{k}, t) = g(t)$, $g_0(\mathbf{r}'(t'), \mathbf{k}'(t')) = g_0(t')$, $\tau_n(\mathbf{r}'(t'), \mathbf{k}'(t')) = \tau(t')$. Thus our equation becomes:

$$\int_{-\infty}^{t} \frac{dt'}{\tau(t')} g_0(t') P(t, t') \tag{14}$$

Now, notice that $P(t, t')$ is the probability of a collision occurring to an electron between time t and t'. Notice that due to the relaxation time approximation, we know

that at any particular instance in time we the probability of an electron collision is given by $\frac{dt}{\tau_n}$. Thus we can generate a differential equation for $P(t, t')$ since:

$$P(t, t') = P(t, t' + dt')(1 - \frac{dt'}{\tau(t')}) \tag{15}$$

If we take the limit of infinitesimal time we get the following equation:

$$\frac{\partial}{\partial t'} P(t, t') = \frac{P(t, t')}{\tau(t')} \tag{16}$$

Notice we can insert this into our equation for $g(t)$ which then becomes:

$$\int_{-\infty}^{t} dt' g_0(t') \frac{\partial}{\partial t'} P(t, t') \tag{17}$$

Finally, if we apply integration by parts we get the following formula:

$$\int_{-\infty}^{t} dt' P(t, t') \frac{d}{dt'} g_0(t') \tag{18}$$

Since we know the form of g_0, if we differentiate and then substitute (a lengthy, unpleasant bit of work) we can obtain the following general formula for the non-equilibrium distribution function.

$$g(t) = g^0 + \int_{-\infty}^{t} dt' P(t, t') [-\frac{df}{d\epsilon} \mathbf{v} \cdot (-e\mathbf{E} - \nabla\mu - \frac{\epsilon - \mu}{T} \nabla T)] \tag{19}$$

VI.   CONDUCTIVITY OF METALS

A.   DC Conductivity

In metals we note that the electric field is generally small, which means that over the average time between scattering τ the change in $\mathbf{k}$ induced by the electric field is negligible. Thus we neglect its effect on $\frac{d\mathbf{k}}{dt}$. Additionally, notice since metals are good thermal conductors the gradient over the metal will also tend to be small and so we may treat the effect of T as a constant. Finally, notice that the chemical potential μ in metals is negligible since it only arises as an artifact of the gradient of the temperature and thus it may also be neglected.

Now that we have found that the effect of the electric field and temperature gradient are neglibile, we should note that the effect of the magnetic field can not be ignored since the magnetic fields that can be commonly generated in metals is large enough to significantly change $\mathbf{k}$ over the relaxation time. However, one thing to note in particular is that the energy is conserved over the magnetic field. Since the $\epsilon(\mathbf{k})$, the only variable in the fermi distribution dependent on time, is conserved this means that the f in our equation for g does not

have any remaining time dependence in our approximations. Therefore, from our equation for g the only time dependent elements left in the integral are $P(t, t')$ and $\mathbf{v}(\mathbf{k}_n(t'))$.

Finally, we make one last approximation in which we assume that the relaxation time is based on the energy of electron, instead of directly on the $\mathbf{k}$. Notice once again that when this is done, the approximation that only the magnetic field is important means that the $\tau(\epsilon_n(\mathbf{k})$ is also not time dependent since $\epsilon_n(\mathbf{k})$ is conserved in magnetic fields. Thus if we refer back to the differential equation for $P(t, t')$ we find that we can now write P as:

$$P(t, t') = e^{-(t-t')/\tau_n(\mathbf{k})} \tag{20}$$

In light of these useful approximations in metals we find that our equation for g has become:

$$g(\mathbf{k}, t) = g^0 + \int_{-\infty}^{t} dt' e^{-(t-t')/\tau_n(\mathbf{k})} [(-\frac{df}{d\epsilon})\mathbf{v} \\ \cdot (-e\mathbf{E} - \nabla\mu - \frac{\epsilon(\mathbf{k}) - \mu}{T}\nabla T)] \tag{21}$$

Our interest is to calculate the conductivity of the metal without temperature gradients or an external electric field, just as did for the Drude-Sommerfeld model. Thus all the terms except for the exponential lose their dependence on time due to our approximation or since we have assumed them to be constant like the electric field and the temperature. Thus the rather complex integral in eqn 21. evaluates quite simply to:

$$g(\mathbf{k}) = g^0(\mathbf{k}) - e\mathbf{E} \cdot \mathbf{v}(\mathbf{k})\tau(\epsilon(\mathbf{k}))(-\frac{\partial f}{\partial \epsilon}) \tag{22}$$

Since we now know the electron density for a given band and $\mathbf{k}$ are are now in the position to calculate the current which is the amount of charge moving through a surface over some unit time. This means that our current equation is given by:

$$\mathbf{j} = \int \frac{d\mathbf{k}}{4\pi^3}\mathbf{v}(\mathbf{k})g \tag{23}$$

Where we have integrated over the entire space of unique $\mathbf{k}$, or over a single unit cell in k space. This is the current density of a single energy band. Plugging in g we find the equation to have the following form:

$$\mathbf{j} = e^2\mathbf{E} \int \frac{d\mathbf{k}}{4\pi^3}\mathbf{v}(\mathbf{k})^2\tau(\epsilon(\mathbf{k}))(-\frac{\partial f}{\partial \epsilon}) \tag{24}$$

We left off the g_0 term since we know it does not contribute to the current, since it is the equilibrium solution. Remember that the conductivity is given by: $\mathbf{j} = \sigma\mathbf{E}$ this implies that the conductivity for band n is given by:

$$\sigma(n) = e^2\mathbf{E} \int \frac{d\mathbf{k}}{4\pi^3}\mathbf{v}(\mathbf{k})^2\tau(\epsilon(\mathbf{k}))(-\frac{\partial f}{\partial \epsilon}) \tag{25}$$

To find the total conductivity we simply sum over the contributions to conductivity from all available bands.

Thus this is the conductivity of a metal with band structure ϵ_n.

B. Insulators vs. Conductors

Notice that $\frac{\partial f}{\partial \epsilon}$ is basically 0 everywhere except for at the Fermi temperature what it becomes very large. Thus what we find is that only the bands that are close in energy to ϵ_f are significantly contributing to the conduction. This begins to shed some light on why some elements are conductors and others insulators. The conductors are the metals where the Fermi temperature lands in the middle of an energy band thus allowing for the electrons in the band to contribute to the conductivity. However, if the fermi temperature lands between two bands which happens to insulators then very few to none of the electrons will contribute to the conductivity and we observe the insulation properties of the insulator. Finally, we see this effect in semiconductors where the bands are sufficiently close to the fermi temperature but not part of them so the crystal acts as both a conductor and an insulator. Notice that this effect was not considered in the Drude-Sommerfeld model at all!

VII. CONCLUSION

In this paper we first considered the conductivity of metals using the classical Drude model and its early quantum mechanical extension the Drude-Sommerfeld model. These models modelled the electrons in a metal as forming an electron gas. The Drude model used the Boltzmann distribution for the energies of the electrons in this gas. While Sommerfeld included the fermionic nature of electrons and used the Fermi-Dirac distribution. Once this model of the metal had been constructed external electric fields were added to the model classically and thus the conductiviy, which is the ratio of current produced, compared to electric field applied. These models had some significant problems such as a lack of accounting for insulators vs. conductors, and why only some electrons seem to conduct in a metal and not all of them. These problems arose due to the neglect of the models to account for the lattice that the electrons resided in, other than through scattering effects. This is why when Bloch discovered the Bloch Theorem an upgrade to these models was immediately discovered since the Bloch electrons took into account the periodic nature of the lattice. This lead to many interesting effects such as the energy band structure of allowed electrons in metals. Then with the addition of classical electromagnetic fields this a new model for the dynamics of electrons was developed using Bloch electrons instead of free electrons as was done in the Drude-Sommerfeld model. This model is called the semiclassical model. With this model we then recalculated the conductivity of metals and found that due to the band structure of metals we could predict if it would be a conductor, semiconductor, or an insulator which was an exciting new result that was not possible under the older models.

[1] Ashcroft, N. W., Mermin, N. D. (1976). Solid state physics. New York: Holt, Rinehart and Winston.

[2] Baierlein, Ralph. Thermal physics. New York: Cambridge UP, 1999.

[3] Bloch, F. (). Über die Quantenmechanik der Elektronen in Kristallgittern. Zeitschrift für Physik, 52, 555-600.

[4] Drude, P. "Zur Elektronentheorie Der Metalle." Annalen Der Physik 306.3 (1900): 566-613. Wiley Online Library. Web. 1 May 2014.

[5] Shankar, Ramamurti. Principles of quantum mechanics. 2nd ed. New Delhi: Springer(India), 2010.

[6] Thomson, J. J. "Xl." Philosophical Magazine Series 5 44.269 (1897): 293-316. Philosophical Magazine. Web. 1 May 2014.

Use of the WKB Approximation Method in Characterizing the Probability and Energy of Nuclear Fusion Reactions

James M. Penna

Department of Physics, 77 Massachusetts Ave., Cambridge, MA 02139-4307

(Dated: May 7, 2014)

The potential of an atomic nucleus is developed as a model exactly solvable using the WKB method. The results are used to find the tunneling probability through the potential and to calculate the parameters of fusion reactions.

I.   INTRODUCTION AND HISTORICAL BACKGROUND

Nuclear fusion has long been a physical process that has turned science on its head multiple times, redefining known physics and causing scientists across the globe to embark on huge quests to harness its power. The historical basis for the physical problem comes from the efforts of scientists to meaningfully answer the rather childish question, "Why does the sun shine?"

The first problem that beleaguered scientists was that the actual properties of the sun were largely unknown, including it's composition and age. Though earlier scientists such as Helmholtz and Mayer had proposed answers to this question, the first solid calculations of the sun's energy and age were produced by William Thompson, better known as Lord Kelvin. Lord Kelvin's calculations were based on the idea of the sun's gravitational energy being the cause of its radiation, as he had calculated that if the sun were to burn via chemical reactions the sun's lifetime would be roughly 3000 years, an absurdly small timescale (and obviously false as the Egyptians had the sun to worship and build pyramids by the light of). After calculating the gravitational energy of an object of the sun's size and using its radiation rate, he calculated the overall lifetime of the sun to be about 30 million years. It was with no small amount of vitriol that Kelvin used this result to attack Charles Darwin's theory of natural selection and erosion-based estimates of the earth's age, which he disagreed with. Citing his result he stated " What then are we to think of such geological estimates as [Darwin's] 300,000,000 years for the "denudation of the Weald?" The " denudation of the Weald " here refers to the erosion of a valley calculated by Darwin in order to give scale to the Earth's age. [1]

Unfortunately for Lord Kelvin, as renown as he is, his criticism of Darwin turned out to be less than merited. The true answer to the sun's power came with the discovery of radiation and the formulation of Einstein's most famous result, the equation $E = mc^2$. This was the key to the sun's power, but the answer sstill remained behind two locks. The first lock was the result of spectrographic measurements of the sun that gave the first hints of its composition. Measurements yielded that the sun is composed of mostly hydrogen and helium, with varying small percentages of heavier elements. The second was the discovery that the helium-4 nucleus, though made

of of four nucleons, was ever-so-slightly lighter than the mass of four constituent nucleon, such as hydrogen nuclei. It was Arthur Eddington who fit the lock and key together, deducing that in some nuclear process, mass was being converted to energy through the conversion of hydrogen to helium.

This process is known to us today as nuclear fusion, but by the classical laws of physics, this process should be impossible. As a toy model we will look at the simplest case of fusion, between two hydrogen-1 nuclei. According to classical electrostatic laws, the force between them can be represented by the equation for Coloumb's law:

$$F(r) = k_e \frac{q_e^2}{r^2} \tag{1}$$

where $k_e = 8.9876 \times 10^9 \frac{N \times m^2}{C^{-2}}$, the SI-unit Coloumb constant, q_e is the charge of the proton, 1.602×10^{-19} C. If we were to evaluate this equation for $r = 1.535 \times 10^{-18}$ meters, i.e. the distance of two adjacent protons, we would get a force of 4.168 meganewtons repelling the two protons. As described by classical electrodynamics, nuclear fusion should not occur, so in order to accurately explain the phenomenon, quantum mechanics must be introduced.

With the advent of quantum mechanics, it became clear that classical forces did not exactly scale to the quantum level. One such non-classical phenomenon is that of quantum tunneling. For a given potential barrier $V(x)$, it is impossible for a particle of $E < V(x)$ to traverse the barrier according to classical calculations. However, when solving the Schrödinger equation for precisely such a potential, there is a small probability that a particle of $E < V(x)$ can indeed traverse the barrier to the other side, the "classically forbidden" region. For a slowly varying potential, one such that $V(x)$ is relatively continuous and does not greatly vary in value across distance, it is possible to apply a method known as the Wentzel-Kramers-Brillouin (WKB) Approximation or Method. The WKB approximation allows the Schrödinger equation to be approximately solved over such slowly-varying potentials for a "semiclassical" solution. The method itself and the formalism associated with it will be developed in the next section.

In 1928, the concept of tunneling and the WKB approximation were applied to the problem of alpha emission by the noted physicist George Gamow. Previously it

227

was not understood how a positively charged alpha particle could remain confined in the nucleus given such a massive potential barrier. However, through use of the WKB approximation it became clear that alpha emission could be explained by tunneling. Conversely, the opposite process of nuclei coming together and fusing was also described this way. Thus the purpose of this paper shall be to:

- Develop the components of the WKB Method needed to do the calculation in Section II.

- Establish a model of the nuclear potential and solve the Schrödinger equation for the potential using the WKB method in order to derive the probability of fusion on the microscopic level in Section III.

- Use the derived probability to calculate the reaction cross-section, reaction rates and reaction energy of a plasma system in which fusion occurs in Section IV.

II.   THE WKB METHOD AND FORMALISM

Here I shall introduce the WKB approximation and list the relevant connection formulae to be ussed in the following derivation. For the purpoe of brevity I will omit the full derivation of the WKB approximation and the connect formulae, but they should be readily accessible and familiar to anyone with a rigorous understanding of basic quantum mechanics. For the complete treatment, one should refer to Griffiths, Chapter 8. [2]

Given a spacially-varying potential $V(x)$, we can apply the WKB approximation if the following condition is satisfied:

$$\lambda(x)|\frac{dV(x)}{dx}| << \frac{[p(x)]^2}{m} \qquad (2)$$

where $\lambda(x)$ is the De Broglie wavelength associated with the wavefunction, $V(x)$ is the potential over space, and $p(x)$ is the momentum associated with the wavefunction. [3]

For this potential the one-dimensional Schrödinger equation can be written as

$$\frac{d^2\psi}{d^2x} = -k^2\psi \qquad (3)$$

where $k = \sqrt{\frac{2m}{\hbar^2}(E - V(x))}$, E being the energy of the incoming particle, m being its mass, and $V(x)$ being the potential we are looking at. Solving this second order differential equation one yields solutions of the type below:

$$\psi(x) = \frac{C}{\sqrt{k(x)}} \exp(\pm i \int_r^a k(x)\,dx) \qquad (4)$$

This is the wave function in the so-called "classically-allowed" region, where the energy of the particle exceeds that of the potenial. However, during the treatment of the nuclear potential, we must also consider the "classically forbidden" region in which $E < V(x)$, where classically it would be impossible for a particle to travel. However, these regions still do also give valid solutions to the Schrodinger equation even if not classically admissible.

One of the most important aspects of the WKB approximation is its ability to connect two different regions, both allowed and forbidden, through use of the connection formula. The key assumption is recasting the potential as an approximately linear function at the point where the two regions meet, $V(x) \approx E + V'(0)x$. The derivation that follows is once again too tedious to cover here, but the basic logic is that because the lengthscale of the slowly-varying potential is much longer than the area in which the wavefunction transits between regions a simple linear form can be used to simplify analysis. The end result is a set of relations between the wavefunctions in each area known as the connection formulae. In going from the classically allowed region to a classically forbidden region such that $V(x < a) < E, V(x > a) > E$ our connection formula is:

$$\frac{2A}{\sqrt{k(x)}} \cos\left(\int_x^a k(x)\,dx - \frac{\pi}{4}\right) +$$
$$\frac{B}{\sqrt{k(x)}} \sin\left(\int_r^a k(x)\,dx - \frac{\pi}{4}\right) \Leftrightarrow$$
$$\frac{A}{\sqrt{|p(x)|}} \exp\left(-\int_a^x |p(x)|\,dx\right) + \qquad (5)$$
$$\frac{B}{\sqrt{|p(x)|}} \exp\left(\int_a^x |p(x)|\,dx\right)$$

Note the order of the limits of integration give the direction of the wave, traveling into the classically forbidden region. Going in an opposite direction, forbidden to allowed such that $V(x < b) > E, V(x > b) < E$, our connection formula is:

$$\frac{A}{\sqrt{|p(x)|}} \exp\left(-\int_x^b |p(x)|\,dx\right) +$$
$$\frac{B}{\sqrt{|p(x)|}} \exp\left(\int_x^b |p(x)|\,dx\right) \Leftrightarrow$$
$$\frac{2A}{\sqrt{k(x)}} \cos\left(\int_b^x k(x)\,dx - \frac{\pi}{4}\right) + \qquad (6)$$
$$\frac{B}{\sqrt{k(x)}} \sin\left(\int_b^x k(x)\,dx - \frac{\pi}{4}\right)$$

Again, the order of integration indicate the region into which we are moving. These connection formulae become key to solving the problem of tunneling and describing the mechanism by which fusion happens.

III.   APPLICATION OF THE WKB METHOD TO THE NUCLEAR POTENTIAL

The connection formula shown above is essential to solving the barrier problem. The potential we consider for the problem of nuclear tunneling must take into account both the electrostatic repulsion of the Coulomb force and the attractive force of the nuclear potential. Such a potential can be modeled below by:

$$V(x) = \begin{cases} \frac{Z_1 Z_2 e^2}{4\pi\epsilon_0 R} & \text{if } r \geq R \\ -V_o & \text{if } r < R \end{cases} \qquad (7)$$

where R is the radius of the atomic nucleus being fused with, and Z_1 and Z_2 are the atomic numbers of the nuclei colliding. The exact form of the nuclear potential varies between nuclear reactions but can usually be approximated by a deep potential well $-V_0$ [3] This was the same approximation made in Gamow's 1928 paper on the tunneling of an alpha particle from a heavy nucleus [4] (though in this case, we are going to flip Gamow's work on its head, or at least in its direction). As we shall see, thanks to the connection formulas, we will never need to deal with it directly for the first part of our calculation.A graph of this toy model of the nuclear potential is seen in Figure [1]. With this graph, we can very clearly distinguish the classically allowed regions $r < R$ and $r > b$ from the classically forbidden region in $R, r < b$. Looking first at the classically allowed region I, the region where $r > b$ on the right, we see that the wave function takes the form in one dimension:

$$\psi(x) \approx \frac{A}{\sqrt{k(x)}} \exp\left(\pm i \int_b^r k(x)\, dx\right) \qquad (8)$$

with $k(x)$ defined as above in the connection formula, though this time we have the explicit potential to work with.In order to simplify our calculations, we shall be continuing the treatment in one dimension only - however, since the Coloumb potential is inversely linear and radially symmetric, a one dimensional approximation and calculation will be suitable for our purposes.

Now looking at the classically forbidden region, $r < b$ as seen in to Figure [1], previous intuition informs us that the wave fuction takes the form of a decaying exponential. Specifically the WKB approximation gives the form of the wavefunction on the other side of the barrier via the connection formula:

$$\psi(x) \approx \frac{A}{\sqrt{|p(x)|}} \exp\left(-\int_r^b |p(x)|\, dx\right) + \\ \frac{B}{\sqrt{|p(x)|}} \exp\left(\int_r^b |p(x)|\, dx\right) \qquad (9)$$

Note here that I am using the notation from Griffiths such that $|p(x)| = |k(x)|$ for the case where $E < V(r)$
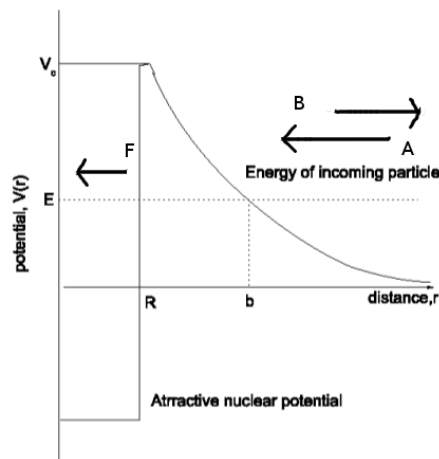

FIG. 1: A sketch of the nuclear potential we are modeling. The Coloumb force is responsible for the positive upwards sloping portion and the nuclear force is here represented as a deep well. R represents the nuclear radius and b represents the distance of closest approach between two nuclei. The incoming plane wave A, the reflected plane wave B, and the transmitted plane wave F, from the solutions to the Schrodinger equation in one dimension, are shown here. A and F are used to find the transmission coefficient which will in turn be used to find the probability of transmission. Adopted from Aziz et. al. [3]

and $k(x)$ becomes imaginary.This solution is a decaying exponential rather than the oscillatory behavior we see in the classically allowed region.

With the wave amplitudes and arrows labeled in Figure [1] providing the visual queue to refresh our memories. On one side of the barrier, we see the intuitive behavior of a reflection of the incoming low energy wave, but we also see the transmission of one component of the incoming free wave on the other side of the barrier, in the other classically allowed region $r < R$, where R is the nuclear radius. The square of the amplitudes of the transmitted wave over the amplitude of the incoming wave gives the probability of transmission, or transmission coefficient $T = \frac{|F|^2}{|A|^2}$.

Using the connection formula as mentioned in the second section, we can equate the wave function of the classically forbidden region to that of the classically allowed region $r < R$. The resultant wavefunction looks similar to the one in equation (7), though granted with the limits of integration instead being from r to R. Thus by dividing the wave function squared amplitudes for the regions, we obtain for the transmission coefficient :

$$T = \exp\left(-2\int_b^R |p(x)|\,dx\right) =$$
$$\exp\left(-2\int_b^R \sqrt{\frac{2m}{\hbar^2}(V(r)-E)}\,dx\right) \quad (10)$$

The integral in the exponential above is often referred to as the Gamow factor γ, the result of Gamow's original work on tunneling in 1928 and also the result of the calculation in Aziz, Yusof, and Kassim in [3]. Despite the seemingly-impossible to pass electrostatic barrier, there is a probability of the particle passing through it, depending on its energy. For the electrostatic potential for $V(r > R)$ specified in (2),this integral can be solved exactly and gives the probability of an incoming particle tunneling through the Coloumb barrier. Here we will depart from the calculation used by Gamow and we will instead look to the calculation done by Aziz et. al.

When the Coloumb potential is inserted and the integral in T is expanded out, we see that the probability of the particle tunneling is [3]:

$$P(E) = \exp-\left(\frac{8Z_1 Z_2 e^2 \mu b}{\hbar^2}\right) \times$$
$$\arccos\left(\left(\frac{E}{V}\right)^{1/2} - \left(\frac{E}{V}\right)^{1/2}\left(1-\frac{E}{V}\right)^{1/2}\right). \quad (11)$$

In which again Z_1 and Z_2 are the atomic numbers of the elements being fused, μ is the reduced mass of the two nuclei, $\frac{m_1 m_2}{m_1 + m_2}$, and b is a parameter representing classically the closest approach between two nuclei, just outside of the atomic radii. Though both Gamow and Aziz et. al. use the low energy approximation in order to either simplify the arccos term away or use a logarithm to get rid of higher terms, we cannot do this just yet. In order to establish valid parameters and energy scales for approximations to take place, we must first look into the actual reactions we are trying to explore, those of nuclear fusion.

IV. NUCLEAR PHYSICS AND CHARACTERIZING LARGE-SCALE FUSION REACTIONS

Having established the cause of nuclear fusion and a suitable mathematical expression to characterize its probability of occurring, it is time to start looking at fusion in a physical setting. Fusion reactions in nature happen on an enormous scale in stars, a far-cry from the simple two-particle model we had built our model upon. It is from the sun we shall first draw intuition and information from.

It has been established through thousands of years of empirical evidence that the sun is hot. Precisely how hot,

however, has only been relatively recently known, despite Lord Kelvin's best efforts. The sun's core is where fusion takes place at about an average of 1.5×10^7 K [5], or in terms of average particle energy, about 1.3 keV. Even in the hottest fusion reactors on Earth, average nucleon energy will not exceed an energy scale on the order of 10 KeV. This relatively small energy scales means that for real life fusion reactions, we may neglect the arccos term as it will go to unity. The probability now becomes the exponential:

$$P(E) = \exp-\left(\frac{2\pi Z_1 Z_2 e^2}{E}\right) \quad (12)$$

However, in large scale nuclear reactions, it becomes next to useless to discuss individual probabilities. Instead, the concept of a reaction cross section must be introduced. Just as scattering in quantum mechanics or macroscopic processes uses a cross section to describe the relative reaction between incoming particle flux and a target, nuclear physics uses the cross section σ_f to characterize the likelihood of a fusion reaction occurring between two particles. The cross section becomes a more physically useful parameter as it can be used to characterize properties of a whole system of fusing particles and also provides a unitless parameter to characterize fusion reactions by. Simply speaking, the cross section can be expressed as:

$$\sigma(E) = \frac{S(E)}{E}P(E) \quad (13)$$

where $S(E)$ is the astrophysical S-factor [5]. The S factor cannot be derived purely from theory -it is a parameter of nuclear reactions with units of energy that has not been theoretically derived and must be measured empirically at each energy. In the case of the fusion reaction scales we are examining, from 1-10 KeV, the S factor is known to vary very slowly, making the derived probability the dominant term in the cross section.

The cross section safely parameterized, we will now direct our attention to deriving the energies at which these reactions occur in a more physical environment than our artificial toy potential model. In a hot plasma or other sufficiently warm, dense collection of light nuclei (such as, conveniently enough, that found in the sun) the energies of said nuclei fall into a Maxwell-Boltzmann distribution of the approximate form:

$$\phi(E) = \phi(v) \propto E \exp\left(-E/kT\right) \quad (14)$$

(For the full form refer to Berulani, pg. 344, eq. 12.14 [5]). E is the energy of the reaction. T is the particle temperature and k is the familiar Boltzmann's constant The thermally averaged rate of the fusion reaction $\langle\sigma v\rangle$ can now be found, knowning both the cross section and how the particles are distributed according to their energies. The explicit calculation is:
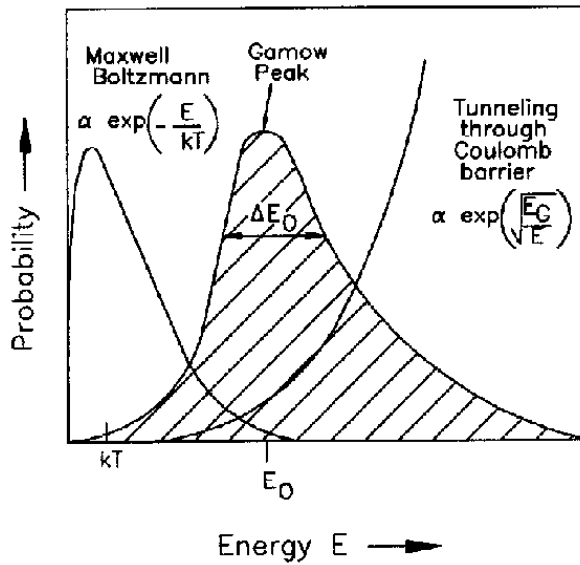
FIG. 2: A sketch of the Gamow factor, and the cross-section. When calculating the reaction rate this peak will dominate the other terms in the integral equation at the energy E_0. This is referred to as the Gamow peak, the "ideal" energy for fusion reactions. Adapted from: http://inspirehep.net/record/827392/plots

$$\langle \sigma v \rangle = (\frac{8}{\pi \mu})(kT)^{-3/2} \int_0^\infty \sigma(E) \exp\left(-\frac{E}{kT}\right) \qquad (15)$$

One may notice, given the form of the cross-section, that the integrand has a term proportional to

$$\exp\left(-\frac{E}{kT} - \frac{u}{\sqrt{E}}\right) \qquad (16)$$

with $u = \sqrt{2\mu\pi^2}\frac{Z_1 Z_2 e^2}{\hbar^2}$. This term implies that there is in fact a peak energy at which the reaction rate is maximized, the so-called Gamow peak that can be seen in Figure [2]. The calculation shall be omitted here for virtue of being messy but the intermediate steps are referred to in Aziz et. al. [3] The end result is quite neat, with an energy that ends up being dependent on the temperature, the size of the nuclei and a few physical parameters:

$$E_o = 1.22(Z_1^2 Z_2^2 \mu T_6^2)^{1/3} keV \qquad (17)$$

where μ is again the reduced mass and T_6 is temperature expressed in millions of degrees Kelvin. The energy needed for the nuclear reaction has been completely characterized from the derivation of the coefficients in the WKB approximation - arguably this is one of the most startlingly effective and important results of quantum mechanics (no fusion means no reaction to provide the energy for sunlight, and sunlight is rather important for life on earth).

With the energy required for the reaction characterized, we may take a look at the opposite end of the equation, the energy produced in the reaction. As mentioned in the discussion of the potential model, within the range of the nuclear radius there is a powerful attractive force that allows nucleons to be bound together despite the powerful Coloumb force repelling the protons in a nucleus. This nuclear force is a consequence that arises from the strong force interactions between quarks in nucleons. The nuclear force is very poorly characterized - to date there are no known universal constraints or parameters on it and any model or problem involving the nuclear force must be dealt with as an individual case. However, for our purposes, merely knowing that the force exists is enough.

The fusion of nuclei is an energy-releasing process, and this energy comes from the release of binding energy from the nuclear force as the separate nucleons are once again re-joined (if this process seems counter-intuitive, consider that it takes net energy to break apart a nucleus into its constituent nucleons - therefore the individual nucleons have stored binding energy they can release by binding once more).

Calculating this release of binding energy does not need to involve a complex study of the nuclear force or QCD (it is not the author's intent to win the Nobel Prize with this paper). It merely requires knowledge of the mass-energy equivalence principle and a little subtraction. The fusion reaction we shall consider is the fusion between a deuteron and a triton, known as a D-T reaction. The D-T reaction is of particular interest as its cross section is much higher than that of other common fusion reactions. This makes it the most important fusion reaction in fusion energy research as it is the most-easily producible. A D-T reaction will produce an alpha particle and a neutron, and by calculating the mass difference between the reactants and products using the following equation

$$B(Z,N) = (\sum m_r(Z,N) - \sum m_p(Z,N))c^2 \qquad (18)$$

we can calculate the binding energy released. The Z in the equation is the atomic number whereas the N is the number of neutrons. For the D-T reaction, a direct calculation of this change in binding energy yields 9.5 MeV. However the actual energy released is a little less than twice that, at 17.6 MeV - this simple formula does not take into account the change in rest masses of the products and reactants moving at relativistic speeds. Plugging in the relevant atomic numbers at 100 million Kelvin, the Gamow peak energy needed for a deuteron to fuse with a triton is roughly 2.8 MeV, less than one-sixth what the reaction would produce. Fusion is an incredibly energetic process with astounding returns on energy, a tempting fact which has led the nuclear fusion power

community into the joint effort of harnessing that energy for humanity.

V. CONCLUSION AND DISCUSSION

The derivation in this paper demonstrates the enormous utility of toy models in solving quantum mechanical systems and the power of approximate methods. By using a model based off of basic knowledge of nuclear physics, we were able to piece together the wavefunction across the nuclear region with the WKB approximation, use the wavefunction amplitudes to derive the transmission coefficient and found the probability of transmission. The direct derivation of the tunneling probability and the fusion cross section that is parameterized by it was a huge win for nuclear physics and stellar astrophysics. To have a reliable expression for it based on the Gamow factor has helped to enable the whole of experimental fusion physics. Knowing the temperature and energy of these reactions allowed for the development of the hydrogen bomb and the design of fusion reactors such as the tokomak, currently mankind's best hope at attaining power from sustainable fusion. Gamow's original work was the key stepping stone that allowed other physicists such as Hans Bethe and [4] to derive the reaction chains of stellar fusion reactions such as the CNO cycle, truly answering the question "Why do the stars shine?" Quantum mechanics is a powerful tool with which many physical systems in nature can be solved, and nuclear fusion has proven to be one of them. Using the techniques of the WKB approximation we have shown it is possible to characterize the workings of even the mightiest stars starting with their smallest constituents.

[1] J.D. Burchfield, Lord Kelvin and The Age of the Earth Chicago: University of Chicago Press, 1990)

[2] D.J. Griffiths, Introduction to Quantum Mechanics, 2nd Ed. (Pearson Prentice Hall, Upper Saddle River, NJ, 2005)

[3] A. Aziz, N. Yusof, H. Kassim, The Effective Energy in Nuclear Reactions from Exact Probability by Using the WKB Approximation 1017, 225 (2008); doi: 10.1063/1.2940632

[4] G. Gamow, Quantum Theory of the Atomic Nucleus ZP, 51, 204

[5] Carlos A. Bertulani, Nuclear Physics in A Nutshell (Princeton University Press, Princeton, NJ, 2007)

Dirac Equation and its Application to the Hydrogen Atom

Anirudh Prabhu

Massachusetts Institute of Technology, 77 Massachusetts Ave., Cambridge, MA 02139-4307

(Dated: May 2, 2014)

The need for and subsequent discovery of the Dirac equation was born out of the necessity to unite special relativity with quantum mechanics. Our investigation of the Dirac equation begins with a historical introduction that provides motivation for our subsequent treatment of the equation. Following the historical preface, we provide a derivation of the Dirac equation for a free electron and discuss its important aspects and implications. This derivation introduces useful concepts including the Dirac spinor, gamma matrices, and antimatter. We then consider the Dirac equation describing an electron in an electric field, in particular, the hydrogen atom potential. Finally, we use the Dirac equation to investigate the energy spectrum of the hydrogen atom and discuss this spectrum in relation to results obtained using perturbation theory in non-relativistic quantum mechanics.

I. NOTATION AND CONVENTIONS

For this treatment, we will use natural units, in which, $\hbar = c = 1$. The presentation of relativity and tensors will be limited to its utility in describing basic processes in special relativity. We will use the following convention for the metric tensor

$$\eta_{\mu\nu} = \begin{pmatrix} 1 & 0 & 0 & 0 \\ 0 & -1 & 0 & 0 \\ 0 & 0 & -1 & 0 \\ 0 & 0 & 0 & -1 \end{pmatrix}$$

With greek letter $(\mu, \nu, \rho, \dots)$ running over 0, 1, 2, 3 and latin letters $(i, j, k, \dots)$ running over 1, 2, 3 unless otherwise stated. We now introduce covariant and contravariant four-vectors.

$$x^\mu = (x^0, \mathbf{x}), \ x_\mu = \eta_{\mu\nu} x^\mu = (x^0, -\mathbf{x})$$

Based on the notion of upper and lower indices, we will introduce Einstein's summation notation. Whenever there is the same index both as an upper index and a lower index, that index is summed from 0 to 3 or 1 to 3 depending on whether it is a Greek or Latin letter. Along the same vein, we may define the derivative operator

$$\partial_\mu = \frac{\partial}{\partial x^\mu} = \left(\frac{\partial}{\partial t}, \nabla \right)$$

Which is a four-dimensional gradient operator.

II. INTRODUCTION

The late 1800s and early 1900s saw great advancement in theoretical physics. In 1890, apparent doublets were observed in the hydrogen spectrum. This phenomenon became later known as the fine structure of hydrogen. The discovery was largely ignored until 1916, when Arnold Sommerfeld treated it (to high experimental accuracy) using both quantum mechanics and special relativity, even before the explicit discovery of the Schrödinger equation [7]. After this treatment, several experimentalists set out to measure the fine structure. Some of these included Merton and Nicholson (1917), Geddes (1922), and Hansen (1925). The most thorough results of the era were given by Kent et. al (1927), following the discovery of the Schrödinger equation[7].

Concurrently, in his 1905 paper, *On the Electrodynamics of Moving Bodies* Einstein postulated the theory of Special Relativity, part of which describes particles moving at speeds comparable to the speed of light. The next few decades saw the development of quantum theory. In 1925, Erwin Schrödinger wrote the Schrödinger equation, which written in its general form is

$$i\frac{\partial \Psi(x,t)}{\partial t} = \hat{H} \Psi(x,t) \tag{1}$$

Here $\Psi(x,t)$ represents the quantum state of a particle, and $\hat{H}$ is the Hamiltonian of the system. This equation describes how a non-relativistic quantum particle evolves in time. Shortly after the discovery of this equation, Oskar Klein and Walter Gordon wrote down an equation that purported to describe the quantum theory of a relativistic electron. The equation was derived from the principles of special relativity and the Schrödinger equation. In particular, the relativistic energy is given by $E^2 = |\mathbf{p}|^2 + m^2$. In quantum theory, momentum is described by operator $\hat{p} = -i\nabla$ and the energy is described by the Hamiltonian operator given by (1). Combining the relativistic energy equation with the operator forms of energy and momentum, led to the Klein-Gordon equation.

$$\begin{aligned} E^2 &= |\mathbf{p^2}| + m^2 \\ -\frac{\partial^2}{\partial t^2}\Psi(x,t) &= \left(-\nabla^2 + m^2 \right) \Psi(x,t) \\ 0 &= \left(\frac{\partial^2}{\partial t^2} - \nabla^2 + m^2 \right) \Psi(x,t) \tag{2} \end{aligned}$$

In the equation above, (2) is a form of the Klein-Gordon equation, more commonly written in the form

$$\left(\partial_\mu \partial^\mu + m^2\right) \Psi(x,t) = 0 \qquad (3)$$

This equation was widely accepted as the relativistic generalization of the Schrödinger equation and was considered viable for describing an electron. However, there were a few physical problems associated with this equation.

A. Negative Energy

Note that the fundamental solutions to (3) are $e^{\pm i p_\mu x^\mu}$, where $p^\mu = (E, \vec{p})$ [4]. However, since (3) is second-order, the solutions admit negative-energy solutions as demonstrated below. Plugging our fundamental solutions into (3), we get that

$$
\begin{aligned}
0 &= \left(p_\mu p^\mu - m^2\right) \\
&= (E^2 - |\mathbf{p}|^2 - m^2) \\
E &= \pm\sqrt{p^2 + m^2}
\end{aligned}
$$

Which means that the energy can take a negative value. The underlying cause for this problem of negative energy comes about due to the fact that (3) is second order in time, an issue that greatly bothered Dirac [3].

B. Other Problems

Another physical problem with the the Klein-Gordon equation is related to its associated probability density. In analogy with the concepts of probability density and probability current in non-relativistic quantum mechanics, we can define the quantities

$$\rho = \frac{i}{2m}\left(\Psi^*\partial_t\Psi - \Psi\partial_t\Psi^*\right), \ \ \vec{J} = -\frac{i}{2m}\left(\Psi^*\nabla\Psi - \Psi\nabla\Psi^*\right)$$

that satisfy the continuity equation $\frac{\partial \rho}{\partial t} + \nabla \cdot \vec{J} = 0$. But notice something troubling: the probability density for the Klein-Gordon equation $\rho = \frac{i}{2m}\left(\Psi^*\partial_t\Psi - \Psi\partial_t\Psi^*\right) = \frac{1}{m}\text{Im}(\Psi\partial_t\Psi^*)$, which is not positive definite. This means ρ cannot be interpreted as a probability density.

Dirac's major contention with the Klein-Gordon was that it was not first order in time. He was quoted as saying [3]

> "The linearity [of the wave equation] in $\frac{\partial}{\partial t}$ was absolutely essential for me. I just couldn't face giving up the transformation theory"

Compelled by the the problems of negative energy, the positive definiteness of the probability density, and the order of the equation, Dirac went about trying to develop an equation for the electron that solved these apparent inconsistencies.

III.   THE DIRAC EQUATION

The ultimate goal of this paper is to examine the spectrum of the hydrogen atom using the Dirac equation. To do so, we will first derive the Dirac equation for a free spin-1/2 particle, using which we will derive the equation that describes a spin-1/2 particle in an electromagnetic field.

A.   Free Spin-1/2 Particle

It is our intent to find an equation that is first order in both temporal and spatial derivatives. This involves taking the "square root" of (3). Based on the form of (3) and our desire to have first-order equations, we can ansatz the following factorization [1].

$$\left(\partial_\mu \partial^\mu + m^2\right) \Psi(x,t) = \qquad (4)$$

$$\left(\sum_{\mu=0}^{3} \alpha_\mu \partial^\mu - \beta\right)\left(\sum_{\nu=0}^{3} \alpha_\nu \partial_\nu + \beta\right)\Psi(x,t)$$

Here α_μ are arbitrary coefficients to be specified. Note a slight notational peculiarity. We have the index ν twice in the bottom. However, we do not intend for α_ν to be a four-vector and hence ν is simply a label of the α's. This is why we have included explicitly the sums, rather than using Einstein's summation notation. For simplicity, let us set $\alpha_0 = 1$. We have just made several assumptions, but if we are able to attain equation (3) by these means, all assumptions become justified. Expanding (4) gives

$$0 = \qquad\qquad\qquad\qquad\qquad\qquad (5)$$

$$\left(\sum_{\mu,\nu=0}^{3} \alpha_\mu \alpha_\nu \partial^\mu \partial_\nu - \sum_{i=1}^{3}\{(\alpha_i\beta + \beta\alpha_i)\partial_i\} - \beta^2\right)\Psi(x,t)$$

In order for (5) to take the same form as (3), we must impose some conditions on α_i and β. Let us look at the first (double) sum in (5). This term must be equal to $\partial^\mu \partial_\mu$ (the sum here is suppressed). For this condition to hold, we must have that $\alpha_i \alpha_j = \delta_{ij}$ where δ_{ij} is the Kronecker delta function. Notice that in (4), we could have done the multiplication from the other side, in which case we would have gotten $\alpha_j \alpha_i = \delta_{ij}$. It follows that $\{\alpha_i, \alpha_j\} = 2\delta_{ij}$ Moving onto the second term, we recall that (3) contains no first derivatives which means

that $\alpha_i\beta + \beta\alpha_i = 0$. Finally, we want $-\beta^2 = m^2$. Consolidating our conditions, we get that

$$\{\alpha_i, \alpha_j\} = 2\delta_{ij} \tag{6}$$
$$\{\alpha_i, \beta\} = 0 \tag{7}$$
$$\beta^2 = -m^2 \tag{8}$$

Here is the first departure from conventional thought. Note that if α_i and β are simply numbers (6), (7), and (8) are incompatible. Note that (7) implies either α_i or β vanishes, which would violate either (6) or (8). A possible solution to this conundrum is to extend our consideration from scalars to matrices. It can be shown that the most restrictive space for these quantities is the set of 4×4 matrices [2].

From (8), we may write $\beta = im\alpha_4$, with $\alpha_4^2 = 1$. With this simplification, conditions (6)-(8) can be condensed to a single condition

$$\alpha_i, \alpha_j = 2\delta_{ij}, \ (i = 1, 2, 3, 4) \tag{9}$$

There are several sets of matrices that satisfy (9), however we will use the convention in [2], namely

$$\alpha_i = \begin{pmatrix} 0 & \sigma_i \\ \sigma_i & 0 \end{pmatrix} \ (i = 1, 2, 3) \quad \alpha_4 = \begin{pmatrix} I_2 & 0 \\ 0 & -I_2 \end{pmatrix} \tag{10}$$

With our coefficients determined by (10), we can finally write our first-order equation from (4), given by

$$\partial_0 + \vec{\alpha} \cdot \nabla + im\alpha_4 = 0$$
$$p_0 - \vec{\alpha} \cdot \vec{p} - m\alpha_4 = 0 \tag{11}$$

Where $\vec{\alpha} = (\alpha_1, \alpha_2, \alpha_3)$ and $\vec{p} = (p_1, p_2, p_3)$

B. Solutions and Antimatter

We can now analyze (11) in more detail. Firstly, notice that the operator on the left hand side of (11) is a four-dimensional matrix. For this to be able to act on Ψ, it must be a four-component object. The object that describes the solution to the Dirac equation is called a *spinor* [4]. A spinor is an element of a complex vector space The spinor solution to (11) is given by $\Psi(x,t) = u\exp{(i(px - Et))}$, where u is a constant 4-spinor. Plugging this into the Dirac equation, we get two independent, positive-energy solutions for u [5]

$$u_1 = \begin{pmatrix} 1 \\ 0 \\ \frac{p_3}{E+m} \\ \frac{p_1+ip_2}{E+m} \end{pmatrix}, \ u_2 = \begin{pmatrix} 0 \\ 1 \\ \frac{p_1-ip_2}{E+m} \\ \frac{-p_3}{E+m} \end{pmatrix}$$

However, we also have two similar solutions for the negative energies, making a total of four independent solutions. These negative energy solutions confounded Dirac for several years. He had attempted to remedy this conundrum by proposing his "Hole Theory," which stated that the negative-energy states were normally filled by one electron each (in accord with the Pauli-Exclusion Principle), which means they are unavailable [3]. This interpretation was not exactly correct. Instead, we interpret these negative energy states as electron antiparticles, also known as positrons [4].

C. Electron in an Electromagnetic Field

Section **IIIB** was devoted to formulating the relativistic equation for a free spin-1/2 particle. We are interested in studying an electron in an electromagnetic field (particularly, the one formed by the hydrogen atom). In quantum mechanics and special relativity, an electromagnetic field is represented by a four-vector

$$A^\mu = (\Phi, \vec{A})$$

Where Φ is the scalar potential and $\vec{A}$ is the electromagnetic vector potential. We can obtain the more common electric and magnetic fields by the identities

$$\vec{E} = -\nabla\Phi - \frac{\partial\vec{A}}{\partial t}$$
$$\vec{B} = \nabla \times \vec{B}$$

The motion of an electron in an electromagnetic field described by A^μ is described by making the following substitution in the free particle Lagrangian

$$p^\mu \longrightarrow p^\mu - eA^\mu$$

Where e is the positron charge [5]. We can use this substitution to modify (11), giving us the Dirac equation in an electromagnetic field

$$0 = (p^0 - e\Phi) - \vec{\alpha} \cdot \left(\vec{p} - e\vec{A}\right) - m\alpha_4$$
$$p^0 = \vec{\alpha} \cdot \left(\vec{p} - e\vec{A}\right) + m\alpha_4 + e\Phi \tag{12}$$

Since p^0 is the energy operator, $p^0 \to \hat{H}$, and $\vec{p} \to -i\nabla$. With this is mind, we can write the Hamiltonian of the electron in an electromagnetic field.

$$\hat{H} = -i\vec{\alpha} \cdot \nabla - e\alpha \cdot \vec{A} + m\alpha_4 + e\Phi \tag{13}$$

Recall that, as in the case of non-relativistic quantum mechanics, we wish to solve the time-independent

Schrödinger equation $\hat{H}\psi = E\psi$. Here, we wish to solve the exact same equation, with the Hamiltonian given by (13). Consolidating everything, we get that the equation of interest is

$$-i\vec{\alpha}\cdot\nabla\Psi - e\alpha\cdot\vec{A}\Psi + m\alpha_4\Psi + e\Phi\Psi = E\Psi \quad (14)$$

This is the general form of the relativistic equation for an electron in an electromagnetic field. We can now use this formalism to construct and solve the equation for the hydrogen atom. Before launching into this consideration, we will make a few comments that will explain the consequences of the Dirac equation and some concepts that will aid our discussion of the hydrogen atom.

D. Spin and the Dirac Equation

Crucial to our treatment of the hydrogen atom will be the effects of spin. We have asserted that the Dirac equation describes a spin-1/2 particle. This can be seen directly from the Dirac equation. In this theory, the equation of interest is

$$i\frac{\partial\Psi}{\partial t} = H\Psi = -i\vec{\alpha}\cdot\nabla\Psi + m\alpha_4\Psi \quad (15)$$

This is simply (11) (or (13) with the four-potential set to zero). Note that $[H, \vec{p}] = 0$, which means momentum is a constant in time. This, however, is not true for the angular momentum defined as

$$\vec{L} = \vec{r}\times\vec{p} = -i\vec{r}\times\nabla$$

Let us attempt to calculate the commutator of the angular momentum with the Hamiltonian. This will give us insight into the true conserved quantity.

$$\begin{aligned}
[H, L_i] &= -[\vec{\alpha}\cdot\nabla, \epsilon_{ijk}r_j\nabla_k] \\
&= -\epsilon_{ijk}\alpha_\ell[\nabla_\ell, r_j\nabla_k] \\
&= -\epsilon_{ijk}\alpha_\ell\delta_{\ell j j}\nabla_k \\
&= -\epsilon_{ijk}\alpha_j\nabla_k \\
&= -\vec{\alpha}\times\nabla \quad (16)
\end{aligned}$$

Note that we are summing over repeated indices in this calculation. By virtue of the commutation relations satisfied by the α matrices, we notice that [5]

$$[H, \vec{\sigma}] = 2\vec{\alpha}\times\nabla \quad (17)$$

Where $\vec{\sigma} = (\sigma_1, \sigma_2, \sigma_3)$. From (16) and (17), we can construct the conserved quantity

$$\begin{aligned}
[H, \vec{J}] &= 0 \\
\vec{L} + \frac{\hbar}{2}\vec{\sigma} &= \hbar\vec{J} \quad (18)
\end{aligned}$$

Equation (18) is identical to the one we attain in non relativistic quantum mechanics $\vec{L} + \vec{S} = \vec{J}$. Here $\vec{S}$ is the spin operator and $\vec{J}$ is the total angular momentum (orbital plus spin) operator. Notice that for this equation, we have restored the $\hbar$'s to make the connection with the non-relativistic equation. Looking at the spin term, it is clear that $\frac{1}{2}\hbar\vec{\sigma}$ describes the angular momentum of a spin-1/2 particle, justifying our claim.

IV. HYDROGEN ATOM

The purpose of the previous section was to obtain the equation describing an electron in an electromagnetic field. We can now consider the electron in an hydrogen atom potential. Starting with (14), we make a few clarifications to get to our equation of interest. Firstly, note that the potential for the hydrogen atom is given by $\Phi = -e/r$ which means $e\Phi = -e^2/r$. In addition, an important property of electromagnetic theory is that the vector $\vec{A}$ is simply a gauge that we can pick arbitrarily so long as its curl is $\vec{B}$. For initial considerations, there is no magnetic field experienced by the electron, so we may fix $\vec{A}$ to be zero [5]. This reduces (14) to

$$H = -i\vec{\alpha}\cdot\nabla\Psi + m\alpha_4 - \frac{e^2}{r} \quad (19)$$

Where α_4 is given in (10). Just as in section **IIIC**, we define the total angular momentum operator $\vec{J} = \vec{L} + \vec{S}$. In exact analogy with the total angular momentum operator in non-relativistic quantum mechanics, we can define J_z (with corresponding eigenvalues j_z) as the z-component of $\vec{J}$ in (18) and $\vec{J}^2$. We need to construct a complete set of commuting observables in order to continue with this calculation. To completely specify a state of the electron, we need to construct a complete set of commuting observables. As in the non-relativistic case, we could consider the set J^2, J_z, S. However, in this case, $\vec{S}$ does not commute with the Hamiltonian. In its stead, we introduce another operator, which encodes the same information and commutes with the Hamiltonian [5].

$$K = \alpha_4\vec{\sigma}\cdot\vec{J} - \frac{1}{2}\alpha_4 \quad (20)$$
$$\begin{aligned}
K^2 &= L^2 + \vec{\sigma}\cdot\vec{J} + 1 \\
&= J^2 + \frac{1}{4} \quad (21)
\end{aligned}$$

It can be shown that this operator commutes with the Hamiltonian and it accounts for the spin component of the angular momentum. The eigenvalues of K^2 are $k^2 = j(j+1) + \frac{1}{4} = (j+\frac{1}{2})^2 \implies k = \pm(j+\frac{1}{2})$. With this in mind, we will try to rewrite the Hamiltonian in terms of K. The only term we need to consider is the $\vec{\alpha}\cdot\nabla$ term. We want an equation in the polar radial variable r. In

order to do this, we use the identity given by equation 32 in [2].

$$(\vec{\sigma} \cdot \vec{A})(\vec{\sigma} \cdot \vec{B}) = (\vec{A} \cdot \vec{B}) + i(\vec{\sigma} \cdot (\vec{A} \times \vec{B})) \quad (22)$$

By use of (22), we get that

$$\begin{aligned} (\vec{\sigma} \cdot \vec{r})(\vec{\sigma} \cdot \vec{p}) &= \vec{\sigma} \cdot (\vec{r} \times (\vec{r} \times \nabla)) \\ &= (\vec{\sigma} \cdot \vec{r})(\vec{r} \cdot \nabla) - r^2(\vec{\sigma} \cdot \nabla) \end{aligned}$$

Here we have used the fact that $\vec{r} \cdot \vec{L} = 0$. Using this result and some computation (for full calculation, see [5]), we settle on the Hamiltonian in polar coordinates.

$$H = i(\vec{\alpha} \cdot \vec{r})\left(\frac{\alpha_4 K}{r^2} - \frac{1}{r^2} - \frac{1}{r}\frac{\partial}{\partial r}\right) + m\alpha_4 - \frac{e^2}{r} \quad (23)$$

A. Solving the Equation

Plugging in the explicit forms of β and α_r and using a two-component representation of the spinor

$$\Psi = \begin{pmatrix} \psi_1 \\ \psi_2 \end{pmatrix}$$

We get the following matrix equation for these components.

$$\begin{aligned} \frac{\partial}{\partial r}\begin{pmatrix} \psi_1 \\ \psi_2 \end{pmatrix} &= \begin{pmatrix} \frac{-(1-k)}{r} & -\left(E+m+\frac{\alpha}{r}\right) \\ \left(E-m-\frac{\alpha}{r}\right) & \frac{-(1+k)}{r} \end{pmatrix}\begin{pmatrix} \psi_1 \\ \psi_2 \end{pmatrix} \\ &\equiv M(r)\begin{pmatrix} \psi_1 \\ \psi_2 \end{pmatrix} \end{aligned} \quad (24)$$

Where α is the fine structure constant. Before attempting to solve this equation, let us examine its asymptotic properties. Note that as $r \to \infty$, we get the following simple equation

$$\frac{\partial}{\partial r}\begin{pmatrix} \psi_1 \\ \psi_2 \end{pmatrix} = \begin{pmatrix} 0 & -(E+m) \\ E-m & 0 \end{pmatrix}\begin{pmatrix} \psi_1 \\ \psi_2 \end{pmatrix}$$

The solutions to this equation go as $\psi_\pm \sim e^{\pm ipr}$, recalling that $p = \sqrt{E^2 - m^2}$. With this in mind, and by defining functions $f_1(r), f_2(r)$

$$\begin{aligned} f_1(r) &= ure^{ipr} \\ f_2(r) &= vre^{ipr} \end{aligned}$$

we can construct the matrix equation

$$\frac{\partial}{\partial r}\begin{pmatrix} f_1 \\ f_2 \end{pmatrix} = \begin{pmatrix} ip+\frac{k}{r} & -\left(E+m+\frac{\alpha}{r}\right) \\ \left(E-m+\frac{\alpha}{r}\right) & ip-\frac{k}{r} \end{pmatrix}\begin{pmatrix} f_1 \\ f_2 \end{pmatrix}$$

We proceed to solve this differential equation using a series expansion [2]

$$\begin{aligned} f_1 &= \sum_{s=0}^{\infty} a_s r^s \\ f_2 &= \sum_{s=0}^{\infty} b_s r^s \end{aligned} \quad (25)$$

Substituting these expansions into (24), we get the following recursion relations

$$\begin{aligned} \alpha a_s - (E-m)a_{s-1} &= -ipb_{s-1} + (k+s)b_s \quad (26) \\ \alpha b_s + (E+m)b_{s-1} &= ipa_{s-1} + (k-s)a_s \quad (27) \end{aligned}$$

Solving these recursion relations gives us

$$\begin{aligned} a_s &= \frac{(E-m)\alpha + ip(k+s)}{(E-m)\alpha^2 + (E-m)(s^2-k^2))}c_s \\ b_s &= \frac{ip\alpha(E-m)(k-s)}{(E-m)\alpha^2 + (E-m)(s^2-k^2))}c_s \\ c_{s+1} &= \frac{((E-m)^2 + p^2)\alpha + 2ip(E-m)s}{(E-m)\alpha^2 + (E-m)(s^2-k^2))}c_s \end{aligned}$$

Where $c_s \equiv (E-m)a_{s-1} - ipb_{s-1}$. In order to prevent the solution from blowing up, we suppose that $c_s \neq 0$ for some $s = n + \epsilon$ for $n \in 1, 2, 3, \dots$ [5]. This supposition gives us the equations

$$\begin{aligned} 0 &= \alpha^2 + \epsilon^2 - k^2 \quad (28) \\ 0 &= ((E-m)^2 + p^2)\alpha + 2(\epsilon+n)ip(E-m) \quad (29) \end{aligned}$$

From (28), it follows that $\epsilon = \sqrt{k^2 - \alpha^2}$ and

$$\begin{aligned} (n+\epsilon)^2 &= \left(\frac{((E-m)^2 + p^2)^2}{-4p^2(E-m))}\right) \\ &= \left(\frac{((E-m)^2 + E^2 - m^2)^2}{4(m^2-E^2)(E-m))}\right) \\ &= \frac{E^2\alpha^2}{(m^2-E^2)} \end{aligned} \quad (30)$$

Combining (30) and the fact that $\epsilon = \sqrt{k^2 - \alpha^2}$, we obtain the desired result.

$$E = \frac{mc^2}{\sqrt{1 + \frac{\alpha^2}{(n+\sqrt{k^2-\alpha^2})^2}}} \quad (31)$$

Notice that we have restored c in this equation. The reason for this is that we would like to compare this result to the non-relativistic case.

B. Comparison to Non-Relativistic Case

In order to investigate this comparison, we would like to make a few clarifications about the expression derived in (31). Recall that the k's are the eigenvalues of the K operator. It can be shown (see [2]) that the principle quantum number, N is related to n and k by $N = n + |k|$. With this in mind, we can expand (31) in powers of $\alpha \sim \frac{1}{137}$ to get

$$E = mc^2 \left(1 - \frac{\alpha^2}{2N^2} + \frac{\alpha^4}{8N^4} \left(3 - \frac{4N}{|k|} \right) \right) \qquad (32)$$

Where the second term is what we get without any corrections in non-relativistic quantum mechanics. The third term corresponds to the fine-structure term. Recalling from (21) and the discussion following it, $k = \pm(j + \frac{1}{2})$ which means $|k| = j + \frac{1}{2}$. This gives us

$$E = mc^2 \left(1 - \frac{\alpha^2}{2N^2} + \frac{\alpha^4}{8N^4} \left(3 - \frac{4N}{j + \frac{1}{2}} \right) \right) \qquad (33)$$

Which is miraculously the exact expression obtained in [6].

V. CONCLUSIONS

Without the conception of the Dirac equation, the fine structure shift in the hydrogen atom can be derived by considering three separate effects: relativistic correction, spin-orbit coupling, and the *Darwin Shift* [6]. The Dirac equation equation elucidates many puzzling questions that challenged the early theories of relativistic quantum mechanics. In particular, it solved the problems of negative energy solutions, linearity of the time derivative, and the positive definiteness of the probability density. However, what is truly amazing about this equation is that it is able to predict to high experimental accuracy the shift in the energy levels of the hydrogen atom in a manner that agrees exactly with what was derived using perturbation theory in non-relativistic quantum mechanics.

VI. ACKNOWLEDGEMENTS

[1] Shankar, Ramamurti. Principles of Quantum Mechanics. New York: Plenum, 1994. Print.
[2] Dirac, P. A. M. The Principles of Quantum Mechanics. Oxford: Clarendon, 1981. Print.
[3] Pais, Abraham. Inward Bound: Of Matter and Forces in the Physical World. Oxford: Clarendon, 1986. Print.
[4] Peskin, Michael Edward, and Daniel V. Schroeder. An Introduction to Quantum Field Theory. Reading, MA: Addison-Wesley, 1995. Print.
[5] Dyson, Freeman J., and David Derbes. Advanced Quan-

tum Mechanics. Hackensack, NJ: World Scientific, 2007. Print.
[6] Harrow, Aram. "8.06 Spring 2014 Lecture Notes." Massachusetts, Cambridge. Reading.
[7] Kragh, Helge. "The Fine Structure of Hydrogen and the Gross Structure of the Physics Community." Historical Studies in the Physical Sciences 15.2 (1985): 67-125. Web. 30 Apr. 2014.

Measurement and *Verdamnte Quantenspringerei*: the Quantum Zeno paradox

Yihui Quek

MIT Physics Department., 77 Massachusetts Ave., Cambridge, MA 02139
(Dated: May 1, 2014)

In the Quantum version of the Zeno paradox, frequent measurements of a quantum state will inhibit transitions to another quantum state due to wave function collapse. This Quantum Zeno Effect was observed in 1990 by Itano et al[2] on an induced transition between two $^9Be^+$ ground state hyperfine levels. In 2014, it was found by Signoles and Haroche[3] that it is possible to not only halt the evolution of the quantum system; but also tailor its evolution *within a customizable border* around a degenerate Hilbert space. This paper reviews the theory and experiments of both QZE and QZD, two phenomena that elucidate the true meaning of quantum measurement.

I. INTRODUCTION

What is a measurement? Even in 490-430BC, the Eleatian philosopher Zeno demonstrated the counterintuitive nature of measurement with his arrow paradox, which concludes that an arrow in flight at any one instant in time cannot be moving. It is not moving to where it is not - for no time has elapsed for it to make such a movement. Neither is it moving to where it is, because it is already there. But, if at every instant of time the arrow is not moving, then motion is impossible.

The quantum version of this is known as the Quantum Zeno Effect(QZE). Just as an arrow whose motion is scrutinized at every instant of time never reaches its target, it is experimentally possible to inhibit transitions between quantum states by frequent measurements. The first half of the paper is devoted to understanding the 1990 experimental implementation of QZE by Itano [2], with the aim of impressing upon readers the causal relationship between measurement and wavefunction collapse, a relationship whose nature tormented Schrödinger in the nascent days of Quantum Theory (he described measurement as 'damned quantum jumping' – *verdamnte quantenspringerei*).

Qualitatively, the experiment goes as follows: Starting off in an initial state that we want to confine the particle in, we repeatedly ask the particle "Have you decayed yet?". Importantly, we make the interrogation at very short time intervals, namely T/n where $n \longrightarrow \infty$. We will see later that in the quantum world, 'asking' translates to *projecting* the state onto exactly one of the eigenstates of the measurement operator. Between t=0 and the first interrogation, the state might have evolved into some superposition of eigenstates due to environmental influence, but measurement – i.e. wavefunction collapse – eliminates this decoherence.

If we are to achieve our goal of confining the particle in the initial state, we must ensure that the 'asking' yields the answer 'not decayed' (a null measurement). We capitalize on the key fact that the probability of decay is *quadratic* at short time scales. Then, because we interrogate at short time scales, the probability of decay is vanishingly small, and the probability of the particle not having decayed (which is our desired outcome) approaches 1.

Readers will be able to gain some mathematical intuition for this in Section II. Following the description of the experiment in Section III, we will lay down a more rigorous mathematical framework in terms of density operators for the QZE in Section IV, from which the step to Quantum Zeno Dynamics(QZD) is merely an allowance for a multi-dimensional subspace of evolution. This is easy to conceive of mathematically, but the experimental implementation, which we consider in Section V is full of subtleties, and we will try to understand the basics of the Signoles and Haroche experiment of 2014 [3] in Section V.

II. QUANTUM ZENO EFFECT

There are two ways that the state of a quantum system can change in time. Firstly, the state could evolve in time according to the time-dependent Schrödinger Equation, $i\hbar\frac{\partial|\psi\rangle}{\partial t} = H|\psi\rangle$. H is the Hamiltonian of the system, usually the result of environmental factors beyond our control. Alternatively, one could *measure* the system, *forcing* a state collapse. The state collapses into the eigenstate $|i\rangle$ of the measurement operator Q corresponding to the measured eigenvalue q: $Q|i\rangle = q|i\rangle$. Prior to the measurement the state may be in a superposition of operator eigenstates, but after the measurement the state is found (with certainty) in the eigenstate to which it has collapsed.

Now we consider a situation that incorporates both pictures: a given system that starts off in state $|\psi_0\rangle = |\psi(t=0)\rangle$ is unstable, evolving *unitarily* in time due to some time-independent Hamiltonian H. If we measure it after a time t, the state will have evolved into

$$|\psi(t)\rangle = e^{iHt}|\psi(0)\rangle \qquad (1)$$

Here we have set $\hbar$ to 1, and we will do so in all subsequent discussions. We will henceforth be interested in whether, at any future time t, the system is in the state $|\psi_0\rangle$ in which it started out – whether it has "survived". To this end we (following [9]) define two useful parameters: the "survival" amplitude $\mathcal{A}(t)$ and the probability $\mathscr{P}(t)$ that the state has survived, which is the amplitude

squared:

$$\mathcal{A}(t) = \langle\psi_0|\psi(t)\rangle = \langle\psi_0|e^{-iHt}\psi_0\rangle \qquad (2a)$$

$$\mathcal{P}(t) = |\mathcal{A}(t)|^2 = |\langle\psi_0|e^{-iHt}\psi_0\rangle|^2 \qquad (2b)$$

Now take t to be an infinitesimally small period of time, δt. Then, expanding the exponential and taking out the time dependence from the inner product, the above two equations become:

$$\mathcal{A}(\delta t) = 1 + i\delta t\langle\psi_0|H|\psi_0\rangle - \frac{1}{2}\delta t^2\langle\psi_0|H^2|\psi_0\rangle + ... \tag{3a}$$

$$\mathcal{P}(\delta t) = 1 - \delta t^2\langle H^2\rangle_0 + \delta t^2\langle H\rangle_0^2 + O(\delta t^4)$$

$$= 1 - \frac{\delta t^2}{\tau_z^2} + O(\delta t^4) \tag{3b}$$

where we define a timescale, the *Zeno time*, τ_z:

$$\frac{1}{\tau_z^2} \equiv \langle H^2\rangle_0 - \langle H\rangle_0^2 \tag{4}$$

Physically-oriented readers might want to gain some intuition for the meaning of the Zeno time. Consider a Hamiltonian that has both a free and interaction part, which are diagonal and off-diagonal respectively: $H = H_0 + H_{int}$. Then, $\langle H_{int}\rangle_0 = 0$ and if the initial state is an eigenstate of the free Hamiltonian $H_0|\psi_0\rangle = \omega_0|\psi_0\rangle$, the Zeno time depends solely on H_{int}:

$$\frac{1}{\tau_z^2} = \langle H_{int}^2\rangle_0 = \sum_n \langle\psi_0|H_{int}|\psi_n\rangle\langle\psi_n|H_{int}|\psi_0\rangle \tag{5}$$

where we use the Completeness Relation for the second equality. This form is analogous to Fermi's Golden Rule, which gives the inverse lifetime γ of a decaying quantum system under a perturbation W, which we associate with H_{int}.

$$\gamma = 2\pi\sum_f |\langle\psi_f|W|\psi_0\rangle|^2\delta(\omega_f - \omega_0) \tag{6}$$

In any case, the probability of survival is now *quadratic* in this characteristic time. We can now capitalize on the quadratic-time regime to make the probability of decay, $1 - \mathcal{P}(\delta t)$, negligible. That is, the probability of making a transition to any state $|\psi_0'\rangle$ other than the initial state , is

$$\mathcal{P}(|\psi_0\rangle \to |\psi_0'\rangle) \approx 1 - \left[1 - \left(\frac{\delta t}{\tau_z}\right)^2\right] = \left(\frac{\delta t}{\tau_z}\right)^2 \tag{7}$$

which is negligible because δt is small. Formally, if we divide our total amount of time, T, into N infinitesimal subintervals τ such that $T = N\tau$, then the probability of survival $\mathcal{P}(T)$ after the total time T consisting of N subintervals of length τ is now a product of the probabilities of survival after each τ subinterval:

$$\mathcal{P}(T) = [\mathcal{P}(\tau)]^N = \left[\mathcal{P}\left(\frac{T}{N}\right)\right]^N$$

$$= \left[1 - \left(\frac{T}{N\tau_z}\right)^2\right]^N \tag{8}$$

$$\xrightarrow{\text{N large}} \approx exp\left[-\frac{1}{N}\left(\frac{T}{\tau_z}\right)^2\right] \xrightarrow{N\to\infty} 1$$

where we have replaced δt in equation (12) with the small time interval $\frac{T}{N}$ in the second line. That is all well and good, but let us take a step back and compare this with the experimental framework we have outlined in the introduction. Where did we perform the "asking" at intervals of $\frac{T}{N}$? The answer is that it is implicit in (8). If we had let the particle evolve for a long time T with no regular interrogation, $\mathcal{P}(T)$ is merely eq (2b) with large t, where the Taylor expansion of the exponential is no longer valid and $\mathcal{P} < 1$. Instead, we collapse the state after every $\tau = \frac{T}{N}$, in effect 'resetting' the state to its initial with high probability given in eqn 12. In order for the state to have survived after a long time T, there is only one path available to it: it must survive at every infinitesimal subinterval τ. Probability of survival after T, $\mathcal{P}(T)$, is therefore a product of the probabilities of survival at the end of each τ.

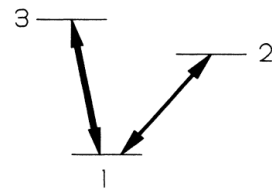## III. EXPERIMENTAL REALIZATION OF QUANTUM ZENO EFFECT

FIG. 1: Simplified energy level diagram for the Quantum Zeno Effect, taken from [2]. Level 2 is an excited metastable state that seldom decays to Level 1. On the other hand, the $1 \to 3$ transition is strongly allowed.

In 1990, a landmark experiment using laser-cooled trapped $^9Be^+$ ions was performed by Itano and Wineland at NIST [2] that experimentally demonstrated the validity of the QZE. Referring to the level structure shown in figure 1, the ion starts off in level 1, and the experiment aims to prevent the "decay transition" from level $1 \longrightarrow$ level 2. In terms of the formalism of the previous section, $|\psi_0\rangle$ is level 1 (and level 3, as we will see below) and $|\psi_0'\rangle$ is level 2. Then, in order to simulate the environmental forces causing the decay, H is artificially applied – a radiofrequency(rf) drive pulse having the frequency $\Omega = \frac{E_2 - E_1}{\hbar}$. Because this exactly corresponds

to the energy separation between the two states, an ion subject to this drive would tend to undergo the $1 \longrightarrow 2$ decay. In the interaction picture, H is of the form

$$H = H_{int} = \Omega\sigma_x = \begin{pmatrix} 0 & \Omega \\ \Omega & 0 \end{pmatrix} \qquad (9)$$

The sole purpose of level 3 is results verification. If we were able to directly count the populations of ions in level 1 and level 2, then level 3 would not be necessary. Lacking such capabilities, we must instead exploit the fact that once an ion has 'decayed' to level 2, it is 'shelved' there forever (no photons are emitted or absorbed). On the other hand, ions in levels 1 and 3 are free to cycle from one to the other, emitting or absorbing a photon in the process. We create this freedom by coupling levels 1 and 3 via a strongly allowed transition, while there is no such coupling between levels 1 and 2. In effect, we now know what is going on in the ion: if it fluoresces, we has succeeded (because the atom is oscillating between levels 1 and 3, and has not gone over to the 'dark' side, ie. level 2).

To recapitulate, the aim is to prevent the $1 \longrightarrow 2$ transition via frequent measurements. Each measurement will project the ion onto either level 1 or 2. It is easy to understand this experiment using the simple concept of a spin-half particle rotating in a B-field. We make the association $|1\rangle = |+\rangle = \begin{pmatrix} 1 \\ 0 \end{pmatrix}$ and $|2\rangle = |-\rangle = \begin{pmatrix} 0 \\ 1 \end{pmatrix}$. Then, the spin vector representing the state is $|\vec{n}\rangle = \cos(\frac{\theta}{2})|+\rangle + \sin(\frac{\theta}{2})e^{i\phi}|-\rangle$. Recalling the form of unitary time evolution, the Hamiltonian forms a rotation operator $R_{\sigma t}(\vec{x}) = e^{-iH_{\text{int}}t} = e^{-i\Omega t\sigma_x}$. This has the effect of causing the spin to precess about the x-axis at angular frequency Ω, which we term the Rabi frequency. Then because the spin starts out in $|+\rangle = |z; +\rangle$ (level 1), its state just before the first measurement at τ^- is

$$|\psi(\tau)\rangle = e^{-i\Omega\tau\sigma_x}|+\rangle = \cos(\frac{\Omega\tau}{2})|+\rangle + \sin(\frac{\Omega\tau}{2})e^{i\frac{\pm\pi}{2}}|-\rangle$$

$$= \begin{pmatrix} \cos(\frac{\Omega\tau}{2}) \\ \pm i\sin(\frac{\Omega\tau}{2}) \end{pmatrix} \qquad (10)$$

and the vector describing the direction is $\vec{n} = (0, -\sin\Omega\tau, \cos\Omega\tau)$ (the spin has precessed ever so slightly in the y-z plane). But the measurement projects the ion back along the z-axis, so only the z-component remains: $\vec{n} = (0, 0, \cos\Omega\tau)$. The aim of QZE is to make this as close to $\vec{n} = (0, 0, 1)$ as possible, which will only be the case if τ is short (we choose $\tau = \frac{2\pi}{N\Omega}$, N large, since the driving pulse is a π-pulse)! Substituting this into eqn (10), $\mathscr{P}_1(\tau) = cos^2(\frac{\pi}{N})$ and $\mathscr{P}_1(T) = [\mathscr{P}_1(\tau)]^N = cos^N(\frac{\pi}{N})$, which goes to 1 as $N \longrightarrow \infty$.

There is another way to look at this: consider what happens to the density matrix describing the two-level system (i.e. only 1 ion) each time we make a measurement. The density matrix of a spin-$\frac{1}{2}$ particle $|\vec{n}\rangle$ is

$$\rho = \frac{I + \vec{n}.\vec{\sigma}}{2} = \frac{1}{2}\begin{pmatrix} 1 + n_z & n_x - in_y \\ n_x + in_y & 1 - n_z \end{pmatrix} \qquad (11)$$

An important concept is that we can immediately see $\mathscr{P}(t)$ from the expectation of the density matrix on the corresponding state vector, in other words, *the diagonal matrix elements*:

$$\mathscr{P}_1(t) = \rho_{11}; \mathscr{P}_2(t) = \rho_{22} \qquad (12)$$

. In particular, the z-component of $\vec{n}$ is given by $n_z = \rho_{11} - \rho_{22} = \mathscr{P}_1 - \mathscr{P}_2$. n_x and n_y are going to be 0 right after each measurement because the ion is unambiguously either $|+\rangle$ with probability 1 or $|-\rangle$ with probability 1. This means that ρ *for just one ion* will be **purely diagonal**: if the ion has been projected to level 1, ρ is $\begin{pmatrix} 1 & 0 \\ 0 & 0 \end{pmatrix}$; if it has been projected to level 2, $\begin{pmatrix} 0 & 0 \\ 0 & 1 \end{pmatrix}$.

If we consider a system of many ions, some will have been projected into level 1, $|+\rangle$ and others (if we are doing our experiment right, not too many) into level 2, $|-\rangle$. Whatever the proportions are, note that if we take ensemble average of all the ions' density matrices right after any measurement, there will be no off-diagonal elements whatsoever, since there are no off-diagonal elements ρ of any single ion. **Measurement introduces decoherence and destroys the off-diagonal elementsof ρ.**

IV. DENSITY MATRIX FORMALISM; STEPS TOWARDS QZD

Having understood the evolution of the density matrix in the case where the initial state is in a one-dimensional subspace, it is easy to generalize the picture to multiple dimensions, which will take us into the realm of QZD. The aim of QZD is slightly different from QZE; rather than prevent transition to another energy eigenstate as in QZE, QZD aims to prevent transitions to another subspace of the operator. For example, choose the total angular momentum operator, $\hat{J}^2$. Recall that each eigenstate $|J, m_J\rangle$ is characterized by two quantum numbers: J, the total angular momentum, and J_z, its projection onto the z-axis. For every value of J, J_z is allowed to run from $[-J, J]$. The aim of QZD is then to confine the particle within a J subspace; ie. we force the total angular momentum to stay constant, but let its projection onto the z-axis vary.

Since we are now working with many degenerate eigenstates, it will behoove us to study the density matrix of the entire system under unitary time evolution. That is, we will want to generalize the 1D discussion in section II. However, we will find that many principles used in the 1D case are equally applicable here.

Let the total Hilbert space be $\mathcal{H}$, with dimension m. Then, the initial density matrix is assumed to belong to an s-dimensional Hilbert space $\mathcal{H}_P$, with $s < m$. The measurement therefore corresponds to determining whether the system is still in $\mathcal{H}_P$. We want to ask the state 'Have you evolved into this particular eigenstate of

$\hat{A}$, $|a_i\rangle$?' A meaningful answer to this question is the density operator of the system, which encodes the probability of being in each eigenstate of each subspace – for instance, in the two-level system, $\text{Prob}(|+\rangle) = \langle+|\rho|+\rangle = \rho_{11}$. What happens to the density operator after a measurement? Recall what happened in QZE for one particle:

$$\frac{1}{2}\begin{pmatrix} 1 + n_z & n_x - in_y \\ n_x + in_y & 1 - n_z \end{pmatrix} \xrightarrow{\text{measurement}} \begin{pmatrix} 1 & 0 \\ 0 & 0 \end{pmatrix} \text{ or } \begin{pmatrix} 0 & 0 \\ 0 & 1 \end{pmatrix} \tag{13}$$

That is, knowing the measurement projected the particle into the $|+\rangle$ eigenstate means we know that the new ρ corresponds to the first of the options above. This can be re-expressed as

$$\rho_{nodecay} = \begin{pmatrix} 1 & 0 \\ 0 & 0 \end{pmatrix} = \Big[\text{Prob}(|+\rangle)\Big]|+\rangle\langle+| = \langle+|\rho|+\rangle\,|+\rangle\langle+|$$

$$= \Big[|+\rangle\langle+|\Big]\rho\Big[|+\rangle\langle+|\Big] = \mathcal{P}_+\rho\mathcal{P}_+ \tag{14}$$

where $\mathcal{P}_+$ is the projection operator $|+\rangle\langle+|$. Since an 'undecayed' measurement in QZE corresponds to projection onto exactly 1 eigenstate, $\text{Prob}(\text{undecayed}) = \text{Prob}|+\rangle = 1$. But this is not true in QZD, for the measurement projects the state into subspaces, not single eigenstates. Hence, an 'undecayed' measurement in QZE means that the state is in the subspace but could be in *any superposition* of its constituent eigenstates, and projection onto $\mathcal{H}_P$ (represented by the s-dim block in ρ) looks like:

$$\begin{pmatrix} d_{11} & \cdots & d_{1s} & \cdots & d_{1m} \\ d_{21} & \cdots & d_{2s} & \cdots & d_{2m} \\ \vdots & \ddots & \vdots & & \vdots \\ d_{s1} & \cdots & d_{ss} & \cdots & d_{sm} \\ \vdots & \ddots & \vdots & & \vdots \\ d_{m1} & \cdots & d_{ms} & \cdots & d_{mm} \end{pmatrix} \mapsto \begin{pmatrix} D_{11} & \cdots & D_{1s} & \cdots & 0 \\ D_{21} & \cdots & D_{2s} & \cdots & 0 \\ \vdots & \ddots & \vdots & & \vdots \\ D_{s1} & \cdots & D_{ss} & \cdots & 0 \\ \vdots & \ddots & \vdots & & \vdots \\ 0 & \cdots & 0 & \cdots & 0 \end{pmatrix} \tag{15}$$

Generalizing eqn (14) (still considering only one particle) to the multi-dimensional subspace in QZD spanned by $|d_i\rangle's$,

$$\rho_{new} \equiv \sum_{j=1}^{m} c_j |d_j\rangle \sum_{i=1}^{m} c_i^* \langle d_i| \qquad \text{By definition of } \rho$$

$$= \mathcal{N} \sum_{i,j\in\mathcal{H}} |d_j\rangle \underbrace{\langle d_j|\rho|d_i\rangle}_{c_j c_i*} |d_i\rangle \quad \text{Matrix expansion of (15)}$$

$$= \mathcal{N}\mathcal{P}\rho\mathcal{P} \qquad \mathcal{N}: \text{ some normalization} \tag{16}$$

where $\mathcal{P}$ is the projection operator onto all eigenstates of $\mathcal{H}_P$, that is, $\mathcal{P} = \sum_{i\in\mathcal{H}_P} |d_i\rangle\langle d_i|$. Since the state starts off in $\mathcal{H}_P$ however, projecting it onto $\mathcal{H}_P$ at t=0 will not change it:

$$\rho_0 = \mathcal{P}\rho_0\mathcal{P} \tag{17}$$

$$Tr[\rho_0\mathcal{P}_i] = \langle\mathcal{P}_i\rangle = 1 \tag{18}$$

and these are our initial conditions.

A. From 0 to τ^-, then measurement

For this and the following subsection, we present the analysis given by Facchi and Pascazio in [14]. Consider what happens up to time τ^-, before any measurements. The state has undergone purely unitary time evolution described by

$$\rho(\tau) = U(\tau)\rho_0 U^\dagger(\tau) \tag{19}$$

We perform a measurement at time τ. Now, if measurement at τ reveals that the state has not decayed, it means the state has been projected onto $\mathcal{H}_P$, and ρ is now, according to eqn (16):

$$\rho(\tau^-) \mapsto \mathcal{P}\rho(\tau)\mathcal{P} = \mathcal{P}U(\tau)\rho_0 U^\dagger(\tau)\mathcal{P}$$

$$= \mathcal{N}_{\text{no decay}}V(\tau)\rho_0 V^\dagger(\tau) \tag{20}$$

where $V(\tau) \equiv \mathcal{P}U(\tau)\mathcal{P}$ and we have used eqn (17).
Just as in 27, we can thus define the survival probability, $\mathscr{P}(t)$. This is exceptionally easy to compute given $\rho(t)$ (by analogy with eqn (12)):

$$\mathscr{P}_{\text{no decay}}(t) = Tr\left[\rho(\tau)\mathcal{P}\right] = Tr\left[U(\tau)\rho_0 U^\dagger(\tau)\mathcal{P}\right]$$

$$= Tr\left[\mathcal{P}U(\tau)(\mathcal{P}\rho_0\mathcal{P})U^\dagger(\tau)\mathcal{P}\right]$$

$$= Tr\left[V(\tau)\rho_0 V^\dagger(\tau)\right] \tag{21}$$

using equations (17) and $\mathcal{P}\mathcal{P} = \mathcal{P}$, as well as the cyclic property of traces. Since this is the probability of being undecayed, we have to *divide $\rho_{no\ decay}$ by this* to get the normalization $\mathcal{N}$.
Since there is also a probability that the state *has* decayed into $\mathcal{H}_P^\perp = \mathcal{H}_Q$ where $\mathcal{H}_P \bigoplus \mathcal{H}_Q = \mathcal{H}$. Replicating the steps of eqn (20), it is straightforward to compute that the density matrix and probability of decay are then

$$\rho(\tau^-) \mapsto \mathcal{N}_{decay}V_{QP}(\tau)\rho_0 V_{QP}^\dagger(\tau) \tag{22}$$

$$\mathscr{P}_{\text{decay}}(t) = Tr\left[V_{QP}(\tau)\rho_0 V_{QP}^\dagger(\tau)\right] \tag{23}$$

where again, $\mathcal{N}_{decay} = 1/Tr\left[V_{QP}(\tau)\rho_0 V_{QP}^\dagger(\tau)\right]$. Of course, we do not know *a priori* what answer the measurement is going to yield: all we know are the probabilities of either outcome. So the density matrix that we can write down *a priori* is

$$\begin{pmatrix} \dfrac{V(\tau)\rho_0 V^\dagger(\tau)}{Tr[V(\tau)\rho_0 V^\dagger(\tau)]} & 0 \\ \hline 0 & \dfrac{V_{QP}(\tau)\rho_0 V_{QP}^\dagger(\tau)}{Tr[V_{QP}(\tau)\rho_0 V_{QP}^\dagger(\tau)]} \end{pmatrix} \tag{24}$$

And this expression is equally applicable to one particle as it is to many particles.

B. After N time intervals, T

Now, just as in the 1D case, we repeat the above analysis for many successive time intervals. Then, to represent many repeated cycles of measurement-unitary evolution-measurement, we define a new operator

$$V_N(T) = [\mathcal{P}U(\frac{T}{N})\mathcal{P}]^N \qquad (25)$$

. It is easy to see that the density matrix is now:

$$\rho_N(T) = \mathcal{N}V_N(T)\rho_0 V_N^\dagger(T) \qquad (26)$$

where

$$\mathcal{N} = 1/\mathscr{P}_N(t) = 1/Tr[V_N(t)\rho_0 V_N^\dagger(t)] \qquad (27)$$

is the normalizing probability of the state having survived after N time intervals. We want to compute ρ_N and $\mathscr{P}_N$ in the limit $N \longrightarrow \infty$(i.e. frequent interrogations), so we define

$$U_Z \equiv \lim_{N\to\infty} V_N \qquad (28)$$

which we can compute as follows

$$V_N(T) = [\mathcal{P}e^{iH\frac{T}{N}}\mathcal{P}]^N$$

$$= \mathcal{P}[1 - i\mathcal{P}H\mathcal{P}\frac{T}{n} + O\left(\frac{1}{N^2}\right) + ...]^N$$

$$\stackrel{N\to\infty}{\longrightarrow} U_Z(t) = \mathcal{P}e^{-i\mathcal{P}H\mathcal{P}T} = \mathcal{P}e^{-i\mathcal{H}_Z t} \qquad (29)$$

defining the Zeno Hamiltonian as $\mathcal{H}_Z = \mathcal{P}H\mathcal{P}$. Equipped with $U_Z(T)$, it becomes simple to evaluate the asymptotic probability of remaining undecayed, $\lim_{N\to\infty} \mathscr{P}_N(T)$:

$$\lim_{N\to\infty} \mathscr{P}_N(t) = Tr\left[U_Z(T)\rho_0 U_Z^\dagger(T)\mathcal{P}\right]$$

$$= Tr\left[\underbrace{\mathcal{P}\mathcal{P}}_{\mathcal{P}}e^{-i\mathcal{H}_Z t}\rho_0 U_Z^\dagger\right] \qquad \text{Use eqn (29)}$$

$$= Tr\left[U_Z\rho_0 U_Z^\dagger\right] = Tr[\rho_0] = 1$$

and ρ will be block-diagonal with only the block representing the $\mathcal{H}_P$ subspace non-zero, ie. like the RHS of eq 15.

V. EXPERIMENTAL IMPLEMENTATION OF QUANTUM ZENO DYNAMICS

Here we give a brief summary of the experiment done by Signoles and Haroche (henceforth S&H) to illustrate QZD. Atomic angular momentum, J, can be represented as an vector evolving on the tip of a Bloch sphere of radius J. The z-component of angular momentum, J_z, is then the projection of this arrow onto the z-axis, and J_z

can take on any integer values from $[-J, J]$. In Signoles's notation, the eigenstates are $|J, J - k\rangle$ with $k = 0 \cdots 2J$ (where J_z is now represented by J-k).

While it is not hard to conceive of measurement 'projecting' a general state onto a single eigenstate (QZE), it is less clear how to selectively project onto the multiple states of a subspace. The key innovation of S&H is to impose a 'Limiting Latitude'(LL) on the Bloch sphere via a 'Zeno' microwave pulse, such that the atom can have values of J_z that correspond to being above the LL, but not below. This LL, along with the energy-level diagram, are shown in Figure 2. Note that S&H do not directly perform their experiments on angular momentum states: they choose a subspace of the Stark manifold of a Rydberg atom [11] (the terms 'Stark effect' and 'Rydberg atom' are explained in the footnote [15]), equivalent to a spin J=25. Here we make the association $|n_e, k\rangle = |J, J - k\rangle$. The state in bold in
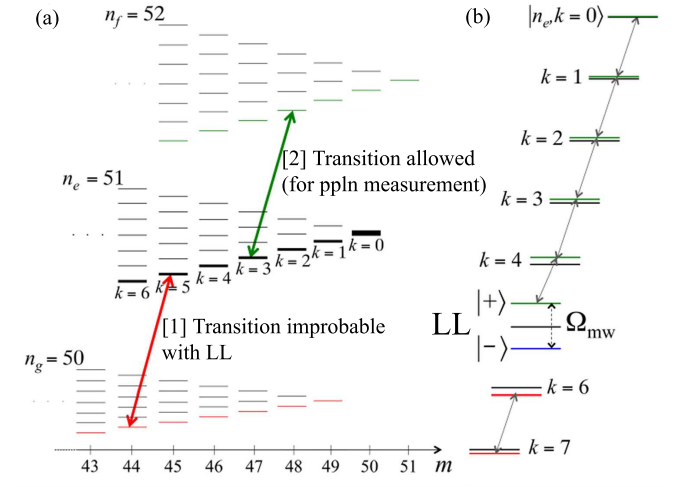

FIG. 2: (a) Energy level diagram of three adjacent Stark manifolds of a Rydberg atom with Principal Quantum Numbers $n_g = 50, n_e = 51, n_f = 52$. The n_g manifold allows us to impose the LL, so that atoms can only evolve within the subspace spanned by $ket n_e, k \leq 5$ (so they cannot even evolve to $ket n_e, k > 5$, needless to say the n_g manifold). The n_f manifold is analogous to level 3 (in the sense that it is only there for results verification) (b) Limiting Latitude arises from an admixture of energy levels from two different manifolds. (Source of diagrams:[3])

figure 2 is the initial state $|n_e = 51, k = 0\rangle$ which corresponds to $|J = 25, m_J = J - k = 25\rangle$, and this is the state with maximal J_z. The aim of the experiment is to try to keep the atom within the $k \leq 5$ subspace of the $n_e = 51$ Rydberg manifold. The Hamiltonian H that causes the unitary evolution (whose effects we want to counteract) is a radio-frequency drive field, given by $\hat{V} = \frac{\hbar\Omega_{rf}}{2}\sqrt{(k+1)(n_e - k - 1)}|n_e, k+1\rangle\langle n_e, k| + h.c.$. Since Ω_{rf} is tuned to the separation between adjacent k-levels within the $n_e = 51$ manifold, the RF field therefore induces evolution up and down the 'ladder' in bold in fig-

ure 2 within the $n_e = 51$ subspace. In the Bloch sphere representation, this is evolution along a meridian of the sphere. While the z-component of this angular momentum is therefore changing constantly, the total angular momentum remains fixed at J=25.

The aim is to prevent the state from exploring the entire ladder by imposing a LL at $k_p = 5$. The 'frequent interrogation' of QZE now translates into frequent imposition of the 'Zeno' microwave field that creates the LL, which in turn prevents decay. This field is resonant on the $|n_e, k_p = 5\rangle \rightarrow |n_g, k_p = 5\rangle$ transition. Hence it admixes these two states from different manifolds into two *dressed states* separated by a large energy gap Ω_{mw}, much larger than the coupling matrix element between adjacent k states $\sim \sqrt{n_e}\Omega_{rf}$ (recall that the probability of transition in PT $\sim 1/\text{detuning}^2$). Effectively, evolution to $|n_e, k > 5\rangle$ is now highly improbable! We will justify this statement in the Appendix, but for now, let us study the results, contrasting the evolution of the populations in the $|n_e, k \leq 5\rangle$ subspace with and without QZD, in figure 4 (but see footnote [16]):

Note that without QZD (figure 4(a)), the state can be seen to be climbing down the ladder of states first introduced in figure 2: the lines representing the different k values (and thus different rungs of the ladder) display population peaks at successively later times. But with QZD, instead of the usual decay of initial populations, the presence of the LL causes a 'revival' of the initial populations starting from around $0.76\mu s$, the point of time at which the $k = 5$ line peaks and the spin hits the LL. For interest's sake, we show a plot of the system's inverted Q distribution[12] (which essentially reconstructs the system's density matrix from measurements) and gives a pictorial representation of the evolution on the Bloch sphere in Fig 3.
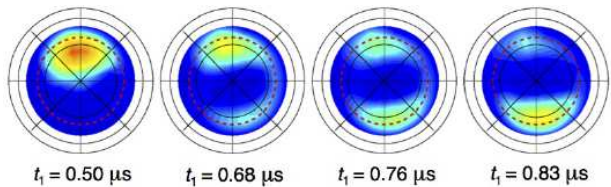

FIG. 3: Looking down from the North Polar Cap of the Bloch sphere at successive times - QZD has confined the motion inside the Limiting Latitude (dashed circle). Notice the 'bouncing off the wall' effect at $t \approx 0.76\mu s$: instantaneously, the spin is in a quantum superposition of two (coherent) spin states with opposite azimuthal phases. This is in effect a Schrödinger Cat State (refer to [13] for details) that can function as a qubit basis state.(All diagrams on this page are from [3])

VI.   CONCLUDING REMARKS

Just as this paper started by describing Zeno's paradox, it will end by describing a paradox inherent to this discussion: the question of whether measurement deter-
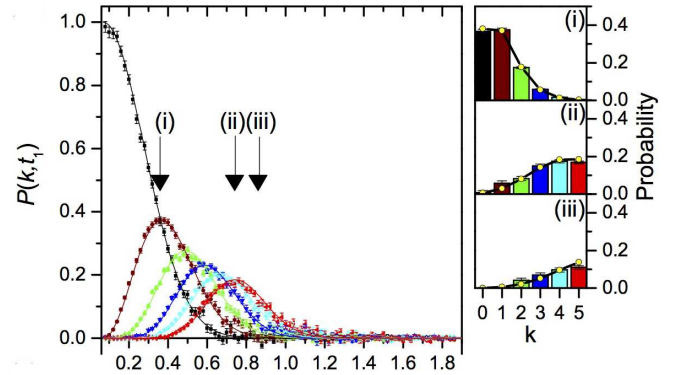
(a)Without QZD, the probability of being in each of the eigenstates of the $n_e, k \leq 5$ manifold decrease monotonically over a time t_1 due to transitions to other states within and without the manifold. The insets present the color code for the different values of $k \leq 5$, while the solid lines correspond to theoretical expectations from numerical simulation.
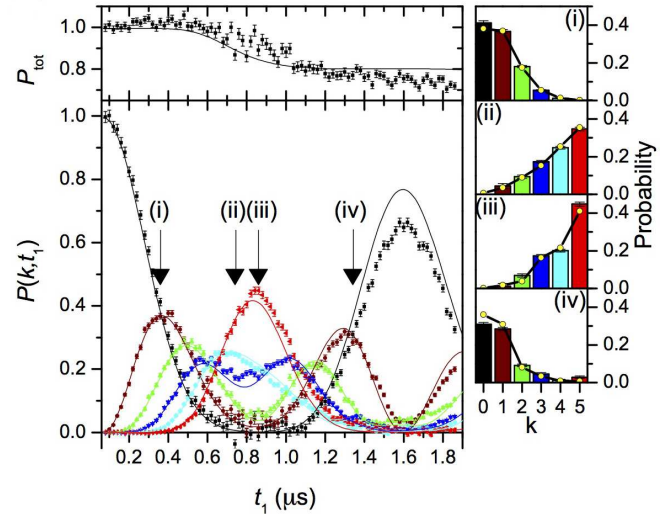
(b)With QZD (selecting $k_z = 5$), the probability of being in the $\mathcal{H}_N$ subspace oscillates sinusoidally in time. The top frame gives the total population P_{tot} of $\mathcal{H}_n$,which never goes below 0.8 of the original. Data points are in good agreement with expectation (solid lines).

FIG. 4: Evolution of the spin state populations for k≤5

mines the quantum state. Although this paper belabors the idea that wavefunction collapse via measurement is a real effect, one might wonder whether the observed tracks of particles in a bubble chamber [1], where the particle decays *despite what one might consider continuous measurement*, directly contradicts this conclusion. One possible resolution is described by [1]: in the Von Neumann interpretation where measurement is an interaction with the measuring instrument, only if the measurement is sufficiently energetic (as in QZE) can it 'freeze' an object in its initial state; mere observation of a decaying particle is not energetic enough and hence does not alter the quantum state. We will leave the interpretation to the philosophers; for us, it will suffice to appreciate this beau-

tiful melding of theory and experiment and note that the future is bright: QZD holds great interest for Quantum Information Processing because it allows one to tailor evolution within a subspace such that it is robust against decoherence.

VII. ACKNOWLEDGMENTS

The author is eternally grateful to Professors Aram Harrow and Barton Zwiebach for setting good Quantum fundamentals in 8.05 and 8.06.

APPENDIX A: HOW IS THE LIMITING LATITUDE IMPOSED?

We impose the 'Limiting Latitude' by splitting two states ($|n_e, k_p\rangle$ and $|n_g, k_p\rangle$, henceforth $|e0\rangle = |e\rangle|0\rangle$ and $|g1\rangle = |g\rangle|1\rangle$) that are coupled by a'Zeno' RF pulse with frequency ω_z into two dressed states separated by a large Ω_{mw}. This can be understood in terms of the familiar Jaynes-Cummings Hamiltonian that describes atom-photon interactions (we assume one photon per mode):

$$\hat{\mathcal{H}} = \frac{1}{2}\hbar\omega_0(|g\rangle\langle g| + |e\rangle\langle e|) + ...$$
$$... \hbar\omega_z(\hat{a}^\dagger\hat{a} + \frac{1}{2}) + \frac{\hbar\Omega_{mw}}{2}(|e\rangle\langle g|\hat{a} - |g\rangle\langle e|\hat{a}^\dagger) \quad \text{(A1)}$$

For simplicity, we take $\omega_z = \omega_0$ (the incident radiation is *on resonance* with the natural energy separation). The first term is the Hamiltonian of the unperturbed atom, the second term is the Hamiltonian of the Zeno RF pulse, and the last term, H_{int} represents the interaction between the two in the Rotating Wave Approximation. The effect of applying the Zeno pulse (H_{int}) is to break the degeneracy that $|e0\rangle$ and $|g1\rangle$ enjoy without any interaction: the eigenvalue of $|e0\rangle$ is clearly $\hbar\left(\frac{\omega_0}{2} + (0 + \frac{1}{2})\omega_0\right)$ and that of $|g1\rangle$, $\hbar\left(-\frac{\omega_0}{2} + (0 + \frac{3}{2})\omega_0\right)$, which are the same. In the model of the spin-half particle precessing in a B-field, degeneracy is equivalent to no applied B-field and no precession. But H_{int} introduces off-diagonal terms in the Hamiltonian equivalent to some σ_x and σ_y. This creates an axis of spin precession in the xy-plane and therefore, new eigenstates are created: the 'up' and 'down' states of the new axis. These are the 'dressed states' on either side of the LL, whose energy separation is $\hbar\Omega_{mw}$ (please refer to [6] for the general idea). The key idea of QZD is to make Ω_{mw} much larger than the natural frequency separation between states $|n_e, k \leq 5\rangle$ and $|n_e, k > 5\rangle$, ω_0. Defining the detuning Δ to be $\Omega_{mw} - \omega_0$, we recall from Time-Dependent Perturbation Theory that the probability of transition to another state is proportional to $1/\Delta^2$. Hence, by making Δ massive, the probability of transition 'across' the LL is vanishingly small.

[1] B. Misra and E.C.G. Sudarshan *The Zeno Paradox in quantum theory* J. Math. Phys. 18, 756 (1977)

[2] Wayne M. Itano, D. J. Heinzen, J. J. Bollinger, and D. J. Wineland, *Quantum Zeno effect* Phys. Rev. A 41, 2295, Published 1 March 1990

[3] Adrien Signoles, Adrien Facon, Dorian Grosso, Igor Dotsenko, Serge Haroche, Jean-Michel Raimond, Michel Brune, Sebastien Gleyzes, *Confined quantum Zeno dynamics of a watched atomic arrow* , Published February 4 2014

[4] Zeno's Paradoxes, Stanford Encyclopedia of Philosophy: http://plato.stanford.edu/entries/paradox-zeno/

[5] M. Porrati and S. Putterman, *Wave-function collapse due to null measurements: The origin of intermittent atomic fluorescence* Phys. Rev. A 36, 2, 1987

[6] Claude Cohen-Tannoudji, Jacques Dupont-Roc, Gilbert Grynberg, *Atom-Photon Interactions: Basic Processes and Applications* John Wiley & Sons, Inc., 1992

[7] Cohen-Tannoudji, Diu, Laloë, *Quantum Mechanics* Vol I. and II., Hermann, Paris, France, 1977

[8] F. Schfer, I. Herrera, S. Cherukattil, C. Lovecchio, F.S. Cataliotti, F. Caruso, A. Smerzi, *Experimental realization of Quantum Zeno Dynamics*

[9] Saverio Pascazio, *All you ever wanted to know about the quantum Zeno effect in 70 minutes* Open Sys. Information Dyn. 21, 1440007 (2014)

[10] Barton Zwiebach, 8.05 typewritten notes, Chapter 6

[11] C.T.W. Lahaye, W. Hogervorst, and W. Vassen *Stark manifolds of barium Rydberg states*, Z. Phys. D -Atoms, Molecules and Clusters, 7, 37-45 (1987)

[12] G. S. Agarwal *State reconstruction for a collection of two-level systems*, PHYSICAL REVIEW A, VOLUME 57, NUMBER 1, JANUARY 1998

[13] H. Jeong and T.C. Ralph *Schrödinger Cat States for Quantum Information Processing*, book chapter of "Quantum Information with Continuous Variables of Atoms and Light" (Imperial College Press)

[14] Facchi, P. & Pascazio, S. *Quantum Zeno dynamics: mathematical and physical aspects*, J. Phys. A 41, 493001 (2008).

[15] A Rydberg atom is basically an atom with one valence electron in a highly excited state. The high-n (and therefore, high J) state is necessary in order to observe the large *J*-degeneracies required for QZD. The term 'Stark effect' describes the shift in energies when an atom is placed in a high enough electric field. In this case, the high electric field was necessary to excite the atom into the Rydberg state, and the Stark effect is an unintended consequence that just shifts the energy levels by an amount linear in the electric field strength.

[16] In QZE, we had a state $|3\rangle$ whose presence allowed us to count the number of atoms that had not decayed to state $|2\rangle$. Here, the $|n_f\rangle$ manifold serves a similar purpose. A π-microwave pulse tuned to the $|n_e, k_p\rangle \rightarrow |n_f, k_p\rangle$ transition excites undecayed atoms to the $n_f = 52$ manifold whereupon their levels can be measured by field ionization (which only resolves the $|n_f\rangle$ states).

Lattice Vibrations, Phonons, and Low Temperature Specific Heats of Solids

Nick Rivera

Department of Physics, 77 Massachusetts Ave., Cambridge, MA 02139-4307

(Dated: May 2, 2014)

In this paper, we will consider the problem of diagonalizing the Hamiltonian of the monatomic harmonic crystal. We start by thinking of the problem classically, i.e; by modeling the ions as undergoing small oscillations about the points of a 3D Bravais lattice. In particular, we derive the classical Hamiltonian for the crystal and discuss the problem of finding the normal modes of the crystal. We then quantize the classical Hamiltonian and diagonalize it via a normal mode transformation. We will interpret the solution of this problem using the language of occupation number representations and show that the excitations of the crystal can be thought of as the addition of noninteracting bosonic particles (phonons) to a vacuum state. Using this bosonic picture of the normal modes, we derive a formula for the specific heat of a monatomic crystal at low temperatures using Bose-Einstein statistics and show that it correctly predicts that this specific heat is proportional to T^3.

I. INTRODUCTION

In this paper, we examine the spectrum of the harmonic crystal. The harmonic crystal is a system of N identical ions whose equilibrium positions are the points of a Bravais lattice in three dimensions. N is on the order of Avogadro's number in physical solids. These ions interact with all of the other ions in the crystal via a pair potential function that depends only on the distance between ions. Is it possible for us to find the eigenenergies of the system? At first sight, this many-body problem looks intractable, and one of the surprises of this many-body problem is that it can be understood very cleanly in terms of *phonons*. A phonon is a single excitation of the harmonic crystal and is suggestive of a "particle of sound". Phonons allow us to simply understand properties of solids such as specific heat, electrical conductivity, thermal conductivity, indirect band gap transitions, superconductivity, and many others [1].

We will show in this paper that the energy eigenstates of the harmonic crystal are formally identical to the energy eigenstates of a harmonic oscillator. In fact, we will show that for a monatomic lattice (only one type of ion), the system is equivalent to a 3N-dimensional harmonic oscillator (i.e; one with 3N different spring constants). In other words, that the energy eigenkets of the harmonic crystal are of the form $|n_1, n_2, ..., n_{3N}\rangle$. Each of these numbers represents the level of excitation of one of the 3N different harmonic oscillators.

Furthermore, we will show that each of these excitations can be associated with a boson. We will demonstrate the mathematical equivalence of the harmonic crystal states with the states of non-interacting bosons by examining a system of non-interacting bosons and writing their states in the *occupation number representation*. We will show that we can define creation and annihilation operators for the bosonic system that make it formally identical to a harmonic oscillator. And because the harmonic oscillator is formally identical to the harmonic crystal, we can establish a complementary picture of excitations of the harmonic crystal in terms of

identical bosons, called phonons.

Using this boson picture of the collective vibrations of the lattice, we will derive the specific heat of a monatomic solid (for simplicity) at low temperature and show that using this picture correctly predicts a T^3 dependence.

II. SETUP AND MATHEMATICAL BACKGROUND

The monatomic harmonic crystal refers to a system in which we have N identical ions of mass M interacting via a pairwise potential function ϕ. The N ions have as their equilibrium positions the points of a Bravais lattice. We want to find the eigenenergies of this systemn

A. Bravais Lattices

A Bravais lattice (BL) is a set consisting of all points in $\Re^3$ with position vectors $\vec{R}$ of the form $\vec{R} = n_1\vec{a_1} + n_2\vec{a_2} + n_3\vec{a_3}$, where the n_is are integers and the $\vec{a_i}$s are linearly independent. The $\vec{a}$ vectors are called lattice directions. Equivalently, a BL is an array of discrete points with an arrangement and orientation that appears exactly the same from whichever point the array is viewed. See [1] for more discussion on this. Using the second definition, we can quickly see that this set of points invariant under translation by $\vec{R}$.

If the number of points in a lattice is finite, then a translation of the lattice will move some points out of the region of the lattice and this is distinguishable from the original lattice. Thus, no physical lattice is a BL. However, we can turn a finite lattice into a BL if we implement periodic, or Born von Karman, boundary conditions. In other words, we say that the point $\vec{R}$ is equivalent to the point $\vec{R} + N_i\vec{a_i}$ for i = 1,2,3 and N_i being some integer for each i. This "wraps the system around itself" along the three lattice directions. As an example of this, consider the 1D case. The periodic boundary

condition implies that the point x is equivalent to the point $x + Na$. While periodic boundary conditions are not physical, it is intuitively clear that for large N_i, the fact that our boundaries aren't physically accurate can't change the physics of the crystal in it's interior. For further discussion of this point, see [1]. Now that we have defined a BL, we can go ahead and setup the classical Hamiltonian.

B. The Classical Hamiltonian

Suppose that each ion has as its equilibrium position a unique Bravais lattice vector, $\vec{R}$. And suppose that the displacement of an ion at $\vec{R}$ is $\vec{u}(\vec{R})$. The $\vec{u}$s are called lattice coordinates. Finally, we assume that any two ions whose equilibrium positions at $\vec{R}$ and $\vec{R}'$ respectively interact via a pair potential of the form $\phi(\vec{r}, \vec{r}') = \phi(|\vec{r} - \vec{r}'|)$, where $\vec{r} = \vec{R} + \vec{u}(\vec{R})$. $\vec{r}$ is the position of an ion with respect to a fixed origin. In order to solve the quantum mechanical problem of lattice vibrations, we will write down the classical Hamiltonian and quantize it. The classical Hamiltonian, H_c of the N particle system is given by

$$H_c = \sum_{\vec{R}} \frac{\vec{P}^2(\vec{R})}{2M} + U, \qquad (1)$$

where $\vec{P}(\vec{R}) = M\dot{\vec{r}} = M\dot{\vec{u}}(\vec{R})$ and U is the potential energy of the system. The $\sum_{\vec{R}}$ denotes a sum over all vectors in the BL. The potential energy of the system is sum of the potential energy between each pair of ions. We can write this as:

$$U = \frac{1}{2} \sum_{\vec{R}, \vec{R}'} \phi(\vec{r} - \vec{r}')$$

$$= \frac{1}{2} \sum_{\vec{R}, \vec{R}'} \phi((\vec{R} - \vec{R}') + (\vec{u}(\vec{R}) - \vec{u}(\vec{R}'))). \qquad (2)$$

The factor of $\frac{1}{2}$ comes from the fact that we've double-counted pairs of ions by including contributions from the $[\vec{R}, \vec{R}']$ term of the sum and the $[\vec{R}', \vec{R}]$ term. These both correspond to an interaction between an ion whose equilibrium position is $\vec{R}$ and an ion whose equilibrium position is $\vec{R}'$. This expression for U however, is completely intractable unless we make approximations. We will simplify it using the harmonic approximation. This requires Taylor expanding each ϕ in the sum in powers of $\vec{u}(\vec{R}) - \vec{u}(\vec{R}')$. For convenience, let $\vec{a} \equiv \vec{u}(\vec{R}) - \vec{u}(\vec{R}')$ and $\vec{x} \equiv \vec{R} - \vec{R}'$. Then

$$\phi(\vec{x} + \vec{a}) = \phi(\vec{x}) + \nabla\phi\Big|_{\vec{a}=0} \cdot \vec{a}$$

$$+ \frac{1}{2} \sum_{i,j=1,2,3} a_j \frac{\partial^2\phi}{\partial x_i \partial x_j}\Big|_{\vec{a}=0} a_i + O(a^3). \qquad (3)$$

When the all of the ions are in their equilibrium positions, $\vec{a} = 0$ and the force between any pair of ions is zero. The force between any two particles, modulo a minus sign, is the gradient of the potential with respect to the coordinates of any of the two particles. Therefore, the second term in the Taylor expansion vanishes because that gradient is just the force between two particles at their equilibrium positions. We can take the first term to vanish as well, because we're free to shift the potential energy by a constant. Finally, in the harmonic approximation, we assume that the a_is are small enough such that we can ignore terms higher than second order in a. Working in this regime, we can simplify (2) by substituting for ϕ the third term in (3). Doing this substitution and writing $\vec{a}$ in terms of the $\vec{u}$s and $\vec{R}$s, we get

$$U = \frac{1}{4} \sum_{\vec{R}, \vec{R}', i, j} (u_i(\vec{R}) - u_i(\vec{R}')) \frac{\partial^2\phi}{\partial x_i \partial x_j}\Big|_{\vec{R} - \vec{R}'} (u_j(\vec{R}) - u_j(\vec{R}')). \qquad (4)$$

I claim that (4) is equivalent to the expression:

$$U = \frac{1}{2} \sum_{\vec{R}, \vec{R}', i, j} u_i(\vec{R}) D_{ij}(\vec{R} - \vec{R}') u_j(\vec{R}'), \qquad (5)$$

where

$$D_{ij}(\vec{R} - \vec{R}') \equiv \left(\delta_{\vec{R}, \vec{R}'} \sum_{\vec{R}''} \frac{\partial^2\phi}{\partial x_i \partial x_j}\Big|_{\vec{R} - \vec{R}''} \right) - \frac{\partial^2\phi}{\partial x_i \partial x_j}\Big|_{\vec{R} - \vec{R}'} \qquad (6)$$

This can be verified by substituting (6) into (5) and comparing it with a version of (4) in which the summand is expanded into terms each quadratic in $\vec{u}$. Plugging (5) into (1) gives us the classical Hamiltonian in the form that we will use in order to solve for the spectrum of the quantum harmonic crystal.

C. Normal Modes of the Harmonic Crystal

Before quantizing the classical Hamiltonian, we will discuss "solving the classical harmonic crystal", which means finding the normal modes of oscillation of the crystal. We do this because it will give us intuition for the quantum problem.

We would like to solve Newton's equations of motion for the harmonic crystal. They read:

$$M\ddot{u}_i(\vec{R}, t) = -\frac{\partial U}{\partial u_i(\vec{R})} = -\sum_{\vec{R}', j} D_{ij}(\vec{R} - \vec{R}') u_j(\vec{R}', t)$$

Or in matrix form,

$$M\ddot{\vec{u}}(\vec{R}, t) = -\sum_{\vec{R}'} D(\vec{R} - \vec{R}') \vec{u}(\vec{R}', t). \qquad (7)$$

In a system of N oscillators with 3N position degrees of freedom, we expect there to be normal mode solutions

(3N of them) in which all of the ions are oscillating with the same frequency. We know from classical mechanics that these normal modes form a basis for all of the solutions of Newton's equations in this system. Thus, without loss of generality, we look for trial solutions of the form $\vec{u}(\vec{R}, t) = \vec{A}(\vec{R})e^{-i\omega t}$. Because of our periodic boundary conditions, we can expand $\vec{u}$ in a three dimensional Fourier series. Any function, $f(\vec{R})$, that is periodic with respect to three linearly independent vectors, $N_1\vec{a}_1$, $N_2\vec{a}_2$, and $N_3\vec{a}_3$ can be written in the following form: $\vec{f}(\vec{R}) = \sum_{\vec{k}} \vec{C}_{\vec{k}} e^{i\vec{k}\cdot\vec{R}}$. This expansion has the property that the only $\vec{k}$s that appear in the sum are those such that $e^{i\vec{k}\cdot(aN_1\vec{a_1}+bN_2\vec{a_2}+cN_3\vec{a_3})} = 1$, where a,b, and c, are integers. As a check of this, we see that upon replacing $\vec{R}$ in the Fourier sum by $\vec{R}+(aN_1\vec{a_1}+bN_2\vec{a_2}+cN_3\vec{a_3})$ with a,b,c being integers, the sum is unchanged, and hence the function is indeed periodic in each of the $N_i\vec{a}_i$s. A more careful treatment of periodicity in higher dimensions is given in almost any book on solid state physics, see [1,2] for example.

Therefore, the exponentials $e^{i\vec{k}\cdot\vec{R}}$ form a basis for the position dependence of the solutions. Thus we can let $\vec{A}(\vec{R}) = \vec{\epsilon}e^{i\vec{k}\cdot\vec{R}}$ and take a superposition over all $\vec{k}$ in the Fourier series expansion to find more general solutions. Adding the time-dependence to $\vec{A}(\vec{R})$, we are left with a trial solution of the form:

$$\vec{u}(\vec{R}, t) = \vec{\epsilon}e^{i(\vec{k}\cdot\vec{R}-\omega t)}. \tag{8}$$

The vector $\vec{\epsilon}$ is called a polarization vector because it represents the direction of oscillation of the ions in the trial solution. The $\vec{k}$s that appear in the trial solutions are the vectors that show up in the Fourier expansion of $\vec{u}(\vec{R})$. They are called wavevectors. Plugging (8) into (7), we get that we find a solution whenever $\vec{\epsilon}$ satisfies the 3D eigenvalue equation:

$$M\omega^2\vec{\epsilon} = \sum_{\vec{R}} D(\vec{R} - \vec{R}')e^{-i\vec{k}\cdot(\vec{R}-\vec{R}')}\vec{\epsilon}$$

$$\equiv \sum_{\vec{x}} D(\vec{x})e^{-i\vec{k}\cdot\vec{x}}\vec{\epsilon} \equiv D(\vec{k})\vec{\epsilon} \tag{9}$$

where $\vec{x}$ still runs over the entire BL. $D(\vec{k})$ is called the *dynamical matrix*. It is shown in [1] that the dynamical matrix is real-symmetric. It is a theorem of linear algebra that any real-symmetric three-dimensional matrix can be diagonalized such that the three eigenvectors are real and orthonormal [1]. For each $\vec{k}$, there are three eigenvectors, labeled $\vec{\epsilon}_s(\vec{k})$ and three eigenvalues, $M\omega_s^2(\vec{k})$. The s label is an eigenvector index (s=1,2,3) for fixed $\vec{k}$, and is called the polarization index. We've broken the problem of finding normal modes into separate eigenproblems for each $\vec{k}$. Since the system has 3N normal modes, we expect to solve N eigenproblems. However, the Fourier series expansion has an infinite number of terms. Thus for this

to be consistent with a finite number of normal modes, there must be redundancies in the Fourier series. Indeed, there are. Although I won't prove it, it turns out that there are in fact N non-redundant terms in the Fourier series [1]. We have everything we need to solve for the spectrum of the quantum harmonic crystal.

III. THE SPECTRUM OF THE HARMONIC CRYSTAL

To quantize the classical Hamiltonian, we will need to turn the lattice coordinates and momenta of the ions into operators and find commutation relations between the momenta and the lattice coordinates. We also need to find commutation relations between different lattice coordinate operators and between different momentum operators. These will be derived using the canonical commutation relations, namely: $[r_i(\vec{R}), P_j(\vec{R}')] = i\hbar\delta_{ij}\delta_{\vec{R},\vec{R}'}$, and $[r_i(\vec{R}), r_j(\vec{R}')] = [P_i(\vec{R}), P_j(\vec{R}')] = 0$, where $r_i(\vec{R})$ is the ith component of the position vector of the ion whose equilibrium position is $\vec{R}$, and $P_i(\vec{R})$ is the ith component of that ion's momentum. Remembering that $\vec{r} = \vec{R} + \vec{u}(\vec{R})$, it directly follows that $[u_i(\vec{R}), P_j(\vec{R}')] = i\hbar\delta_{ij}\delta_{\vec{R},\vec{R}'}$. It also directly that $[u_i(\vec{R}), u_j(\vec{R}')] = 0$. The problem is now fully quantum.

To proceed, I will define *phonon creation and annihilation operators* as follows:

$$a_{\vec{k},s} = \frac{1}{\sqrt{N}} \sum_{\vec{R}} e^{-i\vec{k}\cdot\vec{R}}\vec{\epsilon}_s(\vec{k}) \cdot \left[\sqrt{\frac{M\omega_s(\vec{k})}{2\hbar}}\vec{u}(\vec{R}) + i\sqrt{\frac{1}{2M\hbar\omega_s(\vec{k})}}\vec{P}(\vec{R})\right]$$

$$\tag{10}$$

$$a_{\vec{k},s}^{\dagger} = \frac{1}{\sqrt{N}} \sum_{\vec{R}} e^{i\vec{k}\cdot\vec{R}}\vec{\epsilon}_s(\vec{k}) \cdot \left[\sqrt{\frac{M\omega_s(\vec{k})}{2\hbar}}\vec{u}(\vec{R}) - i\sqrt{\frac{1}{2M\hbar\omega_s(\vec{k})}}\vec{P}(\vec{R})\right],$$

$$\tag{11}$$

where the $\vec{\epsilon}_s(\vec{k})$ and $\omega_s(\vec{k})$ are defined to be the polarization vectors and the eigenfrequencies of the dynamical matrix (9). The definition of these operators is suggestive of a transformation into normal mode coordinates because we're defining an a and an $a^{\dagger}$ for each wavevector $\vec{k}$ and each polarization, s. To get the commutation relations between the creation and annihilation operators, I need to invoke another identity involving three dimensional Fourier series (see [1] for proof). In particular, the identity reads

$$\sum_{\vec{R}} e^{i\vec{k}\cdot\vec{R}} = \begin{cases} N & \text{if } e^{i\vec{k}\cdot\vec{R}} = 1 \text{ for all } \vec{R} \in \text{BL} \\ 0 & \text{otherwise} \end{cases}. \tag{12}$$

Using this identity, the commutation relations for $\vec{u}$ and $\vec{P}$, and the orthonormality of the polarization vectors, we get the algebra of the harmonic oscillator, namely:

$$[a_{\vec{k},s}, a_{\vec{k}',s'}^{\dagger}] = \delta_{\vec{k},\vec{k}'}\delta_{s,s'} \tag{13}$$

$$\text{and } [a_{\vec{k},s}, a_{\vec{k}',s'}] = [a_{\vec{k},s}^{\dagger}, a_{\vec{k}',s'}^{\dagger}] = 0. \tag{14}$$

At this point, solving for the spectrum is llike solving for the spectrum of the 1D harmonic oscillator. We must express the $\vec{u}$s and $\vec{P}$s in the Hamiltonian terms of the creation/annihilation operators. The algebra involved in doing this is cumbersome and not worth showing given how unsurprising the result is (a little bit more of the algebra is shown in [1]). The result of this process is the final Hamiltonian given by:

$$H = \sum_{\vec{k},s} \hbar \omega_s(\vec{k}) \left(a_{\vec{k},s}^{\dagger} a_{\vec{k},s} + \frac{1}{2} \right). \qquad (15)$$

This is an immense simplification! With a Hamiltonian of this form and the algebra given by (13) and (14), we automatically have a problem mathematically equivalent to a 3N-dimensional harmonic oscillator whose individual frequencies are indexed by $(\vec{k}, s)$. In particular, we can write the energy eigenstates as $\left| n_{\vec{k}_1,s_1}, n_{\vec{k}_1,s_2}, n_{\vec{k}_1,s_3}, ..., n_{\vec{k}_N,s_1}, n_{\vec{k}_N,s_2}, n_{\vec{k}_N,s_3} \right\rangle$, where each $n_{\vec{k},s}$ is an integer quantum number labeling the state. By the algebra of the harmonic oscillator, we know that these states are given by:

$$\left| n_{\vec{k}_1,s_1}, n_{\vec{k}_1,s_2}, n_{\vec{k}_1,s_3}, ..., n_{\vec{k}_N,s_1}, n_{\vec{k}_N,s_2}, n_{\vec{k}_N,s_3} \right\rangle = \quad (16)$$

$$\left[\Pi_{\vec{k},s} \frac{1}{\sqrt{n_{\vec{k},s}!}} (a_{\vec{k},s}^{\dagger})^{n_{\vec{k},s}} \right] |0,0,0,...,0,0,0\rangle,$$

where $|0,0,0,...,0,0,0\rangle$ denotes the ground state of the system. The corresponding energy is $E = \sum_{\vec{k},s} \hbar \omega_s(\vec{k}) \left(n_{\vec{k},s} + \frac{1}{2} \right)$.

This was a lot of work in order to get the spectrum. We would like to spend some time understanding the solution. The most generally accepted interpretation of (16) is that it is a state ket corresponding to a system of $\sum_{\vec{k},s} n_{\vec{k},s}$ identical non-interacting particles called phonons. Each phonon has a wavevector and a polarization (just like a photon!) and carries an energy $\hbar \omega_s(\vec{k})$ (the function $\omega_s(\vec{k})$ is called the dispersion relation or just the dispersion sometimes). Furthermore, I claim that they are bosons. We will support this interpretation by defining the occupation number representation for identical bosons. We will then show from our analysis of the occupation number representation that the states of the harmonic crystal are mathematically equivalent to the states of identical non-interacting bosons. The next section will be devoted to developing a few formal tools needed to support our claim.

IV. THE ALGEBRA OF IDENTICAL BOSONS

Suppose that we have a system of N non-interacting identical bosons. Now consider just one of these bosons. We define the single-particle states to be the states in the Hilbert space of this particle. Let's denote these states $|\psi\rangle$. To construct the states of the N particle system, we have to take a symmetrized sum of tensor products of the single-particle states. This is because boson states must always be symmetric with respect to particle exchange. In particular, if we have an N-particle state in which a particle is in state $|\psi_1\rangle$, a second is in $|\psi_2\rangle$, ..., and an Nth particle is in state $|\psi_N\rangle$, then the appropriately symmetrized state, called $|\psi_1, \psi_2, ..., \psi_N\rangle$, to within a normalization constant, is given by:

$$|\psi_1, \psi_2, ..., \psi_N\rangle = \sum_P \left| \psi_{P(1)} \right\rangle \otimes \left| \psi_{P(2)} \right\rangle \otimes ... \otimes \left| \psi_{P(N)} \right\rangle, \qquad (17)$$

where the sum over P denotes a sum over permutations of strings of the form $P(1)P(2)...P(N)$, with P(j) being an integer between 1 and N, inclusive [3,4]. From now on, I will omit the tensor product symbol. This state should be thought of as the N-particle state constructed from permutations of product states of the form $|\psi_1\rangle$, $|\psi_2\rangle$, ... $|\psi_N\rangle$. Note that in this list, there are always N kets since we have an N-particle state but two ψs with different indices could very well refer to the same state, since two bosons can occupy the same state. For example, we could have a state $|\phi, \phi, \phi\rangle$ which is a three-particle state in which all three particles are in the single particle state $|\phi\rangle$.

Now we would like to define two operators that can take us from N particle states to $N \pm 1$ particle states. These are called bosonic creation and annihilation operators, respectively. We define the bosonic creation operator, $b_{\phi}^{\dagger}$ (from now on, just the creation operator) as follows: $b_{\phi}^{\dagger} |\psi_1, \psi_2, ..., \psi_N\rangle = |\phi, \psi_1, \psi_2, ..., \psi_N\rangle$. In other words, we go from a symmetrized N particle state with states $|\psi_1\rangle$, $|\psi_2\rangle$, ... $|\psi_N\rangle$ to the symmetrized $N+1$ particle state with states $|\phi\rangle, |\psi_1\rangle, |\psi_2\rangle, ... |\psi_N\rangle$. From this, we immediately get that $[b_{\phi_1}^{\dagger}, b_{\phi_2}^{\dagger}] = 0$. The reason is as follows: consider the states $b_{\phi_1}^{\dagger} b_{\phi_2}^{\dagger} |\psi_1, \psi_2, ..., \psi_N\rangle$ and $b_{\phi_2}^{\dagger} b_{\phi_1}^{\dagger} |\psi_1, \psi_2, ..., \psi_N\rangle$. These are just $|\phi_1, \phi_2, \psi_1, \psi_2, ..., \psi_N\rangle$ and $|\phi_2, \phi_1, \psi_1, \psi_2, ..., \psi_N\rangle$, respectively, by definition. Going back to the definition of these states in (17), it is clear that they are exactly the same! This is because the sum of all products of permutations of states $|\phi_1\rangle, |\phi_2\rangle, |\psi_1\rangle, |\psi_2\rangle, ... |\psi_N\rangle$ is precisely the same as the sum of all products of permutations of states $|\phi_2\rangle, |\phi_1\rangle, |\psi_1\rangle, |\psi_2\rangle, ... |\psi_N\rangle$. Furthermore, defining the annihilation operator to the adjoint of the creation operator (i.e; $b_{\phi} = (b_{\phi}^{\dagger})^{\dagger}$) and taking the adjoint of $[b_{\phi_1}^{\dagger}, b_{\phi_2}^{\dagger}] = 0$, we get that $[b_{\phi_1}, b_{\phi_2}] = 0$.

These commutation relations are suggestive of a harmonic oscillator algebra. To prove this, we now need to find the commutation relations between creation and annihilation operators. To do this, we will need to know what the annihilation operator does. Our intuition suggests that it will turn an N-particle state into an $N-1$-

particle state. Let's verify this. In order to verify it, I will need to invoke a formula for the inner product of two N-particle boson states, which is proven in [3]. It reads:

$$\langle \chi_1, ..., \chi_N | \psi_1, ..., \psi_N \rangle = \begin{vmatrix} \langle \chi_1 | \psi_1 \rangle & ... & \langle \chi_1 | \psi_N \rangle \\ \vdots & ... & \vdots \\ \langle \chi_N | \psi_1 \rangle & ... & \langle \chi_N | \psi_N \rangle \end{vmatrix}_+ ,$$
(18)

where the (+) subscript denotes that we are evaluating a permanent. Evaluating a permanent is like evaluating a determinant except "with no minus signs" when doing a cofactor expansion. Recall that when evaluating a determinant using a cofactor expansion (also called an expansion by minors), alternating terms pick up a minus sign. Using this, we would like to evaluate the inner product $\langle \chi_1, ..., \chi_{N-1} | b_\phi | \psi_1, ..., \psi_N \rangle$. This is equal to $\left\langle \psi_1, ..., \psi_N | b_\phi^\dagger | \chi_1, ..., \chi_{N-1} \right\rangle^*$. Using the definition of the creation operator and (18), we get that this is equal to

$$\begin{vmatrix} \langle \psi_1 | \phi \rangle & \langle \psi_1 | \chi_1 \rangle & ... & \langle \psi_1 | \chi_{N-1} \rangle \\ \vdots & & ... & \vdots \\ \langle \psi_N | \phi \rangle & \langle \psi_N | \chi_1 \rangle & ... & \langle \psi_N | \chi_{N-1} \rangle \end{vmatrix}_+^* .$$

Doing a cofactor expansion along the column of ϕs, this is equal to

$$\sum_{k=1}^N \langle \phi | \psi_k \rangle \begin{vmatrix} \langle \psi_1 | \chi_1 \rangle & ... & \langle \psi_1 | \chi_{N-1} \rangle \\ \vdots & (\text{no } \psi_k) & \vdots \\ \langle \psi_N | \chi_1 \rangle & ... & \langle \psi_N | \chi_{N-1} \rangle \end{vmatrix}_+^* ,$$

where "no ψ_k" means that we remove all terms from the permanent with ψ_k in it before evaluating it. When we pull the $\langle \phi | \psi_k \rangle$ term out, we evaluate the permanent obtained by deleting the row and column that we pulled $\langle \phi | \psi_k \rangle$ from. Writing the permanents as inner products of $N-1$-particle states, and pulling out the $\langle \chi_1, ..., \chi_{N-1} |$ (because our analysis works for arbitrary $\langle \chi_1, ..., \chi_{N-1} |$), we arrive at:

$$b_\phi | \psi_1, ..., \psi_N \rangle = \sum_{k=1}^N \langle \phi | \psi_k \rangle | \psi_1, ...(\text{no } \psi_k), ..., \psi_N \rangle .$$
(19)

This is a sum of states with $N-1$ particles, as expected. It can be shown relatively easily by direct computation of the commutator that $[b_{\phi_1}, b_{\phi_2}^\dagger] = \langle \phi_1 | \phi_2 \rangle$ [3]. Now we say the following: let the single-particle states ϕ be states belonging to an orthonormal basis $|i\rangle$ for i = 1,2,3,.... In other words, $|\phi_1\rangle = |m\rangle$ and $|\phi_2\rangle = |n\rangle$ (recall that the numerical indices are just particle labels). Then we get that the inner product in the commutator of the previous line is δ_{mn}.

The last formal tool that I will introduce is called the *occupation number representation*. Consider states of the form (17) except now each $|\psi\rangle$ is instead a state in the orthonormal basis defined in the above paragraph. In

general, a state in the occupation number representation can be expressed as $|n_1, n_2, n_3, ...\rangle$, where n_1 denotes the number of particles in the first orthonormal basis state, n_2 the number in the second, and so on. As a example, suppose we have the orthonormal basis described above and we have a state that looks like $|1, 1, 1, 3, 10, 2014\rangle$. This ket corresponds to a six-particle state with three particles in the state $|1\rangle$, one in the state $|3\rangle$, etc. The occupation number representation is another way of writing these kinds of states. In the occupation number representation, the six-particle state above would be expressed as $|3, 0, 1, ...1, ..., 1, 0, 0, ...\rangle$, where the ones are in the third, tenth, and 2014th place.

It can be shown the bosonic creation/annihilation operators act very simply on states in the occupation number basis. In particular, by using the commutation relations that we derived, it can be shown that:

$$b_i^\dagger | n_1, ..., n_i, ... \rangle = \sqrt{n_i + 1} | n_1, ..., n_i + 1, ... \rangle \qquad (20)$$
$$b_i | n_1, ..., n_i, ... \rangle = \sqrt{n_i} | n_1, ..., n_i - 1, ... \rangle \qquad (21)$$
$$| n_1, n_2, ... \rangle = \left[\Pi_i \frac{1}{\sqrt{n_i!}} (b_i^\dagger)^{n_i} \right] | 0, 0, ... \rangle , \qquad (22)$$

where $b_i^{(\dagger)}$ denotes an operator that removes (adds) a particle to the orthonormal basis state, i. This is amazing! We started with N identical bosons. We showed that we could express N-particle basis states of the space of N-particle states in terms of an occupation number representation with a simple interpretation. Each entry in the state ket tells us the number of bosons in a particular orthonormal basis state. Furthermore, we have shown that there are bosonic creation and annihilation operators that can change the number of particles in each state (equations (20) and (21)) and furthermore, they satisfy the harmonic oscillator algebra. We then showed that the states in the occupation number representation can be obtained by acting on a vacuum state (zero-particle state) with creation operators (equation (22)). The final thing to note is that the normalization constants that creation and annihilation operators introduce when they act on occupation number states are exactly the same as the constants that the harmonic oscillator creation/annihilation operators introduce when they act on the number eigenstates of the oscillator. Thus the problem of the harmonic crystal is mathematically identical to the problem of non-interacting identical bosons. We formally have the same states with the same operators with the same algebra!

In particular, we can view the problem of the harmonic crystal in terms of the following *complementary picture* [4]: the harmonic crystal states, given by (16) are states written in the occupation number representation. Each entry of the ket, $n_{\vec{k},s}$, represents exactly that number of some bosonic particle, called a phonon, in an orthonormal basis state whose energy is $\hbar \omega_s(\vec{k})$ (recall that the energy of the harmonic crystal increases by $\hbar \omega_s(\vec{k})$ when $n_{\vec{k},s}$ increases by 1). The total number of phonons in a

harmonic crystal state is given by $\sum_{\vec{k},s} n_{\vec{k},s}$. We have replaced the complicated vibrations of an entire lattice with non-interacting particles. Like particles that we're used to, they carry energy, and can scatter off of other particles. And we can develop some intuition for what new phenomena occur in solids just by thinking of them as particles that have energy and momentum, which can be absorbed or emitted when energy is moved into or out of the normal modes of the harmonic crystal. Using this bosonic particle picture, we can understand many properties of lattice vibrations in solids with relative ease. We will focus only on the specific heats of solids at low temperature.

V. SPECIFIC HEATS OF MONATOMIC METALS AT LOW TEMPERATURE

One of the biggest failures of classical physics in the 19th century was its failure to predict the temperature dependence of the specific heat of metals. Classical physics predicts that the specific heat of a solid is a temperature-independent constant equal to 3R per mole of metal, where R is the universal gas constant. This prediction is called the *Law of Dulong and Petit* and is only true at high temperatures, where the equipartition theorem can correctly describe the vibrations of a solid. [1]. The next attempt at calculating the specific heat of solids due to lattice vibrations was made by Einstein. Einstein modeled the ions in a metal as independent harmonic oscillators with the same frequency [5]. This assumption is of course incorrect. The harmonic crystal is full of phonons each with different frequencies $\omega_s(\vec{k})$. It is unsurprising given this knowledge that Einstein's prediction of the specific heat of metals has the wrong temperature dependence at low-T. In particular, he predicted that the specific heat would decay exponentially fast with temperature as $T \to 0$. It took Debye to get the correct result at low temperatures. He did this by thinking of the harmonic crystal as phonons in a box and by thinking of the statistical mechanics of the system as analogous to the statistical mechanics of photons in a box (i.e; blackbody radiation) [5]. Our derivation is different from that of Debye, but we will get the same answer. This derivation closely follows the derivation of low-T specific heats done in [1].

Because phonons are bosons, they obey Bose-Einstein statistics. Therefore, the number of phonons with energy $\hbar\omega_s(\vec{k})$ in thermal equilibrium is given by:

$$n_{\vec{k},s} = \frac{1}{e^{\beta\hbar\omega_s(\vec{k})} - 1},\qquad(23)$$

where $\beta = \frac{1}{kT}$, in which k is Boltzmann's constant and T is the temperature. Notice that we've set the chemical potential to zero because phonons can be added and removed by adding energy to the system. Dumping energy into normal modes will increase the excita-

tion numbers $n_{\vec{k},s}$ of the system. In our particle picture this corresponds to the addition of phonons to the crystal. The total energy of the phonons is given by $E_{tot} = \sum_{\vec{k},s} \frac{\hbar\omega_s(\vec{k})}{e^{\beta\hbar\omega_s(\vec{k})} - 1}$. We need to evaluate this because the specific heat is given by the derivative of the total energy with respect to temperature. It turns out that for a large enough crystal, the sum can be replaced by an integral over k-vectors. As $V \to \infty$, the spacing between k points goes to zero and the summand can't vary significantly between two k-points. Therefore we can replace the sum by an integral. Namely,

$$E_{tot} = \frac{V}{8\pi^3} \sum_s \int d^3\vec{k} \, \frac{\hbar\omega_s(\vec{k})}{e^{\beta\hbar\omega_s(\vec{k})} - 1}.\qquad(24)$$

To evaluate this integral, we will need to make several approximations. First, we need an approximate form of the dispersion relation. It turns out that for small $|\vec{k}|$ in the region of non-redundant $\vec{k}$'s, $\omega_s(\vec{k}) = c(\hat{k})|\vec{k}|$, where $c(\hat{k})$ is a direction dependent constant. See [1] for a proof. The next approximation is the low-T approximation. In other words, that the characteristic thermal energy kT corresponds only to frequencies where the dispersion relation is to very good approximation linear. Where the dispersion is nonlinear, the energy is much larger than kT. Therefore, there are nearly no contributions to the integral from values of $\vec{k}$ such that the dispersion is nonlinear. We can express (24) as

$$E_{tot} = \frac{V}{8\pi^3} \sum_s \Big(\int_{\text{linear region}} d^3\vec{k} \, \frac{\hbar\omega_s(\vec{k})}{e^{\beta\hbar\omega_s(\vec{k})} - 1}$$
$$+ \int_{\text{non-linear region}} d^3\vec{k} \frac{\hbar\omega_s(\vec{k})}{e^{\beta\hbar\omega_s(\vec{k})} - 1}\Big),\qquad(25)$$

where "(non)-linear region" denotes the region in k-space where the dispersion is (not) approximately linear. Because of the low-T approximation, we can approximate the energy using the first term of (25) with $\omega_s(\vec{k}) = c(\hat{k})|\vec{k}|$. We can also extend the limits of this integral to infinity because we're at low temperatures. Because the edge of the linear region corresponds to a place where the energy $\hbar c|\vec{k}|$ is much above kT, integrating energies beyond that, even assuming a linear dispersion, make an exponentially vanishing contribution to the integral. Thus we're left with the integral:

$$E_{tot} = \frac{V}{8\pi^3} \sum_s \int_{\text{all k}} d^3\vec{k} \, \frac{\hbar c(\hat{k})|\vec{k}|}{e^{\beta\hbar c(\hat{k})|\vec{k}|} - 1}.$$

The specific heat is given by the derivative of E_{tot} respect to temperature. Integrating in spherical coordinates, we get that the specific heat capacity is

$$C = \frac{\partial}{\partial T} \frac{V}{8\pi^3} \sum_s \int d\Omega \int_0^\infty d|\vec{k}| \, \frac{\hbar c_s(\hat{k})|\vec{k}|^3}{e^{\beta\hbar c_s(\hat{k})|\vec{k}|} - 1}.\qquad(26)$$

Doing a substitution $x = \beta \hbar c_s(\hat{k})|\vec{k}|$, defining $\frac{1}{c^3} = \frac{1}{3}\sum_s \int \frac{d\Omega}{4\pi} \frac{1}{(c_s(\hat{k}))^3}$ and using the identity $\int_0^\infty dx \frac{x^3}{e^x - 1} = \frac{\pi^4}{15}$, we finally arrive at:

$$C = \frac{2\pi^2 V k}{5}\left(\frac{kT}{\hbar c}\right)^3, \qquad (27)$$

which is the result we desired, and one consistent with measurements of the specific heats of solids at low temperatures. We have successfully solved the problem that plagued classical physics using a boson picture of the normal mode vibrations of the lattice.

VI.   SUMMARY AND CONCLUSION

We started with what at first a very complicated system. We had a lattice with N ions and every ion was interacting with every other ion via a linear restoring force. On the face of it, we were working with the Hamiltonian in (1) with U being given by (5). But through a normal mode transformation, we managed to get to (15),

giving us a problem formally identical to that of a 3N dimensional harmonic oscillator. We then showed that the excitations of this system correspond to the addition of bosonic particles to a gas. We called these bosonic particles phonons. Using the intuition that these collective vibrations of the lattice were bosons, we were able to calculate the specific heat of a solid at low-T using Bose-Einstein statistics and correctly obtained a T^3 dependence for the specific heat.

When we replace a many-body problem by non-interacting bosons, we call these bosons collective excitations. Sometimes they are called quasiparticles. Quasiparticles/collective excitations have consistently been an enormous simplifying tool in problems in many-body physics and the reason is simple. We don't have good intuition for the dynamics of $\approx 10^{23}$ particles. But we do have good intuition for the dynamics of non-interacting particles. And we can use this intuition to predict at least qualitatively phenomena that occur in many-body systems. In some cases, it's even useful for quantitative calculations, like what we did in calculating phononic contribution to the specific heat of a metal at low-T.

---

[1] N. Ashcroft and D. Mermin, *Solid State Physics* (Saunders College, Philadelphia, 1976), Chapters 22 and 23 for information on the classical and harmonic quantum crystal, pages 135-136 for information on periodic boundary conditions and k-space volumes, and appendices D and F for information on 3D Fourier series.
[2] C. Kittel, *Introduction to Solid State Physics, 8th Edition* (John Wiley & Sons, Inc., 2005), pages 27-30.
[3] R. P. Feynman, *Statistical Mechanics: A Set of Lectures* (Westview Press, 1998), pages 160-174.

[4] A. Altland, B. Simons, *Condensed Matter Field Theory* (Cambridge University Press, 2010), pages 23-24 for information on phonons and complementary pictures, and 40-46 for the formalism of dealing with identical bosons including identities involving the bosonic annihilation/creation operators.
[5] D. V. Schroeder, *An Introduction to Thermal Physics* (Addison Wesley, 2000), pages 307-312.

The Hyperfine Splitting of Hydrogen and its Role in Astrophysics

Devyn M. Rysewyk

Massachusetts Institute of Technology

(Dated: May 1, 2014)

The 21cm line of hydrogen originates from a photon that is emitted due to the spin flip transition of the electron in the ground state of the hydrogen atom. It derived by use of time-independent perturbation theory, magnetic dipole moments, spherical harmonics, and knowledge of spin. It was predicted by Van de Hulst in 1945 and observed by Ewen and Purcell in 1951. Since then, astronomers have utilized this spectral line for their work. The 21cm line is used to measure the velocity and distance of neutral hydrogen clouds which ultimately measures the rotation dynamics and the structure of galaxies.

I. INTRODUCTION

The 21cm line of hydrogen was first theorized by Van de Hulst in 1945; however, it wasn't until 1951 when it was first observed by Ewen and Purcell [5][6]. Since then, astrophysicists have used the 21cm line in astrophysics since neutral hydrogen is the most abundant element in the universe. When a photon is emitted from the hyperfine transition of hydrogen, it has a wavelength of 21cm. Since this is in the microwave length of light, it is not affected by interstellar gas and dust, unlike optical light. Radio astronomers use this to their advantage in determining the structure and dynamics of galaxies.

II. HISTORY

The prediction and observation of the 21cm line of hydrogen began with the desire for discovering the structure of our galaxy, the Milky Way. Jan Oort, a Dutch astronomer, had been working on this problem for several years. He was studying the structure and rotation of the galaxy using visible light [5]. Visible light is blocked by interstellar clouds and dust, which unfortunately, the galactic plane is littered with. Oort realized that he would have to utilize another wavelength of light to study the structure and rotation of the galaxy.

At the time, Grote Reber was working in radio astronomy. Oort heard of his work and asked if there were any radio spectral lines that existed that could be used [5]. Hendrick Van de Hulst was a student of Oort's at the time, and Oort assigned him this project. Van de Hulst immediately thought of hydrogen because it is very abundant in the universe. With further calculations, he predicted the 21cm line of hydrogen in 1945 [5].

In 1950, Harold Ewen was designing an antenna to observe the 21cm line of hydrogen, supervised by Edward Purcell. He had to use a mixer and a receiver in order to reduce the background noise [6]. He put the antenna outside of a window at Harvard University and waves traveled through a waveguide to the mixer and the receiver. Once his antenna was set up, he observed the 21cm line of hydrogen in 1951. Since then, many astronomers and astrophysicists have used the 21cm hydrogen line to determine the structure and dynamics of the Milky Way and other galaxies.

III. DERIVATION OF THE 21CM RADIATION

A. Time-Independent Perturbation Theory

Perturbation theory is used in quantum mechanics when a Hamiltonian is adjusted by a small perturbation. Changes in the wavefunctions and energy eigenvalues can be approximated by using perturbation theory. The perturbed hamiltonian is defined as:

$$H = H_0 + \delta H \tag{1}$$

where H_0 is the original hamiltonian and δH is the small perturbation. The wavefunction and energy shifts are written as $\psi_m^{m'}$ and $E_m^{m'}$ respectively where m labels the wavefunction and its corresponding energy eigenvalue and m' indicates up to which order the wavefunction or energy eigenvalue has been corrected through perturbation theory. The first-order wavefunction shift can be calculated by [1]:

$$\psi_n^1 = \sum_{m \neq n} \frac{\langle \psi_m^0 | \delta H | \psi_n^0 \rangle}{E_n^0 - E_m^0} \psi_m^0 \tag{2}$$

where $\psi_{m,n}^0$ and $E_{m,n}^0$ are the wavefunctions and energy eigenvalues of the original Hamiltonian, H_0. The first-order energy shift can be calculated by [1]:

$$E_n^1 = \langle \psi_n^0 | \delta H | \psi_n^0 \rangle \tag{3}$$

The wavefunction and energy shifts can be approximated to higher orders, but for the purpose of this problem, only first-order perturbation theory will be used.

B. The Perturbing Hamiltonian

For the hydrogen atom, the original Hamiltonian of the electron is [2]:

$$H_0 = \frac{p^2}{2m_e} - \frac{e^2}{4\pi\epsilon_0 r} \tag{4}$$

253

where m_e is the mass of the electron and e is the charge of the electron. The proton in the hydrogen nucleus can be considered a magnetic dipole. The magnetic dipole moment of a proton is [1]:

$$\boldsymbol{\mu}_p = \frac{g_p e}{2m_p} \boldsymbol{S}_p \tag{5}$$

where m_p is the mass of a proton, S_p is the spin operator of a proton, and g_p is the gyromagnetic ratio of a proton. The magnetic dipole produces a magnetic field that is given by [1]:

$$\boldsymbol{B} = \frac{\mu_0}{4\pi r^3}[3(\boldsymbol{\mu}_p \cdot \hat{r})\hat{r} - \boldsymbol{\mu}_p] + \frac{2\mu_0}{3}\boldsymbol{\mu}_p \delta^3(\boldsymbol{r}) \tag{6}$$

where the magnetic dipole is at the origin and the magnetic field is evaluated at $\boldsymbol{r}$.

The perturbation of an electron in a magnetic field is given by [2]:

$$\delta H_{HF} = -\boldsymbol{\mu}_e \cdot \boldsymbol{B} \tag{7}$$

where $\boldsymbol{\mu}_e$ is the dipole moment of an electron. The dipole moment of an electron is given by [1]:

$$\boldsymbol{\mu}_e = -\frac{g_e e}{2m_e}\boldsymbol{S}_e \tag{8}$$

where g_e is the gyromagnetic ratio of an electron. Plugging $\boldsymbol{\mu}_e$ and $\boldsymbol{B}$ into Eq. 7, the hyperfine perturbation is [1]:

$$\begin{aligned}
\delta H_{hf} &= \frac{\mu_0 g_p g_e e^2}{16\pi m_p m_e r^3}[3(\boldsymbol{S}_p \cdot \hat{r})(\boldsymbol{S}_e \cdot \hat{r}) - \boldsymbol{S}_p \cdot \boldsymbol{S}_e] \\
&\quad + \frac{\mu_0 g_p g_e e^2}{6 m_p m_e}\boldsymbol{S}_p \cdot \boldsymbol{S}_e \delta^3(\boldsymbol{r})
\end{aligned} \tag{9}$$

where the 21cm radiation will be derived by calculating δH_{hf}.

C.   The 21cm Radiation

From spherical harmonics, the ground state wavefunction of the hydrogen atom is [2]:

$$\psi_{1,0,0} = \frac{1}{\sqrt{\pi a_0^3}}e^{-\frac{r}{a_0}} = |1,0,0\rangle \tag{10}$$

where a_0 is the Bohr radius, $a_0 = \frac{4\pi \epsilon_0 \hbar^2}{m_e e^2}$. Using Eq. 3 and plugging in Eq. 9 and Eq. 10, the first order energy shift is:

$$\begin{aligned}
E_{hf}^1 &= \langle \psi_{1,0,0}| \delta H |\psi_{1,0,0}\rangle = \langle \delta H\rangle \\
&= \frac{\mu_0 g_p g_e e^2}{16\pi m_p m_e}\left\langle \frac{3(\boldsymbol{S}_p \cdot \hat{r})(\boldsymbol{S}_e \cdot \hat{r}) - \boldsymbol{S}_p \cdot \boldsymbol{S}_e}{r^3}\right\rangle \\
&\quad + \frac{\mu_0 g_p g_e e^2}{6 m_p m_e}\langle \boldsymbol{S}_p \cdot \boldsymbol{S}_e\rangle |\psi_{1,0,0}(0)|^2
\end{aligned} \tag{11}$$

The first term in E_{hf}^1 goes to zero:

$$\left\langle \frac{3(\boldsymbol{S}_p \cdot \hat{r})(\boldsymbol{S}_e \cdot \hat{r})}{r^3}\right\rangle = \int_0^\infty \frac{|\psi_{1,0,0}|^2}{r^3}r^2 dr \times$$

$$\iint 3(\boldsymbol{S}_p \cdot \hat{r})(\boldsymbol{S}_e \cdot \hat{r})\sin\theta d\theta d\phi$$

$$= 3\frac{4\pi}{3}(\boldsymbol{S}_p \cdot \boldsymbol{S}_e)\int_0^\infty \frac{|\psi_{1,0,0}|^2}{r^3}r^2 dr$$

$$\left\langle -\frac{\boldsymbol{S}_p \cdot \boldsymbol{S}_e}{r^3}\right\rangle = -\int_0^\infty \frac{|\psi_{1,0,0}|^2}{r^3}r^2 dr \times$$

$$\iint \boldsymbol{S}_p \cdot \boldsymbol{S}_e \sin\theta d\theta d\phi$$

$$= -4\pi(\boldsymbol{S}_p \cdot \boldsymbol{S}_e)\int_0^\infty \frac{|\psi_{1,0,0}|^2}{r^3}r^2 dr$$

$$\to \left\langle \frac{3(\boldsymbol{S}_p \cdot \hat{r})(\boldsymbol{S}_e \cdot \hat{r}) - \boldsymbol{S}_p \cdot \boldsymbol{S}_e}{r^3}\right\rangle = 0$$

Knowing that $|\psi_{1,0,0}(0)|^2 = 1/(\pi a_0^3)$, E_{hf}^1 can be simplified to [1]:

$$E_{hf}^1 = \frac{\mu_0 g_p g_e e^2}{6\pi m_p m_e a_0^3}\langle \boldsymbol{S}_p \cdot \boldsymbol{S}_e\rangle \tag{12}$$

We can change the dot product into something more useful by completing the square:

$$\begin{aligned}
\boldsymbol{S}_p \cdot \boldsymbol{S}_e &= \frac{1}{2}(S^2 - S_e^2 - S_p^2) \\
S^2 |s,m\rangle &= \hbar^2 s(s+1)|s,m\rangle \\
S_e^2 |s,m\rangle &= \hbar^2 s_e(s_e+1)|s,m\rangle \\
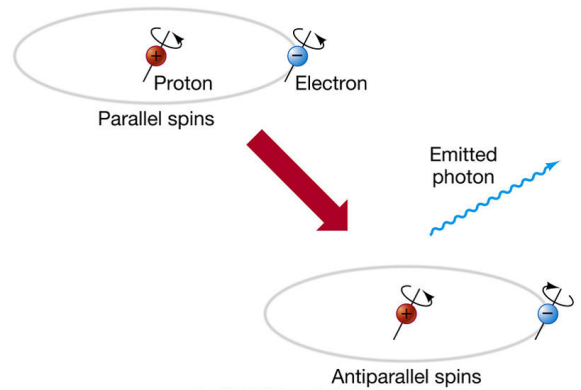S_p^2 |s,m\rangle &= \hbar^2 s_p(s_p+1)|s,m\rangle
\end{aligned}$$

FIG. 1: The triplet state is when the proton and the electron have parallel spins and the singlet state is when the proton and the electron have antiparallel spins [9].

where $\boldsymbol{S} = \boldsymbol{S}_e + \boldsymbol{S}_p$, $s = 0$ or 1, $s_e = \frac{1}{2}$, and $s_p = \frac{1}{2}$. When $s = 0$, the spins of the proton and the electron are

antiparallel. This is called the singlet state. When $s = 1$, the spins of the proton and the electron are parallel. This is called the triplet state. These states can be seen in Fig. 1. Using the fact that:

$$\langle \boldsymbol{S}_p \cdot \boldsymbol{S}_e \rangle = \frac{\hbar^2}{2}(s(s+1) - s_e(s_e+1) - s_p(s_p+1))$$

$$= \begin{cases} \frac{\hbar^2}{4} & \text{triplet} \\ -\frac{3\hbar^2}{4} & \text{singlet} \end{cases} \quad (13)$$

the final answer for the first order energy shift is:

$$E_{hf}^1 = \frac{\mu_0 g_p g_e e^2 \hbar^2}{6\pi m_p m_e a_0^3} \begin{cases} \frac{1}{4} & \text{triplet} \\ -\frac{3}{4} & \text{singlet} \end{cases} \quad (14)$$

This result differs from the results of [1] and [2] only by how the fundamental constants were laid out. This splitting of energy can be seen in Fig. 2. The energy difference
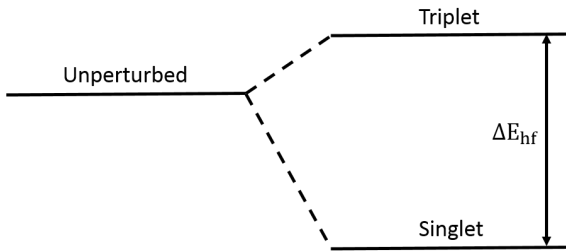

FIG. 2: The triplet state is when the proton and the electron have antiparallel spins and the singlet state is when the proton and the electron have parallel spins [1].

between the triplet state and the singlet state is the energy of the photon that is emitted from the hyperfine transition. This energy difference is:

$$\Delta E_{hf} = \frac{\mu_0 g_p g_e e^2 \hbar^2}{6\pi m_p m_e a_0^3} \quad (15)$$

Knowing that $g_p = 5.59$ and $g_e = 2$, the energy difference is $\Delta E_{hf} = 5.882 \times 10^{-6}$ eV. The energy of this photon can be converted into a frequency, or a wavelength [1]:

$$\nu = \frac{\Delta E_{hf}}{h} = 1420 \text{ MHz}$$

$$\lambda = \frac{hc}{\Delta E_{hf}} = 21 \text{ cm}$$

IV. ROLE IN ASTROPHYSICS

Astrophysicists use the 21cm line of hydrogen to probe galaxies because neutral hydrogen is the most abundant element in the universe and it is not affected by interstellar clouds or dust [4]. After the prediction and subsequent observation of the 21cm line of hydrogen, astronomers have been able to study the structure and dynamics of the galaxy in great detail.
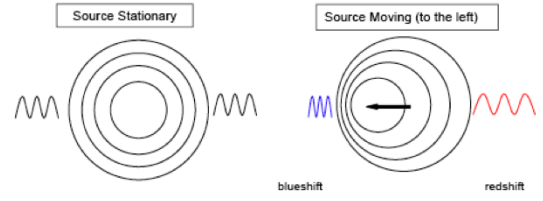
A. The Doppler Effect

FIG. 3: Observed light from a moving source has a lower or higher frequency than if the source was stationary [11].

Before discussing the role that the 21cm line has in astrophysics, we must know what the doppler effect is. The light originating from a moving object will appear to have a lower or higher frequency than when the object is stationary. When the light-emitting source is moving towards an observer, the frequency of the light is higher than the original frequency. This means that the light is shifted towards the blue end of the electromagnetic spectrum, or it is blueshifted. This can be seen in Fig. 3. When the source is moving away from an observer, the
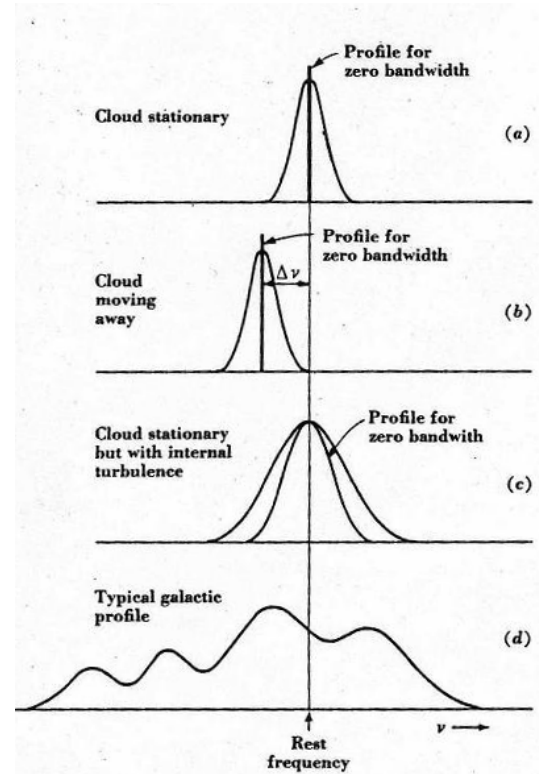

FIG. 4: The top three figures show idealized hydrogen doppler shift profiles and the bottom figure shows a typical observed hydrogen doppler shift profile [4].

frequency of the light is lower than the original frequency, or it is redshifted.

In astronomy, doppler shift is used to calculate the velocity of light-emitting sources. For radio astronomy in particular, a radio telescope is used to obtain doppler shift profiles. Ewen used a rectangular antenna to detect the 21cm line. Today, radio astronomers use a parabolic antenna. The signal travels from the sky into a series of band pass filters and amplifiers which focuses the signal around 1420 MHz, or 21 cm. Once the signal is focused around 1420 MHz, the signal travels to a mixer and a receiver which reduces the amount of background noise in the signal. The signal is then sent to a computer where the hydrogen-line profiles can be seen.

There are three idealized hydrogen profiles that can be seen. To the observer, the neutral hydrogen cloud can look stationary. When the cloud is stationary, the center of doppler shift profile will be at the rest frequency, 1420 MHz. The cloud can be moving with a velocity that can be determined. The center of the doppler shift profile will be some frequency, ν away from the rest frequency. The radial velocity can then be calculated by:

$$v_r = \left(\frac{\nu - \nu_0}{\nu} \right) c \qquad (16)$$

where v_r is the radial frequency, c is the speed of light, ν is the observed frequency, and ν_0 is the rest frequency, 1420 MHz. The cloud can also be stationary with internal motion inside of the cloud [4]. This is when the center of the doppler shift profile is centered around the rest frequency, but the profile is a bit wider than when there is no internal motion in the cloud. These three hydrogen profiles can be seen in Fig. 4. Observed hydrogen profiles have a combination of the idealized hydrogen profiles and multiple clouds in one profile. This can also be seen in Fig. 4.

B. Structure and Dynamics of the Milky Way

The observed hydrogen profiles taken at different galactic longitudes translate into doppler shifts. The doppler shifts allow for the radial velocities of the neutral hydrogen clouds to be calculated by using Eq. 16. Using the complex galactic geometry seen in Fig. 5, the rotational velocity of the neutral hydrogen clouds can be calculated using [3]:

$$\theta_{rot} = v_r - v_{lsr} + (\theta_{sun} + v_e)\sin l \qquad (17)$$

where θ_{rot} is the rotational velocity, $\theta_{sun} = 220 \ \frac{\text{km}}{\text{s}}$ is the rotational velocity of the sun, l is the galactic longitude, v_e is the velocity of the earth, and v_{lsr} is the velocity of the local standard of rest. v_{lsr} describes the mean motion of stars in the solar neighborhood.

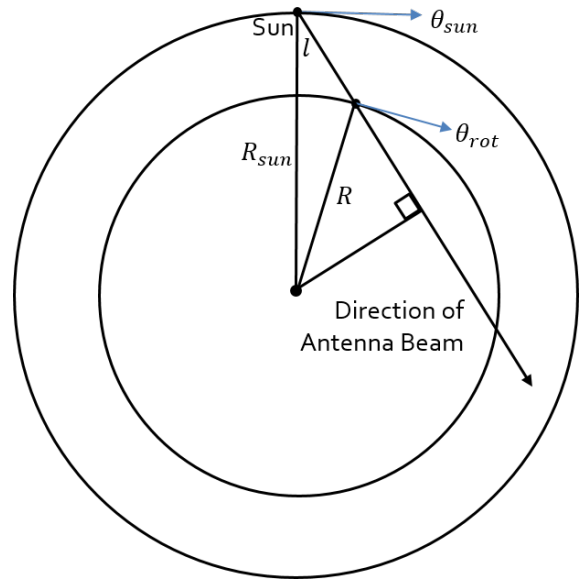The rotation of the galaxy depends on the mass distribution. An example of a mass distribution is a solid

FIG. 5: Galactic geometry [3].

body, or a uniform sphere. The rotation curve of a solid body gives a velocity that is proportional to the radius:

$$
\begin{aligned}
F &= ma \\
\frac{GMm}{r^2} &= \frac{mv^2}{r} \\
\frac{G\frac{4}{3}\pi r^3 \rho}{r^2} &= \frac{v^2}{r} \\
v &\propto r
\end{aligned}
$$

where m is the mass of a star inside of a galaxy, r is the distance between the center of the galaxy and the star, $M = \frac{4}{3}\pi r^3 \rho$ is the enclosed mass of the galaxy at radius r, and ρ is a constant density. Another mass distribution is the Keplerian mass distribution, or a central mass. The rotation curve of a central mass gives:

$$
\begin{aligned}
\frac{GMm}{r^2} &= \frac{mv^2}{r} \\
v &\propto \frac{1}{\sqrt{r}}
\end{aligned}
$$

The Keplerian mass distribution models the luminous matter in the Milky Way. Examples of these mass distributions and the rotational velocity curve of the Milky Way can be seen in Fig. 6 and Fig. 7, respectively. However, the rotation curve of the Milky Way does not match the Keplerian mass distribution curve. This means that there is a lot more matter in the galaxy than we can actually see. This matter is called dark matter. Plotting the rotational velocity curve of the Milky Way using the 21cm line of hydrogen is one way to give evidence that dark matter exists in the galaxy.

The galactic geometry used to calculate the rotational velocity can also be used to calculate the radius of the
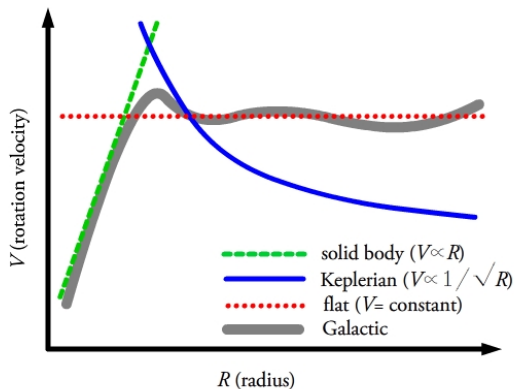
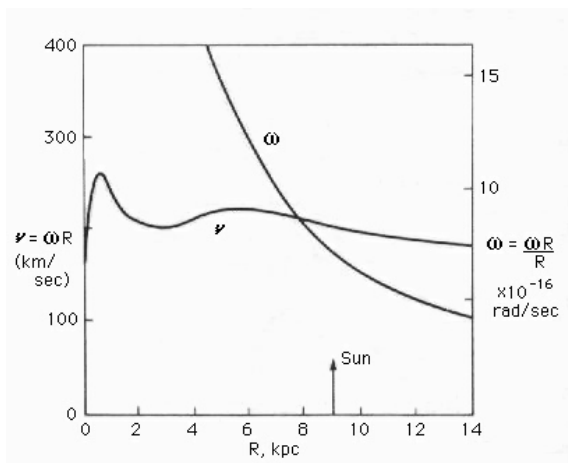FIG. 6: Examples of different mass distributions [9].

FIG. 7: The observed rotational velocity, v, and the angular velocity, ω of the Milky Way as a function of radius from the center of the galaxy [4].
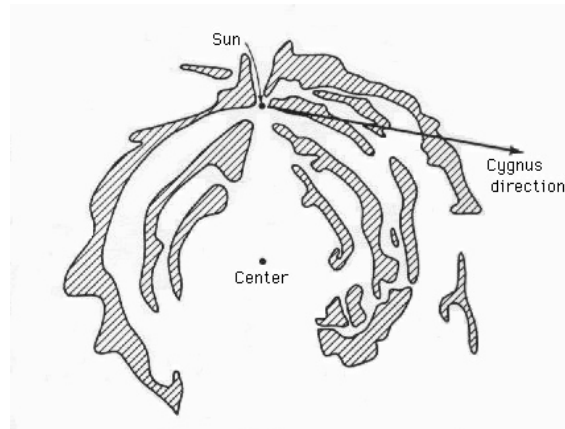

FIG. 8: A map of the neutral hydrogen in the Milky Way plotted by Kerr and Westerhout in 1964 using the 21cm line of hydrogen. [4].

specifically, the time during reionization. Reionization occurred from about 400 million years to a billion years after the big bang. Galaxies and quasars started to form at the beginning of reionization. Quasars are galaxies with a supermassive blackhole at the center. The supermassive blackhole at the center takes in mass at a high rate, and therefore is highly luminous. The 21cm radiation has been used in order to probe these early galaxies and quasars. 21cm absorption has been detected from early galaxies and quasars [7] and the gas density, velocity profiles, ionization state, and temperature profiles have been modeled for dwarf galaxies that formed in the beginning of reionization [8]. The evolution of these dwarf galaxies could also be detected, and therefore, through the use of the 21cm line of hydrogen, astrophysicists aim to understand the thermal history of the universe [8].

neutral hydrogen clouds using [3]:

$$R = R_{sun} \sin l \qquad (18)$$

where $R_{sun} = 8$ kpc is the radius of the sun from the center of the galaxy. Knowing the radii and the galactic positions of these clouds, the neutral hydrogen in the galaxy can be mapped. The distribution of the neutral hydrogen in the Milky Way is shown in Fig. 8. The areas of dense neutral hydrogen clearly show the spiral arms within the galaxy. This led to the classification of the Milky Way as a spiral galaxy [4].

C. Early Galaxies

The 21cm line of hydrogen has applications beyond that of studying our own galaxy. Recently, the hyperfine transmission has been used to probe the early universe,

V. CONCLUSION

Through time-independent perturbation theory, magnetic dipole moments, spherical harmonics, and spin, the 21cm line of hydrogen was derived. When Van de Hulst predicted the 21cm line in 1945 and Ewen and Purcell observed the line in 1951, they had made a significant advancement in the field of astronomy and astrophysics. The 21cm line of hydrogen has proven to be very useful in measuring properties of not only the Milky Way, but other galaxies as well. Molecular hydrogen can also be used to study galaxies; despite that it is far less abundant that neutral hydrogen [4]. The structure and dynamics of the Milky Way can also be determined by measuring the distance to stars within the galaxy using stellar parallax [10]. With all of these techniques in determining the structure and dynamics of galaxies, astronomers continue to make advances in the field of astrophysics.

Acknowledgments

---

[1] Griffiths, David, *Introduction to Quantum Mechanics*, 2004: Pearson Prentice Hall.

[2] Gasiorowicz, Stephen, *Quantum Physics*, 2003: John Wiley & Sons, Inc.

[3] Mihalas, Dimitri and James Binney, *Galactic Astronomy*, 1968: Freeman, San Fransisco.

[4] Kraus, John and et. al., *Radio Astronomy*, 1986: Cygnus-Quasar.

[5] NRAO, *Oort & Van de Hulst*, 2003: http://www.nrao.edu/whatisra/hist_oortvandehulst.shtml

[6] NRAO, *Ewen & Purcell*, 2011: http://www.nrao.edu/whatisra/hist_ewenpurcell.shtml

[7] N. Gupta, R. Srianand, P. Noterdaeme, P. Petitjean and S. Muzahid, "21-cm absorption from galaxies at z=0.3," arXiv:1308.4141 [astro-ph.GA].

[8] Y. Xu, A. Ferrara and X. Chen, "The earliest galaxies seen in 21 cm line absorption," Mon. Not. Roy. Astron. Soc. **410**, 2025 (2011) [arXiv:1009.1149 [astro-ph.CO]].

[9] *Interstellar Medium*, 2013: http://physics.uoregon.edu/~jimbrau/astr122/notes/chapter18.html

[10] M. J. Reid, K. M. Menten, A. Brunthaler, X. W. Zheng, T. M. Dame, Y. Xu, Y. Wu and B. Zhang *et al.*, "Trigonometric Parallaxes of High Mass Star Forming Regions: the Structure and Kinematics of the Milky Way," Astrophys. J. **783**, 130 (2014) [arXiv:1401.5377 [astro-ph.GA]].

[11] Sherman, Reid, *A Doppler Shift Speed Gun*, 2007: http://cfcpwork.uchicago.edu/kicp-projects/nsta/2007/sherman/doppler.htm

Solving Neutrino Oscillation with Matrix Mechanics

William Spitzer
(Dated: May 2, 2014)

Our understanding of neutrinos has improved since their initial discovery. Experimentally, we have discovered the fact that neutrinos can oscillate between different flavors in its lifetime. Theoretically, we can represent the oscillation in the form of a matrix. We will explore how to utilize the neutrino oscillation matrix in order to calculate the probability of a flavor evolving into another flavor in its time evolution. We will also consider a solution with four neutrino flavors as a possible solution to the LSND anomaly.

I. INTRODUCTION

The neutrino was first theorized by Wolfgang Pauli in 1930 as an idea created to resolve the problems involved with an early model for the nucleus of an atom.[1] It was initially called the neutron and described as a neutral particle with a mass like that of the electron. Some inspiration for this theory came from the need of a neutral particle to fix the model of the nucleus and the process of radioactive decays. A resolution to the nucleus model appeared when James Chadwick discovered what we now know as the neutron, and Pauli's neutron, renamed as the neutrino, became discarded as a solution to this problem. The neutrino would be ignored until several years later in 1934, when Fermi was working on his theory of weak interactions, which included the problem of energy conservation in the mechanism of beta decay. In beta decay, Fermi found that the end products seemed to have a lower energy than the initial state. He concluded that the missing energy could be explained in the form of a neutral particle and reintroduced the neutrino as a solution. His theory was verified when in 1937 the muon neutrino was discovered from cosmic rays.[2]

In the 1950's, experiments showed that in some weak processes, particles could violate parity in decay. Parity is the reversal in sign of a spatial coordinate of a particle. This idea is similar to that of left and right handed particles. Other than parity, the particles in these processes were found to hold the exact same properties as each other. This result hinted at the possibility that a particle could change its parity through these weak interactions. As more became known about the neutrino, various anomalies began to appear. These anomalies suggested that neutrinos could be particles that could change between different states, or flavors as they are now known. One such anomaly that prompted this idea was the inconsistency between theoretical neutrino detection and experimental neutrino detection from the sun.

In this paper, we will explore how the theory of neutrino oscillation came about and the matrix created to help calculate these oscillations. In sections II, we give discuss the solar neutrino problem that led to the theory of neutrino oscillation. In section III, we introduce the Pontecorvo-Maki-Nakagawa-Sakata Matrix used in calculating neutrino oscillations. In section IV, we compute the two-flavor neutrino oscillation as a demonstration of the calculation process. In section V, we calculate the full three-flavor neutrino oscillation and compare the transition probabilities from different starting neutrino flavors. In section VI, we discuss the current state of neutrino theory and anomalies that have yet to be resolved. Finally in section VII, we consider the possibility of a fourth neutrino and its effect on neutrino oscillations.

II. SOLAR NEUTRINO PROBLEM

The solar neutrino problem was a major inconsistency in neutrino theory that eventually led to neutrino oscillation theory. The nuclear process that fuels the sun, hydrogen fusion, releases large quantities of electron neutrinos which can be detected via liquid detectors. However, the first detections of solar neutrinos found a much lower flux of electron neutrinos than expected: approximately a third of the predicted value. Physicists proposed several explanations such as the nuclear processes slowing down in the solar core, but these were all rejected due after advancements in the ability to measure data from the sun. This problem puzzled physicists until they discovered the possibility of neutrino oscillation.

Put forth by Bruno Pontecorvo in his 1968 paper, the idea of neutrino oscillation is explained by neutrino masses[3]. If neutrinos exist in flavor states that are superpositions of different neutrino mass states, then it is possible that over a long enough period of time or distance, the neutrino could change its mass by oscillating from one flavor to another. Therefore, in the case of solar neutrinos, it is possible that the neutrinos emitted by the sun change their flavor over the course of the journey from the sun to the earth. Years later, three different flavors of neutrinos were detected from the sun which matched his predictions. The electron neutrino was detected in 1969, the muon neutrino in 1973, and the tau neutrino in 1995[2]. With experimental data backing up the idea, neutrino oscillation became a well accepted theory in particle physics.

III. PMNS MATRIX

The theory of neutrino oscillation was developed by Bruno Pontecorvo.[3] With the discovery of the different

flavors of neutrinos, Pontecorvo developed a matrix that could be used to give a time dependent solution of neutrino oscillation which can then be used to calculate the transition probabilities between the different flavors of neutrinos. In our current theory in the standard model, we have flavor eigenstates $|v_e\rangle$, $|v_\mu\rangle$, and $|v_\tau\rangle$, and mass eigenstates $|v_1\rangle$, $|v_2\rangle$, and $|v_3\rangle$. The flavor eigenstates are related to the mass eigenstates in the following form.

$$|v_f\rangle = U_{fm}|v_m\rangle \qquad (1)$$

where f and m represents the flavor and mass eigenstates. The matrix U is called the Pontecorvo Maki Nakagawa Sakata (PMNS) matrix. We will use this matrix to calculate the transition probabilities between different neutrino flavors.

IV. TWO FLAVOR NEUTRINO OSCILLATION

We will first begin by working through the two state example in order to understand how to calculate neutrino oscillations using matrices. For the two state example, we will use the flavor eigenstates $|v_e\rangle$, $|v_\mu\rangle$ and mass eigenstates $|v_1\rangle$, $|v_2\rangle$. The PMNS matrix relating the two bases is the rotation matrix in two dimensions about an angle θ. For two flavors, the flavor and mass eigenstates will be related by the single rotation angle θ as shown in figure 1 [4].
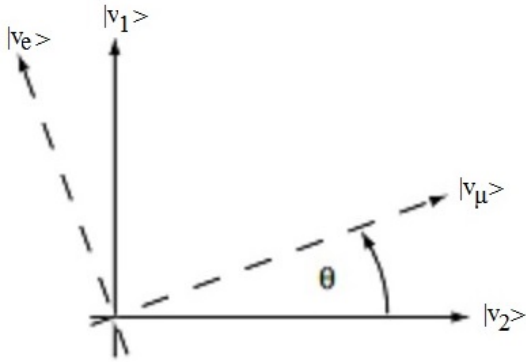

FIG. 1. The neutrino flavor eigenstates are a rotation of its mass eigenstates. The angle θ is the mixing angle between the two bases[4].

For higher dimensions, the PMNS matrix will still be an angular rotation matrix between the flavor eigenstates and mass eigenstates. However, we will have $c(n,2) = \frac{n(n-1)}{2}$ rotation angles to consider. When we perform the calculation using three and four neutrino flavors, we will have more rotation angles involved. For two flavor states, we can write the equation relating the flavor eigenstates and mass eigenstates as follows

$$\begin{pmatrix} v_e \\ v_\mu \end{pmatrix} = \begin{pmatrix} \cos\theta & \sin\theta \\ -\sin\theta & \cos\theta \end{pmatrix} \begin{pmatrix} v_1 \\ v_2 \end{pmatrix} \qquad (2)$$

The next step will be to consider time evolution. This will have the form

$$|v_e(t)\rangle = cos(\theta)e^{-i\frac{E_1 t}{\hbar}}|v_1\rangle + sin(\theta)e^{-i\frac{E_2 t}{\hbar}}|v_2\rangle \qquad (3)$$

$$|v_\mu(t)\rangle = -sin(\theta)e^{-i\frac{E_1 t}{\hbar}}|v_1\rangle + cos(\theta)e^{-i\frac{E_2 t}{\hbar}}|v_2\rangle \qquad (4)$$

We will be assuming neutrinos are relativistic, so the energies will be in the form $E_1 = \sqrt{p^2c^2 + m_1^2 c^4}$ and $E_2 = \sqrt{p^2c^2 + m_2^2 c^4}$ where $p \gg m_1, m_2$. After setting $\hbar = 1$ and $c = 1$, we will expand to second order of the mass term to get $E_1 = \frac{m_1^2 + 2p^2}{2p}$ and $E_2 = \frac{m_2^2 + 2p^2}{2p}$ and extract the E_1 time dependence as a phase factor. Let $\alpha = \frac{m_1^2 + 2p^2}{2p}$ and $\beta = \frac{m_1^2 - m_2^2}{2p}$ to simplify the equations.

$$|v_e\rangle = e^{-i\alpha t}(cos(\theta)|v_1\rangle + sin(\theta)e^{i\beta t}|v_2\rangle) \qquad (5)$$

$$|v_\mu\rangle = e^{i\alpha t}(-sin(\theta)|v_1\rangle + cos(\theta)e^{i\beta t}|v_2\rangle) \qquad (6)$$

Ignoring the phase, the time evolution has left the difference of the masses on the $|v_2\rangle$ mass term. This term is important because the transition probability will depend on time and the frequency of the transitions will depend on the difference in the square of the masses. Now we wish to find the probability of finding a particular flavor after some time t given a starting neutrino flavor. We can calculate these probabilities using the formulas $P(v_e \rightarrow v_\mu) = |\langle v_\mu|v_e\rangle|^2$ and $P(v_\mu \rightarrow v_e) = |\langle v_e|v_\mu\rangle|^2$.

$$P(v_e \rightarrow v_\mu) =$$
$$|(-sin(\theta)\langle v_1| + cos(\theta)\langle v_2|)\cdot$$
$$(e^{-i\alpha t}(cos(\theta)|v_1\rangle + sin(\theta)e^{i\beta t}|v_2\rangle))|^2$$
$$= 2sin^2(\theta)cos^2(\theta)(1 - cos(\beta t))$$
$$= sin^2(2\theta)sin^2(\frac{\beta t}{2}) \qquad (7)$$

$$P(v_\mu \rightarrow v_e) =$$
$$|(cos(\theta)\langle v_1| + sin(\theta)\langle v_2|)\cdot$$
$$(e^{-i\alpha t}(-sin(\theta)|v_1\rangle + cos(\theta)e^{i\beta t}|v_2\rangle))|^2$$
$$= 2sin^2(\theta)cos^2(\theta)(1 - cos(\beta t))$$
$$= sin^2(2\theta)sin^2(\frac{\beta t}{2}) \qquad (8)$$

We see that the transition probabilities are identical which is expected since we arbitrarily named the flavor eigenstates. The transition probability is only dependent on β which is the difference between the squares of the two neutrino masses. We can substitute back for $\frac{\beta t}{2}$ using $\beta = \frac{m_1^2 - m_2^2}{2p} = \frac{\Delta m^2}{2E}$ and $t = x$ for relativistic neutrinos. We will also include $\hbar$ and c and substitute $\hbar c = 197eV \cdot$

nm to get a dimensionless value for the second sine term.

$$P_{trans} = sin^2(2\theta)sin^2(\frac{\Delta m^2 x}{4E})$$

$$= sin^2(2\theta)sin^2(\frac{\Delta m^2 c^4 x}{4E\hbar c})$$

$$= sin^2(2\theta)sin^2(\frac{1.27\Delta E_v^2 x}{E}) \qquad (9)$$

We will plot the probability P against $\frac{x}{E}$ for both neutrino flavors using $\Delta E_v^2 = 2*10^{-3}eV^2$ and $sin^2(2\theta) = .95$. ΔE_v^2 is the difference in the square of the energies of the neutrino masses and $sin^2(2\theta)$ is the mixing angle according to experimental results for atmospheric neutrinos[5]. We normalized the distance by the energy of the neutrinos.
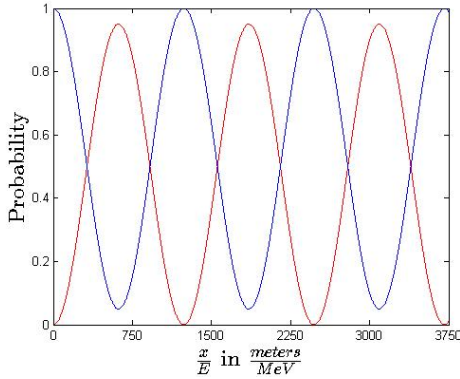

FIG. 2. Probability of finding a neutrino flavor at a distance $\frac{x}{E}$ after starting in a flavor state $|v_e\rangle$. The curve starting at P = 1 represents $P(v_e \rightarrow v_e)$ and the curve starting at P = 0 represents $P(v_e \rightarrow v_\mu)$.

We see that the transition probability is maximized at $\frac{x}{E} \approx 600$ which is when $sin^2(\frac{\beta t}{2}) \approx \pi/2$.

V.   THREE FLAVOR NEUTRINO OSCILLATION

We now move on to the full PMNS 3 by 3 matrix with v_e, v_μ, v_τ are the flavor eigenstates and v_1, v_2, v_3 are the mass eigenstates.

$$\begin{pmatrix} v_e \\ v_\mu \\ v_\tau \end{pmatrix} = \begin{pmatrix} U_{e1} & U_{e2} & U_{e3} \\ U_{\mu1} & U_{\mu2} & U_{\mu3} \\ U_{\tau1} & U_{\tau2} & U_{\tau3} \end{pmatrix} \begin{pmatrix} v_1 \\ v_2 \\ v_3 \end{pmatrix} \qquad (10)$$

The PMNS matrix will be the product of the three rotation matrices possible in a three state system.

$$\begin{pmatrix} c_{12}c_{13} & s_{12}c_{13} & s_{13}e^{-i\delta} \\ -s_{12}c_{23} - c_{12}s_{23}s_{13}e^{i\delta} & c_{12}c_{23} - s12s_{23}s_{13}e^{i\delta} & s_{23}c_{13} \\ s_{12}s_{23} - c_{12}c_{23}s_{13}e^{i\delta} & -c_{12}s_{23} - s12c_{23}s_{13}e^{i\delta} & c_{23}c_{13} \end{pmatrix}$$

where $s_{ij} = sin(\theta_{ij})$, $c_{ij} = cos(\theta_{ij})$, θ_{ij} are the mixing angles between the masses i and j, and δ is a phase that is nonzero if the neutrino oscillation breaks CP symmetry[6]. CP symmetry refers to charge parity symmetry and states that if a particle is interchanged with its antiparticle, then it will act the same under the laws of physics if the parity is flipped. Particles, such as neutrinos, that violate this symmetry are said to break the CP symmetry. The time evolutions of these flavors will then have the form

$$|v_f(t)\rangle = \Sigma_{n=1}^3 e^{-iE_n t/\hbar}U_{fn}|v_n\rangle \qquad (11)$$

for each flavor f. From here, we can calculate the transition probabilities. We will use $|v_f1\rangle$ as our starting flavor eigenstate and $|v_f2\rangle$ as our ending flavor eigenstate. The full expansion of the transition probabilities is much larger so we will not show them here.

$$P(v_{f1} \rightarrow v_{f2}) = |\Sigma_{n=1}^3 U_{f1n}U_{f2n}^* e^{-i(m_n^2)\frac{L}{2E}}|^2 \qquad (12)$$

With these equations, we can calculate the probabilities and plot them again. For these probabilities, we expect to see three curves that oscillate at slightly different periods. We will use $sin^2(2\theta_{12}) = 0.857$, $sin^2(2\theta_{13}) = 0.095$, $sin^2(2\theta_{23}) = 0.95$, $\Delta m_{21}^2 = 7.5 \cdot 10^{-5}eV^2$, $\Delta m_{31}^2 = 2.4 \cdot 10^{-3}eV^2$, and $\Delta m_{32}^2 = 2.32 \cdot 10^{-3}eV^2$. These values have been determined from experimental data that has been fit according to the theoretical predictions for the neutrino oscillation equations that we have determined. The experimental values for the angles and mass differences with errors are shown below[6].

$$sin^2(2\theta_{12}) = 0.857 \pm 0.024$$
$$sin^2(2\theta_{23})\rangle 0.95$$
$$sin^2(2\theta_{13}) = 0.095 \pm 0.010$$
$$\Delta m_{21}^2 = (7.5 \pm 0.2) \cdot 10^{-5}eV^2$$
$$|\Delta m_{21}^2| = (2.32^{+0.12}_{-0.08}) \cdot 10^{-3}eV^2$$

The plot of the transition probabilities for v_e and v_μ are shown here.

These plots are interesting in several ways. First, the probability curves for v_e have small oscillations on top of them, while the curves for v_μ have large oscillations on top. This oscillation arises from the different θ values that are present in a three dimensional matrix; we can clearly see the effect of a larger θ value.

Second, the transition probability $P(v_e \rightarrow v_e)$ is never 0 which means that the v_e flavor can always be measured no matter where it is measured at, while $P(v_\mu \rightarrow v_\mu)$ does hit 0 sometimes. However, the other two transition probabilities in the v_e plots have points at which they are approximately 0 which means that the v_e flavor is almost guaranteed to be measured. Despite the fact that $P(v_\mu \rightarrow v_\mu)$ does hit 0, both $P(v_e \rightarrow v_e)$ and $P(v_\mu \rightarrow v_\mu)$ probabilities return to 1 periodically, which is expected since it should return to its original state after some time.
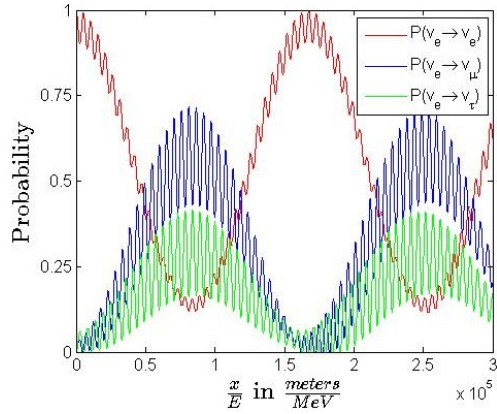
FIG. 3. Probability of finding a neutrino flavor at a distance $\frac{x}{E}$ after starting in a flavor state $|v_e\rangle$.
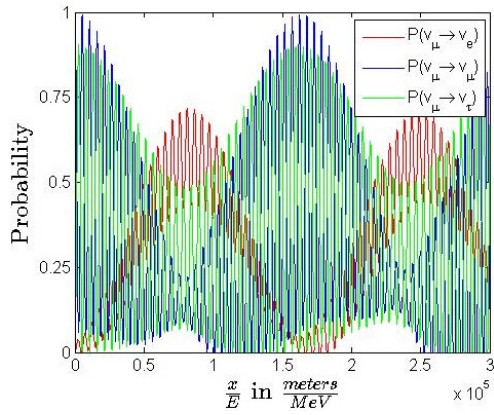

FIG. 4. Probability of finding a neutrino flavor at a distance $\frac{x}{E}$ after starting in a flavor state $|v_\mu\rangle$.

Finally, the shape of the transition probability of the electron flavor is distinctly different compared to the transition probabilities of muon flavor and tau flavor. In both figures, the tau and the muon transition probabilities have similar shapes and cover the same areas at the same time. This result suggests that the tau and muon neutrinos have similar proportions of mass eigenstates and the mass eigenstates consist of similar proportions of muon and tau flavor states. We see in figure 5 that the model of the neutrino masses do have mass eigenstate compositions with almost equal quantities of muon and tau neutrino flavors. This fact is interesting because it means that the v_e neutrino is different in some way compared to the other two flavors.

The diagram of masses in figure 5 shows the current theoretical positions of the neutrino mass eigenstates in comparison with each other. These masses are based on experimental values for the square of the difference in masses. As a result, there are two models that could pos-
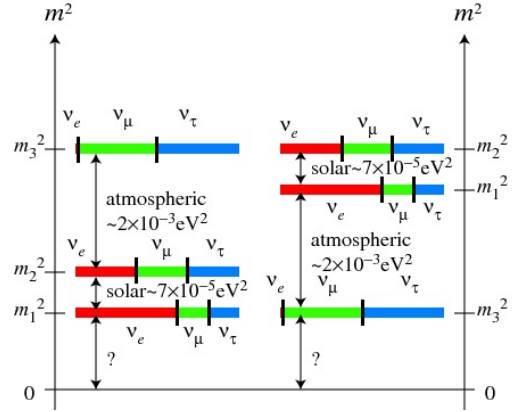

FIG. 5. Composition of the neutrino mass eigenstates in terms of the neutrino flavor eigenstates[7].

sibly describe the relationship between the mass eigenstates. Experiments to determine the value of Δm_{32} are underway to identify the correct model.

VI. THE STANDARD MODEL AND THE LSND ANOMALY

Currently there are three neutrino flavors that are known to exist: electron, mu, and tau neutrinos. The existence of these neutrino flavors fit well with the Standard Model, a theoretical model that connects three of the four fundamental forces of nature: weak, strong, and electromagnetic nuclear forces. The existence of the three neutrino flavors were predicted from the electron, muon, and tau particles, which gave the flavors their names. However, the Standard Models predicted that the neutrinos lacked mass, contradicting the fact that neutrinos undergo oscillations. If instead, we use the Standard Model as guide to assign masses to the neutrino flavors, then it would make sense to consider v_e the lightest, followed by v_μ, and v_τ the heaviest based on the masses of the electron, muon, tau particles. Because the masses of the neutrino flavors are not known, we cannot determine whether or not this is accurate. Thus, the Standard Model does not fully explain the properties of neutrinos and can be improved upon.

In addition to mass problem from the Standard Model, neutrino masses also create problems in experimental detections. There are several experimental anomalies that the current theory of neutrinos cannot explain. The most puzzling of these anomalies, the Liquid Scintillator Neutrino Detector(LSND) anomaly, gave results of neutrino energy differences that differed from theoretical predictions by several orders of magnitude. The LSND was a detector set in Los Alamos Meson Physics Facility that aimed to find neutrino oscillations from v_μ anti-neutrinos that came from a proton target[8]. They managed to de-

tect a difference in neutrino mass; however, this mass difference was on the order of ≈ 1 eV compared to other experimental values on the order of $\approx 10^{-5}$ to 10^{-3} eV.

A possible solution to these problems is the existence of sterile neutrinos, a different type of neutrino that does not interact via interactions other than gravity[9]. By adding in an additional neutrino with a different mass from the existing neutrino flavors, the large mass difference found in the LNSD detection could be explained. However, if a fourth neutrino flavor is discovered, then the current 3 by 3 matrix used to calculate neutrino oscillations will need to be adjusted.

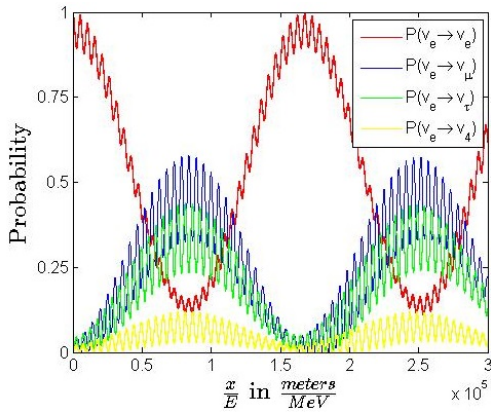## VII. FOUR FLAVOR NEUTRINO OSCILLATION

FIG. 6. Probability of finding a neutrino flavor at a distance $\frac{x}{E}$ after starting in a flavor state $|v_e\rangle$ for four neutrino flavor eigenstates.

Using the same framework that we have used to calculate the two and three state neutrino oscillations, we will also use to calculate the four state neutrino oscillation. We will begin by calculating the PMNS matrix. This matrix will be a product of all the rotations possible in a four state system. If we consider the WXYZ plane, we can have WX, WY, WZ, XY, XZ, and YZ rotations for a total of 6 possible rotation matrices. The matrix will not be presented because it is very large. We then follow equation 12 to calculate the transition probabilities. We will use the values $sin^2(2\theta_{12}) = 0.857$, $sin^2(2\theta_{13}) = 0.095$, $sin^2(2\theta_{14}) = 0.01$, $sin^2(2\theta_{23}) = 0.95$, $sin^2(2\theta_{24}) = 0.1$, $sin^2(2\theta_{34}) = 0.9$, $\Delta m_{21}^2 = 7.5 \cdot 10^{-5} eV^2$, $\Delta m_{31}^2 = 2.4 \cdot 10^{-3} eV^2$, $\Delta m_{41}^2 = \Delta m_{42}^2 = \Delta m_{43}^2 = 1 eV^2$, and $\Delta m_{32}^2 = 2.32 \cdot 10^{-3}$. The angular values were chosen to be similar to the three state case and the mass difference values were chosen based on the LSND predicted values. The main difference is that the transition probability $P(v_e \rightarrow v_\mu)$ has gone down. The point where the transition probability $P(v_e \rightarrow v_4)$ is maximal is where the transition probability $P(v_e \rightarrow v_e)$ is the lowest, so this point could be used as an experimental starting point.

VIII. CONCLUSION

We have investigated the calculations of neutrino oscillations using the PMNS matrix in the two flavor neutrino example to understand how neutrino oscillations work out mathematically. Following this, we were able to calculate neutrino oscillations for three flavors and to produce a plot of neutrino oscillations given initial conditions on the rotation angles and mass differences between the neutrino eigenstates. However, neutrino oscillation is still not a completely understood subject. Although we can accurately predict some phenomenon of neutrino oscillations, we still lack concrete answers to others such as the LSND anomaly. If a fourth neutrino is found, it could solve the problem of the LNSD anomaly and provide possibilities to consider for other currently unsolved questions including the nature of dark matter. We have demonstrated the changes necessary to be made to the PMNS in order to correctly account for a fourth neutrino and an example of its effect on neutrino oscillations.

[1] A. Gouvea, TASI Lectures on Neutrino Physics, (2004), pg 3-6.
[2] I. Anicin, The Neutrino, (2005), pg 1-11.
[3] B. Pontecorvo, Neutrino Experiments and the Problem of Conservation of Leptonic Charge, (Soviet Physics Jetp 1967), pg 1-2.
[4] D. Smith, Calculating the Probability for Neutrino Oscillation, (2001), pg 1-16.
[5] B. Kayser, Neutrino Mass, Mixing, and Flavor Change, (2005), pg 7.
[6] X. Qian et al, Unitary Tests of the Neutrino Mixing Matrix, (2013), pg 1-2.
[7] S. King et al, Neutrino Mass and Mixing with Discrete Symmetry (2013).
[8] C. Athanassopoulos, The Liquid Scintillator Neutrino Detector and LAMPF Neutrino Source, (1996), pg 1-4.
[9] A. Strumia, Interpreting the LSND Anomaly, (2002), pg 1-3.

Describing Quantum and Stochastic Networks using Petri Nets

Adam Strandberg
(Dated: 2 May 2014)

We discuss the basics of stochastic petri nets, the rate equation, the master equation, and the connections between stochastic and quantum mechanics. Unless otherwise noted, everything is drawn from work by John Baez and Jacob Biamonte in [1].

I. STOCHASTIC PETRI NETS

In many fields, one encounters a network of connected objects that can react to form new objects. Examples include

- chemistry: networks of chemical reactions

- physics: particle creation and annihilation

- biology: predator-prey relationships

- computer science: resource flow and queuing

Stochastic petri nets are mathematical objects designed to model the evolution of these networks over time, assuming that each reaction happens randomly at some specified rate.

A **petri net** consists of a set S of species and a set T of transitions, together with two fuctions $s, t : T \to \mathbb{N}^S$. These specify the source and target of each transition. [2] (Note: we can equivalently say that a petri net is a directed multigraph whose nodes are multisets of species and whose edges are transitions between those multisets.) In a graphical representation, species are indicated by circles, while transitions are indicated by boxes. For each transition τ, there is an arrow from each species in $s(\tau)$ to τ, and an arrow from τ to each species in $t(\tau)$.

A **stochastic petri net** is a petri net equipped with a function $r : T \to \mathbb{R}$, specifying the rate of each reaction. Oftentimes, the transitions are labelled by their rates.

II. THE RATE EQUATION

In chemistry, statistical mechanics and biology, we are concerned with the overall concentration of particles in given states. For example, when calculating the acidity of a solution, we care about the relative amounts of H^+, OH^-, and H_2O.

We define a **classical state** $x(t)$ to be a map $S \to \mathbb{R}$ specifying the expected value or concentration of each species. (Note: the variable t is overloaded throughout this paper, referring both to time and to the target function. We trust that it will be unambiguous in context.) The rate equation gives a systematic method for determining the time evolution of classical states given a petri net. Namely, we want an equation such that given a stochastic petri net and a state $x(0)$, we can find $\frac{d}{dt}x(t)$. For the time being, we will take this as a given rule with

heuristic motivation. Later we will see the conditions under which this equation arises from considering stochastic evolution.

To understand the rate equation, we must first define vector exponentiation, which is a sort of generalization of a dot product. In the dot product, we multiply elementwise and then sum; here we exponentiate elementwise and then take the product. If we have two vectors $x = (x_1, x_2, ...x_n) \in X^A, y = (y_1, y_2, ...y_n) \in Y^A$, such that exponentiating elements of X by elements of Y is well defined, then we define

$$x^y \equiv x_1^{y_1} x_2^{y_2} ... x_n^{y_n} \qquad (1)$$

Note that $x^y \in X$. Note also that this quantity is basis-dependent, unlike the dot product. As a concrete example, take $x, y \in \mathbb{R}^2$, with $x = (1, 2), y = (3, 4)$. Then, we have

$$x^y = (1^3)(2^4) = 16$$

To motivate the form of the equation, we note that the amount of a species can only change via some transition. Each transition τ will happen at a rate given by the number of ways it could possibly happen (given by combinatorial consideration) times a rate constant (given by $r(\tau)$). How many ways can a reaction happen? To have a reaction with inputs $s(\tau)$, you need to pick $s_i(\tau)$ objects from each species $i \in S$. If we assume that the objects are all distinguishable, and you pick with replacement, the number of ways to do this given a number of things $x(t)$ is $\prod_{i \in S} x_i(t)^{s_i(\tau)}$, or in our new notation, $x(t)^{s(\tau)}$. The assumption of picking with replacement seems wrong: if you need two H^+ ions to make H_2O, you can't use the same ion twice! However, the rate equation is used to describe systems with large numbers of interacting particles, and when you have large numbers picking a few things without replacement is almost the same as picking a few things with replacement.

Next, we need to find out how much stuff gets moved around each time a transition occurs. This is straightforward enough: the change in a species is just the amount of that species output by the transition minus the amount used up: $t_i(\tau) - s_i(\tau)$. We can combine everything we know so far into one compact equation, the rate equation:

$$\frac{d}{dt}x(t) = \sum_{\tau \in T} r(\tau)\big(t(\tau) - s(\tau)\big)x(t)^{s(\tau)} \qquad (2)$$
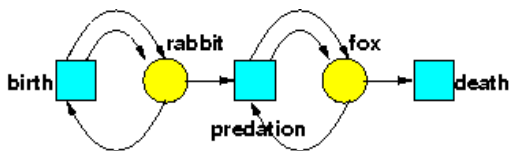
FIG. 1: An example of a predator/prey relationship, represented as a stochastic petri net [1]

For clarity, let's parse this bit by bit. The left-hand side is a vector specifiying the rate of change of each species. The right-hand side is also a vector that says that for each transition, take the base rate of the transition times the amount the transition changes the species by, then multiply by the number of ways the transition can happen given the stuff you have. Sum over all transitions and you're done.

Example II.1. Consider the stochastic petri net in figure II.1:

This is a toy model of a predator/prey relationship: rabbits can make more rabbits, foxes can eat a rabbit in order to have enough energy to reproduce, and foxes can also just die. There are obviously issues with this model, one of which is that rabbits don't reproduce via binary fission, but the qualitative behavior of the model is sufficiently interesting that real biologists actually study it.

Let $x_R(t)$ and $x_F(t)$ denote the concentrations of rabbits and foxes, respectively. Let α, β, and γ be the rates at which birth, predation and death occur. The rates are then given by

$$\frac{d}{dt}x_R(t) = \alpha(x_R^2 - x_R) - \beta x_R x_F$$

$$\frac{d}{dt}x_F(t) = \beta(x_F^2 - x_R x_F) - \gamma x_F$$

III. THE MASTER EQUATION

While the rate equation is great for cases in which you have a large number of interacting objects (for instance, chemicals in solution), it is not the full story. Since we consider the transitions as random processes, we want to have a system that, given a probability distribution over the number of objects of each species, tells us how this full probability distribution evolves. This will have the advantage of being able to describe systems with small numbers of objects of each species, as well as developing powerful analogies with quantum mechanics.

To describe the probability distribution over numbers of objects of species, we use formal power series. A formal power series given a species $i \in S$ is just a series $\big(\Psi(z_i)\big)(t) = \sum_{n_i=0}^{\infty} \psi_{n_i}(t)z_i^{n_i}$, where $\psi_n(t) \in \mathbb{R}$. The

formal variable z does not have any particular meaning; it's just a tool we use. We interpret this formal power series as such: z_i^n represents the basis vector corresponding to n objects of species i, and $\psi_{i,n}$ is the probability that there are this n objects of species i. Consider a petri net with three species, denoted A, B, and C. Say that you start out believing at time zero that there's a 60% chance you have 5 of species A, and a 40% chance you have 1 of species A, 2 of species B, and 16 of species C. This state would be represented as

$$\big(\Psi(z_A, z_B, z_C)\big)(0) = 0.6z_A^5 + 0.4z_A z_B^2 z_C^{16}$$

We can condense this notation by defining two vectors, $z = (z_1, z_2...z_{|S|})$ and $n = (n_1, n_2...n_{|S|})$. We can then express the power series as $\Psi(z)(t) = \sum_{n \in \mathbb{N}^S} \psi_n z^n$. Since we are interpreting the ψ_n as probabilities, we should enforce that $\psi_n(t) \geq 0 \forall n, t$ and $\sum_{n \in \mathbb{N}^S} \psi_n = 1$. (We will see later how the requirement for non-negative probabilities plays in.) A power series that has these properties is called a **stochastic state**.

Given a stochastic state, how do we figure out the time evolution of the state? Taking a cue from quantum mechanics, we assume there exists a linear operator on the space of power series called the Hamiltonian (H), such that

$$\frac{d}{dt}\Psi(z)(t) = H\Psi(z)(t) \tag{3}$$

We define the **creation operator** $a_i^\dagger$ on a species i such that $a_i^\dagger z_i^{n_i} = z_i^{n_i+1}$. If we have a state in which there are definitely n_i objects of species i, applying the creation operator to that state gives a state with $n_i + 1$ objects (hence the name).

The **annihilation operator** a_i is given by $a_i z_i^{n_i} = \frac{d}{dz_i}z_i^{n_i} = n_i z_i^{n_i-1}$. If we are in a definite state with n_i objects, this brings us to a state with $n_i - 1$ objects, but why the factor of n_i? This is due to the fact that there are n_i ways to choose which object to annihilate, as opposed to creating an object, in which there is only one choice. If this is confusing, it will become clearer when we look at the master equation.

For notational convenience, we define vectors of operators $a^\dagger$ and a such that $a^\dagger = (a_1^\dagger, a_2^\dagger...a_{|S|}^\dagger), a = (a_1, a_2...a_{|S|})$.

(Note to self: what are other reasons H should be a linear operator?)

The Hamiltonian is given by

$$H = \sum_{\tau \in T} r(\tau)\big(a^{\dagger t(\tau)} - a^{\dagger s(\tau)}\big)a^{s(\tau)} \tag{4}$$

Example III.1. Consider again the petri net from example II.1. We denote the annihilation operators for rabbits and foxes as a_R and a_F, respectively. The Hamiltonian is then

$$H = \alpha(a_R^{\dagger 2} - a_R^\dagger)a_R + \beta(a_F^{\dagger 2} - a_R^\dagger a_F^\dagger)a_R a_F + \gamma(1 - a_F^\dagger)a_F$$

Let $r^m f^n$ denote a state with r rabbits and f foxes. Assume we start in a state in which we are certain there are two rabbits and one fox. We have $\Psi(0) = r^2 f$. The rate of change at time zero is then

$$\frac{d}{dt}\Psi(0) = H\Psi(0)$$

$$\frac{d}{dt}\Psi(0) = \left(\alpha(a_R^{\dagger 2} - a_R^\dagger)a_R + \beta(a_F^{\dagger 2} - a_R^\dagger a_F^\dagger)a_R a_F + \gamma(1 - a_F^\dagger)a_F\right)r^2 f$$

$$\frac{d}{dt}\Psi(0) = \alpha(a_R^{\dagger 2} - a_R^\dagger)2rf + \beta(a_F^{\dagger 2} - a_R^\dagger a_F^\dagger)2r + \gamma(1 - a_F^\dagger)r^2$$

$$\frac{d}{dt}\Psi(0) = \alpha(2r^3 f - 2r^2 f) + \beta(2rf^2 - 2r^2 f) + \gamma(r^2 - fr^2)$$

This expression looks ugly, but it has a nice interpretation. At a rate α, we are gaining probability that there will be three rabbits and one fox ($r^3 f$). Total probability is conserved, so we lose probability at the same rate from the state with two rabbits and one fox ($r^2 f$). The factor of two comes from the fact that there are two ways to pick one rabbit from a collection of two distinguishable rabbits. Similarly, we gain probability that there is one rabbit and two foxes at the cost of probability theat there are two rabbits and one fox. Through the "death" transition, we gain probability there is one fewer fox at the cost of probability that it stays the same.

A. Eigenvectors of the Hamiltonian and Negative Probabilities

In quantum mechanics, it proves very useful to find the energy eigenstates of the Hamiltonian. Energy eigenstates behave simply under time evolution: they just rotate with a complex phase! Consider the eigenstates ϕ_n such that

$$H\phi_n(t) = \lambda_n \phi_n(t) \tag{5}$$

Since H is an operator over a complex vector space, its eigenvectors span the space, and any state $\psi(t)$ can be expressed as a linear combination of (normalized) eigenvectors: $\psi(t) = \sum_n c_n \psi_n(t)$. It is then trivial to get the solution for all time given an initial condition:

$$\varphi(t) = U(t)\varphi(0) = e^{iHt}\varphi(0)$$

$$\varphi(t) = \sum_n c_n e^{i\lambda_n t}\phi_n(0) \tag{6}$$

We can verify that this evolution is in fact unitary:

$$|\varphi(t)|^2 = \sum_{m,n} c_m c_n^* \delta_{mn} e^{i(\lambda_m - \lambda n)t}$$

$$|\varphi(t)|^2 = \sum_m c_m c_m^* = |\varphi(0)|^2$$

Since this is so useful in quantum mechanics, let us try to apply the same idea to stochastic mechanics. Given a formal power series at time zero $\Psi(0)$, we can express the time evolution as

$$\Psi(t) = U(t)\Psi(0) = e^{Ht}\Psi(0)$$

$$\Psi(t) = \sum_n c_n e^{\lambda_n t}\Psi_n(0) \tag{7}$$

There is a problem here. While the evolution of an eigenstate in the quantum picture was guaranteed to be unitary, the evolution in the stochastic picture is not stochastic unless $\lambda_n = 0$. For any other value the probability exponentially blows up or decays. Didn't we say earlier that probability should be conserved by the master equation? That's still true, but it only applies to valid stochastic states. The issue is that the eigenvectors are not valid stochastic states: they can have negative components.

The use of negative probabilities to solve problems whose solutions can only have non-negative probabilities is analogous to the use of complex analysis in the solution of real differential equations. While the solutions cannot take on those values, the steps to solving the problem are most easily broken down into components using those values.

Negative probabilities have also been used in describing quantum mechanics For example, the Wigner quasiprobability distribution, which was developed by Eugene Wigner in 1932 as a way to extend classical probability distributions for systems in thermal equilibrium to quantum ones, can specifiy some joint configurations as having negative probability (hence the use of the term "quasiprobability"). [3]

IV. NOETHER'S THEOREM

Given a Hamiltonian H, an observable O, and any analytic function $f : \mathbb{R} \to \mathbb{R}$, then

$$[O, H] = 0$$

if and only if

$$\frac{d}{dt}\langle f(O)\rangle(t) = 0$$

A. Case Study: Ion Channels and Antiparticles

Brain function is mediated by neurons, which fire action potentials to send signals. In order to function properly, a neuron needs to precisely control the voltage across its membrane by selectively allowing ions, such as Na$^+$ and K$^+$, to pass through ion channels. These channels open up when the cell needs to become more or less polarized. However, the channels need to have a high degree of specificity for one type of ion in order to function properly. They do this by having a site in the middle of the channel where only one ion can bind at a time, for which the binding affinity is highly tuned to the size of the ion. [4]

A naive approach to modelling this system is shown in the following diagram: an extracellular ion (E) flows into the channel (C) and then becomes an intracellular ion (I). There are two problems here. The first is that we only allow ions to flow from the outside of the cell to the inside of the cell. This is mostly to make the example cleaner, but it's worth noting that there are some ion channels that act like diodes in that most of the current only flows in one direction. The larger problem is that an arbitrary number of ions are allowed to be in the channel at the same time. To get around this, we use a formal trick and introduce an "antichannel" species, called $C^\dagger$ in suggestive analogy with antiparticles in quantum mechanics. We then make it so that an ion exiting the channel creates an antichannel ion, and a particle can only enter the channel if it destroys an antichannel ion. We therefore expect that the number of channel ions plus the number of antichannel ions should remain constant. Let's use Noether's theorem to prove it.

Let the observable N_{chan} be the number of C plus the number of $C^\dagger$:

$$N_{chan} = N_C + N_{C^\dagger} = a_C^\dagger a_C + a_{C^\dagger}^\dagger a_{C^\dagger} \qquad (8)$$

The Hamiltonian for this petri net is

$$H = \alpha(a_C^\dagger - a_E^\dagger a_{C^\dagger}^\dagger)a_E a_{C^\dagger} + \beta(a_I^\dagger a_{C^\dagger}^\dagger - a_C^\dagger)a_C \qquad (9)$$

We note that for each species $i, j \in S$, $[N_i, a_j] = -\delta_{ij}a_i$ and $[N_i, a_j^\dagger] = \delta_{ij}a_i^\dagger$. We also note that for any operators

A, B and C, we have $[A, BC] = [A, B]C + B[A, C]$. Using these facts gives

$$[N_C, H] = \alpha[N_C, a_C^\dagger a_E a_{C^\dagger}] + \beta[N_C, a_I^\dagger a_{C^\dagger}^\dagger a_C] = \alpha a_C^\dagger a_E^\dagger a_{C^\dagger}^\dagger - \beta a_I^\dagger a_{C^\dagger}^\dagger$$

$$[N_{C^\dagger}, H] = \alpha[N_{C^\dagger}, a_C^\dagger a_E a_{C^\dagger} + \beta[N_{C^\dagger}, a_I^\dagger a_{C^\dagger}^\dagger a_C] = -\alpha a_C^\dagger a_E^\dagger a_{C^\dagger}^\dagger + \beta a_I^\dagger$$

Adding these together gives

$$[N_{chan}, H] = 0. \qquad (10)$$

Now we know that if we start out in a state in which $\langle N_{chan}\rangle = 1$, for all time we will have $0 \le \langle N_C\rangle \le 1$, accurately modelling the fact that we have a single binding site.

A. GUIDE TO NOTATION

Variable	Meaning	Type
a_i	annihilation operator	$P \to P$
a	annihilation operator	$S \to (P$
$a_i^\dagger$	creation operator	$P \to P$
$a^\dagger$	creation operator	$S \to (P$
H	Hamiltonian	$P \to P$
N_i	number operator	$P \to P$
N	number operator	$S \to (P$
$\langle O\rangle$	expectation value of observable O	$\mathbb{R}$
P	space of formal power series on S	$\mathbb{R}^S \to \mathbb{R}$
r	rate constant	$T \to \mathbb{R}_{\ge 0}$
s	source	$T \to \mathbb{N}^S$
t	time	$\mathbb{R}$
t	target	$T \to \mathbb{N}^S$
x	classical state	$\mathbb{R} \to (S$
ϕ_n	eigenvector of Hamiltonian with eigenvalue λ_n	$\mathbb{R} \to (\mathbb{N}^S$
φ	quantum state	$\mathbb{R} \to (\mathbb{N}^S$
ψ_n	probability of n objects	$\mathbb{R}$
Ψ	stochastic state	$\mathbb{R} \to (\mathbb{R}^S_{\ge}$

[1] J. Baez and J. Biamonte, *A Course on Quantum Techniques for Stochastic Mechanics* (ArXiv, 2013).
[2] J. Desel, *Unifying Petri Nets* (Springer-Verlag, 2001), chap. What is a Petri Net?
[3] E. Wigner, Phys. Rev. **40**, 749 (1932).
[4] K. et. al., *Principles of Neural Science* (McGraw-Hill, 2013), chap. 5, 5th ed.

The Path Integral Formulation of Quantum Mechanics

Phong T. Vo[*]

Department of Physics, Massachusetts Institute of Technology, Cambridge, Massachusetts 02139

(Dated: May 2, 2014)

In this paper, we derive the Feynman path integral via finite discretization, from which we recover the Schrodinger equation as a demonstration of consistency. With all the basic elements introduced, we then pause to examine more closely the mathematical structure of the Feynman path integral in relation to its Euclidean analog. Next, we apply this formulation to solving the free particle and the harmonic oscillator. Furthermore, we also emphasize applications in statistical mechanics. We conclude by briefly surveying the diverse utility of the path integral.

I. INTRODUCTION

The early pioneers of quantum mechanics, including Erwin Schrodinger, Paul Dirac, and Werner Heisenberg, focused their efforts on describing quantum dynamics through the governing Hamiltonian. Although certainly a remarkably fruitful approach, it proved difficult when applied directly to the renormalization of quantum electrodynamics. The unsatisfactory state of knowledge in the 1930's intrigued the then-youthful Richard P. Feynman to seek the solution that ultimately led him to the discovery of a new formulation of quantum mechanics.

As an undergraduate at MIT, Feynman was puzzled by the self-interaction of a charge with its own electromagnetic field [1]. He proposed that perhaps a charge does not interact with its own field at all. In fact, the concept of field to him is auxiliary, although useful, in describing what is fundamentally action-at-a-distance. As a consequence, this viewpoint necessitated that a radiating charge must experience radiative reaction [2]. Working with John Wheeler, his graduate advisor at Princeton University, to make this picture of radiative reaction consistent, Feynman found that a combination of both advanced and retarded solutions to Maxwell's equations was needed [3, 4].

With this new theory of electrodynamics, Feynman looked for a consistent quantum picture. He needed a formulation that not only considers the current state of a system, but also its past and future [2], a feature that the Hamiltonian approach lacks. The classical principle of least action provided Feynman with an answer, but it needed alterations to be consistent with quantum mechanics. So he began searching for such a theory.

At the dawn of his search, Feynman was guided by a proposal of Dirac in a 1933 paper [2] which claims that

$$\text{``}(q_t|q_T) \text{ corresponds to } \exp\left[i \int_T^t Ldt/h\right]\text{.''} \quad (1)$$

Feynman ultimately found that the probability of a particle initially at position and time (x_i, t_i) getting to a final position and time (x_f, t_f) depends on all paths connecting the two events. Each path contributes equally to the probability, but with a different complex phase given by the classical action of the path in units of $\hbar$.

This is distinctly different from classical mechanics in that a classical particle travels between two space-time coordinates precisely by one path, the one that minimizes the action. As quantum mechanics is inherently probabilistic, this discrepancy is perhaps not too surprising. In fact, we can gain some intuition for this viewpoint by considering an electron in the two-slit experiment [5]. We know the initial location of the electron from the emitter and its final destination at the detector. Which slit the electron goes through is an ill-defined concept, however. Thus, to find the probability that the electron gets to the detector, we must add contributions from both slits.

This approach of summing over all paths is elegantly described by the Feynman path integral, the central theme of this manuscript. In the pages to come, we will derive the path integral and apply it to different quantum systems as illustration of its utility.

II. THE PRINCIPLE OF LEAST ACTION

Before we formally define the path integral in quantum mechanics, we first recall a basic result of relevance from classical theory. The principle of least action states that the path which a classical particle takes from an initial location and time (x_i, t_i) to a final location and time (x_f, t_f) is the one that minimizes the action defined as

$$S = \int_{t_i}^{t_f} \mathcal{L}(x, \dot{x}, t)dt, \quad (2)$$

where $\mathcal{L}(x, \dot{x}, t)$ is the Lagrangian describing the particle, defined as the difference between the particle's kinetic energy, $K(\dot{x})$, and potential energy, $V(x,t)$, x is a generalized spatial variable, $\dot{x}$ is the corresponding generalized velocity, and t denotes time [5, 6].

The action S is a functional whose value depends on the particular path of the particle. So to minimize S, we must consider all possible paths, and the one for which S is minimal is the physical path. To find the physical path, we use the calculus of variations. Let $\tilde{x}(t)$ be the actual path of the particle. Consider another path slightly perturbed by $\delta x(t)$ from the actual path. By virtue that $\tilde{x}(t)$ minimizes S, to first order, the differential change in S about $\tilde{x}(t)$ vanishes

$$\delta S = S[\tilde{x}(t) + \delta \tilde{x}(t)] - S[\tilde{x}(t)] = 0. \quad (3)$$

Evaluating the action while imposing this constraint leads us to the *Euler-Lagrange equation*

$$\frac{d}{dt}\left[\frac{\partial \mathcal{L}}{\partial \dot{x}}\right] - \frac{\partial \mathcal{L}}{\partial x} = 0. \quad (4)$$

In classical mechanics, given a Lagrangian, we can predict the unique path of the particle using Eq. 4.

———
[*] Email address: vophong@mit.edu

III. DERIVATION OF THE PATH INTEGRAL

In quantum mechanics, we pose a slightly different question regarding the path of a particle with a given Lagrangian than that in classical mechanics. Instead of looking for a specific, unique path which the particle must take, we seek to find the probability of the particle being at (x_f, t_f) knowing its initial condition at (x_i, t_i). Richard Feynman conjectured that, in fact, all paths that the particle can take from (x_i, t_i) to (x_f, t_f) contribute equally to the probability amplitude, but each with a different complex phase given by the classical action in units of $\hbar$. Said differently, suppose we have the wavefunction $\psi(x+\delta x, t)$; we are interested in finding the wavefunction $\psi(x, t+\delta t)$, where δx and δt denote infinitesimally small changes in position and time respectively. As derived in Refs. [2, 7], Feynman proposed that

$$\psi(x, t+\delta t) = \frac{1}{A} \int \exp\left(\frac{i}{\hbar} \int_t^{t+\delta t} \mathcal{L}dt'\right) \psi(x+\delta x, t)d(\delta x),$$
(5)

where the overall integral is the sum over all paths, and A is a normalization constant to be determined. Assuming that for a particle of mass m

$$\mathcal{L} = \frac{1}{2}m\dot{x}^2 - V(x, t) \approx \frac{1}{2}m\left(\frac{\delta x}{\delta t}\right)^2 - V(x, t),$$
(6)

we have

$$\psi(x, t+\delta t) = \left\{\int \exp\left(i\frac{\delta t}{\hbar}\left[\frac{m}{2}\left[\frac{\delta x}{\delta t}\right]^2 - V(x, t)\right]\right)\right.$$
$$\left. \times \frac{\psi(x+\delta x, t)d(\delta x)}{A}\right\}.$$
(7)

Now, we expand $\psi(x+\delta x, t)$ about $\delta x = 0$ and find

$$\psi(x, t+\delta t) = \frac{1}{A}\exp\left(-\frac{i\delta t}{\hbar}V(x, t)\right) \times$$
$$\int \exp\left(\frac{im}{2\hbar}\frac{\delta x^2}{\delta t}\right)\left(\psi(x, t) + \delta x\frac{\partial\psi}{\partial x} + \frac{\delta x^2}{2}\frac{\partial^2\psi}{\partial x^2} + ...\right)d(\delta x).$$
(8)

We are now left with integrals of the form

$$\int \frac{\delta x^n}{n!}\exp\left(\frac{im}{2\hbar}\frac{\delta x^2}{\delta t}\right)d(\delta x) \qquad n = 0, 1, 2, ...,$$

which have analytic solutions [2]. Substituting in the integrals, we find, to first order in δt,

$$\psi(x, t+\delta t) = \frac{\sqrt{\frac{2i\pi\hbar\delta t}{m}}}{A}e^{-\frac{i\delta t V}{\hbar}}\left(\psi(x, t) + \frac{i\hbar\delta t}{2m}\frac{\partial^2\psi}{\partial t^2}\right).$$
(9)

Now, if we let $\delta t \to 0$, then physical intuition requires that $\psi(x, t+\delta t) \to \psi(x, t)$ because the evolution of the wavefunction is continuous. We consequently must have

$$A = \sqrt{\frac{2i\pi\hbar\delta t}{m}}.$$
(10)

Substituting in A and performing Taylor expansion for $\psi(x, t+\delta t)$ and $e^{-i\delta t V/\hbar}$ about $\delta t = 0$, we find that

$$\psi(x, t)+\delta t\frac{\partial\psi}{\partial t} = \psi(x, t)+\frac{i\hbar\delta t}{2m}\frac{\partial^2\psi}{\partial t^2}-\frac{i\delta t V}{\hbar}\psi(x, t)+\mathcal{O}(\delta t^2).$$
(11)

Simplifying Eq. 11 and taking the limit as $\delta t \to 0$ yield

$$i\hbar\frac{\partial\psi(x, t)}{\partial t} = -\frac{\hbar^2}{2m}\frac{\partial^2\psi(x, t)}{\partial x^2} + V(x, t)\psi(x, t),$$
(12)

which is precisely the *time-dependent Schrodinger equation*. Thus, we see that this formulation based on the sum over all paths is equivalent to that of wave mechanics. The wavefunction we find using Feynman's method encodes the same information as that solved through the Schrodinger equation.

Having shown its consistency, we can now generalize this result to find the wavefunction $\psi(x_f, t_f)$ at arbitrary space and time coordinates from $\psi(x_i, t_i)$ [5]. First, we partition the interval $t_f - t_i$ into N equal subintervals of length δt. We denote the time interval limits as $t_0, t_1, t_2, ..., t_N$. Likewise, we partition the corresponding spacial intervals such that $x_0 = x(t_0) = x_i$, $x_1 = x(t_1)$, $x_2 = x(t_2)$, ..., $x_N = x(t_N) = x_f$. We can now define $\psi(x_N, t_N)$ iteratively

$$\psi(x_N, t_N) \approx \frac{1}{A}\int e^{\frac{i}{\hbar}\mathcal{S}(x_N, x_{N-1})}\psi(x_{N-1}, t_{N-1})dx_{N-1},$$
(13)

where $\mathcal{S}(x_N, x_{N-1}) = \int_{t_{N-1}}^{t_N}\mathcal{L}dt'$ is the classical action. Iterating Eq. 13 $N-1$ times, we obtain

$$\psi(x_N, t_N) \approx \frac{1}{A^{N-1}}\iint ... \int \prod_{k=1}^{N}\exp\left(\frac{i}{\hbar}\mathcal{S}(x_k, x_{k-1})\right)\psi(x_0, t_0)dx_{N-1}...dx_2 dx_1.$$
(14)

To make our notation more compact, we note that

$$\prod_{k=1}^{N}\exp\left(\frac{i}{\hbar}\mathcal{S}(x_k, x_{k-1})\right) = \exp\left(\frac{i}{\hbar}\mathcal{S}(x_f, x_i)\right).$$

Additionally, we define a new infinite-dimensional inte-

gral operator $\mathcal{D}[x(t)]$ by

$$\int_{x_0}^{x_N}\mathcal{D}[x(t)] = \lim_{\delta t \to 0}\left(\frac{m}{2i\pi\hbar\delta t}\right)^{\frac{N-1}{2}}\int ... \int dx_{N-1}...dx_1,$$
(15)

Furthermore, we now adopt the Dirac bra-ket notation for simplicity by using the position base ket in the Heisen-

berg picture $|x_N, t_N\rangle$ for the state represented in position by $\psi(x_N, t_N) = \langle x_N, t_N|\psi\rangle$ as in Refs. [8, 9]. Thus, in the continuum limit as $\delta t \to 0$, we finally obtain *Feynman's path integral*

$$\langle x_N, t_N|x_0, t_0\rangle = \int_{x_0}^{x_N} \mathcal{D}[x(t)] \exp\left(\frac{i}{\hbar}\mathcal{S}(x_f, x_i)\right). \quad (16)$$

Eq. 16 is also known as the *Minkowski path integral*. In the Schrodinger picture, with a time-independent Hamiltonian H, we have

$$\langle x_N, t_N|x_0, t_0\rangle = \langle x_N|e^{-\frac{i(t_f - t_0)H}{\hbar}}|x_0\rangle,$$

showing that the path integral yields the matrix elements of the time-evolution operator. This interpretation is consistent with our motivation, in that the path integral allows us to evaluate the probability amplitude at some space-time coordinate given initial conditions.

In our new notation, the probability of finding the particle at (x_f, t_f) from (x_i, t_i) is simply $|\langle x_N, t_N|x_0, t_0\rangle|^2 dx_N$. To simplify the notation, we define the *propagator* as

$$K(x_f, t_f, x_i, t_i) = \langle x_f, t_f|x_i, t_i\rangle, \quad (17)$$

and note some of its properties. With this definition, we need not resort to Feynman's path integral for insight. Rather, we can use the Heisenberg picture to understand its properties as noted in Ref. [8] and then compare them to the path integral formulation as a check of consistency.

First, the propagator is nothing more than the *kernel* of Schrodinger's equation in the sense that given $K(x_f, t_f, x_i, t_i)$, we can convolve it against an initial wavefunction to find the final wavefunction. That is

$$\psi(x_f, t_f) = \langle x_f, t_f|\psi\rangle = \int \langle x_f, t_f|x_i, t_i\rangle\langle x_i, t_i|\psi\rangle dx_i$$
$$= \int K(x_f, t_f, x_i, t_i)\psi(x_i, t_i)dx_i.$$

From Eqs. 14 and 16, this property should also be apparent from the path integral approach. The physical intuition behind the kernel is that it is a distribution function that counts how much of the wavefunction at (x_i, t_i) makes its way to (x_f, t_f). So to get the total amplitude at (x_f, t_f), we must sum all contributions from every initial (x_i, t_i), hence we integrate over all paths as shown [5].

Second, we see that

$$\lim_{t_f \to t_i} K(x_f, t_f, x_i, t_i) = \delta(x_f - x_i), \quad (18)$$

where δ is the Dirac delta function. To make this more clear, we use the Schrodinger picture to write

$$K(x_f, t_f, x_i, t_i) = \sum_n \langle x_f|n\rangle\langle n|x_i\rangle \exp\left(-\frac{iE_n(t_f - t_i)}{\hbar}\right),$$

where $H|n\rangle = E_n|n\rangle$, and H is the Hamiltonian. Taking the limit as $t_f \to t_i$, and using the completeness of the eigenstates of N and the orthonormality of the position states, we have

$$\lim_{t_f \to t_i} K(x_f, t_f, x_i, t_i) = \sum_n \langle x_f|n\rangle\langle n|x_i\rangle = \delta(x_f - x_i).$$

Again, this property is apparent from the path integral formulation. At a fixed time t, the probability that the particle is at its initial coordinate is, of course, one. And the probability that the particle is anywhere else is zero. Thus, we see that the path integral formulation is consistent with the Schrodinger and Heisenberg pictures of conventional quantum mechanics.

It remains to explore how this formulation yields the classical result in the limit as $\hbar \to 0$. In light of Eq. 14, we see that when $\hbar$ is very small, the exponential oscillates rapidly, contributing mostly destructive interference between adjacent paths [2, 5, 8]. In other words, when integrated against dx_i, the positive and negative contributions of $e^{\frac{i\mathcal{S}}{\hbar}}$ tend to cancel out. The only exception is the path that, when perturbed slightly, remains unchanged to first order. That is, we have $\delta\mathcal{S} = 0$, precisely corresponding to the classical path that satisfies the least action principle. In the limit as $\hbar \to 0$, only a narrow strip of paths very close to this path survives from destructive inference and manifests in measurements as the true (classical) path of the particle.

At this point, we have examined most of the basic salient features of the path integral formulation. Namely, we have recovered the Schrodinger equation from this approach, checked it against the Schrodinger and Heisenberg pictures of quantum mechanics, and demonstrated that the path integral reduces to the classical path in the limit as $\hbar \to 0$.

IV.   THE EUCLIDEAN PATH INTEGRAL

Having derived the path integral in Eq. 16, we need to now examine whether the path integral is mathematically well-defined. Here, we follow the approach in [10, 11]. There are at least two apparent convergence issues that must be resolved. The first is convergence in the limit as $\delta t \to 0$. But even more crucial is convergence of the discretized iterated integrals. The rapidly oscillating complex exponential (which does not converge absolutely) can potentially be a source of problems when integrated. Consider, for example, the integral

$$\int_{-\infty}^{\infty} e^{ix}dx = \int_{-\infty}^{\infty} (\cos x + i \sin x)dx$$

that clearly diverges due to the integrand's oscillation.

Mathematicians have shown that under certain assumptions, the path integral is well-behaved, i.e. it converges [12]. For instance, it has been shown that the path integral converges for Lagrangians whose potentials are in the class of C^∞ functions [13], of which the harmonic oscillator potential is a member [14]. But it turns out that the path integral as defined by Eq. 16 is not, in general, a well-behaved mathematical operation. Instead, the notion of the path integral needs to be made rigorous by other means. In this section, we briefly summarize one such means which will play a dominant role in the discussion of statistical mechanics.

Although not rigorous, we take as our motivation to aim to eliminate the oscillating complex exponential that does not converge. Thus, instead of integrating the Lagrangian in real time, we define an imaginary time such

that $t_E = it$. The exponential of the discretized classical action becomes

$$\exp\left(-\frac{1}{\hbar}\sum_{i=1}^{N}\left[\frac{1}{2}m\frac{(x_i - x_{i-1})^2}{\delta t_E} + \delta t_E V(x_i)\right]\right),$$

where we have used that $\delta t_E = i\delta t$. In the limit that $N \to \infty$, we obtain

$$\exp\left(-\frac{1}{\hbar}\int_{t_{E,i}}^{t_{E,f}}\left[\frac{1}{2}m\frac{dx}{dt_E} + V(x)\right]dt_E\right) = \exp\left(-\frac{1}{\hbar}\mathcal{S}_E\right), \tag{19}$$

where $\mathcal{S}_E$ is the Euclidean action. We can, of course, go through the same procedure of discretizing time and iteratively integrate the contributions of all paths as we have done in the previous section. This time, for every finite N time intervals, we have absolute convergence of the integrals. So in the limit as $N \to \infty$, we typically have a well-behaved path integral in the end. We omit the detailed calculation and quote the result here

$$\langle x_f | e^{-\beta H} | x_0 \rangle = \int_{x_i}^{x_f}\mathcal{D}[x(t_E)]\exp\left(-\frac{1}{\hbar}\mathcal{S}_E(x_f, x_i)\right), \tag{20}$$

where we have used $e^{-\frac{i}{\hbar}(t_f - t_i)H} = e^{-\frac{1}{\hbar}(t_{E,f} - t_{E,i})H}$, and without loss of generality, we choose the initial imaginary time $t_{E,i} = 0$ and final imaginary time $t_{E,f} = \hbar\beta$ to get $e^{-\beta H}$. Eq. 20 is known as the *Euclidean path integral.*

In contrast to the Minkowski path integral, the Euclidean path integral is well-defined. But the two are intricately linked by a linear transformation of time. Thus, we can rigorously define the Feynman path integral (in its form as a Minkowski integral) by an analytic continuation of the Euclidean path integral [15]. With this new definition, issues with convergence can be avoided.

V. THE FREE PARTICLE

In this section, we apply the path integral approach to the basic one-dimensional free particle for demonstration of the method. Evaluating the path integral for even simple systems can be rather cumbersome. It is thus reasonable that through all of this, the reader becomes doubtful of the utility of this method. We emphasize, however, that the real utility of the path integral will become apparent when we briefly explore quantum statistical mechanics. Here, we follow the method in [11].

Consider the free-particle Lagrangian

$$\mathcal{L} = \frac{1}{2}m\dot{x}^2. \tag{21}$$

Without loss of generality, we find the propagator for a particle of mass m that starts at the origin at time $t = 0$

$$K(x, t, 0, 0) = \int_0^x \exp\left(\frac{i}{\hbar}\frac{m}{2}\int_0^t \dot{x}^2 dt'\right)\mathcal{D}[x(t)]. \tag{22}$$

Without a force, we know that the classical path of the particle is $x_c(t') = \frac{x}{t}t'$, where c denotes classical. The actual path is then just some deviation $\delta x(t')$ from the classical path $x(t') = x_c(t') + \delta x(t')$. The velocity is then $\dot{x} = \dot{x_c} + \dot{\delta x} = \frac{x}{t} + \dot{\delta x}$. Thus, we can write the action as

$$\frac{2}{m}\mathcal{S}(x) = \int_0^t \dot{x}^2 dt' = \int_0^t (\dot{x_c} + \dot{\delta x})^2 dt'$$
$$= \int_0^t \dot{x_c}^2 dt' + \int_0^t \dot{\delta x}^2 dt' = \frac{2}{m}\mathcal{S}(x_c) + \frac{2}{m}\mathcal{S}(\delta x) \tag{23}$$

where we have used that

$$\int_0^t \dot{x_c}\frac{d\delta x}{dt'}dt' = \frac{x}{t}\int_0^t d\delta x = \frac{x}{t}(\delta x[t] - \delta x[0]) = 0.$$

With this, the propagator becomes

$$K(x, t, 0, 0) = \int_0^x \exp\left(\frac{i}{\hbar}\frac{m}{2}\int_0^t (\dot{x_c}^2 + \dot{\delta x}^2)dt'\right)\mathcal{D}[x(t)]$$
$$= \exp\left(\frac{i}{\hbar}\mathcal{S}(x_c)\right)\int_0^x \exp\left(\frac{i}{\hbar}\mathcal{S}(\delta x)\right)\mathcal{D}[\delta x(t)]. \tag{24}$$

The classical action is simply $\mathcal{S}(x_c) = \frac{mx^2}{2t}$. We expect the path integral with respect to δx to only depend on t because the arbitrary endpoints are always zero. Thus, we write the propagator in a more suggestive form of

$$K(x, t, 0, 0) = \exp\left(i\frac{mx^2}{2t\hbar}\right)f(t),$$

with some function $f(t)$ to be determined, and exploit orthonormality that as $t \to 0$, we have

$$\lim_{t \to 0} K(x, t, 0, 0) = \delta(x),$$

where $\delta(x)$ is the Dirac delta function. Using one of the approximations of the Dirac Delta function

$$\delta(x) = \lim_{t \to 0}\left(\frac{m}{2i\pi\hbar t}\right)^{1/2}\exp\left(i\frac{mx^2}{2t\hbar}\right), \tag{25}$$

we can read off the propagator as

$$K(x, t, 0, 0) = \left(\frac{m}{2i\pi\hbar t}\right)^{1/2}\exp\left(i\frac{mx^2}{2t\hbar}\right). \tag{26}$$

If we repeat the same procedure above to find the Euclidean path integral, we arrive at

$$K_E(x, t_E, 0, 0) = \left(\frac{m}{2\pi\hbar t_E}\right)^{1/2}\exp\left(-\frac{mx^2}{2t_E\hbar}\right). \tag{27}$$

K_E becomes delocalized as $t_E \to \infty$, which in terms of statistical mechanics, models the occupation of the ground state as $T \to 0$. We shall make this notion more precise later. In fact, K_E in this case is exactly the kernel of the one-dimensional heat equation. Under closer inspection of the Schrodinger equation, this result should not be surprising. When t is mapped to t_E, we have

$$i\hbar\frac{\partial K}{\partial t} \to \frac{\partial K_E}{\partial t_E} = \frac{\hbar}{2m}\frac{\partial^2 K_E}{\partial x^2},$$

the one-dimensional heat equation. The analogy holds also for any form of the Hamiltonian, except then, the heat equation is non-homogeneous.

VI.   QUANTUM STATISTICAL MECHANICS

We have already seen with the Euclidean path integral an expression (Eq. 20) reminiscent of the partition function. Defining $\beta = \frac{1}{k_B T}$, where k_B is Boltzmann's constant, and T is the temperature in the canonical ensemble, Eq. 20 is in fact related to the matrix elements of the density matrix. In this section, we highlight applications of the path integral in statistical mechanics using the approach of Refs. [5, 16].

Recall that in the canonical ensemble, the probability, $p(E_i)$, of finding a state with energy E_i at fixed temperature T is given by

$$p(E_i) = \frac{e^{-\beta E_i}}{Z}, \tag{28}$$

where $Z = \sum_i e^{-\beta E_i}$ is the partition function that normalizes the probability distribution. The partition function allows us to compute many of the fundamental thermodynamic quantities governing the system. For instance, the internal energy $U(T)$ is

$$U(T) = \sum_i E_i p(E_i) = -\frac{\partial \ln Z}{\partial \beta}. \tag{29}$$

Introducing a new normalization factor $F(T)$ such that $p(E_i) = e^{-\beta(E_i - F)}$, we get that

$$F(T) = -k_B T \ln Z, \tag{30}$$

where $F(T)$ is the Helmholtz free energy. Thus, it follows from the first and second law of thermodynamics that the entropy $S(T)$ is

$$S(T) = -\frac{\partial F}{\partial T} = k_B \ln Z + \frac{U(T)}{T}. \tag{31}$$

From Eqs. 29, 30, and 31, it is clear that our task is to calculate the partition function. In this section, we explore the utility of the path integral in computing the partition function for statistical quantum systems.

As we have seen, using the path integral ultimately involves computing the kernel with the integrand being the exponential of the classical action. In statistical mechanics, this integrand is the density matrix. Recall that a density matrix ρ of an ensemble of energy eigenstates $|n\rangle$, each occurring with probability p_i is

$$\rho = \sum_i p_i |i\rangle\langle i| = \frac{1}{Z} \sum_i e^{-\beta E_i} |i\rangle\langle i| = \frac{e^{-\beta H}}{Z}. \tag{32}$$

In coordinate representation, we have

$$\rho(x_f, x_i) = \langle x_f | \rho | x_i \rangle = \frac{1}{Z} \sum_i e^{-\beta E_i} \psi(x_f)\psi(x_i)^*, \tag{33}$$

where ψ is the energy eigenfunction in position representation. It is clear then that

$$Z = \sum_i e^{-\beta E_i} = \text{Tr}\left[e^{-\beta H}\right]. \tag{34}$$

Thus, we have

$$\rho = \frac{e^{-\beta H}}{\text{Tr}\left[e^{-\beta H}\right]} = \frac{\tilde{\rho}}{\text{Tr}\left[e^{-\beta H}\right]}, \tag{35}$$

where we adopt the convention that $\tilde{\rho} = e^{-\beta H}$ is the unnormalized statistical density matrix. It is not difficult to see then that

$$-\frac{\partial \tilde{\rho}}{\partial \beta} = H\tilde{\rho}. \tag{36}$$

We observe that $\tilde{\rho}$ satisfies the heat equation with respect to β just as the Euclidean kernel does with respect to imaginary time. Therefore, we can immediately write the path integral for the density matrix

$$\tilde{\rho}(x_f, x_i, u) = \int_{x_i}^{x_f} \Phi[x(u)]\mathcal{D}[x(u)], \tag{37}$$

where

$$\Phi[x(u)] = \exp\left(-\frac{1}{\hbar} \int_0^u \left[\frac{1}{2}m\dot{x}(u)^2 + V[x(u)]\right] du\right), \tag{38}$$

and $u = \beta\hbar$. From Eq. 37, we can easily compute the partition function

$$Z = \text{Tr}[e^{-\beta H}] = \int \tilde{\rho}(x, x)dx, \tag{39}$$

from which we can obtain important thermodynamic quantities.

VII.   THE HARMONIC OSCILLATOR

In this section, we utilize the insight gained from statistical mechanics to explore the properties of the quantum harmonic oscillator using the path integral formalism. We shall first calculate the Minkowski path integral and then perform a change of time at the end. We will use Fourier analysis to calculate the path integral [5].

Consider the Lagrangian for the harmonic oscillator for a particle of mass m and frequency ω

$$\mathcal{L} = \frac{1}{2}m\dot{x}^2 - \frac{1}{2}m\omega^2 x^2. \tag{40}$$

The propagator is

$$K(x, t, 0, 0) = \int_0^x \exp\left(\frac{im}{2\hbar} \int_0^t \left[\dot{x}^2 - \omega^2 x^2\right] dt'\right) \mathcal{D}[x(t)]. \tag{41}$$

As before, we consider a path slightly perturbed from the classical path such that $x(t) = x_c(t) + \delta x(t)$. Inserting this observation in Eq. 41 and expanding, we find that the cross terms involving $x_c(t)$ and $\delta x(t)$ integrate to zero. Thus, we arrive at

$$K(x, t, 0, 0) = \exp\left(\frac{i}{\hbar}\mathcal{S}(x_c)\right) \int_0^x \exp\left(\frac{i}{\hbar}\mathcal{S}(\delta x)\right) \mathcal{D}[\delta x(t)], \tag{42}$$

where

$$\mathcal{S}(x_c) = \frac{1}{2}m \int_0^t \left[\dot{x_c}^2 - \omega^2 x_c^2\right] dt', \tag{43}$$

and

$$\mathcal{S}(\delta x) = \frac{1}{2}m \int_0^t \left[\dot{\delta x}^2 - \omega^2 \delta x^2\right] dt'. \tag{44}$$

Now, we observe that the remaining path integral is only dependent on t and not on the arbitrary endpoints as $\delta x(0) = \delta x(t) = 0$. So we can write

$$K(x, t, 0, 0) = \exp\left(\frac{i}{\hbar}\mathcal{S}(x_c)\right) f(t), \qquad (45)$$

for some function $f(t)$ that we now determine. Because $\delta x(0) = \delta x(t) = 0$, it has period t and can be expanded as a Fourier sine series such that

$$\delta x(t') = \sum_n b_n \sin\left(\frac{n\pi t'}{t}\right), \qquad (46)$$

for coefficients b_n. Now, we expand the path integral in terms of b_n in place of δx. First noting that

$$\int_0^t \dot{\delta x}^2 \, dt' = \frac{t}{2}\sum_n \left(\frac{n\pi}{t}\right)^2 b_n^2, \quad \text{and} \quad \int_0^t \delta x \, dt' = \frac{t}{2}\sum_n b_n^2.$$

we get the path integral for δx to be

$$f(t) = J \lim_{N\to\infty}\int \prod_{n=1}^N \exp\left(\frac{im}{2\hbar}\left[\left(\frac{n\pi}{t}\right)^2 - \omega^2\right]b_n^2\right)\frac{db_n}{A}, \qquad (47)$$

where A is the normalization factor as before, and J is a Jacobian determinant associated with the transformation from δx to b_n. Each of the integrals in Eq. 47 is Gaussian and can be integrated. Thus $f(t)$ becomes

$$f(t) \propto \lim_{N\to\infty}\prod_{n=1}^N \left(1 - \left[\frac{\omega t}{n\pi}\right]^2\right)^{-1/2} = \left(\frac{\omega t}{\sin\omega t}\right)^{1/2}. \qquad (48)$$

To find the normalization constant, we note that as $\omega \to 0$, we have $f(t)$ of the free particle in Eq. 25, leading to

$$f(t) = \left(\frac{m\omega}{2\pi i\hbar\sin\omega t}\right)^{1/2}. \qquad (49)$$

To find the propagator, it only remains to evaluate the classical action. We know that the path of the classical particle satisfies the Euler-Lagrange equation (Eq. 4). So we can find $\mathcal{S}(x_c)$ by solving for $x_c(t)$. We omit the calculation, and quote the propagator for the harmonic oscillator in its final form as

$$K(x, t, 0, 0) = \left(\frac{m\omega}{2\pi i\hbar\sin\omega t}\right)^{1/2}\exp\left(\frac{im\omega}{2\hbar\sin\omega t}[x^2\cos\omega t]\right). \qquad (50)$$

If we use any arbitrary initial condition, then

$$K(x_f, t_f, x_i, t_i) = \left(\frac{m\omega}{2\pi i\hbar\sin\omega t}\right)^{1/2} \times$$
$$\exp\left(\frac{im\omega}{2\hbar\sin\omega t}[(x_f^2 + x_i^2)\cos\omega t - 2x_f x_i]\right), \qquad (51)$$

where $t = t_f - t_i$. Encoded in this propagator is the complete information of the time evolution of the harmonic oscillator in some initial state at (x_i, t_i).

To gain additional insight from Eq. 51, we proceed to evaluate the partition function of a system of harmonic oscillators in thermal equilibrium. First, we obtain from

Eq. 51 the density matrix by performing the transformation $t \to -it_E$ and using $\beta = t_E/\hbar$, we have [16]

$$\rho(x_f, x_i) = \left(\frac{m\omega}{2\pi\hbar\sinh\omega\beta\hbar}\right)^{1/2} \times$$
$$\exp\left(\frac{im\omega}{2\hbar\sinh\omega\beta\hbar}[(x_f^2 + x_i^2)\cosh\omega\omega\beta\hbar - 2x_f x_i]\right). \qquad (52)$$

Now, we calculate the partition function [16, 17]

$$Z = \frac{1}{2\sinh\left(\frac{\hbar\omega}{2k_B T}\right)} = \sum_{i=0}^\infty \exp\left(-\frac{(i+1/2)\hbar\omega}{k_B T}\right). \qquad (53)$$

Knowing that the partition function takes the form $Z = \sum_i e^{-E_i/k_B T}$, we can read off the energy levels

$$E_i = \left(i + \frac{1}{2}\right)\hbar\omega, \qquad (54)$$

which agree with the result from other analyses. Additionally, we can obtain from this formulation even more than just the energy levels. Consider the limit as $T \to 0$; we note that the density matrix tends to

$$\sqrt{\frac{m\omega}{\pi\hbar}}\exp\left(\frac{-\hbar\omega}{2k_B T}\right)\exp\left(-\frac{m\omega x_f^2}{2\hbar}\right)\exp\left(-\frac{m\omega x_i^2}{2\hbar}\right), \qquad (55)$$

which agrees with our intuition that as $T \to 0$, the entropy tends to a constant; so only the ground state is occupied. Then noting that in this limit, $\rho(x_i, x_f) \to e^{-\beta E_0}\psi_0(x_f)\psi_0(x_i)^*$, we can read off the ground state wavefunction

$$\psi_0(x) = \left(\frac{m\omega}{\pi\hbar}\right)^{1/4}\exp\left(-\frac{m\omega x^2}{2\hbar}\right). \qquad (56)$$

As shown, using the path integral, we arrived at very important results in statistical mechanics, including the partition function and the density matrix. From these, we were able to confirm the energy levels of the harmonic oscillator as well as its ground state wavefunction.

VIII. FURTHER IMPLICATIONS

It is impossible for a short paper such as this do justice to a topic as broad and profound as the Feynman path integral. Thus, we briefly summarize a few extensions and applications of the path integral here to give the reader a taste of the far-reaching impact of this alternative approach to quantum mechanics.

First, for clarity, our treatment of the path integral has been only done for one-dimensional non-relativistic systems. Most practical systems, however, are fundamentally of higher dimensions. The generalization of Eq. 16 to higher dimensions is straightforward. Recall that for a set of generalized coordinates and velocities, $\{q_1, ...q_N, \dot{q}_1, ..., \dot{q_N}, t\}$, the classical action is simply

$$\mathcal{S} = \int_{t_i}^{t_f}\left(\frac{1}{2}m\sum_{i=1}^N \dot{q_i}^2 - V(q_1, ...q_N, \dot{q}_1, ..., \dot{q_N})\right) dt. \qquad (57)$$

The N-dimensional path integral follows naturally from this generalized classical action.

To make this groundwork fully relativistic is a more difficult matter. It suffices to note though that such an effort led Feynman to the formulation of one of the first successful quantum theories of the interaction of matter with electromagnetic fields. In the non-relativistic limit, we can write the action of such a process as a contribution of three separate actions: one due solely particles, one due to the interaction of particles with fields, and one due to the presence of fields only.

Quantum electrodynamics is one of the hallmarks of the path integral formulation, even though it was certainly not the key ingredient of the theory. In his Nobel Lecture, Feynman noted, "The path-integral formulation of quantum mechanics was useful for guessing at final expressions and at formulating the general theory of electrodynamics in new ways - although, strictly it was not absolutely necessary" [1].

Beyond quantum electrodynamics, the Feynman path integral has also played an important role in the development of quantum field theory [18, 19], and has been often used in condensed matter physics [20]. For example, it has been applied to calculating the interaction of bosons with a fluctuating gauge field [21], to estimating the polaron ground state in a magnetic field [22], and to studying the Anderson-Higgs mechanism [23]. Outside of physics, the path integral has been utilized in diverse fields like finance and materials science [20].

IX. DISCUSSION

The path integral formulation is an alternative approach to quantum mechanics that relies on the classical principle of least action. Throughout this paper, we have shown that the path integral approach is in complete agreement with conventional quantum mechanics. Namely, we have recovered from computing the propagator the Schrodinger equation, implying that all the information encoded in the Schrodinger wavefunction can also be obtained from the propagator. This consistency was seen in the examples as well, as in the case of the harmonic oscillator when we recovered the ground state wavefunction and exact energy levels from the density matrix in the low temperature limit.

Furthermore, the path integral is not merely duplication of known physics. Rather, through this method, we gain additional insight and computational machinery for quantum systems. For instance, when evaluated against imaginary time, the Euclidean path integral quickly yields the density matrix, from which we can obtain all thermodynamic quantities of importance. Conversely, when a system lacks Hamiltonian form, the conventional description of quantum mechanics cannot be easily used to reach any conclusion. In this case, the Feynman path integral may be applied. Such an effort has led, if indirectly, to the development of a consistent theory of quantum electrodynamics.

Feynman is known to insist on finding new ways to solve the same problem [2]. The path integral is certainly a stellar example of the productivity that can spring from such a mentality.

[1] R. P. Feynman, "Nobel lecture: The development of the space-time view of quantum electrodynamics," (2013).

[2] R. P. Feynman, L. M. Brown, and P. A. M. Dirac, *Feynman's thesis: a new approach to quantum theory* (Hackensack, NJ: World Scientific, 2005).

[3] J. A. Wheeler and R. P. Feynman, Rev. Mod. Phys. **17**, 157 (1945).

[4] J. A. Wheeler and R. P. Feynman, Rev. Mod. Phys. **21**, 425 (1949).

[5] R. P. Feynman and A. R. Hibbs, *Quantum mechanics and path integrals*, International series in pure and applied physics (New York: McGraw-Hill, 1965).

[6] L. D. Landau and E. M. Lifshitz, *Mechanics*, Course of theoretical physics: v. 1 (New York: Pergamon Press, 1988).

[7] R. P. Feynman, Rev. Modern Physics **20**, 367 (1948).

[8] J. J. Sakurai and J. Napolitano, *Modern quantum mechanics* (Boston: Addison-Wesley, 2011).

[9] H. Murayama, "Path integral," University Lecture Notes (2006).

[10] V. Kaplunovsky, "Path integral for harmonic oscillator," University Lecture Notes (2005).

[11] K. Cahill, *Physical mathematics* (Cambridge: Cambridge University Press, 2013).

[12] N. Kumano-Go, Sūrikaisekikenkyūsho Kōkyūroku , 5 (2000), microlocal analysis of the Schrödinger equation and related topics (Japanese) (Kyoto, 1999).

[13] These are functions that are infinitely differentiable. Notice that the functions can be unbounded at infinity.

[14] D. Fujiwara, Duke Mathematical Journal **47**, 559 (1980).

[15] This can be done using a Wick rotation.

[16] R. P. Feynman, *Statistical mechanics: a set of lectures*, Advanced book classics (Reading, Mass.: Addison-Wesley, 1998).

[17] E. Wikberg, "Path integral in quantum mechanics," University Lecture Notes (2006).

[18] D. G. C. McKeon and C. Wong, Journal of Mathematical Physics **36** (1995).

[19] S. Sawin, Journal of Mathematical Physics **36** (1995).

[20] H. Kleinert, *Path integrals in quantum mechanics, statistics, polymer physics, and financial markets*, 5th ed. (World Scientific Publishing Co. Pte. Ltd., Hackensack, NJ, 2009).

[21] M. U. Ubbens and P. A. Lee, Phys. Rev. B **49**, 13049 (1994).

[22] D. M. Larsen, Phys. Rev. B **32**, 2657 (1985).

[23] J.-H. She, D. Sadri, and J. Zaanen, Phys. Rev. B **78**, 144504 (2008).

The Methods and Benefits of Squeezing

Troy P. Welton

Physics Department, 77 Massachusetts Ave., Cambridge, MA 02139-4307

(Dated: May 2, 2014)

This paper examines the principal method for the construction of squeezed states and some applications for which they are useful.

I. INTRODUCTION

A squeezed state is a quantum mechanical state that saturates the bound of the Heisenberg uncertainty principle ($\Delta x \Delta p = \hbar/2$). To better understand squeezed states, the simple harmonic oscillator offers a convenient context. It has a Hamiltonian describable in terms of the oscillator's fundamental frequency and its mass. Assume that these parameters instantaneously can be changed without changing the wavefunction of the particle. The new Hamiltonian does not have the same eigenstates as the previous one, so the particle does not evolve trivially. The uncertainties of the position and momentum, which originally are

$$\Delta x = \sqrt{\frac{\hbar}{2m\omega}} \qquad \text{and} \qquad \Delta p = \sqrt{\frac{\hbar m\omega}{2}}, \quad (1)$$

are changed by the reparametrization to be

$$\Delta x' = \sqrt{\frac{\hbar}{2m'\omega'}} \qquad \text{and} \qquad \Delta p' = \sqrt{\frac{\hbar m'\omega'}{2}}. \quad (2)$$

This shows a skew in the uncertainties of position and momentum from the original values that can be rewritten in terms of a parameter γ:

$$\Delta x' = e^{-\gamma}\Delta x \qquad \text{and} \qquad \Delta p' = e^{\gamma}\Delta p \quad (3)$$

$$\text{where } e^{\gamma} = \sqrt{\frac{m'\omega'}{m\omega}}. \quad (4)$$

This new parameter measures how much the uncertainty is skewed toward position or momentum in the Heisenberg uncertainty relation. Mathematically, a squeezed state is described as [6]

$$|\psi(\gamma)\rangle_S \equiv \frac{1}{\sqrt{\cosh(\gamma)}} \exp[-\frac{1}{2}\tanh(\gamma)(\hat{a}^\dagger)^2]|0\rangle. \quad (5)$$

One sees that taking $\gamma \to -\infty$ produces a state proportional to $\exp[\hat{a}^{\dagger 2}]|0\rangle$, which is annihilated by the momentum operator. That means that it must be proportional to $\delta(p)$ in momentum space, or a constant in position space. Taking $\gamma \to \infty$ creates a state proportional to $\exp[-\hat{a}^{\dagger 2}]|0\rangle$, which is annihilated by the position operator and must be proportional to $\delta(x)$. These two conclusions about the wavefunction match with the predictions of Eq. 3, in which position or momentum achieves zero uncertainty under infinite squeezing. This gives the basic function of a squeezed state: The squeezing parameter gives an idea of the uncertainty in each of a conjugate pair of variables. This is true for any conjugate pair that follows an uncertainty relation similar to x and p. Section II describes a graphical representation for squeezed states that allows for probabilistic calculations. Section III gives the prominent application of squeezed states to modern experiments. Section IV examines a theoretical use for squeezed states in quantum computing. Section V shows how one would create a squeezed state.

II. WIGNER FUNCTIONS

A Wigner function, also referred to as a Wigner quasiprobability distribution, gives the closest approximation to a joint probability distribution for conjugate variables in quantum mechanics [5]. The form of a Wigner function is

$$P(x,p) = \frac{1}{\pi\hbar} \int_{-\infty}^{\infty} \psi^*(x+y)\psi(x-y)e^{2ipy/\hbar}\,\mathrm{d}y \quad (6)$$

where x and p, representing the position and momentum respectively, could be replaced by any conjugate pair of variables. This formula has the capacity to represent any number of particles by extending the coordinate and momentum dependence to as many variables as necessary. It is very useful in statistical mechanics for finding the properties of many particles, but it can also be used to quantify probabilities of a single particle system using Eq. 6. The probability of a particle's position or momentum is given by integrating over all momentum or space, respectively. It is easy to see that integrating over momentum in Eq. 6 leaves $|\psi(x)|^2$ and integrating over position gives

$$\left| \int_{-\infty}^{\infty} \psi(x)e^{-ipx/\hbar}\mathrm{d}x \right|^2 \quad (7)$$

which is just the norm-square of the Fourier transform. Thus, integrating with respect to one of the variables gives the correct probability for the other. In this sense, the Wigner representation is more illuminating than a phase space diagram in classical mechanics because it incorporates the aspect of probability that is essential

to quantum mechanics. The one difference between the Wigner distribution and a classical probability distribution is that there is no restriction on the function to remain positive everywhere. The negative values in a Wigner function are indicative of the quantum mechanical nature of this distribution. The change of the function over time also aids to establish a quantum mechanical interpretation for this distribution. It can be shown [5] that the change of a Wigner function over time can be put in the form

$$\frac{\partial}{\partial t}P(x,p) = -\frac{p}{m}\frac{\partial}{\partial x}P(x,p) + \int_{-\infty}^{\infty} P(x,p+j)J(x,j)\mathrm{d}j$$
(8)

Here p represents a number instead of its traditional operator designation and $J(x,p)$ can be interpreted as the probability of a jump in momentum in the amount j for a particle at position x. The probability of the jump takes the form

$$J(x,j) = \frac{i}{\pi\hbar^2} \int_{-\infty}^{\infty} [V(x+y) - V(x-y)]e^{-2iyj/\hbar}\mathrm{d}y \quad (9)$$

This is also the form of a Fourier expansion of the coefficients of the potential V of the system. These jumps or discontinuities are indicative of the transfer of quanta of momentum, which only arises from quantum mechanical considerations.

The canonical picture for the squeezed state in two-dimensional phase space is an ellipse that has a very long major axis and a very narrow minor axis. This means that the squeezed state has a very well defined value for one conjugate variable and is nearly indeterminate in the other. In other words, the uncertainty in one variable is close to zero and the uncertainty of the conjugate variable is very large. The additional visualization of a squeezed state through the lens of a Wigner diagram is shown in Figure 1.

The common phase space variables for squeezed states are amplitude (which is also sometimes written in terms of intensity) and phase. These two variables form a conjugate pair that has an uncertainty relation which is obtainable from the canonical relation of position and momentum. The ellipses formed by taking horizontal slices out of the Wigner function very close to the origin shows the elliptical nature of the phase space in relation to the conjugate variables. The reason to consider the region very close to the origin is that it represents the location of the highest probability.

Now that we know that squeezed states are important for focusing one of a conjugate pair and that they have a propensity towards nonclassicality, we can examine how these features are used in experiment and theory.

III.   QUANTUM NOISE REDUCTION

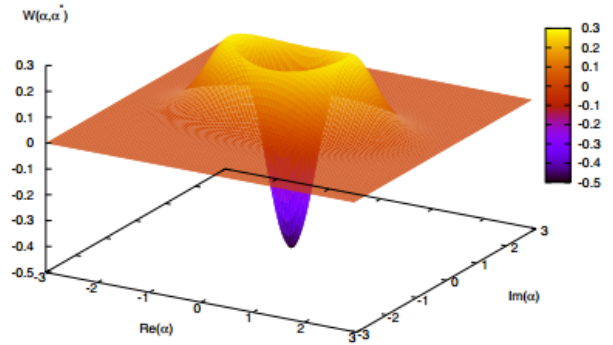The main use of squeezed states in quantum mechanical experiments is in the reduction of quantum noise.

FIG. 1: This plot shows a squeezed state for a specific squeezing parameter γ. The key features of this graph are the probabilities associated with the different regions of the graph and the general shape of the graph in the region very close to the origin. The first feature shows that this state is quantum mechanical because its largest amplitude is negative. Negative values on a Wigner function are associated with quantum mechanical regions. The second feature shows that a phase space diagram (horizontal slice) is an ellipse (focused in one variable). [2]

Consider the picture of a two-dimensional phase space diagram of a conjugate variable pair. Imagine taking this diagram to the limit of squeezing. In phase space, this diagram becomes a line instead of an ellipse. That means that the variation in one of the variables is zero and the variation of the other is very large (the value is indeterminate). Even disregarding the concept of infinite squeezing, very large squeezing creates an ellipse in phase space that is very similar to the line just mentioned. That means that the variation in one variable can be stabilized very precisely if one does not care about its conjugate partner. Using squeezed states, random fluctuations in all electronic and photonic systems can be restricted to produce very clean results. A common fundamental limit to the precision of an electronic or photonic measurement is the shot-noise limit. Shot noise arises from the fluctuations in measurement of discrete particles. Light and electrons carry discrete quanta of momentum and charge, respectively. When considering a weak beam of light or a weak current, the fluctuation in the intensity of the beam can be significant based on the randomness of any such Poissonian system. For a beam of light with high intensity or large currents, the shot noise has a proportionally lower effect because it grows much less rapidly than other sources of noise. This suggests that having a beam of few particles that can still maintain a well regulated amplitude is essential for circumventing the limit imposed by the shot noise level. Squeezed states that are also entangled with each other are very useful for establishing this kind of noise reduction. Fortunately, the standard creation of squeezed states (see Section V) also leaves the resulting states entangled. Therefore, the correlation be-

tween the states can be manipulated to ensure that the amplitude of the signal beam (the light being used in an experiment) remains relatively noiseless.

The most common method for creating squeezed states leaves the states in two different beams separable by polarization. The idle beam (the states not being used in an experiment) can be monitored by a feedback loop so that its amplitude remains very stable. By necessity, the signal beam also maintains a very stable amplitude. The fact that the beams are correlated through entanglement allows for this nondemolition measurement. Having two identical beams allows one to be confident of the accuracy of the experimental amplitude of a beam of light, for example. The reason for this confidence will be explained in Section V when the creation of squeezed states is explained. As early as 1987, experimentalists saw the potential for these states, and the earliest attempts reduced the noise of their measurements by up to 25%, as shown in Figure 2. The plot shows a comparison of the measured noise to the shot noise level for various frequencies in the MHz range.
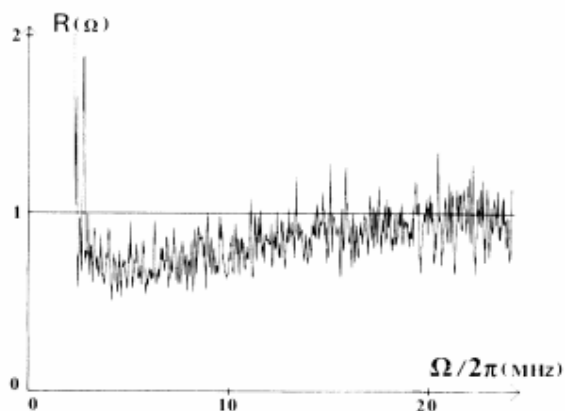

FIG. 2: As early as 1987, scientists were capable of engineering lasers that had lower noise than the shot-noise limit. This figure shows a reduction by as much as 25% at a frequency for light of about 5 MHz. Here the axes represent the frequencies for which light was tested and the comparison of the resulting noise to the shot noise level. [3]

Even though the shot-noise limit is small for most scales, this reduction is very important for interferometry. Interferometry splits a beam of light and sends it in perpendicular directions to reflect off two mirrors and interfere as the beams re-merge at the beam-splitter interface. In the detection of gravitational waves, which deals with length scales on the order of 10^{-19} meters, any reduction of noise is significant. The interferometer is detecting a change in the relative spatial location of the two mirrors, which are tuned to interfere perfectly in the absence of gravitational waves. A gravitational wave passing through the detector reshapes space so that the direction of propagation is elongated and the transverse

direction is shrunk. These differences are very small, as described above, so it is very important to reduce any external factors that might obscure a detection of these extremely small alterations to space.

IV. SQUEEZED STATES IN QUANTUM COMPUTING

Squeezed states are also very important for experiments in quantum computing. One prominent example is the process of quantum teleportation. All the applications below involve EPR beams, which are simply the superposition of two independent beams of squeezed-state light sent through a half-beam splitter. (See Figure 3.)
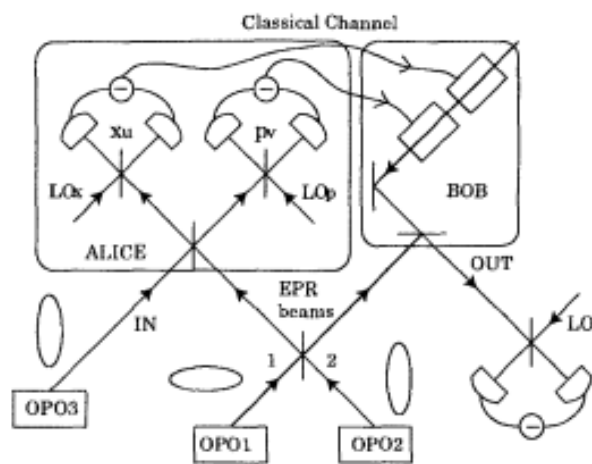

FIG. 3: This figure shows the setup for a quantum teleportation experiment. The squeezed states are created using OPOs (see Section V) and sent to a sending and receiving station. Then another squeezed state is superposed with the beam at the sending station and the classical quantities of position and momentum are measured. These quantities are sent classically to the receiving station and the receiver combines a state with these values to the entangled quantum state originally sent. The output is a reconstructed version of the state introduced at the sending station. The accuracy of the reconstruction depending on the squeezing parameter, γ.

The resulting state is also referred to as a two-mode squeezed vacuum. For clarity, the form of one of the new states is

$$\begin{cases} \hat{x}'_1 = \frac{1}{\sqrt{2}} \left(e^{\gamma} \hat{x}_1 + e^{-\gamma} \hat{x}_2 \right) \\ \hat{p}'_1 = \frac{1}{\sqrt{2}} \left(e^{-\gamma} \hat{p}_1 + e^{\gamma} \hat{p}_2 \right) \end{cases} \tag{10}$$

where the unprimed variables represent the states before mixing and γ is the squeezing factor. The other state is retrieved by replacing the addition in Eq. 10 with subtraction. These squeezed states are important for quantum teleportation because in the limit of perfect squeezing, states can be perfectly reconstructed by a

simple transfer of information about the state's position and momentum. The following example from [4] best illustrates this fact.

Consider an input state that Alice, the sender, wants to teleport to Bob, the receiver. Using the superposition state that she was given (Eq. 10), Alice measures the position and momentum of the input state to be teleported by combining it with the superposition state at a half beam splitter. She obtains the operators $\hat{x}_u = (\hat{x}_{in} - \hat{x}_1')/\sqrt{2}$ and $\hat{p}_v = (\hat{p}_{in} + \hat{p}_1')/\sqrt{2}$ from this mixing, and measures the associated values. She sends these measured values (x_u, p_v) classically to Bob, the receiver. Bob reconstructs the state by applying the operators $\hat{x}_{tel} = \hat{x}_2' + \sqrt{2}\hat{x}_u$ and $\hat{p}_{tel} = \hat{p}_2' + \sqrt{2}\hat{p}_v$. Using Eq. 9, one sees that the reconstructed state takes the form

$$x_{tel} = \hat{x}_{in} - \sqrt{2}e^{-\gamma}\hat{x}_2 \quad \text{and} \quad \hat{p}_{tel} = \hat{p}_{in} + \sqrt{2}e^{-\gamma}\hat{p}_1 \tag{11}$$

The error in the teleportation goes as $e^{-\gamma}$, so in the limit of perfect squeezing, a state can be perfectly reconstructed in a different location only using the classical transfer of two pieces of information.

With these applications in mind, it is necessary to discuss the creation of these states.

V.   OPTICAL PARAMETRIC OSCILLATIONS

The most common method for creating squeezed states is through the use of optical parametric oscillators (OPOs). [3] These devices combine a nonlinear crystal with an optical cavity that acts as a resonator to produce beams of light that are highly correlated in amplitude fluctuations and are, in fact, squeezed. A nonlinear crystal, such as $KTiOPO_4$, can transform one pulse or continuous stream of photons that is passed through it (called the pump beam) into two beams, referred to as the signal and the idle beams. In the process known as downconversion, a single photon from the pump beam is absorbed and two new "twin" (entangled) photons are released in its place. This interaction must obey conservation laws and various other conditions for this to happen. These conditions include energy conservation, momentum conservation, and boundary-condition matching for the optical cavity. The first two conditions can be represented by simple formulas:

$$\omega_p = \omega_s + \omega_i \tag{12}$$

$$\vec{k}_p = \vec{k}_s + \vec{k}_i \tag{13}$$

where the subscripts correspond to the pump, signal, and idle beams, and the variables are frequency ω and wavevector $\vec{k}$. The resonant cavity determines the excitable modes of the signal and idle beams because the beams must match boundary conditions related to the length of the cavity. All of these conditions are only satisfied for specific cavity lengths, restricted by the desired

frequencies and wavevectors. Oscillations only occur in a range of a few nanometers around these specific lengths. Any vibrations that the OPO experiences during the creation of the beams is very detrimental to the output intensity of the beams. In order to stabilize the intensity of the beams, the length of the cavity is variable and is adjusted throughout the experiment to be stabilized at the resonance conditions for the output beams. This is accomplished by monitoring the tiny fraction of the output beams that is transmitted from the cavity through the mirror nearer to the source, back in the direction of the laser. The intensity of this beam is maintained at a constant value by adjusting the cavity length. This portion of the beam is representative of the intensity of the whole beam, so it is an indirect measurement of the overall beam intensity difference over time.

After the beams are emitted from the cavity, the original laser frequency is filtered out, and the other frequencies are separated by a polarizing beam splitter. In common usage in experiment, the amplitude fluctuations in the idle beam are closely measured and the beam's amplitude is stabilized with a feedback loop. Since the creation of the signal and idle beams correlates the amplitude fluctuations (the number of photons in each beam over a long period of time will be approximately the same through the creation mechanism), it does not matter if we measure one of the beams and destroy those states because we know exactly how the other beam will respond to similar corrections. This correlation between the two beams allows the noise from the amplitude to fall much below the shot-noise limit. This is important for increasing the precision of laser amplitudes.
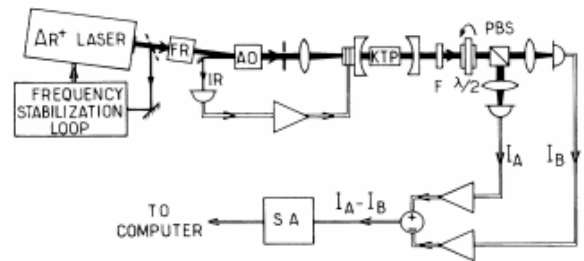

FIG. 4: The figure shows the experimental setup for an optical parametric oscillation/squeezing experiment using $KTiOPO_4$ (KTP) as the crystal. [3]

Figure 4 shows one of the original squeezing experiments. In addition to details described above, this setup has a few other features. The pumping laser is offset from the center of the crystal and the cavity so that the feedback loop can be reflected from the cavity along the axis of propagation without interfering with the laser light. After exiting the cavity (through the back), the two beams are separated based on their polarizations by the polarizing beam splitter, or PBS. FR is a Faraday rotator (to account for the laser's skew). AO is an acousto-optic

modulator to isolate the reflected infrared beam from the laser beam. F is a filter that absorbs the untransformed pump beam and allows the new signal and idle beams to pass through. The beam intensities are converted to currents using InGaAs photodiodes. SA is the spectrum analyzer, which examines the noise, or fluctuation, in the difference in intensity of the two beams by way of the current.

Crystals have properties that can make this process efficient or very inefficient. [1] The crystals used in OPOs are birefringent, which means that different directions of propagation and polarizations of waves have different refractive indices in the crystal. These crystals have preferred axes that specify up to 3 different refractive indices. Combinations of these directions determine the overall refractive index for a given direction. When crystals have two preferred axes with the same index, the polarization is the same along those axes and perpendicular for the other axis. For this experimental setup, the crystal is oriented so that the signal and idle beams have perpendicular polarization for easier discrimination of the two beams. The conversion rate of the pump beam into the signal and idle beams is also related to the properties of the crystal. In general, the conversion between the two over the length of the crystal relates to the phase-matching condition. Mathematically, conversion, or the rate of change of the amplitude of the signal and idle beams over the length of the crystal, is

$$\frac{\partial(A_s + A_i)}{\partial z} = A_p \chi e^{i\Delta k z} \qquad (14)$$

where A represents the amplitude, χ the susceptibility of the crystal (explained below), z the direction of propagation of the beams, and Δk the difference in phase between the pump beam and the sum of the signal and idle beams. The change in amplitude of the output frequencies is positive when $z < \frac{\pi}{\Delta k}$ and negative when $z > \frac{\pi}{\Delta k}$. This presents a problem because a region that is negative converts the signal and idle frequencies into the pump frequency instead of the other way, which would diminish the returns of this experimental setup. Fortunately, there is still one parameter that can save the experiment: χ. The susceptibility of the crystal depends on the direction of propagation (it relates to the birefrin-

gence of the crystal). Therefore, switching the axis of the crystal (exchanging $-z$ with $+z$) changes the sign of χ. Therefore, if one changes the axis of the crystal whenever $z = \frac{\pi}{\Delta k}$, the sign of the amplitude change remains positive. This is accomplished by taking slices of crystal and placing them back to back, so that the orientation is changed periodically. The length at which the crystal axis is changed is referred to as the coherent length of the crystal. The situation just described is shown in Figure 5. The resulting conversion equation is

$$\frac{\partial(A_s + A_i)}{\partial z} = A_p \chi (-1)^n e^{i\Delta k z + n\pi} \qquad (15)$$
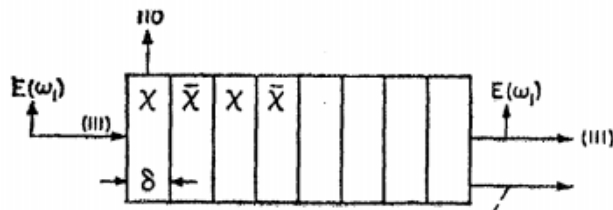
and the result is always positive.

FIG. 5: The electromagnetic wave $E(\omega_1)$ is propagating through a crystal that changes orientation (and susceptibility from χ to $\bar{\chi}$ every coherent length, δ.[1]

VI. CONCLUSIONS

By examining the creation and uses of squeezed states, one sees that the uncertainty description supplied for harmonic oscillators gives a good description of squeezing for any pair of conjugate variables. Squeezing in optical applications focuses the amplitude of the beam as it relates to intensity and ignores all information of phase of that beam. This allows for very precise measurements in areas like interferometry. Position and momentum are still useful parameters for theoretical calculations in quantum computing because these quantities are easy to determine. The key fact to remember about squeezing is that a sudden change to the Hamiltonian of a state can reduce the uncertainty of one variable enough to make useful calculations and calibrations with it.

[1] J. A. Armstrong, N. Bloembergen, J. Ducuing, and P. S. Pershan. Interactions between light waves in a nonlinear dielectric. *Phys. Rev.*, 127:1918–1939, Sep 1962.
[2] Asoka Biswas and G.S. Agarwal. Nonclassicality and decoherence of photon-subtracted squeezed states. In *Quantum Electronics and Laser Science Conference, 2007. QELS '07*, pages 1–2, May 2007.
[3] A. Heidmann, R. J. Horowicz, S. Reynaud, E. Giacobino, C. Fabre, and G. Camy. Observation of quantum noise reduction on twin laser beams. *Phys. Rev. Lett.*, 59:2555–

2557, Nov 1987.
[4] N. Takei, T. Aoki, H. Yonezawa, K. Wakui, T. Hiraoka, and A. Furusawa. Teleportation of a squeezed state. In *Quantum Electronics and Laser Science, 2003. QELS. Postconference Digest*, pages 2 pp.–, June 2003.
[5] E. Wigner. On the quantum correction for thermodynamic equilibrium. *Phys. Rev.*, 40:749–759, Jun 1932.
[6] B. Zwiebach. Quantum dynamics [8.05 course notes]. 2013.

A Brief Introduction to the Path Integral Formalism and its Applications

Max I. Wimberley
MIT
(Dated: May 2, 2014)

We develop the formalism of path integrals in quantum mechanics and put it to use in familiar contexts, such as analysis of the quantum-mechanical free particle and harmonic oscillator. For each of these systems, we compute the general path integral, and use this to obtain information about the time evolution of such a system, as well as the energy spectrum and eigenstates.

I. INTRODUCTION

The path integral in quantum mechanics is a tool with which a complete description (Feynman's "path integral formulation") of quantum mechanics can be built. Conventionally, quantum mechanical systems are characterized by of their Hamiltonians, because the Hamiltonian fully governs the time-evolution of the system in a relatively straightforward way. In the Schrödinger picture, this manifests as the evolution of states over time – the system has a characteristic time evolution operator $U(t_0, t_1)$ (depending only on the Hamiltonian) which, when acting on the state of a system at time t_0, yields the state at time t_1. This picture is fairly abstract, and makes little direct reference to basic physical processes familiar from our experience of the world, such as motion of objects through space.

Perhaps for this reason, it also makes essentially no mention whatsoever of the closely related classical concept of action in Lagrangian mechanics, which is defined in terms of paths in spacetime. Like the Hamiltonian, the quantum-mechanical Lagrangian can straightforwardly be defined, but the analogue of the action is nontrivial. In the 1920s, Dirac developed an informal correspondence between the quantity $e^{iS/\hbar}$, where S is the action for a path between two points (x_0, t_0) and (x_1, t_1) and the transition amplitude $\langle x_0, t_0 | x_1, t_1 \rangle$, remarking that the two were essentially proportional over infinitesimal time intervals. However, it wasn't until 1948 that the action was brought fully into quantum mechanics, when Feynman formulated the famous path integral, and showed that the resulting picture was equivalent to the other theories [2, 3].

In some ways, this new picture of quantum mechanics provides remarkably straightforward physical intuition, as it can informally be described as based on (a more general version of) the following principle: given that a particle is known to be at position x_0 at time t_0, the amplitude for it to be found at x_1 at time t_1 is the "sum over all spacetime paths" between these two points, weighted by the "amplitude" for each path. Of course, the tricky part here is to give meaning to concepts like a "sum over all spacetime paths." This is precisely what the path integral accomplishes.

A. Review of Lagrangian Mechanics

Classically, a system whose state can be specified by coordinates q and $dq/dt = \dot{q}$ (we will work with only one q for simplicity) has dynamics determined by a Lagrangian $L(q, \dot{q}, t)$. The Lagrangian determines an action functional S which associates to each path $q(t)$ (for $t_0 \leq t \leq t_1$) its action

$$S[q(t)] = \int_{t_0}^{t_1} L(q(t), \dot{q}(t), t) dt. \tag{1}$$

The system is then said to obey the *principle of least action*, whereby the path taken between two configurations is that which minimizes the action among all paths between those configurations. This leads to the *variational principle*, $\delta S = 0$ for a path taken by the system; i.e. that "small deformations" of the path yield no variation in the action to first order. Careful examination of the requirement $\delta S = 0$ yields the equations of motion (the Euler-Lagrange equations) for the system; which depend only on the Lagrangian. The Lagrangian determines the dynamics of the system through the associated Euler-Lagrange equations. Typically, we are interested in systems with Lagrangians of the form $L = T - V$, where T is the kinetic energy and V is the potential energy. The corresponding Hamiltonian for such a system is $H = T + V$.

II. MOTIVATING AND DEFINING THE PATH INTEGRAL

A. A Simple Case: Diffraction

Before considering the full path integral, we turn to an example where we can roughly interpret the notion of a "sum over paths" in an elementary way – diffraction of a particle through two slits. This follows the example in [4]. The primary focus here is on gaining intuition for the behavior of the phase $e^{iS[x]/\hbar}$, and how two such phases interfere for different paths.

We suppose a particle of mass m propagates with a momentum localized around some particular value p (thus very delocalized in position space) through a screen with two slits at positions x_1 and x_2 (equidistant from the source of the particle), to a screen some large distance (compared to the slit separation) away (see figure 1).
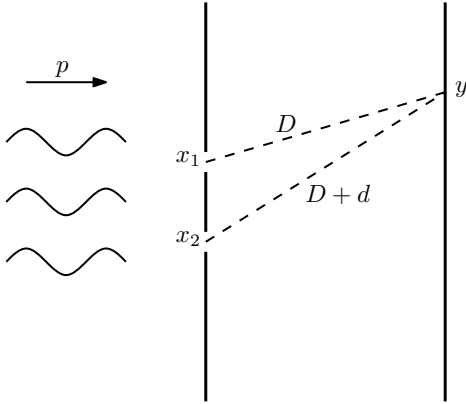
FIG. 1: A particle propagating through two slits at x_1 and x_2, being observed at y.

Now consider a point y on the screen a distance D from x_1 and $D+d$ from x_2. If the particle propagates through slit 1 and then takes a classical trajectory to reach y a time $t = mD/p$ later, the action for this second leg is $S_1 = (p^2/(2m))t = mD^2/(2t)$, since the Lagrangian is just the kinetic energy $p^2/(2m)$, which is constant for this trajectory. On the other hand, for the particle to reach y from x_2 in the same time (this can occur with non-negligible probability for $d \ll D$), the action is instead $S_2 = m(D+d)^2/(2t)$. If we were then to informally apply the notion that the amplitude for the particle to be found at y is the "sum over paths" of $e^{iS/\hbar}$, restricting to these two paths, we would obtain

$$e^{iS_1/\hbar} + e^{iS_2/\hbar} = e^{imD^2/(2\hbar t)} + e^{im(D+d)^2/(2\hbar t)}$$
$$\approx e^{imD^2/(2\hbar t)}\left(1 + e^{imDd/(\hbar t)}\right)$$
$$= e^{imD^2/(2\hbar t)}\left(1 + e^{\frac{ipd}{\hbar}}\right).$$

If we use the de Broglie relation $p = h/\lambda$, the phase in the second factor is $e^{id/(2\pi\lambda)}$, from which we see that constructive and destructive interference happen for $d = n\lambda$ and $d = (n + 1/2)\lambda$ respectively, which is in agreement with the conventional result. This should be seen as a sign that this choice of phase leads to sensible results. Interestingly, it turns out that the true path integral (allowing all paths, not just the classical ones) for the free particle is a normalized version of $e^{iS_c/\hbar}$, where S_c is the action of the classical path, so we were not far off in this approximation.

B. Generalizing to the Continuum Limit

In our previous example, we restricted our integral to a sum of two discrete contributions. However, in general, the paths in the sum are allowed to vary continuously in some nonzero volume of spacetime, thus making the notion of summation over such paths seemingly tricky.

However, Feynman's approach in [1], which serves as the definition used by most other sources regarding the topic, makes it surprisingly straightforward. The trick is to discretize time, and, in a manner reminiscent of the construction of the Riemann integral, consider the quantity we are interested in to be the "infinitesimal time interval" limit.

If we wish to integrate some functional F of paths in spacetime over the paths connecting the points (x_a, t_a) and (x_b, t_b), we can make approximations by subdividing the time interval into N equal segments, defining

$$N\epsilon = t_b - t_a \tag{2}$$
$$\epsilon = t_{i+1} - t_i \tag{3}$$
$$t_0 = t_a \quad t_N = t_b \tag{4}$$
$$x_0 = x_a \quad x_N = x_b. \tag{5}$$

To integrate over all paths in this approximation, then, is simply to integrate over all the intermediate coordinates $x_1, \ldots, x_{N-1}$ (excluding x_0 and x_N so that the path satisfies the boundary conditions), subject to some normalization that ensures that the limit $N \to \infty$ can yield something sensible. If we denote this approximation with N time intervals by $K_N(x_b, t_b; x_a, t_a)$, we then have

$$K_N(x_b, t_b; x_a, t_a) \propto \int \cdots \int dx_1 \cdots dx_{N-1} F[x(t)], \tag{6}$$

where here $x(t)$ is the "continuous" path constructed by interpolating linearly between the coordinates x_i. In our case, the functional F turns out to be the aforementioned phase $e^{iS/\hbar}$, which is supported by the diffraction example. Another way to understand this choice of functional is that it ensures that the contribution of each path is of equal (unitary) magnitude, but it reproduces the classical principle $\delta S = 0$ in the following way: if we consider the limit $\hbar \to 0$, variation of the action from one path to another results in extreme oscillation of the phase. So, roughly, the *stationary phase approximation* tells us that, in this limit, contributions where S varies to first order will cancel out due to this rapid oscillation, leaving only contributions from terms with $\delta S = 0$, which is precisely the classical behavior (this is meant very informally, as a rigorous description of this phenomenon is outside the scope of this paper).

Given that we use this amplitude functional, the only question remaining about our path integral is how it should be normalized. As is noted in [1], this is quite difficult to do in general (i.e. for a general Lagrangian), but for those of the typical form $L = T - V$, the normalization of the approximation with N time steps turns out to be A^{-N}, where

$$A = \sqrt{\frac{2\pi i \hbar \epsilon}{m}}. \tag{7}$$

A quick way of seeing why this is a good choice is to consider the case of the free particle, where the exponent

is a sum of kinetic energy terms that look like

$$\frac{im}{2\hbar}\left(\frac{x_i - x_{i-1}}{\epsilon}\right)^2 \epsilon = \frac{-\pi}{A^2}(x_i - x_{i-1})^2,$$

since the path from x_{i-1} to x_i is taken to have constant velocity in time ϵ, so the action is again just the product of the kinetic energy with the time ϵ. So the integral looks roughly like a product of gaussian integrals with normalization A (this is not exactly true because of the nontrivial way the variables appear in each factor). Later, we will see that this normalization reproduces the Schrödinger picture.

In summary, we define the path integral from (x_a, t_a) to (x_b, t_b) as

$$K(b, a) = \int_{x(t_a)=x_a}^{x(t_b)=x_b} e^{iS[x(t)]/\hbar} \mathcal{D}x(t)$$

$$= \lim_{N \to \infty} \left(\frac{2\pi i \hbar \epsilon}{m}\right)^{-N/2} \int dx_1 \cdots dx_{N-1} e^{iS[x(t)]/\hbar},$$
(8)

where we have written $K(b, a)$ instead of $K(x_b, t_b; x_a, t_a)$ for convenience.

C. Reproducing the Schrödinger Picture

At this point, we have defined the notion of a path integral, but have said little of how it is used to construct a physical (quantum-mechanical) theory. Furthermore, even after the latter point is addressed, the question of how this theory relates to the conventional descriptions – whether it is equivalent (they make exactly the same predictions), stronger or weaker (one theory making all the same predictions as the other, and more which are genuinely novel), or even inconsistent with them (making different predictions regarding the same phenomena) – is of paramount importance. It turns out that the theory is equivalent; we will confirm this insofar as recovering the Schrödinger equation in the path integral formulation. First, however, we must further develop an interpretation of the new theory.

To do this, we will adopt a way of dealing with wave functions in the path integral formulation. As mentioned before, the path integral itself $K(x_b, t_b; x_a, t_a)$ can be thought of, on physical grounds, as representing the amplitude that a particle known to be at x_a at time t_a will be found at x_b at time t_b. We can then think of the former condition as being represented by the wave function $\delta(x - x_a)$ at time t_a, and the latter condition as some other wave function $\psi(x_b)$, since we interpret wave functions as probability amplitudes. So in this theory, ψ here represents the result of evolving $\delta(x - x_a)$. Our statement about the interpretation of K is equivalent to saying $K(x_b, t_b; x_a, t_a) = \psi(x_b)$, i.e. the path integral as a function of x_b is equal to the result of evolving $\delta(x-x_a)$ from t_a to t_b, interpreted as a wavefunction.

In general, if, instead of certainty that the particle is at x_a at time t_a, we have a probability amplitude $\psi_a(x_a)$ that this is true, then we can use the path integral to find the probability amplitude $\psi_b(x_b)$ that the particle is at x_b at time t_b, by integrating the propagation amplitude $K(x_b, t_b; x_a, t_a)$ over all x_a, weighted by the amplitude for the particle to have been at x_a in the first place:

$$\psi_b(x_b) = \int dx_a K(x_b, t_b; x_a, t_a)\psi_a(x_a). \quad (9)$$

(Because of this property, the function K is also often called the kernel.) Again, this can also be described as the "evolved" form of the original wavefunction – we can replace ψ_a and ψ_b with the more familiar notation $\psi(x_a, t_a)$ and $\psi(x_b, t_b)$. This essentially completely specifies our theory in terms of path integrals, as we have defined how an arbitrary state evolves in time.

To recover the Schrödinger equation, we consider infinitesimal time evolution with a Lagrangian given by $L(x, v, t) = (1/2)mv^2 - V(x, t)$, following [1]. According to (9),

$$\psi(x, t + \epsilon) = \int K(x, t + \epsilon; y, t)\psi(y, t)dy \quad (10)$$

$$= \frac{1}{A} \int \exp\left(\frac{i}{\hbar}\epsilon L\left(\frac{x+y}{2}, \frac{x-y}{\epsilon}, t\right)\right)\psi(y, t)dy$$
(11)

$$= \frac{1}{A} \int \exp\left(\frac{i}{\hbar}\frac{m(x-y)^2}{2\epsilon}\right)$$

$$\times \exp\left(-\frac{i}{\hbar}\epsilon V\left(\frac{x+y}{2}, t\right)\right)\psi(y, t)dy.$$
(12)

Obtaining (11) from the previous line is justified as follows: we consider $K(x, t + \epsilon; y, t)$ to be the "final time step" in the discretized approximation of $K(x, t+\epsilon; y, 0)$, and the action in this case is approximately ϵL since ϵ is infinitesimal (i.e. L is approximately constant over the path). At this point, we argue that the phase of the first factor in the integrand varies so rapidly when y is a finite distance from x that the integral can be neglected outside a region $y \sim x + \delta x$, with δx on the order of $\sqrt{2\hbar\epsilon/m}$ (so expanding to first order in ϵ means expanding to second order in δx). Substituting $y = x + \delta x$ and $dy = d[\delta x]$ in (12) and then expanding the second exponential to first order in ϵ then yields the product

$$\left(1 - \frac{i}{\hbar}\epsilon V(x, t)\right)\left(\psi(x, t) + \delta x \frac{\partial\psi}{\partial x} + \frac{(\delta x)^2}{2}\frac{\partial^2\psi}{\partial x^2}\right)$$

in the integral. Again to first order in ϵ, this can be expanded as

$$\psi(x, t) - \frac{i}{\hbar}\epsilon V(x, t)\psi(x, t) + \delta x \frac{\partial\psi}{\partial x} + \frac{(\delta x)^2}{2}\frac{\partial^2\psi}{\partial x^2}.$$

The integral of the first term gives

$$\psi(x, t)\frac{1}{A}\int \exp\left(\frac{im(\delta x)^2}{2\hbar\epsilon}\right)d[\delta x] = \psi(x, t).$$

Similar computations show that the integral of the second term is simply $(-i/\hbar)\epsilon V(x,t)\psi(x,t)$, the third vanishes due to the factor of δx, and the last term gives $(i\hbar\epsilon/(2m))\partial^2\psi/\partial x^2$. Combining all of these, we then have

$$\psi + \epsilon\frac{\partial\psi}{\partial t} = \psi - \frac{i}{\hbar}\epsilon V\psi + \frac{i\hbar\epsilon}{2m}\frac{\partial^2\psi}{\partial x^2},$$

or, after cancelling the ψ's and the factor of ϵ,

$$\frac{\partial\psi}{\partial t} = -\frac{i}{\hbar}\left(-\frac{\hbar^2}{2m}\frac{\partial^2\psi}{\partial x^2} + V\psi\right),$$

which is the Schrödinger equation.

III. APPLICATIONS TO FAMILIAR SYSTEMS

We now turn to the problem of analyzing specific quantum systems in the path integral formulation. We will focus on two of the most fundamental systems, which are frequently among the first analyzed in the Schrödinger formulation – the free particle and the simple harmonic oscillator. Before considering either system in particular, we will derive an important identity here for the kernel, for systems with time-independent Lagrangians (time-independent potentials):

$$K(x_b, t_b; x_a, t_a) = \sum_{n=1}^{\infty} \phi_n(x_b)\phi_n^*(x_a)e^{-\frac{iE_nT}{\hbar}}, \quad (13)$$

Where $T = t_b - t_a$ and ϕ_n are the energy eigenfunctions of the system, which we take to be orthonormal. One way of seeing why this would be true is by the "propagation amplitude" interpretation of K. We have reproduced the Schrödinger equation, so we are confident that the path integral formulation is equivalent to the Schrödinger picture. If this is the case, then we can consider the propagation amplitude in the Schrödinger picture, which should be given by $\langle x_a| U(t_a, t_b) |x_b\rangle$, where $U(t_a, t_b)$ is the time evolution operator. Then we can insert a complete set of energy eigenstate projections $|n\rangle\langle n|$ on either side of U to find

$$K = \sum_n \langle x_a|n\rangle \langle n| U(t_a, t_b) |n\rangle \langle n|x_b\rangle,$$

And it is not too difficult to see that this is in fact the form in (13). Perhaps a slightly more rigorous demonstration starts with the fact that any wavefunction ψ can be expanded in terms of the ϕ_n at time t_a, and then its time evolution is governed by the superposition principle, resulting in the following:

$$\psi(x, t_a) = \sum_{n=1}^{\infty} a_n\phi_n(x), \quad \text{and}$$

$$\psi(x, t_b) = \sum_{n=1}^{\infty} a_n e^{-\frac{iE_nT}{\hbar}}\phi_n(x).$$

If we substitute the relation $a_n = \int dy\phi_n^*(y)\psi(y, t_a)$ which follows from orthonormality, we obtain

$$\psi(x, t_b) = \int dy \sum_{n=1}^{\infty} \phi_n(x)\phi_n^*(y)e^{-\frac{iE_nT}{\hbar}}\psi(y, t_a).$$

On the other hand, (9) says that the same relation holds for K. If we denote the right-hand side of (13) by K', then this means

$$0 = \int dy(K' - K)\psi(y, t_a)$$

For any ψ – this can only be true if $K' - K = 0$. With this, we are prepared to analyze the free particle and the simple harmonic oscillator.

A. The Free Particle

We begin by directly computing the path integral $K(x_b, t_b; x_a, t_a)$ for the free particle, with Lagrangian $L = (1/2)mv^2$. The action for a linear path from (x_a, t_a) to (x_b, t_b) in this case is simply given by $(1/2)mv^2T$ where $T = (t_b - t_a)$ and $v = (x_b - x_a)/T$. This allows us to substitute directly into the definition of the path integral to obtain the expression

$$K = \lim_{\epsilon\to 0} A^{-N} \int dx_1 \cdots dx_{N-1}\exp\left(\frac{im}{2\hbar\epsilon}\sum_{i=1}^{N}(x_i - x_{i-1})^2\right)$$

For a given N, we can actually just perform the integrations explicitly. To integrate over x_1, we factor out all terms except those which involve x_1 and integrate. This gives us a factor of

$$\int dx_1\exp\left(\frac{im}{2\hbar\epsilon}\left[(x_2 - x_1)^2 + (x_1 - x_0)^2\right]\right)$$
$$= \int dx_1\exp\left(\frac{im}{\hbar\epsilon}\left[\left(x_1 - \frac{x_0 + x_2}{2}\right)^2 + \left(\frac{x_2 - x_0}{2}\right)^2\right]\right)$$
$$= \frac{A}{\sqrt{2}}\exp\left(\frac{im}{2\hbar\cdot 2\epsilon}(x_2 - x_0)^2\right)$$

Inside the integral. Then to integrate over x_2, we multiply this by the other term involving x_2, which is $\exp\left((im/(2\hbar\epsilon))(x_3 - x_2)^2\right)$. Completing the square as we did above gives the result

$$\frac{A^2}{\sqrt{3}}\exp\left(\frac{im}{2\hbar\cdot 3\epsilon}(x_3 - x_0)^2\right),$$

And, continuing inductively, after $n - 1$ integrations, we have

$$\frac{A^{n-1}}{\sqrt{n}}\exp\left(\frac{im}{2\hbar\cdot n\epsilon}(x_n - x_0)^2\right),$$

So that after all $N-1$ integrations and multiplying the result by A^{-N}, we finally have

$$\frac{A^{-1}}{\sqrt{N}}\exp\left(\frac{im}{2\hbar\cdot N\epsilon}(x_N-x_0)^2\right)$$
$$=\sqrt{\frac{m}{2\pi i\hbar N\epsilon}}\exp\left(\frac{im}{2\hbar\cdot N\epsilon}(x_N-x_0)^2\right)$$
$$=\sqrt{\frac{m}{2\pi i\hbar(t_b-t_a)}}\exp\left(\frac{im(x_b-x_a)^2}{2\hbar(t_b-t_a)}\right),$$

where the last line uses the definitions of x_0, x_N, and ϵ in (2) and (5).

In the interpretation of K as the evolved form of a position eigenfunction $\delta(x-x_a)$, we see that, over time, the wavefunction spreads out as a widening gaussian centered at x_a, reflecting the fact that the momentum of the particle was completely unconstrained. Furthermore, using a continuous-spectrum analogue of (13), the expression of K as a Fourier transform

$$K=\int dp\, e^{\frac{ip}{\hbar}(x_b-x_a)}e^{-\frac{ip^2}{2m\hbar}(t_b-t_a)}$$

shows that the energy eigenstates are propotional to $e^{ipx/\hbar}$ with corresponding energies $p^2/(2m)$. This is the simplest system of quantum mechanics, so it is good that we have been able to obtain the most fundamental facts about it using the path integral as our primary tool.

B. The Simple Harmonic Oscillator

A more interesting, but still very fundamental system to analyze is the quantum simple harmonic oscillator with Lagrangian given by

$$L=\frac{1}{2}m\dot{x}^2-\frac{1}{2}m\omega^2x^2$$

To compute the path integral for this, we first write the paths from (x_a,t_a) to (x_b,t_b) in the form $x(t)=x_c(t)+y(t)$, where $x_c(t)$ is the classical path from (x_a,t_a) to (x_b,t_b). So $x(t)$ runs through all paths from x_a to x_b as y runs through all loops beginning and ending at 0. Furthermore, the action for a path x can be written

$$S[x(t)]=S[x_c(t)]+\int_{t_a}^{t_b}\left(m\dot{x}_c\dot{y}-m\omega^2x_cy\right)dt$$
$$+\int_{t_a}^{t_b}\left(\frac{1}{2}m\dot{y}^2+\frac{1}{2}m\omega^2y^2\right)dt.$$

However, the second term vanishes, which is actually a direct result of the requirement $\delta S=0$ for the classical path – the action must not vary to first order in y (more explicitly, the first term can be integrated by parts, and then the equation of motion $\ddot{x}_c=-\omega^2x_c$ shows this term vanishes). So the exponential of the first term can be

factored out of the path integral, and the path integral an be expressed as

$$K(b,a)=e^{\frac{iS[x_c]}{\hbar}}\int_0^0\exp\left(\frac{i}{\hbar}\int_{t_a}^{t_b}\frac{m}{2}\left(\dot{y}^2-\omega^2y^2\right)dt\right)\mathcal{D}y(t).$$

The classical path and its associated action can be found straightforwardly by solving the equation $\ddot{x}=-\omega^2x$ with the appropriate boundary conditions, and computing the action explicitly for the result. From this we obtain

$$S[x_c]=\frac{m\omega\left[(x_a^2+x_b^2)\cos(\omega(t_b-t_a))-2x_ax_b\right]}{2\sin(\omega(t_b-t_a))}.$$

To compute the remaining path integral, note that we can shift everything in time so that effectively we have $t_a=0$ and $t_b=T$ (i.e. the quantity we're interested in is only a function $F(T)$ of the difference $T=t_b-t_a$). Then each path under consideration can be treated as periodic with period T (since it returns to 0 at time T), so can be expanded in Fourier series, say $y=\sum_n a_n\sin(n\pi t/T)$. The result can then be computed by considering the action for each individual wave and integrating over the coefficients a_j. This introduces a Jacobian relating the measure $\mathcal{D}y(t)$ to $\prod da_j$, and the integration becomes a product of gaussian integrals in each a_j. This is carried out in detail in [1]; we simply cite the result

$$F(T)=\left(\frac{m\omega}{2\pi i\hbar\sin\omega T}\right)^{1/2}.$$

Combining this with the previous result for $e^{iS[x_c]/\hbar}$ yields the full path integral for the harmonic oscillator.

C. Spectrum of the Harmonic Oscillator

We will examine two different methods for finding the spectrum of the harmonic oscillator in the path integral formulation. The first is described in [1], which makes use of the decomposition (13). For this method, we substitute the expressions

$$i\sin\omega T=\frac{1}{2}e^{i\omega T}\left(1-e^{-2i\omega T}\right),$$
$$\cos\omega T=\frac{1}{2}e^{i\omega T}\left(1+e^{-2i\omega T}\right)$$

Into our expression for the path integral, obtaining

$$\sqrt{\frac{m\omega}{\pi\hbar}}e^{-\frac{i\omega T}{2}}(1-e^{-2i\omega T})^{-\frac{1}{2}}\exp\left(-\frac{m\omega}{2\hbar}(B-C)\right),$$

where

$$B=(x_a^2+x_b^2)\left(\frac{1+e^{-2i\omega T}}{1-e^{-2i\omega T}}\right),\quad\text{and}$$
$$C=\frac{4x_ax_be^{-i\omega T}}{1-e^{-2i\omega T}}.$$

Everything to the right of the factor $e^{-i\omega T/2}$ is a function of $e^{-i\omega T}$, so we can taylor expand in this variable, and the path integral becomes

$$K = e^{-\frac{i\omega T}{2}} \sum_{n=0}^{\infty} \Phi_n(x_a, x_b) e^{-in\omega T}$$

$$= \sum_{n=0}^{\infty} \Phi_n(x_a, x_b) e^{-i\omega(n+1/2)T}.$$

Here the Φ_n represent the coefficients in this expansion, which are functions of x_a and x_b. When computed explicitly, these do indeed factor into the form $\phi_n^*(x_a)\phi_n(x_b)$ as desired (see [1]), but it is difficult and tedious to carry out for general n (though this does tell us that, in principle, the energy eigenfunctions ϕ_n can be found in the new theory by performing these computations). However, since this is in the form of (13), this implies that the energy levels E_n satisfy

$$E_n/\hbar = \omega \left(n + \frac{1}{2} \right),$$

again in agreement with the conventional result.

Another way of recovering the spectrum makes use of an interesting connection to statistical mechanics, which is also discussed in [1]. For a system with energies E_n, an important thermodynamical quantity is the partition function

$$Z = \sum_{n=1}^{\infty} e^{-\beta E_n},$$

Where $\beta = 1/(k_B \mathcal{T})$, with $\mathcal{T}$ the temperature. This function is significant for the role it plays in the probability p_n of observing the system in state n:

$$p_n = \frac{1}{Z} e^{-\beta E_n}.$$

From this, we see that we can find the probability (density) of observing the system at position x is given by

$$P(x) = \frac{1}{Z} \sum_{n=1}^{\infty} \phi_n^*(x)\phi_n(x) e^{-\beta E_n},$$

Since $\phi_n^*(x)\phi_n(x)$ represents the probability density of observing x, given that the system is in state n. Now we notice that the sum is formally identical to the right-hand side of (13), with $x_a = x_b = x$, but with the time interval $t_b - t_a$ replaced by $-i\beta\hbar$ – this is also called a "Wick rotation." If we rewrite K as a function of T, say $K(x_b, t_b; x_a, t_a) = G(x_b, x_a; T)$ (which is always possible for systems with time-independent Lagrangians), then what we are saying is

$$P(x) = \frac{1}{Z} G(x, x; -i\beta\hbar).$$

Then, since P is normalized, integrating over x and multiplying by Z yields

$$Z = \int dx\, G(x, x; -i\beta\hbar).$$

So we can find the partition function for the harmonic oscillator by substituting $-i\beta\hbar$ for $T = t_b - t_a$ in our expression for $K(x_b, t_b; x_a, t_a)$, also setting $x_b = x_a = x$, and integrate over x to obtain the partition function. In our case, the integral is just a gaussian integral (we will omit the computation), and the result is

$$Z = \frac{1}{\sqrt{2(\cosh \beta\hbar\omega - 1)}}.$$

Then if we expand Z in powers of $e^{-\beta\hbar\omega}$ we recover the spectrum of the harmonic oscillator. Note, however, that this approach throws away the information about the wave functions of the eigenstates when we integrate over x.

IV. DISCUSSION

We have defined the Feynman path integral for quantum mechanics and given some motivation for its form; we subsequently showed how it could form the basis for a complete description of quantum mechanics which is equivalent to the Schrödinger (and therefore also Heisenberg) picture. Through analyzing simple but fundamental systems such as the free particle and harmonic oscillator, we learned how to recover important facts in the path integral formulation such as the energy eigenvalues. However, many important subtleties and questions have been left unaddressed. Our analysis actually has a notable weakness – the "time-slicing" definition we used for the path integral specifies a parameterization of the path in terms of time, which makes computing the path integral for potentials which cannot be approximated as quadratic (to low order) essentially intractable using a direct method (it is simply not known, generally, how to compute the integral for such potentials). This is an extremely significant problem because the Coulomb potential, arguably one of the most important examples, cannot be analyzed in this manner. This issue is resolved in [5], by using a different parameterization of the paths.

Additionally, we have not shown much in the way of substantial advantages of the path integral formulation over the "conventional" descriptions, rather focusing on showing that certian problems which are eminently tractable in conventional theories are also doable with path integrals. However, there are advantages to the path integral – particularly when it comes to generalizing non-relativistic quantum theory to more powerful physical theories (particularly quantum field theory). First, as a general principle, it is desirable that the path integral formulation unifies the action principle of Lagrangian mechanics and quantum mechanics, but, as noted by Dirac

[2], this brings with it the more concrete advantage of being more easily made relativistic, as the action S lends itself easily to a relativistic form – in particular, the action can be taken to be Lorentz invariant, while total energy (i.e. the Hamiltonian) is not. At first glance, it may appear that there is still a problem because we have defined the path integral by parameterizing the paths in terms of time, thus breaking symmetry between time and space. However, we are free to reparameterize the path – for example, in terms of some Lorentz-invariant quantity like proper time.

Another advantage in a different vein is the way the path integral for ordinary quantum mechanics serves as a stepping stone for its analogue in quantum field theory, where it actually becomes an object of central interest which is put to diverse uses, one of the most important of which is in describing scattering (for example, finding scattering cross-sections). Most introductions to QFT, such as [4], discuss the application of the QFT-analogue of the path integral to problems of scattering.

If one grants that QFT is, in some sense, a more fundamental description of nature, then the fact that it lends itself well to a description in terms of path integrals arguably indicates that the notion of the path integral itself is somehow a very natural, fundamental physical concept. I hope that the examples reviewed here provide a glimpse into the workings of the path integral which yields some sense of why this might be true.

Acknowledgements

[1] R. P. Feynman and A. R. Hibbs, *Quantum Mechanics and Path Integrals, Emended Ed.* (McGraw-Hill, New York, 1965)

[2] P. A. M. Dirac, *The Principles of Quantum Mechanics, 4th Ed.* (Oxford University Press, 1958)

[3] R. P. Feynman, "Space-Time Approach to Non-Relativistic Quantum Mechanics" (1948). Rev. of Mod. Phys., **20**, 367

[4] M. E. Peskin and D. V. Schroeder, *An Introduction to Quantum Field Theory* (Westview Press, 1995)

[5] I. H. Duru and H. Kleinert, "Solutions of the Path Integral for the H-atom" (1979). *Physics Letters* **84B**(2).

Isospin, Flavor Symmetry, and the Quark Model

David H. Yang
(Dated: May 2, 2014)

We discuss the symmetries of elementary particles coming from the quark model. We start by considering protons and neutrons, which have similar masses and the same strong interactions but different charges. This would be explained by a formalism of "isospin" coming from a $SU(2)$ symmetry. After a general discussion of $SU(2)$ symmetry, we explain isospin symmetry via the quark model of hadrons. As an application, we estimate the ratio of the magnetic moments of the neutron and the proton. Finally, we give a brief overview of $SU(3)$ flavor symmetry and the Eightfold Way.

I. INTRODUCTION

Before the neutron was discovered in 1932, there were only two other "elementary" particles known: the electron and the proton. The neutron has very similar properties to the proton. For one thing, the mass of the neutron and the proton are almost identical. In fact, physicists had earlier been working with a model of the atom consisting only of protons and electrons. So when James Chadwick found the neutron, physicists immediately started trying to explain the similarities between the proton and the neutron.

Within a year, Werner Heisenberg had come up with a proposal. Heisenberg suggested that the proton and the neutron were roughly analogous to the up-spin and down-spin states of a spin-$\frac{1}{2}$ particle. The proton and the neutron would similarly be two states of a single particle. Instead of being up-spin or down-spin, they would be up-"isospin" or down-"isospin". The particle's electromagnetic properties could depend on isospin, and this would slightly alter the mass. But the behavior of the particle under the strong interaction would not depend on its isospin.

Heisenberg did not have an exact understanding of how the strong interaction worked. He only knew that there must be some force stopping the electromagnetic repulsions between protons from blowing up the nucleus. He had no Hamiltonian. But just as spin is a consequence of the rotation symmetry of the universe, isospin would be a consequence of an angular-momentum-like symmetry of the strong interaction's Hamiltonian. This symmetry would give all of the angular momentum formalism in this setting: raising/lowering operators, singlets/multiplets, etc. This kind of symmetry is called a $SU(2)$ symmetry.

As time went on, many more particles were discovered, and physicists needed to somehow organize them. Isospin was a starting point for this organization. By the late 1950s, physicists had found many more isospin families than the proton and neutron. For example, they knew of four Delta baryons, all with very similar masses but with different charges. In the language of isospin, the Delta baryons could be treated as different states of a single isospin-$\frac{3}{2}$ particle. But there were still many different isospin multiplets, so physicists still needed some tool for arranging those multiplets into even bigger multiplets.

This was accomplished in the 1960s when it was discovered that protons and neutrons, previously thought to be elementary particles, were actually composed of smaller particles called quarks. There was an even greater (if less exact) symmetry present, namely flavor symmetry, a $SU(3)$ symmetry, and isospin/flavor symmetry was reinterpreted as a symmetry of quarks. This had as a natural consequence the Eightfold Way, a classification scheme for hadrons. But before sketching these more recent developments, we spell out the classical picture.

In Section II, we define $SU(2)$ symmetry and explain in what sense it is equivalent to rotation symmetry and algebras of angular momentum. We give isospin as an example of a $SU(2)$ symmetry. Then in Section III we explain the quark model of hadrons and reinterpret isospin as coming from an approximate symmetry between up and down quarks. We extend this to strange quarks in Section IV, and give an exposition of $SU(3)$ flavor symmetry. Finally, we say a few words about quantum chromodynamics in Section V.

II. SU(2) SYMMETRY

Consider the spin state space of an electron. This will be a two-dimensional vector space V. A rotation T corresponds to an unitary operator U on V. Composition of unitary operators corresponds to composition of rotations, i.e., the unitary matrix corresponding to rotating by T_1 and then rotating by T_2 is $U_2 U_1$. (Note: We have to consider 360° rotations as different from 0° rotations; a 0° rotation corresponds to the identity matrix I, while a 360° rotation corresponds to the matrix $-I$.)

More generally, assume we have a vector space V and a unitary operator $U(T)$ for every rotation T such that $U(T_2)U(T_1)$ corresponds to rotating by T_1 and then rotating by T_2. We call this data a $SU(2)$ representation.

We claim that a $SU(2)$-representation with vector space V is equivalent to an algebra of angular momentum on V. We will not fully prove this, but we can still get a sense of why this might hold. If we take an infinitesimal rotation T, we will get an infinitesimal unitary matrix $U = 1 + i\epsilon A + O(\epsilon^2)$. For U to be unitary, it must satisfy $U^\dagger U = 1$, or

$$(1 + i\epsilon A + O(\epsilon^2))(1 - i\epsilon A^\dagger + O(\epsilon^2)) = 1 + O(\epsilon^2) \quad (1)$$
$$1 + i\epsilon(A - A^\dagger) = 1 + O(\epsilon^2) \quad (2)$$
$$A^\dagger = A \quad (3)$$

So we see that from an infinitesimal rotation we get a Hermitian operator. We can get back the original rotation by exponentiation. We can now define S_x, S_y, S_Z to be the Hermitian operators corresponding to the infinitesimal rotations at a speed of 1 radian per second around the x, y, z axises. (Note: These are scaled differently than the usual spin operators.) The point is that for any unitary $SU(2)$-representation, these operators will satisfy an algebra of angular momentum, namely

$$[S_i, S_j] = 2i\epsilon_{ijk}S_k \quad (4)$$

We will prove this later. But first we rephrase the definition of a $SU(2)$ representation. Our new definition of a $SU(2)$ representation is a vector space V with a unitary operator $U(T)$ for every unitary 2×2 matrix T such that $U(T_2)U(T_1)$ is the operator corresponding to $T_2 T_1$.

We have a natural representation, given by taking V two-dimensional and defining $U(T)$ to just be T itself. This is called the fundamental representation. In our previous definition, this would correspond to the spin-$\frac{1}{2}$ doublet, i.e., the state space of the electron with rotations acting in the standard way.

It turns out that there is a natural way (which we will not discuss) to associate to each unitary 2×2 matrix a rotation so that composition of matrices becomes composition of rotations. Each rotation will be sent to by 2 different unitary matrices, which reflects the fact that a 360° rotation has a nontrivial effect. This is good: if we work purely with rotations, we always have to keep in mind the distinction between 360° and 0° rotations, while with unitary matrices no such issues occur.

The spin operators S_x, S_y, S_z are defined as the Hermitian operators such that $e^{S_x t}, e^{S_y t}, e^{S_z t}$ correspond to the infinitesimal 2×2 unitary operators $e^{i\sigma_1 t}, e^{i\sigma_2 t}, e^{i\sigma_3 t}$ (t is infinitesimal). This definition corresponds to our previous definition of the spin operators under the correspondance outlined in the previous paragraph.

We can now see why S_x, S_y, S_z satisfy an algebra of angular momentum. We know, as composition corresponds to composition, that

$$e^{itS_x}e^{itS_y}e^{-itS_x}e^{-itS_y}$$

is the unitary operator associated to

$$e^{i\sigma_1 t}e^{i\sigma_2 t}e^{-i\sigma_1 t}e^{-i\sigma_2 t}.$$

We can thus apply Baker-Campbell-Hausdorff to conclude that

$$[S_x, S_y]t^2 + O(t^3)$$

corresponds to

$$[\sigma_1, \sigma_2]t^2 + O(t^3)$$

So $[S_x, S_y]$ must correspond to $2i\sigma_3$, or $[S_x, S_y] = 2iS_z$. And so we see that we indeed get our traditional algebra of angular momentum from a $SU(2)$-representation.

Now that we have summarized the key properties of $SU(2)$-representations, we can explain how isospin can now be interpreted as a $SU(2)$-symmetry. For our vector space V, take the two-dimensional vector space generated by the state of a neutron and the state of a proton. We then take our representation to be the fundamental representation of $SU(2)$. Then we could consider this to be the vector space of "isospin-states" of a single particle, the nucleon. The $SU(2)$ symmetry would give a Hermitian operator S_z, which would have as eigenvectors the states of a neutron and of a proton. For spin, particles whose state space is the fundamental representation are called spin one-half. Using the same terminology in the context of isospin, we call nucleons isospin-$\frac{1}{2}$.

III. THE QUARK MODEL AND MAGNETIC MOMENTS

We now know the structure of two-dimensional isospin representations. But not all isospin vector spaces will be two-dimensional; for example, there are four different Delta baryons, and we would like to consider them as four independent eigenvectors of S_z in some isospin representation. To do, we need some way of generating higher-dimensional representations.

Imagine that we have a representation V. Then we can take its kth tensor power, the tensor product $V \otimes V \cdots \otimes V$ of k copies of V. This sometimes decomposes into smaller representations. For example, if we take the 2nd tensor power of the fundamental representation, we get a direct sum of a three-dimensional representation and a one-dimensional representation. In this way, we can get higher-dimensional representations. It turns out that the third tensor power of the fundamental representation is the direct sum of a four-dimensional representation and two fundamental representations. We would like to say that this is the four-dimensional Delta baryon representation.

Where does a tensor product arise physically? It arises whenever we have multi-particle systems. So one way we could get the Delta baryon representation is if they were composed out of three isospin-$\frac{1}{2}$ particles.

This is indeed the case. In fact, even the proton and neutron turn out not to be elementary. Delta baryons and nucleons are both composed of particles called quarks, of which there are 6 types (called flavors). We temporarily focus on two particular flavors, namely up-quarks and down-quarks. The state space generated by up-quarks and down-quarks is the fundamental representation under isospin. All the isospin families we have

seen are just pieces of a tensor power of the up/down quark doublet.

You cannot isolate a lone quark. All particles we know of that consist purely of quarks contain three quarks, and such a particle is called a baryon. (There are also mesons, which are composed of one quark and one antiquark.) Every particle we have discussed to this point is a baryon. For example, a proton is two up-quarks and a down-quark, while a neutron is two down-quarks and a up-quark. So here, we see that the nucleons (neutrons/protons) correspond to an isospin doublet in the third tensor power of the up/down-quark isospin doublet. This matches up with what we already know: when we take the third tensor power of a spin doublet, we get a spin quartet and two spin doublets. Furthermore, the quartet in the third tensor product corresponds to the Delta baryons.

Simiarly, for mesons, when we tensor the two-dimensional quark representation with the two-dimensional antiquark representation we get a triplet and a singlet. And indeed, we observe a family of three particles corresponding to that triplet, namely the pi mesons. We will not discuss mesons further.

We will derive equations for nucleon states later, so for now we content ourselves with giving the Delta baryon states. For the delta baryon states, we have

$$\begin{aligned}
|\Delta^{++}\rangle &= |uuu\rangle \\
|\Delta^{+}\rangle &= \frac{1}{\sqrt{3}}(|uud\rangle + |udu\rangle + |duu\rangle) \\
|\Delta^{0}\rangle &= \frac{1}{\sqrt{3}}(|udd\rangle + |dud\rangle + |ddu\rangle) \\
|\Delta^{-}\rangle &= |ddd\rangle
\end{aligned}$$

Note that every state is completely symmetric in the three quarks. In general, the kth tensor power of any $SU(2)$ representation will contain a representation with all states completely symmetric.

So how does the quark model explain why neutrons and protons have such similar properties? Well first of all, up and down quarks behave the same in the strong interaction. So neutrons and protons also have the same strong interactions. Furthermore, up and down quarks have much smaller masses than the neutron and proton, so the variation in mass affects the masses of the neutron and proton only a bit. Finally, the charge of the up quark is $\frac{2}{3}e$, while the charge of the down quark is $-\frac{1}{3}e$. Therefore, the neutron is neutral, while the proton has charge $\frac{2}{3}e + \frac{2}{3}e - \frac{1}{3}e = e$.

As another application, we can use the quark model to estimate the magnetic moments of hadrons. In particular, we will estimate the ratio of the magnetic moment of the proton to the magnetic moment of the neutron. If the neutron were elementary, it would have no magnetic moment as it has no charge. But as it is composed of three quarks and each of those quarks has a charge, the neutron has a magnetic moment.

Before we can calculate anything, we need to analyze the state of a proton (or really, the state of a 3 quark system inside the proton.) We make the simplifying assumption that the quarks don't interact in any way. In that case, their relative positions within the proton do not matter, so we simply ignore the position part of their state. Disregarding position, there are three attributes of a quark that we need to take into account. Two are spin and isospin. The third is a more complicated property specific to quarks, called color. The possible color states of an individual quark form a three-dimensional vector space, and the tensor corresponding to a triple of quarks must be totally antisymmetric. As there is only one totally antisymmetric element in the third tensor power of a three-dimensional vector space, the total color vector space is one dimensional and hence we can ignore it.

As quarks are spin-$\frac{1}{2}$, the Pauli exclusion principle tells us that the state of a proton must be antisymmetric with respect to the three quarks in it. As the color part of the state is already antisymmetric, the spin/isospin part must be symmetric. (We are disregarding the position wavefunction here; it turns out that must be symmetric as well.) Furthermore, we know that if we consider the spin-up state of a proton, the z-projections of spin and isospin will both be $\frac{1}{2}$. This tells us that the state must be some linear combination of

$$|u\uparrow u\uparrow d\downarrow\rangle + |u\uparrow d\downarrow u\uparrow\rangle + |d\downarrow u\uparrow u\uparrow\rangle$$

and

$$|u\uparrow u\downarrow d\uparrow\rangle + |u\downarrow u\uparrow d\uparrow\rangle + |u\uparrow d\uparrow u\downarrow\rangle$$
$$+ |u\downarrow d\uparrow u\uparrow\rangle + |d\uparrow u\downarrow u\uparrow\rangle + |d\uparrow u\uparrow u\downarrow\rangle$$

To figure out which linear combination, we need to also use that the total spin is $\frac{1}{2}$. (We could also use that the total isospin is $\frac{1}{2}$, but this turns out to give the same equation.) The total spin being $\frac{1}{2}$ tells us that the raising operator (which will turn the $\downarrow$s into $\uparrow$s) must annihilate the space. Our above two states get sent by (the same multiple of) the raising operator to (respectively)

$$|u\uparrow u\uparrow d\uparrow\rangle + |u\uparrow d\uparrow u\uparrow\rangle + |d\uparrow u\uparrow u\uparrow\rangle$$

and

$$2(|u\uparrow u\uparrow d\uparrow\rangle + |u\uparrow d\uparrow u\uparrow\rangle + |d\uparrow u\uparrow u\uparrow\rangle)$$

so we see that the state of a proton must be

$$\frac{1}{\sqrt{18}}(|u\uparrow u\downarrow d\uparrow\rangle + |u\downarrow u\uparrow d\uparrow\rangle + |u\uparrow d\uparrow u\downarrow\rangle$$
$$+ |u\downarrow d\uparrow u\uparrow\rangle + |d\uparrow u\downarrow u\uparrow\rangle + |d\uparrow u\uparrow u\downarrow\rangle$$
$$- 2|u\uparrow u\uparrow d\downarrow\rangle - 2|u\uparrow d\downarrow u\uparrow\rangle - 2|d\downarrow u\uparrow u\uparrow\rangle)$$

In particular, we see that the down-quark has probability $\frac{1}{3}$ of being up-spin, while the two up-quarks have probability $\frac{5}{6}$ of being up-spin. If we let μ_u denote the magnetic moment of the spin-up up-quark and μ_d denote the magnetic moment of the spin-up down-quark, then we see the expected magnetic moment of an up-quark is $\frac{2}{3}\mu_u$ and the expected magnetic moment of a down-quark is $-\frac{1}{3}\mu_d$. Therefore the expected magnetic moment of a proton is $\frac{4}{3}\mu_u - \frac{1}{3}\mu_d$. Furthermore, as an up-quark has charge -2 times the charge of a down-quark, we expect μ_u to be around $-2\mu_d$. We can thus estimate the magnetic moment of a proton as $-3\mu_d$.

We can repeat this argument for a neutron. We will find that the state of a neutron is

$$\frac{1}{\sqrt{18}}(|d\downarrow d\uparrow u\downarrow\rangle + |d\uparrow d\downarrow u\downarrow\rangle + |d\downarrow u\downarrow d\uparrow\rangle$$
$$+ |d\uparrow u\downarrow d\downarrow\rangle + |u\downarrow d\uparrow d\downarrow\rangle + |u\downarrow d\downarrow d\uparrow\rangle$$
$$- 2|d\downarrow d\downarrow u\uparrow\rangle - 2|d\downarrow u\uparrow d\downarrow\rangle - 2|u\uparrow d\downarrow d\downarrow\rangle)$$

and here the two down-quarks have probability $\frac{1}{6}$ of being up-spin, while the up-quark has probability $\frac{2}{3}$ of being up-spin. The magnetic moment is thus $-\frac{4}{3}\mu_d + \frac{1}{3}\mu_u = -2\mu_d$, and we finally see that the quark model predicts that the ratio between the magnetic moment of the proton and the magnetic moment of the neutron is $\frac{3}{2}$. This heuristic argument fares quite well; the actual ratio is around 1.46.

To get a possible isospin state for the proton and the neutron, we just take only the terms in the above expressions with the fixed spin state $\uparrow\uparrow\downarrow$ or $\uparrow\downarrow\downarrow$. We thus get the expressions

$$\frac{1}{\sqrt{6}}(|duu\rangle + |udu\rangle - 2|uud\rangle)$$

for the proton and

$$\frac{1}{\sqrt{6}}(|udd\rangle + |dud\rangle - 2|ddu\rangle)$$

for the neutron. (Note that these are only one possibility for there states. For example, you could get a different possibility by permuting the three quarks, as the above two expressions are not symmetric.)

IV. $SU(3)$ **FLAVOR SYMMETRY AND THE EIGHTFOLD WAY**

As mentioned before, there are quarks of flavors other than up and down. The other four flavors of quarks are strange, charm, bottom, and top. Up and down quarks are the most common (as the other flavors rapidly decay into them) and have the smallest mass. The quark with the next smallest mass is the strange quark, and we would

like to be able to have an analogue of the isospin story for particles made out of up, down, and strange quarks. In particular, it would be nice if we could group such particles into families of similar mass, just as we grouped the nucleons (neutron/proton) together and the Delta baryons together.

These hopes are answered by something called $SU(3)$ flavor symmetry. What is a $SU(3)$ symmetry? Well now that we have a definition of a $SU(2)$-representation in terms of 2×2 unitary matrices, we can now easily define a $SU(n)$-representation for any n: simply replace 2×2 matrices with $n \times n$ matrices.

And so if we take the three-dimensional vector space spanned by up, down, and strange quarks, it will naturally be a $SU(3)$-representation: the unitary operator corresponding to a unitary 3×3 matrix can just be taken to be itself. This $SU(3)$ symmetry is called flavor symmetry. As before, if we want to predict what flavor symmetry does to hadrons, we should look inside pieces of the (third) tensor power of the quark state space.

The decomposition of $SU(3)$ tensor powers is more complicated than that of $SU(2)$ tensor powers. It can be computed that the third tensor power decomposes into a decuplet (i.e. a $SU(3)$-representation of dimension 10), two octets, and a singlet. The decuplet would have one particle for every combination of up, down, and strange quark, while the octets would have no $|uuu\rangle, |ddd\rangle$, or $|sss\rangle$ but would have two particles composed of one up, one down, and one strange quark. To give a taste, here are the states for the decuplet:

$$|\Delta^{++}\rangle = |uuu\rangle$$
$$|\Delta^{+}\rangle = \frac{1}{\sqrt{3}}(|uud\rangle + |udu\rangle + |duu\rangle)$$
$$|\Delta^{0}\rangle = \frac{1}{\sqrt{3}}(|udd\rangle + |dud\rangle + |ddu\rangle)$$
$$|\Delta^{-}\rangle = |ddd\rangle$$
$$|\Sigma^{*+}\rangle = \frac{1}{\sqrt{3}}(|uus\rangle + |usu\rangle + |suu\rangle)$$
$$|\Sigma^{*0}\rangle = \frac{1}{\sqrt{6}}(|uds\rangle + |dus\rangle + |usd\rangle + |dsu\rangle + |sud\rangle + |sdu\rangle)$$
$$|\Sigma^{*-}\rangle = \frac{1}{\sqrt{3}}(|dds\rangle + |dsd\rangle + |sdd\rangle)$$
$$|\Xi^{*0}\rangle = \frac{1}{\sqrt{3}}(|uss\rangle + |sus\rangle + |ssu\rangle)$$
$$|\Xi^{*-}\rangle = \frac{1}{\sqrt{3}}(|dss\rangle + |sds\rangle + |ssd\rangle)$$
$$|\Omega^{-}\rangle = |sss\rangle$$

As we know that the strange quark has charge $-\frac{1}{3}$, we could calculate the charges of all of these particles. Furthermore, the masses of any two particles in the same family would be close. If they had the same number of strange quarks, the masses would be very close.

In the case of the octet, there were known particles fitting these descriptions that could be nicely organized together. In fact, this organization, called the Eightfold Way, precluded the introduction of the quark model. Indeed, the quark model arose out of attempts to give a conceptual explanation for this organization.

On the other hand, in the case of the decuplet, only nine of the ten particles were known when the Eightfold Way was introduced. The $|sss\rangle$ particle had not yet been discovered. Murray Gell-Mann, one of the (independent) discoverers of the Eightfold Way and the quark model, predicted that there would be a new particle, the omega-minus particle, fitting in the $|sss\rangle$ spot. Such a particle would have charge -1, and Gell-Mann could also predict its mass.

The omega-minus particle was discovered in 1964, only a few years after the introduction of the Eightfold Way. Its discovery essentially confirmed the validity of the Eightfold Way, and Gell-Mann would win a Nobel prize in 1969.

V. CONCLUDING WORDS

We've seen that isospin, flavor symmetry, and quarks are fantastic tools for the classification of hadrons. By decomposing particles into quarks, we can calculate their charge and approximate their mass. Nowadays, we have experimental proofs of quarks, even though no quarks can be isolated.

However, because of the impossibility of isolating quarks, there was a period where the physicality of the quark model was greatly in question. But eventually a theory was proposed for how quarks are confined, or in other words, why quarks always appear inside hadrons. Still no analytic proof of confinement exists, but it is almost certainly true.

Nowadays, quarks play a prominent role in quantum chromodynamics, the quantum field theory of the strong force. Quantum chromodynamics, or QCD, is one of the parts of the Standard Model, the comprehensive description of all forces other than gravity. It describes the dynamics of quarks and gluons, the elementary particles participating in the strong interaction.

[1] Griffiths, Introduction to Elementary Particles
[2] S. Coleman, Aspects of Symmetry
[3] http://www.physics.umd.edu/courses/Phys741/xji/chapter3.pdf
[4] "On the Consequences of the Symmetry of the Nuclear Hamiltonian on the Spectroscopy of Nuclei", E. Wigner

Nuclear Quadrupole Resonance Spectroscopy

William Yashar

Massachusetts Institute of Technology

(Dated: May 2, 2014)

Nuclear Magnetic Resonance (NMR) is a powerful analytical technique that allows researchers to determine the underlying characteristics and compostions of molecules. In order for NMR to properly polarize its samples, however, it relies on the use of superconducting magnets that are highly immobile, expensive, and require cryogenic temperatures in order to operate sufficiently. There has been great interest in instead exploring Nuclear Quadrupole Resonance (NQR) that does not rely on the use of superconducting magnets but instead analyzes the nuclear quadrupole interactions with an Electric Field Gradient (EFG) created by surrounding charges. This report explores the derivation for the quantum expression of the NQR Hamiltonian, assuming that energy of the system can be described by the product of the nuclear electric quadrupole moment and the EFG. As superconducting magnets generate homogeneous fields for acquiring high signal-to-noise data used in NMR analysis, alternative hyperpolarization techniques for NQR spectroscopy are also discussed.

I. INTRODUCTION

The phenomenon of magnetic resonance has become an essential tool in a diverse number of fields since its discovery by Bloch and Purcell 60 years ago[1]. Powerful analytic devices relying on magnetic resonance allow researchers to determine the structures of chemical and biological samples, further revealing their underlying characteristics and compositions. In medicine, magnetic resonance serves as the foundation of magnetic resonance imaging (MRI) technology that allows physicians to acquire a clear picture inside a patient's body while avoiding invasive surgical procedures and the external health risks associated with other imaging systems[2].

Magnetic resonance, however, is not just restricted to studying the human body but has also allowed physical scientists to understand the underlying mechanics of molecules[3]. The magnetic resonance technique that revolutionized the study of chemical characteristics and molecular dynamics is nuclear magnetic resonance (NMR).

NMR and MRI both use resonant radio-frequency pulses to perturb nuclear spins, yielding unique spectra that are indicative of molecular structure[3]. In order to generate a sufficient magnetic field to achieve high spin polarization, however, superconducting magnets are typically required to create a large, homogenous magnetic field. This is problematic, however, in that superconducting magnets are immobile, expensive, and require cryogenic temperatures in order to operate sufficiently.

With these drawbacks in mind, there has been great interest in engineering portable, low-cost, cryogen-free devices utilizing Nuclear Quadrupole Resonance (NQR) spectroscopy instead, often referred to as 'Zero-field NMR'[2]. These spectrometers have the ability to enable chemical analysis at greatly reduced cost in environments not accessible to standard high-field NMR technology.

As in NMR spectroscopy, the primary goal of NQR spectroscopy is to analyze the energy level transitions and spin relaxations of molecules. NQR spectroscopy, however, does not rely on the application of magnetic fields but rather analyzes the nuclear interactions with an Electric Field Gradient (EFG) created by the surrounding charges in the medium. As the nucleus can only interact with the EFG via its electric quadrupole moment, a unique Hamiltonian must be derived in order to conduct tests and collect data using NQR spectroscopy.

Section II outlines the derivation of the NQR Hamiltonian. We start off with a nucleus sitting in a solid which, in the absence of a magnetic field, interacts with the surrounding charges via its nuclear quadrupole moment. Section II A shows that the nucleus orients itself such that it rests in an equilibrium position in which the electric field is zero. As the nuclear quadrupole moment changes the shape of the distribution of the nuclear charges, however, the nuclear interactions with the surrounding EFG is non-zero.

Section II B goes on to outline Das and Hahn's original formulation of the nuclear quadrupole moment and EFG as tensor functions. Das and Hahn composed these functions by parameterizing the nuclear shape by a multipole expansion of the external electric field. These functions are spherically symmetric and transform like the spherical harmonics.

Section II C goes on to fully express the nuclear quadrupole tensor by evaluating the spherical harmonics corresponding to the $\ell=2$ angular momentum states, the first excited interaction states with the EFG. The EFG tensor is fully formulated in Section II D after evaluating two sets of spatial derivatives of the Coulombic potential surrounding the nucleus. Once both the nuclear quadrupole and EFG tensors are fully developed, we take the product of these two tensors to derive the final quantum expression of the NQR Hamiltonian.

II. GENERAL FORMALISM

A. The Nuclear Shape in a Medium

A nucleus sitting in a solid will feel an external electric field generated by charges in the surrounding medium.

The nucleus in turn will rest in an equilibrium position to minimize the electric field and so in the absence of a magnetic field, the first non-zero interactions are with the electric quadrupole moment of the nucleus. Nuclei with a total nuclear spin, I, greater than $\frac{1}{2}$ will posses a non-zero quadrupole moment and will have a nuclear charge distribution resembling either a prolate ("stretched") or an oblate ("squashed") spheroid as shown in Figure 1.
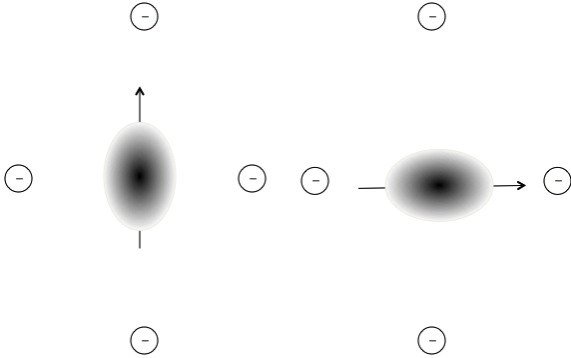

FIG. 1: Two orientations of a non-spherical nucleus interacting with external charges in a surrounding medium. An electric field is generated by charges sitting in lattices surrounding the nucleus. Althogh the nucleus can orient itself such that this electric field is zero, the second set of spatial derivatives of this electric field, called the EFG, is nonzero. The configuration on the left, the prolate spheroid, is lower in energy than that shown on the right, the oblate spheroid.

Although the nucleus can rest in this orientation, the gradient of this electric field, however, is not necessarily zero. The second set of spatial derivatives of the electrostatic potential evaluated at the nucleus is non-zero, however, when interacting with non-spherical nuclei and thus giving rise to the EFG.

B. Outline of Das and Hahn's Tensor Functions

Das and Hahn formulated tensor functions that describe the nucleus interacting with the EFG generated by surrounding charges[4]. Although the derivation of these tensor functions are not derived explicitly in this report, an outline of their steps are explained in this section.

Das and Hahn started by creating an explicit form of the nuclear quadrupole moment. The nuclear shape can be parameterized by a multipole expansion of the external field or potential felt by the nucleus.

$$V(r) = \frac{1}{4\pi} \int \frac{\rho(r')}{|r-r'|} d^3 r' \qquad (1)$$

where $|r-r'|$ is the distance to the observer and $\rho(r')$ describes the density of the charges sitting in the potential. If the observer is sitting very close to this potential or $r' << r$, the potential can be expanded in powers of

r'/r and generate a set of Legendre polynomials [5]. This assumption is valid as nuclei sitting in a lattice will be in close proximity to its surrounding charges. The expansion results in three relevant terms, a first-order overall nuclear charge term, an electric dipole term and an electric quadrupole term.

The nuclear wavefunction has a defined parity, however, so the electric dipole moment is always zero. Moreover, as the nuclear quadrupole moment is non-spherical, only the quadrupole term will interact with the EFG. We can disregard the first term of the power expansion, resulting in the first non-zero interaction term of the potential, the electric quadrupole moment. The nuclear quadrupole is non-spherical and describes the distribution of nuclear charges by

$$eQ = \int \rho r^2 (3\cos^2\theta - 1)d\tau \qquad (2)$$

where ρ is the charge density in a small volume element, $d\tau$, inside the nucleus at a distance r.

As the total potential energy of a nucleus sitting in a lattice is formulated by taking the product of the contributions of the nuclear quadrupole moment and the EFG, Das and Hahn created tensor functions to explicitly define their interactions. If we instead defined equation 2 in terms of the Legendre polynomials, $P_\ell(\cos\theta)$, we can can reformulate the nuclear charge distribution in terms of the spherical harmonics, $Y_\ell^m(\theta,\phi)$. The electric field tensor can be treated similarly, resulting in the nuclear quadrupole tensor and electric field tensor functions, respectively, from Das and Hahn used to derive the NQR Hamiltonian in this report[4].

$$N_\ell^m = \left(\frac{4\pi}{2\ell+1}\right)^{1/2} \sum_i e_i r_i^2 Y_\ell^m(\theta_i, \phi_i) \qquad (3)$$

$$E_\ell^{-m} = \left(\frac{4\pi}{2\ell+1}\right)^{1/2} \sum_j \frac{e_j Y_\ell^m(\theta_j, \phi_j)}{r^{(\ell+1)}} \qquad (4)$$

C. The Nuclear Quadrupole Moment Tensor

The energy level transitions are created by the electric quadrupole moment interacting with the EFG. The Hamiltonian operator can be expressed as the sum of the tensor products that define the electrostatic charge interactions between the nucleus and the external field:

$$\hat{H} = \sum_{\ell=0}^{\infty} \sum_{m=-\ell}^{\ell} N_\ell^m \cdot E_\ell^{-m}$$

where ℓ and m are quantum numbers that describe the azmuthal angular momentum and the magnetic moment

of the nucleus, respectively. This expression for the Hamiltonian can be Taylor expanded considering that the energy level splittings created by the EFG are perturbative. Given that odd ℓ states disrupt the symmetry constraints on the nuclear wavefunction, only the even angular momentum states survive[6].

$$\hat{H} = N_0^0 E_0^0 \;+\; N_1^0 E_1^0 + N_1^{\pm 1} E_1^{\pm 1} + N_2^0 E_2^0$$
$$+ \; N_2^{\pm 1} E_2^{\pm 1} + N_2^{\pm 2} E_2^{\pm 2} + ...$$

The terms with $\ell=0$ correspond to the Coulomb interactions within the system. These interactions are sufficiently high in energy and are not considered[6]. The next nonzero terms are the $\ell=2$ momentum states that describe the nuclear quadrupole interactions. We can solve for each set of nuclear quadrupole states by choosing the corresponding quantum numbers for each state, where $\ell = 2$ and $m = [-2, 2]$, and utilizing the known forms of the spherical harmonics as provided in Equation (5)[7].

$$
\begin{aligned}
Y_2^0(\theta, \phi) &= \frac{1}{4}\sqrt{\frac{5}{\pi}}(3\cos^2\theta - 1) \\
&= \frac{1}{4}\sqrt{\frac{5}{\pi}}\frac{(2z^2 - x^2 - y^2)}{r^2}
\end{aligned}
\tag{5}
$$

where $\{r\}^2 = x^2 + y^2 + z^2$. Both the nuclear quadrupole moment tensor and electronic tensor functions are proportional to the spherical harmonics and can be fully expressed in terms of Cartesian coordinates. When treated as such, the first non-zero nuclear terms are expressed as:

$$N_2^0 = \frac{1}{2}\sum_i e_i(3z_i^2 - (x_i^2 + y_i^2 + z_i^2)) \tag{6}$$

$$N_2^{\pm 1} = \frac{\sqrt{6}}{2}\sum_i e_i z_i(x_i \pm iy_i) \tag{7}$$

$$N_2^{\pm 2} = \frac{\sqrt{6}}{4}\sum_i e_i(x_i \pm iy_i)^2 \tag{8}$$

Further, it is easier to generalize this set of expressions in terms of a general quadrupole moment tensor, Q^m, given that all the first non-zero terms in the Hamiltonian are in the $\ell=2$ angular momentum state.

Moreover, we need to express these relations in terms of the total nuclear spin operator, $\hat{I}$. As the primary goal of NQR spectroscopy is to analyze the spin dyamics of molecules in a medium, the total nuclear spin is used to understand the underlying dynamics and configurations of molecules. Given the general expressions for spin operators, $\hat{I} = (\hat{I}_x^2 + \hat{I}_y^2 + \hat{I}_z^2)$ and $|\hat{I}^2| = I^2$[6], equations (6-8) can be rewritten as:

$$
\begin{aligned}
Q^0 &= \frac{1}{2}\kappa(3\hat{I}_z^2 - \hat{I}^2) \\
Q^{\pm 1} &= \frac{\sqrt{6}}{4}\kappa(\hat{I}_z\hat{I}_\pm + \hat{I}_\pm\hat{I}_z) \\
Q^{\pm 2} &= \frac{\sqrt{6}}{4}\kappa\hat{I}_\pm^2
\end{aligned}
\tag{9}
$$

where the ladder operator is defined as $\hat{I}_\pm = \hat{I}_x \pm i\hat{I}_y$ and κ is a normalization constant resulting from reformulating the nuclear quadrupole moment as a function of the Cartesian spatial operators to a function of the nuclear spin operators.

The total charge of the nucleus is the sum of all the individual charges that constitute the atom, $\sum_i e_i$. As neutrons do not carry charge, only protons and electrons will contribute to the overall charge. If we choose that the maximum component of the nuclear charge aligns along the $\hat{z}$ axis, assigning axial symmetry to the system, κ can be evaluated by[4]:

$$eq \equiv \kappa \langle I, I| \, 3\hat{I}_z^2 - \hat{I}^2 \, |I, I\rangle \tag{10}$$

As the nuclear tensor matrix elements in states $|I, M\rangle$ are formed from a basis of angular momentum eigenstates, the Wigner-Eckhart theorem can be used to calculate κ. This relation is evaluated to find

$$\kappa = \frac{eq}{I(2I-1)} \tag{11}$$

We can plug in this value for κ into Equation (9) to report the final set of expressions for the nuclear quadrupole moment.

$$
\begin{aligned}
Q^0 &= \frac{eq}{2I(2I-1)}(3\hat{I}_z^2 - \hat{I}^2) \\
Q^{\pm 1} &= \frac{\sqrt{6}eq}{4I(2I-1)}(\hat{I}_z\hat{I}_\pm + \hat{I}_\pm\hat{I}_z) \\
Q^{\pm 2} &= \frac{\sqrt{6}eq}{4I(2I-1)}\hat{I}_\pm^2
\end{aligned}
\tag{12}
$$

D.   The Electric Field Gradient Tensor

The electronic tensor functions share a similar form to the nuclear tensor in which they also transform like the spherical harmonics. The electronic tensors differ, however, in that they are not functions of the total nuclear spin operator but rather the Coulombic potential created by the charges surrounding the nucleus. The tensor needs to require that the electric field is generated solely by the charges in the medium and is centered on the nucleus. We can then, at first, treat the electronic tensor function

similarly to that of the nuclear tensor to express the electronic tensor function in Cartesian coordinates, again by using the known forms of the spherical harmonics.

$$
\begin{aligned}
E^0 &= \left(\frac{4\pi}{5}\right)^{1/2} \sum_j \frac{e_j Y_2^0(\theta_j, \phi_j)}{r^3} \\
&= \frac{e}{2} \sum_j \frac{3z_j^2 - r_j^2}{r_j^5} \\
E^{\pm 1} &= \frac{\sqrt{6}e}{2} \sum_j \frac{z_j(x_j \pm iy_j)}{r_j^5} \\
E^{\pm 2} &= \frac{\sqrt{6}e}{4} \sum_j \frac{(x_j \pm iy_j)^2}{r_j^5}
\end{aligned} \tag{13}
$$

From here, the electric field tensor needs to evaluated in terms of the central potential. The electrostatic potential at the nucleus can be modeled like a general coulombic potential, given below:

$$
V(r) = \frac{q^2}{4\pi\epsilon_0 r}
$$

Taking the nucleus to be the origin of the coordinate system, the EFG is given by the second set of spatial derivatives of the Coulombic potential.

$$
\begin{aligned}
V_{ij} &= -\nabla^2 V(r) \\
&= -\begin{pmatrix} V_{xx} & V_{xy} & V_{xz} \\ V_{yx} & V_{yy} & V_{yz} \\ V_{zx} & V_{zy} & V_{zz} \end{pmatrix} \\
&= -\chi \begin{pmatrix} 2x^2 - y^2 - z^2 & 3xy & 3xz \\ 3yx & 2y^2 - x^2 - z^2 & 3yz \\ 3zx & 3zy & 2z^2 - y^2 - x^2 \end{pmatrix}
\end{aligned}
$$

where $V_{ij} = \frac{\partial^2 V}{\partial x_i \partial x_j}$ and $\chi = \frac{q^2}{4\pi\epsilon_0 r^5}$ that describes the volumetric electric field density.

We can choose a proper set of principal axes to diagonalize the matrix in addition to the three components associated with the principal axis directions. Moreover, by using the Laplace equation, $\nabla^2 V(r) = 0$, the resultant matrix created is traceless so that the electric field at the nucleus is produced entirely by the charges external to the nucleus[10]. Using the matrix elements of the EFG, the electric field tensor can be re-evaluated as:

$$
\begin{aligned}
E_2^0 &= \frac{e}{2} \sum_j \frac{3z_j^2 - r_j^2}{r_j^5} \\
&= -\frac{e}{2}\hat{V}_{zz} \\
E_2^{\pm 1} &= \mp\frac{\sqrt{6}e}{6}(\hat{V}_{xz} \pm i\hat{V}_{yz}) \\
E_2^{\pm 2} &= \pm\frac{\sqrt{6}e}{12}(\hat{V}_{xx} - \hat{V}_{yy} \pm 2i\hat{V}_{xy})
\end{aligned} \tag{14}
$$

Finally, Das and Hahn devised an asymmetry paramter, η, to measure the deviation of the EFG from cylindrical symmetry[4].

$$
\eta = \frac{\hat{V}_{xx} - \hat{V}_{yy}}{\hat{V}_{zz}}
$$

The parameter η can vary from 0 to 1 where $\eta=0$ corresponds to symmetry around the $\hat{z}$ axis. We want to align the maximum component of the nuclear potential so that it is symmetric around the nucleus and it aligns with the $\hat{z}$ axis. When $\eta=0$, the components of the EFG tensor are:

$$
\begin{aligned}
V_{xx} &= V_{yy} = -\frac{1}{2}eq \\
V_{zz} &= eq
\end{aligned} \tag{15}
$$

As expected, the maximal component of the EFG tensor aligns along the $\hat{z}$ axis and is symmetric in respect to the other axes. Additionally, the resultant EFG tensor is diagonalized such that all the off-diagonal elements are zero. Using all the redefined parameters, the matrix elements of the EFG tensor and the asymmetry parameter, the electric field tensor functions are evaluated as:

$$
\begin{aligned}
E^0 &= \frac{eq}{2} \\
E^{\pm 1} &= 0 \\
E^{\pm 2} &= \frac{\sqrt{6}eq}{12}\eta
\end{aligned} \tag{16}
$$

We now have all of the relevant expressions to report the final quantum NQR Hamiltonian. The end of Section II B gives the final expressions for the nuclear quadrupole moment tensor function in terms of the total nuclear spin operator, $\hat{I}$. We can combine the nuclear quadrupole tensor with the electronic tensor function, in terms of the EFG matrix elements in Equation (16), to derive the nuclear quadrupole interactions with the surrouding charges. As described in the Hamiltonian in Equation (5), the product of the nuclear quadrupole tensor and the electronic tensor results in the final expression of the NQR Hamiltonian[8].

$$
\hat{H} = \frac{eq}{2I(2I-1)}(3\hat{I}_z^2 - \hat{I}^2 + \frac{\eta}{2}\hat{I}_\pm^2) \tag{17}
$$

III. BEYOND THE HAMILTONIAN: HYPERPOLARIZATION TECHNIQUES FOR NQR SPECTROSCOPY

The utilization of the NQR Hamiltonian is important in that it allows researchers to conduct magnetic resonance spectroscopy without the restrictions created by

using superconducting magnets. Superconducting magnets, although they create high signal-to-noise data by generating a large, homogeneous magnetic field to spin polarize molecules to a high degree of homogeneity, they are largely limited by their immobility and cost. Instead, NQR spectroscopy does not rely on superconducting magnets but rather uses hyperpolarization techniques and direct optical detection of NMR signals to compensate[11].

Using extremely sensitive direct optical detection of the NMR signal amends the low detection efficiency of NMR at low magnetic fields. Hyperpolarization is a technique that allows NQR spectroscopy to be possible, by replacing the thermal equilibrium spin distribution, which produces very low signals at low magnetic fields, with a long-lived non-equilibrium distribution favoring one spin state over the other[11]. When ^{129}Xe is hyperpolarized through means of spin-exchange with optically pumped ^{87}Rb atoms, ^{129}Xe will be polarized by 3 to 4 orders of magnitude more than the maximum value if it was polarized using strong magnets[13]. The hyperpolarized ^{129}Xe, with its greatly enhanced NMR signal, may then be used for probing a variety of phenomenon, such as the presence or lack of biological molecules[12].
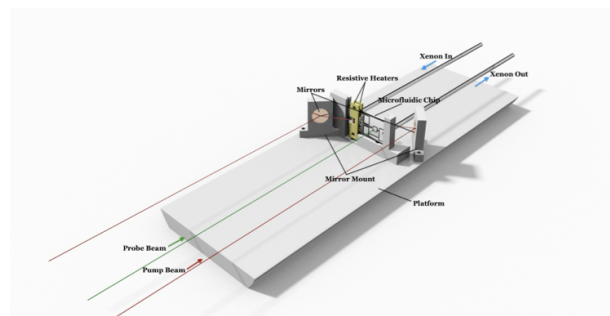

FIG. 2: An experimental model that flows Xenon through a microfluidic chip. Xenon flows in and out through glass tubings attached to the back of the chip. There are two 795 nm lasers that interact with the system: the pump and probe beams. The pump beam transfers its energy to the Rubidium Azide which in turn polarizes the Xenon. The probe beam is guided by the two mirrors and comes through the microfluidic chip perpendicular to the pump beam. We analyze the transferred polarization in the probe beam when it comes out of the magnetometer to detect for hyperpolarization.

This technology can be further miniaturized using standard microfabrication techniques to work on a microfluidic chip[13]. The microfluidic chip that is created is no more than a couple of centimeters wide and a couple of millimeters thick as opposed to high-field NMR spectroscopy where the superconducting magnets can weigh a couple tons.

Optical polarization, however, isnt the only technique of increasing low-field NMR signal-to-noise. Parahydrogen-induced polarization is one particularly effective technique to amplify the low-field NMR signal to

help determine chemical composition[14]. When parahydrogen is added to an analyte via hydrogenation, the non-equilibrium singlet spin polarization is spread throughout the molecule through spin-spin couplings. The spread of spin order is particularly effective at zero to low magnetic fields because the couplings are not truncated by chemical shift differences[12].
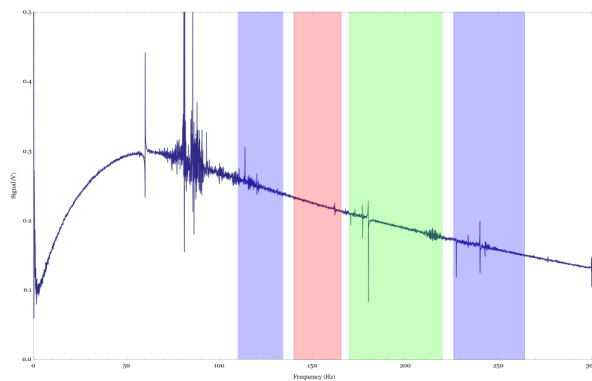

FIG. 3: The spectrum depicts parahydrogen hydrogenating a reference styrene sample, proving that hyperpolzariation can be achieved using parahydrogen as it increased the styrene hyrdogenation signal under no applied magnetic field. The shaded boxes are used to identify the contributions from the α and β isotopermers with ^{13}C on the benzene ring.

Parahydrogen-induced spin polarization is a valuable tool for vastly increasing the intensity of the spectral peaks used to characterize chemical structures in NQR spectroscopy, improving the sensitivity of the technique by orders of magnitude. Increased spin polarization also further extends the applicability of NQR to dilute analytes in solution, also eliminating the need for isotopic labeling[14]. This allows NMR researchers to explore low-field spectra of essential, complex biomolecules including amino acids, peptides, and neurotransmitters.

IV. CONCLUSION

NQR spectroscopy, unlike in NMR, does not rely on the use of magnetic fields to split the energy levels but rather analyzes the effect of an EFG created by charges in a medium on the nuclear quadrupole moment. The first non-zero terms of the Hamiltonian are the terms in which the EFG interacts with the non-spherical moment of the nucleus, the electric quadrupole moment, corresponding to the $\ell=2$ angular momentum states. The nuclear interactions can be described by a tensor function that transforms like the spherical harmonics and is in terms of the total nuclear spin operator, $\hat{I}$. As the components of the nuclear quadrupole tensor are eigenstates of angular momentum, the Wigner-Eckart theorem was used to normalize the quadrupole tensor functions to align the maximum nuclear spin component along the $\hat{z}$ axis.

The electric field tensor function can be treated similarly as it also transforms like the spherical harmonics. It must be expressed, however, in terms of the Coulombic potential surrounding the nucleus. Assigning the EFG so that it is produced entirely by the charges external to the nucleus and the potential is completely symmetric around $\hat{z}$ axis, the final form of the electronic tensor function is expressed in terms of the EFG matrix elements. By combining the final expression for the nuclear quadrupole and EFG field tensors, the full quantum expression for the Hamiltonian is formulated.

The NQR Hamiltonian allows researchers to conduct magnetic resonance analysis without the use of a superconducting magnet. NQR spectroscopy is limited by extremely low thermal spin polarization and poor detection sensitivity so hyperpolarization, the polarization of nuclear spins far beyond thermal equilibrium, is used to generate data with large signal-to-noise in order to conduct NQR spectroscopy.

Two different techniques were explored: optical detection of NMR signals through means of optically pumped ^{87}Rb atoms and the application of parahydrogen. ^{129}Xe can be hyperpolarized by 3 to 4 orders of magnitude more than the maximum value if it was polarized using strong magnets. Moreover, optical detection of NMR signals can be transferred onto a microfluidic chip, opening the door for portable NMR analysis. Further, parahydrogen can be added to an analyte such that the non-equilibrium singlet spin polarization is spread throughout the molecule through spin-spin couplings, thus hyperpolarizing the sample.

[1] F. Bloch, W. W. Hansen, and M. E. Packard. Physical Review, 69:127, 1946.

[2] Dwight G. Nishimura. Principles of Magnetic Resonance Imaging. 1996.

[3] Malcolm H. Levitt. Spin Dynamics: Basics of Nuclear Magnetic Resonance. John Wiley and Sons, 1st edition, 2001.

[4] T. P. Das and E. L. Hahn, "Nuclear Quadrupole Resonance Spectroscopy," Solid State Physics, Supl. 1, (Academic Press, NY, 1958).

[5] D. Ward, Lecture Notes from the Particle and Nuclear Physics module provided by the Department of Physics, University of Cambridge, 2014.

[6] N. R. Cooper, Lecture Notes from the Advanced Quantum Physics module provided by the Department of Physics, University of Cambridge, 2013.

[7] D. A. Varshalovich, A. N. Moskalev, V. K. Khersonskii (1988). *Quantum theory of angular momentum : irreducible tensors, spherical harmonics, vector coupling coefficients, 3nj symbols* (1. repr. ed.). Singapore: World Scientific Pub. p. 155-156. ISBN 9971-50-107-4.

[8] M. Kaplansky, *Applications of Nuclear Quadrupole Resonance Spectroscopy*, (Thesis–McGill University, 1967).

[9] A. Koukoulas, *Investigations in Pulsed Nuclear Quadrupole Resonance Spectroscopy*, (Thesis–McGill University)

[10] S. H. Choh, H. W. Shin, I. Park, H. Ju, J. H. Kim, H. J. Kim, "Calculation of electric field gradient tensor for simple point charge distributions and its application to real systems", *Journal of the Korean Magnetic Resonance Society*, 2003, 7, 16-24.

[11] Burt, Scott, "MRI of Heterogeneous Hydrogenation Reactions Using Parahydrogen Polarization", PhD Thesis, Dept. of Chemistry, Materials Sciences Division, Lawrence Berkeley Lab., Univ. California, Berkeley, CA, 2008

[12] Schroder, L., Lowery, T. J., Hilty, C., Wemmer, D. E., and Pines, A. Molecular imaging using a targeted magnetic resonance hyperpolarized biosensor. Science 314, 446-449 (2006).

[13] Jennifer C. Klein, Adam R. Burr, Bengt Svensson, Daniel J. Kennedy, John Allingham, Margaret A. Titus, Ivan Rayment, and David D. Thomas. Actin-binding cleft closure in myosin II probed by site-directed spin labeling and pulsed EPR. Proceedings of the National Academy of Sciences. 2008, Aug. 25.

[14] Theis, T., Ganssle, Kervern, G., Knappe, S., Kitching, J., Ledbetter, M. P., Budker, D., and Pines, A. Parahydrogen-enhanced zero-field nuclear magnetic resonance. Nature Physics 7, 571575 (2011).

Hidden symmetries of the isotropic harmonic oscillator

QinQin Yu

Physics Department, 77 Massachusetts Ave., Cambridge, MA 02139-4307

(Dated: May 2, 2014)

The isotropic harmonic oscillator has many degeneracies in its energy spectrum, which increase in number at higher dimensions. These degeneracies are explained by symmetries of the Hamiltonian, some of which are obvious, and others of which seem "hidden." One way to organize the degeneracies is using angular momentum; however, we find that this organization is insufficient in explaining all of the degeneracies. The symmetry of an N dimensional harmonic oscillator in general can be understood in terms of the special unitary SU(N) group, which we will develop. This formalism will be used to derive and understand the conserved operators of the 2D and 3D harmonic oscillator.

I. INTRODUCTION

Problems in quantum mechanics that have symmetry will exhibit degeneracies. Some problems have a natural way to organize these degeneracies; one example is into angular momentum states. Our intuition is that these problems have rotational symmetry, and thus angular momentum. However, it may be that some of these symmetries may be hidden as angular momentum. This means that their associated operators satisfy the algebra of angular momentum, but do not have the antisymmetric property of true angular momentum operators. One example of this type of problem is the isotropic harmonic oscillator.

In general, a symmetry is represented by an operator G, that commutes with the Hamiltonian of the system

$$[H, G] = 0. \tag{1}$$

It is known that the expectation value of such an operator does not change over time [6]. For the isotropic harmonic oscillator, we can construct operators J_i that both commute with H *and* satisfy the algebra of angular momentum. These operators obey the commutation relations

$$[J_i, J_j] = i\hbar\epsilon_{ijk}J_k \tag{2}$$
$$i, j, k = 1, 2, 3.$$

We can choose a basis that is an eigenstate of $J^2 = J_x^2 + J_y^2 + J_z^2$ and J_z and label the respective eigenvalues by j and m. In this basis, we can write raising and lowering operators J_+ and J_-

$$J_\pm |j, m\rangle = \hbar\sqrt{j(j+1) - m(m \pm 1)} |j, m \pm 1\rangle \tag{3}$$

that relate states with different angular momenta. The J_+ and J_- operators are related to J_x and J_y by

$$J_\pm = \frac{J_x \pm iJ_y}{\sqrt{2}}. \tag{4}$$

We run into a problem when we try to use only these "angular momentum" operators to explain the symme-

tries of the isotropic harmonic oscillator. [1] We first notice that there are only three of these operators: J_x, J_y, and J_z. However, the number of symmetries in an N-dimensional isotropic harmonic oscillator is not always three. In fact, for some values of N, the number of symmetries is not even a multiple of three.[2] We will also show that for some values of N, writing the eigenstates in the angular momentum basis still leaves unexplained degeneracies. Thus, these "angular momentum" operators can not completely explain the symmetries in the isotropic harmonic oscillator.

The origin of these fake "angular momentum" operators is not immediately obvious. In this short paper, we will construct and explain the conserved operators in the isotropic harmonic oscillator, using the 2D and 3D cases as examples to build intuition. We will first construct the conserved operators that satisfy the algebra of angular momentum in the 2D and 3D case. We will then construct the additional conserved operators using symmetries of the special unitary group SU(N) of group theory. Finally, we will give the conserved operators a physical explanation. This includes identifying which of the operators that satisfy the algebra of angular momentum are true angular momentum operators and which are "hiding" as angular momentum.

II. REVIEW OF THE HARMONIC OSCILLATOR

We will first review the derivations of the energy spectrum for the 2D and 3D harmonic oscillators and build their operators that satisfy the algebra of angular momentum. Understanding the 2D and 3D cases provides good intuition for understanding and organizing the of degeneracies associated with the symmetries of the harmonic oscillator, which we can then explain.

---

[1] We use quotation marks here because we will later discover that not all of these operators are true angular momentum operators.

[2] It is a coincidence that the 3D harmonic oscillator is rotationally symmetric in 3 dimensions. However, the 2D harmonic oscillator is rotationally symmetric in only 1 direction.

A. 2D

We start with the Hamiltonian of the 2D harmonic oscillator

$$H = \frac{1}{2m}(p_x^2 + p_y^2) + \frac{1}{2}mw^2(x^2 + y^2). \quad (5)$$

The Hamiltonian takes a more intuitive form when we define raising and lowering operators

$$a_x \equiv \sqrt{\frac{mw}{2\hbar}}\left(x + i\frac{p_x}{2m}\right) \quad (6)$$

$$a_x^\dagger \equiv \sqrt{\frac{mw}{2\hbar}}\left(x - i\frac{p_x}{2m}\right)$$

and similarly a_y and $a_y^\dagger$. We rewrite the Hamiltonian as

$$H = \hbar w(N_x + N_y + 1) \quad (7)$$

where $N_x \equiv a_x^\dagger a_x$ and $N_y \equiv a_y^\dagger a_y$ are the number operators. We see that the number operators commute with the Hamiltonian, which means that the operators can be simultaneously diagonalized. Thus, acting with the number operator on the energy eigenstates does not change their energies. We can relabel the states by the eigenvalues of the number operator states, n_x and n_y. We already see that there are degeneracies in the energy spectrum, because for the 2nd energy level, $\{n_x, n_y\} = \{1,1\}, \{2,0\}$, and $\{0,2\}$ all give states with the same energy.

Now we want to look for the operators that satisfy the algebra of angular momentum. We start by noticing that the classical z-angular momentum operator commutes with H

$$\ell = xp_y - yp_x = i\hbar(a_y^\dagger a_x - a_y a_x^\dagger) \quad (8)$$
$$[H, \ell] = 0.$$

We would like to choose a basis that is also an eigenstate of ℓ, in order to organize the energy eigenstates by their ℓ eigenvalue. Thus, we are looking to rewrite ℓ as a product of linear combinations of a_x, a_y, $a_x^\dagger$, and $a_y^\dagger$. We find inspiration in circularly polarized light, where the electric field points in $x \pm iy$ and has angular momentum $\pm\hbar$. Thus, we can try a similar construction [4]

$$a_R \equiv \frac{1}{\sqrt{2}}(a_x - ia_y) \quad (9)$$

$$a_L \equiv \frac{1}{\sqrt{2}}(a_x + ia_y).$$

Indeed, by multiplying out, we find that

$$\ell = \hbar(a_R^\dagger a_R - a_L^\dagger a_L) = \hbar(N_R - N_L). \quad (10)$$

where we have defined $N_R \equiv a_R^\dagger a_R$ and $N_L \equiv a_L^\dagger a_L$. Rewriting H in terms of N_R and N_L gives:

$$H = \hbar w(N_L + N_R + 1). \quad (11)$$

We can label the eigenstates states by n_L and n_R and can visualize them quite nicely by organizing them by their H and ℓ eigenvalues (see Figure 1). We see that $\{N_R, H\}$ and $\{N_L, H\}$ form a complete set of commuting observables (CSCO).
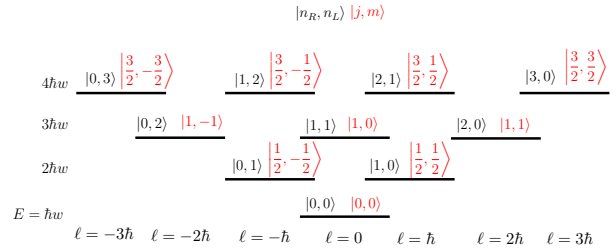

FIG. 1: Energy spectrum of the 2D harmonic oscillator. The different representations are labeled in black and red.

We are now ready to construct the angular momentum operators. We notice that within each degenerate level, the ℓ eigenvalues jump by $2\hbar$. The z component of angular momentum *should* jump by $\hbar$. [3] If we divide ℓ by 2, then it gives the correct difference in eigenvalues:

$$J_z = \frac{1}{2}\ell = \frac{\hbar}{2}(a_R^\dagger a_R - a_L^\dagger a_L) = i\frac{\hbar}{2}(a_x^\dagger a_y - a_y^\dagger a_x) \quad (12)$$

where in the last expression, we have used the definitions of a_R and a_L. This picture also fits with the multiplet states. The first three energy levels in Figure 1 contain 1, 2, and 3 degenerate states. This can be explained by total angular momentum values of 0, $\frac{1}{2}$, and $\frac{3}{2}$, which are multiplets of 1, 2, and 3 states respectively. We can relabel these states with the quantum numbers j, the total angular momentum number, and m, the z component of the angular momentum:

$$J^2 |j,m\rangle = \hbar^2 j(j+1) |j,m\rangle \quad (13)$$
$$J_z |j,m\rangle = \hbar m |j,m\rangle.$$

We see that the states can be completely specified by $\{J^2, J_z\}$, so they form a CSCO.

By inspecting Figure 1, we see that we can move from $|j,m\rangle$ to $|j,m+1\rangle$ by raising n_R by one and lowering n_L by one. The opposite is true of moving from $|j,m\rangle$ to $|j,m-1\rangle$. We construct the raising and lowering operators

$$J_+ = \hbar a_R^\dagger a_L$$
$$J_- = \hbar a_L^\dagger a_R. \quad (14)$$

---

[3] We can show this using the commutation relation $[J_z, J_\pm] = \pm\hbar J_\pm$. If f is an eigenfunction of J_z with eigenvalue μ, then $J_z(J_\pm f) = [J_z, J_\pm]f + J_\pm J_z f = (\hbar + \mu)(L_\pm f)$. Thus, we have a ladder of states whose J_z eigenvalues are separated by $\hbar$ [6].

From J_+ and J_- we can construct the J_x and J_y operators

$$J_x = \frac{J_+ + J_-}{2} = \frac{\hbar}{2}(a_R^\dagger a_L + a_R a_L^\dagger)$$
$$= \frac{\hbar}{2}(a_x^\dagger a_x - a_y a_y^\dagger) \qquad (15)$$
$$J_y = \frac{J_+ - J_-}{2} = \frac{\hbar}{2i}(a_R^\dagger a_L - a_R a_L^\dagger)$$
$$= \frac{\hbar}{2}(a_x^\dagger a_y + a_x a_y^\dagger).$$

We can easily check that J_x, J_y and J_z satisfy the commutation relation in Equation 2, but we don't know yet whether they are all true angular momentum operators.

We expected to find only one angular momentum operator, because the 2D harmonic oscillator is rotationally symmetric in one dimension, which we've arbitrarily chosen here as the z axis. At first sight, the J_x and J_y operators seem to have no physical significance. These extra "angular momentum" operators result from additional symmetries, which we will construct and understand in Section III.

B.   3D

The 3D problem offers a more rich energy spectrum and thus a more interesting organization of states. These additional degeneracies result from the additional symmetries in the problem. Some of these extra degeneracies are explained by the extra two dimensions of rotational invariance. We set up the problem in a similar way to the 2D case. We begin again with the Hamiltonian

$$H = \frac{1}{2m}(p_x^2 + p_y^2 + p_z^2) + \frac{1}{2}mw^2(x^2 + y^2 + z^2). \quad (16)$$

We again define raising and lowering operators a_x, a_y, a_z and $a_x^\dagger, a_y^\dagger, a_z^\dagger$ in the same way as we did in Equation 7. The Hamiltonian can be rewritten as

$$H = \hbar w(N_x + N_y + N_z + \frac{3}{2}). \qquad (17)$$

We can label the states with n_x, n_y, and n_z. Let us check again the degeneracies of the 2nd energy level ($N_x + N_y + N_z = 2$). We find that this includes the states $\{n_x, n_y, n_z\} = \{1,1,0\}, \{1,0,1\}, \{0,1,1\}, \{2,0,0\}, \{0,2,0\}$, and $\{0,0,2\}$. When we compare this to the degeneracies of the same energy level in the 2D case, we see that the 3D harmonic oscillator does indeed have more degenerate states.

We will look for an angular momentum representation by starting with the same analogy to the classical z-angular momentum operator (see Equation 12). We define a_L and a_R in the same way as in Equation 9, and a_z remains unchanged. We can also define N_R and N_L in the same way and $N_z \equiv a_z^\dagger a_z$. We relabel the states as
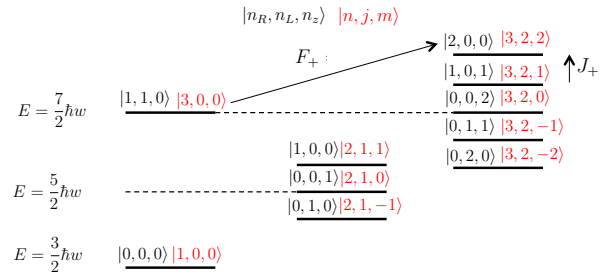

FIG. 2: Energy spectrum of the 3D harmonic oscillator. The different representations are labeled in black and red. Multiplet states have the same energy and are represented by multiple states directly above one another.

$|n_R, n_L, n_z\rangle$. The operators $\{N_R, N_L, N_z\}$ form a CSCO [3]. Figure 2 shows the energy spectrum.

We see now that each energy level contains one or more sets of angular momentum states with the same ℓ eigenvalue, which forms a multiplet of states. This is different from the 2D H.O., where the degenerate states in each energy level had a distinct ℓ eigenvalue. This seems to suggest that the 3D H.O. has an additional angular momentum representation. We relabel the states by $|n, j, m\rangle$, according to the convention of the hydrogen atom, where n indicates the energy level, j is the orbital angular momentum number, and m is the z component of the angular momentum. For instance, we see that the $n = 3, j = 2$ multiplet contains 5 states, just as we expect. However, we also note that the multiplets of the same energy level are separated by j values of ± 2, rather than ± 1. Constructing the angular momentum operators that give these eigenvalues is not so easy for the 3D case. We will do so in Section III C.

III.   SYMMETRIES

We would like to understand the underlying symmetry that generates the angular momentum operators of the 2D case and derive those for the 3D case. It seems so far that they have only been near-random constructions of conserved operators. To be more systematic in looking for symmetries, we inspect the Hamiltonian. We notice that the Hamiltonian of the harmonic oscillator only depends on norms of operators, meaning $a^\dagger a$, p^2, and x^2. Thus, an operator that conserves the length of another operator will be a conserved quantity of the harmonic oscillator. These operators are the unitary operators U with the properties

$$U^\dagger U = 1 \qquad (18)$$
$$a^\dagger (U^\dagger U)a = a^\dagger a.$$

Since the Hamiltonian H is a function of $a^\dagger a$, it remains unchanged when acted on by U

$$U^\dagger H(a^\dagger a)U = H. \qquad (19)$$

We can write an N-dimensional unitary operator as

$$U = e^{i\Omega} \tag{20}$$

where Ω is an N-dimensional Hermitian operator [2].

The number of conserved quantities will be the number of independent parameters of Ω. An N dimensional Hermitian operator has N^2 independent parameters [1]. Thus we expect N^2 conserved quantities. [4] The multiplication of any two of these conserved quantities will yield another conserved quantity. Thus, they form a group, in mathematical language [5]. This group of operators is called the special unitary group SU(N), where "special" means the operator has determinant 1, and N means it has N dimensions. Thus, we see that the N-dimensional harmonic oscillator is a representation of the SU(N) group.

We will now construct the conserved quantities for a general N-dimensional harmonic oscillator, and then we will examine in detail the 2D and 3D cases.

A.   SU(N)

The goal of this section is to mathematically derive the conserved operators, and then we will give them physical interpretations when discussing the 2D and 3D cases. To construct the conserved quantities, we inspect the Hamiltonian. We notice that the following quantities are conserved

$$Q_{ij} = a_i^\dagger a_j \tag{21}$$
$$i, j = 1, 2, ..., N$$

because they creates one quantum and destroys one quantum, keeping the sum of the number operator eigenvalues the same. Thus, the conserved unitary operators of the Hamiltonian will be linear combinations of Q_{ij}. Since $i, j = 1, 2, ..., N$, there will be N^2 linear combinations of Q_{ij}. This is the number of conserved quantities that we are expecting.

However, we notice that for the linear combination $\sum Q_{ii}$ is the just the Hamiltonian up to an additive constant. This conserved operator can be interpreted as just the conservation of energy. We can also understand this by considering $\sum Q_{ii}$ in the $a_i^\dagger a_j$ basis as the identity operator. Thus, acting with $\sum Q_{ii}$ operator just gives every operator an overall phase. Since we cannot detect overall phases, we expect this to be a conserved quantity. In the language of group theory, $\sum Q_{ii}$ is a part of the one dimension unitary group U(1). We will disregard

this symmetry in looking for the remaining symmetries, which now number $N^2 - 1$.

Now we turn our attention back to Q_{ij}. A unitary operator has the additional property of being Hermitian. Although Q_{ij} are conserved, they are not Hermitian. This can easily be fixed with linear combinations of Q_{ij}

$$M_{ij} = i(a_i^\dagger a_j - a_j^\dagger a_i)$$
$$T_{ij} = a_i^\dagger a_j + a_j^\dagger a_i, \qquad i \neq j \tag{22}$$
$$S_2 = a_1^\dagger a_1 - a_2^\dagger a_2$$
$$S_3 = a_1^\dagger a_1 + a_2^\dagger a_2 - 2a_3^\dagger a_3$$
$$...$$

where we have grouped the linear combinations into the antisymmetric combinations M_{ij}, and the symmetric combinations T_{ij} and S [5]. We've written S in a way to avoid making a linear combination of H, which we have already accounted for.

We can now count up the number of operators. For an N-dimensional harmonic oscillator, there are $\binom{N}{2} = \frac{(N-1)N}{2}$ possible M_{ij} operators. For T_{ij} there are again $\frac{(N-1)N}{2}$ possibilities. There are $N - 1$ possibilities of S. We find the total number of conserved Hermitian matrices to be:

$$\frac{(N-1)N}{2} + \frac{(N-1)N}{2} + N - 1 = N^2 - 1 \tag{23}$$

Thus, all of these operators account for the conserved quantities we were expecting.

A nice interpretation of the antisymmetric operators M_{ij} can be seen by rewriting M_{ij} in terms of x_i and p_i using Equation 6

$$M_{ij} = x_i p_j - x_j p_i, \tag{24}$$

up to a factor. We can check that this rewritten operator makes sense because we expected an operator that's antisymmetric in i, j and is Hermitian. We now notice that M_{ij} is just a component of the angular momentum! We have known all along that angular momentum is antisymmetric, and since the M_{ij}'s are antisymmetric, it is natural then that they are the angular momentum operators. Thus, we interpret M_{ij} as representations of rotational symmetries.

Now we can look specifically at the 2D and 3D cases and identify the real and fake angular momentum operators. Additionally, the interpretation of T_{ij} and S is more easily done by looking specifically at specific cases.

---

[4] We can quickly check this for $N = 2$. The most general 2 by 2 Hermitian operator has $4 = 2 \times 2$ independent parameters 3 from linear combinations of the Pauli matrices, and 1 from the identity matrix.

B.   SU(2)

We will now write the conserved operators of the 2D case and compare them to the J_x, J_y, and J_z operators

that we constructed earlier. The conserved Hermitian operators are

$$M_{12} = i\frac{\hbar}{2}(a_x^\dagger a_y - a_y^\dagger a_x)$$

$$T_{12} = \frac{\hbar}{2}(a_x^\dagger a_y + a_y^\dagger a_x) \tag{25}$$

$$S_2 = \frac{\hbar}{2}(a_x^\dagger a_x - a_y^\dagger a_y)$$

We find $2^2 - 1 = 3$ operators, as we had expected.

From Equations 12 and 15, we see that $M_{12} = J_z$, $T_{12} = J_x$, and $S_2 = J_y$. Therefore, only J_z is a representation of angular momentum, as discussed above. We now see that J_x and J_y are other conserved operators hiding as angular momentum! How then can we give them a physical interpretation? We will appeal to the classical 2D harmonic oscillator. The orbits are ellipses that do not precess (we can think of rolling a marble down a circular ramp.). [5] Thus, there are two conserved quantities: the ratio of the major to minor axis of the orbit and its orientation. This is the best that we can do to understand the quantum 2D H.O. Since the orbits do not take a shape, we cannot say find a physical quantity that is associated with T_{12} and S_2 being conserved. However, the symmetry is an analogy to the classical harmonic oscillator orbits not precessing.

C.   SU(3)

Whereas earlier we had trouble constructing the angular momentum operators, we can now easily construct them from the possible antisymmetric conserved quantities M_{ij}

$$M_{12} = i\frac{\hbar}{2}(a_x^\dagger a_y - a_y^\dagger a_x) = J_z$$

$$M_{23} = i\frac{\hbar}{2}(a_y^\dagger a_z - a_z^\dagger a_y) = J_x \tag{26}$$

$$M_{31} = i\frac{\hbar}{2}(a_z^\dagger a_x - a_x^\dagger a_z) = J_y.$$

We can check that J_x, J_y, and J_z follow the algebra of angular momentum. We can also find the J_+ and J_- operators that move between states of different m quantum numbers. This accounts for 3 conserved operators, all of which are real angular momentum operators.

The remaining 9 - 3 - 1 = 5 conserved operators come

_____

[5] Central potentials $\frac{1}{r^\alpha}$ with α = -1 and 2 possess this unique quality. Thus, the harmonic oscillator potential and the Coulomb/gravitational potentials have orbits that do not precess

from the 5 symmetric operators:

$$T_{12} = \frac{\hbar}{2}(a_x^\dagger a_y + a_y^\dagger a_x)$$

$$T_{23} = \frac{\hbar}{2}(a_y^\dagger a_z + a_z^\dagger a_y) \tag{27}$$

$$T_{31} = \frac{\hbar}{2}(a_z^\dagger a_x + a_x^\dagger a_z)$$

$$S_2 = a_x^\dagger a_x - a_y^\dagger a_y$$

$$S_3 = a_x^\dagger a_x + a_y^\dagger a_y - 2a_z^\dagger a_z$$

A nice way to interpret two of these symmetric operators comes from noticing that each energy level also has different j multiplets (see Figure 2). Thus, we are able to construct and operator $F_\pm$ that moves between these multiplets, and from there construct a second algebra of angular momentum. By inspecting the $|n,l,m\rangle$ states, we notice that between the highest m state of one multiplet and the highest m state of the next multiplet we have $n_R + 1$ and $n_L - 1$. Thus we construct

$$F_+ = a_R^\dagger a_L = \left(\frac{a_x^\dagger + ia_y^\dagger}{\sqrt{2}}\right)\left(\frac{a_x + ia_y}{\sqrt{2}}\right) \tag{28}$$

$$= \frac{1}{2}[(a_x^\dagger a_x - a_y^\dagger a_y) + i(a_x^\dagger a_y + a_y^\dagger a_x)]$$

$$F_- = a_L^\dagger a_R$$

We see now that F_+ and F_- are just a linear combination of T_{12} and S_2. From here, we can construct F_x, F_y, and F_z. Thus, we can interpret the additional degeneracies of the 3D harmonic oscillator as coming from an additional angular momentum representation [2].
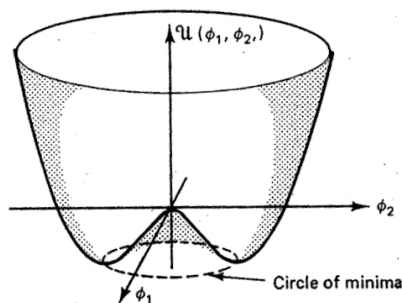

FIG. 3: The Mexican hat potential for SU(2) symmetry breaking in particle physics. Figure taken from W. Mader [8].

IV.   CONCLUSION

The approach of learning the harmonic oscillator without group theory makes the relation of the isotropic harmonic oscillator to SU(N) a pleasant surprise. We see that the N-dimensional harmonic oscillator is just a representation of SU(N) symmetry. This approach easily

reveals the conserved operators, and we realize which "angular momentum" operators are real and which are fake by looking at antisymmetry. We interpret the other conserved operators as additional hidden symmetries, by making an analogy to classical mechanics. For each higher dimensional harmonic oscillator, there are additional degeneracies which can be grouped into more angular momentum representations. We only explored the 2D and 3D cases in detail, but we can now also explain the additional degeneracies of higher dimensional isotropic harmonic oscillators.

A neat application of SU(N) symmetry is in the symmetries of the Lagrangian that describes our universe. In field theory, particles are described by fields. From assuming that the Lagrangian is invariant under transformations of the fields in different dimensions of SU(N), we can derive the fundamental forces. For example, from assuming that the fields are invariant under transformations in SU(1), we derive electromagnetism. From SU(2) symmetry breaking, we derive the electroweak force. We have called it symmetry breaking because SU(2) symmetry would require that all fermions are either massless or have the same mass. Instead of a 2D H.O. representation, imagine a Mexican hat potential, as in Figure 3. Finally, from SU(3) symmetry, we derive the strong force [7].

Thus, SU(N) symmetry finds an application in many problems that only depend on the norms of objects. We have found a way to organize the SU(N) degeneracies into angular momentum states. It is possible that other beautiful organizations exist, and we encourage the reader to explore more.

Acknowledgments

[1] R. Jaffe, Notes on dynamical symmetries of harmonic oscillators.

[2] R. Shankar, *Principles of quantum mechanics* (Plenum Press, 1994).

[3] B. Zwiebach, 8.05 notes on 2D and 3D harmonic oscillators.

[4] B. Zwiebach, "Asymmetric two dimensional oscillator" problem on 8.05 problem set 6.

[5] Discussion with Prof. Jaffe.

[6] D. Griffiths, *Introduction to quantum mechanics* (Pearson Prentice Hall, 2005)

[7] D. Griffiths, *Introduction to elementary particle physics* (Wiley-VCH, 2008) gives a nice derivation of the Dirac Lagrangian and the fundamental forces of nature.

[8] W. Mader, *Leptons and Gauge Bosons* course notes, Technical University of Dresden.

Theory of Superconductivity and the Josephson Effect

Evan Zayas[*]

MIT Department of Physics
(Dated: April 30, 2014)

I will discuss the quantum mechanical phenomenon of superconductivity and its consequences as predicted by B. D. Josephson known as the Josephson effect. I will explore the idea of quantum tunneling across a Josephson junction, and explain the behavior of currents that have been measured experimentally. I will also discuss recent applications of the Josephson effect; namely, its use in experiments to measure the magnetic flux quantum Φ_0 with a great degree of precision. Finally, I will explore the phenomenon of high-temperature superconductivity which is not adequately explained by current theories, and the importance of the Josephson effect in recent efforts to study the mechanism behind high-temperature superconductors.

I. INTRODUCTION

Superconductivity is a phenomenon in which some materials behave as a perfectly diamagnetic conductor when cooled below a critical temperature T_c. It was first discovered in 1911 by the Dutch physicist Heike Kamerlingh Onnes, who was one of the first to study the behavior of materials at temperatures near absolute zero. Using liquid helium, which Onnes himself was the first to create three years earlier, he discovered that the electrical resistance of some metals abruptly vanishes when they are cooled to sufficiently low temperatures. Since its discovery over 100 years ago, superconductivity has been one of the most actively researched fields in physics.

I begin by outlining the theory of superconductivity as proposed by the London brothers, in which I will derive the electromagnetic equations which are fundamental to a superconductor. I will also discuss qualitatively the nature of Cooper pairing and the development of BCS theory, which is now widely accepted as a quantum mechanical description of superconductivity. In sections two and three I consider the quantum mechanical theory of a junction between two superconductors (a Josephson junction) and the predictions set forth by B. D. Josephson regarding this junction - namely, the DC and AC Josephson effects. In section four I will briefly discuss an application of the Josephson effect which has allowed physicists to measure the elementary charge and Planck's constant with great precision. Finally, in section five I explore the phenomenon of high-temperature superconductivity, which remains unexplained to this day.

I.1. The Meissner Effect

When a material undergoes a transition into the superconducting state, it responds to incident magnetic fields in an interesting way. Walther Meissner and Robert Ochsenfeld observed a change in the exterior magnetic field around a superconducting material during this transition; since magnetic flux must be conserved, this implies a change in the interior magnetic field (through the superconductor) as well. Further analysis revealed that when the material reached a superconducting state, the interior field was very nearly equal to zero. This "expulsion" of internal magnetic fields is known as the Meissner effect.

The Meissner effect suggests that the superconducting state cannot be explained simply as a state of perfect conductance because it contradicts the predictions of classical electromagnetic theory. A phenomenological explanation of the Meissner effect was first proposed by Fritz and Heinz London [1], where they consider electrons in a perfect conductor which is under the influence of an electric field $\mathbf{E}$:

$$\mathbf{F} = e\mathbf{E} = m\frac{dv}{dt} \tag{1}$$

Here e is the elementary charge. The current density $\mathbf{J}$ is defined as $\mathbf{J} = env$ where n is the number density of charge carriers. Then, we can easily relate the time derivative of current density to the electric field:

$$\dot{\mathbf{J}} = \frac{ne^2}{m}\mathbf{E} \tag{2}$$

This is the first London Equation, and is commonly written as $\Lambda\dot{\mathbf{J}} = \mathbf{E}$ with $\Lambda \equiv \frac{m}{ne^2}$. Following the process of London, we can use the Maxwell equation $\nabla \times \mathbf{E} = -\frac{1}{c}\dot{\mathbf{B}}$ to obtain:

$$\nabla \times \Lambda\dot{\mathbf{J}} = -\frac{1}{c}\dot{\mathbf{B}} \tag{3}$$

Then, we use the Maxwell equation $\nabla \times \mathbf{B} = \frac{4\pi}{c}\mathbf{J}$ (neglecting the displacement current):

$$\nabla \times (\nabla \times \Lambda\dot{\mathbf{B}}) = -\frac{4\pi}{c^2}\dot{\mathbf{B}} \tag{4}$$

Finally, since div $\mathbf{B} = 0$, we can replace $\nabla \times (\nabla \times \dot{\mathbf{B}})$ with $-\nabla^2\dot{\mathbf{B}}$ and integrate with respect to time, yielding a differential equation in $\mathbf{B}$:

$$\frac{1}{4\pi}\Lambda c^2\nabla^2(\mathbf{B} - \mathbf{B}_0) = \mathbf{B} - \mathbf{B}_0 \tag{5}$$

[*] ezayas@mit.edu

$\mathbf{B}_0$ is the magnetic field at time $t = 0$, the point of transition. The general solution to this equation is given by a superposition of the homogeneous and particular solutions: a trivial particular solution is $\mathbf{B} = \mathbf{B}_0$, which physically means the initial interior magnetic field persists for all time. The homogeneous solution to this equation gives a magnetic field which exponentially decays (we rule out exponential growth as this is unphysical) with a decay constant of $\lambda = \sqrt{\frac{mc^2}{4\pi ne^2}}$. This is called the London penetration depth; numerically, it is typically on the order of 10-100 nanometers. Then, the homogeneous solution is effectively zero at all points except those very near the surface of the superconductor, and the general solution is given simply by the particular solution of $\mathbf{B} = \mathbf{B}_0$.

However, the observational evidence of the Meissner effect contradicts this theory. We know (as did the Londons) that the internal magnetic field in a superconductor is expelled to zero, rather than persisting like this equation would suggest. We conclude from this that Equation 2 is too general; nature should not be governed by an equation which has physical but not-observed solutions. This reasoning motivated the Londons to instead postulate that the homogeneous case of Equation 5 ($\mathbf{B}_0 \to 0$) is the true fundamental equation which describes a superconductor - in other words, it is the replacement for Ohm's law. Then, the exponentially decaying solution is the only solution, and it perfectly predicts the Meissner effect. This is the second London Equation, typically written as:

$$\nabla \times \Lambda\mathbf{J} = -\frac{1}{c}\mathbf{B} \quad (6)$$

One can derive the same results from a quantum mechanical standpoint, with the velocity operator given by [1, 2]:

$$m\hat{\mathbf{v}} = \hat{\mathbf{p}} - \frac{e\mathbf{A}}{c} \quad (7)$$

Where $\hat{\mathbf{p}}$ is the generalized momentum operator and $\mathbf{A}$ is the vector potential defined by $\mathbf{B} = \nabla \times \mathbf{A}$. London argues that we expect the ground state to have zero net momentum[1], and thus we obtain:

$$\mathbf{J} = -\frac{1}{\Lambda c}\mathbf{A} \quad (8)$$

Taking the time derivative gives the first London equation (2) and taking the curl gives the second (6). With

_____

[1] This is apparently shown in an unpublished theorem by Bloch according to F. London [2, 3]. The theorem states that with no applied magnetic field, the most stable state of any electronic system is one with zero current. Although a complete proof of this theorem has never been published, there is little doubt that it is correct. It is also predicted by BCS theory, specifically in the case of boson condensation; see section I.2 entitled 'Cooper Pairs' for more information.

this approach, it is also easy to see why Equation 2 by itself is too general: by taking the time derivative of Equation 8 we lose the information that $\mathbf{B}_0 = 0$, which explains and predicts the Meissner effect.

I.2. Cooper Pairs

While the London Equations explain one observed effect of superconductivity, a more complete theory is needed to explain its origin in the first place. It wasn't until the 1950s when work from John Bardeen [4] and Herbert Fröhlich [5] led Leon Cooper to formulate a situation in which pairs of electrons existing in a bound state could explain the superconducting phenomenon. [6]

When an electron moves through a lattice, it attracts nearby positively charged nuclei; this attraction is manifested as a change in the vibrations of the lattice (phonons). As a result, the space near the electron is (on average) of higher positive charge density than normal. Another electron will be attracted to this area of positive charge, thus forming a bound state with the first electron known as a Cooper pair. It is important to note that although these two electrons are interacting, the average spatial separation between them is quite large, sometimes on the order of 1 micron.[2] This is much greater than the lattice spacing as well as the mean distance between two electrons in the superconductor - consequently, many Cooper pairs will occupy the same space. It is also important to note that while this effect is best described as an interaction between two individual electrons, this description is not entirely accurate. Bardeen [8] remarks that while the paired states become energetically favorable below the critical temperature, electrons constantly move in and out of these pairings as a result of thermal excitation. Even at sufficiently low temperatures the electrons will have some probability to exist "normally", not in a Cooper pair.

The crucial link between Cooper pairs and superconductivity comes from thinking of the pair as a two-particle composite of fermions, which behaves as a boson. Bosons are not restricted by Pauli's exclusion principle, meaning that under the right conditions a large fraction of these Cooper pairs could simultaneously condense into a ground state. Cooper [6] showed that the formation of many paired states leads to an energy spectrum which is continuous except for the ground state, which is separated by an energy gap. Because of this gap to excitations, small perturbations to the system which normally cause electrical resistance will not affect the condensate as a whole; the condensate experiences no resistance and the superconducting state is obtained.

With all of these elements, Bardeen and Cooper assembled the BCS theory with Robert Schrieffer, for which

_____

[2] According to Rohlf. [7]

they received the Nobel Prize in 1972. BCS theory served as the first comprehensive description of superconductivity, and is widely accepted in part because it explains and predicts many aspects of the phenomenon to do with penetration depth, specific heat, and the Meissner effect.[3]

II. QUANTUM MECHANICS OF A JUNCTION BETWEEN TWO SUPERCONDUCTORS

Consider two superconductors which are separated by a thin insulating material, and with a potential difference V (which I will define to be positive for convenience) between them. It is possible for electrons in one superconductor to tunnel across the insulator, provided that the quantum mechanical amplitude does not substantially decay across the junction - this is a familiar example of quantum tunneling. In practice, the insulator must be very thin ($< 50\text{Å}$) to observe this effect. Ivar Giaever [10] discovered that when two superconductors are joined in this way, there is almost zero tunneling current for a sufficiently low potential. For voltages which are considerably higher than this threshold, the current behaves linearly as a function of V as one would expect from Ohm's law. Giaever's results can be explained by the energy gap behavior of Cooper pairs in BCS theory. Since the electrons are condensed into these paired states, individual electrons are not available to tunnel across the barrier. However, when the potential difference is large enough to break the Cooper pairs, the current quickly becomes proportional to V, which describes the familiar process of ohmic tunneling. The threshold voltage is given by $V = \frac{2\Delta}{e}$ where Δ is the energy gap and e is the elementary charge. BCS theory predicts that the energy gap is given approximately[4] by $\Delta \approx 1.764 \, k_B \, T_c$ where k_B is the Boltzmann constant.

A sample plot of Giaever's results is presented in Figure 1. For the $T = 1.6\text{K}$ curve (where the approximation above holds best), the threshold voltage is given by:

$$V = \frac{\Delta}{e} \approx \frac{1.764}{e} \times 7.2\text{K} \; k_B = 1.094\text{mV} \qquad (9)$$

Here we use $V = \frac{\Delta}{e}$ instead of $\frac{2\Delta}{e}$ because only the lead sample is superconducting and not the aluminum. The plot above shows a clear change in behavior in the region near this potential; the current is very nonlinear for voltages near and below the threshold. One might expect

----

[3] There is some debate on that last note. Crucial to the explanation of the Meissner effect is the prediction that the canonical momentum in Equation 7 is zero in the Bose-condensed ground state. Hirsch [9] argues that BCS theory does not predict this to be the case.

[4] Of course, we would expect that as $T \to T_c$ the energy gap goes to zero. This approximation is valid for temperatures which are not extremely close to T_c, and has been supported by experimental results. See Tinkham [2] and Bardeen *et. al.* [11] for more information.
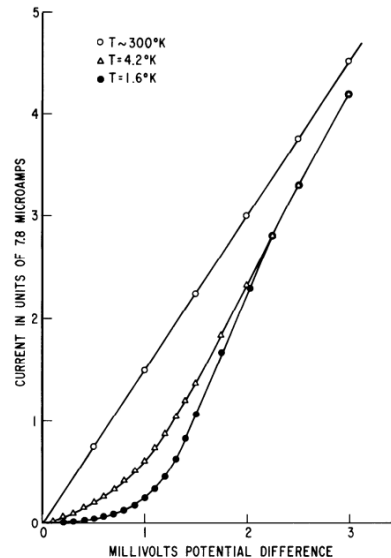

FIG. 1. Current vs. voltage for a junction between aluminum and lead, adopted from Giaever [10]. In this experiment, the lead was superconducting but the aluminum was not, as its critical temperature is very low at 1.2K. The threshold voltage is approximately equal to 1.094 mV.

the current to abruptly drop to zero instead, but recall that even in a superconductor there is a small fraction of electrons which are not in Cooper pairs, as I have already discussed. These electrons can tunnel normally and thus produce a current. Additionally, there is a clear distinction between the curve at 4.2K and 1.6K, which Giaever notes is a consequence of the temperature dependence of Δ.

III. JOSEPHSON'S PREDICTIONS

Following Giaever's research, Brian David Josephson [12] examined the wave functions of electrons tunneling across this junction, which we now call a Josephson junction. We will begin by considering the wavefunction amplitudes at each side of the junction, a procedure which is described also by Feynman [13]:

$$i\hbar\frac{\partial \psi_1}{\partial t} = U_1\psi_1 + K\psi_2$$
$$i\hbar\frac{\partial \psi_2}{\partial t} = U_2\psi_2 + K\psi_1 \qquad (10)$$

These equations assume only that both superconductors are the same material and that K is some characteristic constant of the junction which depends both on the superconductors and the insulator. Then, if a potential is applied across the junction, we have that $U_1 - U_2 = 2qV$.[5]

----

[5] This q is equal to the elementary charge e. I proceed with q

For convenience, we can define the zero-point energy to be the average of U_1 and U_2 such that $U_1 = -U_2$; then, Equation 10 simplifies to:

$$ih\frac{\partial \psi_1}{\partial t} = qV\psi_1 + K\psi_2$$
$$ih\frac{\partial \psi_2}{\partial t} = -qV\psi_2 + K\psi_1 \tag{11}$$

Next we make the following substitutions for ψ_1 and ψ_2:

$$\psi_1 = \sqrt{\rho_1}e^{i\theta_1}$$
$$\psi_2 = \sqrt{\rho_2}e^{i\theta_2} \tag{12}$$

This is a simple and valid way to express any complex number. Of course, it is important to note that $\rho_{1,2}$ and $\theta_{1,2}$ depend on time. Combining equations 11 and 12 yields four more equations (see p. 15 of Feynman [13]) which in turn yield the following expression for the current across the junction:

$$J = \dot{\rho}_1 = -\dot{\rho}_2 = J_0 \sin\left(\delta_0 + \frac{2q}{\hbar}\int V(t)dt\right) \tag{13}$$

Here $J_0 \equiv \frac{2K\sqrt{\rho_1\rho_2}}{\hbar}$ is a new quantity which is characteristic of the junction and $\delta_0 \equiv \theta_2(0) - \theta_1(0)$ is the phase difference between the wavefunctions at time $t = 0$. The consequences of this equation are what we now call the Josephson effects, and are responsible for Josephson's Nobel Prize in 1973.

III.1. DC Josephson Effect

First, let us consider applying a DC voltage: that is, $V(t) = V_0$. Then, the argument of the sine becomes $\delta_0 + \frac{2qV_0}{\hbar}t$. For realistic values of V_0, the frequency of this oscillation is much too fast to measure.[6] Thus, the measured current averages to zero in all cases *except* when V_0 is equal to zero. In this case, the current across the junction is simply given by $J_0 \sin \delta_0$. From this, we conclude that the current should decrease nonlinearly and become very small as $V \to 0$, but at $V = 0$ a small current between $+J_0$ and $-J_0$ (depending on δ_0) should be observed. Figure 2 shows the first published observation of this effect, which is now called the DC Josephson effect.

III.2. AC Josephson Effect

Next, we can consider applying a DC voltage with a small AC component: $V = V_0 + v\cos(\omega t)$. Then, we ob-

————

anyway to avoid confusion with the energy unit electron-volts (eV). Note that Feynman [13] uses $q = 2e$ instead, the charge of a pair.

[6] Take, for example, V_0=1 millivolt. This gives a frequency of 484 GHz, while standard oscilloscopes operate at 1 GHz or lower.
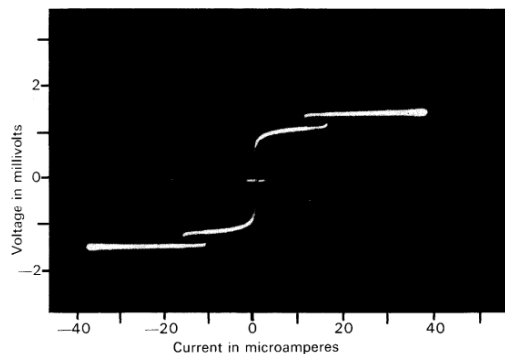

FIG. 2. Plot of voltage vs. current showing both Josephson tunneling and single electron tunneling, adopted from Josephson [14]. Note that the axes here are reversed from those in Figure 1.

tain the following expression for the current from Equation 13:

$$J = J_0 \sin\left(\delta_0 + \frac{2qV_0 t}{\hbar} + \frac{2qvt}{\hbar\omega}\sin(\omega t)\right) \tag{14}$$

Following the process of Richards *et. al.* [15], we may choose $\delta_0 = \frac{\pi}{2}$ for simplicity and expand the sine in the following way:

$$\sin(X\sin\theta) = \sum_{n=-\infty}^{n=\infty} J_n(X)\sin(n\theta)$$

$$\cos(X\sin\theta) = \sum_{n=-\infty}^{n=\infty} J_n(X)\cos(n\theta)$$

$$\Rightarrow \frac{J}{J_0} = \sum_{n=0}^{n=\infty} J_n\left(\frac{\omega_0 v}{\omega V_0}\right) \times$$
$$\left[\cos\left((\omega_0 + n\omega)t\right) + (-1)^n\cos\left((\omega_0 - n\omega)t\right)\right] \tag{15}$$

I have defined $\omega_0 \equiv \frac{2qV_0}{\hbar}$ to simplify the expression. Here J_n is the n-th order Bessel function and $J_{-n}(X) \equiv (-1)^n J_n(X)$. This expression, while somewhat arduous, allows us to see that the term in brackets (sum of cosines) simply describes a beat phenomenon. Once again, the frequency of these beats in general will be much too quick for a feasible measurement, and the current will average to zero. However, if we choose ω such that the beat frequency is very short, we do expect to measure a current. By driving the beat frequency down to zero, we can observe a constant and nonzero current; we call this value of ω a resonant frequency. We observe a current when any harmonic of the resonant frequency coincides with ω_0:

$$n\omega = \omega_0 = \frac{2qV_0}{\hbar} \text{ for } n \in \mathbb{Z}^+ \tag{16}$$

Feynman [13] derives this result with a somewhat simpler approach starting from the assumption that $V \gg v$. Using this, we can expand Equation 14 in a different way using first-order approximations:

$\sin(x + \Delta x) \approx \sin x + \Delta x \cos x$ for small Δx

$$\Rightarrow \frac{J}{J_0} = \sin(\delta_0 + \omega_0 t) + \frac{\omega_0 v}{\omega V_0} \sin(\omega t) \cos(\delta_0 + \omega_0 t) \tag{17}$$

Here I have used the same substitution of ω_0. In this case, the first sine term averages to zero as before and the second term will do the same for non-resonant frequencies. However, if $n\omega = \omega_0$ for some positive integer n then the average current is nonzero and depends on our choice of δ_0.

IV. PRECISE MEASUREMENT OF FUNDAMENTAL CONSTANTS

The AC Josephson effect is useful to experimental physicists because it provides an exact conversion between the resonant frequency and the applied voltage. Recent experiments [15, 16] have shown that it is possible to observe this resonance with incredible precision - in some cases with a fractional uncertainty of order 10^{-8}. By dividing the applied voltage V_0 by the fundamental harmonic ($n = 1$) resonant frequency, we can obtain a numerical value for the quantity $\frac{2e}{h}$:

$$\frac{2e}{h} = 483,597.870(11) \text{ Hz/V} \tag{18}$$

This quantity is also called the Josephson constant, denoted K_J. It is only a function of fundamental constants, meaning it does not depend on the nature of the Josephson junction, the superconducting materials, or the environment of an experiment. This has allowed physicists to measure its value with a great deal of precision; the number quoted above [17] has an uncertainty of only 0.023 parts per million. Additionally, one can use the following relationship to determine the fundamental constant h:

$$h = \frac{8\alpha}{\mu_0 c K_J^2} \tag{19}$$

Here μ_0 is the permeability of free space, α is the fine-structure constant, c is the speed of light and K_J is the Josephson constant. Experiments which study the AC Josephson effect in this way have yielded some of the most precise measurements of the Josephson constant and Planck's constant to date.

V. HIGH-TEMPERATURE SUPERCONDUCTIVITY

BCS theory provided the first widely successful explanation of superconductivity, but more recent experiments have shown that it is likely incomplete. It predicts a theoretical maximum $T_c \approx 30$K, above which the formation of Cooper pairs should be impossible for any material due to thermal energy. In 1986, Georg Bednorz and K. Alex Müller [18] found that Lanthanum Barium Copper Oxide (LBCO) compounds exhibited superconducting properties at 35K. Within the next year, these results had been confirmed many times, Bednorz and Müller had won a Nobel Prize, and the Chinese physicist M. K. Wu [19] had observed superconductivity at 93K, which is particularly significant because a sample at this temperature can be cooled with liquid nitrogen (BP 77K) instead of liquid helium. Since then, high-temperature superconductivity (HTS) has been actively researched by physicists around the world. It remains one of the most prominent unsolved problems in physics.
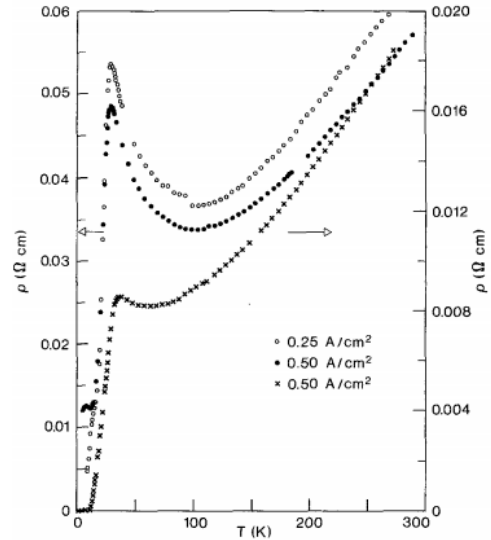

FIG. 3. Resistivity vs. Temperature for compounds in the Ba - La - Cu - O system plotted for various current densities. Adopted from Bednorz and Müller [18], this plot shows superconducting effects at about 35K, which is above the theoretical limit imposed by BCS theory.

V.1. A Possible Qualitative Explanation

Considering the success of BCS theory, it is natural to postulate that the mechanism responsible for HTS is similar. A major component of BCS theory is the idea of Cooper pairing, where electron-phonon interactions create an attractive potential between two electrons which binds the pair together. However, the origin of this attractive potential need not be specified; the formation of Cooper pairs relies only on the fact that there exists *some* attraction between the electrons. Resonating Valence Bond theory (RVB) suggests that in a HTS, this

attraction is caused by spin-density waves rather than by phonons (which can be viewed as charge-density waves). The strength of this attraction depends on the lattice structure of the material; it is strongest when the lattice is nearly antiferromagnetic - that is, when neighboring lattice sites have opposite spins. All currently observed HTS materials are "strong" spin-density systems in this regard.

V.2. Experimental Tests of Cooper Pairing in High-T_c Superconductors

If RVB Theory is correct and high-temperature superconductivity is a consequence of Cooper pairs, then we should already have an understanding of how to model a Josephson junction between two HTS samples. Consider a superconducting ring which consists of one Josephson junction where we choose $\delta_0 = \pi$. Such a setup is called a π-loop, and the junction is called a π-junction. Any superconducting ring will exhibit magnetic flux quantization (see Kirtley and Tsuei [20–22]) - that is, the flux through the loop is given by:

$$\Phi = n\Phi_0 \text{ for } n = 0, 1, 2, ... \quad (20)$$

Where Φ_0 is the magnetic flux quantum $\frac{h}{2e}$, the reciprocal of the Josephson constant K_J. However, in the particular case that the loop has an odd number of π-junctions, we can observe half-integer quantization:

$$\Phi = \left(n + \frac{1}{2}\right)\Phi_0 \text{ for } n = 0, 1, 2, ... \quad (21)$$

This is a consequence of a symmetry that exists in the Cooper pairing mechanism called d-wave symmetry. The electron spins spontaneously align even in the absence of an applied magnetic field, a process known as spontaneous magnetization. Kirtley and Tsuei [20–22] provide some additional insight on this phenomenon. To test whether Cooper pairing is involved in the mechanism for HTS, many experiments have been built to observe this half-integer flux quantization. The results of such experiments thus far have been somewhat inconclusive, most likely due to defects in the superconductor. To circumvent this problem, Kirtley and Tsuei [22] designed an experiment to consider both the "clean" limit (no defects) and the "dirty" limit (maximal defects). From this they have concluded that while it is likely that Cooper pairing is involved with at least some high-T_c superconductors, the extent and nature of its involvement is still unknown.

VI. CONCLUSIONS

The Josephson junction applies the familiar idea of quantum tunneling to an insulating barrier between two superconductors. From the theory of Cooper pairing and the energy gap-to-excitations, we have explored the predictions set forth by Josephson regarding the induced current through a junction in response to DC and AC voltage input. These effects have helped physicists measure the magnetic flux quantum Φ_0 with greater precision than before, and the Josephson junction has proved to be a useful tool in probing the mechanism behind high-temperature superconductors.

VII. ACKNOWLEDGEMENTS

[1] F. London; H. London, *The Electromagnetic Equations of the Supraconductor*. Proc. Roy. Soc. **149**, 866: p. 71 (1935)

[2] Michael Tinkham, *Introduction to Superconductivity*. McGraw-Hill. (1996)

[3] F. London, *Superfluids*. Wiley, New York. (1950)

[4] J. Bardeen, *Wave Functions for Superconducting Electrons*. Phys. Rev. **80**, 4. (1950)

[5] H. Frohlich, Proc. Roy. Soc. (London) **A215**, 291. (1952)

[6] L. Cooper, *Bound Electron Pairs in a Degenerate Fermi Gas*. Phys. Rev. **104**, 4. (1956)

[7] J. W. Rohlf, *Modern Physics from a to Z*. Wiley. (1994)

[8] J. Bardeen, *Electron-Phonon Interactions and Superconductivity*. Cooperative Phenomena, p. 67 (1973)

[9] J. E. Hirsch, *Explanation of the Meissner Effect and Prediction of a Spin Meissner Effect in Low and High T_c Superconductors*. Physica Scripta **80**, 035702. (2009)

[10] L. Esaki and I. Giaever, *Nobel Lectures: Experimental Discoveries Regarding Tunnelling Phenomena in Semiconductors and Superconductors*. (1973)

[11] J. Bardeen, L. N. Cooper, and J. R. Schrieffer, *Theory of Superconductivity*. Phys. Rev. **108**, 5. (1957)

[12] B. D. Josephson, *The Discovery of Tunnelling Supercurrents*. Rev. Mod. Phys. **46**, 2. (1974)

[13] R. Feynman, *Lectures on Physics*, vol. III. Addison-Wesley, New York. (1966)

[14] B. D. Josephson, *Nobel Lecture: Theoretical Predictions of the Properties of a Supercurrent through a Tunnel Barrier, In Particular Those Phenomena which are Generally Known as Josephson Effects*. (1973)

[15] P. Richards, S. Shapiro, and C. Grimes, *Student Laboratory Demonstration of Flux Quantization and the Josephson Effect in Superconductors*. American Journal of Physics **36**, 8. (1968)

[16] J. Clarke, *The Josephson Effect and e/h*. American Journal of Physics **38**, 9. (1970)

[17] *Josephson constant KJ*. 2010 CODATA recommended values. Retrieved 10 January 2012.

[18] J. G. Bednorz and K. A. Müller. *Possible High-T_c Superconductivity in the Ba - La - Cu - O System*. Zeitschrift für Physik B **64**, 2. (1986)

[19] M. K. Wu et. al. *Superconductivity at 93 K in a New Mixed-Phase Y-Ba-Cu-O Compound System at Ambient Pressure*. Phys. Rev. Lett. **58**, 9. (1987)

[20] C. C. Tsuei and J. R. Kirtley. *Half-Integer Flux Quantization in Unconventional Superconductors*. (2011)

[21] C. C. Tsuei and J. R. Kirtley. *Pairing Symmetry in Cuprate Superconductors*. Rev. Mod. Phys. **72**, 4. (2000)

[22] J. R. Kirtley et. al. *Symmetry of the Order Parameter in the High-T_c Superconductor $YBa_2Cu_3O_{7-\delta}$*. Nature **373**, p. 225. (1995)

[23] MIT Department of Physics. *Superconductivity: The Meissner Effect, Persistent Currents and the Josephson Effects*. (2011)

[24] J. Bardeen, L. N. Cooper, and J. R. Schrieffer, *Microscopic Theory of Superconductivity*. Phys. Rev. **106**, p. 162. (1957)

[25] B. D. Josephson, *Possible New Effects in Superconductive Tunnelling*. Phys. Lett. **1**, 7. (1962)

[26] L. Zhou, *The Meissner Effect and the Josephson Effect in Superconductors*. (2013)

[27] L. D. Landau and L. M. Lifshitz, *Quantum Mechanics: Non-Relativistic Theory*. Butterworth-Heinemann. (1976)

[28] A. Leggett, *What DO We Know About High T_c?* Nature Physics **2**, 3. (2006)

The Solar Neutrino Problem and Neutrino Oscillation

Shengen Zhang*
MIT Department of Physics
(Dated: May 2, 2014)

We first introduce the neutrino and a mysterious phenomenon about it , which is usually referred as the solar neutrino problem. Then we present in detail the theory of neutrino oscillation, which gives a reasonable and powerful explanation to the solar neutrino problem.

1. INTRODUCTION

The solar neutrino problem is the discrepancy between the number of solar neutrinos predicted by standard model of solar interior and the number actually measured. Due to technological limit, keeping track of the products of sun's nuclear reaction is by far the best and the only way to study the structure of the sun. In that sense, the discrepancy between the expected and recorded numbers of solar neutrinos is undoubtedly a huge impact upon our understanding about the sun. Therefore, the solar neutrino problem is a crucial and fundamental problem we have to answer before we can proceed in our exploration of the universe. The main purpose of this paper is to present a theory that gives reasonable account for "disappearance" of solar neutrinos.

This paper mainly consists of five sections. The first section is the introduction. The second and third are mostly introductory backgrounds of neutrinos and the solar neutrino problem. The forth section is devoted to a detail illustration of the neutrino oscillation theory, which includes the formulation of the theory, example of calculation as well as experimental evidences that support the theory. The final section is the conclusion.

2. A BRIEF INTRODUCTION OF NEUTRINO

Neutrino was first postulated in 1930 by Wolfgang Pauli to compensate for missing energy of beta decay. Until now, three "flavors" (types) of neutrinos have been discovered. They are electron neutrinos, muon neutrinos and tau neutrinos, each named after their partner leptons.

The name of these spin $\frac{1}{2}$ subatomic particles, "neutrino," which means little neutral one in italian, pretty much summarize their characteristics: electrically neutral and extremely light weighted. Because of these characteristics, neutrinos are not subject to electromagnetic force and gravity, but only responsive to short-range weak force. And this makes them extremely hard to detect.

————

*Electronic address: shengenz@mit.edu

Scientists used to believe, and in fact the standard model of particle today still assumes, that neutrinos were massless and traveling at the speed of light. However, even though the masses of neutrinos are yet to be determined, experiment conducted at the Super-Kamiokande detector in Japan, 1998, proved that neutrinos do have masses. As we would see later in this paper, the mass differences among the mass eigenstates of neutrinos is the core of the neutrino oscillation theory.

3. THE SOLAR NEUTRINO PROBLEM

The sun power generate power through proton-proton fussion, which includes mainly the following three branches:

1) PP1: p + p → D + e^+ + ν_e + 0.26 MeV

2) PP2: ^7Be + e^- → ^7Li + ν_e + 0.80 MeV

3) PP3: ^8B → ^8Be + e^+ + ν_e + 7.2 MeV.

As you can see, electron neutrinos are produced in all three branches of the proton-proton fussion. Because they are electrically neutral and only response to weak interaction, most of the them could easily make it to the earth without any being damped by any material in between.

Studying solar neutrons had always been a good way to visualize what was happening at the core of the sun. However, as the quality of detector improved, scientists noticed a discrepancy between the actual measurement of solar neutrino flux and the prediction according to the standard solar model. Ray Davis and John Bahcall's Homestake experiment in the late 1960s captured an approximately 2/3 loss of solar neutrinos. Similar deficits persisted in subsequent experiments which conducted even with more accurate technologies.

The mysterious disappearance of solar neutrinos is what we call the solar neutrino problem. This is not a good sign to physicists, for it could probably overturn their understanding about interior of the sun. There are generally two types of proposed solutions. One suggests modifying the solar interior model while the other bring up a brand new theory called neutrino oscillation, which is what we are going to discuss today.

4. NEUTRINO OSCILLATION

The concept of neutrino oscillation was first proposed by Bruno Pontecorvo in 1957. By "oscillation," it refer to the periodic shift of a neutrino among its three flavor eigenstates. The theory brought up two brand-new idea. Firstly, neutrinos have masses and secondly, the flavor eigenstates are not the mass eigenstates but rather mixtures (or superpositions) of them. Because the mass eigenstates do not share the same mass, the mixtures is actually changing over time in a periodic pattern. This is saying that an electron neutrino produced by nuclear fusion at the core of the sun could probably end up in a different flavor when it it detected on the earth. If our apparatus we use only detect electron neutrinos, we could definitely experience a loss of solar neutrinos. As a matter of fact, the neutrino oscillation theory is quite a reasonable explanation for the solar neutrino problem, for it is backed by a some subsequent experiments.

4.1. Formulation of the Neutrino oscillation in Vacuum [?]

Let us take a closer look at the formulation of the neutrino oscillation in vacuum . Denote the mass eigenstate of a neutrino by ν_k ($k = 1, 2, 3$), and the flavor eigenstate by ν_α ($\alpha = e, \mu, \tau$). According to theory, the flavor eigenstates can be written as superpositions of mass eigenstates:

$$|\nu_\alpha> = \sum_{k=1}^{3} U_{\alpha,k} |\nu_k> . \qquad (1)$$

Here, U is an unitary matrix that mixes up the mass eigenstates. Because matrix U is unitary, according to CPT invariance, the mass eigenstates can conversely be written as superpositions of the flavor eigenstate:

$$|\nu_k> = \sum_{\alpha=e,\mu,\tau} U_{k,\alpha}^* |\nu_\alpha> . \qquad (2)$$

Because the mass eigenstates have definite energy and mass, using variable separation, we can write down the time-dependent mass eigenstate as

$$|\nu_k(t)> = e^{\frac{-iE_k t}{\hbar}} |\nu_k> . \qquad (3)$$

Combining Equation 1), 2) and 3), we see that, a flavor eigenstate is in fact a superposition of all three flavor states:

$$
\begin{aligned}
|\nu_\alpha(t)> &= \sum_{k=1}^{3} U_{\alpha,k} e^{-iE_k t\hbar} |\nu_k> \\
&= \sum_{\beta=e,\mu,\tau} (\sum_{k=1}^{3} U_{\alpha,k} e^{\frac{-iE_k t}{\hbar}} U_{\beta,k}^*) |\nu_\beta> . \quad (4)
\end{aligned}
$$

And the probability of the transition from state α to state β can be obtained as the square of the inner product of the two states,

$$P_{\nu_\alpha \to \nu_\beta} = |<\nu_\beta|\nu_\alpha>|^2 = |\sum_{k=1}^{3} U_{\alpha,k} e^{\frac{-iE_k t}{\hbar}} U_{\beta,k}^*|^2 . \quad (5)$$

Because the three mass eigenstates are normal to each other, only terms with the same subscript survive. Continue simplifying the above equation, we get,

$$P_{\nu_\alpha \to \nu_\beta} = \sum_{j,k=1}^{3} U_{\alpha,k}^* U_{\beta,k} U_{\alpha,j} U_{\beta,j}^* e^{\frac{-(E_k - E_j)t}{\hbar}} . \quad (6)$$

The complex exponential phase in equation 6) shows that due to discrepancies in mass, and thus in energy, the flavor eigenstates of neutrino are not stable. Instead, it "oscillates" periodically among all three flavor eigenstates.

4.2. The Maki-Nakagawa-Sakata (MNS) Matrix

The unitary matrix U appears in the previous section is the Maki-Nakagawa-Sakata (MNS) Matrix, named after Ziro Maki, Masami Nakagawa and Shoichi Sakata who introduced it in 1962. It basically describes how the mass eigenstates are mixed in construction of specific flavor eigenstates. In the case of three-flavor neutrino oscillation in vacuum, the MNS matrix

$$U =$$

$$\begin{bmatrix} c_{12}c_{13} & s_{12}c_{13} & s_{13}e^{-i\delta_{CP}} \\ -s_{12}c_{23}-c_{12}s_{13}s_{23}e^{i\delta_{CP}} & c_{12}c_{23}-s_{12}s_{13}s_{23}e^{i\delta_{CP}} & c_{13}s_{23} \\ s_{12}s_{23}-c_{12}s_{13}c_{23}e^{i\delta_{CP}} & -c_{12}s_{23}-s_{12}s_{13}c_{23}d^{i\delta_{CP}} & c_{13}c_{23} \end{bmatrix},$$

$$(7)$$

which is 3×3 matrix. The abbreviation c_{ij} stands for $cos\theta_{ij}$, where θ_{ij} is the mixing angle between ν_i and ν_j. $e^{-i\delta_{CP}}$ is a complex phase that responses to CP violation.[?]

The maxing matrix for two-flavor neutrino oscillation is a lot simpler, the 2×2 matrix

$$U = \begin{bmatrix} cos\theta & sin\theta \\ -sin\theta & cos\theta \end{bmatrix} . \qquad (8)$$

We do not have the complex phase this time. The angle θ is simply just the mixing angle between the two chosen flavors.[?]

4.3. Example: Oscillation Between Two Flavor Neutrinos[?]

To obtain a clearer picture, let us go through the calculation of the 2-flavor case.

Suppose we want to calculate the transition probability of a muon neutrino into an electron neutrino at time t after its creation. The MNS matrix in this case would be a 2×2 matrix. The relation between the flavor eigenstates and the mass eigenstates is summarized as the following matrix equations:

$$\begin{bmatrix} \nu_e \\ \nu_\mu \end{bmatrix} = \begin{bmatrix} cos\theta & sin\theta \\ -sin\theta & cos\theta \end{bmatrix} \begin{bmatrix} \nu_1 \\ \nu_2 \end{bmatrix} \qquad (9)$$

and

$$\begin{bmatrix} \nu_1 \\ \nu_2 \end{bmatrix} = \begin{bmatrix} cos\theta & -sin\theta \\ sin\theta & cos\theta \end{bmatrix} \begin{bmatrix} \nu_e \\ \nu_\mu \end{bmatrix}. \qquad (10)$$

Rewriting the above equation in the form of equations 1) and 2), we have

$$|\nu_e> = cos\theta|\nu_1> + sin\theta|\nu_2> \qquad (11)$$

$$|\nu_\mu> = -sin\theta|\nu_1> + cos\theta|\nu_2> \qquad (12)$$

$$|\nu_1> = cos\theta|\nu_e> - sin\theta|\nu_\mu> \qquad (13)$$

$$|\nu_2> = sin\theta|\nu_e> + cos\theta|\nu_\mu> . \qquad (14)$$

Now introduce the time dependences to equation 11) and 12). Then, substitute $|\nu_1>$ and $|\nu_2>$ with equation 13) and 14), we have:

$$\begin{aligned} |\nu_e> &= (cos^2\theta|\nu_e> - cos\theta sin\theta|\nu_\mu>)e^{\frac{-iE_1t}{\hbar}} \\ &+ (sin^2\theta|\nu_e> + sin\theta cos\theta|\nu_\mu>)e^{\frac{-iE_2t}{\hbar}} \quad (15) \end{aligned}$$

and

$$\begin{aligned} |\nu_\mu> &= (-sin\theta cos\theta|\nu_e> + sin^2\theta|\nu_\mu>)e^{\frac{-iE_1t}{\hbar}} \\ &+ (sin\theta cos\theta|\nu_e> + cos^2\theta|\nu_\mu>)e^{\frac{-iE_2t}{\hbar}}. \quad (16) \end{aligned}$$

Now, we can calculate the transition probability of an muon neutrino transforming into an electron neutrino (or the other way around) at time t, simply by squaring the inner product of "$<\nu_e|$" and "$|\nu_\mu>$". Because ν_e and ν_μ are orthonormal, only terms with identical subscript survive, leaving

$$\begin{aligned} P(\nu_\mu \to \nu_e) &= |<\nu_e|\nu_\mu>|^2 \\ &= |-sin\theta cos\theta e^{\frac{-iE_1t}{\hbar}} + sin\theta cos\theta e^{\frac{-iE_2t}{\hbar}}|^2 \\ &= sin^2\theta cos^2\theta(2 - e^{\frac{-i(E_2-E_1)t}{\hbar}} + e^{\frac{i(E_2-E_1)t}{\hbar}}) \\ &= \frac{1}{2}sin2\theta(1 - cos\frac{(E_2-E_1)t}{\hbar}) \quad (17) \end{aligned}$$

Let us carry out some approximations to make our answer more explicit. In general, the energy of a neutrino is $E = \sqrt{p^2c^2 + m^2c^4}$. Because neutrino are traveling at a speed close to the speed of light (not the speed of light), we can approximate E with the first two terms of

its binomial expansion. This gives $E \approx pc + \frac{1}{2}\frac{m^2c^4}{pc}$ and therefore

$$\begin{aligned} P(\nu_\mu \to \nu_e) &= \frac{1}{2}sin2\theta(1 - cos\frac{(E_2-E_1)t}{\hbar}) \\ &= \frac{1}{2}sin2\theta(1 - cos\frac{1}{2}\frac{(m_2^2-m_1^2)c^4t}{pc\hbar}) \\ &= \frac{1}{2}sin2\theta(1 - cos\frac{1}{2}\frac{(\Delta m^2)c^4t}{pc\hbar}) \\ &= \frac{1}{2}sin2\theta sin^2\frac{1}{4}\frac{(\Delta m^2)c^4t}{pc\hbar}. \quad (18) \end{aligned}$$

The sine term of the above equation tells us that the amplitude of transition probability depends on the mixing angle θ. When $\theta = \pi/4$, it reaches its maximum value $1/2$. Similarly, from the sine square term, we can see that the frequency of oscillation depend of Δm^2. The larger the mass difference, the more rapid neutrinos are going to oscillate.

4.4. Evidences of Neutrino Oscillation

Even today, the validity of the neutrino oscillation theory is still doubted by some physicists due to its conflict with the standard model of particle and CP violation, but two strong evidences have been found for the past 2 decades. The first compelling evidence was found at the Super-Kamiokanade detector in Japan, 1998. Comparing two groups of muon neutrinos, one coming directly from the upper atmosphere and the other coming through the earth, experimenters detected a difference in the number of muon neutrinos between the two groups. And that difference depended on the distance traveled by the neutrinos before reaching the detector.[?]

The second and even more compelling evidence was found in 2001 at the Sudbury Neutrino Observatory (SNO) in Canada. The detector used by SNO was sensitive to all three flavor of neutrinos. Even though the number of electron neutrinos was only 35% of the number predicted, the number of all three types of neutrinos detected was in fact consistent with the predicted value. It was quite reasonable to believe neutrino oscillations did take place when he solar neutrinos were traveling to the earth.

5. CONCLUSION

In this paper, we present the solar neutrino problem along with the theory of neutrino oscillation which tries to tackle the problem. The theory suggests that neutrinos have masses, the frequency of oscillation depend upon the mass differences among mass eigenstates. Even though, the well working standard model of particle we use today assume that neutrinos have no masses, the experimental evidences observed by the

Super-Kamiokanade detector and the SNO, in some extend proves reasonability of the neutrino oscillation theory. And I personally believe that, as the advance of technologies and the increase of our understanding about the neutrinos, we would find a way to resolve this conflict.

[1] Carlo Giunti. "Theory of Neutrino Oscillations". http://arxiv.org/pdf/hep-ph/0608101v1.pdf

[2] Jochin Kopp. "Phenomenology of Three-Flavor Neutrino Oscillation. http://www.mpi-hd.mpg.de/phenocond/pdf/diploma-thesis.pdf

[3] I carried the calculation of this section by myself due to the simplicity of the math.

[4] The Super-Kamiokande Collaboration. "Evidence for Oscillation of Atmospheric Neutrino". http://arxiv.org/pdf/hep-ex/9807003v2.pdf

Characterizing the Boundaries of Quantum Mechanics

Hengyun Zhou[*]

MIT Department of Physics
(Dated: April 30, 2014)

In this paper, I will discuss recent progress in quantum information to characterize quantum mechanics and differentiate it from other possible physical theories and mathematical theories. The paper will start from a discussion of Bell's inequalities at the level covered in lecture. It will then move on to a discussion of more experimentally feasible CHSH inequalities and Tsirelson's bound on quantum correlations. Following this will be recent proposals for physical principles to separate quantum mechanics from other stronger nonlocal correlations, including information causality, multipartite quantum information tasks and local orthogonality.

I. Introduction

Ever since its discovery in the early twentieth century, the peculiarities of quantum correlations have generated much interest and investigation. As early as 1935, Einstein, Podolski and Rosen demonstrated that quantum mechanics is inherently nonlocal [1], and they therefore advocated a local realism formalism to attempt to explain the phenomena dubbed quantum.

In 1964 Bell [2], however, showed that quantum mechanics and local realism give rise to experimentally testable differences. Kochen and Specker also showed [3] that the local realism assumption of hidden variables with definite values independent of measurement settings (noncontextuality) is inconsistent with quantum mechanical predictions. Experiments have since tested Bell's inequality and support quantum mechanics [13–15].

These lower bounds on correlation strength naturally led to efforts to characterize the upper boundaries of quantum mechanics. Notable is work by Tsirelson [4] which proved an upper bound to the strength of quantum correlations in Bell inequality settings.

Along the trails of the EPR paradox, Bennett et al. [5] put forward the possibility of quantum teleportation; this idea, however, does not permit super-luminal communication, since classical information needs to be transmitted. Further work also found that while quantum mechanics and entanglement could be exploited to achieve more efficient communication, they were always bounded by the no-signaling principle, which states that no information can be transmitted by local operations.

Popescu and Rohrlich then discovered [6] that mathematically a much richer class of theories exist. They obey the no-signaling principle yet have correlations stronger than quantum mechanics. These theories, however, would make distributed computations require only a trivial amount of communication [7]. Researchers have thus proposed physical principles which might explain the absence of stronger correlations in nature, including "information causality" which limits the amount of information that can be recovered from a certain amount of communication.

Lately, it has also been found that multipartite principles are necessary to completely distinguish the boundaries between quantum mechanics and stronger theories [8]. Quantum games have been devised to illustrate this point, and a new principle named "local orthogonality" has been proposed to characterize quantum correlations in a multipartite setting.

In this paper, we will give a brief introduction to the aforementioned progress in the exciting field of quantum information and provide some physical reasoning as to why these principles hold true.

II. The Boundary Between Classical Correlations and Quantum Correlations

II.1. Review of Quantum Mechanical Expectations

Although entanglement was first discussed as early as 1935 [1], it took another 30 years for people to realize that the distinction between local and quantum correlations has experimentally testable consequences [2].

Before we derive Bell's inequality and the CHSH inequality, let us first review the quantum mechanical expressions for correlation expectations. For simplicity, we consider a spin-1/2 system with a pair of entangled particles in the singlet state $|\Psi\rangle = \frac{1}{\sqrt{2}}(|+\rangle_A|-\rangle_B - |-\rangle_A|+\rangle_B)$.

We then consider the correlation between a pair of measurements performed on part A and B. If A performs a measurement in the $\vec{a}$ direction and B in the $\vec{b}$ direction, then the correlation function is defined as $C(\vec{a}, \vec{b}) = E[A(\vec{a})B(\vec{b})]$, where E denotes expectation value and here we assume $E[A(\vec{a})] = E[B(\vec{b})] = 0$. Correlations are normalized such that perfect correlation corresponds to $C(\vec{a}, -\vec{a}) = 1$. Therefore, in the quantum mechanics formulation we may write our expression in terms of Pauli matrices $C(\vec{a}, \vec{b}) = \langle(\vec{\sigma_A} \cdot \vec{a})(\vec{\sigma_B} \cdot \vec{b})\rangle$.

By spherical symmetry, we take $\vec{a}$ to be in the $\hat{z}$ direction and $\vec{b}$ in the $x - z$ plane at an angle θ to $\vec{a}$. We can then calculate the quantum-mechanical expression

$$
\begin{aligned}
C(\vec{a}, \vec{b}) &= \langle(\vec{\sigma_A} \cdot \vec{a})(\vec{\sigma_B} \cdot \vec{b})\rangle \\
&= \langle\sigma_{zA}(\cos\theta\sigma_{zB} + \sin\theta\sigma_{xB})\rangle \\
&= \frac{1}{2}(\langle+|\langle-| - \langle-|\langle+|)\sigma_{zA}(\cos\theta\sigma_{zB} \\
&\quad + \sin\theta\sigma_{xB})(|+\rangle|-\rangle - |-\rangle|+\rangle) = -\cos\theta \quad (1)
\end{aligned}
$$

* hyzhou@mit.edu

We also note here that when $\vec{a}$ and $\vec{b}$ are approximately the same we have the small angle approximation $C(\vec{a}, \vec{b}) \approx -1 + \theta^2/2$ as $\theta \to 0$.

II.2. Bell's Inequality

Equipped with the quantum-mechanical expectations, we can now proceed to analyze Bell's inequality. In its original form, it states that for any three measurement settings (in our case directions $\vec{a}$, $\vec{b}$ and $\vec{c}$) and for any theory which invokes local hidden variables, the correlation functions are bounded by the nontrivial relation [2]

$$|C(\vec{a}, \vec{b}) - C(\vec{a}, \vec{c})| \leq 1 + C(\vec{b}, \vec{c}) \qquad (2)$$

Before we give a rigorous derivation, we first motivate this relation from general probability considerations, also known as the Wigner-d'Espagnat inequality [9].

Since $C(\vec{a}, \vec{a}) = -1$, we can think of $M(\vec{a}, \vec{b}) = C(\vec{a}, \vec{b}) + 1 \geq 0$ as characterizing the mismatch between $\vec{a}$ and $\vec{b}$. Now consider the mismatch between the three vectors $\vec{a}$, $\vec{b}$ and $\vec{c}$. In a local theory, each mismatch between $\vec{a}$ and $\vec{b}$ must either be due to a mismatch between $\vec{a}$, $\vec{c}$ or between $\vec{b}$, $\vec{c}$. This implies that the mismatch between $\vec{a}$, $\vec{b}$ is no greater than the sum of the other two mismatches, or mathematically

$$M(\vec{a}, \vec{c}) + M(\vec{b}, \vec{c}) \geq M(\vec{a}, \vec{b}) \qquad (3)$$
$$C(\vec{a}, \vec{c}) + C(\vec{b}, \vec{c}) + 2 \geq 1 + C(\vec{a}, \vec{b})$$
$$C(\vec{a}, \vec{b}) - C(\vec{a}, \vec{c}) \leq 1 + C(\vec{b}, \vec{c})$$

By symmetry $C(\vec{a}, \vec{b}) = C(\vec{b}, \vec{a})$, so we see that equation (2) should hold.

To rigorously derive Bell's inequality, we shall need to use the fact that the two parts of the singlet state are perfectly anti-correlated. In the language of hidden variables,

$$C(\vec{a}, \vec{b}) = \int d\lambda A(\vec{a}, \lambda) B(\vec{b}, \lambda) \rho(\lambda) \qquad (4)$$

Here, λ is the hidden variable of the system and $\rho(\lambda)$ a corresponding probability distribution which, in a classical theory, will encode all information about the distributions. $A(\vec{a}, \lambda) = \pm 1$ and $B(\vec{b}, \lambda) = \pm 1$ denote the observed values for a given λ.

Using the anti-correlation properties of a singlet, and writing A_a as a short hand notation for $A(\vec{a}, \lambda)$ etc., we can write the correlations in terms of integrals over outcomes of system A. To prove the inequality, we only need to transform two correlations into the third one using sin-

glet properties. This will lead us to

$$|C(\vec{a}, \vec{b}) - C(\vec{a}, \vec{c})| = |\int d\lambda \rho(\lambda)(A_a B_b - A_a B_c)|$$

$$= |\int d\lambda \rho(\lambda)(-A_a A_b + A_a A_c)|$$

$$= |\int d\lambda \rho(\lambda)(-A_a A_b + A_a A_b A_b A_c)| \qquad (5)$$

$$= |-\int d\lambda \rho(\lambda) A_a A_b (1 - A_b A_c)|$$

$$\leq \int d\lambda \rho(\lambda)(1 - A_b B_c) \qquad (6)$$

$$= 1 + C(\vec{b}, \vec{c})$$

Here in equation (5,6) we have used the fact that the outcomes are ± 1 and in equation (6) we use $1 - A_b A_c \geq 0$. Therefore, we have proved a bound to all local theories. This bound essentially stems from the fact that we are considering a mathematical setup which allows separable descriptions of the two subsystems A and B.

Now we compare to quantum mechanics. For simplicity, we assume that the three vectors $\vec{a}$, $\vec{b}$, $\vec{c}$ are coplanar. Then the inequality becomes $|\cos\theta_{ab} - \cos\theta_{ac}| \leq 1 - \cos\theta_{bc}$. But if we consider the case where $\vec{c}$ is between $\vec{a}$ and $\vec{b}$ with $\theta_{ac} = \theta_{bc} = \frac{1}{2}\theta_{ab} = \theta$, as shown in figure 1, then locality requires $2\cos\theta \leq 1 + \cos 2\theta = 2\cos^2\theta$, which is violated for angles $\theta \in (0, \frac{\pi}{2})$. Therefore, quantum mechanics and local realism have different predictions.
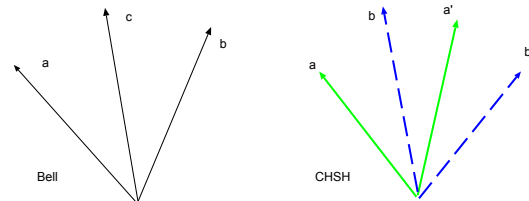

FIG. 1. Figure of the directions of vectors chosen in a measurement. On the left is Bell's inequality, on the right is the CHSH inequality with solid vectors denoting system A and dashed ones denoting system B.

II.3. The CHSH Inequality

The above Bell's inequality is valid for perfectly correlated or anti-correlated states for A and B, since we need to transform measurement results from B to A in our derivation. In actual experiments, however, due to detector efficiency limitations and other factors, we might not always be able to achieve perfect correlations, and therefore we need an inequality which does not rely on this assumption. It was found that a generalization to Bell's inequality - the CHSH inequality proposed in 1969 [10]- can satisfy this by introducing 4 measurement directions,

and moreover, it provides mathematical advantages for generalizing into other no-signaling theories.

The form of the CHSH inequality is the following: (hereon we drop the vector symbols for simplicity)

$$|C(a,b) + C(a',b) + C(a',b') - C(a,b')| \leq 2 \quad (7)$$

An intuitive argument is similar to the one presented in the previous section, in which we consider the mismatches which can occur between different correlations. Once again the mismatch is bounded by the sum of the others, which will lead to the above equation.

A rigorous derivation uses the same idea of transforming one correlation into another, this time by supplementing terms, and then uses the fact that outcomes $|A|, |B| \leq 1$. Following the trails of Bell in his 1987 book [11] and using the same notation as the previous section,

$$\begin{aligned} C(a,b) - C(a,b') &= \int d\lambda \rho(\lambda)(A_a B_b - A_a B_{b'}) \\ &= \int d\lambda \rho(\lambda) A_a B_b (1 - A_{a'} B_{b'}) \\ &\quad - \int d\lambda \rho(\lambda) A_a B_{b'} (1 - A_{a'} B_b) \\ &\leq \int d\lambda \rho(\lambda)(1 - A_{a'} B_{b'} + 1 - A_{a'} B_b) \quad (8) \\ &= 2 - C(a',b) - C(a',b') \end{aligned}$$

where in equation (8) we have used the bounds on outcome values $|A|, |B| \leq 1$. We have therefore proved the CHSH inequality for local realism theories.

The CHSH inequality is violated by quantum mechanics for certain choices of measurement directions. In particular, for the configuration in figure 1, choosing $\theta_{ab} = \theta_{a'b} = \theta_{a'b'} = \frac{\pi}{4}$, $\theta_{ab'} = \frac{3\pi}{4}$ gives $C(a,b) + C(a',b) + C(a',b') - C(a,b') = 2\sqrt{2}$, violating the inequality.

Before we move on to more general no-signaling theories, we note experimental evidence which is overwhelmingly in favor of nonlocal correlations. Using the form of the CHSH inequality which takes photon detector efficiency and the fact that we can only detect one polarization at a time into account [10], Freedman and Clauser [12] were able to experimentally test the inequality (7). Their results are equivalent to finding that $C(a,b) + C(a',b) + C(a',b') - C(a,b') = 2.416 \pm 0.104$ can be achieved, violating Bell's inequality.

In 1982 Aspect et al. performed a similar experiment [13], this time with the polarization directions chosen after the photons were generated to ensure space-like separation. Further experiments by Zeilinger's group and other scientists have closed possible loopholes such as freedom of choice and detector efficiency, further corroborating quantum mechanical results [14, 15].

III. Quantum Correlations and Beyond

III.1. Tsirelson's Bound

While we have seen that local realism imposes restrictions on the possible correlations, we would also like to ask whether quantum mechanics might have any similar restrictions. A natural restriction for any correlation function, not limited to quantum mechanics, is that

$$|C(a,b) + C(a',b) + C(a',b') - C(a,b')| \leq 4 \quad (9)$$

since each correlation function satisfies $|C(a,b)| = |\int d\lambda \rho(\lambda) A_a B_b| \leq |\int d\lambda \rho(\lambda)| = 1$.

This however can not be saturated by quantum mechanics due to the Tsirelson's (Cirel'son) bound [4]. The key to proving this is to recognize that quantum mechanics imposes restrictions on the commutators, so that the different correlation functions are related to each other.

To prove Tsirelson's bound of $2\sqrt{2}$ on the right-hand-side of equation (7), we write the left hand side of the inequality in operator form and define

$$T = A_a B_b + A_{a'} B_b + A_{a'} B_{b'} - A_a B_{b'} \quad (10)$$

As usual, the operators satisfy $A^2 = B^2 = I$. Since the two systems A and B are space-like separated, $[A_a, B_b] = 0$ for any directions $\vec{a}$ and $\vec{b}$.

Since we are interested in the correlations, we wish to generate interference between terms, so we square equation (10) to get

$$\begin{aligned} T^2 &= 4I + \{A_a, A_{a'}\} + \{A_a B_b, A_{a'} B_{b'}\} - \{B_b, B_{b'}\} \\ &\quad + \{B_b, B_{b'}\} - \{A_{a'} B_b, A_a B_{b'}\} - \{A_{a'}, A_a\} \\ &= 4I + (A_a A_{a'} - A_{a'} A_a)(B_b B_{b'} - B_{b'} B_b) \\ &= 4I + [A_a, A_{a'}][B_b, B_{b'}] \quad (11) \end{aligned}$$

where $\{A, B\} = AB + BA$, $[A, B] = AB - BA$ are the anticommutators and commutators.

Local deterministic theories require the commutators to be 0, so we recover the CHSH bound $|T| \leq 2$. In quantum mechanics, the eigenvalues of A and B are ± 1, so $|\langle AB \rangle| \leq 1$. Therefore

$$\langle T \rangle \leq \sqrt{\langle T^2 \rangle} \leq 2\sqrt{2} \quad (12)$$

In general, though, the observables may not necessarily obey the commutation relations which we have exploited in equation (11), and therefore supraquantum correlations might violate Tsirelson's bound.

III.2. Maximally Strong No-signaling Correlations

In fact, it was shown by Popescu and Rohrlich [6] that there exist correlations, now known as PR boxes, that fit into relativity (meaning that they do not allow superluminal communication of information) yet still achieve the maximal CHSH value of $T = C(a,b) + C(a',b) + C(a',b') - C(a,b') = 4$.

Consider a "superquantum" singlet state in which for chosen measurement directions $\vec{a}$ and $\vec{b}$, the correlation function will only depend on the angle $C(a,b) = C(\theta_{ab})$. By symmetry, the outcome probabilities satisfy $P(\uparrow\uparrow) = P(\downarrow\downarrow)$ and $P(\uparrow\downarrow) = P(\downarrow\uparrow)$. Since their sum is 1, we have

$P(\uparrow) = P(\uparrow\uparrow) + P(\uparrow\downarrow) = 1/2$, i.e. the outcome of one measurement contains no information of the other, thus satisfying relativistic causality. The only restriction on the correlation function is that by rotational symmetry $C(\pi - \theta) = -C(\theta)$.
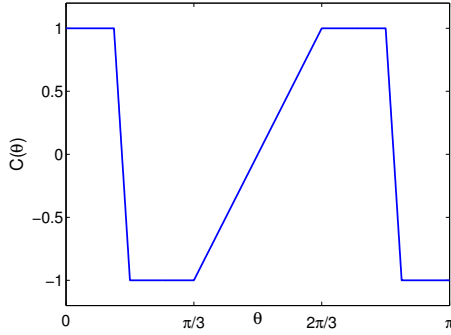

FIG. 2. Figure of the correlation function for a maximally strong no-signaling correlation function as a function of angle

Now, instead of quantum mechanics where $C(a,b) = -\cos\theta_{ab}$, we artificially construct a correlation function as shown in figure 2. From this figure, we see that as long as we construct a suitable function where there exists a point with $C(\theta) = -C(3\theta) = 1$ (in this case $\theta = \pi/12$ suffices), then we can choose a configuration as in figure 1 with angle θ between the vectors and achieve the maximal CHSH value of $T = C(a,b) + C(a',b) + C(a',b') - C(a,b') = 4$.

III.3. Physical Implications of Stronger-than-Quantum Correlations

The preceding example of stronger no-signaling correlations (henceforth called NS correlations) shows that quantum mechanics is not the unique theory which satisfies both nonlocality and relativity. Indeed, there exist a broad class of theories which also satisfy these two principles. Van Dam showed, however, that these correlations will have strong information consequences [7, 16].

Before we look at these consequences, let us first rephrase our previous inequality into the form of a game or an information task, also known as the black-box model.

We imagine two parties, Alice and Bob, sharing two prewired boxes. The boxes might have any kind of correlation, depending on which theory we would like to analyze. The boxes have the functionality that when Alice and Bob each insert an input (x for Alice, y for Bob) into their own side, the box returns a value on each side, denoted as u and v. We shall assume that all values are binary choices in the following discussion, since a general case can be constructed by expanding the number in base 2. Here the values satisfy $x, y, u, v \in \{0, 1\}$.

Now we consider a game in which Alice and Bob need to construct a box that will produce outputs satisfying ($\oplus$ denotes congruence mod 2)

$$u \oplus v = xy \qquad (13)$$

how likely are they to succeed given a certain type of resource that they can share beforehand?

We can in fact easily obtain the result by mapping this problem into the CHSH inequality. In equation (13), to succeed we require $u \oplus v = 0$ when $xy = 0$ (3/4 of the time) and $u \oplus v = 1$ when $xy = 1$ (1/4 of the time). This ratio is precisely that of the signs in the CHSH inequality, and therefore if we map $x = 0, 1$ into $A(a'), A(a)$, $y = 0, 1$ into $B(b), B(b')$ and output $u = 1$ if measurements yield $A = 1$, $u = 0$ if measurements yield $A = -1$ etc., then the success probability of input set a, b is

$$
\begin{aligned}
P_{success}(a,b) &= P(u_a = v_a = 1) + P(u_a = v_a = 0) \\
&= P(A_a = B_b = 1) + P(A_a = B_b = -1) \\
&= \frac{1 - P(A_a \cdot B_b = -1)}{2} + \frac{P(A_a \cdot B_b = 1)}{2} \\
&= \frac{C(a,b) + 1}{2}
\end{aligned}
$$

The total success probability P and the CHSH value T are thus related by

$$
P = \frac{1}{4} \frac{C(a,b) + C(a',b) + C(a',b') - C(a,b') + 4}{2}
$$

One consequence is elimination of communication redundancy in distributed decision problems [7]. For example, suppose Alice and Bob each have two strings $\vec{x}$ and $\vec{y}$ of 0s and 1s and they wish to determine whether the number of incidents where they both have 1 is even or odd (i.e. whether the inner product between the strings is even or odd, which is also why this problem is called the "inner product" problem).

Classically and even quantum mechanically, one side will have to send the entire string over to get the result. However, with PR boxes, the parity of $\sum_i x_i y_i$ is equal to that of $\sum_i u_i + v_i$, so all that Bob needs to know to compute the decision is simply the parity of $\sum_i u_i$, which can be communicated in one bit.

While eliminating this redundancy doesn't seem to go against our direct physical intuitions, the task is known to be the most general communication task [16], and in a sense it is like achieving $P = NP$ in communication tasks.

III.4. Information Causality as a Physical Principle

In 2009, Pawowski et al. [17] extended this idea into a new principle which they termed information causality.

Suppose Alice and Bob receive strings $\vec{x}$ and $\vec{y}$ and are asked to compute a Boolean function $f(\vec{x}, \vec{y})$. Since any Boolean function can be written as a sum $f(\vec{x}, \vec{y}) =$

$\sum_i P_i(\vec{x})Q_i(\vec{y})$, where P_i and Q_i are locally computable quantities, all they need to do is let Alice compute P_i locally and employ the inner product algorithm discussed in the previous section.

For a PR box, if we choose $\vec{y} = (K)$ and $f(\vec{x}, K) = x_K$, where K is some given index, then we see immediately that Bob can access any bit Alice has, though not simultaneously. This seems to imply that they actually have communicated more information than we naturally imagine, and this is where information causality poses a boundary, restricting the amount of information that Bob can recover from his initial resources and Alice's signal bit(s) by m, the information volume communicated.
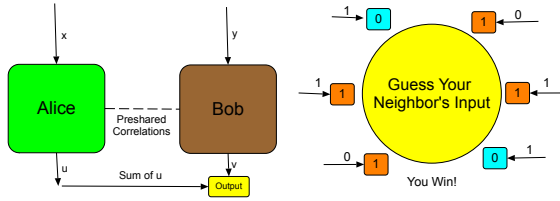

FIG. 3. Figure of the two games we consider in this article. The first one is a distributed computing problem and the second one is the "guess your neighbor's input" game, where the players have won in this particular example.

This formulation can be made more rigorous by using mathematical expressions of entropy and Shannon mutual information, and people have shown [17] that the principle singles out correlations which violate the CHSH inequality stronger than the Tsirelson's bound. These detailed discussions, however, are beyond the scope of this paper.

IV. Multipartite principles

IV.1. Game of "Guess Your Neighbor's Input"

To illustrate interesting consequences of a multipartite setting, we introduce the game of "guess your neighbor's input", first studied by Almeida et al [18]. As the name suggests, the game consists of N people forming a circle for which each person's task is to output the bit that the person to his left received, see figure 3. Formally, the winning probability is

$$\omega = \sum_{\vec{x}} q(\vec{x})P(a_i = x_{i+1}|\vec{x}) \tag{14}$$

where $q(\vec{x})$ denotes the input distribution and $P(\vec{a}|\vec{x})$ denotes the probability of outcome vector $\vec{a}$ given input vector $\vec{x}$.

If there are no shared correlations between the parties, so that each subsystem only has local resources, every player can only make a binary choice according to the input that they have received. Suppose that an output strategy succeeds when a string x is the input, then it will also succeed only for the input $\bar{x}$, where the bar denotes

inverting all input bits and hereon we will omit vector symbols on top to simplify notation. Clearly then, the classical optimal winning probability is given by

$$\omega_c = \max_x[q(x) + q(\bar{x})] \tag{15}$$

Almeida et al. prove that quantum mechanics can not do any better in this task by exploiting an algebraic identity that only relies on the properties of projective operators and does not depend on any commutation features of quantum mechanics.

In quantum mechanics, the N parties will share an entangled state $|\psi\rangle$ beforehand. If we define projection operators $M_{a_i}^{x_i}$ corresponding to projection of the ith person's state onto result a_i if he/she is given x_i, and let $M_x = M_{x_2}^{x_1} \otimes ...M_{x_1}^{x_n}$, then the winning probability ω_q and operators M_x satisfy

$$\omega_q = \sum_x q(x)\langle M_x\rangle \tag{16}$$

$$M_x^2 = M_x \tag{17}$$

$$M_x M_y = 0 \text{ for } x \neq y, \bar{y} \tag{18}$$

Now we may proceed to try and prove $\omega_c \geq \omega_q$. Due to the property in equation (17), we naturally wish to put $\omega_c - \omega_q$ into the form of a sum of squares. Some guessing around and a few mathematical tricks yield

$$\omega_c - \omega_q = \omega_c - \sum_x q(x)M_x$$

$$= (\sqrt{\omega_c} - \sum_x \frac{q(x)}{\sqrt{\omega_c}}M_x)^2 + \sum_x q(x)M_x$$

$$- \sum_x \frac{q(x)^2}{\omega_c}M_x - \sum_x \frac{q(x)q(\bar{x})}{\omega_c}M_x M_{\bar{x}} \tag{19}$$

$$= (\sqrt{\omega_c} - \sum_x \frac{q(x)}{\sqrt{\omega_c}}M_x)^2 + \sum_x \frac{q(x)^2 + q(x)q(\bar{x})}{\omega_c}M_x$$

$$- \sum_x \frac{q(x)^2}{\omega_c}M_x - \sum_x \frac{q(x)q(\bar{x})}{\omega_c}M_x M_{\bar{x}} \tag{20}$$

$$= (\sqrt{\omega_c} - \sum_x \frac{q(x)}{\sqrt{\omega_c}}M_x)^2 + \frac{1}{2}\sum_x \frac{q(x)q(\bar{x})}{\omega_c}(M_x - M_{\bar{x}})^2$$

$$\geq 0 \tag{21}$$

where in the derivations all operators M_x stand for their expectation values $\langle M_x\rangle$ and we have repeatedly made use of identities (17,18). Since $\omega_c - q(x) - q(\bar{x}) \leq 0$ by equation (15), we have also replaced all $q(x)$ by $q(x) + [\omega_c - q(x) - q(\bar{x})]/2$ to make $q(x) + q(\bar{x}) = \omega_c$ in our preceding arguments. The last line in equation (21) follows from the fact that the two terms are sums of Hermitian operators multiplied by nonnegative numbers.

Intuitively, one might guess that the results above are due to the fact that relativity prohibits any local result to reveal information about its neighbor. However here arises the peculiarity of multipartite cases, in that for general no-signaling theories, even though any individual party does not reveal information about its neighbor,

for certain inputs by utilizing established NS correlations they can still collectively improve the winning probability.

A mathematical statement of no-signaling is that the probability distribution of any subset $\{i_1, ..., i_k\}$ should not depend on the choices of the remaining parts, so that mathematically

$$P(a_{i_1}, ..., a_{i_k}|x_1, ..., x_N) = P(a_{i_1}, ..., a_{i_k}|x_{i_1}, ..., x_{i_k}) \quad (22)$$

To find a case where NS correlations do better, we would like to have the inputs correlated to some degree. Therefore, we consider the simple case where $N = 3$, with input distribution

$$q(x) = \begin{cases} 1/2^{3-1}, & x_1 \oplus x_2 \oplus x_3 = 0 \\ 0, & \text{otherwise} \end{cases} \quad (23)$$

Intuitively, the input is strongly correlated: knowing two bits automatically tells us what the third bit is. However, each individual will not be able to extract any information about their neighbor just by looking at what they have received.

Now consider what restrictions the no-signaling principle imposes on these correlations [18]. We are most interested in the terms which appear in the winning probabilities

$$\begin{aligned} \omega = \frac{1}{4}[&P(000|000) + P(110|011) + P(011|101) \\ &+ P(101|110)] \end{aligned}$$
$$\omega_c = \omega_q \leq \frac{1}{4} \quad (24)$$

We also wish to find a bound from the no-signaling principle, so we should try to transform different terms into having the same input and make use of some normalizations. This leads us to

$$P(000|000) \leq \sum_{a_3} P(00a_3|000) = \sum_{a_3} P(00a_3|001)$$
$$P(110|011) \leq \sum_{a_2} P(1a_20|011) = \sum_{a_2} P(1a_20|001)$$
$$P(011|101) \leq \sum_{a_1} P(a_111|101) = \sum_{a_1} P(a_111|001)$$

Here the inequalities follow from probabilities being non-negative and the equalities come from the no signaling condition. Notice how each time we only change one bit, but all three situations can be tuned to have matched inputs.

Writing down similar expressions for each three terms and summing over them we find

$$3[P(000|000)+P(110|011)+P(011|101)+P(101|110)] \leq 4$$

implying that $\omega_{ns} \leq 4/3\omega_c$. Input distributions can indeed be found which saturate this bound [18], though the mathematical constructions are quite complicated and do not have a clear physical intuition. In fact, similar ratios can also be obtained for more parties and they are all bound by 2.

IV.2.   Necessity for a Multipartite Principle

We would like to note that correlations which do not violate Tsirelson's bound for the CHSH inequality could still be stronger than quantum mechanics: the bound only singles out part of the boundary, but there might be other restrictions that make a correlation stronger than any possible quantum correlation.

In fact, Gallego et al. [8] showed that to completely characterize quantum mechanics, any principle which is bipartite, in the sense that when generalizing it to N parties it is applied to a bipartition of the N parties, is insufficient. They managed to construct an example where for any bipartition of the system the result will be the same as a classical local theory, but in multiparty cases it violates the "guess your neighbor's input" bound (24), meaning that it is actually supra-quantum.

IV.3.   Local Orthogonality as a Physical Principle

One of the latest progress in formulating a multipartite physical principle to characterize quantum mechanics is local orthogonality [19].

For a system of n parties with each party having m possible measurements with d outcomes per measurement, two events $e = (a_1, ..., a_n|x_1, ..., x_n)$ and $e' = (a'_1, ..., a'_n|x'_1, ..., x'_n)$ are considered locally orthogonal if for some measurements with the same input, the outcomes are different. A collection of events $\{e_i\}$ is called orthogonal if they are pairwise orthogonal. We would then naturally expect the normalization restriction for any set of orthogonal events

$$\sum_i P(e_i) \leq 1 \quad (25)$$

If there are only two parties then it can be shown that this restriction is equivalent to the no-signaling principle, which seems to be a pretty weak constraint. However the trick of this method is to consider not one copy of this pair, but instead k copies, and then apply local orthogonality to all of these parties. This new set of restrictions is known as LO^k. It turns out that these larger systems will have stronger restrictions which can be plugged back to obtain a bound on the bipartite case.

As an example, we illustrate the method for a PR box. Consider 2 copies of PR boxes, with probability distribution $P(u_1 v_1 u_2 v_2 | x_1 y_1 x_2 y_2)$, then it is possible to construct an inequality from local orthogonality [19]

$$\begin{aligned} P(0000|0000) &+ P(1110|0011) + P(0011|0110) \\ &+ P(1101|1011) + P(0111|1101) \leq 1 \quad (26) \end{aligned}$$

This inequality is violated by PR boxes by a value of 5/4 of the left hand side, since each term is equal to 1/4 (recall that $P(uv|xy) = 1/4$ whenever $u \oplus v = xy$). Therefore, PR boxes are excluded by LO^2.

However, it is known that even LO^∞ does not exclude all stronger-than-quantum correlations [20]. Therefore, it is still an interesting question as to how we might improve these principles to further prune out the nonphysical theories that lie between current boundaries and quantum mechanics.
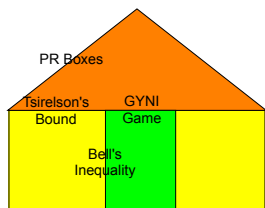

FIG. 4. Schematic of a possible cross section of the correlation polytope. The smallest green region are the local correlations, the larger rectangular region with green and yellow are the quantum correlations, and the outer boundaries characterize all no-signaling correlations. Some boundaries between theories are labeled in the figure as well.

V. Conclusion

In this paper, we have reviewed the various results in characterizing the boundaries of quantum mechanics. Many discoveries have been made over the years to help us understand what quantum mechanics, with all of its fancy yet powerful machinery that has been so successful in explaining the microscopic world, actually means from a physical and information theoretical viewpoint.

Although many of this progress might seem haphazard at first sight, looking back we can see the natural logical development in these works: from Bell's bound on classical physics, people were prompted to find a similar bound on quantum mechanics; this then led to the realization that relativity and nonlocality are insufficient, and that more compelling reasons were needed for quantum mechanics. Then an investigation of what those strong correlations could do led to new physical principles, which imposed further restrictions. When the natural generalizations of these principles to multiparty cases were examined, researchers realized that more was needed, leading to the most recent developments in the field.

If we visualize all of the possible correlations as points in a higher dimensional space (figure 4), with coordinate values corresponding to the input and output values, then each of the inequalities and principles that we have described above can be thought of as imposing one constraint on the permissible points. Over the years, we have been constantly narrowing our range down and providing better explanations for why these bounds hold true. Hopefully, a better understanding of these underlying principles will shed more light on quantum mechanics and physics as a whole, and let us gain a new appreciation of our beautiful world.

Acknowledgements

[1] A. Einstein, B. Podolsky, and N. Rosen, Physical Review 47, 777 (1935).

[2] J.S.Bell, Physics 1, 195 (1964).

[3] S. Kochen and E. Specker, Indiana Univ. Math. J. 17, 59 (1968).

[4] B. S. Cirel'son, Letters in Mathematical Physics 4, 93 (1980).

[5] C. H. Bennett, G. Brassard, C. Crépeau, R. Jozsa, A. Peres, and W. K. Wootters, Phys. Rev. Lett. 70, 1895 (1993).

[6] S. Popescu and D. Rohrlich, Foundations of Physics 24, 379 (1994).

[7] W. V. Dam, Nonlocality & Communication Complexity, Ph.D. thesis, University of Oxford.

[8] R. Gallego, L. E. Würflinger, A. Acín, and M. Navascués, Physical Review Letters 107, 210403 (2011).

[9] J. S. Bell, Le Journal de Physique Colloques 42, C2 (1981).

[10] J. Clauser, M. Horne, A. Shimony, and R. Holt, Physical Review Letters 23, 880 (1969).

[11] J. S. Bell, Speakable and Unspeakable in Quantum Mechanics (Second Edition). (Cambridge Univ Pr, 2004).

[12] S. J. Freedman and J. F. Clauser, Physical Review Letters 28, 938 (1972).

[13] A. Aspect, J. Dalibard, and G. Roger, Physical Review Letters 49, 1804 (1982).

[14] G. Weihs, T. Jennewein, C. Simon, H. Weinfurter, and A. Zeilinger, Physical Review Letters 81, 5039 (1998).

[15] M. Giustina, A. Mech, S. Ramelow, B. Wittmann, J. Kofler, J. Beyer, A. Lita, B. Calkins, T. Gerrits, S. W. Nam, R. Ursin, and A. Zeilinger, Nature 497, 227 (2013).

[16] S. Popescu, Nature Physics 10, 264 (2014).

[17] M. Pawowski, T. Paterek, D. Kaszlikowski, V. Scarani, A. Winter, and M. Zukowski, Nature 461, 1101 (2009).

[18] M. L. Almeida, J.-D. Bancal, N. Brunner, A. Acín, N. Gisin, and S. Pironio, Physical Review Letters 104, 230404 (2010).

[19] T. Fritz, A. B. Sainz, R. Augusiak, J. B. Brask, R. Chaves, A. Leverrier, and A. Acín, Nature communications 4, 2263 (2013).

[20] A. Acín, T. Fritz, A. Leverrier, and A. B. Sainz, (2012), arXiv:1212.4084.

Von Neumann Entropy and Transmitting Quantum Information

Kevin Zhou
(Dated: May 2, 2014)

We introduce the Shannon entropy and its quantum counterpart, the von Neumann entropy. We then exhibit their operational meanings in the context of coding in a noiseless channel, via Shannon's and Schumacher's theorems. We then give a brief overview of the problems of coding in a noisy quantum channel, and the concept of accessible information.

I.   INTRODUCTION

In 1948, Shannon's paper "A Mathematical Theory of Communication" jumpstarted the field of information theory, both defining the Shannon entropy and linking it to limits on communication rates in noiseless and noisy channels. [4] However, it was not until almost 40 years after that the ideas of information theory were applied to quantum mechanics. [3]

Quantum information theory presents a number of features that cannot be reproduced in classical information theory. For example, it is possible for two states to individually not possess definite states, but for the composite system to be in a definite state; this is quantum entanglement. As another example, quantum states that are not orthogonal cannot be perfectly distinguished; classical information theory is the special case where we only transmit orthogonal quantum states.

Despite these differences, results in classical and quantum information theory, along with their proofs, often parallel each other closely. In this paper, we briefly discuss the Shannon entropy and Shannon's source coding theorem, then discuss Schumacher's theorem, its quantum analog. We also consider transmission of information over a noisy channel, which leads to the concept of mutual information and its quantum analog, the Holevo information. [2]

II.   CLASSICAL INFORMATION THEORY

A.   Shannon Entropy

Suppose we want to transmit a message A consisting of letters chosen from the alphabet $\{a_1, \ldots, a_k\}$, with a_i occurring with probability p_i. Further suppose that the letters in our message in our set are chosen independently. How many bits per letter are necessary to transmit the message?

Naively, the answer is $\lg k$, where $\lg$ denotes the base-2 logarithm. This lets us assign a unique binary string, of length $\lg k$, to each letter. However, we already know this is not the case. For example, Morse code transmits 26 distinct letters using only binary dots and dashes, but the average number of dots/dashes used for each letter is less than $\lg 26$ because more common letters, such as E and T, are given shorter representations. (The analogy is not perfect, because Morse code also includes a third

symbol (a pause) to separate letters.)

The idea, which is to give precedence to the more likely letters, is sharpened in Shannon's theorem. We will see that when we consider blocks of many letters at once, we will only have to code a fraction of the total possible blocks to get an arbitrarily high probability of successful transmission. The length of such a "typical" block will be given by the Shannon entropy,

$$H(A) = -\sum_i p(a_i) \lg p(a_i) \tag{1}$$

B.   Mathematical Results

By the convexity of the $\lg$ function, it can be shown that the Shannon entropy $H(A)$ is maximized when all the probabilities are equal to $1/k$. In this case, it is equal to $\lg k$, which intuitively fits with our discussion in the previous section; if none of the letters are privileged over the others, coding is as difficult is possible, we cannot do better than the naive code.

Moreover, as one of the p_i approaches 1, the Shannon entropy approaches 0. This is also plausible, because when $p_i = 1$ we will know that the message consists only of the letter a_i before it is even sent.

The weak law of large numbers will be useful. Suppose we have N independent, identically distributed random variables $x_1, \ldots, x_n$ with mean $\overline{x}$ and finite variance. Then for any $\delta, \epsilon > 0$, there exists an N_0 so that for $N > N_0$,

$$P\left(\left|\frac{\sum_i x_i}{N} - \overline{x}\right| > \delta\right) < \epsilon \tag{2}$$

C.   Shannon's Source Coding Theorem

We now quantify the notion of a "typical" block. Consider the random variable on letters $f(a) = -\lg p(a)$. By definition, its mean value is $H(A)$. Considering a block $\alpha = a_1 a_2 \ldots a_N$ of N letters, the sum of the values of this random variable is equal to

$$
\begin{aligned}
f(a_1) + \ldots + f(a_N) &= -(\lg p(a_1) + \ldots + \lg p(a_N)) \\
&= -(\lg p(a_1) p(a_2) \ldots p(a_N)) \\
&= -(\lg p(\alpha))
\end{aligned}
$$

322

where $p(\alpha)$ is the probability of the block α occurring. Applying Eq. (2), we find that for any $\epsilon, \delta > 0$,

$$P\left(\left|\frac{-\lg p(\alpha)}{N} - H(A)\right| > \delta\right) < \epsilon \qquad (3)$$

for sufficiently large N. Define a typical block to be one that satisfies this inequality. How many typical blocks are there? This is constrained by the fact that the sum over all blocks $\sum_\alpha p(\alpha)$ must be 1. The above tells us that the probability of a typical block satisfies $p(\alpha) > 2^{-N(H(A)-\delta)}$. This means there are at most $2^{N(H(A)+\delta)}$ typical blocks.

This gives us our protocol: only code the typical blocks, each of which requires $N(H(A) + \delta)$ bits. Define the fidelity F as the change of successful transmission, $1 - \epsilon$. As ϵ and δ go to zero, we attain a code that expresses the message with perfect fidelity, using on average $H(A)$ bits per letter. [6] This is the forward direction of Shannon's source coding theorem.

We now sketch a proof of the converse. Suppose there was a scheme that encoded a block of length N using on average R bits per letter, where $R < H(A)$. Then we can code a maximum of 2^{NR} blocks. All these blocks should be typical blocks, since the total contribution from the atypical blocks goes to zero. However, applying Eq. (3), we find that the probability of a typical block is at most $2^{-N(H(A)+\delta)}$. That means the probability that our scheme works is bounded by

$$2^{NR}2^{-N(H(A)+\delta)} = 2^{N(R-H(A)+\delta)}$$

For sufficiently large N, we may set $\delta < |R - H(A)|/2$, which shows that the probability of successful transmission goes to zero. This completes the proof of Shannon's theorem.

The coding scheme we have exhibited, though it is optimal by certain standards, lacks many practical features. It requires a codebook of exponential size to decode the typical blocks (which defeats the point of a data compression algorithm), and it requires the probability distribution to be known in advance. However, it serves as a reference point for compression efficiency, similarly to how the Carnot efficiency does the same in thermodynamics. It then serves as a point of comparison for practical algorithms like Huffman coding (which requires little space) and *universal coding* schemes, which do not need to know the probability distribution.

III. NOISELESS QUANTUM CHANNEL

A. Von Neumann Entropy

Suppose we now want to transmit a message consisting of quantum states $|a\rangle$ with probability $p(a)$. We know

that, for the purposes of any measurement, this ensemble is completely specified by the density matrix

$$\rho = \sum_a p(a) |a\rangle \langle a| \qquad (4)$$

and all quantities should be written in terms of it. We claim that the analog of the Shannon information in this context is the *von Neumann entropy*, [5]

$$S(\rho) = -\text{tr}(\rho \lg \rho). \qquad (5)$$

As justification, suppose that all the states we are sending are orthogonal. In this case our message is equivalent to a classical one, so our expression should reduce to the Shannon entropy. This is indeed the case. If we work in the $|a\rangle$ basis, ρ is diagonal with $p(a)$ on the diagonal entries. Then ρ^k is diagonal with diagonal entries $p(a)^k$, which means $f(\rho)$ is diagonal with diagonal entries $f(p(a))$ by applying Taylor series. Then $\rho \lg \rho$ has diagonal entries $p(a) \lg p(a)$, and taking the trace reproduces the Shannon entropy. In general, however, $S(\rho) \leq H(A)$, where $H(A)$ is computed from the $p(a)$.

Next, consider the case of a pure state, $\rho = |a\rangle \langle a|$. Then $\rho^2 = \rho$. Now consider a function of ρ that can be expanded in a Taylor series. Then

$$f(\rho) = \sum a_k \rho^k = \left(\sum a_k\right) \rho = f(1)\rho.$$

Because $\lg 1 = 0$, this shows that the von Neumann entropy of a pure state is zero, which is also plausible. In this case, there is only one possible state that is sent, so we already know the message.

Another useful property will be invariance under unitary evolution. If the quantum state $|\psi\rangle$ is subjected to a unitary evolution U, then the density operator ρ becomes $U\rho U^\dagger$. Then the von Neumann entropy stays the same because

$$\begin{aligned}
\text{tr}\left(f(U\rho U^\dagger)\right) &= \text{tr}\left(\sum a_k (U\rho U^\dagger)^k\right) \\
&= \text{tr}\left(\sum a_k U\rho^k U^\dagger\right) \\
&= \text{tr}\left(U f(\rho) U^\dagger\right) \\
&= \text{tr}\left(U^\dagger U f(\rho)\right) = \text{tr}\left(f(\rho)\right)
\end{aligned}$$

where we have used the cyclic property of the trace. Note that we have already implicitly used this property when we chose to work in the $|a\rangle$ basis, because taking $U\rho U^\dagger$ is equivalent to a change of basis.

B. Fidelity

The quantum analog of the classical coding problem is as follows: given a message characterized by a density matrix ρ, how many *qubits* per letter are necessary

to transmit the message with high *fidelity*? Before we continue, we have to define two new terms.

A *qubit* is an arbitrary two state system. When we transmit a message using k qubits, we are representing it as a vector in a 2^k-dimensional Hilbert space.

To motivate the definition of fidelity, suppose we attempt to transmit the state $|\psi\rangle$ and our partner receives the density matrix w. The projection operator $\pi = |\psi\rangle \langle\psi|$ acts as a validation test; its expectation value is equal to the probability that a test that w matches $|\psi\rangle$ returns true. For an operator A, the expectation value of A is

$$\langle A \rangle = \text{tr}(A\rho) \qquad (6)$$

Accounting for the different possibilities for $|\psi\rangle$, we define the fidelity [7]

$$F = \sum_a p(a)\text{tr}(\pi_a w_a) \qquad (7)$$

Note that this is consistent with our previous definition of fidelity. In classical information theory, a string with an incorrect bit contributed zero to the fidelity. In this case, a bit flip is equivalent to sending a qubit state orthogonal to the intended state, which makes the projection zero, also contributing nothing.

C.   Schumacher's Theorem

Schumacher's Theorem states that the most efficient possible high fidelity encoding scheme, requires on average $S(\rho)$ qubits per letter. Parallel to Shannon's theorem, we will achieve this by only sending the components of states that lie within a "typical subspace".

Because ρ is Hermitian, we may choose a orthogonal basis where it is diagonal. That is, we can choose orthogonal $|\varphi_i\rangle$ so that ρ is equivalent to sending the state $|\varphi_i\rangle$ with probability p_i. Because $S(\rho)$ is invariant under a change of basis, we know that $-\sum p_i \lg p_i = S(\rho)$. Because the quantum states are orthogonal, this is equivalent to sending classical states, so we may borrow from the proof of Shannon's theorem.

Consider sending a block of N letters, represented by the density matrix $\rho^N = \rho \otimes \ldots \otimes \rho$. Now apply Eq. (3). The eigenvectors take the place of blocks of letters, the eigenvalues take the place of probabilities (because tr $\rho = 1$, they also sum to 1), and the von Neumann entropy $S(\rho)$ takes the place of the Shannon entropy $H(X)$.

Performing all these substitutions, we conclude that there are at most $2^{N(S(\rho)+\delta)}$ typical eigenvectors, where a typical eigenvector has a eigenvalue λ that satisfies $2^{-N(S(\rho)-\delta)} \geq \lambda \geq 2^{-N(S(\rho)+\delta)}$. Moreover, the sum of the eigenvalues of all other eigenvectors is less than ϵ. Define the typical subspace Λ to be the space spanned by the typical eigenvectors, and let $\Lambda^\perp$ be its orthogonal complement.

Schumacher's coding protocol is then as follows.

1. Taking the input block, perform a measurement that projects the state into either Λ or $\Lambda^\perp$. [8]

2. Perform a unitary operation U that takes all typical eigenvectors to a state of the form $|\psi\rangle \otimes |0\rangle \otimes \ldots \otimes |0\rangle$, where $|\psi\rangle$ is a state of $N(S(\rho)+\delta)$ qubits. This is possible because the subspace of such states has dimension $2^{N(S(\rho)+\delta)}$, which was our bound on the number of typical eigenvectors.

3. Send only $|\psi\rangle$ and discard the other qubits.

4. When $|\psi\rangle$ is received, append the appropriate number of $|0\rangle$ qubits and then perform U^{-1}.

The last three steps do not affect the fidelity, but they give us a concrete way to package the information in fewer qubits. The number of qubits per letter is $S(\rho)+\delta$ which limits to $S(\rho)$, as desired. However, we must also show that the fidelity can be made arbitrarily high.

Let **E** be the operator that projects onto the typical subspace. Because the typical eigenvectors' eigenvalues add up to at least $1 - \epsilon$, we know that $\text{tr}(\rho^N \mathbf{E}) > 1 - \epsilon$. When we apply the measurement in step (1) to the pure state $|\varphi\rangle \langle\varphi|$, the result is a density matrix,

$$\rho' = \mathbf{E} |\varphi\rangle \langle\varphi| \mathbf{E} + \rho_j \langle\varphi| (1 - \mathbf{E}) |\varphi\rangle \qquad (8)$$

where ρ_j is the "junk" state that we send if we failed in step 1.

Because the typical eigenvectors do not have anything to do with the states in the alphabet, the fidelity will likely be less than 1 for any of the states in the alphabet. However, we are interested in the fidelity averaged across all possible block states, we apply Eq. (7), which yields

$$\begin{aligned} F &= \sum p_i \langle\varphi_i| \rho'_i |\varphi_i\rangle \\ &= \sum p_i \langle\varphi_i| \mathbf{E} |\varphi_i\rangle \langle\varphi_i| \mathbf{E} |\varphi_i\rangle + \text{"junk" terms} \\ &\geq \sum p_i (\langle\varphi_i| \mathbf{E} |\varphi_i\rangle)^2 \end{aligned}$$

where we have used the fact that the junk terms must contribute a nonnegative amount to the fidelity. We now wish to get a bound on F in terms of ϵ.

For any real number x, we have

$$(x-1)^2 \geq 0 \;\rightarrow\; x^2 \geq 2x - 1 \qquad (9)$$

Applying this to our previous equation yields

$$\begin{aligned} F &\geq \sum p_i (2 \langle\varphi_i| \mathbf{E} |\varphi_i\rangle - 1) \\ &= 2 \,\text{tr}(\rho^n \mathbf{E}) - 1 \\ &> 2(1 - \epsilon) - 1 = 1 - 2\epsilon. \qquad (10) \end{aligned}$$

Thus, as ϵ is taken to zero, we get arbitrarily good fidelity. This concludes the proof of correctness of Schumacher's protocol. We must also prove that we cannot do better than $S(\rho)$ qubits per letter; this is proven in the same way the converse of Shannon's theorem is proven.

IV.   ACCESSIBLE INFORMATION

A.   Mutual Information

The concept of mutual information appears when communicating over a noisy channel. Suppose that when we attempt to send the letter x in an alphabet X, the channel randomly outputs a letter y in an alphabet Y, with the probabilities characterized by conditional probabilities $f(y|x)$. How much information can we learn about x, given y?

When we receive y, we use Bayes rule to update our prior distribution $p(x)$ to $p(x|y)$. We know that $p(x|y) = p(x,y)/p(y)$. Then, taking the log and expectation value of both sides,

$$\langle -\log(p(x|y)) \rangle = \langle -\log p(x,y) \rangle - \langle -\log p(y) \rangle \quad (11)$$

The left hand side is the Shannon information of the posterior distribution. We call this quantity $H(X|Y)$, the conditional entropy; it is the amount of additional bits needed to determine x. The right hand side is, by definition, $H(X,Y) - H(Y)$.

The quantity we want is the amount of information about X which we gained; this is equal to $H(X) - H(X|Y)$. We thus define the mutual information as

$$\begin{aligned} I(X;Y) &= H(X) - H(X|Y) & (12) \\ &= H(X) + H(Y) - H(X,Y) & (13) \end{aligned}$$

where the latter equality shows that I is symmetric in X and Y.

B.   Holevo Bound

We now consider the analogous question in a noisy quantum channel. Suppose we are attempting to send states $|x\rangle$ characterized by a probability distribution $p(x)$. However, due to the noise in the channel, the recipient instead gets a mixed state ρ_x. Denote the ensemble $\{\rho_x, p_x\}$ by $\mathcal{E}$. The recipient then performs a measurement which gives result y characterized by conditional probabilities $p(y|x)$.

Here, the information the recipient is trying to get is *classical* information. The measurement gives a definite result, and this gives us some number of bits of knowledge about the preparation x that was used to send the state. This is in contrast with the previous section, where the focus was having the recipient end up with the correct quantum state; in that case, the recipient might have no idea what that state actually is.

The situation is already more complex than in the classical case. For example, suppose there is no noise at all, and we are trying to send one of two nonorthogonal states $|\varphi\rangle$ and $|\psi\rangle$. Then it is impossible for the recipient to tell with certainty which state he has received, since any possible measurement may give the wrong result.

One possibility is that the recipient may try to boost his chances of success by cloning (making copies of) the received state. Then as long as the mutual information isn't zero, he will be able to distinguish between the two states arbitrarily accurately by making more copies. However, this is forbidden by the *no-cloning* theorem, which states that it is impossible to accurately duplicate quantum states! [1]

Here, the amount of information gain $I(X;Y)$ depends on the measurement scheme. We define the Holevo information as

$$\chi(\mathcal{E}) = S(\rho) - \sum_x p_x S(\rho_x) \quad (14)$$

where ρ is the density matrix $\sum p_x \rho_x$. The Holevo bound states that the accessible information, which is the maximum possible value of $I(X;Y)$ over all measurement schemes, is at most $\chi(\mathcal{E})$. Note that $S(\rho) \leq H(X)$ in general, this means that we can't get more than n bits of classical information out of n qubits! This is, at first glance, a rather surprising conclusion.

Switching back to the context of data compression, consider an alternate scenario when we are intentionally sending mixed states ρ_x with probability p_x (through a noiseless channel). Then $\chi(\mathcal{E})$ is the minimum number of qubits per letter needed to send the message with high fidelity; this is the analog of Schumacher's theorem for mixed states.

V.   CONCLUSION

Quantum information theory presents many new features not found in classical information theory. In this paper, we have considered theoretical bounds on data transmission through noiseless quantum channels, as well as the practical issue of accessible information.

There are many questions that remain. We have not mentioned how one would actually encode mixed states, or when the Holevo bound may be attained. We have also ignored the transmission of entangled states, which open up many new possibilities. Finally, one might want to develop practical algorithms for these tasks. An everyday application of quantum information theory may soon come from quantum cryptography, and its subfield, quantum key distribution.

[1] CH Bennett and DP DiVincenzo. Quantum information and computation. *Nature*, 404(6775):247 – 255, 2000.

[2] Michael A. Nielsen and Isaac L. Chuang. *Quantum Computation and Quantum Information.* Cambridge University Press, 2000.

[3] Benjamin Schumacher. Quantum coding. *Phys. Rev. A*, 51:2738–2747, Apr 1995.

[4] Claude Elwood Shannon. A mathematical theory of communication. *ACM SIGMOBILE Mobile Computing and Communications Review*, 5(1):3–55, 2001.

[5] Mark M. Wilde. From classical to quantum shannon theory. *CoRR*, abs/1106.1445, 2011.

[6] It is not difficult to modify this into a procedure that is guaranteed to never fail. For example, we can pad the codes for each block with a bit that is 0 if the following block is a typical one (in which case we use the code described above) or 1 if it is it not (in which we use the naive

code described earlier). Then the number of bits per letter is bounded by $((1-\epsilon)(N(H(A)+\delta)+1)+\epsilon(N \lg k+1))/N$, which also limits to $H(A)$. However, this is not a very important point, because we would like to keep the idea of fidelity for later use.

[7] In some papers, the fidelity is instead defined as $\sqrt{F}$. Moreover, we're using a special case of the fidelity (which in general is defined between two density matrices), comparing a density matrix and a pure state.

[8] If we get $\Lambda^\perp$, the procedure has failed, though we can continue with the steps anyway. In fact, it doesn't matter what we do, just like it does not matter what we do with the atypical strings in the classical case. We'll later show that as ϵ is taken to zero, the effect on the fidelity will go to zero, because this will almost never happen.